

**PHYSICAL CHEMISTRY OF
MACROMOLECULES**

Second Edition

PHYSICAL CHEMISTRY OF MACROMOLECULES

Basic Principles and Issues

Second Edition

S. F. SUN

St. John's University
Jamaica, New York



A Wiley-Interscience Publication
JOHN WILEY & SONS, INC.

Copyright © 2004 by John Wiley & Sons, Inc. All rights reserved.

Published by John Wiley & Sons, Inc., Hoboken, New Jersey.

Published simultaneously in Canada.

No part of this publication may be reproduced, stored in a retrieval system, or transmitted in any form or by any means, electronic, mechanical, photocopying, recording, scanning, or otherwise, except as permitted under Section 107 or 108 of the 1976 United States Copyright Act, without either the prior written permission of the Publisher, or authorization through payment of the appropriate per-copy fee to the Copyright Clearance Center, Inc., 222 Rosewood Drive, Danvers, MA 01923, 978-750-8400, fax 978-646-8600, or on the web at www.copyright.com. Requests to the Publisher for permission should be addressed to the Permissions Department, John Wiley & Sons, Inc., 111 River Street, Hoboken, NJ 07030, (201) 748-6011, fax (201) 748-6008.

Limit of Liability/Disclaimer of Warranty: While the publisher and author have used their best efforts in preparing this book, they make no representations or warranties with respect to the accuracy or completeness of the contents of this book and specifically disclaim any implied warranties of merchantability or fitness for a particular purpose. No warranty may be created or extended by sales representatives or written sales materials. The advice and strategies contained herein may not be suitable for your situation. You should consult with a professional where appropriate. Neither the publisher nor author shall be liable for any loss of profit or any other commercial damages, including but not limited to special, incidental, consequential, or other damages.

For general information on our other products and services please contact our Customer Care Department within the U.S. at 877-762-2974, outside the U.S. at 317-572-3993 or fax 317-572-4002.

Wiley also publishes its books in a variety of electronic formats. Some content that appears in print, however, may not be available in electronic format.

Library of Congress Cataloging-in-Publication Data:

Sun, S. F., 1922-

Physical chemistry of macromolecules : basic principles and issues / S. F. Sun.—2nd ed.
p. cm.

Includes bibliographical references and index.

ISBN 0-471-28138-7 (acid-free paper)

1. Macromolecules. 2. Chemistry, Physical organic. I. Title.

QD381.8.S86 2004

547'.7045—dc22

2003063993

Printed in the United States of America.

10 9 8 7 6 5 4 3 2 1

CONTENTS

Preface to the Second Edition	xv
Preface to the First Edition	xix
1 Introduction	1
1.1 Colloids, 1	
1.2 Macromolecules, 3	
1.2.1 Synthetic Polymers, 4	
1.2.2 Biological Polymers, 7	
1.3 Macromolecular Science, 17	
References, 17	
2 Syntheses of Macromolecular Compounds	19
2.1 Radical Polymerization, 19	
2.1.1 Complications, 21	
2.1.2 Methods of Free-Radical Polymerization, 23	
2.1.3 Some Well-Known Overall Reactions of Addition Polymers, 23	
2.2 Ionic Polymerization, 25	
2.2.1 Anionic Polymerization, 25	
2.2.2 Cationic Polymerization, 27	
2.2.3 Living Polymers, 27	
2.3 Coordination Polymerization, 30	
2.4 Stepwise Polymerization, 32	

- 2.5 Kinetics of the Syntheses of Polymers, 33
 - 2.5.1 Condensation Reactions, 34
 - 2.5.2 Chain Reactions, 35
- 2.6 Polypeptide Synthesis, 40
 - 2.6.1 Synthesis of Insulin, 43
 - 2.6.2 Synthesis of Ribonucleus, 48
- 2.7 DNA Synthesis, 48
- References, 50
- Problems, 50

3 Distribution of Molecular Weight 52

- 3.1 Review of Mathematical Statistics, 53
 - 3.1.1 Binomial Distribution, 53
 - 3.1.2 Poisson Distribution, 54
 - 3.1.3 Gaussian Distribution, 55
- 3.2 One-Parameter Equation, 56
 - 3.2.1 Condensation Polymers, 57
 - 3.2.2 Addition Polymers, 58
- 3.3 Two-Parameter Equations, 59
 - 3.3.1 Normal Distribution, 59
 - 3.3.2 Logarithm Normal Distribution, 60
- 3.4 Types of Molecular Weight, 61
- 3.5 Experimental Methods for Determining Molecular Weight and Molecular Weight Distribution, 64
- References, 65
- Problems, 65

4 Macromolecular Thermodynamics 67

- 4.1 Review of Thermodynamics, 68
- 4.2 ΔS of Mixing: Flory Theory, 71
- 4.3 ΔH of Mixing, 75
 - 4.3.1 Cohesive Energy Density, 76
 - 4.3.2 Contact Energy (First-Neighbor Interaction or Energy Due to Contact), 79
- 4.4 ΔG of Mixing, 81
- 4.5 Partial Molar Quantities, 81
 - 4.5.1 Partial Specific Volume, 82
 - 4.5.2 Chemical Potential, 83
- 4.6 Thermodynamics of Dilute Polymer Solutions, 84
 - 4.6.1 Vapor Pressure, 87
 - 4.6.2 Phase Equilibrium, 89
- Appendix: Thermodynamics and Critical Phenomena, 91
- References, 92
- Problems, 93

5 Chain Configurations **96**

- 5.1 Preliminary Descriptions of a Polymer Chain, 97
- 5.2 Random Walk and the Markov Process, 98
 - 5.2.1 Random Walk, 99
 - 5.2.2 Markov Chain, 101
- 5.3 Random-Flight Chains, 103
- 5.4 Wormlike Chains, 105
- 5.5 Flory's Mean-Field Theory, 106
- 5.6 Perturbation Theory, 107
 - 5.6.1 First-Order Perturbation Theory, 108
 - 5.6.2 Cluster Expansion Method, 108
- 5.7 Chain Crossover and Chain Entanglement, 109
 - 5.7.1 Concentration Effect, 109
 - 5.7.2 Temperature Effect, 114
 - 5.7.3 Tube Theory (Reptation Theory), 116
 - 5.7.4 Images of Individual Polymer Chains, 118
- 5.8 Scaling and Universality, 119
- Appendix A Scaling Concepts, 120
- Appendix B Correlation Function, 121
- References, 123
- Problems, 124

6 Liquid Crystals **127**

- 6.1 Mesogens, 128
- 6.2 Polymeric Liquid Crystals, 130
 - 6.2.1 Low-Molecular Weight Liquid Crystals, 131
 - 6.2.2 Main-Chain Liquid-Crystalline Polymers, 132
 - 6.2.3 Side-Chain Liquid-Crystalline Polymers, 132
 - 6.2.4 Segmented-Chain Liquid-Crystalline Polymers, 133
- 6.3 Shapes of Mesogens, 133
- 6.4 Liquid-Crystal Phases, 134
 - 6.4.1 Mesophases in General, 134
 - 6.4.2 Nematic Phase, 135
 - 6.4.3 Smectic Phase, 135
 - 6.4.3.1 Smectic A and C, 136
 - 6.4.4 Compounds Representing Some Mesophases, 136
 - 6.4.5 Shape and Phase, 137
 - 6.4.6 Decreasing Order and ΔH of Phase Transition, 138
- 6.5 Thermotropic and Lyotropic Liquid Crystals, 138
- 6.6 Kerr Effect, 140
- 6.7 Theories of Liquid-Crystalline Ordering, 141
 - 6.7.1 Rigid-Rod Model, 141
 - 6.7.2 Lattice Model, 142
 - 6.7.3 De Genne's Fluctuation Theory, 144

- 6.8 Current Industrial Applications of Liquid Crystals, 145
 - 6.8.1 Liquid Crystals Displays, 146
 - 6.8.2 Electronic Devices, 147
- References, 149

7 Rubber Elasticity **150**

- 7.1 Rubber and Rubberlike Materials, 150
- 7.2 Network Structure, 151
- 7.3 Natural Rubber and Synthetic Rubber, 152
- 7.4 Thermodynamics of Rubber, 154
- 7.5 Statistical Theory of Rubber Elasticity, 158
- 7.6 Gels, 162
- References, 163
- Problems, 164

8 Viscosity and Viscoelasticity **165**

- 8.1 Viscosity, 165
 - 8.1.1 Capillary Viscometers, 166
 - 8.1.2 Intrinsic Viscosity, 170
 - 8.1.3 Treatment of Intrinsic Viscosity Data, 172
 - 8.1.4 Stokes' Law, 176
 - 8.1.5 Theories in Relation to Intrinsic Viscosity of Flexible Chains, 176
 - 8.1.6 Chain Entanglement, 179
 - 8.1.7 Biological Polymers (Rigid Polymers, Inflexible Chains), 181
- 8.2 Viscoelasticity, 184
 - 8.2.1 Rouse Theory, 187
 - 8.2.2 Zimm Theory, 190
- References, 192
- Problems, 193

9 Osmotic Pressure **198**

- 9.1 Osmometers, 199
- 9.2 Determination of Molecular Weight and Second Virial Coefficient, 199
- 9.3 Theories of Osmotic Pressure and Osmotic Second Virial Coefficient, 202
 - 9.3.1 McMillan–Mayer Theory, 203
 - 9.3.2 Flory Theory, 204
 - 9.3.3 Flory–Krigbaum Theory, 205
 - 9.3.4 Kurata–Yamakawa Theory, 207
 - 9.3.5 des Cloizeaux–de Gennes Scaling Theory, 209
 - 9.3.6 Scatchard's Equation for Macro Ions, 213

Appendix A	Ensembles, 215
Appendix B	Partition Functions, 215
Appendix C	Mean-Field Theory and Renormalization Group Theory, 216
Appendix D	Lagrangian Theory, 217
Appendix E	Green's Function, 217
References,	218
Problems,	218

10 Diffusion 223

10.1	Translational Diffusion, 223
10.1.1	Fick's First and Second Laws, 223
10.1.2	Solution to Continuity Equation, 224
10.2	Physical Interpretation of Diffusion: Einstein's Equation of Diffusion, 226
10.3	Size, Shape, and Molecular Weight Determinations, 229
10.3.1	Size, 229
10.3.2	Shape, 230
10.3.3	Molecular Weight, 231
10.4	Concentration Dependence of Diffusion Coefficient, 231
10.5	Scaling Relation for Translational Diffusion Coefficient, 233
10.6	Measurements of Translational Diffusion Coefficient, 234
10.6.1	Measurement Based on Fick's First Law, 234
10.6.2	Measurement Based on Fick's Second Law, 235
10.7	Rotational Diffusion, 237
10.7.1	Flow Birefringence, 239
10.7.2	Fluorescence Depolarization, 239
References,	240
Problems,	240

11 Sedimentation 243

11.1	Apparatus, 244
11.2	Sedimentation Velocity, 246
11.2.1	Measurement of Sedimentation Coefficients: Moving-Boundary Method, 246
11.2.2	Svedberg Equation, 249
11.2.3	Application of Sedimentation Coefficient, 249
11.3	Sedimentation Equilibrium, 250
11.3.1	Archibald Method, 251
11.3.2	Van Holde–Baldwin (Low-Speed) Method, 254
11.3.3	Yphantis (High-Speed) Method, 256
11.3.4	Absorption System, 258
11.4	Density Gradient Sedimentation Equilibrium, 259
11.5	Scaling Theory, 260

References, 262

Problems, 263

12 Optical Rotatory Dispersion and Circular Dichroism 267

12.1 Polarized Light, 267

12.2 Optical Rotatory Dispersion, 267

12.3 Circular Dichroism, 272

12.4 Cotton Effect, 275

12.5 Correlation Between ORD and CD, 277

12.6 Comparison of ORD and CD, 280

References, 281

Problems, 281

13 High-Performance Liquid Chromatography and Electrophoresis 284

13.1 High-Performance Liquid Chromatography, 284

13.1.1 Chromatographic Terms and Parameters, 284

13.1.2 Theory of Chromatography, 289

13.1.3 Types of HPLC, 291

13.2 Electrophoresis, 300

13.2.1 Basic Theory, 300

13.2.2 General Techniques of Modern Electrophoresis, 305

13.2.3 Agarose Gel Electrophoresis and Polyacrylamide
Gel Electrophoresis, 307

13.2.4 Southern Blot, Northern Blot, and Western Blot, 309

13.2.5 Sequencing DNA Fragments, 310

13.2.6 Isoelectric Focusing and Isotachopheresis, 310

13.3 Field-Flow Fractionation, 314

References, 317

Problems, 318

14 Light Scattering 320

14.1 Rayleigh Scattering, 320

14.2 Fluctuation Theory (Debye), 324

14.3 Determination of Molecular Weight and Molecular Interaction, 329

14.3.1 Two-Component Systems, 329

14.3.2 Multicomponent Systems, 329

14.3.3 Copolymers, 331

14.3.4 Correction of Anisotropy and Depolarization
of Scattered Light, 333

14.4 Internal Interference, 333

14.5 Determination of Molecular Weight and Radius of
Gyration of the Zimm Plot, 337

Appendix Experimental Techniques of the Zimm Plot, 341

References,	345	
Problems,	346	
15 Fourier Series		348
15.1 Preliminaries,	348	
15.2 Fourier Series,	350	
15.2.1 Basic Fourier Series,	350	
15.2.2 Fourier Sine Series,	352	
15.2.3 Fourier Cosine Series,	352	
15.2.4 Complex Fourier Series,	353	
15.2.5 Other Forms of Fourier Series,	353	
15.3 Conversion of Infinite Series into Integrals,	354	
15.4 Fourier Integrals,	354	
15.5 Fourier Transforms,	356	
15.5.1 Fourier Transform Pairs,	356	
15.6 Convolution,	359	
15.6.1 Definition,	359	
15.6.2 Convolution Theorem,	361	
15.6.3 Convolution and Fourier Theory: Power Theorem,	361	
15.7 Extension of Fourier Series and Fourier Transform,	362	
15.7.1 Lorentz Line Shape,	362	
15.7.2 Correlation Function,	363	
15.8 Discrete Fourier Transform,	364	
15.8.1 Discrete and Inverse Discrete Fourier Transform,	364	
15.8.2 Application of DFT,	365	
15.8.3 Fast Fourier Transform,	366	
Appendix,	367	
References,	368	
Problems,	369	
16 Small-Angle X-Ray Scattering, Neutron Scattering, and Laser Light Scattering		371
16.1 Small-Angle X-ray Scattering,	371	
16.1.1 Apparatus,	372	
16.1.2 Guinier Plot,	373	
16.1.3 Correlation Function,	375	
16.1.4 On Size and Shape of Proteins,	377	
16.2 Small-Angle Neutron Scattering,	381	
16.2.1 Six Types of Neutron Scattering,	381	
16.2.2 Theory,	382	
16.2.3 Dynamics of a Polymer Solution,	383	
16.2.4 Coherently Elastic Neutron Scattering,	384	
16.2.5 Comparison of Small-Angle Neutron Scattering with Light Scattering,	384	

16.2.6	Contrast Factor, 386	
16.2.7	Lorentzian Shape, 388	
16.2.8	Neutron Spectroscopy, 388	
16.3	Laser Light Scattering, 389	
16.3.1	Laser Light-Scattering Experiment, 389	
16.3.2	Autocorrelation and Power Spectrum, 390	
16.3.3	Measurement of Diffusion Coefficient in General, 391	
16.3.4	Application to Study of Polymers in Semidilute Solutions, 393	
16.3.4.1	Measurement of Lag Times, 393	
16.3.4.2	Forced Rayleigh Scattering, 394	
16.3.4.3	Linewidth Analysis, 394	
	References, 395	
	Problems, 396	
17	Electronic and Infrared Spectroscopy	399
17.1	Ultraviolet (and Visible) Absorption Spectra, 400	
17.1.1	Lambert–Beer Law, 402	
17.1.2	Terminology, 403	
17.1.3	Synthetic Polymers, 405	
17.1.4	Proteins, 406	
17.1.5	Nucleic Acids, 409	
17.2	Fluorescence Spectroscopy, 412	
17.2.1	Fluorescence Phenomena, 412	
17.2.2	Emission and Excitation Spectra, 413	
17.2.3	Quenching, 413	
17.2.4	Energy Transfer, 416	
17.2.5	Polarization and Depolarization, 418	
17.3	Infrared Spectroscopy, 420	
17.3.1	Basic Theory, 420	
17.3.2	Absorption Bands: Stretching and Bending, 421	
17.3.3	Infrared Spectroscopy of Synthetic Polymers, 424	
17.3.4	Biological Polymers, 427	
17.3.5	Fourier Transform Infrared Spectroscopy, 428	
	References, 430	
	Problems, 432	
18	Protein Molecules	436
18.1	Protein Sequence and Structure, 436	
18.1.1	Sequence, 436	
18.1.2	Secondary Structure, 437	
18.1.2.1	α -Helix and β -Sheet, 437	
18.1.2.2	Classification of Proteins, 439	
18.1.2.3	Torsion Angles, 440	
18.1.3	Tertiary Structure, 441	
18.1.4	Quarternary Structure, 441	

18.2	Protein Structure Representations, 441	
18.2.1	Representation Symbols, 441	
18.2.2	Representations of Whole Molecule, 442	
18.3	Protein Folding and Refolding, 444	
18.3.1	Computer Simulation, 445	
18.3.2	Homolog Modeling, 447	
18.3.3	De Novo Prediction, 447	
18.4	Protein Misfolding, 448	
18.4.1	Biological Factor: Chaperones, 448	
18.4.2	Chemical Factor: Intra- and Intermolecular Interactions, 449	
18.4.3	Brain Diseases, 450	
18.5	Genomics, Proteomics, and Bioinformatics, 451	
18.6	Ribosomes: Site and Function of Protein Synthesis, 452	
	References, 454	
19	Nuclear Magnetic Resonance	455
19.1	General Principles, 455	
19.1.1	Magnetic Field and Magnetic Moment, 455	
19.1.2	Magnetic Properties of Nuclei, 456	
19.1.3	Resonance, 458	
19.1.4	Nuclear Magnetic Resonance, 460	
19.2	Chemical Shift (δ) and Spin–Spin Coupling Constant (J), 461	
19.3	Relaxation Processes, 466	
19.3.1	Spin–Lattice Relaxation and Spin–Spin Relaxation, 467	
19.3.2	Nuclear Quadrupole Relaxation and Overhauser Effect, 469	
19.4	NMR Spectroscopy, 470	
19.4.1	Pulse Fourier Transform Method, 471	
19.4.1.1	Rotating Frame of Reference, 471	
19.4.1.2	The 90° Pulse, 471	
19.4.2	One-Dimensional NMR, 472	
19.4.3	Two-Dimensional NMR, 473	
19.5	Magnetic Resonance Imaging, 475	
19.6	NMR Spectra of Macromolecules, 477	
19.6.1	Poly(methyl methacrylate), 477	
19.6.2	Polypropylene, 481	
19.6.3	Deuterium NMR Spectra of Chain Mobility in Polyethylene, 482	
19.6.4	Two-Dimensional NMR Spectra of Poly- γ -benzyl-L-glutamate, 485	
19.7	Advances in NMR Since 1994, 487	
19.7.1	Apparatus, 487	
19.7.2	Techniques, 487	
19.7.2.1	Computer-Aided Experiments, 487	
19.7.2.2	Modeling of Chemical Shift, 488	
19.7.2.3	Protein Structure Determination, 489	

19.7.2.4	Increasing Molecular Weight of Proteins for NMR study, 491	
19.8	Two Examples of Protein NMR, 491	
19.8.1	A Membrane Protein, 493	
19.8.2	A Brain Protein: Prion, 494	
	References, 494	
	Problems, 495	
20	X-Ray Crystallography	497
20.1	X-Ray Diffraction, 497	
20.2	Crystals, 498	
20.2.1	Miller Indices, <i>hkl</i> , 498	
20.2.2	Unit Cells or Crystal Systems, 502	
20.2.3	Crystal Drawing, 503	
20.3	Symmetry in Crystals, 504	
20.3.1	Bravais Lattices, 505	
20.3.2	Point Group and Space Group, 506	
20.3.2.1	Point Groups, 507	
20.3.2.2	Interpretation of Stereogram, 509	
20.3.2.3	Space Groups, 512	
20.4	Fourier Synthesis, 515	
20.4.1	Atomic Scattering Factor, 515	
20.4.2	Structure Factor, 515	
20.4.3	Fourier Synthesis of Electron Density, 516	
20.5	Phase Problem, 517	
20.5.1	Patterson Synthesis, 517	
20.5.2	Direct Method (Karle–Hauptmann Approach), 518	
20.6	Refinement, 519	
20.7	Crystal Structure of Macromolecules, 520	
20.7.1	Synthetic Polymers, 520	
20.7.2	Proteins, 523	
20.7.3	DNA, 523	
20.8	Advances in X-Ray Crystallography Since 1994, 525	
20.8.1	X-Ray Sources, 525	
20.8.2	New Instruments, 526	
20.8.3	Structures of Proteins, 526	
20.8.3.1	Comparison of X-Ray Crystallography with NMR Spectroscopy, 527	
20.8.4	Protein Examples: Polymerase and Anthrax, 528	
	Appendix Neutron Diffraction, 530	
	References, 532	
	Problems, 533	
	Author Index	535
	Subject Index	543

PREFACE TO THE SECOND EDITION

In this second edition, four new chapters are added and two original chapters are thoroughly revised. The four new chapters are Chapter 6, Liquid Crystals; Chapter 7, Rubber Elasticity; Chapter 15, Fourier Series; and Chapter 18, Protein Molecules. The two thoroughly revised chapters are Chapter 19, Nuclear Magnetic Resonance, and Chapter 20, X-Ray Crystallography.

Since the completion of the first edition in 1994, important developments have been going on in many fields of physical chemistry of macromolecules. As a result, two new disciplines have emerged: materials science and structural biology. The traditional field of polymers, even though already enlarged, is to be included in the bigger field of materials science. Together with glasses, colloids, and liquid crystals, polymers are considered organic and soft materials, in parallel with engineering and structural materials such as metals and alloys. Structural biology, originally dedicated to the study of the sequence and structure of DNA and proteins, is now listed together with genomics, proteomics, and molecular evolution as an independent field. It is not unusual that structural biology is also defined as the field that includes genomics and proteomics.

These developments explain the background of our revision.

Chapters 6 and 7 are added in response to the new integration in materials science. In Chapter 6, after the presentation of the main subjects, we give two examples to call attention to readers the fierce competition in industry for the application of liquid crystals: crystal paint display and electronic devices. Within the next few years television and computer films will be revolutionalized both in appearance and in function. Military authority and medical industry are both looking for new materials of liquid crystals. The subject rubber elasticity in

Chapter 7 is a classical one, well known in polymer chemistry and the automobile industry. It should have been included in the first edition. Now we have a chance to include it as materials science.

Chapters 18–20 constitute the core of structural biology. Chapter 18 describes the most important principles of protein chemistry, including sequence and structure and folding and misfolding. Chapters 19 and 20 deal with the two major instruments employed in the study of structural biology: nuclear magnetic resonance (NMR) spectroscopy and x-ray crystallography. Both have undergone astonishing changes during the last few years. Nuclear magnetic resonance instruments have operated from 500 MHz in 1994 to 900 MHz in the 2000s. The powerful magnets provide greater resolution that enables the researchers to obtain more detailed information about proteins. X-ray crystallography has gained even more amazing advancement in technology: the construction of the gigantic x-ray machine known as the synchrotron. Before 1994, an x-ray machine could be housed in the confines of a research laboratory building. In 1994 the synchrotron became as big as a stadium and was first made available for use in science.

Chapter 15, Fourier Series, was given in the previous edition as an appendix to the chapter entitled Dynamic Light Scattering. Now it also becomes an independent chapter. This technique has been an integral part of physics and electrical engineering and has been extended to chemistry and biology. The purpose of this chapter is to provide a background toward the understanding of mathematical language as well as an appreciation of this as an indispensable tool to the new technologies: NMR, x-ray crystallography, and infrared spectroscopy. Equally important, it is a good training in mathematics. On the other hand, in this edition the subject of dynamic light scattering is combined with the subjects of small-angle x-ray scattering and neutron scattering to form Chapter 16.

In addition to the changes mentioned above, we have updated several chapters in the previous edition. In Chapter 5, for example, we added a section to describe the images of individual polymer chains undergoing changes in steady shear. This is related to laser technology.

Although the number of chapters has increased from 17 in the previous edition to 20 in this edition, we have kept our goal intact: to integrate physical polymer chemistry and biophysical chemistry by covering principles and issues common to both.

This book is believed to be among the pioneers to integrate the two traditionally independent disciplines. The integration by two or more independent disciplines seems to be a modern trend. Since our book was first published, not only two newly developed subjects have been the results of integrations (i.e., each integrates several different subjects in their area), but also many academic departments in colleges and universities have been integrated. In the old days, for example, we have departments with a single term: Physics, Chemistry, Biology, and so forth; now we have departments with two terms of combined subjects: Chemistry and Biochemistry, Biochemistry and Molecular Biophysics, Chemistry and Chemical Biology, Biochemistry and Molecular Biophysics, Anatomy and Structural Biology, Materials Science and Engineering, Materials and Polymers. For young science students,

the integrated subjects have broader areas of research and learning. They are challenging and they show where the jobs are.

There are no major changes in the homework problems except that two sets of problems for Chapters 7 and 15 are added in this edition. A solution manual with worked out solutions to most of the problems is now available upon request to the publisher.

S. F. SUN

Jamaica, New York

ACKNOWLEDGMENTS

The author is greatly indebted to Dr. Emily Sun for reading the manuscript and making many helpful suggestions; to Caroline Sun Esq. for going over in detail all the six chapters and for valuable consultations; to Patricia Sun, Esq. for reading two new chapters and providing constant encouragement.

This book is dedicated to my wife, Emily.

PREFACE TO THE FIRST EDITION

Physical chemistry of macromolecules is a course that is frequently offered in the biochemistry curriculum of a college or university. Occasionally, it is also offered in the chemistry curriculum. When it is offered in the biochemistry curriculum, the subject matter is usually limited to biological topics and is identical to biophysical chemistry. When it is offered in the chemistry curriculum, the subject matter is often centered around synthetic polymers and the course is identical to physical polymer chemistry. Since the two disciplines are so closely related, students almost universally feel that something is missing when they take only biophysical chemistry or only physical polymer chemistry. This book emerges from the desire to combine the two courses into one by providing readers with the basic knowledge of both biophysical chemistry and physical polymer chemistry. It also serves a bridge between the academia and industry. The subject matter is basically academic, but its application is directly related to industry, particularly polymers and biotechnology.

This book contains seventeen chapters, which may be classified into three units, even though not explicitly stated. Unit 1 covers Chapters 1 through 5, unit 2 covers Chapters 6 through 12, and unit 3 covers Chapters 13 through 17. Since the materials are integrated, it is difficult to distinguish which chapters belong to biophysical chemistry and which chapters belong to polymer chemistry. Roughly speaking, unit 1 may be considered to consist of the core materials of polymer chemistry. Unit 2 contains materials belonging both to polymer chemistry and biophysical chemistry. Unit 3, which covers the structure of macromolecules and their separations, is relatively independent of units 1 and 2. These materials are

important in advancing our knowledge of macro molecules, even though their use is not limited to macromolecules alone.

The book begins with terms commonly used in polymer chemistry and biochemistry with respect to various substances, such as homopolymers, copolymers, condensation polymers, addition polymers, proteins, nucleic acids, and polysaccharides (Chapter 1), followed by descriptions of the methods used to create these substances (Chapter 2). On the basis of classroom experience, Chapter 2 is a welcome introduction to students who have never been exposed to the basic methods of polymer and biopolymer syntheses. The first two chapters together comprise the essential background materials for this book.

Chapter 3 introduces statistical methods used to deal with a variety of distribution of molecular weight. The problem of the distribution of molecular weight is characteristic of macromolecules, particularly the synthetic polymers, and the statistical methods are the tools used to solve the problem. Originally Chapter 4 covered chain configurations and Chapter 5 covered macromolecular thermodynamics. Upon further reflection, the order was reversed. Now Chapter 4 on macromolecular thermodynamics is followed by Chapter 5 on chain configurations. This change was based on both pedagogical and chronological reasons. For over a generation (1940s to 1970s), Flory's contributions have been considered the standard work in physical polymer chemistry. His work together with that of other investigators laid the foundations of our way of thinking about the behavior of polymers, particularly in solutions. It was not until the 1970s that Flory's theories were challenged by research workers such as de Gennes. Currently, it is fair to say that de Gennes' theory plays the dominant role in research. In Chapter 4 the basic thermodynamic concepts such as χ , θ , ψ , and κ that have made Flory's name well known are introduced. Without some familiarity with these concepts, it would not be easy to follow the current thought as expounded by de Gennes in Chapter 5 (and later in Chapters 6 and 7). For both chapters sufficient background materials are provided either in the form of introductory remarks, such as the first section in Chapter 4 (a review of general thermodynamics), or in appendices, such as those on scaling concepts and correlation function in Chapter 5.

In Chapters 6 through 17, the subjects discussed are primarily experimental studies of macromolecules. Each chapter begins with a brief description of the experimental method, which, though by no means detailed, is sufficient for the reader to have a pertinent background. Each chapter ends with various theories that underlie the experimental work.

For example, in Chapter 6, to begin with three parameters, ρ (shear stress), ϵ (shear strain), and E (modulus or rigidity), are introduced to define viscosity and viscoelasticity. With respect to viscosity, after the definition of Newtonian viscosity is given, a detailed description of the capillary viscometer to measure the quantity η follows. Theories that interpret viscosity behavior are then presented in three different categories. The first category is concerned with the treatment of experimental data. This includes the Mark-Houwink equation, which is used to calculate the molecular weight, the Flory-Fox equation, which is used to estimate thermodynamic quantities, and the Stockmayer-Fixman equation, which is used to

supplement the intrinsic viscosity treatment. The second category describes the purely theoretical approaches to viscosity. These approaches include the Kirkwood-Riseman model and the Debye-Buche model. It also includes chain entanglement. Before presenting the third category, which deals with the theories about viscosity in relation to biological polymers, a short section discussing Stokes' law of frictional coefficient is included. The third category lists the theories proposed by Einstein, Peterlin, Kuhn and Kuhn, Simha, Scheraga and Mendelkern. With respect to viscoelasticity, Maxwell's model is adopted as a basis. Attention is focused on two theories that are very much in current thought, particularly in connection with the dynamic scaling law: the Rouse model and the Zimm model. These models are reminiscent of the Kirkwood-Riseman theory and the Debye-Buche theory in viscosity but are much more stimulating to the present way of thinking in the formulation of universal laws to characterize polymer behavior.

Chapter 7, on osmotic pressure, provides another example of my approach to the subject matter in this book. After a detailed description of the experimental determination of molecular weight and the second virial coefficient, a variety of models are introduced each of which focuses on the inquiry into inter- and intramolecular interactions of polymers in solution. The reader will realize that the thermodynamic function μ (chemical potential) introduced in Chapter 4 has now become the key term in our language. The physical insight that is expressed by theoreticians is unusually inspiring. For those who are primarily interested in experimental study, Chapter 7 provides some guidelines for data analysis. For those who are interested in theoretical inquiry, this chapter provides a starting point to pursue further research. Upon realizing the difficulties involved in understanding mathematical terms, several appendices are added to the end of the chapter to give some background information.

Chapters 8 through 12, are so intermingled in content that they are hardly independent from each other, yet they are so important that each deserves to be an independent chapter. Both Chapters 8 and 9 are about light scattering. Chapter 8 describes general principles and applications, while Chapter 9 discusses advanced techniques in exploring detailed information about the interactions between polymer molecules in solutions. Chapters 10 and 11 are both about diffusion. Chapter 10 deals with the general principles and applications of diffusion, while Chapter 11 describes advanced techniques in measurement. However, diffusion is only part of the domain in Chapter 11, for Chapter 11 is also directly related to light scattering. As a matter of fact, Chapters 8, 9, and 11 can be grouped together. In parallel, Chapters 10 and 12, one about diffusion and the other about sedimentation, are closely related. They describe similar principles and similar experimental techniques. Knowledge of diffusion is often complementary to knowledge of sedimentation and vice versa.

It should be pointed out that all the chapters in unit 2 (Chapters 6 through 12) so far deal with methods for determining molecular weight and the configuration of macromolecules. They are standard chapters for both a course of polymer chemistry and a course of biophysical chemistry. Chapters 13 through 17 describe some of the important experimental techniques that were not covered in Chapters 6 through 12.

Briefly, Chapter 13, on optical rotatory dispersion (ORD) and circular dichroism (CD), describes the content of helices in a biological polymer under various conditions, that is, in its native as well as in its denatured states. The relationship between ORD and CD is discussed in detail. Chapter 14 provides basic knowledge of nuclear magnetic resonance phenomena and uses illustrations of several well-known synthetic polymers and proteins. Chapter 15, on x-ray crystallography, introduces the foundations of x-ray diffractions, such as Miller indices, Bravais lattices, seven crystals, 32 symmetries, and some relevant space groups. It then focuses on the study of a single crystal: the structure factor, the density map, and the phase problem. Chapter 16, on electron and infrared spectroscopy, provides the background for the three most extensively used spectroscopic methods in macromolecular chemistry, particularly with respect to biological polymers. These methods are ultraviolet absorption, fluorimetry, and infrared spectra. Chapter 17 belongs to the realm of separation science or analytical chemistry. It is included because no modern research in polymer chemistry or biophysical chemistry can completely neglect the techniques used in this area. This chapter is split into two parts. The first part, high-performance liquid chromatography (HPLC), describes key parameters of chromatograms and the four types of chromatography with an emphasis on size-exclusion chromatography, which enables us to determine the molecular weight, molecular weight distribution, and binding of small molecules to macromolecules. The second part, electrophoresis, describes the classical theory of ionic mobility and various types of modern techniques used for the separation and characterization of biological materials. Chapter 17 ends with an additional section, field-flow fractionation, which describes the combined methods of HPLC and electrophoresis.

In conclusion, the organization of this book covers the basic ideas and issues of the physical chemistry of macromolecules including molecular structure, physical properties, and modern experimental techniques.

Mathematical equations are used frequently in this book, because they are a part of physical chemistry. We use mathematics as a language in a way that is not different from our other language, English. In English, we have words and sentences; in mathematics, we use symbols (equivalent to words) and equations (equivalent to sentences). The only difference between the two is that mathematics, as a symbolic language, is simple, clear, and above all operative, meaning that we can manipulate symbols as we wish. The level of mathematics used in this text is not beyond elementary calculus, which most readers are assumed to have learned or are learning in college.

In this book, derivations, though important, are minimized. Derivations such as Flory's lattice theory on the entropy of mixing and Rayleigh's equation of light scattering are given only because they are simple, instructive, and, above all, they provide some sense of how an idea is translated from the English language to a mathematical language. The reader's understanding will not be affected if he or she skips the derivation and moves directly to the concluding equations. Furthermore, the presentation of the materials in this book has been tested on my classes for many years. No one has ever complained.

The selection of mathematical symbols (notations) used to designate a physical property (or a physical quantity) poses a serious problem. The same letter, for example, α or c , often conveys different meanings (that is, different designations). The Greek letter α can represent a carbon in a linear chain (α atom, β atom, . . .), one of the angles of a three-dimensional coordinate system (related to types of crystals), the expansion factor of polymer molecules in solutions (for example, $\alpha^5 - \alpha^3$), the polarizability with respect to the polarization of a molecule, and so on. The English letter c can represent the concentration of a solution (for example, g/mL, mol/L), the unit of coordinates (such as a , b , c), and so on. To avoid confusion, some authors use different symbols to represent different kinds of quantities and provide a glossary at the end of the book. The advantage of changing standard notation is the maintenance of consistency within a book. The disadvantage is that changing the well-known standard notation in literature (for example, S for expansion factor, T for polarizability, instead of α for both; or d for a unit coordinate, j for the concentration of a solution, instead of c for both), is awkward, and may confuse readers. In addressing this problem, the standard notations are kept intact. Sometimes the same letters are used to represent different properties in the same chapter. But I have tried to use a symbol to designate a specific property as clearly as possible in context by repeatedly defining the term immediately after the equation. I also add a prime on the familiar notations, for example, R' for gas constant and c' for the velocity of light. Readers need not worry about confusion.

At the end of each chapter are references and homework problems. The references are usually the source materials for the chapters. Some are original papers in literature, such as those by Flory, Kirkwood, Debye, Rouse, Des Cloizeau, deGennes, Luzzati, and Zimm, among others; and some are well-known books, such as those of Yamakawa and Hill, in which the original papers were cited in a rephrased form. Equations are usually given in their original forms from the original papers with occasional modifications to avoid confusion among symbols. It is hoped that this will familiarize readers with the leading literature. Homework problems are designed to help readers clarify certain points in the text.

A comment should be made on the title of the book, *Physical Chemistry of Macromolecules: Basic Principles and Issues*. The word “basic” refers to “fundamental,” meaning “relatively timeless.” In the selection of experimental methods and theories for each topic, the guideline was to include only those materials that do not change rapidly over time, for example, Fick’s first law and second law in diffusion, Patterson’s synthesis and direct method in x-ray crystallography, or those materials, though current, that are well established and frequently cited in the literature, such as the scaling concept of polymer and DNA sequencing by electrophoresis. The book is, therefore, meant to be “a course of study.”

I wish to thank Professor Emily Sun for general discussion and specific advice. Throughout the years she has offered suggestions for improving the writing in this book. Chapters 1 through 12 were read by Patricia Sun, Esq., 13 through 17 by Caroline Sun, Esq., and an overall consultation was provided by Dr. Diana Sun. I am greatly indebted to them for their assistance. A special note of thanks goes to Mr. Christopher Frank who drew the figures in chapter 11 and provided comments

on the appendix, and to Mr. Anthony DeLuca and Professor Andrew Taslitz, for improving portions of this writing. Most parts of the manuscript were painstakingly typed by Ms. Terry Cognard. For many years, students and faculty members of the Department of Chemistry of Liberal Arts and Sciences and the Department of Industrial Pharmacy of the College of Health Science at St. John's University have encouraged and stimulated me in writing this book. I am grateful to all of them.

S. F. SUN

*Jamaica, New York
February 1994*

Contents of the First Edition

- Chapter 1. Introduction
- Chapter 2. Syntheses of Macromolecular Compounds
- Chapter 3. Distribution of Molecular Weight
- Chapter 4. Macromolecular Thermodynamics
- Chapter 5. Chain Configurations
- Chapter 6. Viscosity and Viscoelasticity
- Chapter 7. Osmotic Pressure
- Chapter 8. Light Scattering
- Chapter 9. Small Angle X-Ray Scattering and Neutron Scattering
- Chapter 10. Diffusion
- Chapter 11. Dynamic Light Scattering
- Chapter 12. Sedimentation
- Chapter 13. Optical Rotatory Dispersion and Circular Dichroism
- Chapter 14. Nuclear Magnetic Resonance
- Chapter 15. X-Ray Crystallography
- Chapter 16. Electronic and Infrared Spectroscopy
- Chapter 17. HPLC and Electrophoresis

1

INTRODUCTION

Macromolecules are closely related to colloids, and historically the two are almost inseparable. Colloids were known first, having been recognized for over a century. Macromolecules were recognized only after much fierce struggle among chemists in the early 1900s. Today, we realize that while colloids and macromolecules are different entities, many of the same laws that govern colloids also govern macromolecules. For this reason, the study of the physical chemistry of macromolecules often extends to the study of colloids. Although the main topic of this book is macromolecules, we are also interested in colloids. Since colloids were known first, we will describe them first.

1.1 COLLOIDS

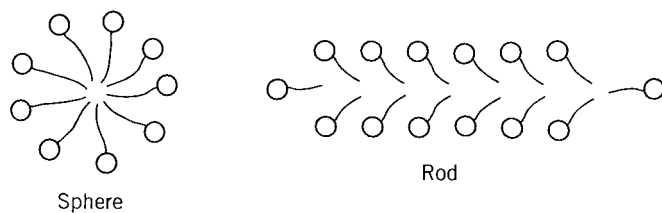
When small molecules with a large surface region are dispersed in a medium to form two phases, they are in a colloidal state and they form colloids. The two phases are liquid–liquid, solid–liquid, and so on. This is not a true solution (i.e., not a homogeneous mixture of solute and solvent), but rather one type of material dispersed on another type of material. The large surface region is responsible for surface activity, the capacity to reduce the surface or interface tensions.

There are two kinds of colloids: lyophobic and lyophilic. Lyophobic colloids are solvent hating (i.e., not easily miscible with the solvent) and thermodynamically unstable, whereas the lyophilic colloids are solvent loving (i.e., easily miscible with the solvent) and thermodynamically stable. If the liquid medium is water, the

2 INTRODUCTION

lyophobic colloids are called hydrophobic colloids and the lyophilic colloids are called hydrophillic colloids. Three types of lyophobic colloids are foam, which is the dispersion of gas on liquid; emulsion, which is the dispersion of liquid on liquid; and sol, which is the dispersion of solid on liquid.

An example of lyophilic colloids is a micelle. A micelle is a temporary union of many small molecules or ions. It comes in shapes such as spheres or rods:



Typical micelles are soaps, detergents, bile salts, dyes, and drugs. A characteristic feature of the micelle is the abrupt change in physical properties at a certain concentration, as shown in Figure 1.1. The particular concentration is called the critical micelle concentration (CMC). It is at this concentration that the surface-active materials form micelles. Below the CMC, the small molecules exist as individuals. They do not aggregate.

Two micelle systems of current interest in biochemistry and pharmacology are sodium dodecylsulfate (SDS) and liposome. SDS is a detergent whose chemical formula is

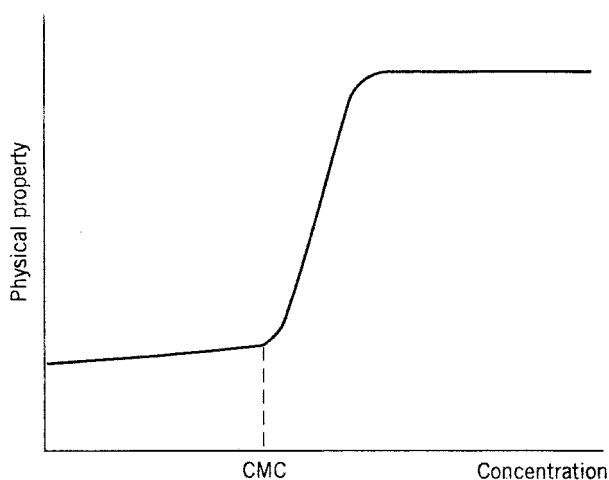
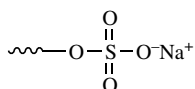
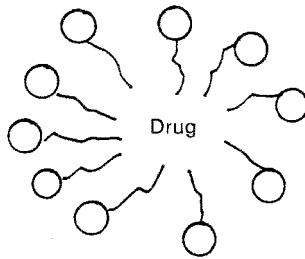


FIGURE 1.1 Critical micelle concentration.

The surface activity of this detergent causes a protein to be unfolded to a linear polypeptide. It destroys the shape of the protein molecule, rendering a spherical molecule to a random coil. SDS binds to many proteins. The binding is saturated at the well-known 1.4-g/g level, that is, at the concentration of SDS exceeding 0.5 mM. Above this level SDS starts self-association and binding is reduced. At 8.2 mM, SDS forms micelles, with an aggregation number of 62 and a micellar molecular weight of 18,000.

Liposome is believed to be one of the best devices for the controlled release of drugs. There are three kinds of liposomes:

1. Uncharged (ingredients: egg lecithin–cholesterol, weight ratio 33 : 4.64 mg)
2. Negatively charged (ingredients: egg lecithin–cholesterol–phosphatidic acid–dicetyl phosphate, ratio 33 : 4.46 : 10 : 3.24 mg)
3. Positively charged (ingredients: egg lecithin–cholesterol–stearylamine, ratio 33 : 4.46 : 1.6 mg)



The surface of the micelle liposome is similar to that of membrane lipids; it does no harm to the body when administered.

1.2 MACROMOLECULES

The physical properties of macromolecules, such as sedimentation, diffusion, and light scattering, are very similar to those of colloids. For generations macromolecules have been regarded as associated colloids or lyophilic colloidal systems. But macromolecules are not colloids. Colloids are aggregations of small molecules due to the delicate balance of weak attractive forces (such as the van der Waals force) and repulsive forces. The aggregation depends on the physical environment, particularly the solvent. When the solvent changes, the aggregation may collapse. Macromolecules are formed from many repeating small molecules which are connected by covalent bonds. Each macromolecule is an entity or a unit, not an aggregation. As the solvent changes, the properties of a macromolecule may change, but the macromolecule remains a macromolecule unless its covalent bonds are broken.

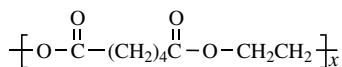
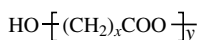
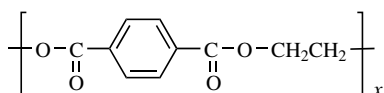
Basically there are two types of macromolecules: synthetic polymers and biological polymers. Synthetic polymers are those that do not exist in nature; they are man-made molecules. Biological polymers do exist in nature, but they can also

be synthesized in the laboratory. Synthetic polymers have a very small number of identical repeating units, usually one or two in a chain, whereas biological polymers have more identical repeating units in a chain, particularly proteins and enzymes, which have a variety of combinations (i.e., amino acids). Synthetic polymers carry flexible chains; the molecules are usually not rigid. Biological polymer chains are more ordered; the molecules are, in general, rigid. The rigidity depends on the nature of the chains and their environment. Relatively speaking nucleic acids are more rigid than proteins.

Recently, more similarity has been observed between the two types of macromolecules. For example, synthetic polymers, which are usually considered to be in the form of flexible random coils, can now be synthesized with the Ziegler–Natta catalysts to have stereoregularity. Furthermore, synthetic polymers can be designed to have helices, just like proteins and nucleic acids. As our knowledge of macromolecules increases, the sharp distinction between synthetic polymers and biological polymers becomes more and more arbitrary.

1.2.1 Synthetic Polymers

In 1929, Carothers classified synthetic polymers into two classes according to the method of preparation used: condensation polymers and addition polymers. For condensation (or stepwise reaction) polymers, the reaction occurs between two polyfunctional molecules by eliminating a small molecule, for example, water. The following are examples of condensation polymers:



Polyester (fiber)

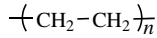


Polyurethane (fiber)

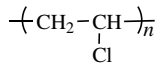


Polyurea

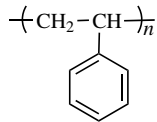
Addition (or chain reaction) polymers are formed in a chain reaction of monomers which have double bonds. The following are examples of addition polymers:



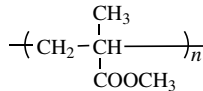
Polyethylene



Poly(vinyl chloride)



Polystyrene

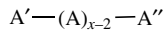


Poly(methyl methacrylate)

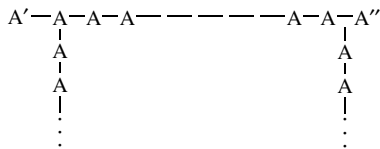
Polymers may be classified into two structural categories: linear polymers and branched polymers. Linear polymers are in the form



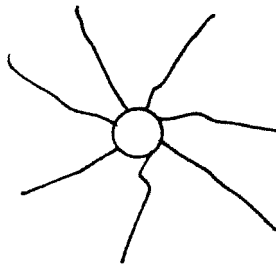
or



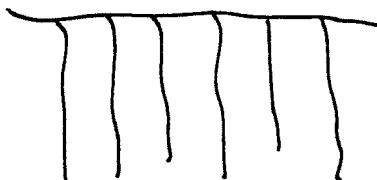
where A is the structural unit, x is the degree of polymerization, and A' , A'' are end groups of A. An example of a linear polymer is linear polystyrene. Branched polymers are in the form



Two of the most well-known branched polymers are the star-shaped polymer

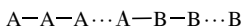


and the comb-shaped polymer

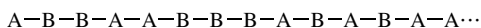


which both have various numbers of arms. Examples are star-shaped polystyrene and comb-shaped polystyrene.

In terms of repeating units there are two types of polymers: homopolymers and copolymers. A homopolymer is one in which only one monomer constitutes the repeating units, for example, polystyrene and poly(methyl methacrylate). A copolymer consists of two or more different monomers as repeating units, such as the diblock copolymer



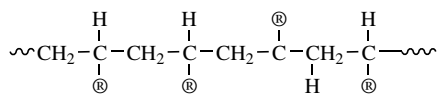
and the random or static copolymer



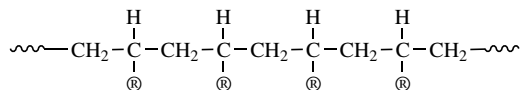
An example is the polystyrene-poly(methyl methacrylate) copolymer.

In terms of stereoregularity synthetic polymers may have *trans* and *gauche* forms, similar to some small molecules (e.g., ethane). Because of the steric position of substituents along the chain, the heterogeneity of the chain structure may be classified into three forms:

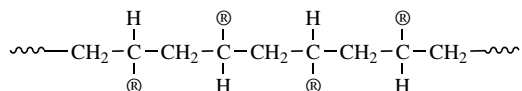
1. *Atactic polymers*—no regularity of R groups; for example,



2. *Isotactic polymers*—regularity of R groups; for example,



3. *Syndiotactic polymers*—regularity involves *trans* and *gauche* forms in a uniform manner; for example,



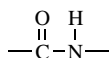
The isotactic and syndiotactic polymers can be synthesized using Ziegler–Natta catalyst.

Synthetic polymers that are commercially manufactured in the quantity of billions of pounds may be classified in three categories: (1) plastics, which include thermosetting resins (e.g., urea resins, polyesters, epoxides) and thermoplastic resins (e.g., low-density as well as high-density polyethylene, polystyrene, polypropylene); (2) synthetic fibers, which include cellulose (such as rayon and acetate) and noncellulose (such as polyester and nylon); and (3) synthetic rubber (e.g., styrene–butadiene copolymer, polybutadiene, ethylene–propylene copolymer).

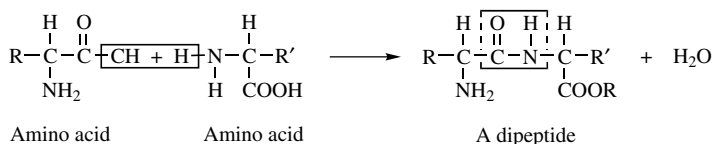
1.2.2 Biological Polymers

Biological polymers are composed of amino acids, nucleotides, or sugars. Here we describe three types of biological polymers: proteins and polypeptides, nucleic acids, and polymers of sugars.

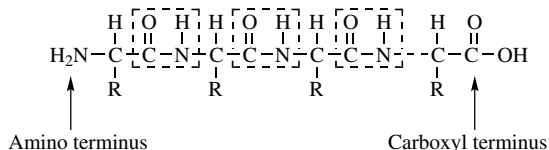
Proteins and Polypeptides Amino acids are bound by a peptide bond which is an amide linkage between the amino group of one molecule and the carboxyl group of another. It is in the form



For example,



A polypeptide is in the form



A protein is a polypeptide consisting of many amino acids (Table 1.1). A protein with catalytic activities is called an enzyme. All enzymes are proteins, but not all proteins are enzymes. A hormone is also a polypeptide (e.g., insulin) and is closely related to proteins.

TABLE 1.1 Amino Acids*Aliphatic Amino Acids (major amino acids contributed to a hydrophobic region)*

Glycine (Gly)	$\text{H}_2\text{N}-\text{CH}_2-\text{COOH}$
Alanine (Ala)	$\begin{array}{c} \text{H} \\ \\ \text{CH}_3-\text{C}-\text{COOH} \\ \\ \text{NH}_2 \end{array}$
Valine (Val)	$\begin{array}{c} \text{CH}_3-\text{CH}-\text{CH}-\text{COOH} \\ \quad \\ \text{CH}_3 \quad \text{NH}_2 \end{array}$
Leucine (Leu)	$\begin{array}{c} \text{CH}_3-\text{CH}-\text{CH}_2-\text{CH}-\text{COOH} \\ \quad \quad \\ \text{CH}_3 \quad \quad \text{NH}_2 \end{array}$
Isoleucine (Ileu)	$\begin{array}{c} \text{CH}_3-\text{CH}_2-\text{CH}-\text{CH}-\text{COOH} \\ \quad \quad \quad \\ \quad \quad \text{CH}_3 \quad \text{NH}_2 \end{array}$

Hydroxy Acids

Serine (Ser)	$\begin{array}{c} \text{CH}_2-\text{CH}-\text{COOH} \\ \quad \\ \text{OH} \quad \text{NH}_2 \end{array}$
Threonine (Thr)	$\begin{array}{c} \text{CH}_3-\text{CH}-\text{CH}-\text{COOH} \\ \quad \\ \text{OH} \quad \text{NH}_2 \end{array}$

Aromatic Amino Acids (UV region)

Phenylalanine (Phe)	$\begin{array}{c} \text{C}_6\text{H}_5-\text{CH}_2-\text{CH}-\text{COOH} \\ \quad \quad \\ \quad \quad \text{NH}_2 \end{array}$
Tyrosine (Tyr)	$\begin{array}{c} \text{HO}-\text{C}_6\text{H}_4-\text{CH}_2-\text{CH}-\text{COOH} \\ \quad \quad \quad \quad \\ \quad \quad \quad \quad \text{NH}_2 \end{array}$

Heterocyclic Group

Tryptophan (Try)	$\begin{array}{c} \text{C}_8\text{H}_6\text{N}_2-\text{CH}_2-\text{CH}-\text{COOH} \\ \quad \quad \quad \quad \\ \quad \quad \quad \quad \text{NH}_2 \end{array}$
------------------	---

Sulfur-Containing Amino Acids (cross-linkage)

Cysteine (Cys)	$\begin{array}{c} \text{CH}_2-\text{CH}-\text{COOH} \\ \quad \\ \text{SH} \quad \text{NH}_2 \end{array}$
Methionine (Met)	$\begin{array}{c} \text{CH}_3-\text{S}-\text{CH}_2-\text{CH}_2-\text{CH}-\text{COOH} \\ \quad \quad \quad \quad \\ \quad \quad \quad \quad \text{NH}_2 \end{array}$

TABLE 1.1 (Continued)

<i>Acidic Amino Acids (potentiometric titration)</i>	
Aspartic acid (Asp)	$\text{HOOC}-\text{CH}_2-\underset{\text{NH}_2}{\text{CH}}-\text{COOH}$
Glutamic acid (Glu)	$\text{HOOC}-\text{CH}_2-\text{CH}_2-\underset{\text{NH}_2}{\text{CH}}-\text{COOH}$
<i>Basic Amino Acids (potentiometric titration)</i>	
Lysine (Lys)	$\underset{\text{NH}_2}{\text{CH}_2}-\text{CH}_2-\text{CH}_2-\text{CH}_2-\underset{\text{NH}_2}{\text{CH}}-\text{COOH}$
Arginine (Arg)	$\text{H}_2\text{N}-\overset{\text{H}}{\underset{\text{H}}{\text{N}}}=\overset{\text{H}}{\text{N}}-\text{CH}_2-\text{CH}_2-\text{CH}_2-\underset{\text{NH}_2}{\text{CH}}-\text{COOH}$
Histidine (His)	$\text{HC}=\underset{\text{N}}{\underset{\text{H}}{\text{C}}}-\underset{\text{NH}}{\text{CH}}-\underset{\text{NH}_2}{\text{CH}}-\text{COOH}$
<i>Imino Acids</i>	
Proline (Pro)	$\begin{array}{c} \text{H}_2\text{C}-\text{CH}_2 \\ \quad \\ \text{H}_2\text{C}-\text{N}-\text{CH}-\text{COOH} \\ \\ \text{H} \end{array}$
Hydroxyproline (Hyp)	$\begin{array}{c} \text{HO}-\text{HC}-\text{CH}_2 \\ \quad \\ \text{H}_2\text{C}-\text{N}-\text{CH}-\text{COOH} \\ \\ \text{H} \end{array}$
<i>Carboxamide</i>	
Asparagine	$\text{O}=\overset{\text{NH}_2}{\text{C}}-\text{CH}_2-\overset{\text{NH}_2}{\underset{\text{H}}{\text{C}}}-\text{COOH}$
Glutamine	$\text{O}=\overset{\text{NH}_2}{\text{C}}-\text{CH}_2-\text{CH}_2-\overset{\text{NH}_2}{\underset{\text{H}}{\text{C}}}-\text{COOH}$

There are two types of proteins: simple and conjugated. Simple proteins are described in terms of their solubility in water into five groups (old description*):

1. *Albumins*—soluble in water and in dilute neutral salt solutions
2. *Globins*—soluble in water (e.g., hemoglobins)

*For new description, see Chapter 18.

10 INTRODUCTION

3. *Globulins*—insoluble in water, but soluble in dilute neutral salt solutions (e.g., γ -globulins)
4. *Prolamines*—soluble in 70% ethyl alcohol, insoluble in water
5. *Histones*—strongly basic solutions, soluble in water

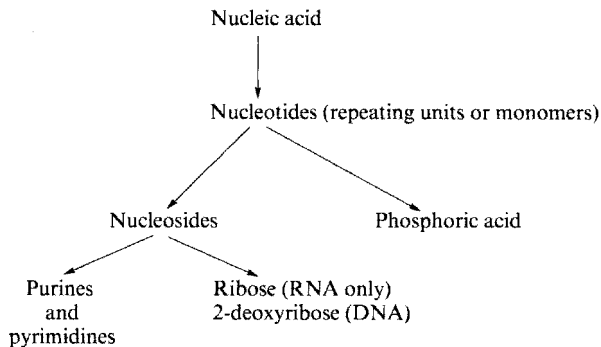
Conjugated proteins are described by the nonprotein groups:

1. *Nucleoproteins*—a basic protein such as histones or prolamines combined with nucleic acid
2. *Phosphoproteins*—proteins linked to phosphoric acid (e.g., casein in milk and vitellin in egg yolk)
3. *Glycoproteins*—a protein and a carbohydrate [e.g., mucin in saliva, mucoids in tendon and cartilage, interferon, which is a human gene product made in bacteria using recombinant deoxyribonucleic acid (DNA) technology]
4. *Chromoproteins*—a protein combined with a colored compound (e.g., hemoglobin and cytochromes)
5. *Lipoproteins*—proteins combined with lipids (such as fatty acids, fat, and lecithin)
6. *Membrane proteins*—proteins embedded in the lipid core of membranes (e.g., glycohorin A)

Proteins may be found in three shapes:

1. Thin length (e.g., collagen, keratin, myosin, fibrinogen)
2. Sphere (e.g., serum albumin, myoglobin, lysozyme, carboxypeptidase, chymotrypsin)
3. Elastic (e.g., elastin, the main constituent of ligament, aortic tissue, and the walls of blood vessels)

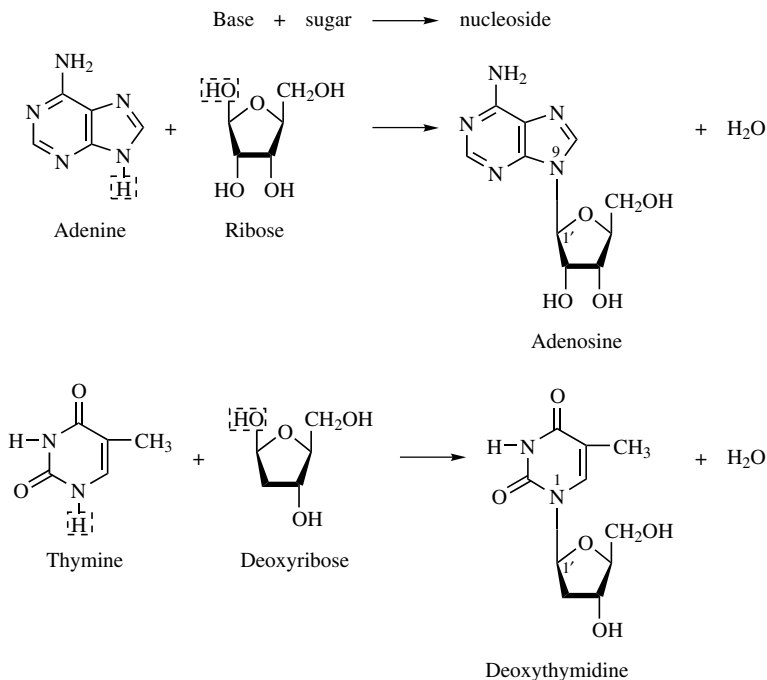
Nucleic Acids Nucleic acids consist of nucleotides, which in turn consist of nucleosides:



The major repeating units (nucleotides) are shown in Table 1.2. Each nucleotide consists of a base, a sugar, and a phosphate. There are only five bases, two sugars, and one phosphate from which to form a nucleotide. These are shown in Table 1.3. A nucleoside is a nucleotide minus the phosphate.

For illustrative purpose, we give two chemical reactions for the formation of nucleoside and one chemical reaction for the formation of a nucleotide:

Formation of nucleosides:



Formation of a nucleotide:

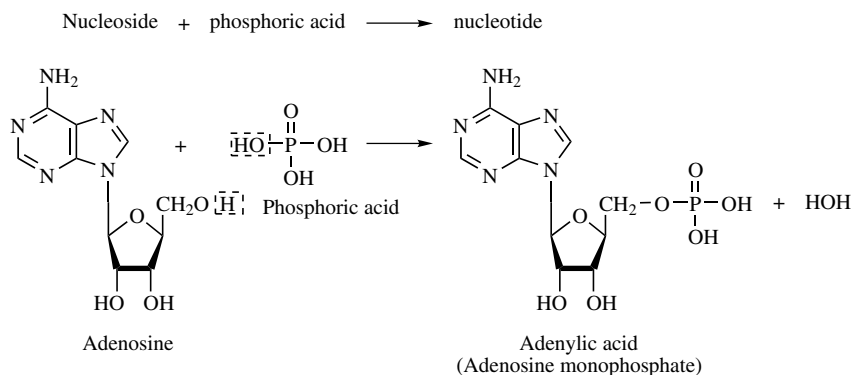
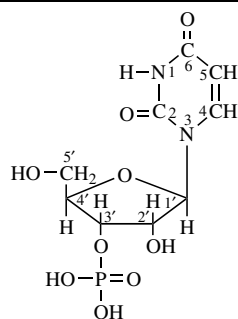
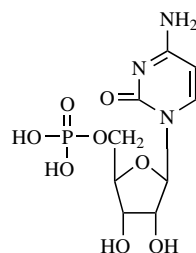


TABLE 1.2 Major Nucleotides

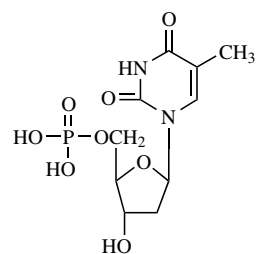
Uridylic acid (uridine-3'-phosphate)



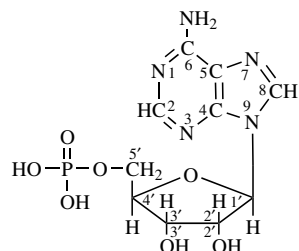
Cytidylic acid (cytidine-5'-phosphate)



Deoxythymidylic acid (deoxythymidine-5'-phosphate)



Adenylic acid (adenosine-5'-phosphate)



Guanylic acid (guanosine-5'-phosphate)

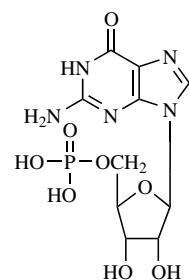
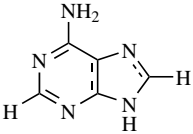
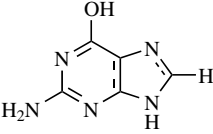
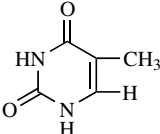
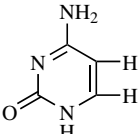
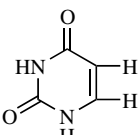
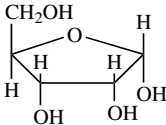
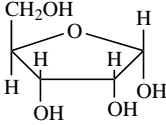
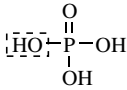


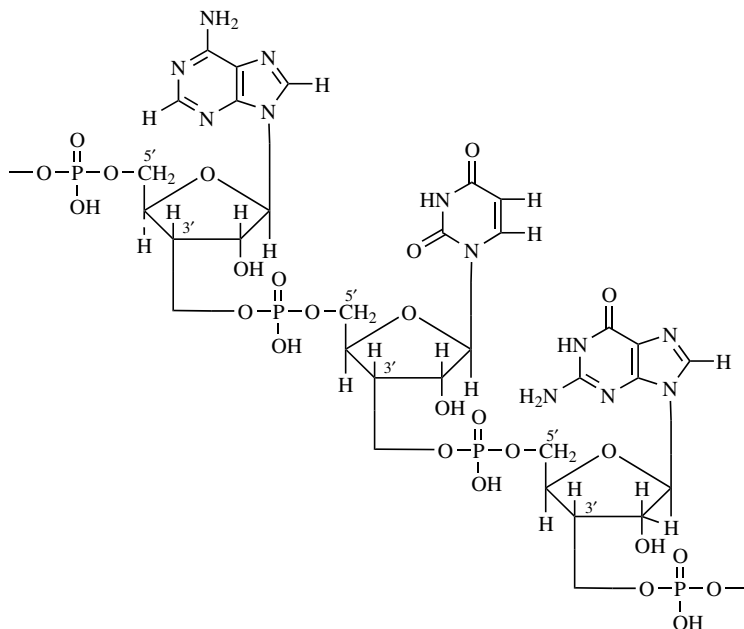
TABLE 1.3 Repeating Units of Nucleic Acids

<i>Five Bases</i>	
Adenine (A)	
Guanine (G)	
Thymine (T) (DNA only)	
Cytosine (C)	
Uracil (U) (RNA only)	
<i>Two Sugars (a pentose in furanose form)</i>	
Ribose (RNA only)	
2-Deoxyribose (DNA only)	
<i>One Phosphate</i>	
Phosphate	

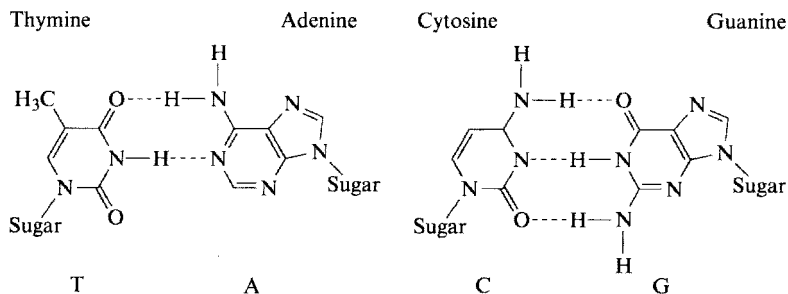
DNA Nucleotides are sequentially arranged to form a DNA molecule through 3',5' or 5',3' sugar-phosphate bonds:



that is,



Each DNA molecule consists of two strands twisted by hydrogen bonds between the two base pairs. The base pairing occurs between T and A and between C and G:



The overall structure of DNA is believed to follow the Watson-Crick model (Figure 1.2).

RNA Ribonucleic acid (RNA) is a single-stranded nucleic acid. (There are exceptions, of course. See Chapter 18.) It contains the pentose ribose, in contrast

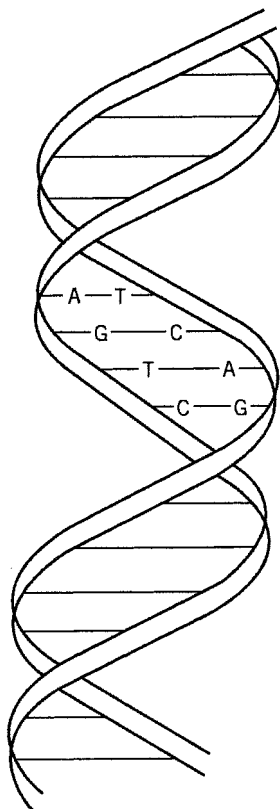


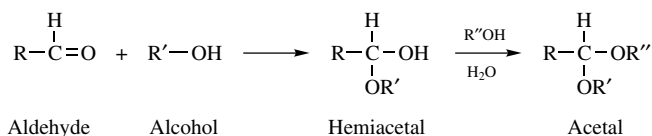
FIGURE 1.2 Watson-Crick model of DNA.

to the 2-deoxyribose of DNA. It has the base uracil instead of thymine. The purine-pyrimidine ratio in RNA is not 1 : 1 as in the case of DNA. There are three types of RNA, based on their biochemical function:

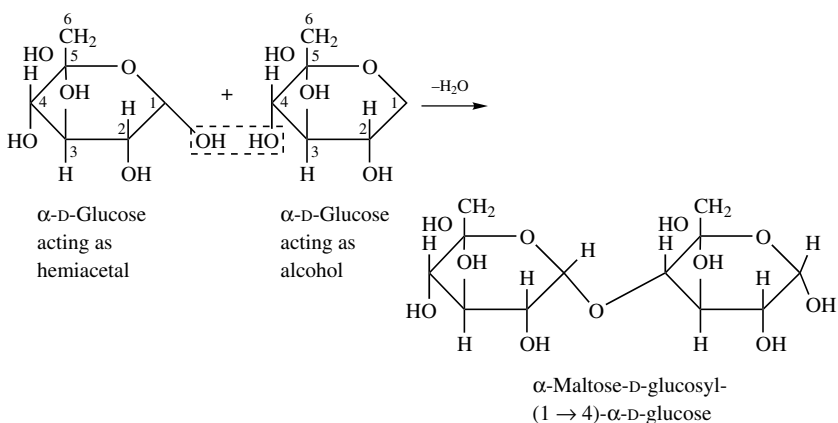
1. *Messenger RNA* (mRNA)—very little intramolecular hydrogen bonding and the molecule is in a fairly random coil
2. *Transfer RNA* (tRNA)—low molecular weight, carrying genetic information (genetic code), highly coiled, and with base pairing in certain regions
3. *Ribosomal RNA* (rRNA)—spherical particles, site for biosyntheses

Polymers of Sugars Polymers of sugars are often called polysaccharides. They are high-molecular-weight (25,000–15,000,000) polymers of monosaccharides. The synthesis of polysaccharides involves the synthesis of hemiacetal and acetal. When an aldehyde reacts with an alcohol, the resulting product is hemiacetal. Upon

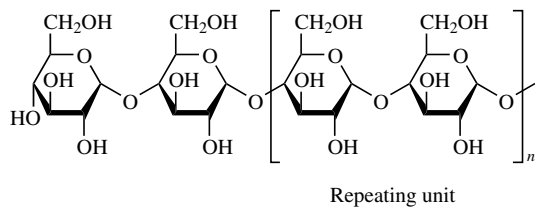
further reaction with an alcohol, a hemiacetal is converted to an acetal. The general mechanism of acetal formation is shown in the following reaction:



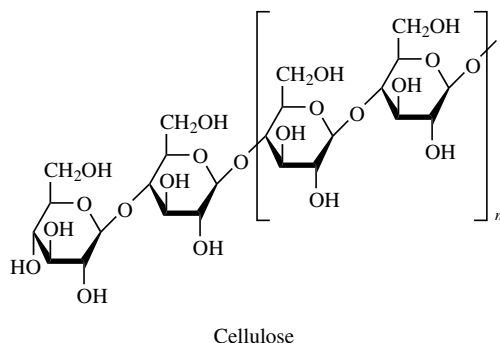
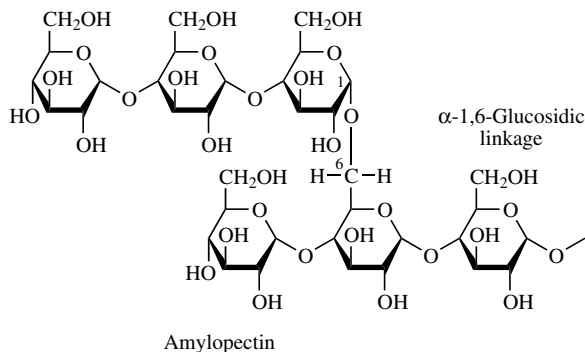
The sugar linkage is basically the formation of acetals:



Among the well-known polysaccharides are the three homopolymers of glucose: starch, glycogen, and cellulose. Starch is a mixture of two polymers: amylose (formed by α -1,4-glycosidic linkage) and amylopectin (a branched-chain polysaccharide formed by α -1,4-glycosidic bonds together with some α -1,6-glycosidic linkage). Glycogen is animal starch, similar to amylopectin but more highly branched. Cellulose is a fibrous carbohydrate composed of chains of D-glucose units joined by β -1,4-glycosidic linkages. The structures of amylose, amylopectin, and cellulose are shown in the following formulas:



Amylose



1.3 MACROMOLECULAR SCIENCE

Three branches of science deal with colloids and macromolecules: colloid science, surface science, and macromolecular science. Colloid science is the study of physical, mechanical, and chemical properties of colloidal systems. Surface science deals with phenomena involving macroscopic surfaces. Macromolecular science investigates the methods of syntheses in the case of synthetic polymers (or isolation and purification in the case of natural products such as proteins, nucleic acids, and carbohydrates) and the characterization of macromolecules. It includes, for example, polymer chemistry, polymer physics, biophysical chemistry, and molecular biology. These three branches of science overlap. What one learns from one branch can often be applied to the others.

The subject matter covered in this book belongs basically to macromolecular science. Emphasis is placed on the characterization of macromolecules (synthetic and biological polymers). Hence, the material also belongs to the realm of physical chemistry.

REFERENCES

Adamson, A. W., *Physical Chemistry of Surfaces*, 2nd ed. New York: Wiley-Interscience, 1967.

Billmeyer, F. W., Jr., *Textbook of Polymer Chemistry*, 2nd ed. New York: Wiley, 1985.

Carothers, W. H., *J. Am. Chem. Soc.* **51**, 2548 (1929).

Helenius, A., and K. Simons, *Biochim. Biophys. Acta* **415**, 29 (1975).

Shaw, D. J., *Introduction to Colloids and Surface Chemistry*, 2nd ed. Stoneham, MA: Butterworth, 1978.

Tanford, C., *The Hydrophobic Effect*. New York: Wiley, 1981.

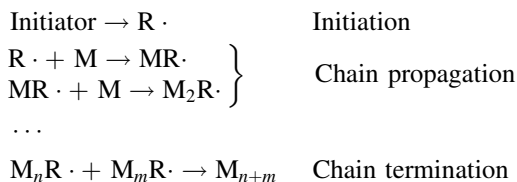
2

SYNTHESES OF MACROMOLECULAR COMPOUNDS

The first three sections of this chapter deal with addition polymerization, the fourth with condensation polymerization, the fifth with kinetics of the syntheses of polymers, the sixth with polypeptide synthesis, and the seventh with nucleic acid synthesis. Readers should be familiar with these subjects before going on to the major topics of this book. The chapter itself could be considered as a book in miniature on synthetic chemistry. Important synthetic methods and well-known chemical compounds are covered.

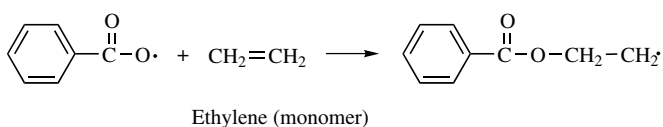
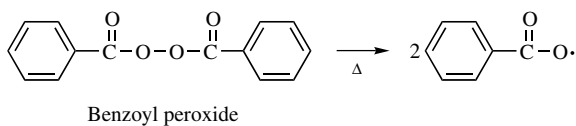
2.1 RADICAL POLYMERIZATION

The general reaction scheme for free-radical polymerization can be expressed as follows:

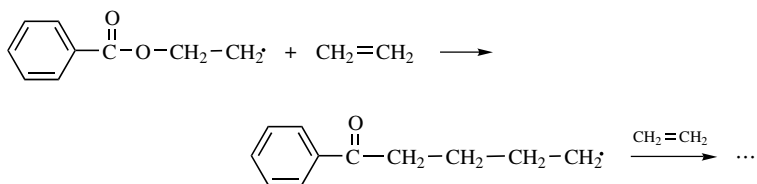


where M represents a monomer molecule and R· a free radical produced in the initial step. An example of free-radical polymerization is the synthesis of polyethylene:

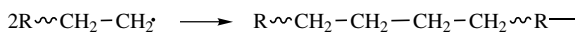
Initiation:



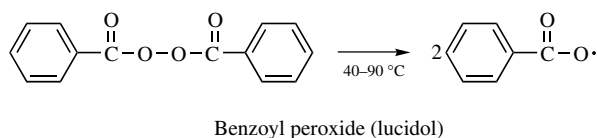
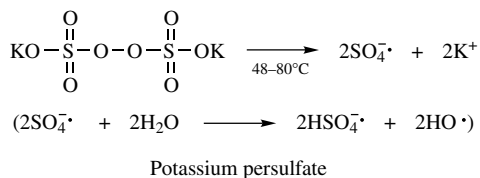
Propagation:

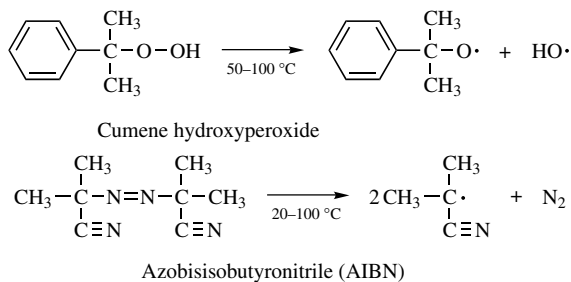


Termination:



Most of the initiators are peroxides and aliphatic azo compounds, such as the following:

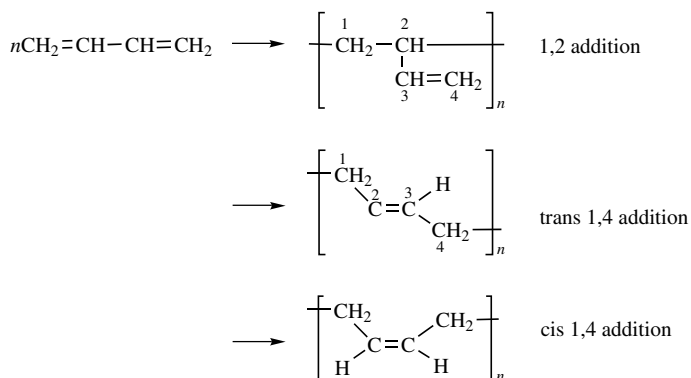




2.1.1 Complications

Free-radical polymerization often involves complications. Complications may occur during propagation, chain transfer, and chain termination.

Complications in Propagation When there is more than one unsaturated bond in the monomers, propagation can occur in a different mechanism, thereby affecting the chain structure. For example, in the synthesis of polybutadiene, polymerization can lead to three different products:



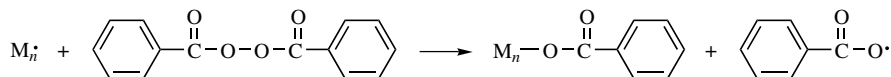
The three polymers have different properties. 1,2-Polybutadiene is a hard and rough crystalline compound; 1,4-polybutadiene is not. The crystalline and glass transition temperatures for *cis*- and *trans*-1,4-polybutadiene are markedly different: T_g is -108°C for *cis* and -18°C for *trans*; T_m is 1°C for *cis* and 141°C for *trans*. The glass transition temperature T_g is the temperature below which an amorphous polymer can be considered to be a hard glass and above which the material is soft or rubbery; T_m is the crystalline melting point where the crystallinity completely disappears.

The mechanism that the reaction follows depends, among other factors, on the solvent and the temperature. Phenyllithium in tetrahydrofuran favors 1,2 polymers, whereas lithium dispersion or phenyllithium in paraffinic hydrocarbons such as heptane as a solvent favors 1,4 polymers. A higher temperature favors

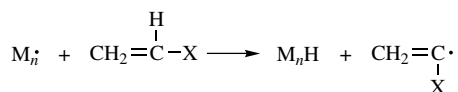
1,2 polymers; at low temperature the products are predominantly 1,4 repeating units.

Complications in Chain Transfer The reactivity of a radical can be transferred to the monomer, polymer, or solvent or even to the initiator, as the following examples show:

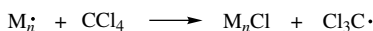
Transfer to initiator:



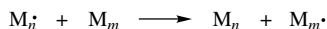
Transfer to monomer:



Transfer to solvent:



Transfer to polymer:



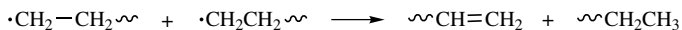
Chain transfer is the termination of a polymer chain without the destruction of the kinetic chain. Chain transfer does not affect the overall rate of polymerization but does affect the molecular weight distribution of polymer products. It is related to the efficiency of synthesizing the polymer within a designated range.

Complication in Chain Termination Termination may occur by recombination or by disproportionation:

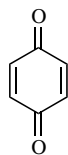
Recombination:



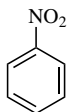
Disproportionation:



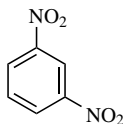
Recombination strengthens the chain length, whereas disproportionation gives short chains. Termination could also be carried out with an inhibitor, such as



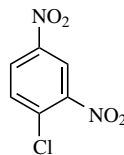
Quinone



Nitrobenzene



Dinitrobenzene



Dinitrochlorobenzene

as well as phenyl- β -naphthalamine, O_2 , NO, nitroso compounds, sulfur compounds, amines, and phenols.

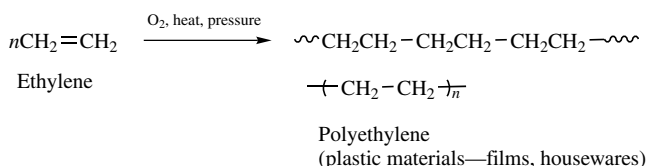
2.1.2 Methods of Free-Radical Polymerization

There are various ways to carry out free-radical polymerization. Here we mention a few of them:

1. *Bulk polymerization*—synthesis without solvent
2. *Solution polymerization*—synthesis with (inert) solvent
3. *Precipitation polymerization*—using solvent (such as methanol) to precipitate out the polymer
4. *Suspension polymerization*—adding an initiator to the suspension in aqueous solution
5. *Emulsion polymerization*—adding an initiator (such as potassium persulfate) to the emulsion of water-insoluble monomers (such as styrene) in aqueous soap solution

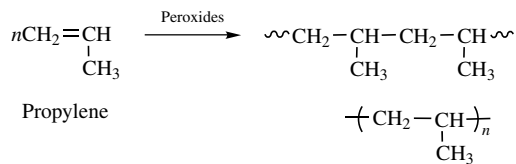
2.1.3 Some Well-Known Overall Reactions of Addition Polymers[†]

The following are the overall reactions for the synthesis of typical (also well-known in our daily life) polymers. All of them undergo the mechanism of addition polymerization.

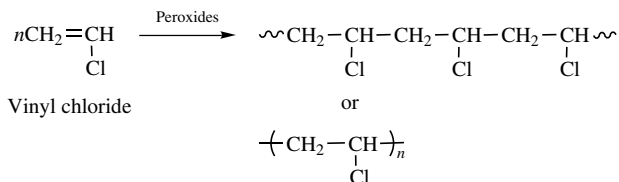


[†]Since 1994 plastics have been heavily used in the building and construction industry and have been competing with traditional stalwarts such as concrete, wood, steel, and glass. Some applications in certain types of window frames and house siding have grown dramatically. Plastics most widely used are polyvinyl chloride (PVC) polyethylene, and polystyrene. Engineering plastics used in construction include polycarbonate, acetals, and polyphenyl oxide. Other than for building and construction, polyurethane is used for insulation. PVC goes into pipes for water mains and sewers. It is also fashioned to be film and sheet as well as wire and cable.

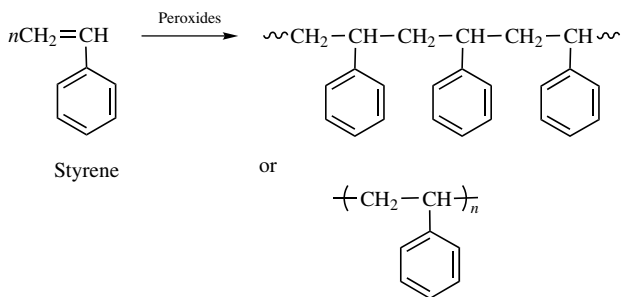
Recently, plastics are able to be made electrically conductive. They behave like metals or semiconductors known as conjugate polymers. The well-known conjugate polymers which can be made (Continued)



Polypropylene
(ropes, appliance parts)

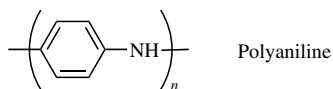


Poly(vinyl chloride) [floor coverings, phonograph records, plastic pipes (when plasticized with high-boiling esters), raincoats, upholstery fabrics]

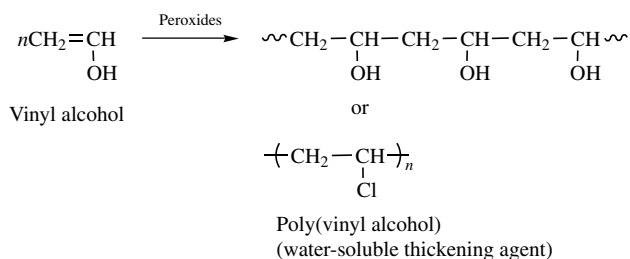
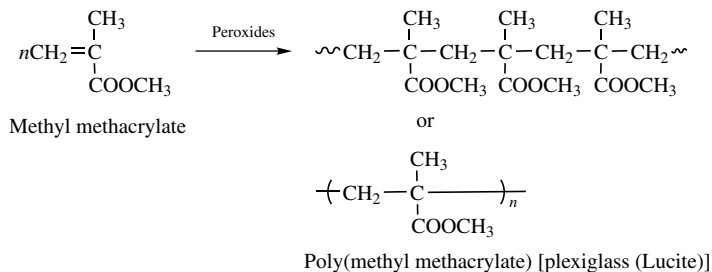


Polystyrene (coffee cups, packages, insulation)

† (Continued) conductive include



The mechanism can easily be understood by illustrating the coating of polyacetylene with iodine. In one exposure to iodine, the polymer chain loses an electron, leaving a hole or positive charge, while the pilfered electron resides on the counterion I_3^- . When such a hole is filled by an electron jumping in from a neighboring position, a new hole is created. As the cascade continues, the positive charge can migrate down the conjugated chain.



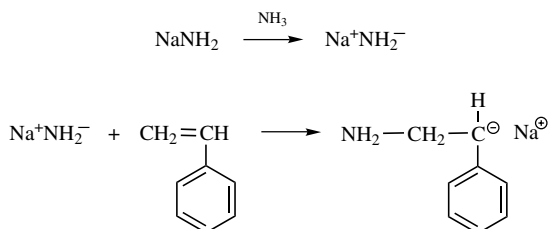
2.2 IONIC POLYMERIZATION

The two types of ionic polymerizations are anionic and cationic. The former involves carbanions C^- and the latter involves carbonium C^+ ions. Catalysts and cocatalysts are needed in ionic polymerization.

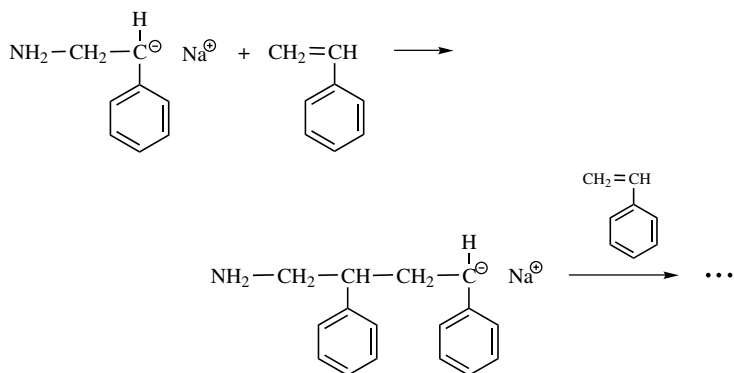
2.2.1 Anionic Polymerization

The catalysts for anionic polymerization are alkali metals, alkali metal amides, alkoxides, and cyanides. The cocatalysts are organic solvents, such as heptane. An example of anionic polymerization is the synthesis of polystyrene:

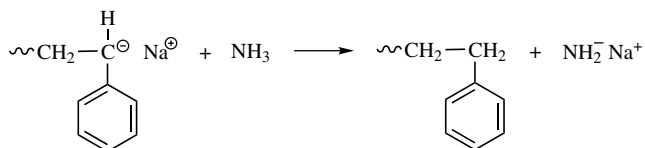
Initiation:



Propagation:

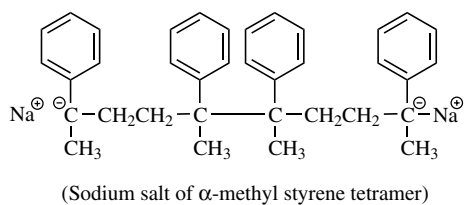


Termination:

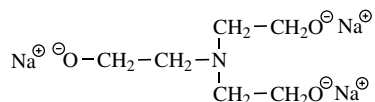


The chain growth in anionic polymerization does not necessarily have to go in one direction, as shown in the above example. It can go through two, three, four, or more directions, depending on the catalysts:

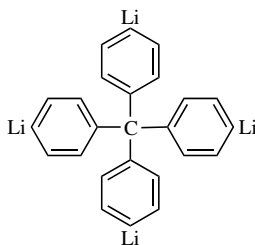
Two-way growth—bivalent ions used as initiator:



Three-way growth—polyfunctional initiator:



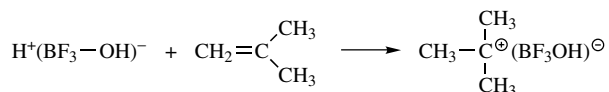
Four-way growth—polyfunctional initiator:



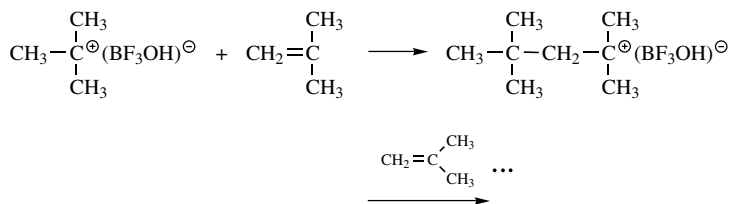
2.2.2 Cationic Polymerization

The catalysts for cationic polymerization are Lewis acids and Friedel–Crafts catalysts such as BF_3 , AlCl_3 , and SnCl_4 and strong acids such as H_2SO_4 . The cocatalysts are, for example, water and isobutene. An example of cationic polymerization is the synthesis of isobutene:

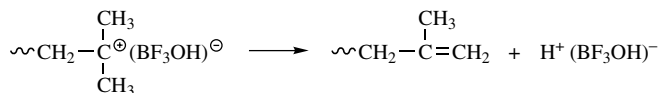
Initiation:



Propagation:



Termination:



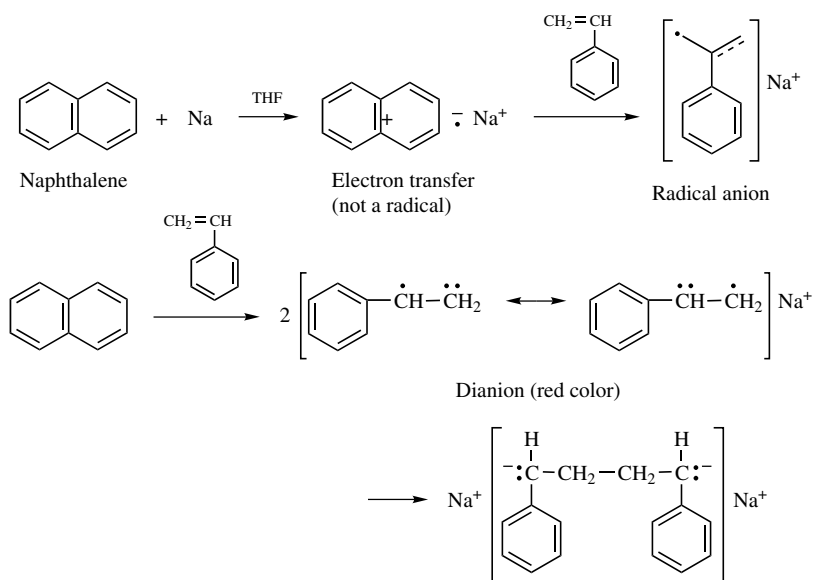
2.2.3 Living Polymers

Anionic polymerization is terminated not by the reaction of two growing species but by chain transfer to the solvent or to impurities present in the system. If an

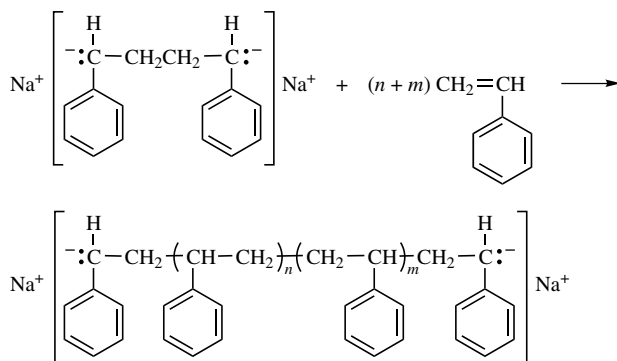
inactive solvent (such as tetrahydrofuran or dioxane) is chosen and the impurities are removed, the polymerization will not stop until all the monomers are consumed. Such a polymer, if kept in an appropriate condition, would always have a reactive end. If additional monomers are introduced to the system, the polymer keeps growing. The polymer is therefore called a living polymer. To meet these requirements, synthesis is usually performed under high vacuum and the product is also kept in a container sealed under high vacuum.

An example is the polymerization of styrene with sodium naphthalene at a pressure of 1×10^{-6} mm Hg:

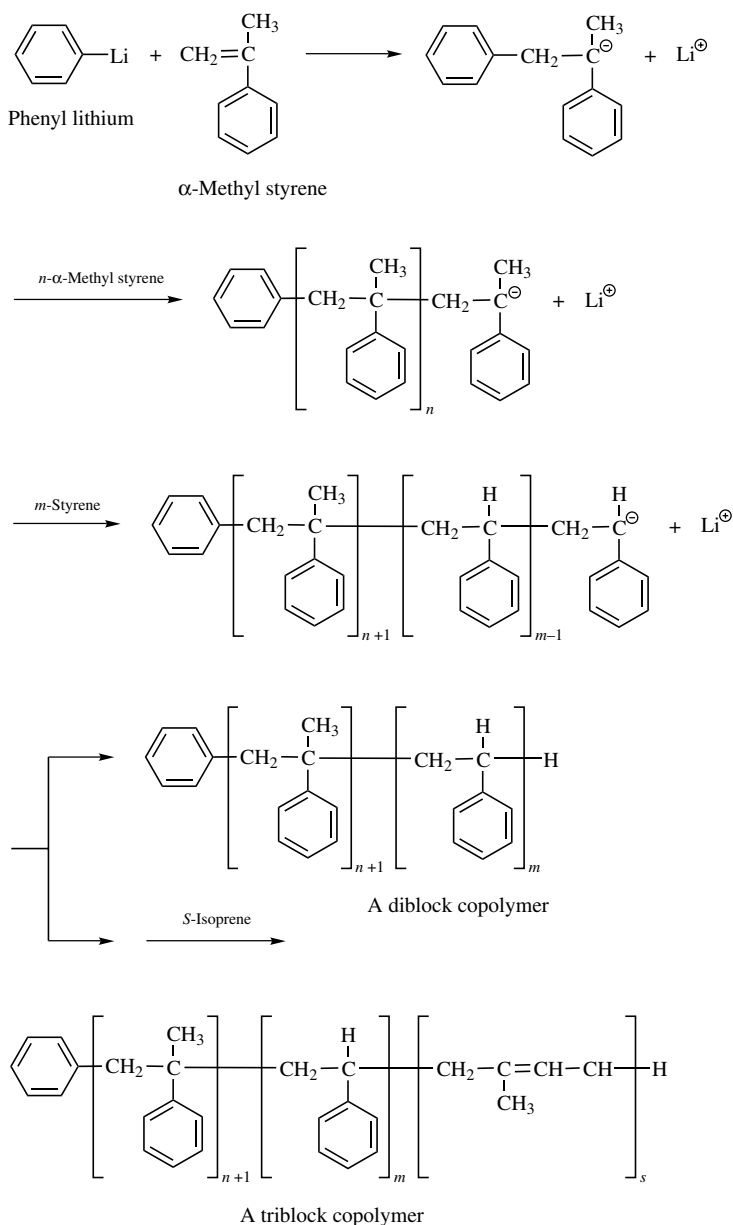
Initiation via electron transfer:



Propagation at both ends:



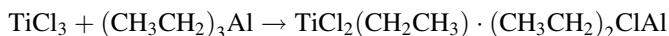
Since there is no chain transfer involved, preparation through living polymer results in a narrow distribution of molecular weight. It is the best way to synthesize di- and triblock copolymers, star-shaped and comb-shaped polymers, and homopolymers with high molecular weight. The following is an example of the synthesis of di- and triblock copolymers:



2.3 COORDINATION POLYMERIZATION

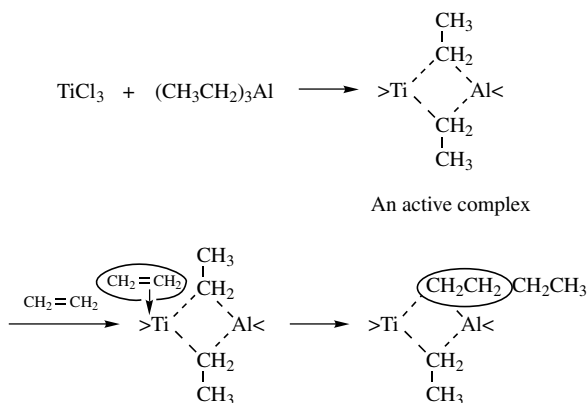
Coordination polymerization is also called stereospecific or stereoregular polymerization. The essential feature is a directing force to a growing chain end. Coordination polymerization is carried out using a catalyst called the Ziegler–Natta catalyst. Typical Ziegler–Natta catalysts are transition metal halides, such as TiX_4 , TiX_3 , VX_4 , VX_3 , VOX_3 , Co, and Ni complexes, and organometallic compounds, such as AlR_3 , AlR_2X , ZnR_2 , and LiR .

It is generally believed that the following oxidation–reduction reaction is responsible for chain growth:

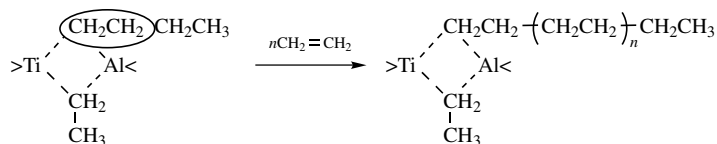


Titaniumtrichloride (a transition metal salt) reacts with triethylaluminum (a metal alkyl) to form an active catalyst, a titanium complex holding an ethyl group. If an alkene, such as ethylene, is introduced, the alkene attaches itself to titanium by a π bond. With the alkene and ethyl both held by the metal, the alkene unit inserts itself between the metal and the ethyl group. There is now an *n*-butyl group (in the case of ethylene) attached to the titanium. The bonding site where ethylene was held is vacant. The catalyst is ready to work again and the process continues until the insertion of hydrogen. The long chain then separates from the metal and a molecule of polyethylene has been formed. The mechanism may be better described in equations:

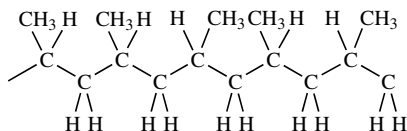
Initiation:



Propagation:



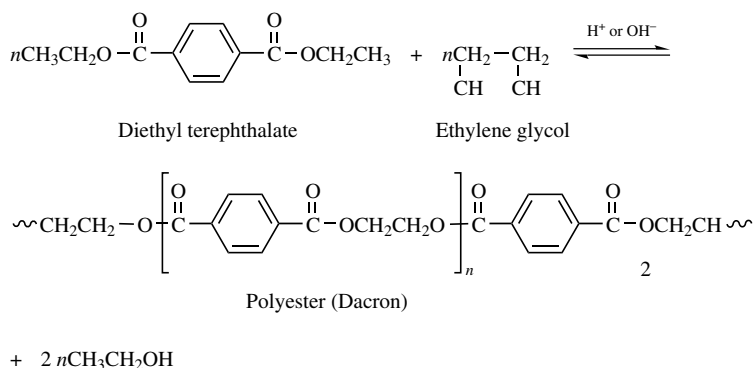
Atactic polypropylene:



2.4 STEPWISE POLYMERIZATION

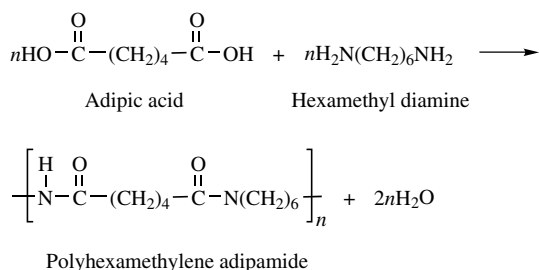
In stepwise polymerization, there is no initiation, propagation, or termination as is the case in chain reaction polymerization. The polymerization depends entirely on the individual reactions of the functional groups of monomers. The four types of stepwise polymerization are the synthesis of polyester, polyamide, polyurethane, and polycarbonate.

1. Polyester is synthesized by the direct reaction of a diacid and a diol at high temperatures. An example is the synthesis of Dacron:



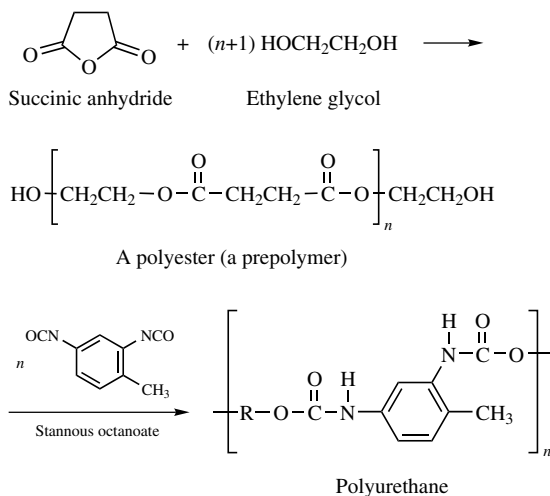
Polyester is used for clothing and tire cord.

2. Polyamide is synthesized using two difunctional monomers. An example is the synthesis of 66 nylon:



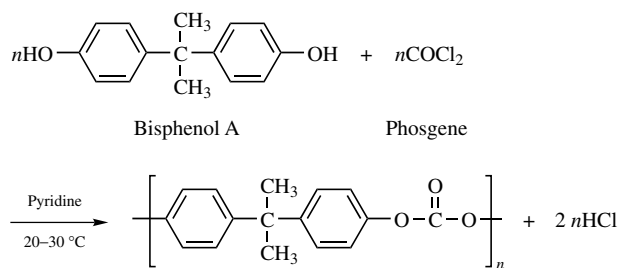
The number n is usually between 50 and 65, corresponding to a molecular weight of 12,000–15,000. Like polyester, nylon is used for clothing and tire cord.

3. Polyurethanes, also called polycarbamates, are synthesized by the reaction of a diisocyanate with a diol. Experiments are usually carried out in solutions. The following is an example of polyurethane synthesis:



Polyurethane is used for rubber (vulcollanes), elastic fibers (Lycra), hard or elastic forms (Moltoprene), stain, flooring, and wood and fabric coating.

4. Polycarbonate is synthesized by the reaction of the simplest diacidchloride, phosgene, with bisphenol A in the presence of a base:



Property: electric resistance.

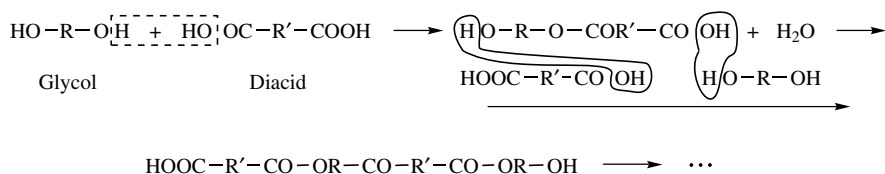
2.5 KINETICS OF THE SYNTHESIS OF POLYMERS

The kinetics of a condensation reaction is similar to those of small molecular reactions. It is basically a simple order reaction (first order, second order, or third

order). On the other hand, free-radical polymerization, ionic polymerization, and coordination polymerization are all chain reactions. Their mechanism is very complicated.

2.5.1 Condensation Reactions

A typical condensation polymerization may run as follows:



Let A represent HO—R—OH and B represent COOH—R'—COOH. Then the rate law of condensation polymerization is a simple third-order reaction:

$$\frac{-d[B]}{dt} = k[B]^2[A]$$

If $[B] = [A] = c$, where c is the concentration in moles per liter, then

$$\frac{-dc}{dt} = kc^3$$

Upon integration, we obtain

$$2kt = \frac{1}{c^2} + \text{const}$$

Let P be the extent of reaction, or probability that the functional groups will react, that is, the fraction of the functional groups that has reacted at time t ; then

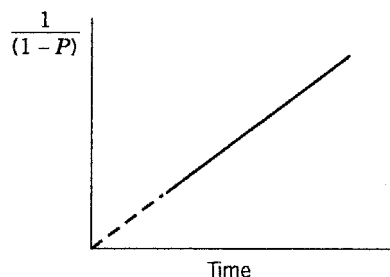
$$c = c_0(1 - P)$$

where c is the concentration of monomers at any time t and c_0 is the initial concentration. The quantity $1 - P$ is the probability that the groups will not react. Substituting c into the previous equation, we obtain

$$2c_0^2kt = \frac{1}{(1 - P)^2} + \text{const}$$

The degree of polymerization DP for condensation reaction can be defined in terms of $1 - P$ by the equation $DP = 1/(1 - P)$.

If we plot $1/(1 - P)^2$ versus t (time), a linear graph is obtained:



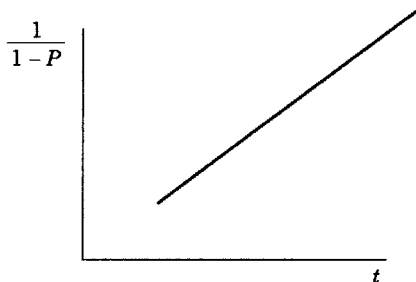
The rate constant k can be obtained from the slope. The third-order reaction can be reduced to the second-order reaction if a strong acid catalyst is added to the reaction system. The rate equation then becomes

$$-\frac{dc}{dt} = kc^2$$

and

$$c_0 k' t = \frac{1}{1 - P} + \text{const}$$

The plot of $1/(1 - P)$ versus t yields a straight line:



2.5.2 Chain Reactions

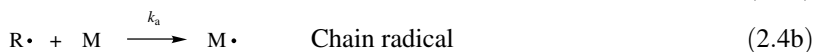
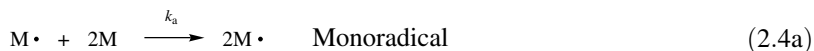
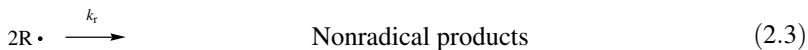
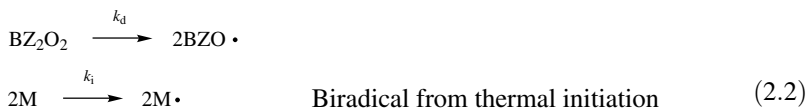
The mechanism of the basic feature of a chain reaction may be illustrated by that of a free-radical reaction, particularly the polymerization of styrene, which has been extensively investigated for years by many investigators. Here we describe the mechanism proposed by Mayo and co-workers (1951, 1959).

A free-radical reaction may go through all or some of the following steps:

Initiation:



for example,

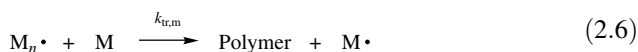


Monoradicals and chain radicals are the same. The chain has not propagated as yet; hence, both equations are labeled (2.4). BZ_2O_2 is benzoyl peroxide. The term k_d is the rate constant of the decomposition of peroxide, k_i is the rate constant of the thermal initiation of the biradical, k_r is the rate constant of the first-order recombination of radicals from the peroxide, and k_a is the rate constant of the reaction of these radicals with monomer:

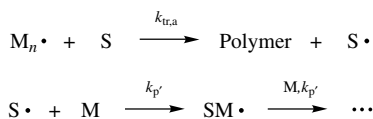
Propagation:



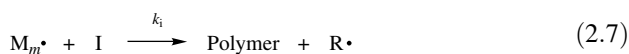
Chain transfer to monomer:



Chain transfer to solvent:

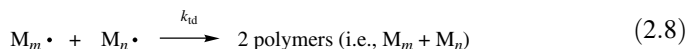


Chain transfer to initiator:

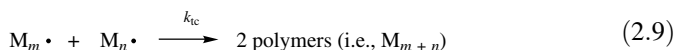


where k_p is the rate constant of propagation, k_{tr} is the rate constant of transfer, and k_i is the rate constant of the chain transfer to the initiator.

Termination:



where k_{td} is the rate constant of termination by disproportionation,



where k_{tc} is the rate constant of termination by coupling.

The rate of initiation R_i is

$$R_i = \frac{d[M \cdot]}{dt} = 2fk_d[I]$$

where f is the efficiency of the initiation and is given in the expression

$$f = \frac{k_a[2R \cdot][M]}{k_r[2R \cdot] + k_a[2R \cdot][M]} = \frac{1}{(k_r/k_a[M]) + 1} \quad (2.10)$$

The value of f ranges between 0.5 and 1 and is usually 0.70. The rate of termination is

$$R_t = -\frac{d[M \cdot]}{dt} = 2k_t[M \cdot]^2$$

where $k_t = k_{td} + k_{tc}$. At steady state, $R_i = R_t$, that is,

$$[M \cdot] = \left(\frac{k_i[M]^2 + k_d f [I]}{k_t} \right)^{1/2}$$

The overall rate is

$$-\frac{d[M]}{dt} = k_p[M \cdot][M] = k_p \left(\frac{k_i[M]^2 + k_d f [I]}{k_t} \right)^{1/2} [M] \quad (2.11)$$

Since k_i is usually small, we may assume that $k_i = 0$. Equation (2.11) then becomes

$$-\frac{d[M]}{dt} = k_p \left(\frac{fk_d}{k_t} \right)^{1/2} [M][I]^{1/2} \quad (2.12)$$

This is the rate law of free-radical polymerization. In general, the polymerization is in $\frac{1}{2}$ order with respect to $[I]$ and first order with respect to $[M]$. However, it depends on f . If f is low, k_i is no longer negligible, and the polymerization could be in $\frac{3}{2}$ order with respect to $[M]$ while still in $\frac{1}{2}$ order with respect to $[I]$.

Of particular interest is the study of chain transfer during the process of chain propagation. Let us define the degree of addition polymerization DP as

$$\begin{aligned} \text{DP} &= \frac{\text{rate of polymerization } (R_p)}{\text{half the rate of formation of chain ends}} \\ &= \frac{k_p[\text{M}\cdot][\text{M}]}{fk_d[\text{I}] + k_{\text{tr,I}}[\text{M}\cdot][\text{I}] + k_{\text{tr,m}}[\text{M}\cdot][\text{M}] + k_{\text{tr,s}}[\text{M}\cdot][\text{S}] + k_{\text{td}}[\text{M}\cdot]^2} \end{aligned}$$

where $k_{\text{tr,I}}$ is the rate constant of chain transfer to the initiator and $k_{\text{tr,I}}[\text{M}\cdot][\text{I}] = k_t[\text{M}\cdot][\text{I}]$. Similarly, $k_{\text{tr,m}}$ is the rate constant of chain transfer to the monomer, and $k_{\text{tr,m}}[\text{M}\cdot][\text{M}] = k_{\text{tr,m}}[\text{M}_n\cdot][\text{M}]$; $k_{\text{tr,s}}$ is the rate constant of chain transfer to the solvent, and $k_{\text{tr,s}}[\text{M}\cdot][\text{S}] = k_{\text{tr,s}}[\text{M}_n\cdot][\text{S}]$. Taking the reciprocal of DP and neglecting the solvent effect, we have

$$\frac{1}{\text{DP}} = \frac{k_{\text{tr,I}}[\text{M}\cdot][\text{I}] + k_{\text{tr,m}}[\text{M}\cdot][\text{M}] + k_d f[\text{I}] + k_{\text{td}}[\text{M}\cdot]^2}{k_p[\text{M}\cdot][\text{M}]} \quad (2.13)$$

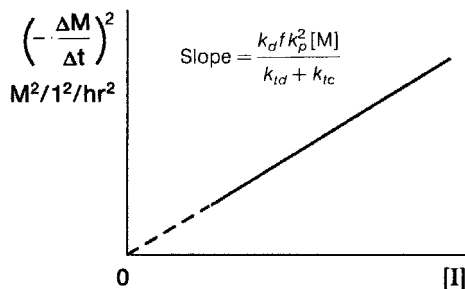
which leads to

$$\begin{aligned} \frac{1}{\text{DP}} &= c_M + \frac{c_1[\text{I}]}{[\text{M}]} + \frac{k_d f[\text{I}]}{-d[\text{M}]/dt} + \frac{k_{\text{td}}(k_i[\text{M}]^2 + k_d f[\text{I}])}{(-d[\text{M}]/dt)(k_t)} \\ &= c_M + \frac{c_1[\text{I}]}{[\text{M}]} + \frac{k_d f[\text{I}]}{-d[\text{M}]/dt} + \frac{k_{\text{td}}(-d[\text{M}]/dt)}{k_p^2[\text{M}]^2} \end{aligned} \quad (2.14)$$

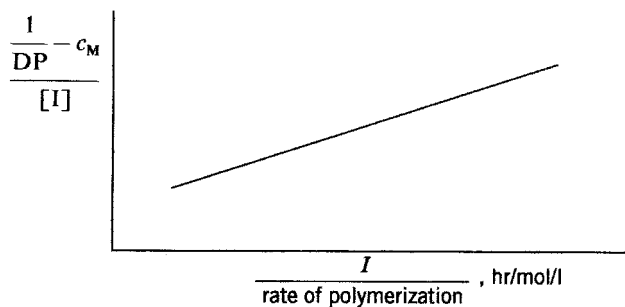
where $c_M = k_{\text{tr}}/k_p$ and $c_1 = k_i/k_p$. If the solvent effect is stressed, the reciprocal of DP is in the form [from the equation for $[\text{M}\cdot]$ and Eq. (2.12)]

$$\frac{1}{\text{DP}} = \frac{R_p k_t}{k_p^2[\text{M}]^2} + \frac{k_{\text{tr,m}}}{k_p} + \frac{k_{\text{tr,s}}[\text{S}]}{k_p[\text{M}]} \quad (2.15)$$

Equations (2.12), (2.14), and (2.15) can be experimentally tested. From Eq. (2.12) we plot



at the same monomer concentration, that is, $[\text{M}]$ is constant. From Eq. (2.14) we plot (assuming $k_{\text{td}} = 0$)



If the value of c_M is known, for example, $c_M = 6 \times 10^{-5}$ for polymerization of styrene, we obtain

$$\begin{aligned} \text{Slope} &= k_d f \\ \text{Intercept} &= \frac{c_I}{[M]} \end{aligned}$$

In obtaining this plot, we assume, of course, that all chains are terminated by coupling, that is, $k_{td} = 0$.

In the use of Eq. (2.15) we assume that $k_{tr,m}$ is negligible. This can be done by running the experiments of uncatalyzed polymerization at different initial monomer concentrations. Assuming that $R_p \propto [M]^2$, Eq. (2.15) becomes

$$\frac{1}{DP} = \left(\frac{k_t}{k_p^2} + \frac{k_{tr,m}}{k_p} \right) + \frac{k_{tr,s}[S]}{k_p[M]}$$

The plot of $1/DP$ versus $[S]/[M]$ will yield

$$\text{Slope} = \frac{k_{tr,s}}{k_p}$$

which is the solvent transfer constant. The effect of solvent is shown in Figure 2.1.

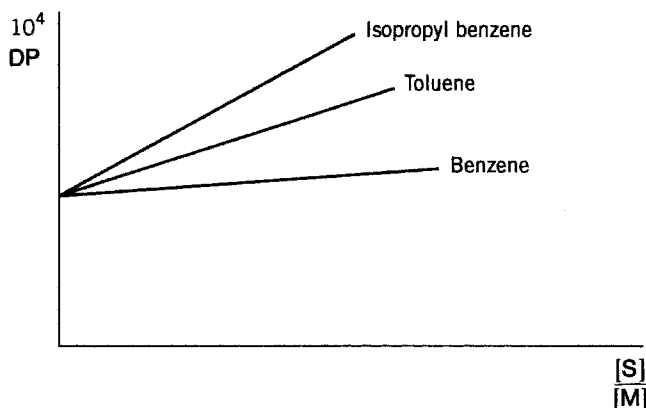


FIGURE 2.1 Effect of solvent on styrene polymerization at 100°C.

It is customary to define the chain length ν as the number of monomer units consumed per active center:

$$\nu = \frac{R_p}{R_i} = \frac{R_p}{R_t} \quad (\text{steady state})$$

$$\nu = \frac{k_p [M]}{2k_t [M\cdot]}$$

$$\nu = \frac{k_p^2 [M]^2}{2k_t R_p}$$

$$\nu = \frac{k_p [M]}{2(fk_d k_t)^{1/2} [I]^{1/2}}$$

In general, the chain length is related to DP, this is, $\nu \sim \text{DP}$. The proportionality constant depends on the mode of termination: For termination by coupling, $\text{DP} = 2\nu$, and for termination by disproportionation, $\text{DP} = \nu$.

On the basis of the above mechanism, we can write a simple equation to describe the probability p that a polymer radical $M_n\cdot$ may undergo transfer rather than addition of another monomer:

$$1 - p = \frac{k_{tr}[A]}{k_p[M] + k_{tr}[A]}$$

where A can be an initiator, a solvent, a radical, or even a monomer. The degree of polymerization \bar{x}_n may be written as before:

$$\bar{x}_n = \frac{1}{1 - p}$$

The chain termination by coupling can be described by

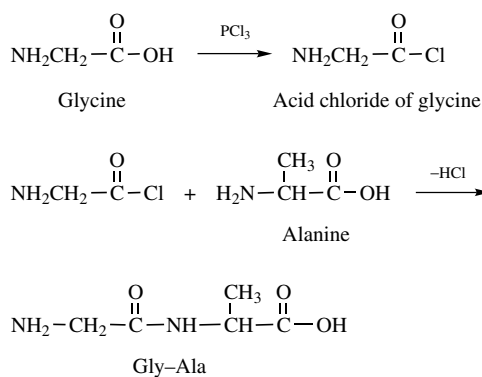
$$1 - p = \frac{2k_t [M\cdot]}{k_p [M] + 2k_t [M\cdot]}$$

$$\bar{x}_n = \frac{2}{1 - p} = 2 + \frac{k_p [M]}{k_t [M\cdot]}$$

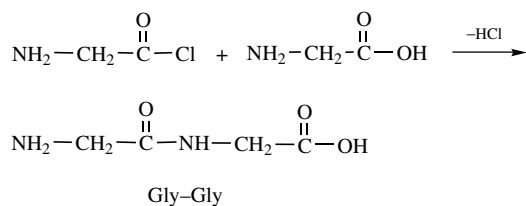
2.6 POLYPEPTIDE SYNTHESIS

Polypeptide synthesis is basically the work of coupling of two amino acids or peptides in sequence. The most frequently used reagent for coupling is acid

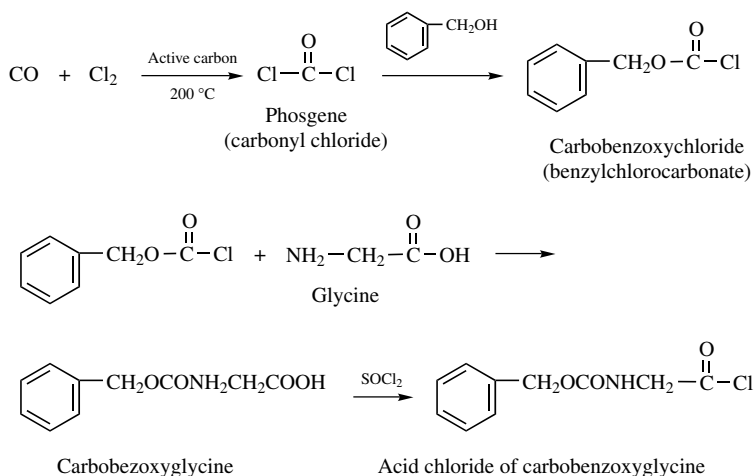
chloride. An example is the coupling of Gly and Ala:



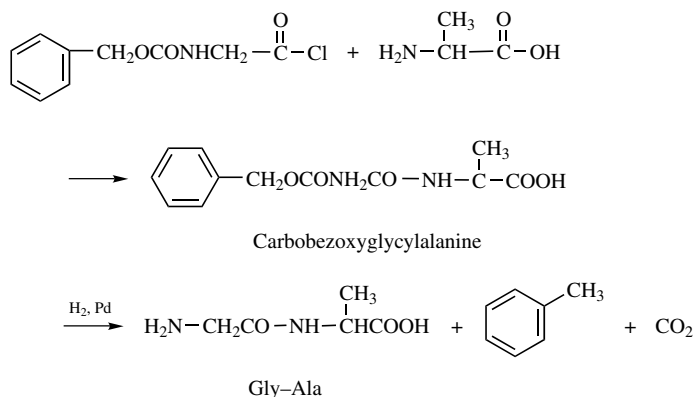
However, the side reaction of coupling glycine often occurs also:



To avoid the side reaction, a protecting or blocking group must be substituted on the amino function of the group, for example, $-\text{NH}_2-$:

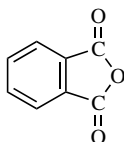
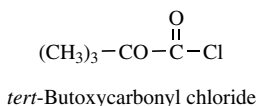


Once the amino group is protected, we can couple Gly and Ala without a side reaction:



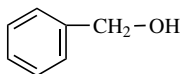
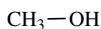
Since amino acids and peptides often possess a variety of chemically reactive substituents (in addition to amino groups ---NH_2), such as carboxyl groups (---COOH), thiol groups (---SH), and hydroxy groups (---OH), a number of chemical blocking reagents other than carbobenzoxy chloride must be used. The following are some examples:

To block an N terminal:

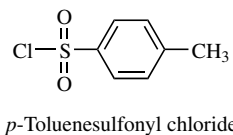


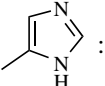
Phthalic anhydride

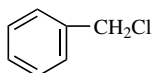
To block a C terminal:



To block a side-chain amino group:



To block side chains $-\text{COOH}$, $-\text{SH}$, $-\text{OH}$, and  :

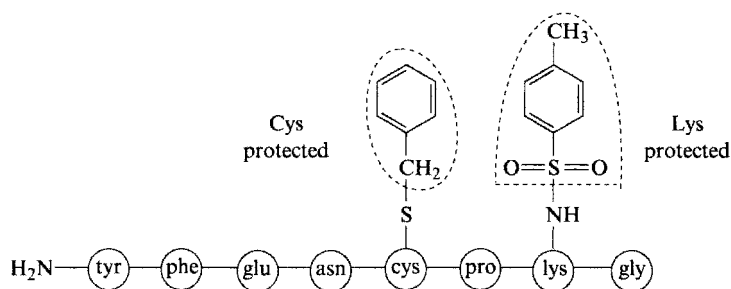


Benzyl chloride

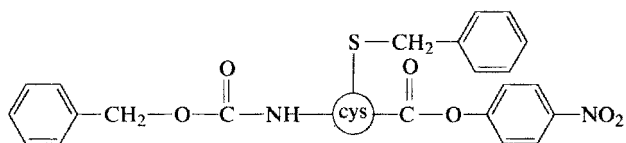
Suppose we have a polypeptide available:



and we want to add one group, Cys, to Tyr (N terminal). We first protect the Cys and Lys groups in the given polypeptide:



Then we activate the C terminal end of an independent protected Cys,



which will undergo coupling as shown in Figure 2.2.

Polypeptide synthesis is one of the exciting and challenging areas in modern chemistry. Here we describe the two most well-known polypeptide syntheses: the synthesis of insulin and the synthesis of ribonuclease.

2.6.1 Synthesis of Insulin

The synthesis of insulin was reported by three groups: Zahn (1963), Katsoyannis and Dixon (1964), and Niu et al. (1965). Insulin consists of an A chain and a B chain:

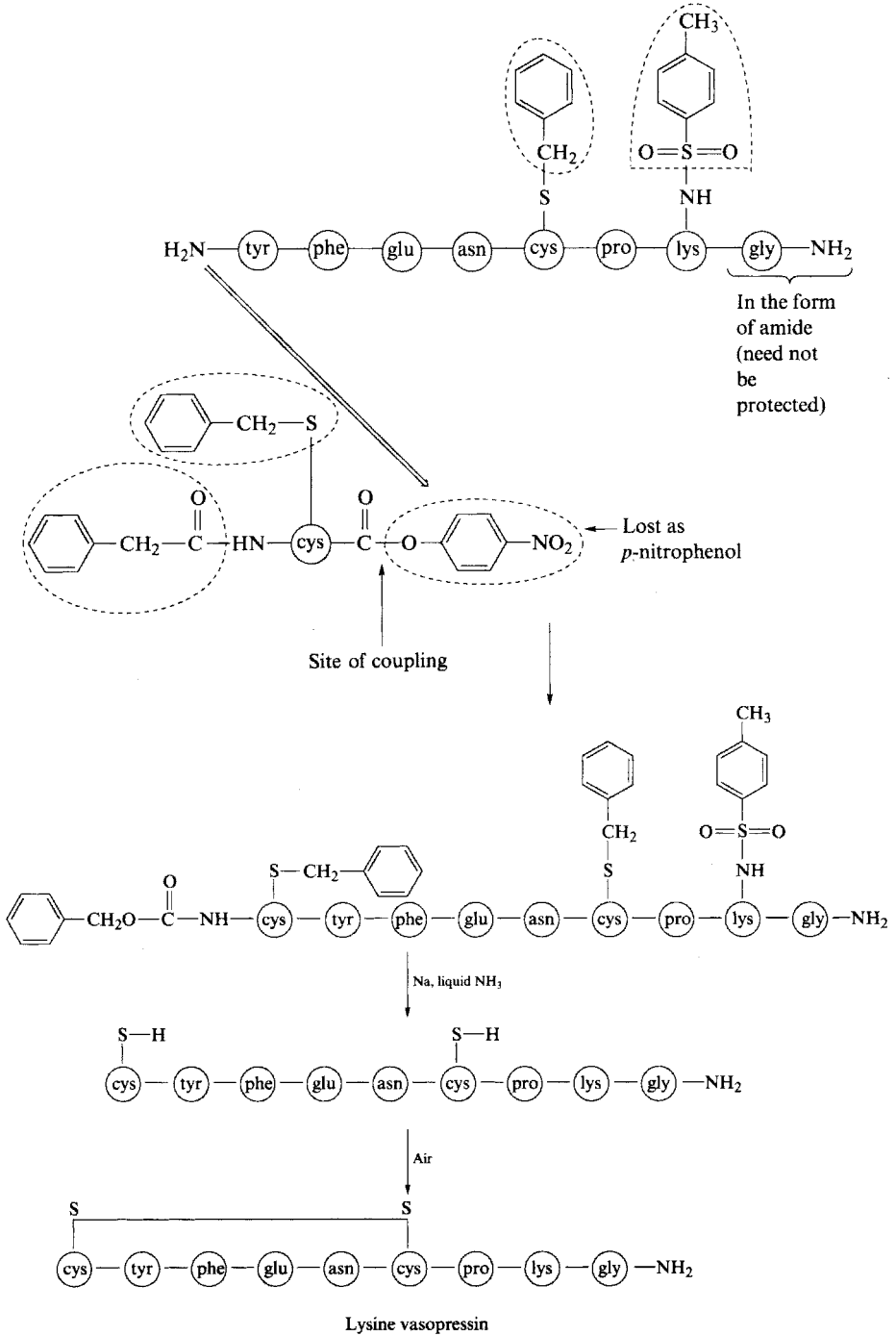
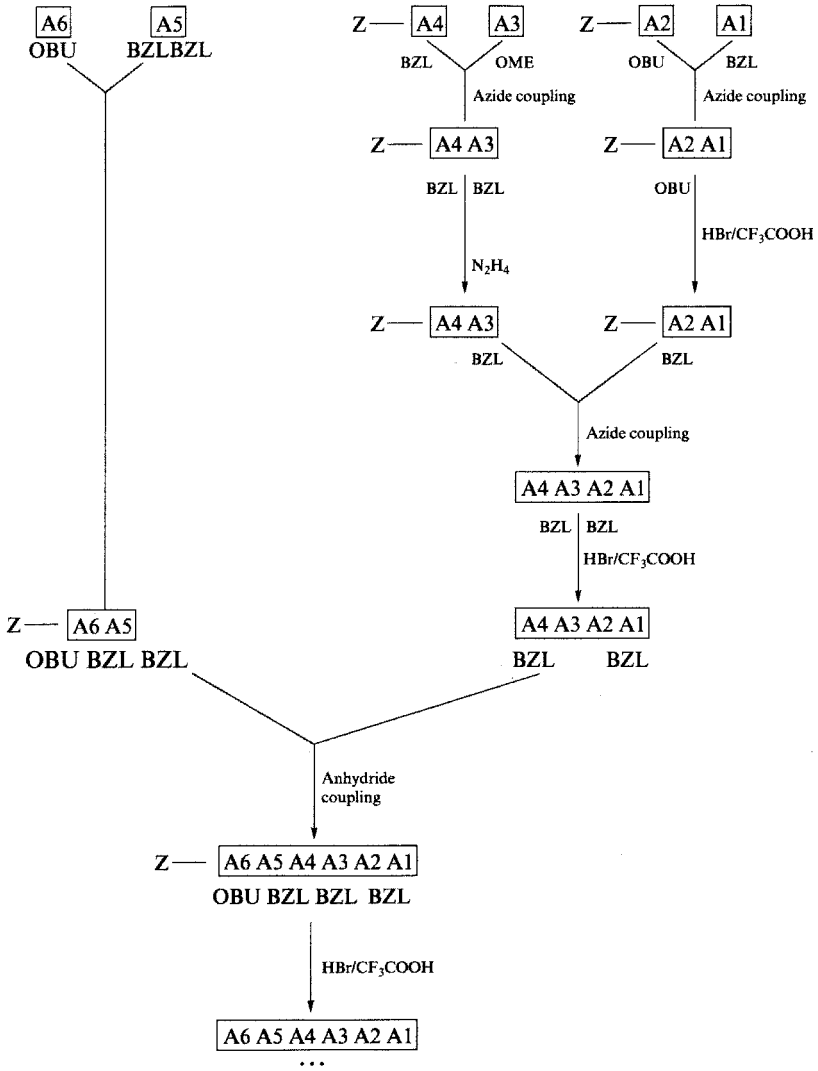


FIGURE 2.2 Coupling of polypeptides. [Source: Wingrove and Caret (1981).]



Abbreviations: BZL, benzyl; OBU, butyl ester; OME, methyl ester; A, amino acid; Z, benzyloxy-carbonyl.

FIGURE 2.3 Synthesis of insulin. [Source: Vollmert (1973).]

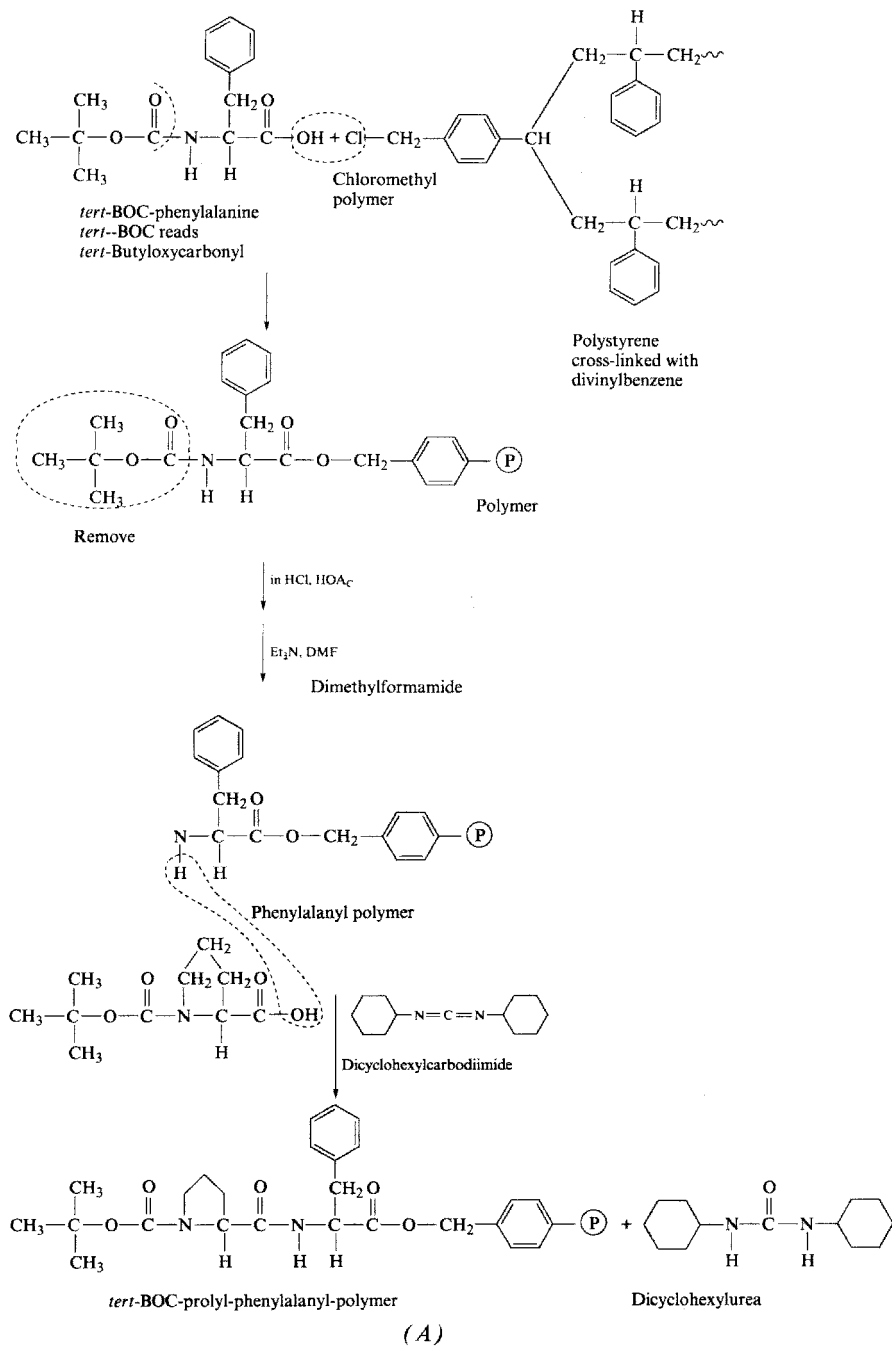


FIGURE 2.4 (a) First steps of ribonuclear synthesis. (b) General diagram. [Source: Merrifield (1963).]

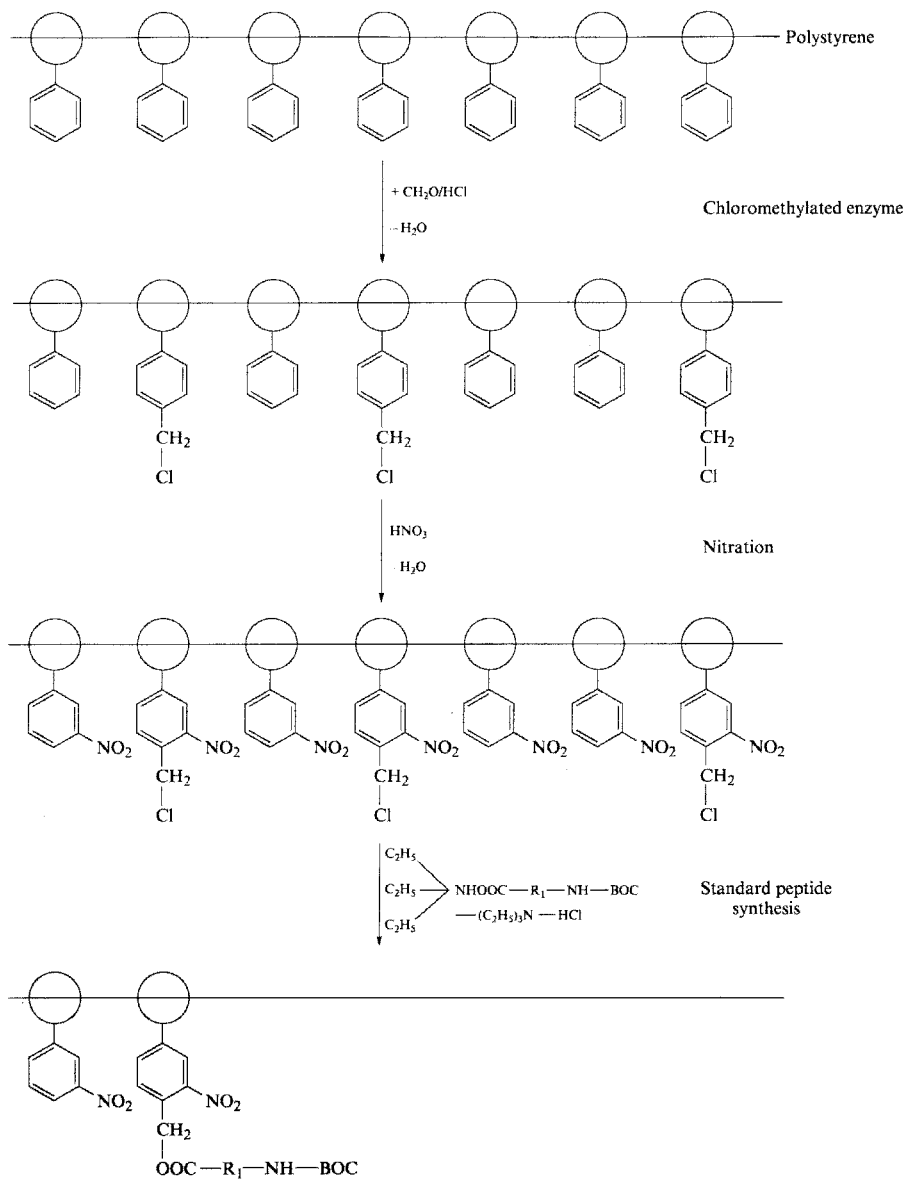
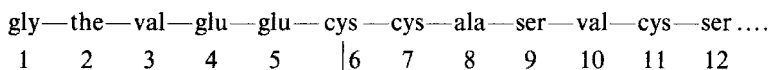


FIGURE 2.4 (Continued)

A chain



|

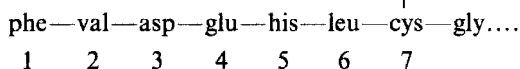
S

|

S

|

B chain



The scheme of the synthesis is illustrated in Figure 2.3.

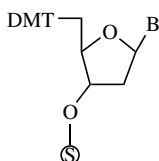
2.6.2 Synthesis of Ribonucleus

The successful synthesis of ribonucleus is attributed to Merrifield (1963), who designed the solid-phase method in polypeptide chemistry. The method starts with the synthesis of a polymeric material (polystyrene). The polymer is chloromethylated and nitrated. The first amino acid is attached to the CH_2 group of the chloromethyl polystyrene by esterification. Then the other amino acids are added step by step (Figure 2.4).

2.7 DNA SYNTHESIS

There are three methods for synthesizing DNA: phosphate diester, phosphate triester, and phosphite triester. To illustrate, we describe the phosphite triester method. This method is parallel to Merrifield's synthesis of ribonucleus in the sense that the strategy involves adding mononucleotides in sequence to a deoxynucleoside, which is covalently attached to a polymeric material. The polymeric material is usually silica based, such as Vydak, Fractosil, and poreglass. It consists of coupling a deoxynucleoside that contains a 3'-*p*-nitrophenylsuccinate ester with an amino group attached to the polymer support.

The starting material is a compound that contains a deoxynucleoside covalently joined to silica gel (S) through an amide bond:



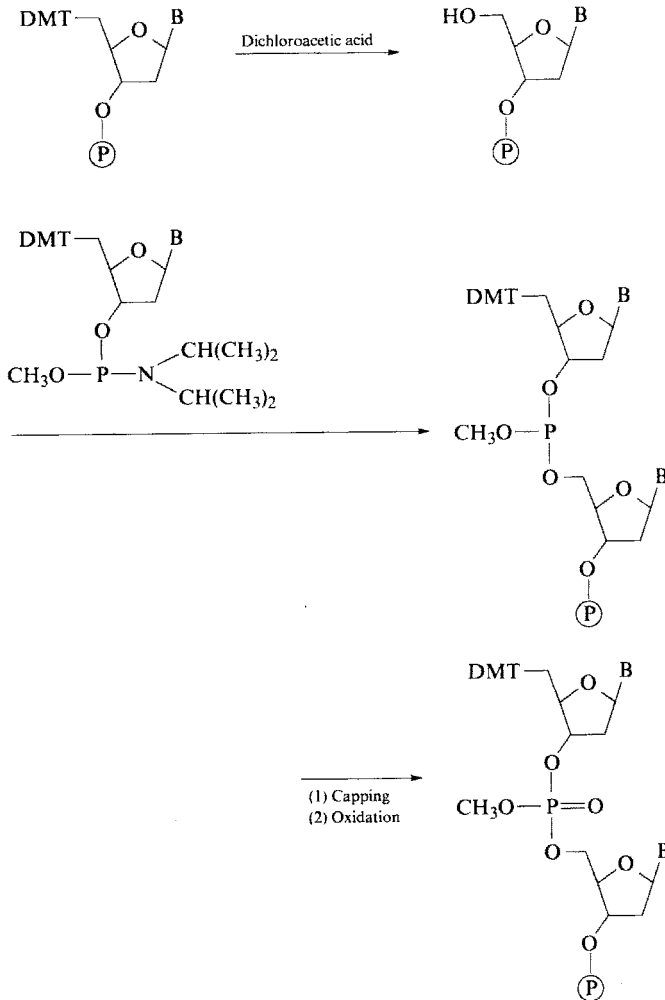


FIGURE 2.5 Capping of unreactive deoxynucleoside followed by oxidation of the phosphite triester to the phosphate triester. [Source: Caruthers (1985).]

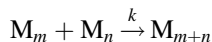
where B is the thymine or appropriately protected adanine, cytosine, or guanine and DMT is the dimethoxytrityl. The site for synthesis is DMT. A certain amount of dichloroacetic acid is added to remove the DMT, and then the condensation reaction is allowed to occur with another DMT-protected deoxynucleoside 3'-phosphoramidite. Finally, capping of the unreactive deoxynucleoside, or acylation, is followed by oxidation of the phosphite triester to the phosphate triester, thereby adding one nucleotide in the cycle in a 3' to 5' direction. The overall reaction is given in Figure 2.5.

REFERENCES

- Caruthers, M. H., *Science* **230**, 281 (1985).
- Dostal, H., and R. Raff, *Monatsh. Chem.* **68**, 188 (1936a).
- Dostal, H., and R. Raff, *Z. Phys. Chem. B* **32**, 11 (1936b).
- Flory, P. J., *Principles of Polymer Chemistry*. Ithaca, NY: Cornell University Press, 1953.
- Laidler, K. J., *Chemical Kinetics*. New York: McGraw-Hill, 1965, pp. 425–426.
- Lenz, R. W., *Organic Chemistry of Synthetic Polymers*. New York: Wiley, 1967.
- Mayo, F. R., *J. Chem. Ed.* **36**, 157 (1959).
- Mayo, F. R., R. A. Gregg, and M. S. Matheson, *J. Am. Chem. Soc.* **73**, 1691 (1951).
- Merrifield, R. B., *J. Am. Chem. Soc.* **85**, 2149 (1963).
- Odian, G., *Principles of Polymerization*, 2nd ed. New York: Wiley, 1981.
- State of the Art Symposium: Polymer Chemistry, *J. Chem. Ed.* **58** (1981).
- Szwarc, M., pp. 303–325 in H. F. Mark (Ed.), *Encyclopedia of Polymer Science and Technology*, Vol. 8. New York: Wiley, 1968.
- Vollmert, B., *Polymer Chemistry*. New York: Springer, 1973.
- Wingrove, A. S., and R. L. Caret, *Organic Chemistry*. New York: Harper & Row, 1981.

PROBLEMS

- 2.1** Plot the extent of conversion P (x coordinate) versus the degree of polymerization DP (y coordinate) and interpret the resulting graph.
- 2.2** In condensation polymerization, if 99% of one of functional groups has reacted (and, therefore, 99% of the other groups), what is the average degree of polymerization?
- (a) No monofunctional impurity is involved.
- (b) Three percent impurity is involved.
- 2.3** The mechanism of condensation polymerization may be expressed as



where M_m and M_n represent a chain containing m and n monomers, respectively, and k is the rate constant. Show that the fraction of functional groups f that is reacted at time t can be given by

$$f = \frac{[M_1]_0 kt}{2 + [M_1]_0 kt}$$

where $[M_1]_0$ is the initial concentration of monomers (Dostal and Raff, 1936a,b; cited in Laidler, 1965).

- 2.4** Following are the data of polymerization of styrene by benzoyl peroxide at 60°C:

[BZ ₂ O] (mL)	$-\Delta[M]/\Delta t$ (m/Lh ⁻¹)	Molecular Weight
0.0001265	0.0181	800,774
0.0002525	0.0248	714,737
0.000500	0.0328	641,264
0.001010	0.0466	485,738
0.0200	0.203	121,750
0.0800	0.404	53,052

- (a) Calculate the degree of polymerization of each polymer product.
- (b) Assuming the value of c_M to be 6×10^{-5} , determine the constant of chain transfer with benzoyl peroxide $c_I = k_I/k_p'$ and the constant of the decomposition of radical d_d . The parameter c_M is the chain transfer with styrene monomer, $c_M = k_{tr}/k_p$. The fraction of the radicals f that is successful in initiating chains is 0.70 (70%) (Mayo et al., 1951).

3

DISTRIBUTION OF MOLECULAR WEIGHT

For small molecules, such as ethane, there is no problem of molecular weight distribution. All ethane molecules have the same molecular weight. The problem exists for macromolecules, especially synthetic polymers. Not all polymer molecules of the same compound will have the same molecular weight, even if they are prepared the same way. In step polymerization (condensation reaction), any two molecular species (monomer and monomer, monomer and growing polymer, growing polymer and growing polymer) can react and stop at any moment. As a result, different species of polymer molecules, ranging from those with very long chains to those with very short chains, exist simultaneously. Similarly, in a chain reaction (addition polymerization), a radical, an anionic, or a cationic reactive center adds a monomer unit to a growing polymer. The termination could occur at any stage: chain radical combination, chain radical disproportionation, and chain transfer to monomer, to solvent, or to any impurity. All of these reactions produce polymer molecules with different chain lengths.

While the problem of molecular weight distribution is serious with synthetic polymers, it is not so with proteins and nucleic acids. However, biological polymers in aqueous solutions under certain conditions often form dimers and trimers; thus, the solution may not be homogeneous either; for example, most bovine serum albumin (BSA) samples contain 10% of dimers. Knowledge about the distribution of molecular weight may apply equally to biological polymers. Since molecular weight is directly related to the size of the chain, the approach to the distribution problem is statistical in nature.

3.1 REVIEW OF MATHEMATICAL STATISTICS

To explain the rationale behind the proposals for describing molecular weight distribution, a simple review of mathematics and statistics is given in this section. The following equations are useful in formulating statistical distribution:

Factorial:

$$N! = (N)(N - 1)(N - 2) \cdots (1)$$

Combination:

$$C_n^N = \binom{N}{n} = \frac{N!}{(N - n)!n!}$$

Binomial theorem:

$$(a + b)^N = \sum_{n=0}^{\infty} \binom{N}{x} a^{N-n} b^n = \sum_{n=0}^{\infty} \frac{N!}{(N - n)!n!} a^{N-n} b^n$$

Three types of distributions are frequently used in statistics: binomial, Poisson, and Gaussian. They are all relevant to the study of molecular weight distribution.

3.1.1 Binomial Distribution

Let N be the total number of events independent of each other, p be the probability of success, and x be the number of successful events out of N . Then $1 - p$ is the probability of failure and $N - x$ is the number of events that fail. The probability that exactly x events will succeed from the group of N is

$$f(x) = \binom{N}{x} p^x (1 - p)^{N-x} \quad 0 \leq x \leq n \quad (3.1)$$

where $f(x)$ refers to the binomial distribution because it is closely related to the binomial theorem.

The binomial distribution function is not continuous; hence, to calculate the average (mean value of \bar{x}), we have to use operator summation instead of integration:

$$\bar{x} = \sum_{x=0}^N x f(x) = \sum x \binom{N}{x} p^x (1 - p)^{N-x} = Np = m$$

Note:

$$\begin{aligned} \bar{x} &= \sum_{x=0}^N xf(x) \\ \bar{x}^2 &= \sum_{x=0}^N x^2f(x) \\ \bar{x}^3 &= \sum_{x=0}^N x^3f(x) \\ &\vdots \end{aligned}$$

3.1.2 Poisson Distribution

The terms in Eq. (3.1) may be rearranged in the form

$$f(x) = \binom{N}{x} p^x (1-p)^{N-x} = \frac{N!}{(N-x)!x!} p^x \frac{(1-p)^N}{(1-p)^x}$$

Consider three conditions:

1. The total number of events N is large and x is small. For the first approximation

$$\frac{N!}{(N-x)!} = (N)(N-1)(N-2) \cdots (N-x+1) \simeq N^x$$

Then

$$\frac{N!}{(N-x)!x!} p^x = \frac{(Np)^x}{x!}$$

2. The probability of success p is small. Hence, the factor $(1-p)^x$ is nearly equal to unity, $(1-p)^x = 1$.
3. Take the average value of m (the number of successful events) from the binomial distribution:

$$Np = m$$

from which we obtain

$$N = \frac{m}{p}$$

When we apply all three of these conditions, Eq. (3.1) becomes

$$f(x) = \frac{m^x}{x!} (1-p)^{m/p}$$

Note the definition of e :

$$\lim_{p \rightarrow 0} (1 + p)^{1/p} = e \Rightarrow \{[1 + (-p)]^{m/-p}\}^{-1} - 1 = e^{-m}$$

Hence we have

$$f(x) = \frac{m^x e^{-m}}{x!} \quad x = 0, 1, 2, 3, \dots \tag{3.2}$$

Equation (3.2) represents the Poisson distribution and $f(x)$ is the Poisson distribution function. Like binomial distribution, Poisson distribution is not continuous. To calculate the average (mean) value of \bar{x} , we must use the operator summation. The value of m that is the product of N_p plays a characteristic role in Poisson distribution. An important assumption is that the distribution $f(x)$ is through the area with uniform probability. In comparison, the binomial distribution has a much wider spread from the lowest value to the highest value than the Poisson distribution.

3.1.3 Gaussian Distribution

The Gaussian distribution is also called the normal distribution or normal error distribution. It is associated with a limiting form of binomial distribution. The conditions for the Gaussian distribution are N very large and $p = \frac{1}{2}$, that is, the probability of success is $\frac{1}{2}$ and the probability of failure is $\frac{1}{2}$; the chances for success and failure are absolutely at random, no bias. The Gaussian distribution is a continuous function:

$$f(x) = \frac{1}{\sqrt{2\pi}\sigma} e^{-(x-m)^2/2\sigma^2} \tag{3.3}$$

where x is a continuous variable rather than an integer as with the binomial and Poisson distributions and σ is the standard deviation. The Gaussian distribution is based on two parameters: m (mean) and σ^2 (variance). As shown in Figure 3.1, if m

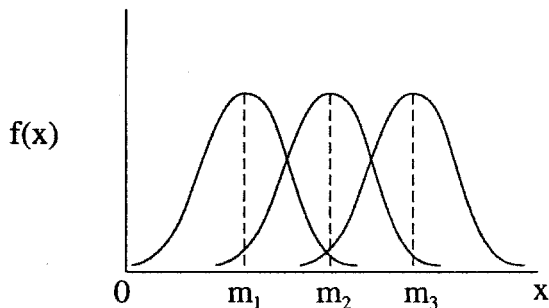


FIGURE 3.1 Gaussian distribution curve: σ constant.

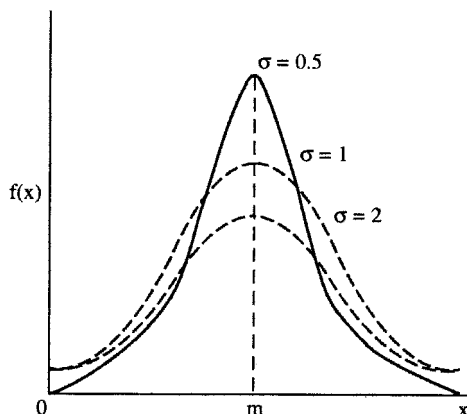


FIGURE 3.2 Gaussian distribution curve: m constant.

changes while σ is constant, the curve shifts to the right or left without changing its shape. If the standard deviation σ changes while m is constant, the shape of the curve changes (Figure 3.2). Note that in the Gaussian distribution $f(x)$ is a density function and $\int_{-\infty}^{\infty} f(x) dx = 1$. The area A under the curve is represented by

$$A = \frac{1}{\sqrt{2\pi}\sigma} \int_{-\infty}^{\infty} e^{-(x-m)^2/2\sigma^2} dx$$

If $y = (x - m)/\sigma$, then

$$A = \frac{1}{\sqrt{2\pi}} \int_{-\infty}^{\infty} e^{y^2} dy$$

Transforming this expression into polar coordinates, we obtain

$$A^2 = \frac{1}{2\pi} \int_0^{2\pi} \int_0^{\infty} r e^{-r^2/2} dr d\theta = 1$$

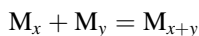
So the area is the same whether σ is 0.5, 1, or 2. To calculate the average (mean) value of \bar{x} , we use the operator integration, not summation, as in the case of the binomial and Poisson distributions.

3.2 ONE-PARAMETER EQUATION

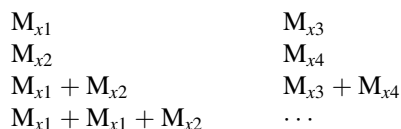
To illustrate our discussion so far, we describe the molecular weight distribution with a one-parameter equation first suggested by Flory (1936, 1940).

3.2.1 Condensation Polymers

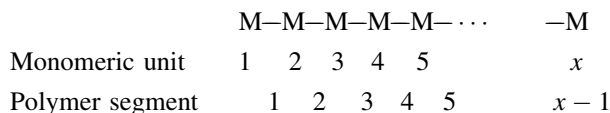
Condensation polymers are those produced by a reaction of the type



where M is a monomer and x and y are integers from zero to infinity. The growing polymer M_x can be terminated by adding a monomer ($y = 1$), a dimer ($y = 2$), or another growing polymer ($y = n$). That is, the product of the condensation polymer is a mixture of various sizes:



Consider one single-polymer molecule:



The number of monomeric units is always one unit larger than the number of segments. If x is large, the difference is negligible.

The probability that the functional group of the first unit has reacted is equal to p , for the second unit it is equal to p^2 , for the third unit it is equal to p^3 , and so on. For the $x - 1$ unit the probability is p^{x-1} that the molecule contains at least $x - 1$ reactive groups, or at least x units. The probability that the x th unit has not reacted is $1 - p$. That is, the probability for the last (x th) unit to be terminated is $1 - p$. Then the probability that among the x monomeric units $x - 1$ units have reacted and one (the end unit) has not reacted is

$$n_x = p^{(x-1)}(1 - p) \quad (3.4)$$

where n_x is called the number average distribution or most probable distribution of polymer molecules. It is very close to the binomial distribution, but it is not the binomial distribution because there is no combination term $\binom{N}{x}$. The term n_x may also be considered the probability that the molecule consists of exactly x units.

If N_0 is the total number of monomers (e.g., OH—R—COOH units) and N is the total number of macromolecules, then the total number of x -mers is

$$N_x = Np^{(x-1)}(1 - p) = Nn_x$$

and the total number of macromolecules is

$$N = N_0(1 - p)$$

Hence

$$N_x = N_0(1-p)^2 p^{(x-1)}$$

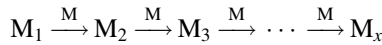
If w is the mass of a monomer unit, then the total mass of N_0 monomers is N_0w . The mass of one x -mer is xw ; the mass of N_x x -mers is $N_x xw$. We now have the ratio

$$w_x = \frac{N_x xw}{N_0 w} = x(1-p)^2 p^{(x-1)} \quad (3.5)$$

where w_x is the weight fraction of the x -mer. Equation (3.4) describes the number average distribution n_x , and Eq. (3.5) describes the weight average distribution function w_x .

3.2.2 Addition Polymers

Addition polymers are obtained from a reaction process of the type



The monomers M are added to the growing chain one at a time. According to the Poisson distribution, the probability of finding x events within a fixed interval of specified length is statistically independent of the number of other events. This clearly fits the description of addition polymerization. Hence, we have

$$n_x = \frac{e^{-m} m^{x-1}}{(x-1)!} \quad (3.6)$$

$$w_x = \frac{[m/(m+1)]x e^{-m} m^{x-2}}{(x-1)!} \quad (3.7)$$

The number average degree of polymerization \bar{x}_n can be derived:

$$\begin{aligned} \bar{x}_n &= \sum_{x=1}^{\infty} x n_x = \sum_{x=1}^{\infty} \frac{x e^{-m} m^{x-1}}{(x-1)!} \\ &= e^{-m} \sum_{x=1}^{\infty} \frac{x m^{x-1}}{(x-1)!} \end{aligned}$$

Note:

$$\sum_{x=1}^{\infty} \frac{x A^{x-1}}{(x-1)!} = (1+A) \exp A$$

Hence

$$\bar{x}_n = e^{-m}(1+m)e^m = m+1$$

Similarly, we can derive the weight average degree of polymerization:

$$\begin{aligned}\bar{x}_w &= \sum_{x=1}^{\infty} xw_x = \sum_{x=1}^{\infty} \frac{x[m/(m+1)]x e^{-m} m^{x-2}}{(x-1)!} \\ &= \frac{m}{m+1} e^{-m} \sum_{x=1}^{\infty} \frac{x^2 m^{x-2}}{(x-1)!} \\ &= \frac{1}{m+1} e^{-m} \sum_{x=1}^{\infty} \frac{x^2 m^{x-1}}{(x-1)!}\end{aligned}$$

Note:

$$\begin{aligned}\sum_{x=1}^{\infty} \frac{x^2 A^{x-1}}{(x-1)!} &= (1+3A+A^2) \exp A \\ \bar{x}_w &= \frac{1}{m+1} e^{-m}(1+3m+m^2)e^m \\ &= \frac{1}{m+1}(1+3m+m^2)\end{aligned}$$

The ratio x_w/x_n for the Poisson molecular weight distribution is

$$\frac{\bar{x}_w}{\bar{x}_n} = \frac{[1/(m+1)](1+3m+m^2)}{m+1} = \frac{1+3m+m^2}{1+2m+m^2} = 1 + \frac{m}{(m+1)^2}$$

The second term is always less than 0.5. This indicates a very narrow molecular weight distribution, much narrower than that of a condensation polymer.

3.3 TWO-PARAMETER EQUATIONS

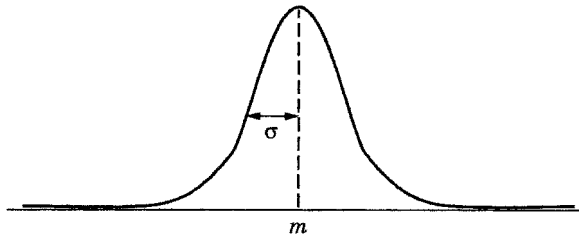
Since there are numerous ways for synthesizing polymers, a molecular weight distribution does not always follow a one-parameter equation. Even the condensation polymers do not necessarily follow the most probable distribution, nor do addition polymers follow the Poisson distribution. In many cases we naturally consider classical statistics, the normal distribution.

3.3.1 Normal Distribution

The normal (or Gaussian) distribution is given by

$$n_x = \frac{1}{\sqrt{2\pi}\sigma} e^{-(x-m)^2/2\sigma^2} \quad (3.8)$$

where the two parameters are m and σ . The standard deviation σ is the half width of the normal curve:



Here, the weight average distribution is given by

$$w_x = \frac{x}{m} n_x$$

The number average degree of polymerization is identical with the mean:

$$\bar{x}_n = \int_{-\infty}^{\infty} x n_x dx = m$$

and the weight average degree of polymerization is

$$\bar{x}_w = \frac{\sigma^2}{m} + m$$

where

$$\sigma^2 = \int_{-\infty}^{\infty} (x - m)^2 n_x dx$$

3.3.2 Logarithm Normal Distribution

The normal distribution function extends to both the positive and negative sides. To avoid the negative molecular weights (which do not exist), an assumption is made that the logarithm of the molecular weight is normally distributed. Thus, we replace x by $\ln x$ and m by $\ln m$. Then the weight distribution becomes

$$w_{\ln x} = \frac{1}{\sqrt{2\pi}\sigma} \exp\left(\frac{-(\ln x - \ln m)^2}{2\sigma^2}\right) \tag{3.9}$$

and

$$\int_1^{\infty} w_{\ln x} d \ln x = 1$$

Now, the average degrees of polymerization are

$$\bar{x}_n = m \exp\left(\frac{-\sigma^2}{2}\right) \quad \bar{x}_w = m \exp\left(\frac{\sigma^2}{2}\right)$$

from which we can show that

$$m = (\bar{x}_n \bar{x}_w)^{1/2} \quad \frac{\bar{x}_w}{\bar{x}_n} = \exp \sigma^2$$

where

$$\sigma^2 = \int_0^\infty (\ln x - \ln m)^2 w_x dx$$

and

$$w_x = \frac{1}{x\sqrt{2\pi}\sigma} \exp\left(\frac{-(\ln x - \ln m)^2}{2\sigma^2}\right)$$

$$\int_0^\infty w_x dx = 1$$

3.4 TYPES OF MOLECULAR WEIGHT

There are at least four types of molecular weight: number average, weight average, z average, and intrinsic viscosity. The number average molecular weight is given by

$$\bar{M}_n = M_0 \bar{x}_n$$

where M_0 is the molecular weight of the structural unit. For example,

$$\bar{x}_n = \sum xp^{x-1}(1-p) = \frac{1}{1-p}$$

$$\bar{M}_n = \frac{M_0}{1-p}$$

The weight average molecular weight is given by

$$\bar{M}_w = M_0 \bar{x}_w$$

For example,

$$\bar{x}_w = \sum xw_x = \sum x^2 p^{x-1} (1-p)^2 = \frac{1+p}{1-p}$$

$$\bar{M}_w = M_0 \left(\frac{1+p}{1-p} \right)$$

The z average molecular weight is given by

$$M_z = \frac{\int_{x_0}^{x_n} M_{zx} z \, dx}{\int_{x_0}^{x_n} z \, dx}$$

or

$$M_z = \frac{\int_{x_0}^{x_n} M_{zx} z f(x) (dx/x)}{\int_{x_0}^{x_n} z f(x) (dx/x)}$$

The z value and the $z + 1$ value of molecular weight are obtained by successively taking all the differences between the reading for a certain line and a reference line under the experimental curve. They are often related to the evaluation of an area that corresponds to the molecular weight. In the ultracentrifuge sedimentation experiment, the z value and the $z + 1$ value of molecular weight are often the results of such evaluation.

The intrinsic viscosity $[\eta]$ (see Chapter 8) may be expressed as

$$[\eta] = K \bar{x}_v^a$$

where K and a are constants. The value of \bar{x}_v can be calculated as follows:

$$\bar{x}_v = \left[\frac{\sum_{x=1}^{\infty} x^{1+a} F(x)}{\sum_{x=1}^{\infty} x F(x)} \right]^{1/a}$$

$$\bar{x}_v = \left(\frac{\sum_{x=1}^{\infty} x^a w_x}{\sum_{x=1}^{\infty} w_x} \right)^{1/a}$$

where $F(x)$ is the fraction of molecules of size x . If $f(x)$ is not continuous, we have

$$\sum F(x_i) = 1$$

If $f(x)$ is continuous, we have

$$\int_0^{\infty} F(x) \, dx = 1$$

Note that

$$M_v = M_0 \bar{x}_v$$

As a comparison of the types of molecular weight, we let N_i be the number of molecules of kind i (i being the degree of polymerization) present in the mixture, M_i be their molecular weight, and c_i be the concentration or weight. Then,

$$\begin{aligned}\bar{M}_n &= \frac{\sum_i N_i M_i}{\sum_i N_i} = \frac{\sum_i c_i}{\sum_i c_i / M_i} \\ \bar{M}_w &= \frac{\sum_i N_i M_i^2}{\sum_i N_i M_i} = \frac{\sum c_i M_i}{\sum c_i} \\ \bar{M}_z &= \frac{\sum_i N_i M_i^3}{\sum_i N_i M_i^2} = \frac{\sum c_i M_i^2}{\sum c_i M_i} \\ \bar{M}_{z+1} &= \frac{\sum_i N_i M_i^4}{\sum_i N_i M_i^3} = \frac{\sum c_i M_i^3}{\sum c_i M_i^2} \\ \bar{M}_v &= \left(\frac{\sum_i N_i M_i^{1+a}}{\sum_i N_i M_i} \right)^{1/a}\end{aligned}$$

The average degree of polymerization \bar{i} is related to the average molecular weight by

$$\bar{M} = M_0 \bar{i}$$

where M_0 is the molecular weight of the repeating unit. Therefore, we may compare various types of average degree of polymerization corresponding to average molecular weight as follows:

$$\begin{aligned}\bar{i}_n &= \frac{\sum w_i}{\sum (w_i / i)} \\ \bar{i}_w &= \frac{\sum w_i i}{\sum w_i} \\ i_{zx} \cong \bar{i}_z &= \frac{\sum w_i i^2}{\sum w_i i} \\ \bar{i}_{(z+1)x} \cong \bar{i}_{z+1} &= \frac{\sum w_i i^3}{\sum w_i i^2}\end{aligned}$$

where w_i denotes the average mass in grams of molecules of size i . In general,

$$M_n < M_w < M_z < M_{z+1} < M_v$$

If there is no molecular weight distribution, namely, if the molecular weight of all species in a sample is the same, then

$$\bar{M}_n = \bar{M}_w = \bar{M}_z = \bar{M}_{z+1} = \bar{M}_v$$

The ratio \bar{M}_w / \bar{M}_n , called the polydispersity, is a useful measure of the spread of a polymer distribution. Larger values of \bar{M}_w / \bar{M}_n indicate a very wide spread, with

substantial amounts of materials at both extremes. When $M_w/M_n = 1$, all polymeric molecules have the same molecular weight and there is no spreading.

3.5 EXPERIMENTAL METHODS FOR DETERMINING MOLECULAR WEIGHT AND MOLECULAR WEIGHT DISTRIBUTION

Here we list some of the well-known experimental methods for determining molecular weight and molecular weight distribution. Details are discussed in later chapters.

1. Number average molecular weight and molecular weight distribution
 - a. Osmotic pressure
 - b. Intrinsic viscosity
2. Weight average molecular weight and molecular weight distribution
 - a. Ultracentrifuge sedimentation
 - b. Diffusion
 - c. Light scattering
3. z and $z + 1$ average molecular weight and molecular weight distribution
 - a. Ultracentrifuge sedimentation

Methods 1–3 are all primary methods.

4. Secondary methods
 - a. Fractional precipitation
 - b. Gel permeation chromatography
 - c. High-performance liquid chromatography (HPLC)
 - d. Electrophoresis

The following are some useful sum terms:

$$\sum_{x=1}^{\infty} p^{x-1} = \frac{1}{1-p} \quad p < 1$$

$$\sum_{x=1}^{\infty} xp^{x-1} = \frac{1}{(1-p)^2} \quad p < 1$$

$$\sum_{x=1}^{\infty} x^2 p^{x-1} = \frac{1+p}{(1-p)^3} \quad p < 1$$

$$\sum_{x=1}^{\infty} \frac{A^{x-1}}{(x-1)!} = \exp A$$

$$\sum_{x=1}^{\infty} \frac{x A^{x-1}}{(x-1)!} = (1+A) \exp A$$

$$\sum_{x=1}^{\infty} \frac{x^2 A^{x-1}}{(x-1)!} = (1+3A+A^2) \exp A$$

REFERENCES

- Feller, W., *An Introduction to Probability Theory and Its Applications*, Vol. 1. New York: Wiley, 1950.
- Flory, P. J., *J. Am. Chem. Soc.* **58**, 1877 (1936).
- Flory, P. J., *J. Am. Chem. Soc.* **62**, 1561 (1940).
- Flory, P. J., *Principles of Polymer Chemistry*. Ithaca, NY: Cornell University Press, 1953.
- Mood, A. M., *Introduction to the Theory of Statistics*. New York: McGraw-Hill, 1950.
- Peebles, L. H., Jr., *Molecular Weight Distribution in Polymers*. New York: Wiley-Interscience, 1971.

PROBLEMS

- 3.1** Show that (a) the equation $\bar{r}_n = \sum_1^{\infty} rp^{r-1}(1-p)$ leads to the equation $\bar{r}_n = 1/(1-p)$ and (b) the equation $\bar{r}_w = \sum_1^{\infty} r^2 p^{r-1}(1-p)^2$ leads to $r_w = (1+p)/(1-p)$, where \bar{r}_n is the number average degree of polymerization and \bar{r}_w is the weight average degree of polymerization.
- 3.2** Show that $\bar{x} = m$ for the binomial, Poisson, and normal distributions.
- 3.3** The most probable distribution function of the molecular weight of condensation polymers is given by

$$w_r = rp^{r-1}(1-p)^2$$

- (a) Plot w_r (in the range between 0 and 0.20) versus r (in the range between 0 and 50) for $p = 0.5, 0.8, 0.9$.
- (b) Plot $w_r(0 \leq w_r \leq .04)$ versus $r(0 \leq r \leq 250)$ for $p = 0.9$ (Flory, 1936).
- 3.4** The Poisson distribution of the molecular weight of addition polymers (which do not have termination) is given by

$$w_r = \frac{\gamma}{\gamma + 1} e^{-\gamma} \frac{r\gamma^{r-2}}{r-1}!$$

- Plot w_r in percentage ($0 \leq w_r \leq 6$) versus $r(0 \leq r \leq 140)$ for $\gamma = 50, 100, 500$ (Flory, 1940).
- 3.5** Show that the mole fraction distribution X_x is the same as the number average distribution n_x , that is, $X_x = n_x$.
- 3.6** Show that the number average molecular weight M_n is given by

$$M_n = \frac{\sum M_i N_i}{\sum N_i} = M_0 \sum_1^{\infty} X n_x = \frac{M_0}{1-p}$$

and that the weight average molecular weight M_w is given by

$$M_w = \frac{\sum M_i^2 N_i}{\sum M_i N_i} = M_0 \sum X_{w_x} = M_0 \frac{1+p}{1-p}$$

where M_0 is the molecular weight of a monomer unit.

- 3.7** Consider a solution containing equal numbers of molecules of molecular weights 50×10^3 , 100×10^3 , 200×10^3 , and 400×10^3 . Calculate \bar{M}_n , \bar{M}_w , and \bar{M}_z . Assume that the solution contains equal weight concentrations of the four species and calculate \bar{M}_n , \bar{M}_w , and \bar{M}_z .
- 3.8** A protein sample consists of 90% by weight of 100,000 molecular weight material and 10% by weight of dimer of 200,000 molecular weight. Calculate \bar{M}_w and \bar{M}_n .

4

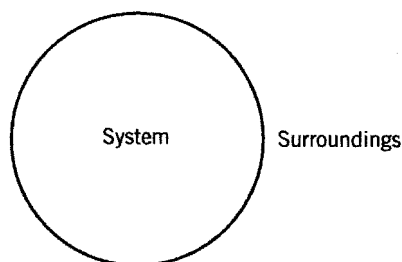
MACROMOLECULAR THERMODYNAMICS

In describing the thermodynamic behavior of a system (here, macromolecules), the three most important state functions to be specified are ΔS , ΔH , and ΔG . When applied to solutions, the partial molar quantities of these three functions, particularly $\Delta\bar{G}$ (the chemical potential), must be added as the bases for the interpretation of polymer phenomena. In this chapter we begin with a brief review of the principles of thermodynamics in general. This is basically a review of thermodynamic terms. Since Flory, among others, laid the foundation of physical polymer chemistry, we describe in detail his lattice theory of ΔS of mixing, his concept of contact energy ΔH of mixing, and his utilization of ΔG and $\Delta\bar{G}$ in the treatment of dilute polymer solutions. His contribution to creating and explaining the two parameters χ_1 and θ has left a deep imprint in polymer language for many generations to come. We believe that it is beneficial for a reader or research worker to become familiar with Flory's work before embarking on any advanced subject. In conjunction with Flory's concept of contact energy, we also describe Hildebrand's concept of the solubility parameter δ , not only for comparison, but also for application.

Chapters 4 and 5 are closely related in providing fundamental principles of modern polymer physical chemistry. Chapter 4 duly emphasizes Flory's work and Chapter 5 emphasizes de Gennes' work. de Gennes' work, in a sense, refutes some of Flory's theory and orients polymer physical chemistry in a new direction.

4.1 REVIEW OF THERMODYNAMICS

Let us first define two important terms in thermodynamics: system and surroundings. Any material body (e.g., 1 mol of gas, 500 mL of a protein solution) under study is called a system or a thermodynamic system. With respect to a given system, the rest of the world is called the surroundings. In a diagram, a system and its surroundings may be expressed as



A system plus its surroundings is called the universe. Thermodynamics is the science of the change of energy in a system with regard to its surroundings.

We choose three parameters to characterize a system: P (pressure), V (volume), and T (temperature). For convenience, a fourth parameter is also chosen, C (the heat capacity), which is closely related to T . With P , V , and T as three independent variables and C as an auxiliary variable given, we can now define two thermodynamic quantities, w (work) and q (heat), in a differential equation form:

$$dw = P dV \quad dq = C dT$$

The letter w refers to work done on or by the system, and q refers to the heat (energy) entering or released from the system. Whether “done on or by” or “entering or released from,” w or q is always related to the surroundings. The quantities w and q have positive or negative signs. The convention we follow is shown in Figure 4.1. If heat enters the system from the surroundings, q is positive; if

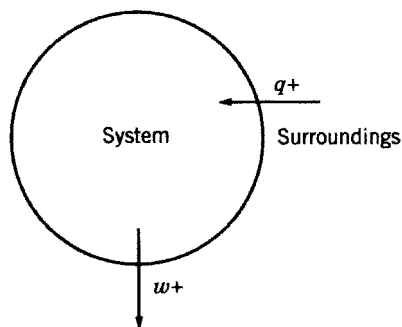


FIGURE 4.1 Convention of the sign of q and w .

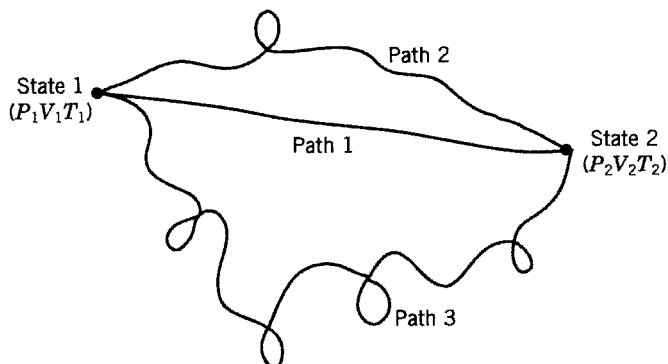


FIGURE 4.2 Path of the change in a thermodynamic state.

heat is released from the surroundings, q is negative. Similarly, if work is done on the surroundings by the system, w is positive; if work is done on the system by the surroundings, w is negative.

We say that the state of a system is known if the three independent variables are specified. For example, 1 mol of gas is in state 1 when we know the exact values of P_1 , V_1 , and T_1 . Similarly, the same 1 mol of gas is in state 2 if we know the exact values of P_2 , V_2 , and T_2 . The change in a system occurs when the values change from P_1 , V_1 , and T_1 to P_2 , V_2 , and T_2 . We say that the system changes from state 1 to state 2. In calculus, the term *path* is used to mean the route of change from state 1 to state 2. This term is important to our discussion because the two quantities dw and dq both depend on the path, as shown in Figure 4.2.

A system can follow many paths to change from state 1 to state 2. In Figure 4.2, path 1 is shorter than path 2, which is shorter than path 3. Consequently, for a system to arrive at state 2 from state 1, path 1 requires much less work (dw) and energy (dq) than path 2 or path 3 if other conditions are equal. In chemistry, examples of paths are constant volume, constant temperature, and constant pressure.

An interesting fact is that while dw and dq both depend on the path, the combination of the two quantities in the form of $dq - dw$ is independent of the path. The combination $dq - dw$ depends only on the states involved. If the change occurs from state 1 through a certain path back to state 1 as shown in Figure 4.3, then dq

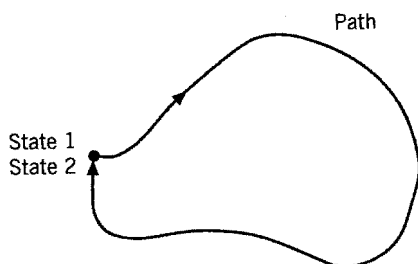


FIGURE 4.3 Path of a state from one position back to the original position.

and dw are not zero, but $dq - dw$ is zero, because there is no change in state. Because of its importance, we introduce a special term, dE , to represent $dq - dw$:

$$dE = dq - dw \quad (4.1)$$

This is the first law of thermodynamics. The term E represents internal energy.

All processes by which changes occur in a system from one state to another may be classified into two types: reversible and irreversible. A reversible process from state 1 to state 2 consists of an infinite number of equilibrium states; an irreversible process does not. That is, a system can change back to any previous equilibrium state in the reversible process but not in the irreversible process if the change of energy is reversed in direction. Now, while dq_{rev} (the infinitesimal change in heat in a reversible process) depends on the path, the quantity dq_{rev}/T (i.e., dq_{rev} multiplied by a factor $1/T$, which in mathematics is called the integrating factor) is independent of the path. The quantity dq_{rev}/T is the change in entropy dS :

$$dS = \frac{dq_{\text{rev}}}{T} \quad (4.2)$$

This is the second law of thermodynamics. The term S represents entropy. Note that dq is not necessarily equal to dq_{rev} . It may be equal to dq_{irrev} . The calculation of dq_{irrev} is more complicated than that of dq_{rev} .

These two laws form the basis of equilibrium thermodynamics. In this chapter, the term thermodynamics is understood to mean equilibrium thermodynamics; we do not consider nonequilibrium thermodynamics here. The quantities dE and dS are state functions because their values depend only on the change in states; they are independent of path.

It is very difficult to measure E . For practical purposes three more measurable thermodynamic quantities are introduced, all of which are based on the above two laws:

$$H = E + PV \quad G = H - TS \quad A = E - TS$$

where H is the enthalpy or heat content, G is the Gibb's free energy, and A is the Helmholtz free energy. When these three quantities are written in differential form, we have to specify conditions for simplicity:

At constant pressure:

$$dH = dE + P dV \quad (4.3)$$

At constant temperature:

$$dG = dH - T dS \quad (4.4)$$

$$dA = dE - T dS \quad (4.5)$$

All five quantities (dE , dS , dH , dG , and dA , or in integral forms, ΔE , ΔS , ΔH , ΔG , and ΔA) are state functions; they do not depend on the path. Among the five, Eq. (4.4) is the most important in the study of macromolecules. It is usually put in integrated form:

$$\Delta G = \Delta H - T \Delta S \quad (4.6)$$

where ΔG is an indicator as to whether the change of state is favorable or not. If ΔG is negative, the change is favored and will occur spontaneously; if ΔG is positive, the change is not favored and large amounts of energy are needed to force the state to change; if $\Delta G = 0$, the system is at equilibrium. The term ΔH is the energy term. If ΔH is negative, energy will be released when a change occurs, for example, when a bond is broken or formed. If ΔH is positive, energy must be supplied from the surroundings for a change to occur. The term $T \Delta S$ is related to the molecular configuration. If $\Delta S = 0$, there is no change in configuration. If ΔS is positive, a spontaneous change in the configuration of the molecules occurs.

In the above description, the state is specified by P , V , and T because historically thermodynamics starts with the observation of change in the properties of gases. A gas is described or specified by P , V , and T only. If we deal with solutions (a system of two or more components), we have to introduce one more independent variable, n , the number of moles of a component, which we discuss in later sections.

We begin our study of macromolecular thermodynamics by discussing these three basic quantities: ΔS , ΔH , and ΔG . Our interpretation of the change in a polymeric system is based on the change in the values of ΔS , ΔH , and ΔG . A change in the properties of the polymer always occurs whenever there is a change in the surroundings (environment). In later sections we discuss two more thermodynamic quantities: \bar{v} , the partial specific volume, and μ , the chemical potential. Both are related to the behavior of polymer solutions.

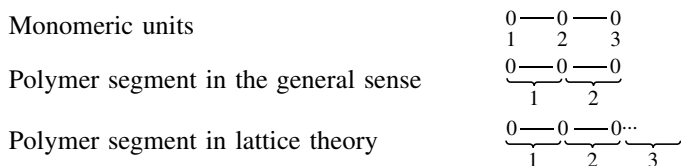
4.2 ΔS OF MIXING: FLORY THEORY

The Flory model[†] for ΔS of mixing a polymer chain with solvents has been influential in polymer chemistry for several decades. The model assumes the validity of the lattice theory to describe the change in the molecular configuration of the polymer in the presence of a solvent, just as it describes the patterns of the crystal structure of molecules. The central point is the filling of lattice sites in a three-dimensional space by polymer segments and solvent molecules; that is, how many ways can we fill up the lattice sites?

Consider a binary solution consisting of two types of molecules, the polymer chain and the solvent, and neglect the interaction potential existing between polymer segments. Here the meaning of *segment* is slightly different from that

[†]Huggins (1942(a) and (b)) proposed a similar model to calculate ΔS_m . The Flory model is, therefore, also named the Flory–Huggins model. The same idea was also expressed by Miller (1943).

described in previous chapters. The emphasis here is on the space that a polymer segment occupies. Thus, a segment is not a structural or monomeric unit. A segment is defined as "that portion of a polymer molecule requiring the same space as a molecule of solvent" (Flory, 1953). The difference may be shown as follows:



Assume that the polymer segment in a chain and the solvent molecule are of equal volume. Let us fill lattice sites, one segment or one solvent molecule per site. While the solvent molecules can be placed in any unoccupied site available, the possibilities for placing the segment are limited, not only by the availability of sites, but by linkage to adjacent segments. Figure 4.4 shows the random filling of the sites.

Let y be the number of segments in a chain, that is, the ratio of molar volumes of solute to solvent, n_1 the number of solvent molecules, n_2 the number of solute chain molecules, and n_0 the total number of lattice sites. Then

$$n_0 = n_1 + yn_2$$

Suppose i polymer molecules (chains) have been inserted previously at random. Now consider the insertion of the $(i + 1)$ th polymer. There are $n_0 - yi$ vacant cells

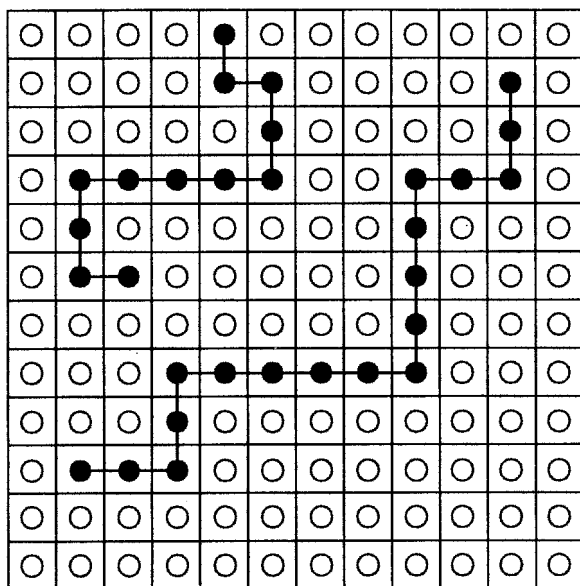


FIGURE 4.4 Random filling of the sites: ●, polymer segment; ○, solvent molecule.

for the first segment of molecule $i + 1$. Let z be the lattice coordination number or number of cells that are first neighbors to a given cell in a three-dimensional space. The range of z is from 6 to 12: $z = 6$ for a regular cubic lattice, $z = 12$ for a hexagonal lattice. Let f_i be the probability that a given site adjacent to the first segment is occupied (not available). Then $1 - f_i$ is the probability that a given site is available for a segment. The number of ways that the $(i + 1)$ th polymer molecule (chain) would fill the cell sites, v_{i+1} , may be expressed as follows:

$$\begin{aligned}
 v_{i+1} &= \underbrace{(n_0 - yi)}_{\text{Vacant for the first segment}} \underbrace{z(1 - f_i)}_{\text{Second}} \underbrace{(z - 1)(1 - f_i)}_{\text{Third}} \underbrace{(z - 1)(1 - f_i)}_{\text{Fourth}} \cdots \\
 &\quad \underbrace{(z - 1)(1 - f_i)}_{(y-2)\text{th}} \\
 &= (n_0 - yi)z(z - 1)^{y-2}(1 - f_i)^{y-1}
 \end{aligned}$$

where, for example, z represents six sites if the coordination number is 6.

The segments of the $(i + 1)$ th polymer molecule have been so far treated as if they were distinguishable. But they are indistinguishable, in that we cannot distinguish configurations that involve the interchange of polymer segment positions. For that reason, we have to introduce the term $1/n_2!$ And the number of ways in which all the polymer molecules n_2 could be arranged in the lattice is

$$\Omega = \frac{1}{n_2!} \prod_{i=1}^{n_2} v_i = \frac{1}{n_2!} \prod_{i=0}^{n_2-1} v_{i+1}$$

Let \bar{f}_i be the average probability of a site not available. We make a simple approximation,

$$1 - f_i \cong 1 - \bar{f}_i = \frac{\text{number of sites available}}{\text{total number of sites}} = \frac{n_0 - yi}{n_0}$$

Hence,

$$v_{i+1} = (n_0 - yi)z(z - 1)^{y-2} \left(\frac{n_0 - yi}{n_0} \right)^{y-1}$$

Replacing the lone factor z by $z - 1$, we obtain

$$v_{i+1} = (n_0 - yi)^y \left(\frac{z - 1}{n_0} \right)^{y-1}$$

With a second approximation,

$$(n_0 - yi)^y = (n_0 - yi)(n_0 - yi) \cdots (n_0 - yi) \cong \frac{(n_0 - yi)!}{[n_0 - y(i + 1)]!}$$

we have

$$v_{i+1} = \frac{(n_0 - yi)!}{[n_0 - y(i+1)]!} \left(\frac{z-1}{n_0}\right)^{y-1}$$

and

$$\begin{aligned} \Omega &= \frac{1}{n_2!} \prod_{i=0}^{n_2-1} v_{i+1} \\ &= \frac{1}{n_2!} \left\{ \frac{n_0!}{(n_0 - y)!} \frac{(n_0 - y)!}{(n_0 - 2y)!} \frac{(n_0 - 2y)!}{(n_0 - 3y)!} \cdots \frac{[n_0 - (n_2 - 1)y]!}{(n_0 - n_2y)!} \right\} \left(\frac{z-1}{n_0}\right)^{n_2(y-1)} \\ &= \frac{1}{n_2!} \frac{n_0!}{(n_0 - n_2y)!} \left(\frac{z-1}{n_0}\right)^{n_2(y-1)} \end{aligned}$$

Using the Boltzmann–Planck law, the entropy of configuration of polymer molecules can be expressed as

$$S_{\text{conf}} = k \ln \Omega$$

Introducing Stirling's formula,

$$\ln n! = n \ln n - n$$

and replacing n_0 with $n_1 + yn_2$, we obtain

$$\begin{aligned} S_{\text{conf}} &= \underbrace{-kn_1 \ln \left(\frac{n_1}{n_1 + yn_2}\right) + kn_2 \ln \left(\frac{yn_2}{n_1 + yn_2}\right)}_{\Delta S_{\text{mix}}} \\ &\quad + \underbrace{kn_2 \ln y - kn_2(y-1) \ln \left(\frac{z-1}{e}\right) - kn_2 \ln y}_{\Delta S_{\text{diso}}} \end{aligned}$$

where ΔS_{mix} is the entropy of mixing (of polymer and solvent) and ΔS_{diso} is the entropy of disorientation of polymer molecules. What is important to us is the expression of the entropy of mixing ($\Delta S_{\text{mix}} \equiv \Delta S_{\text{m}}$):

$$\Delta S_{\text{m}} = -k(n_1 \ln \phi_1 + n_2 \ln \phi_2) \quad (4.7)$$

where ϕ_1 and ϕ_2 are volume fractions:

$$\phi_1 = \frac{n_1}{n_1 + yn_2} \quad \phi_2 = \frac{yn_2}{n_1 + yn_2}$$

Equation (4.7) gives the final result of the Flory model of ΔS of mixing. The importance of this model is to explain the very large deviation in the behavior of polymer solutions experimentally observed from that of an ideal solution. An ideal solution is defined as a solution that obeys the Raoult's law:

$$p_1 = x_1 p_1^\circ$$

where p is the vapor pressure, x is the mole fraction, and the superscript ($^\circ$) refers to the substance in its pure phase. Van't Hoff describes the ΔS of mixing for an ideal solution as

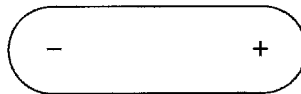
$$\Delta S_m = -k(n_1 \ln x_1 + n_2 \ln x_2)$$

When we compare Eq. (4.7) with Van't Hoff's equation, we notice that for polymer solutions we cannot use mole fraction x as an independent variable to describe the ΔS of mixing. Instead, we have to use volume fraction ϕ as an independent variable. The mole fraction x_i does not give room for molecular interaction, whereas the volume fraction ϕ_i depends very much on molecular interactions.

4.3 ΔH OF MIXING

Again, in comparison with an ideal solution for which $\Delta H_{\text{mix}} = 0$, polymer solutions cannot have $\Delta H_{\text{mix}} = 0$. In polymer solutions there is an interaction not only between the macromolecule (chain) and the solvent but also between the polymer segments themselves within the chain. The former is called intermolecular interaction and the latter is called intramolecular interaction.

All the interactions, whether intermolecular or intramolecular, are essentially electrostatic in origin. If the molecules carry charge (electrolytes), the interaction is Coulombic. Even if the molecule is neutral, electrons are in motion all the time around the centers of atoms and their bonds. Under certain environments the centers of positive and negative charges do not coincide, thus turning the molecule into a dipole:



Hence, there are always dipole–dipole interactions between molecules. As a result, there is always a weak force, called the van der Waals force, existing between molecules. Before we describe ΔH_{mix} , we first discuss the van der Waals force as a background.

The van der Waals force involves three factors: permanent dipole–permanent dipole interaction, induced dipole interaction, and dispersion effect. The permanent dipole–permanent dipole interaction exerts an orientation effect. It may be expressed as

$$E = -\frac{\mu_1 \mu_2}{r^3} [2 \cos \theta_1 \cos \theta_2 - \sin \theta_1 \sin \theta_2 \cos(\phi_1 - \phi_2)]$$

where E is the interaction energy, μ_1 and μ_2 refer to the dipole moments of two permanent dipoles, and r , θ , and ϕ (here) are spherical polar coordinates. A permanent dipole in one molecule can induce a dipole in another molecule. The interaction energy E may be expressed in the form

$$E = -\frac{1}{r^6}(\alpha_1\mu_2^2 + \alpha_2\mu_1^2)$$

where α_1 and α_2 refer to the polarizability of molecules 1 and 2. The interaction energy of dispersion effect may be expressed as

$$E = -\frac{3\alpha_1\alpha_2 h\nu_{0,1} \times h\nu_{0,2}}{2r^6 h\nu_{0,1} + h\nu_{0,2}}$$

where ν_0 is the frequency of a molecule in its unperturbed state and h is Planck's constant.

We now introduce two approaches of ΔH of mixing for macromolecules: cohesive energy density and contact energy. Both are related to van der Waals' force.

4.3.1 Cohesive Energy Density

The van der Waals equation of real gas is

$$\left(P + \frac{n^2a}{V^2}\right)(V - nb) = nR'T$$

where R' is the gas constant, a is the van der Waals constant, n is the number of moles, b is the excluded volume, and a/V^2 represents the attractive force between the two molecules. In 1906 van Laar derived a parallel equation to describe the heat involved in the vapor pressure of a binary liquid mixture:

$$\Delta H_m = \frac{n_1 V_1 n_2 V_2}{n_1 V_1 + n_2 V_2} \left(\frac{a_1^{1/2}}{V_1} - \frac{a_2^{1/2}}{V_2} \right)$$

where V is the volume and subscripts 1 and 2 refer to solvent and solute molecules, respectively.

Scatchard (1931) and Hildebrand (1933) independently suggested that this equation, with some modification, can equally be valid to describe the energy ΔE involved in the mixing of solute and solvent. They derived a similar equation:

$$\Delta E = (n_1 V_1 + n_2 V_2) \left[\left(\frac{\Delta E_1^v}{V_1} \right)^{1/2} - \left(\frac{\Delta E_2^v}{V_2} \right)^{1/2} \right]^2 \phi_1 \phi_2 \quad (4.8)$$

where ΔE^v is the energy of vaporization and all the other symbols in the equation were defined previously. Hildebrand called the quantity $\Delta E^v/V$ (the energy of vaporization per milliliter) a measure of “internal pressure” and used the symbol $\delta = (\Delta E^v/V)^{1/2}$, which is now called the solubility parameter, a measurable quantity. Thus, we have

$$\left(\frac{\Delta E^v}{V}\right)^{1/2} = \delta = \frac{a^{1/2}}{V}$$

The term E_m/V (hence $\Delta E^v/V$) is also called the cohesive energy density (E being cohesive energy).

Hildebrand further derived an equation to relate the heat of mixing ΔH_{mix} with the solubility parameter δ , which is now called the Hildebrand equation:

$$\Delta H_m = V_m(\delta_1 - \delta_2)^2\phi_1\phi_2 \tag{4.9}$$

where V_m is the volume of the solution. Both δ_1 and δ_2 are measurable quantities. They can be used to estimate qualitatively whether a compound can be dissolved in a solvent. As a rough rule of thumb, a polymer is miscible with the solvent if the following condition is satisfied:

$$(\delta_2 - 1.1) < \delta_1 < (\delta_2 + 1.1) \tag{4.10}$$

The solubility parameters δ_1 of some solvents are given in Table 4.1; the solubility parameters of some polymers are given in Table 4.2.

TABLE 4.1 Values of Solubility Parameter δ_1 of Some Common Solvents

Solvent	δ_1 (25°C)	V_1 (25°C) (mL)
<i>N</i> -Pentane	7.05	116
<i>N</i> -Hexane	7.3 (7.24)	132
<i>N</i> -Heptane	7.45	147
Ethyl ether	7.5	105
Cyclohexane	8.2	109
Carbon tetrachloride	8.65 (8.58)	97
Toluene	8.9	107
Benzene	9.15	89
Chloroform	9.3 (9.24)	81
Acetone	9.71	
Acitic acid	10.5	
Acetonitrile	11.9	
Ethanol	14.3	
Ethylene glycol	16.3	
Water	23.3	

Source: Hildebrand and Scott (1950).

TABLE 4.2 Values of Solubility Parameter δ_2 of Some Common Polymers

Polymer	δ_2
Polyisobutylene	8.1
Polystyrene	9.2
Poly(vinyl chloride)	9.5
Polyethylene	7.9
Poly(methyl methacrylate)	9.1
Poly(ethylene terephthalate)	10.7
66 Nylon	13.6
Polyacrylonitrile	15.4

Source: Hildebrand and Scott (1950).

Several experimental methods can be used to determine δ_1 and δ_2 . Since the values of δ_1 are tabulated in the literature for many common solvents and the values of δ_2 for a newly prepared polymer often need to be determined, we confine our discussion to two methods for determining δ_2 . One measures the density ρ and the other measures the refractive index n . We can determine δ_2 for a polymer of known structure by measuring the density ρ using the equation

$$\delta_2 = \rho \frac{\sum k'}{M} \quad (4.11)$$

where M is the molecular weight of the polymer and k' is the molar attraction constant of the structural configuration of the repeating unit in the polymer chain. The typical values of the molar attraction constants k' are given in Table 4.3. We

TABLE 4.3 Molar Attraction Constants k' , (cal/cm³)^{1/2}/mol

Group	k'
—CH ³	148
—CH ² —	131.5
)CH—	86
)C(32
CH ² =	126.5
—CH ² =	121.5
)C=	84.5
)C=O	263

Source: Hoy (1976) and Billmeyer (1984).

can determine δ_2 by measuring the refractive index n of the polymer solution using the equation

$$\delta_2 = 30.3 \frac{n^2 - 1}{n^2 + 2}$$

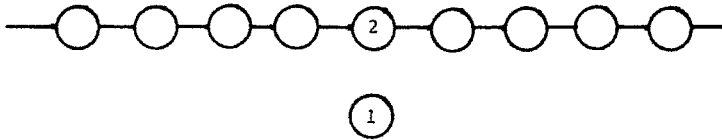
For solubility of solids in liquid, Hildebrand and Scatchard independently derived another equation, now called the Hildebrand–Scatchard equation:

$$\log \frac{1}{x_2} = \frac{\Delta H_m^F}{4.575} \left(\frac{T_m - T}{T_m T} \right) - \frac{\Delta C_p}{4.575} \frac{T_m - T}{T} + \frac{\Delta C_p}{1.987} \log \frac{T_m}{T} + \frac{V_2}{4.575 T} (\delta_1 - \delta_2)^2 \phi_1^2 \tag{4.12}$$

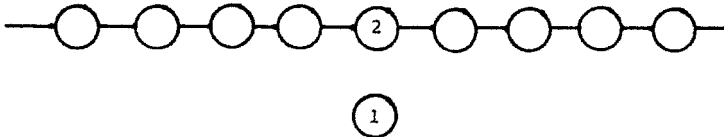
where x_2 is the mole fraction solubility, ΔH_m^F is the heat of fusion at the melting point T_m in kelvins, ΔC_p is the difference between the heat capacities of solid and liquid, T is the temperature of solution in kelvins, and V_2 is the molar volume of the solute as a hypothetical supercooled liquid. This equation is often used in pharmacology among other fields.

4.3.2 Contact Energy (First-Neighbor Interaction or Energy Due to Contact)

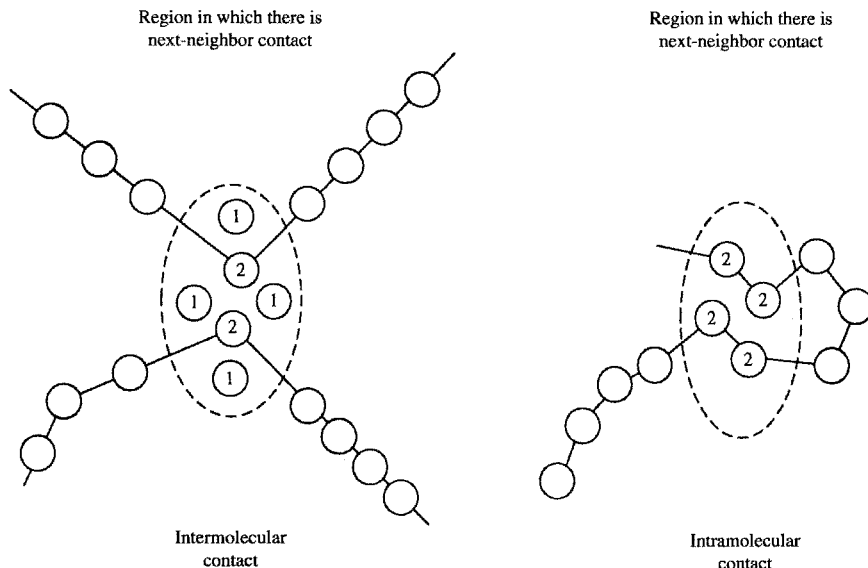
Flory advanced the idea of contact energy as the cause of the heat of mixing for polymer solutions. Consider a structural unit in a chain molecule and label it with a number 2:



Consider also another chain with the same labeling:



Let number 1 refer to the solvent molecule and number 2 refer to any structural unit with 3 as its next neighbor, 4 next to 3, and so forth. We focus on structural unit 2. Within the same chain, 2 and 3 are the next neighbors, but 2 and 4 and 2 and 5 are not. Structural unit 2 of one chain can have next-neighbor contact with structural unit 2 of other chains as well as with solvent molecule n_1 :



First-neighbor contact is called short-range interaction and non-first-neighbor contact is called long-range interaction. For short-range interaction there are three types of first-neighbor contact, 1-1, 1-2, 2-2, and three corresponding kinds of energy: w_{11} , w_{12} , and w_{22} . The energy associated with mixing solute (polymer segments) and solvent is Δw_{12} , defined as

$$\Delta w_{12} = w_{12} - \frac{1}{2}(w_{11} + w_{22})$$

The total 1-2 pairs contact is given by

$$z y n_1 \phi_2 \equiv z n_1 \phi_1$$

where n_1 is the number of the solvent molecules, z is the coordination number, y is the number of segments per polymer chain ($y = V_2/V_1$), and V_2 and V_1 are the molar volumes of polymer and solvent, respectively. The product of the total number of contact pairs and Δw_{12} is the result that we are looking for, namely, the heat of mixing ΔH_m . The equation is

$$\Delta H_m = z \Delta w_{12} y_1 n_1 \phi_2$$

where y_1 is the number of segments that have contacted with solvent molecules. This is the van Laar expression.[†]

We may group the terms into a new form:

$$\Delta H_m = kT \chi_1 n_1 \phi_2 \quad (4.13)$$

[†]It is interesting to note that both Hildebrand and Flory's theories were originated from van Laar's work.

where

$$\chi_1 = \frac{z \Delta w_{12} y_1}{kT}$$

It should be pointed out that the equation of ΔH_m in terms of Δw_{12} is not important because it is not feasible to calculate Δw_{12} as such. Equation (4.13) in terms of χ_1 is important in polymer chemistry: ΔH_m here is called the contact energy. A dimensionless quantity, χ_1 characterizes the interaction energy per solvent molecule divided by kT (k being the Boltzman constant). The term ΔH_m is also called the Flory interaction energy. The physical meaning of χ_1 is

$$kT\chi_1 = (\text{energy of the solvent in solution}) - (\text{energy of the solvent in its pure state})$$

In the literature of polymer chemistry, the two parameters δ_2 (the solubility parameter of polymer) and χ_1 (the interaction energy of the solvent) are frequently investigated. Both are measurable quantities. The quantity ΔH_m , on the other hand, is only of secondary importance.

4.4 ΔG OF MIXING

Once ΔS_m and ΔH_m are known, ΔG_m can easily be calculated. Thus, according to Hildebrand,

$$\begin{aligned}\Delta S_m &= -R'(x_1 \ln x_1 + x_2 \ln x_2) \\ \Delta H_m &= V_m(\delta_1 - \delta_2)^2 \phi_1 \phi_2 \\ \Delta G_m &= R'T(x_1 \ln x_1 + x_2 \ln x_2) + V_m(\delta_1 - \delta_2)^2 \phi_1 \phi_2\end{aligned}$$

According to Flory,

$$\begin{aligned}\Delta S_m &= -k(n_1 \ln \phi_1 + n_2 \ln \phi_2) \\ \Delta H_m &= kT\chi_1 n_1 \phi_2 \\ \Delta G_m &= kT \left[\underbrace{(n_1 \ln \phi_1 + n_2 \ln \phi_2)}_{\text{Combinatory term}} + \underbrace{\chi_1 n_1 \phi_2}_{\text{Contact term}} \right]\end{aligned}\tag{4.14}$$

Equation (4.14) is further explored in Section 4.6.

4.5 PARTIAL MOLAR QUANTITIES

When we deal with solutions, we need another independent variable to specify the composition of the system, in addition to P , V , and T . This additional independent variable is n , the number of moles of a component in the system. A thermodynamic

property in which n is chosen as an independent variable is called the partial molar quantity. Consider an extensive property g :

$$g = g(T, P, n_1, n_2, \dots)$$

The partial molar quantity of the i th component is defined as

$$g_i = \left(\frac{\partial g}{\partial n_i} \right)_{T, P, n_j \neq n_j}$$

Applying Euler's theorem, we have

$$g = n_1 g_1 + n_2 g_2 + \dots = \sum n_i g_i$$

In macromolecular chemistry, two partial molar quantities are especially important: partial molar volume (particularly partial specific volume) and partial molar free energy, also called chemical potential. The partial specific volume \bar{v}_i is defined as

$$\bar{v}_i = \left(\frac{\partial v}{\partial w_i} \right)_{T, P, w_j \neq w_j}$$

(where w_i is the weight in grams). The partial molar Gibbs free energy, also called the chemical potential μ , is defined as

$$\bar{G}_i = \mu_i \left(\frac{\partial G}{\partial n_i} \right)_{T, P, n_j \neq n_j}$$

Partial molar volume $\bar{V}_i = (\partial V / \partial n_i)_{T, P, n_j \neq n_j}$ and partial specific volume \bar{v}_i are closely related; one is expressed in moles and the other is expressed in grams.

4.5.1 Partial Specific Volume

An exact description of partial specific volume in terms of molecular structure is not known. The parameter \bar{v}_i alone does not seem to be clear enough to characterize the behavior of the component i in the solution in relation to its size, shape, and chemical reactivity. However, it is an indispensable quantity which permits interpretation of other experimental parameters, such as light scattering, diffusion, and sedimentation, as we will see later.

The experimental methods for measuring partial specific volume include density gradient columns, pycnometry, the magnetic flotation methods, and the vibration method. Regardless of which method we use, the measurement is often tedious and difficult. In protein chemistry, instead of measurement, a reasonable estimation of \bar{v}

TABLE 4.4 Partial Specific Volume of Amino Acid Residue, \bar{v}_i

Amino Acid	\bar{v}_i (mL/g)	Amino Acid	\bar{v}_i (mL/g)
Glycine	0.64	Cysteine	0.61
Alanine	0.74	Methionine	0.75
Valine	0.86	Aspartic acid	0.60
Leucine	0.90	Glutamic acid	0.66
Isoleucine	0.90	Lysine	0.82
Serine	0.63	Arginine	0.70
Threonine	0.70	Histidine	0.67
Phenylalanine	0.77	Proline	0.76
Tyrosine	0.71	Hydroxyproline	0.68
Tryptophan	0.74	Glutamine	0.67

is sometimes obtained by using the equation

$$\bar{v}_p = \frac{\sum \bar{v}_i w_i}{\sum w_i} \quad (4.15)$$

where \bar{v}_p is the partial specific volume of protein, \bar{v}_i is the partial specific volume of amino acid i , and w_i is the weight percent of the i th amino acid residue in the protein. The values of \bar{v}_i are presented in Table 4.4.

4.5.2 Chemical Potential

The chemical potential μ is related to a measurable quantity, the activity a , which is also called the effective concentration:

$$\begin{aligned} \mu_i &= \mu_i^\circ + R'T \ln a_i \\ &= \mu_i^\circ + R'T \ln y_i x_i \end{aligned}$$

where i refers to the i th component, μ_i° is the chemical potential in the reference state ($a_i = 1$) and is a function of temperature and pressure only, y_i is the activity coefficient, and x_i is the mole fraction. For a very dilute solution, $y_i \rightarrow 1$, we have

$$\mu_i = \mu_i^\circ + R'T \ln x_i$$

Consider a two-component system in which $x_1 \gg x_2$. We can write

$$\ln x_1 = \ln(1 - x_2) = -x_2 - \frac{1}{2}x_2^2 - \dots$$

Note:

$$\ln(1 - x) = -x - \frac{1}{2}x^2 - \frac{1}{3}x^3 - \frac{1}{4}x^4 - \dots$$

Substituting the expanded $\ln x_1$ term into the equation of chemical potential, we have

$$\mu_1 - \mu_1^\circ = -R'T(x_2 + \frac{1}{2}x_2^2 + \dots)$$

Now the mole fraction of component 2 can be converted to the concentration c_2 (in grams per milliliter) by the following approximation:

$$x_2 = \frac{n_2}{n_1 + n_2} = \frac{(\text{g}/M_2)/\text{mL}}{(n_1 + n_2)/\text{mL}}$$

where M_2 is the molecular weight of the solute (i.e., polymer). Since $n_1 + n_2 \simeq n_1$, we have

$$x_2 = \frac{\text{g}/\text{mL}}{M_2} \frac{\text{mL}}{n_1} = \frac{c_2}{M_2} V_1^\circ$$

where V_1° is the molar volume in milliliters of solvent.

The equation of $\mu_1 - \mu_1^\circ$ then becomes

$$\mu_1 - \mu_1^\circ = -R'TV_1^\circ \left[\left(\frac{1}{M_2} \right) c_2 + \left(\frac{V_1^\circ}{2M_2^2} \right) c_2^2 + \dots \right]$$

or

$$\mu_1 - \mu_1^\circ = -R'TV_1^\circ \left(\frac{1}{M_2} + A_2c_2 + A_3c_2^2 + \dots \right) \quad (4.16)$$

Compare Eq. (4.16) with the virial equation for 1 mol of gas,

$$PV = R'T(1 + A_2P + A_3P^2 + \dots)$$

we realize that A_2 is the second virial coefficient, A_3 is the third virial coefficient, and so forth. Equation (4.16) will be used in the interpretation of osmotic pressure (Chapter 9) and light scattering (Chapter 14).

4.6 THERMODYNAMICS OF DILUTE POLYMER SOLUTIONS

We now differentiate Flory's equation of ΔG_m ,

$$\Delta G_m = kT(n_1 \ln \phi_1 + n_2 \ln \phi_2 + \chi_1 n_1 \phi_2)$$

with respect to n_1 of solvent molecules, keeping in mind that ϕ_1 and ϕ_2 are both of functions of n_1 ,

$$\phi_1 = \frac{n_1}{n_1 + n_2y} \quad \phi_2 = \frac{n_2y}{n_1 + n_2y}$$

and multiply by Avogadro's number N_A to obtain the chemical potential per mole. We find

$$\mu_1 - \mu_1^\circ = R'T \left[\ln(1 - \phi_2) + \left(1 - \frac{1}{y}\right)\phi_2 \right] + R'T\chi_1\phi_2^2 \quad (4.17)$$

Expanding the term $\ln(1 - \phi_2)$ in series leads to

$$\mu_1 - \mu_1^\circ = -R'T \left[\left(\frac{1}{2} - \chi_1\right)\phi_2^2 + \frac{1}{3}\phi_2^3 + \dots \right] \quad (4.18)$$

But we know that

$$\mu_1 - \mu_1^\circ = \Delta\bar{H}_1 - T \Delta\bar{S}_1 \quad (4.19)$$

(from $\Delta\bar{G}_1 = \Delta\bar{H}_1 - T \Delta\bar{S}_1$), where $\Delta\bar{H}_1$ is the partial molar enthalpy and $\Delta\bar{S}_1$ is the partial molar entropy. For that reason, Flory defined these terms as

$$\Delta\bar{H}_1 = R'T\kappa_1\phi_2^2 \quad \Delta\bar{S}_1 = R'\psi_1\phi_2^2$$

where κ_1 is the heat-of-dilution parameter and ψ_1 is the entropy-of-dilution parameter. Then Eq. (4.19) becomes

$$\begin{aligned} \mu_1 - \mu_1^\circ &= R'T\kappa_1\phi_2^2 - R'T\psi_1\phi_2^2 \\ &= -R'T(\psi_1 - \kappa_1)\phi_2^2 \end{aligned} \quad (4.20)$$

Comparison of Eq. (4.18) with Eq. 4.20) leads to

$$\kappa_1 - \psi_1 = \chi_1 - \frac{1}{2} \quad (4.21)$$

This is equivalent to assuming that χ_1 consists of two parts, the entropy and the enthalpy. Flory further defined the ideal temperature θ by

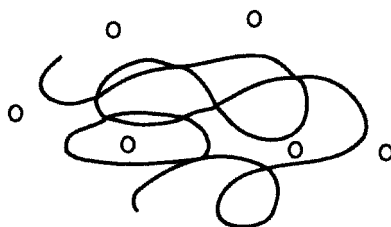
$$\theta = \frac{\kappa_1 T}{\psi_1} \quad (4.22)$$

We then have

$$\psi_1 - \kappa_1 = \psi_1 \left(1 - \frac{\theta}{T} \right) \quad (4.23)$$

Equations (4.21), (4.22), and (4.23) have formed an important background in polymer chemistry for several decades. We shall further discuss the physical meanings of χ_1 and θ in later chapters. Here we briefly describe how they are related to the quality of solvent in polymer solutions. The value of χ_1 is useful for indicating whether a solvent is good or poor for a particular polymer: A good solvent has a low value of χ_1 , while a poor solvent has a high value of χ_1 . The borderline is $\chi_1 = \frac{1}{2}$.

In good solvents molecular interaction between the polymer segment and solvent molecule is favored. Solvent molecules can pass through the holes or cavities formed by a polymer chain, as shown in the following diagram (\circ is a solvent molecule):



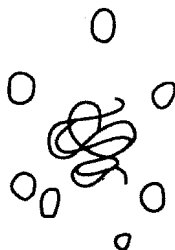
At the same time two polymer segments compete for space occupation. No segment allows the other segment of the same chain to be too close because of a repulsive force of polymer segments against each other. This repulsive force results in the excluded volume u , which is defined as

$$u = \int_0^\infty \frac{U(r)}{kT} r^2 dr$$

where $U(r)$ is the potential existing between the two segments, r is the distance, and k is the Boltzmann constant. The overall polymer molecule is in an extended conformation. Its end-to-end distance (its size), which we describe in Chapter 5, is large; that is, the polymer chain occupies a large space in the solution.

In poor solvents, molecular interaction between the polymer segment and solvent molecule is not favored. The polymer segment does not attract the solvent molecule to pass through the holes or cavities created by the polymer chain. To resist the approaching solvent molecules, the polymer segments reduce their resistance against each other and an attractive force develops between them. Consequently, the excluded volume gets smaller. The overall polymer shrinks and the end-to-end distance becomes smaller. If a particular temperature θ is set [Eq. (4.22)], then the polymer molecule further shrinks to a state in which the

attractive force cancels the repulsive force. The polymer molecule now exists in a compact form:



Such a state is called the θ state (theta state). At the θ state, the excluded volume effect vanishes and the dimensions of the polymer molecule are called unperturbed dimensions. Thus, the θ state is also called the unperturbed state or the (pseudo) ideal state.

It should be pointed out that for experimental reasons we group the following three terms together: good solvent, poor solvent, and θ temperature. We could have θ temperature for good solvents as well as for poor solvents. But the θ temperature for good solvents is often in a range where the experiment is difficult or inconvenient to carry out, for example, 100 K. On the other hand, the θ temperature for poor solvents is often in a range that is convenient for experiments, for example, 20–80°C. For this reason the θ temperature is often associated with poor solvents and poor solvents are often called theta solvents. As mentioned before, it is only with respect to a given polymer that the solvent is good or poor. For example, cyclohexane is poor solvent for polystyrene but a good solvent for poly(methyl methacrylate). Table 4.5 lists good solvents, poor solvents, and θ temperature for a few common polymers.

The experimental methods used for the study of thermodynamic parameters such as χ_1 and θ of a polymer in dilute solutions are numerous. Among them are intrinsic viscosity, light scattering, diffusion, sedimentation, vapor pressure, and phase equilibrium. Here we discuss vapor pressure and phase equilibrium, leaving the other methods for later chapters.

4.6.1 Vapor Pressure

The classical way to describe thermodynamic properties of a solution, such as vapor pressure and osmotic pressure, is to describe the behavior of solvent activity a_1 over the whole concentration range. By definition,

$$\ln a_1 = \frac{\mu_1 - \mu_1^\circ}{R'T}$$

which, using Flory's equation, can be expressed as

$$\ln a_1 = \ln(1 - \phi_2) + \left(1 - \frac{1}{y}\right)\phi_2 + \chi_1\phi_2^2 \quad (4.24)$$

TABLE 4.5 Solvents for Some Common Polymers

Polymer	Good Solvent	Poor Solvent	
		Solvent	θ Temperature ($^{\circ}\text{C}$)
Polyisobutylene	Cyclohexane	Anisole	105
		Benzene	24
Polypropylene	Benzene, cyclohexane	1-Chloronaphthalene	74
Polystyrene	Benzene, toluene	Cyclohexane	34
		Toluene/methanol	
		76.9/23.1	25
		75.2/24.8	34
		72.8/27.2	45
		<i>trans</i> -Decalin	20.5
Poly(vinyl chloride)	Cyclohexane	Benzyl alcohol	155.4
Poly(vinyl acetate)	Dioxane	Ethanol	56.9
Poly(methyl methacrylate)	Benzene, cyclohexane	<i>n</i> -Butyl chloride	35.4
		3-Heptanone	33.7
		3-Octanone	71
		<i>n</i> -Propanol	84.4

The parameter $\ln a_1$ can be determined by measuring the vapor pressure of the solvent in the polymer solution, p_1 , and in its pure phase, p_1° :

$$\ln a_1 = \frac{p_1}{p_1^{\circ}}$$

Since ϕ_1 and ϕ_2 are known from the preparation of the solution and y can be calculated from V_1 and V_2 , χ_1 can be calculated from Eq. (4.24) once the value of a_1 is determined by vapor pressure measurement. The two other thermodynamic parameters, $\Delta\bar{H}_1$ and $\Delta\bar{S}_1$, can be calculated using the following equations:

$$\Delta\bar{H}_1 = R'T\chi_1\phi_2^2 \quad (4.25)$$

$$\Delta\bar{S}_1 = -R' \left[\ln(1 - \phi_2) + \left(1 - \frac{1}{y}\right)\phi_2 \right] \quad (4.26)$$

The quantities $\Delta\bar{H}_1$ and $\Delta\bar{S}_1$ can also be calculated from the temperature coefficient of the activity a_1 :

$$\Delta\bar{H}_1 = -R'T \left(\frac{\partial \ln a_1}{\partial T} \right)_{P, \phi_2} \quad (4.27)$$

$$\Delta\bar{S}_1 = -R' \left(\frac{\partial (T \ln a_1)}{\partial T} \right)_{P, \phi_2} \quad (4.28)$$

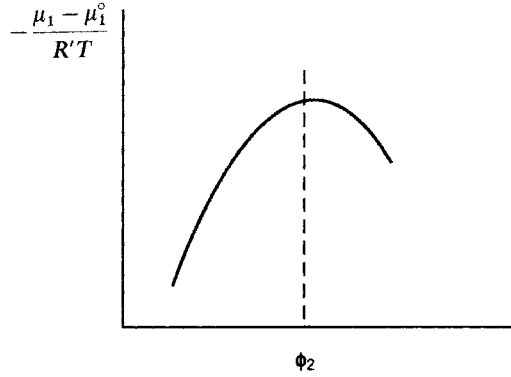


FIGURE 4.5 Phase separation curve.

Thus, we can check whether χ_1 gives a reasonable value to characterize the interaction between the solvent and solute in dilute polymer solutions.

4.6.2 Phase Equilibrium

Equation (4.18) can be put in a slightly different form:

$$\frac{\mu_1 - \mu_1^\circ}{R'T} = -\phi_2 - \frac{\phi_2^2}{2} - \frac{\phi_2^3}{3} + \dots + \phi_2 - \frac{1}{y}\phi_2 + \chi_1\phi_2^2 \quad (4.29)$$

If we plot $-(\mu_1 - \mu_1^\circ)/(R'T)$ versus ϕ_2 , we obtain a curve like the one shown in Figure 4.5. The curve is a phase separation curve, in which a maximum, a minimum, or an inflection will be shown. The conditions for incipient phase separation are

$$\left(-\frac{\partial\mu_1}{\partial\phi_2}\right)_{T,P} = 0 \quad \left(\frac{\partial^2\mu_1}{\partial\phi_2^2}\right)_{T,P} = 0$$

Differentiating Eq. (4.29) to obtain $(\partial\mu_1/\partial\phi_2)_{T,P}$ and equating to zero, we obtain

$$\frac{1}{1-\phi_2} - \frac{1}{1-y} - 2\chi_1\phi_2 = 0 \quad (4.30)$$

Further differentiating to obtain $(\partial^2\mu_1/\partial\phi_2^2)_{T,P}$ and equating to zero will lead to

$$\frac{1}{(1-\phi_2)^2} - 2\chi_1 = 0 \quad (4.31)$$

Eliminating χ_1 from Eqs. (4.30) and (4.31), we have

$$\phi_2 = \frac{1}{1+y^{1/2}}$$

For large y , the equation of ϕ_2 can further be reduced to

$$\phi_2 = \frac{1}{y^{1/2}} \quad (4.32)$$

We now substitute Eq. (4.32) into Eq. (4.31):

$$\chi_1 = \frac{(1 + y^{1/2})^2}{2y} = \frac{1}{2y} + y^{-1/2} + \frac{1}{2}$$

or

$$\chi_1 - \frac{1}{2} = \frac{1}{2y} + y^{-1/2}$$

This leads to

$$-\psi_1 \left(1 - \frac{\theta}{T} \right) = \frac{1}{2y} + \frac{1}{y^{1/2}}$$

At the temperature where phase separation occurs, we have $T = T_c$, where T_c is the critical temperature. We thus have

$$\frac{1}{T_c} = \frac{1}{\theta} \left[1 + \frac{1}{\psi_1} \left(\frac{1}{y^{1/2}} + \frac{1}{2y} \right) \right] \quad (4.33)$$

For large y ($1/2y \simeq 0$), Eq. (4.33) becomes

$$\begin{aligned} \frac{1}{T_c} &= \frac{1}{\theta} \left(1 + \frac{1}{\psi_1 y^{1/2}} \right) \\ &= \frac{1}{\theta} \left(1 + \frac{b}{M^{1/2}} \right) \end{aligned} \quad (4.34)$$

where

$$\begin{aligned} b &= \frac{(V_1^\circ/\bar{v}_2)^{1/2}}{\psi_1} \\ y &= \frac{M\bar{v}_2}{V_1^\circ} \end{aligned} \quad (4.35)$$

The terms V_1° (the molar volume of the solvent), \bar{v}_2 (the partial specific volume of the polymer molecule), and M (the molecular weight of the polymer) have their usual meanings. Thus, if we determine the consolute temperatures for a series of

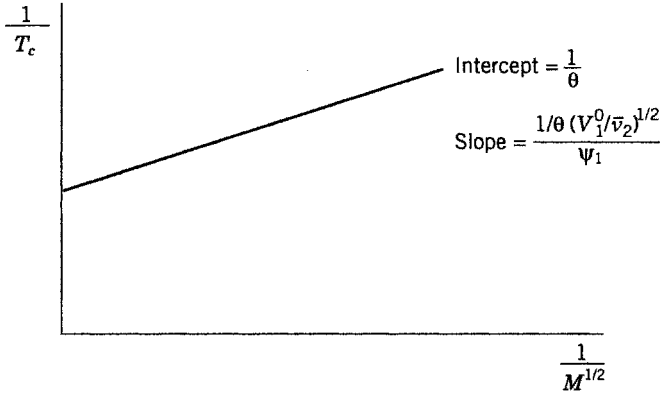


FIGURE 4.6 Phase equilibrium plot for determining θ and Φ_1 .

fractions covering an extended range in molecular weight, we can determine the θ temperature by extrapolating these critical temperatures to infinite molecular weight (Figure 4.6).

APPENDIX: THERMODYNAMICS AND CRITICAL PHENOMENA

The direct application of thermodynamics to the study of polymer solutions has been demonstrated in Flory's theories of ΔS_{mix} and ΔH_{mix} , as described in this chapter. Here, as a prelude to Chapter 5, we describe the connection of thermodynamics and critical phenomena in phase transition. The study of phase transition is one of the most challenging problems in statistical mechanics. Phase transition such as liquid-gas transition and magnetism transition involves an order parameter. For liquid-gas transition the order parameter is the density ρ , and for magnetism transition the parameter is the magnetism M . Above the critical temperature, both of the order parameters vanish:

$$\begin{aligned}
 \rho_{(\text{liquid})} - \rho_{(\text{gas})} &\neq 0 && \text{for } T < T_c \\
 &= 0 && \text{for } T > T_c \\
 M &\neq 0 && \text{for } T < T_c \\
 &= 0 && \text{for } T > T_c
 \end{aligned}$$

Even though the phase transition (liquid-gas) and the magnetism transition are different phenomena, there is a one-to-one correspondence between the two parameters:

$$\rho \leftrightarrow M$$

Near the critical point (critical temperature) almost all physical quantities (such as ρ and M) obey some sort of power laws:

$$\rho \sim (T_c - T)^\alpha \quad M \sim (T_c - T)^\beta$$

The exponents α and β are called critical exponents. We discuss power laws and critical exponents on polymer configurations in the next chapter. Here we point out that all these laws have their roots in the concept of thermodynamic equilibrium. Consider the equation

$$A = E - TS \quad (\text{or } G = H - TS)$$

where A is the free energy, E is the internal energy, T is the temperature, and S is the entropy. The equation implies that to reach equilibrium A must be minimized ($A \rightarrow 0$). At high temperature, the term TS dominates and the minimum value of A is related to the maximum value of S , which, in turn, leads the system into a disordered state. The order parameter is zero. At low temperatures the internal energy parameter E is the dominating factor. The state with the minimum internal energy is the ordered state. Hence, the order parameter is not zero.

REFERENCES

- Aminabhavi, T. M., and P. Munk, *Macromolecules* **12**, 1186 (1979).
 Bawn, C. E. H., R. F. J. Freeman, and A. R. Kamaliddin, *Trans. Faraday Soc.* **46**, 677 (1950).
 Billmeyer, F. W., Jr., *Textbook of Polymer Chemistry*, New York: Wiley, 1984.
 Brandrup, J., and E. N. Immergut, *Polymer Handbook*, 2nd ed. New York: Wiley-Interscience, 1975.
 Cohn, J., and J. T. Edsall, *Proteins, Amino Acids and Peptides*. New York: Reinhold, 1943.
 Dayhoff, M. O., G. E. Perlmann, and D. A. MacInnes, *J. Am. Chem. Soc.* **74**, 2515 (1952).
 Flory, P. J., *J. Chem. Phys.* **9**, 660 (1941); **10**, 51 (1942).
 Flory, P. J., *Principles of Polymer Chemistry*. Ithaca, NY: Cornell University Press, 1953.
 Flory, P. J., and T. G. Fox, Jr., *J. Am. Chem. Soc.* **73**, 1915 (1951).
 Hildebrand, J. H., and R. L. Scott, *The Solubility of Non-Electrolytes*. New York: Reinhold, 1950.
 Hildebrand, J. H., and S. E. Wood, *J. Chem. Phys.* **1**, 817 (1933).
 Hoy, K. L., *J. Paint Technol.* **42**, 76 (1976).
 Huggins, M. L., *J. Chem. Phys.* **9**, 440 (1941).
 Huggins, M. L., *J. Phys. Chem.* **46**, 151 (1942a).
 Huggins, M. L., *J. Am. Chem. Soc.* **64**, 1712 (1942b).
 Krause, S., and E. Cohn-Ginsberg, *J. Phys. Chem.* **67**, 1479 (1963).
 Lawson, D. D., and J. D. Ingham, *Nature* **223**, 614 (1969).
 Martin, A., and M. J. Miller, *J. Pharm. Sci.* **71**, 439 (1982).

- Miller, A. R., *Proc Cambridge Philos. Soc.* **38**, 109 (1942).
 Miller, A. R., **39**, 54, 131 (1943).
 Newing, M. J., *Trans. Faraday Soc.* **46**, 613 (1950).
 Scatchard, G., *Chem. Rev.* **8**, 321 (1931).
 Schultz, A. R., and P. J. Flory, *J. Am. Chem. Soc.* **74**, 4767 (1952).
 van Laar, J. J., *Sechs Vorträge über das Thermodynamische Potential*. Braunschweig, 1906.
 Wall, F. T., *Chemical Thermodynamics* 3rd ed. San Francisco: Freeman, 1974.
 Yalkowsky, S. H., and S. C. Valvani, *J. Pharm. Sci.* **92**, 912 (1980).

PROBLEMS

- 4.1** The values of the solubility parameter δ_1 in $(\text{cal}/\text{cm}^3)^{1/2}$ are given as follows:

<i>n</i> -Hexane	7.24
Carbon tetrachloride	8.58
Benzene	9.15
Acetone	9.71
Methanol	14.5

The solubility parameters δ_2 in $(\text{cal}/\text{cm}^3)^{1/2}$ are 8.6 for polystyrene and 9.1 for poly(methyl methacrylate). Predict by calculation whether each of the two polymers will dissolve in the above five solvents.

- 4.2** Let $\phi_i = N_i V_i / \sum N_i V_i$, where the subscript i refers to the i th component in solution (e.g., for a two-component system, 1—solvent, 2—solute), ϕ_i is the volume fraction, N is the number of moles, and V is the partial molar volume. Let the notations be changed:

$$\Delta W_{12} = h_{12} \quad \chi_1 = g_{12}$$

Show that Flory's equations of ΔG_m and ΔH_m can be transformed into

$$\Delta G_m = R'T \left[\sum_{i=1}^2 N_i \ln \phi_i + \left(\sum_{i=1}^2 N_i V_i \right) \phi_1 \phi_2 \left(\frac{g_{12}}{V_1} \right) \right]$$

$$\Delta H_m = R' \left(\sum_{i=1}^2 N_i V_i \right) \phi_1 \phi_2 \left(\frac{h_{12}}{V_1} \right)$$

(Aminabhavi and Munk, 1979).

- 4.3** Derive the equation

$$\mu_1 - \mu_1^\circ = R'T \left[\ln(1 - \phi_2) + \left(1 - \frac{1}{y} \right) \phi_2 + \chi_1 \phi_2^2 \right]$$

4.4 Derive the equation

$$\psi - \kappa_1 = \psi \left(1 - \frac{\theta}{T} \right)$$

- 4.5 Silicone, $\text{CH}_3[(\text{CH}_3)_2\text{SiO}]_n\text{Si}(\text{CH}_3)_3$, and benzene are mixed in the following proportion: $\phi_1 = 0.2, 0.4, 0.6, 0.7, 0.8$. Calculate $\Delta\bar{S}_1$ and plot $\Delta\bar{S}_1/\phi_2^2$ versus ϕ_2 using

$$\Delta\bar{S}_1 = -R' \left[\ln(1 - \phi_2) + \left(1 - \frac{1}{y} \right) \phi_2 \right] \quad (\text{Flory})$$

$$\Delta\bar{S}_1 = -R' \left[\ln(1 - \phi_2) - \frac{z}{2} \ln \left[1 - \frac{2}{z} \left(1 - \frac{1}{n} \right) \phi_2 \right] \right] \quad (\text{Miller})$$

Compare the results of the two equations. Assume that $y = n = 100$, $z = 4$ (Newing, 1950).

- 4.6 Measurement of the lowering of vapor pressure by silicones (consisting of 100 structural units, $y = 100$) in benzene yields the following set of data:

ϕ_1	0.0843	0.171	0.266	0.356	0.427	0.820
a_1	0.400	0.635	0.850	0.940	0.955	0.995

Calculate χ_1 values and plot χ_1 versus ϕ_2 .

- 4.7 Precipitation temperature–concentration measurement on fractions of different molecular weight (MW) of isotactic poly(methyl methacrylate) in acetonitrile yields the following set of data:

T_c (°C)	16.3	18.2	21.2	22.0	23.4
MW	0.90×10^5	1.61×10^5	2.62×10^5	4.56×10^5	5.35×10^5

Using these data determine θ (the Flory temperature) and ψ_i (the entropy parameter) (Krause and Cohn-Ginsberg, 1963).

- 4.8 Critical temperatures T_c for polystyrene (molecular weight 89,000) in cyclohexane solutions with volume fractions ϕ_2 were determined by observing the solutions to be turbid on cooling. Data were obtained as follows:

ϕ_2	0.17	0.20	0.28	0.32
T_c (°C)	22.5	21.8	17.5	15

What is the θ temperature of polystyrene in cyclohexane? (See Flory and Fox, 1951).

- 4.9 From the measurements of amino acid analysis, the weight percent of amino acid residues in insulin was found as follows:

Amino Acid	Weight Percent of Amino Acid Residues
Serine	2.96
Threonine	2.26
Leucine and isoleucine	25.88
Cystine	11.56
Tyrosine	11.25
Histidine	9.46
Arginine	2.73
Lysine	1.10
Glutamic acid	13.80
Glutamine	12.43

Estimate the partial specific volume of the protein.

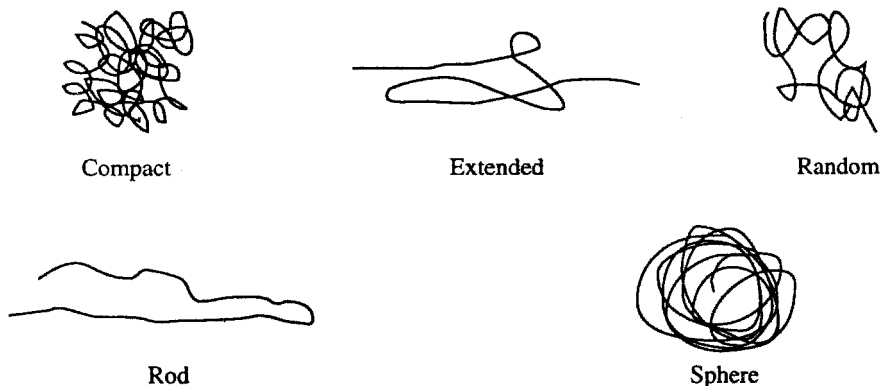
5

CHAIN CONFIGURATIONS

Flory's influence on polymer chemistry is again detailed in this chapter. His interpretation of the polymer chain configurations in terms of the expansion factor α (or swelling ratio) constitutes the central point of general polymer chain dynamics. Before we introduce Flory's theory, we describe the random-flight model of chain configurations; after we introduce Flory's theory, we describe the two-parameter theory (α and z). We then focus on the new idea of complex dumping and internal movements of polymer chain molecules. This new challenge came from various related areas, among them the development of renormalization group theory, the modern concept of chaos, and the universality of critical exponents on scaling laws. Along with Flory's work, we discuss in detail de Gennes' work on chain configurations. It was de Gennes' theories that pointed to similarities between motion of long chains and magnetic movements undergoing a phase transition. His theories of semidilute solution and reptation in the entangled chain have stimulated new approaches and new ways of interpreting chain configurations. This chapter also covers many other important topics on chain configurations. As is our normal way of presentation, background materials are given first, namely, random-walk statistics and a description of the Markov chain. In the appendices we provide the mathematics of the scaling relation and correlation function.

5.1 PRELIMINARY DESCRIPTIONS OF A POLYMER CHAIN

A polymer chain consists of many structural units (repeating units or monomeric units). The chain may take on many different configurations, for example:



The configurations are restricted by chemical bonds. The double bond $C=C$ has little or no rotational freedom. The single bond $C-C$, which has rotational freedom, is constrained due to geometric reasons. The interaction among the hydrogen or other atoms leaves certain rotational angles preferred on energetic grounds, as in the case of a small molecule, ethane. The two well-known configurations of ethane are shown in Figure 5.1. The staggered configuration is more stable than the eclipsed because it offers the least interaction. A molecule may possess a variety of structures, but certain configurations are preferred because of the interference and restrictions imposed by rotational angles under certain conditions.

Figure 5.2 shows a simple model of a chain consisting of four carbons connected with three single $C-C$ bonds. Carbons C_1 , C_2 , and C_3 lie on a plane; that is, they

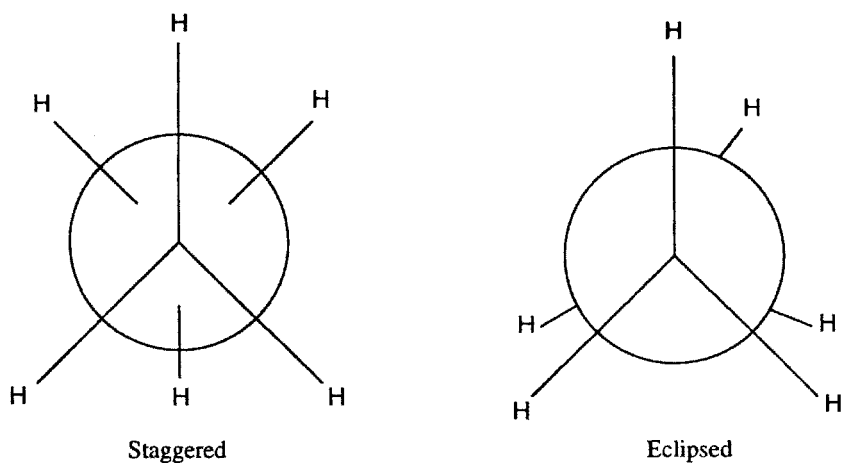


FIGURE 5.1 The two configurations of ethane.

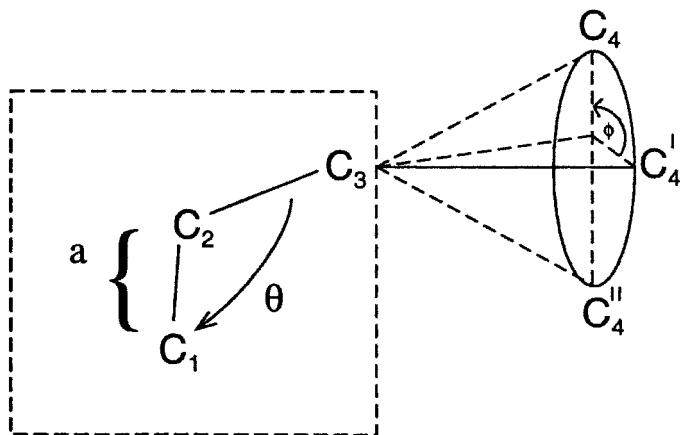


FIGURE 5.2 Simple model of a four-carbon chain.

are constrained in a planary position. Carbon C_4 may not necessarily be on the same plane. It can take many positions, for example, C_4 , C'_4 , and C''_4 , and the C_3 - C_4 bond is free to rotate about C_3 or about the entire C_1 - C_2 - C_3 plane.

Thus, the configuration of the four-carbon chain is determined by three parameters: the bond length a , the rotational angle θ , and the hindrance angle ϕ . This model can be applied to chains containing any number of carbons greater than 3. But, as the number of bonds increases in a chain, the situation becomes more complicated.

The modern approach to chain configuration is to use techniques from probability theory or statistical mechanics. For the first approximation, chain configuration is studied in terms of its distribution of chain length only, ignoring θ and ϕ as independent variables. The second assumption is that chains are supposed to be completely in the form of a random coil, ignoring other molecular shapes such as spheres and rods. Furthermore, since we cannot investigate polymer molecules in the gaseous phase, the study of configuration and its relationship to molecular properties has to be confined to polymers dissolved in solutions. According to Kuhn (1930), chemical bonds of polymers in solution (or in melts) are flexible, and this flexibility gives rise to the variety of properties. In Sections 5.2 and 5.3, we discuss the configuration of an ideal (or rather oversimplified) polymer chain that is based on the above assumptions. From Section 5.4 on, we introduce more advanced theories that are no longer entirely based on the above assumptions. For the most part, these theories are presented in chronological order, which also happens to follow the logical order. Recent advances strongly suggest that many properties of polymer solutions depend on the configuration of the chain, rather than on the nature of the chain atoms.

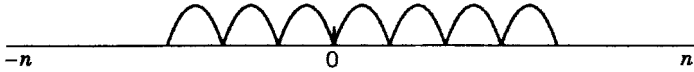
5.2 RANDOM WALK AND THE MARKOV PROCESS

The model of random walk is closely related to the Bernoulli trials. It has been utilized in physics and chemistry as an approximation to one-dimensional diffusion

and Brownian motion. When the theory was advanced by Markov, random walk became a special case of what is now called the Markov chain.

5.2.1 Random Walk

For simplicity we describe first the one-dimensional random walk (see Chandrasekhar, 1943). Consider n steps of random walk along an axis, with each step either in the forward or the backward direction. Each step has equal probability $\frac{1}{2}$:



The two extremes are all n steps directed to the right (positive) or all n steps directed to the left (negative) from the origin 0 along one dimension (x axis). Most probably n steps end in between n and $-n$ since the walk is random. Let n_+ be the positive step, n_- be the negative step, and m be the last step. Then m is the distance from the origin and $m = n_+ - n_-$ or $m = n_- - n_+$. If $n_+ = n_-$, $m = 0$. We take

$$m = n_+ - n_- \tag{5.1}$$

where

$$n_+ + n_- = n \tag{5.2}$$

From Eqs. (5.1) and (5.2), we obtain

$$n_+ = \frac{n + m}{2} \quad n_- = \frac{n - m}{2}$$

That is, among n steps of random walk,

$$\frac{n + m}{2} \text{ steps are in the positive direction}$$

$$\frac{n - m}{2} \text{ steps are in the negative direction}$$

The probability of leading to the value of m after n steps of random walk can be expressed in terms of $w(n, m)$, which is the Bernoulli probability (or the Bernoulli distribution).[†] Thus, for the random-walk distribution (probability distribution)

[†]*Mathematical Note:* Suppose that there are only two possible outcomes to a trial, success or failure. Let p be the probability of success; then $1 - p$ will be the probability of failure. The probability that among n trials there are k successes is

$$w(n, k) = \binom{n}{k} p^k (1 - p)^{n-k}$$

where

$$\binom{n}{k} = \frac{n!}{k!(n - k)!}$$

and $w(n, k)$ is called the Bernoulli probability. It is identical to the binomial function.

equation, we have

$$w(n, m) = \frac{n!}{((n+m)/2)!((n-m)/2)!} \left(\frac{1}{2}\right)^n \quad (5.3)$$

By using Stirling's formula,

$$\log n! = (n + \frac{1}{2}) \log n - n + \frac{1}{2} \log 2\pi$$

Eq. (5.3) is converted to

$$\begin{aligned} \log w(n, m) &= \left(n + \frac{1}{2}\right) \log n - \frac{1}{2}(n+m+1) \log \left[\frac{n}{2} \left(1 + \frac{m}{n}\right)\right] \\ &\quad - \frac{1}{2}(n-m+1) \log \left[\frac{n}{2} \left(1 - \frac{m}{n}\right)\right] - \frac{1}{2} \log 2\pi \\ &\quad - n \log 2 \end{aligned}$$

Since $m \ll n$, we can use the series expansion

$$\log(1+x) = x - \frac{1}{2}x^2 + \frac{1}{3}x^3 - \dots$$

to convert Eq. (5.3) further:

$$\begin{aligned} \log w(n, m) &= \left(n + \frac{1}{2}\right) \log n - \frac{1}{2} \log 2\pi - n \log 2 - \frac{1}{2}(n+m+1) \\ &\quad \times \left(\log n - \log 2 + \frac{m}{n} - \frac{m^2}{2n^2}\right) - \frac{1}{2}(n-m+1) \\ &\quad \times \left(\log n - \log 2 - \frac{m}{n} - \frac{m^2}{2n^2}\right) \end{aligned}$$

Simplifying, we obtain

$$\log w(n, m) = \frac{1}{2} \log n + \log 2 - \frac{1}{2} \log 2\pi - \frac{m^2}{2n}$$

Taking exponential functions on both sides, we get

$$w(n, m) = \left(\frac{2}{\pi n}\right)^{1/2} \exp\left(\frac{-m^2}{2n}\right) \quad (5.4)$$

This is exactly the Gaussian distribution function. Instead of m , we now introduce the net displacement x from the starting point as the variable; that is, we change the

variable:

$$x = ma$$

where a is the length of step. We realize that $w(n, x) \Delta x = w(n, m)(\Delta x/2a)$; hence, we obtain

$$w(n, x) = \frac{1}{(2\pi na^2)^{1/2}} \exp\left(\frac{-x^2}{2na^2}\right)$$

Here Δx represents the intervals along the straight line and $w(n, x) \Delta x$ is the probability that the random walk ends in the interval between x and $x + \Delta x$ after n steps. Thus, we conclude that the random walk is governed by a distribution function $w(n, x)$ which is Gaussian in nature.

5.2.2 Markov Chain

An important feature of the random-walk theory is that in a sequence of trials each trial is independent of the others. Markov advanced the theory by generalizing the condition that the outcome of any trial may depend on the outcome of the preceding trial; that is, the probability of an event is conditioned by the previous event. This idea clearly fits the description of the configuration of a polymer chain.

Let us first change the term “random walk” into “random flight” because the latter term is used more often in polymer chemistry, though both terms mean the same thing. Consider the configurations of a given chain characterized by the position vector \mathbf{R} , as shown in Figure 5.3. The general problem of random flight of a Markov chain may be expressed as follows. After N displacements, the position \mathbf{R} of the particle is given by

$$\mathbf{R} = \sum_{i=1}^N \mathbf{r}_i \quad i = 1, \dots, N$$

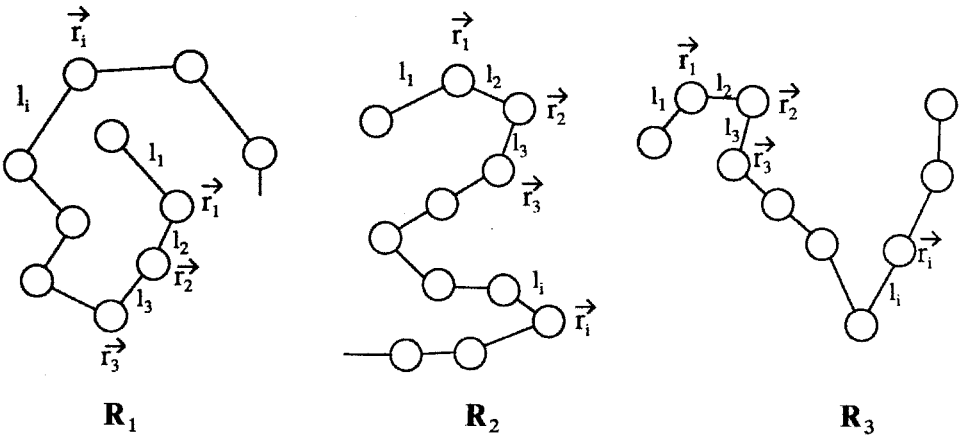


FIGURE 5.3 Configurations of a chain.

where \mathbf{r}_i refers to the individual displacement. The probability $\tau_i(x_i, y_i, z_i)$ that the i th displacement is found between \mathbf{r}_i and $\mathbf{r}_i + d\mathbf{r}_i$ is

$$\tau_i(x_i, y_i, z_i) dx_i dy_i dz_i = \tau_i d\mathbf{r}_i$$

According to the fundamental limit theorem (an extension of the Bernoulli theorem by Laplace) if an event A occurs m times in a series of n independent trials with constant probability p and if $n \rightarrow \infty$, then the distribution function tends to be

$$\frac{1}{\sqrt{2\pi}} \int_{-\infty}^u e^{-(1/2)u^2} du$$

as a limit. That is, the distribution function tends to be a normal (Gaussian) function. The term u here is a dummy variable. It has no physical meaning. Markov further extends it to the sums of dependent variable, in our case, \mathbf{R} and $\Sigma \mathbf{r}_i$. We take a special case of τ_i as the Gaussian distribution of displacement \mathbf{r}_i , that is, $\tau_i(\mathbf{r}_i)$:

$$\tau_i = \left(\frac{3}{2\pi l_i^2} \right)^{3/2} \exp\left(-\frac{3r_i^2}{2l_i^2} \right) \tag{5.5}$$

where l is the length of displacement. Applying the displacement of \mathbf{r}_i to \mathbf{R} , we have

$$w_N(\mathbf{R}) = \left(\frac{3}{2\pi N \langle l^2 \rangle} \right)^{3/2} \exp\left(-\frac{3R^2}{2N \langle l^2 \rangle} \right)$$

where $w_N(\mathbf{R}) d\mathbf{R}$ is the probability that after N displacements the particle lies in the interval between \mathbf{R} and $\mathbf{R} + d\mathbf{R}$ and $\langle l^2 \rangle$ is the mean-square displacement. If all the individual displacements have the same length, then the distribution function is

$$\tau_i = \frac{1}{4\pi l^3} \delta(|\mathbf{r}_i|^2 - l_i^2)$$

where δ is the Dirac function,

$$r_{ij} = \begin{cases} 0 & \text{if } i \neq j \\ 1 & \text{if } i = j \end{cases}$$

and the probability function is

$$w(\mathbf{R}) = \left(\frac{3}{2\pi N l^2} \right)^{3/2} \exp\left(\frac{-3R^2}{2N l^2} \right) \tag{5.6}$$

5.3 RANDOM-FLIGHT CHAINS

We assume that each bond between the two monomeric units of a polymer has a constant length a and that τ_i is the bond probability. This enables the configuration of a polymer molecule in the form of a flexible random coil to be described in terms of a Markov chain; namely, the probability $w(R) dR$ that after N displacements the position of the particle lies between R and $R + dR$ can be described by Eqs. (5.5) and (5.6). All we have to do is to change r_i to r in Eq. (5.5) and l_i to a in Eq. (5.6) and to rewrite the two equations as follows:

$$\tau(\mathbf{r}) = \left(\frac{3}{2\pi a^2}\right)^{3/2} \exp\left(\frac{-3r^2}{2a^2}\right) \quad (5.7)$$

$$w(R) = \left(\frac{3}{2\pi Na^2}\right)^{3/2} \exp\left(\frac{-3R^2}{2Na^2}\right) \quad (5.8)$$

With the distribution function $w(R)$ available, we can now calculate the mean-square end-to-end distance $\langle R^2 \rangle$ of a polymer chain in the following way:

$$\langle R^2 \rangle = \int_0^\infty R^2 w(R) 4\pi R^2 dR = Na^2 \quad (5.9)$$

the function $w(R)$ is being normalized,

$$\int_0^\infty w(R) 4\pi R^2 dR = 1$$

The root-mean-square end-to-end distance of a chain is the square root of $\langle R^2 \rangle$:

$$\langle R^2 \rangle^{1/2} = N^{1/2} a$$

The radius of gyration $\langle S^2 \rangle^{1/2}$, which is the root-mean-square distance of an end from the center of gravity, is related to the root-mean-square end-to-end distance by

$$\langle S^2 \rangle^{1/2} = \frac{1}{\sqrt{6}} \langle R^2 \rangle^{1/2}$$

or

$$\frac{\langle S^2 \rangle}{\langle R^2 \rangle} = \frac{1}{6}$$

Equation (5.9) represents an ideal polymer chain, a random-flight chain. It is also regarded as a freely jointed chain. To apply Eq. (5.9) to the real chain, several

modifications have been suggested by various investigators. Here we list three of them.

1. On the basis of statistical reason, for Eq. (5.9) to be true, the value of a must be large and that of N must be small. One way to solve this problem is to introduce a proportionality constant c , which is called the characteristic ratio. Equation (5.9) is modified to the form

$$\langle R^2 \rangle = cNa^2 \quad (5.10)$$

If $c = 1$, the chain is, needless to say, ideal. If $c \neq 1$, we must correct our estimation of the value of $\langle R^2 \rangle$. Thus, the value of c provides some information on the dimension of a polymer chain in relation to its deviation from ideality: The larger the value of c , the larger the chain extended.

2. In case the bond angles θ of a chain are restricted but rotations about the bonds are not restricted, it is suggested that Eq. (5.9) be further modified:

$$\langle R^2 \rangle_f = cNa^2 \frac{1 - \cos \theta}{1 + \cos \theta} \quad (5.11)$$

Such a chain is often called a freely rotating chain.

3. We can write the random-flight chain in a more general way:

$$\langle R^2 \rangle = \sum_{i=1}^N \langle \mathbf{r}_i^2 \rangle + 2 \sum_{1 \leq i < j \leq N} \langle \mathbf{r}_i \mathbf{r}_j \rangle \quad (5.12)$$

where $\langle \mathbf{r}_i \mathbf{r}_j \rangle$ is the correlation factor (see Appendix B). In obtaining Eq. (5.9), we tacitly assume that

$$\langle \mathbf{r}_i \mathbf{r}_j \rangle = 0 \quad \text{for } i \neq j$$

and that

$$\langle \mathbf{r}_i^2 \rangle = a^2$$

However, this assumption is not true because we neglect the excluded volume effect which is expressed in the terms $\langle \mathbf{r}_i \mathbf{r}_j \rangle$. That is, we should not assume that $\langle \mathbf{r}_i \mathbf{r}_j \rangle \neq 0$ for $i \neq j$. Hermans (1950) and Grimley (1952) suggested independently that we include $\langle \mathbf{r}_i \mathbf{r}_j \rangle$ ($i \neq j$) in Eq. (5.9). Hermans' equation is

$$\langle R^2 \rangle = Na^2 \left[1 + 0.78 \left(\frac{\beta_0}{a^3 N^{1/2}} \right) \right] \quad (5.13)$$

where β_0 is the volume excluded to one segment by the another. Grimley's equation is almost identical to Hermans', except for the numerical coefficient:

$$\langle R^2 \rangle = Na^2 \left[1 + 0.143 \left(\frac{\beta_0}{a^3 N^{1/2}} \right) \right] \quad (5.14)$$

In both cases, as $N \rightarrow \infty$, $\langle R^2 \rangle \rightarrow Na^2$.

5.4 WORMLIKE CHAINS

The wormlike chain model is an extension of the random-flight chain model. It was proposed by Kratky and Porod (1949) for the purpose of interpreting the experimental data of small-angle x-ray scattering (see Chapter 16) from biological polymers. It is well known that biological polymers such as proteins and DNA have stiff chains. The wormlike chain resembles a freely rotating chain: The chain consists of N bonds of fixed length joined at fixed bond angles θ . All bond lengths and all bond angles are taken to be equal. The chain can rotate freely about single bonds. The general expression for the mean-square end-to-end distance of such a chain is

$$\langle R^2 \rangle = Na^2 \left[\frac{1 - \cos \theta}{1 + \cos \theta} + \frac{2 \cos \theta}{N} \frac{1 - (1 - \cos \theta)^N}{(1 + \cos \theta)^2} \right] \quad (5.15)$$

The wormlike chain is a limiting case of such a chain, namely, $a \rightarrow 0$ and $\theta \rightarrow \pi$. The chain is characterized by the contour length L , defined as

$$L = Na$$

and the persistence length $(2\lambda)^{-1}$, defined as

$$(2\lambda)^{-1} = \frac{a}{1 + \cos \theta}$$

By substituting the two parameters, L and $(2\lambda)^{-1}$, into Eq. (5.15) and simplifying, we obtain the general expression of $\langle R^2 \rangle$ for the wormlike chain:

$$\langle R^2 \rangle = \frac{L}{\lambda} - \frac{1}{2\lambda^2} (1 - e^{-2\lambda L}) \quad (5.16)$$

Unlike other flexible chains, the dimensions of the wormlike chain are greatly influenced by the shape of the molecules. The parameter λ is a measure of the chain stiffness.

5.5 FLORY'S MEAN-FIELD THEORY

Flory pointed out that volume exclusion must cause $\langle R^2 \rangle$ to increase. The amount of increase can be expressed by the expansion factor α^2 , defined as

$$\alpha^2 = \frac{\langle R^2 \rangle}{\langle R^2 \rangle_0} \quad (5.17)$$

where $\langle R^2 \rangle$ is the mean-square end-to-end distance of the chain, which has been perturbed by the excluded volume effect, and $\langle R^2 \rangle_0$ is the distance for the unperturbed chain, that is, the ideal chain, ($\langle R^2 \rangle_0 = Na^2$). Thus, the value of $\langle R^2 \rangle_0$ can only be used as a reference. Once the value of $\langle R^2 \rangle_0$ is known, the value of $\langle R^2 \rangle$, which is the real chain dimension, should solely depend on the value of α . To understand the average dimension of a chain over various configurations, we need to understand α .

Consider the segments of a chain, x in number, which pervade a volume V . Let ρ be the segment density, which is uniform throughout the volume V . Then $\rho = x/V$ within V and $\rho = 0$ outside V . The volume is related to $\langle R^2 \rangle$ by

$$V = A \langle R^2 \rangle^{3/2}$$

where A is the proportionality constant. The probability that an arbitrary distribution of the centers of segments within V is

$$P_{(i)} \cong \prod_{i=1}^x \left(1 - \frac{i\beta}{V} \right) \cong \exp \left(\frac{-\beta x^2}{2V} \right) = \exp \left(\frac{-\beta x^2}{2A \langle R^2 \rangle_0^{3/2} \alpha^3} \right)$$

where β is the volume excluded by a segment. In terms of the conventional parameter z , defined as

$$z = \left(\frac{3}{2\pi} \right)^{3/2} \left(\frac{\langle R^2 \rangle_0}{x} \right)^{-3/2} x^{1/2} \beta$$

we have

$$P_{(i)} = \exp \left[-2^{1/2} \left(\frac{\pi}{3} \right)^{3/2} A^{-1} z \alpha^{-3} \right] \quad (5.18)$$

Equation (5.18) describes the average density corresponding to $\langle R^2 \rangle$. (*Note:* This is the major point of mean-field theory; see Chapter 9, Appendix E.) The distribution of chain vector \mathbf{R} for the unperturbed chain is assumed to be Gaussian in nature, that is,

$$w(\mathbf{R}) d\mathbf{R} = \text{const} \times \exp \left(\frac{-3R^2}{2\langle R^2 \rangle_0} \right) d\mathbf{R}$$

The probability $p_{(ii)}$ of a set of configurations corresponding to $\langle R^2 \rangle$ relative to the probability of a set of configurations corresponding to $\langle R^2 \rangle_0$ is

$$P_{(ii)} = \frac{(d\mathbf{R})}{(d\mathbf{R})_0} \exp \left[\frac{-3(\langle R^2 \rangle - \langle R^2 \rangle_0)}{2\langle R^2 \rangle_0} \right] = \alpha^3 \exp \left[-\frac{3}{2}(\alpha^2 - 1) \right]$$

The combined probability leads to

$$P_{(i)}P_{(ii)} = \alpha^3 \exp \left[-2^{1/2} \left(\frac{\pi}{3} \right)^{3/2} A^{-1} z \alpha^{-3} - \frac{3}{2}(\alpha^2 - 1) \right]$$

Maximizing the expression of $P_{(i)}P_{(ii)}$ (i.e., setting $\partial P_{(i)}P_{(ii)}/\partial \alpha = 0$) and solving for α give

$$\alpha^5 - \alpha^3 = 2^{1/2} \left(\frac{\pi}{3} \right)^{3/2} A^{-1} z \quad (5.19a)$$

or

$$\alpha^5 - \alpha^3 = Bx^{1/2}\beta \quad (5.19b)$$

where

$$B = \left(\frac{\langle R^2 \rangle_0}{x} \right)^{-3/2} (2A)^{-1}$$

The quantity B is a constant for a given series of polymer homologs. Equations (5.19a) and (5.19b) are Flory's theory to describe the polymer chain configuration. de Gennes commented that because of the assumption of Gaussian distribution with respect to $\langle R^2 \rangle_0$, Flory's theory is still intrinsically a random-flight chain in nature.

5.6 PERTURBATION THEORY

Perturbation theory (Zimm et al., 1953; Yamakawa, 1971) is an extension of Flory's theory. It is based on mathematical analysis of the transition probability, which indicates that the excluded volume effect on $\langle R^2 \rangle$ becomes asymptotically proportional to a power of N higher than the first. Flory's term α may be expanded in a power series by the excluded volume parameter z . The underlying idea is to describe α as a universal function of z . For this reason, the theory is also called the two-parameter (α and z) theory. So far it has only partially reached this goal, because it is a many-body problem and the mathematics involved are difficult.

5.6.1 First-Order Perturbation Theory

In this theory the coupling parameter method is used to derive an equation for the distribution function. The coupling parameter method considers only those configurations in which a single pair of segments is interacting. It neglects the higher order approximations for multiple contacts. The following equations are the results obtained by Zimm and co-workers (1953):

$$\alpha_R^2 = 1 + \frac{4}{3}z + \dots \quad (5.20)$$

where

$$z = \left(\frac{3}{2\pi a^2} \right)^{3/2} \beta N^{1/2} = \left(\frac{3}{2\pi \langle R^2 \rangle_0} \right)^{3/2} \beta N^{1/2}$$

$$\beta = \int 1 - g(\mathbf{R}_{ij}) d\mathbf{R}_{ij}$$

The term $g(\mathbf{R}_{ij})$ is defined as

$$g(\mathbf{R}_{ij}) = \exp \left[-\frac{w(R_{ij})}{kT} \right]$$

where $w(R_{ij})$ is the pair potential of mean force between the i th and j th segments as a function of R_{ij} . The parameter β is expected to have large positive values in good-solvent systems and to have small positive, zero, or negative values in poor-solvent systems. In terms of Flory's expressions, the first-order perturbation theory can be rephrased:

$$\alpha_R^5 - \alpha_R^3 = \frac{4}{3}z \quad \alpha_S^5 - \alpha_S^3 = \frac{134}{105}z \quad (5.21)$$

5.6.2 Cluster Expansion Method

In this theory the single-contact term, the double-contact term, and so forth are taken into consideration. The cluster diagrams developed by Ursell (1927) and Mayer et al. (1940, 1945) are employed to calculate the mean-square end-to-end distance. Here we give the results obtained by Yamakawa (1971):

$$\alpha_R^2 = 1 + 1.333z - 2.075z^2 + 6.459z^3 - \dots \quad (5.22)$$

$$\alpha_S^2 = 1 + 1.276z + \dots \quad (5.23)$$

In term's of the Flory theory, the two-parameter theory of Yamakawa may be expressed as

$$\alpha^5 - \alpha^3 = 2.60z \quad (5.24)$$

At small z ,

$$\alpha^2 = 1 + 2.60z - \dots \quad (5.25)$$

5.7 CHAIN CROSSOVER AND CHAIN ENTANGLEMENT

5.7.1 Concentration Effect

So far our description of the random-coil chain basically assumes a dilute solution and we have not yet defined the term dilute solution. It has been discovered that when the concentration increases to a certain point, interesting phenomena occur: chain crossover and chain entanglement. Chain crossover refers to the transition in configuration from randomness to some kind of order, and chain entanglement refers to the new statistical discovery of the self-similar property of the random coil (e.g., supercritical conductance and percolation theory in physics). Such phenomena also occur to the chain near the theta temperature. In this section, we describe the concentration effect on chain configurations on the basis of the theories advanced by Edwards (1965) and de Gennes (1979). In the next section, we describe the temperature effect, which is parallel to the concentration effect.

In 1966, S. F. Edwards proposed classifying the concentrations of polymer solutions into three broad types in terms of the total number of micromolecules (monomers) N , the number of polymer chains n , the effective length l of a micromolecule, the excluded volume per micromolecule u' , and the total volume V . The length of the single chain L is defined as

$$L = \frac{N}{n}l$$

The three types of concentration can be described as follows:

1. Dense solutions in which $V/N < u'$
2. Intermediate concentrations in which

$$L^{9/5}u'^{3/5}l^{-3/5} > \frac{V}{n} > u'$$

3. Dilute solutions in which

$$\frac{V}{n} < L^{9/5}u'^{3/5}l^{-3/5}$$

Edwards discussed intermediate concentrations in detail, for this is the region in which chain crossover and chain entanglement occur. To describe this region, he introduced two derived quantities:

$$\xi = \left(\frac{12nu'L}{Vl^3} \right)^{-1/2} \quad g = \left(\frac{u'L}{l} \right)^{1/3}$$

We thus have four basic quantities— $l_0 = (u')^{1/3}$, l , $r_0 = (V/n)^{1/3}$, and $r_1 = (Ll)^{1/2}$ —and two derived quantities— ξ and g . The quantity ξ is now called the screen length and the quantity g^3 is the effective volume of the molecules in one chain. Edwards showed that the intermediate region exists provided that

$$l_0 < l \ll g < r_0 < \xi < r_1$$

Edwards reached a conclusion for the mean-square end-to-end distance of a polymer in intermediate solution by giving

$$\langle r^2 \rangle = c_2 \left(\frac{u'}{l} \right)^{2/5} L^{6/5} \quad (5.26)$$

where c_2 is a numerical constant. This equation is very similar to Flory's equation,

$$\langle R^2 \rangle \sim N^{12/10} \quad (5.27)$$

but Edwards and Flory used different approaches. Flory adopted the mean-field model and the chain is intrinsically Gaussian, as we mentioned before. Edwards adopted the self-consistent argument and the chain is not Gaussian.

A more detailed and elegant description of the concentration effect on the chain configuration is offered by de Gennes, particularly in the intermediate region. de Gennes pointed out that at a certain concentration the behavior of a polymer chain is analogous to the magnetic critical and tricritical phenomena. He applied a method to study chain behavior similar to that used by Wilson (1971) to study magnetic critical and tricritical phenomena, namely, the adoption of renormalization group theory to derive equations (Chapter 9, Appendix D). The techniques focus on the length scale L as a basic parameter on which polymer properties are related and the power laws are obtained for asymptotic behavior by taking $N \rightarrow \infty$. de Gennes classifies the concentration c into three categories: the dilute solution c' , the semidilute solution c^* , and the concentrated solution c'' . They are related in the following way:

$$c' < c^* < c''$$

The concentration c^* is equivalent to the critical point where the crossover phenomenon occurs from randomness to order. It is also equivalent to p_c (the critical probability) in the percolation theory, where the crossover phenomenon occurs from the finite cluster (such as a macromolecule containing a finite number of monomers) to the infinite cluster (such as the network of an entangled macromolecule, which extends from one end to the other). The three regions are characterized by three important quantities: the number of statistical elements per chain N , the number of statistical elements per unit volume ρ (density), and the correlation or screen length ξ .

Dilute Solutions In a dilute solution c' , a polymer chain behaves like a small hard sphere, that is, a single blob, with a radius r in the form of a power law:

$$r \sim N^{\nu} \quad \text{and} \quad \nu = \frac{3}{d+2} \quad \text{for } d \leq 4 \quad (5.28)$$

where ν is an excluded volume exponent (or the critical exponent for the mean dimension of a polymer chain) and d is the dimensionality ($d = 1, 2, 3, \dots$). For example, for $d = 3$, $\nu = \frac{3}{5}$. Each polymer in a dilute solution is an isolated chain. Here, the length scale L is represented by the radius r and is equal to the correlation length ξ , that is, $r = \xi$. The chain concentration is equal to ρ/N ; that is, the coils are separated from each other.

Semidilute Solutions As concentration increases, the blobs begin to overlap each other. There are interchain interactions; that is, the chains begin to interpenetrate. If the concentration is increased to a point slightly higher than c^* , the coils become entangled and a network of mesh ξ is formed. The parameter ξ now refers to the distance between two entanglement points or two intersection points. At the entangled point it can no longer be distinguished which chain is tangled with which other chain. Yet, just as in fractal geometry and percolation theory, at such a random state, a strange phenomenon happens: An individual long chain (originally one blob, that is, in dilute solution) can be visualized as a succession of sequences of well-ordered and isolated blobs.

The formation of the long chain in the entanglement may be sketched as in Figure 5.4. In the dilute solution region (1), an individual polymer chain A may be

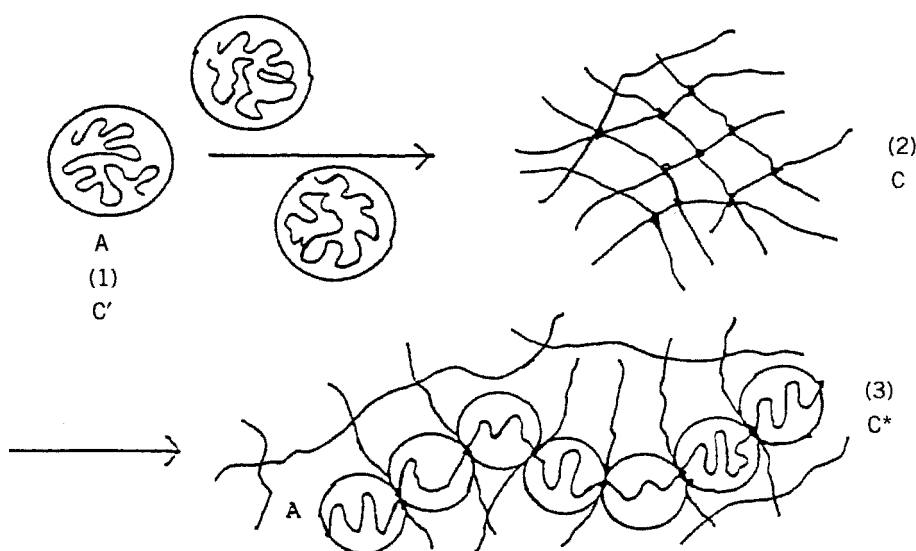


FIGURE 5.4 Chain entanglement.

conceived as confined in a blob of radius r or ξ . In the semidilute solution region (2), many chains interpenetrate into each other to form a mesh of size ξ . In (3), still in the semidilute solution region but with a slightly higher than c^* , the same individual chain A is now in the form of a succession of subchains or a sequence of blobs of radius ξ . The parameter ξ (the correlation length) is equivalent to the mean-free path between two collisions in the kinetic theory of gas.

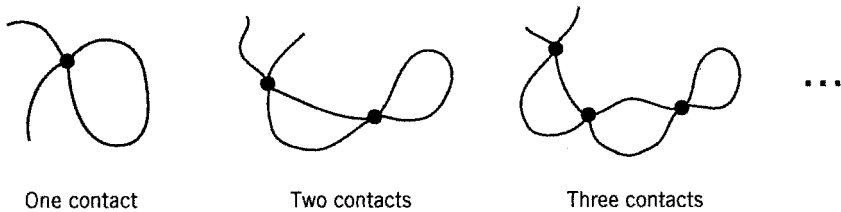
The concentration c^* can be defined by (a power law)

$$c^* = \frac{\rho^*}{u'} \sim N^{1-\nu d} \tag{5.29}$$

where ρ^* is the overlap threshold density and u' is the excluded volume parameter, which involves monomer–monomer interactions. The degree of interpenetration as shown in (2) in Figure 5.4 can be measured in terms of ρ/ρ^* .

Assume that we are dealing with polymers in good solvents and in the semidilute solution. If r is a scale to measure, then the chain entanglement shows the following properties. At $r > \xi$, that is, outside the blob, the repulsive interactions between monomers are “screened out” by other chains in the solution so that the whole chain is composed of blobs connected in an ordinary random walk without excluded volume effect. Overall, the chain follows Gaussian statistics. At $r < \xi$, that is, within the blob, the chain does not interact with other chains, but there is a strong excluded volume effect.

In a semidilute solution the system dynamics are controlled by interaction contacts:



The end-to-end distance or radius of gyration (R or S) is no longer important. It is the screen length ξ (the diameter of blob), which is related to R , that plays an important role. The concentration dependence of ξ is obtained from the scaling relationship,

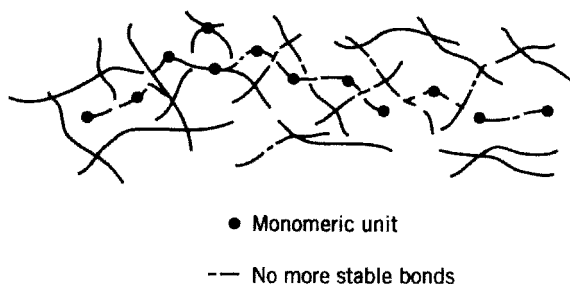
$$\xi \sim R \left(\frac{c}{c^*} \right)^x \tag{5.30}$$

If $R \sim M^{-3/5}$ and $c^* \sim M^{-4/5}$, then $x = -\frac{3}{4}$ (where M is the molecular weight). We thus have the power law

$$\xi \sim c^{-3/4} \tag{5.31}$$

This power law, Eq. (5.31), is the central theme of the scaling theory for understanding entangled polymer chains in good solvents. Furthermore, at concentration c^* , the screen length ξ is equal to the coil size.

Concentrated Solutions In the concentrated solution c'' , the length ξ is smaller than the coil size. When the concentration is very high, ρ equals unity and ξ becomes of order 1, which is comparable to the monomer size, as shown in the following diagram:



where ● is a monomeric unit and the dashed line indicates no more stable bonds. Here the chain collapses, or is better said to be in a collapsed state.

Comments on Flory's Theory by de Gennes According to de Gennes, Flory did not realize the existence of the critical point c^* in the polymer solution. His mean-field theory of α in the dilute polymer solution leads, indeed, to a correct expression of scaling law,

$$R \sim N^{-6/5}$$

because luckily the errors introduced in ΔS_{mix} and ΔH_{mix} for a polymer chain canceled out. Flory's approach to the polymer solution problem is basically wrong. According to de Gennes, he neglected the changes in the pair correlation function $g(\mathbf{r})$ that occur when we incorporate the effects of excluded volume. For a correct approach, we must not neglect the correlations between all pairs of monomers. The pair correlation may be defined as

$$g(\mathbf{r}) = \frac{1}{2}[\langle c(0)c(\mathbf{r}) \rangle - c^2]$$

de Gennes' own theory may be summarized in a slightly different way when correlation function is taken into consideration. In the dilute polymer solutions, coils are separated, while in the more concentrated solutions, coils overlap. At the threshold ($c = c^*$), the coils begin to be densely packed. In terms of correlation function $g(\mathbf{r})$, for $\mathbf{r} < \xi$ (i.e., inside the blob), we have

$$g(\mathbf{r}) \cong \frac{1}{r^{4/3} a^{5/3}}$$

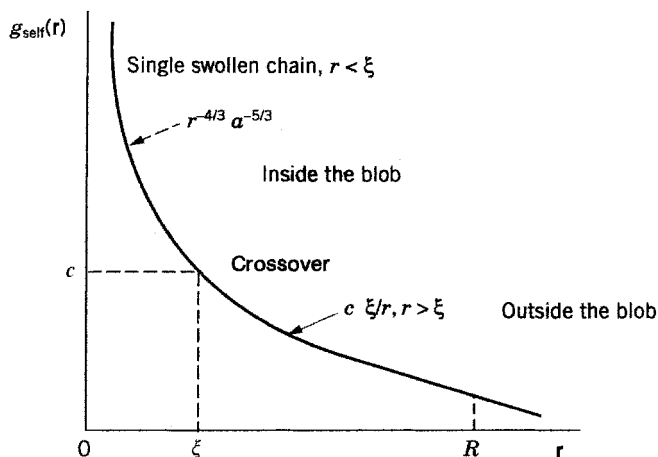


FIGURE 5.5 Description of crossover phenomena; r is scale of measure.

where a is the length of a statistical unit (equivalent to bond length). For $r > \xi$ (i.e., outside the blob), where the chain begins to feel the effects of surrounding chains,

$$g(\mathbf{r}) = c \frac{\xi}{r}$$

The two coils cross over smoothly at $r = \xi$. For $r > R$ (where R is the overall size of the chain),

$$g(\mathbf{r}) \rightarrow 0$$

In Figure 5.5, the crossover is shown as a smooth curve.

5.7.2 Temperature Effect

The conformation[†] of a single polymer chain in solutions is affected by temperature just as much as by concentration. de Gennes pointed out that the θ point is in fact a tricritical point. Experimentally, while it is difficult to find the sharp point of c^* , it is easy to find the sharp point of θ for a particular polymer solution system. The

[†] We agree with Flory in the use of the terms configuration and conformation. Flory said, "The term *conformation* connotes form and a symmetrical arrangement of parts. The alternative term, *configuration*, is perhaps the more general of the two in referring to the disposition of the parts of the object in question without regard for shape and symmetry." (Flory, 1969, p. 15). For practical reasons, he considered these two terms interchangeable. In recent literature of polymer science, both terms are used. Authors customarily used the term conformation with respect to temperature effect. We use both terms in this chapter so that readers will feel comfortable with both.

equation of $\alpha^5 - \alpha^3$ developed by Flory on the basis of mean-field approximation is modified by de Gennes with the new approach, renormalization group theory, to describe the effect of temperature on chain configuration which is parallel to concentration effect. de Gennes' equation is given as

$$\underbrace{\alpha^5 - \alpha^3}_{(i)} - \underbrace{\frac{y}{\alpha^3}}_{(ii)} = \underbrace{kN^{1/2} \frac{w_1}{a^3}}_{(iii)} \quad (5.32)$$

where

$$y = k^2 w_2 a^{-6}$$

In these equations y is a parameter ($y = 0, 0.01, 0.038, 0.1, 1$), w_1 and w_2 are successive virial coefficients, N is the number of monomers along the chain, k is a numerical constant, and a is the monomer length. Equation (5.32) can be used to describe the single-chain behavior in infinite dilution. But, instead of using the concentration c as a scaling variable, here we choose T as a scaling variable.

According to Perzynski et al. (1982), Eq. (5.32) can be interpreted as follows: The term $\alpha^5 - \alpha^3$ (term i) describes the elasticity of the chains. The negative term $-\alpha^3$ prohibits large swelling. Term i is important when $T > \theta$. The term y/α^3 (term ii) describes a hard-core repulsion and slows down the collapse of the chain. Term ii is important when $T < \theta$. Term iii is proportional to the reduced temperature τ , defined as

$$\tau = \begin{cases} \frac{T-\theta}{T} & \text{for } T > \theta \\ \frac{\theta-T}{\theta} & \text{for } T < \theta \end{cases}$$

This term is important both for $T > \theta$ (the swelling of the chain) and $T < \theta$ (the contraction of the chain). It is a description of the crossover phenomena (Figure 5.5).

We can now introduce a reduced variable that involves temperature: $\tau\sqrt{N}$. The expansion factor α is simply a function of this single reduced variable $\tau\sqrt{N}$:

$$\alpha = f(\tau\sqrt{N})$$

At the θ temperature, $f(\tau\sqrt{N}) \cong 1$ and $\tau\sqrt{N} \ll 1$. We have

$$R \sim R_\theta \sim N^{1/2} \quad (\text{Gaussian chain})$$

At $T < \theta$, $f(\tau\sqrt{N}) \cong (\tau\sqrt{N})^{-1/3}$ and $\tau\sqrt{N} \gg 1$, and we have

$$R \sim N^{-1/3} \tau^{-1/3} \quad (\text{globule chain})$$

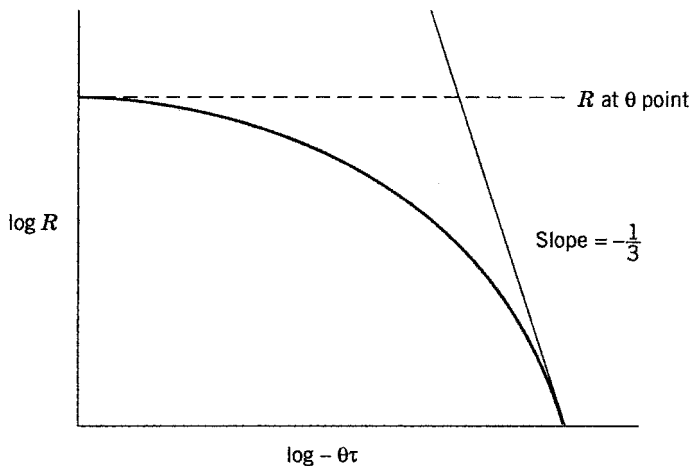


FIGURE 5.6 Collapse state.

The collapse state at which Eq. (5.32) is aimed can be visualized by plotting the experimental data of $\log R$ versus $\log(-\theta\tau)$, as shown in Figure 5.6. At $T > \theta$, $f(\tau\sqrt{N}) \cong (\tau\sqrt{N})^{3/5}$, and $\tau\sqrt{N} > 1$, we have

$$R \sim N^{3/5}$$

The value of R decreases slowly at first as the temperature decreases. At a very narrow range of the temperature $\theta - T$, the value of R rapidly drops, which is an indication of the collapse state of the polymer chain.

The question is, what about the combined effects of concentration and temperature on the chain conformation? This has been described in terms of the coexistence curve, which is shown in Figure 5.7. The coexistence curve describes the states of temperature and solute concentration at which the attractive parts of segment-segment interactions just begin to dominate. The polymer begins to form aggregates, but no phase separation occurs as yet.

5.7.3 Tube Theory (Reptation Theory)

Tube theory describes the motion of a chain in an entanglement of mesh ξ . It was originally proposed by de Gennes (1971) and was advanced by Doi and Edwards (1978). A chain in the entanglement is viewed as the chain being confined in an environment densely filled with the strands of other chains, which, in a sense, form a tube. It is the center line of the tube that tracks the current chain conformation. The chain can move laterally, but the displacements can take place only by diffusion along its contour.

The short-range interaction of the chain segments causes the molecule to accommodate with the tube; that is, the length of the chain is identical with the

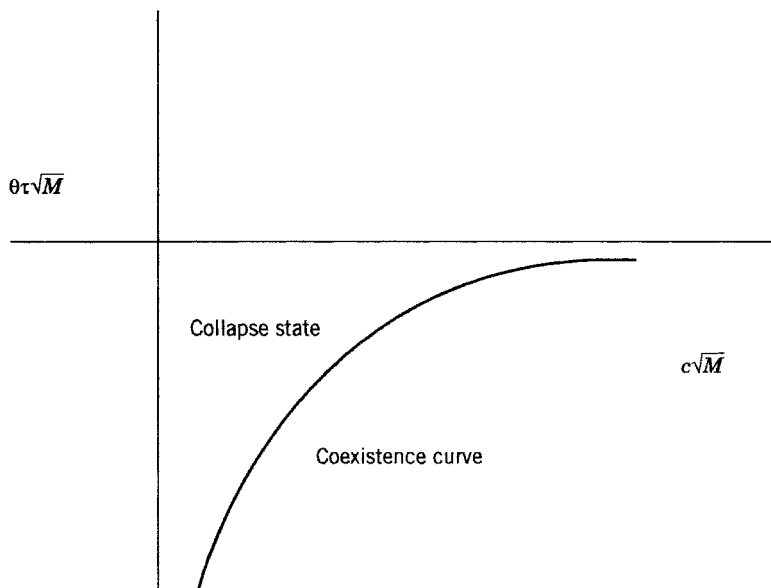


FIGURE 5.7 Coexistence curve: combined effects of concentration and temperature.

mesh size ξ . The long-range interaction, however, makes the chain capable of sliding along the contour like a snake until it finally escapes from the tube. This process is called reptation. The entangled chains rearrange their conformations from time to time by reptation. In technical terms, reptation is a curvilinear diffusion along their own contour. The important parameters in this model are the tube diameter ξ and the tube or curvilinear length L (see Figure 5.8).

The tube diameter and the tube length are related by

$$L = \left(\frac{N}{g}\right)^{1/2} \xi$$

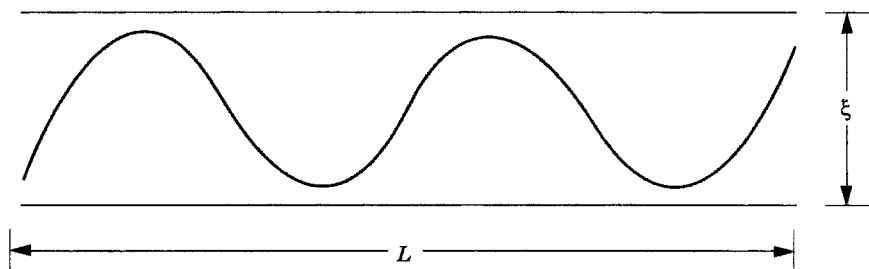


FIGURE 5.8 Reptation model.

where N is the total number of chains in consideration and g is the number of monomers in a subunit. Let μ_t be the mobility of the chain along the tube and μ_1 the mobility of one unit. Then

$$\mu_t = \left(\frac{N}{g}\right)\mu_1$$

But

$$\mu_1 = \frac{1}{\eta_s \xi}$$

where η_s is the solvent viscosity. The diffusion coefficient D (Chapter 10) is related to μ_t in terms of the mean-square distance by

$$D = kT\mu_t = \frac{kT}{\eta_s \xi} \frac{g}{N} \quad (5.33)$$

Assume that the primitive path of the chain in the tube is a random-walk sequence of N steps with step length ξ . Then we have

$$R = \left(\frac{N}{g}\right)^{1/2} \xi \quad (5.34)$$

Thus, L , the end-to-end vector of the tube, and R , the root-mean-square end-to-end distance, coincide. The reptation time T_R , which is the time for the chain to renew its configuration, is related to L by

$$T_R D \sim L^2 \quad (5.35)$$

The tube theory has been applied successfully to the mechanical properties in concentrated polymer liquids. It also has been proved useful for analyzing the motion of DNA in a gel which includes the effect of molecular fluctuations.

5.7.4 Images of Individual Polymer Chains

According to tube theory, the coil of a polymer molecule can be stretched into a long chain. This has been recently confirmed by Chu and co-workers (1997, 1999) with three slightly different experimental techniques.

- (a) *Laser tweezer*—This is based on the observation that the laser beam attracts the electrons of chain molecules. By attaching a polystyrene bead, for example, to the end of a DNA molecule, the chain was driven by optical tweezers and gravitational force to stretch to its limit.



FIGURE 5.9 See color insert. Conformation-dependent rate of stretching. Image spaced every 0.13 Å at the highest strain rate investigated. (Source: T. T. Perkins, D. E. Smith, and S. Chu, *Science* **276**, 2016 (1997). With permission from AAAS. Original in color.)

- (b) *Longitudinal shear flow*—Very dilute chains (e.g., DNA molecule) were inserted into a longitudinal shear cell. One of them was being watched in its distorted form and the duration of torture was counted.
- (c) *Steady shear flow*—Here the coil is directly observed by using video fluorescence microscopy on the conformational dynamics of individual flexible polymers.

Figure 5.9 shows images of single DNA chains tagged with fluorescent markers.

In Figure 5.9, four of the seven chain-stretching configurations were observed. The seven chains are dumbbell, half dumbbell, folded, uniform, kinked, coiled, and extended. The configurations from top to bottom are dumbbell, kinked, half dumbbell, and folded. Sometimes two chains display different behaviors even though they suffered the same length of stretching time stress. Dumbbell chains elongate quickly. Folded chains are like a hairpin along the stretching direction and elongate more slowly.

These experiments confirm that a long chain moves not only by discrete segments, but also as a whole molecule. The movement is like that of snake. Even in a tangled environment, an individual chain molecule can move about as a whole by diffusion just as reptation predicted.

The results also indicate that identical polymers beginning from the same state can uncoil in different ways and get hung up in strange knots and bends.

5.8 SCALING AND UNIVERSALITY

To summarize what we have discussed so far, the configuration of a polymer chain depends on two basic quantities: molecular weight M (which, in turn, is related to

the number of polymeric links N) and the end-to-end distance R or radius of gyration S (which, in turn, is related to both inter- and intramolecular interactions). At the asymptotic region there is not much difference between R and S .

Although the random motion of a flexible polymer chain is complex, recent theoretical developments predict that the universal behavior should be observed in certain dynamic regimes. Such a behavior is related to the critical exponents as expressed in power laws.

The universal laws of current interest for a polymeric system are in the form

$$p \sim M^{\nu}$$

where p refers to R_g , R_H , A_2 , or $[\eta]$, M is the molecular weight, and ν is the critical exponent. These laws govern which scale we choose to measure the macrostructure of a system. Experimentally, R_g is the radius of gyration, which is an average measure of the size of the macromolecule. The instrument used to measure R_g is light scattering. The term R_H is also the radius of gyration, but it is a measure of the hydrodynamic size of a polymer as it drifts through a fluid. The instruments that measure R_H are ultracentrifuge sedimentation and diffusion (e.g., laser light scatterings). The second virial coefficient, A_2 , is a direct measure of the excluded volume effect. The instrument that best measures this quantity is osmotic pressure. The term $[\eta]$ is the intrinsic viscosity due to the rate of dissipated energy in shear flow of the polymer solution, which is another measure of the hydrodynamic volume of a power law.

Since M is related both to N (the number of links) and c (the concentration), the independent variable M can be converted to N or c , and the power laws are in the form

$$p \sim N^{\nu} \quad \text{or} \quad p \sim c^{\nu}$$

The quantities N and c vary from material to material (or from system to system), but the exponent ν stays the same. The exponent ν is the most crucial term describing the state of the polymeric system (e.g., randomness, crossover, order). It is the critical exponent that describes the universal behavior of polymer chains, and it is independent of the details of the materials and the models that we use.

Chapters 8–11, 14, and 16 describe the experimental methods that, in addition to the classical exposition, are closely related to current thinking on universal laws that govern polymer behavior.

APPENDIX A SCALING CONCEPTS

Scaling Relationship

For any two quantities A and B that are related,

$$A = f(B) \quad \text{or} \quad B = g(A)$$

and that characterize a regime (e.g., a molecular system), we can write their relationship in the form of a power law:

$$A \sim B^{\nu} \quad (\text{or } B \sim A^{\nu'})$$

where ν (or ν') is the exponent of the scaling variable (A or B). If a regime is in chaos (in a random state), the power law has a special meaning; namely, ν represents a critical value, which may be called the fractal dimension, the critical correlation length or the measure, and with which we observe an order in randomness. The value ν can be determined experimentally or by computer simulation.

Dimensions of a Polymer Chain

In a very dilute solution c' with a good solvent, the polymer molecule swells and its size can be expressed (in terms of mean-square end-to-end distance) by

$$\langle R^2 \rangle \sim N^{2\nu}$$

(ν being the excluded volume effect exponent). When the solution is very concentrated (c''), the chain, which is not collapsed yet, is in the ideal (or unperturbed) state and its size can be expressed as

$$\langle R^2 \rangle \sim N$$

In between we have a semidilute solution c^* with the threshold density ρ^* . A given chain now has two different sizes:

$$\langle R^2 \rangle \sim N^{-(2\nu-1)/(d\nu-1)} \quad (\text{inside the blob})$$

$$\langle R^2 \rangle \sim N \quad (\text{outside the blob})$$

APPENDIX B CORRELATION FUNCTION

Let x and y be two independent variables and $P_1(x)$ and $P_2(y)$ be probability density distributions. Then the joint probability distribution of x and y , $P(x, y)$, is related to $P_1(x)$ and $P_2(y)$ by

$$P(x, y) \, dx \, dy = P_1(x)P_2(y) \, dx \, dy$$

If, however, x and y are not independent, then $P_1(x)$ and $P_2(y)$ can still be correlated provided that there exists a function $g(x, y)$, called the correlation function, such that

$$P(x, y) \, dx \, dy = P_1(x)P_2(y)g(x, y) \, dx \, dy$$

Example 1

Consider the expression

$$\int_0^t e^{-\zeta(t-t')/m} f(t') dt'$$

where ζ is the frictional coefficient, m is the mass, and t and t' are different times. Neither t nor t' is an independent variable; $t - t'$ is a variable of interest. Let $\rho = t - t'$. Then

$$\int_0^t e^{-\zeta(t-t')/m} f(t') dt' = \int_0^t e^{-\zeta\rho/m} f(t - \rho) d\rho$$

We introduce another dummy variable σ such that

$$\sigma = t - t'$$

Although both ρ and σ are expressed in terms of $t - t'$, they are not equal; they are two different variables. Squaring the function, we obtain

$$\int_0^t d\rho \int_0^t d\sigma e^{-\zeta\rho/m} e^{-\zeta\sigma/m} \langle f(t - \rho) f(t - \sigma) \rangle$$

If we impose a condition that $f(t)$ is random, then the function $\langle f(t - \rho) f(t - \sigma) \rangle$ depends only on the time interval $|\rho - \sigma|$. We now have

$$g(|\rho - \sigma|) \equiv \langle f(t - \rho) f(t - \sigma) \rangle$$

The function in the form $\langle f(t - \rho) f(t - \sigma) \rangle$ is called the autocorrelation function. It involves double integrals.

Example 2

Let the two functions be

$$x_1(t) = \int_0^t f(t') dt' \quad x_2(t) = \int_0^t f(t'') dt''$$

Here t , t' , and t'' are not true independent variables, but the time interval $|t'' - t'|$ is. The parameter t'' is equivalent to ρ and t' is equivalent to σ in the previous example. Hence, the functions Δx_1 and Δx_2 are correlated by

$$\langle [\Delta x(t)]^2 \rangle = \int_0^t dt' \int_0^t dt'' \langle f(t') f(t'') \rangle$$

Again, if t is completely at random, the expression $\langle f(t')f(t'') \rangle$ is the correlation function. If $\sigma \equiv t'' - t'$, we can write the autocorrelation function (Berry et al., 1980) as

$$g(f) \equiv \langle f(t')f(t' + \sigma) \rangle = \langle t(0)t(\sigma) \rangle = \langle f(t' - \sigma)f(t') \rangle$$

REFERENCES

- Berry, R. S., S. A. Rice, and J. Ross, *Physical Chemistry*, New York: Wiley, 1980.
- Chandrasekhar, S., *Rev. Mod. Phys.* **15**, 1 (1943).
- de Gennes, P. G., *J. Chem. Phys.* **55**, 572 (1971).
- de Gennes, P. G., *Phys. Lett. A* **38**, 399 (1972).
- de Gennes, P. G., *J. Phys. Lett.* **36**, L-55 (1975).
- de Gennes, P. G., *Macromolecules* **9**, 564 (1976).
- de Gennes, P. G., *Scaling Concepts in Polymer Physics*. Ithaca, NY: Cornell University Press, 1979.
- Doi, M., and S. F. Edwards. *J. Chem. Soc. Faraday Trans. II*, **74**, 1789, 1802, 1818 (1978).
- Doi, M., and S. F. Edwards, *The Theory of Polymer Dynamics*, New York: Oxford University Press, 1988.
- Edwards, S. F., *Proc. Phys. Soc. London* **85**, 613 (1965); **88**, 265 (1966).
- Feller, W., *An Introduction to Probability Theory and Its Applications*. New York: Wiley, 1950.
- Fixman, M., *J. Chem. Phys.* **23**, 1656 (1955).
- Flory, P. J., *Principles of Polymer Chemistry*. Ithaca, NY: Cornell University Press, 1953.
- Flory, P. J., *Statistical Mechanics of Chain Molecules*. New York: Interscience, 1969; Hanser Publishers, new edition, 1989.
- Flory, P. J., *Science* **188**, 1268 (1975).
- Freed, K. F., *Renormalization Group Theory of Macromolecules*. New York: Wiley, 1987.
- Graessley, W. W., *Adv. Polym. Sci.* **16**, 1 (1974).
- Grimley, T. B., *Proc. R. Soc. London Ser. A* **212**, 339 (1952).
- Hermans, J. J., *Rec. Trav. Chim.* **69**, 220 (1950).
- Kac, M., *Am. Math. Monthly* **54**, 369 (1947).
- Kratky, O., and G. Porod, *Rec. Trans. Chim.* **68**, 1106 (1949).
- Kuhn, W., *Ber.* **63**, 1503 (1930).
- Kurata, M., *J. Polym. Sci. A* **2-6**, 1607 (1968).
- Leger, L., H. Hovel, and F. Rondelez, *Macromolecules* **14**, 1732 (1981).
- Mandelbrot, B. B., *The Fractal Geometry of Nature*. New York: Freeman, 1982.
- Mayer, J. E., and M. G. Mayer, *Statistical Mechanics*. New York: J Wiley, 1940.
- McMillan W. G., and J. E. Mayer, *J. Chem. Phys.* **13**, 276 (1945).
- Miyaki, Y., Y. Einaga, and H. Fujita, *Macromolecules* **6**, 1180 (1978).
- Nierlich, M., J. P. Cotton, and B. Farnoux, *J. Chem. Phys.* **69**, 1379 (1978).

- Noolandi, J., G. W. Slater, H. A. Lim, and J. L. Viovy, *Science* **243**, 1456 (1989).
 Perkins, T. T., D. E. Smith, and S. Chu, *Science* **275**, 2016 (1997).
 Perzynski, R., M. Adam, and M. Delsanti, *J. Phys.* **43**, 129 (1982).
 Smith, D. E., H. P. Babcock, and S. Chu, *Science* **283**, 1724 (1999).
 Stauffer, D., *Introduction to Percolation Theory*. London: Taylor & Francis, 1985.
 Sun, S. F., C. C. Chow, and R. A. Nash, *J. Chem. Phys.* **93**, 7508 (1990).
 Sun, S. F., and J. Fan, *Polymer* **34**, 655 (1993).
 Sun, S. F., and J. Fan, *Polymer* **38**, 563 (1997).
 Ursell, H. D., *Proc. Cambridge Phil. Soc.* **23**, 685 (1927).
 Uspensky, J. V., *Introduction to Mathematical Probability*. New York: McGraw-Hill, 1937.
 Wilson, K. G., *Phys. Rev. B* **4**, 3174, 3184 (1971).
 Yamakawa, H., *Modern Theory of Polymer Solutions*. New York: Harper & Row, 1971.
 Yamakawa, H., and M. Fujii, *Macromolecules* **7**, 128 (1974).
 Zimm, B. H., *J. Chem. Phys.* **14**, 164 (1946).
 Zimm, B. H., W. H. Stockmayer, and M. Fixman, *J. Chem. Phys.* **21**, 1716 (1953).

PROBLEMS

- 5.1** The distribution for a random chain in one dimension (random walk) may be expressed in the form of Bernoulli's equation:

$$w(n, m) = \left(\frac{1}{2}\right)^n \frac{n!}{[(n+m)/2]![(n-m)/2]!}$$

where $w(n, m)$ is the probability of m displacements out of n steps. Using Stirling's formula,

$$n! = \sqrt{2\pi} \frac{n^{n+1/2}}{e^n}$$

show that Bernoulli's equation can be converted to

$$w(n, m) = \left(\frac{2}{\pi n}\right)^{1/2} \left[1 - \left(\frac{m}{n}\right)^2\right]^{-(n+1)/2} \left(\frac{1 - m/n}{1 + m/n}\right)^{m/2}$$

which, in turn, can be converted to a Gaussian distribution function (or normal error function):

$$w(n, m) = \left(\frac{2}{\pi n}\right)^{1/2} e^{-m^2/2n}$$

Assume that $|m/n| \ll 1$. *Hint:* $(1 + x)^m = 1 + mx + \dots \quad x \ll 1$:

$$\lim_{h \rightarrow 0} (1 + h) \frac{1}{h} = e$$

5.2 Suppose a person walks from the origin in one dimension one unit step each, forward or backward. The probability for each direction is $\frac{1}{2}$. Find the probability function of the person being at each of the possible points between $-n$ and n (where n is the number of total steps). *Hint:* $x = \sum_{i=1}^n x_i$, where x is the net displacement after n steps and x_i are the individual steps.

5.3 Show that the root-mean-square end-to-end distance is

$$\langle R^2 \rangle^{1/2} = N^{1/2} a$$

if the probability function $w(R)$ for an ideal polymer chain (random-flight chain) is given by

$$w(R) = \left(\frac{3}{2\pi Na^2} \right)^{3/2} \exp\left(\frac{-3R^2}{2Na^2} \right)$$

5.4 Show that for wormlike chains

$$\begin{aligned} \lim_{\lambda L \rightarrow \infty} \langle R^2 \rangle &= \frac{L}{\lambda} && \text{for random flights} \\ \lim_{\lambda L \rightarrow 0} \langle R^2 \rangle &= L^2 && \text{for rods} \end{aligned}$$

(*Source:* Yamakawa, 1971.)

5.5 (a) For the random-flight chain model, Kurata (1968) derived an equation to relate α_R with z :

$$\frac{1}{5}(\alpha_R^5 - 1) + \frac{1}{3}(\alpha_R^3 - 1) = \frac{4}{3}z$$

where

$$\alpha_R = \frac{\langle R^2 \rangle^{1/2}}{\langle R^2 \rangle_0^{1/2}}$$

Show that at large z

$$\alpha_R^2 = (\text{const})z^{2/5}$$

(b) The parameter z is defined as

$$z = \left(\frac{1}{4\pi} \right)^{3/2} \frac{\beta}{M_0^2 A^{3/2}} M^{1/2},$$

where A' is a constant and β is the binary cluster intergral. Since z is proportional to $M^{1/2}$ for a given polymer-solvent system, the plot of α_R^2 versus $M^{1/5}$ should be linear. Plot the following data of polystyrene in benzene to test the theory:

In benzene at 25°C		In cyclohexane at 34.5°C	
MW $\times 10^{-6}$	$\langle R^2 \rangle^{1/2}$ (nm)	MW $\times 10^{-6}$	$\langle R^2 \rangle_0^{1/2}$ (nm)
56	50	55	22
39	39	38	18
31	35	32	16
23	29	23	14
15	23	15	11
9	16	9	87

(c) An empirical equation was suggested where by

$$\alpha_R^2 = (1.64)z^{2/5}$$

Plot $(1.64)z^{2/5}$ versus $z^{2/5}$ for z from 6 to 40 and read the values of z for α_R^2 in part (b) (Miyaki, 1978).

- 5.6** The radius of gyration for a polystyrene (MW 30×10^6) in benzene solution was found to be 1010 Å in a semidilute solution. Estimate the overlapping concentration c^* in grams per cubic centimeters.
- 5.7** The theoretical equation of the end-to-end distance $R(\rho)$ for a polymer in a semidilute solution may be expressed in the form

$$R^2(\rho) = \frac{N}{\rho(\xi)} \xi^2 \sim N\rho^{(1-2\nu)/(\nu d-1)}$$

Show that this equation can be reduced to an equation that can be tested experimentally in the form

$$R^2(c) \sim M_w c^{-1/4} \quad \text{for } d = 3$$

that is,

$$\frac{R^2(c)}{M_w} \sim c^{-.25}$$

Note: $\rho(\xi) \sim \xi^{1/\nu}$.

6

LIQUID CRYSTALS

A liquid crystal is a special kind of material. It is a liquid because it is a fluid, but it is also a crystal because it is an ordered solid. It is a material in a state between liquid and solid. The simplest kind of liquid crystal consists of a single semirigid or mesogenic core attached to one or two terminal alkyl chains. It is the anisotropic interaction between the cores, normally of phenyl rings through short unsaturated linkages, that results in the liquid-crystal behavior.

It is well known that matter exists in three different states depending upon the temperature: solid, liquid, and gas. Between the crystalline solid and the isotropic liquid (normal, isotropic liquid) there actually exists a series of transitions as temperature increases, giving rise to several new phases. These new phases have mechanical, optical, and structural properties and are referred to as liquid-crystalline phases. Materials isolated from these phases are liquid crystals. A liquid crystal may, therefore, be as an intermediate phase or mesomorphic (meaning in between) phase which has liquidlike order in at least one direction and possesses a degree of anisotropy (also a kind of order).

There are two major ways to describe the arrangement of molecules in a liquid crystal:

1. *Orientalional order*—the symmetry axes of the ordering objects parallel to a well-defined spatial direction, \vec{n} , called the director
2. *Positional order*—an integer number of lattice translational vectors which makes the system invariant under translation

In the crystalline state, the constituent molecules or ions are ordered in their orientation or position or both. The liquid-crystal materials combine the properties of both the crystalline state (optical and electrical anisotropy) and the pure liquid state (fluidity).

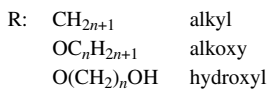
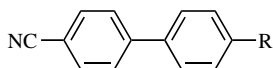
Although liquid crystals have been known for at least two decades, it is only in the last four or five years that these materials have become hot subjects both in academia and in industry.

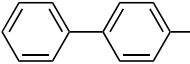
6.1 MESOGENS

Liquid-crystalline molecules are also called mesogens. It is the mesogenic core (phenyl rings) that is responsible for the packing of the molecules in an ordered arrangement and for the geometry (e.g., anisotropy, rigidity) of the compounds. There are various kinds of mesogens which contain six-member rings interlinked at para positions. At least one of them is the aromatic ring. The following lists some typical ones.

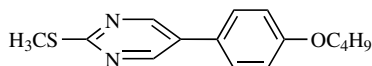
1. Mesogens that contain two rings:

a. Two aromatic rings:



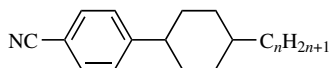
The group  is a cyanobiphenyls. An example is 4'-n-alkyl-4-cyanobiphenyl.

b. One aromatic ring and one pyrimidine ring:



for example, 2-methylthio-5-(4'-n-butyloxyphenyl)pyrimidine. (*Note:* Here n means normal.)

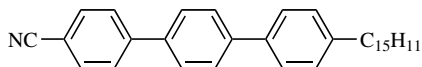
c. One aromatic and one aliphatic ring:



for example, *trans*-4-*n*-alkyl-(4'-cyanophenyl)cyclohexanes.

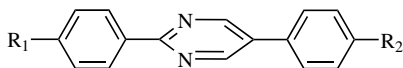
2. Mesogens that contain three rings:

a. Three aromatic rings:



for example, 4-cyano-4'-*n*-pentyl-*p*-terphenyl.

b. Two aromatic rings and one pyrimidine ring:

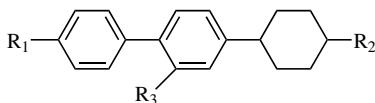


R₁: H₉C₄O-

R₂: -H

for example, 2,5-diphenyl pyrimidines.

c. Two aromatic and one aliphatic rings:



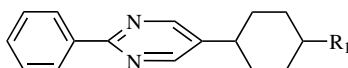
R₁: -H

R₂: -C₃H₃

R₃: -H

for example, biphenylcyclohexanes.

d. One aromatic ring, one pyrimidine ring, and one aliphatic ring:

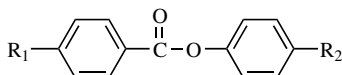


R₁: H₅C₂-

for example, 5-(4'-alkyl-cyclohexyl)-2-(4''-cyanophenyl)pyrimidines.

3. Mesogens that contain functional groups between the rings:

a. Phenyl benzoates:

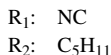
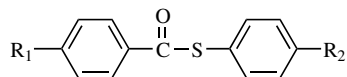


R₁: H₁₁C₅ or NC

R₂: CN

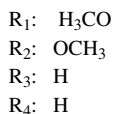
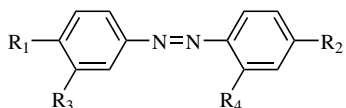
for example, mesogenic phenyl benzoates.

b. Phenyl thiobenzoates:



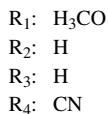
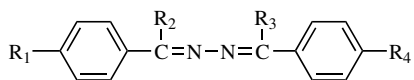
for example, mesogenic phenyl thiobenzoates.

c. Azo and azoxyl compounds:



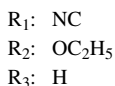
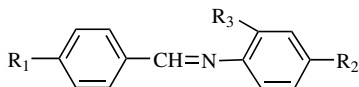
for example, mesogenic azo and azoxy compounds.

d. Azines:



for example, mesogenic azines.

e. Benzylidene anilines:



for example, mesogenic benzylidene anilines.

6.2 POLYMERIC LIQUID CRYSTALS

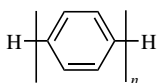
Polymeric liquid crystals consist of mesogenic subunits which are connected together with flexible links forming what are known as the main-chain polymer

liquid crystals. Alternatively, the mesogenic subunits can be attached to the polymer chains as side groups. These are known as side-chain polymer liquid crystals. In addition, there is another class called segmented-chain polymer crystals.

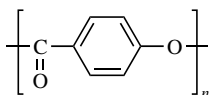
The segmented chains may contain mesogenic compounds in repeating units or low-molecular-weight liquid crystals (LMWLCs) in repeating units. The segmented chains can also be in the form of main chains and side chains. We begin with the description of LMWLCs and then extend to main-chain, side-chain and segmented-chain liquid polymers in that order.

6.2.1 Low-Molecular-Weight Liquid Crystals

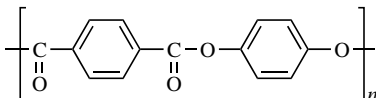
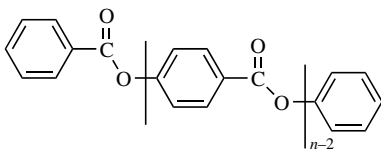
LMWLCs are often used as models for theoretical calculations and experimental observations of the behavior of liquid-crystalline polymers. Several homologous series of mesogenic compounds are classified as LMWLCs. Among them are



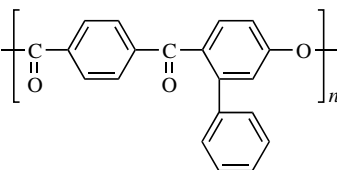
$n = 4,5,6$
p-Phenylene series



$n = 3,4,5$
poly (*p*-oxybenzoate) series



poly (1,4-phenylene terephthalate)



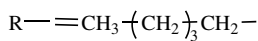
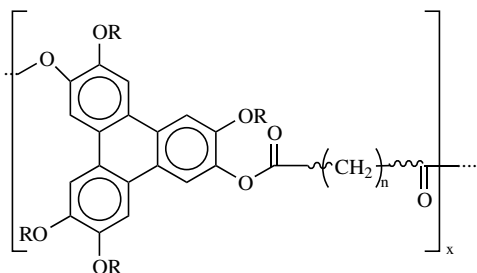
poly (1,4-phenylene terephthalate)

6.2.2 Main-Chain Liquid-Crystalline Polymers

The main-chain liquid crystalline polymers are polymers in which the anisometric units are aligned head to tail:

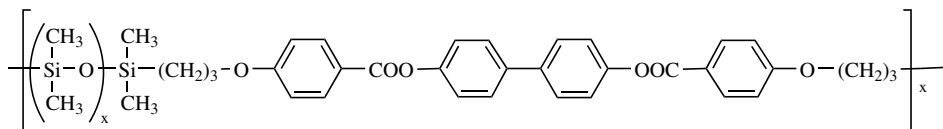


The main chain as a whole functions as the mesogen. Examples are



n 10, 14, 20

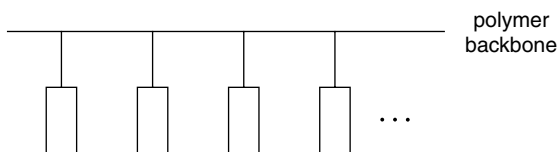
main chain polyester



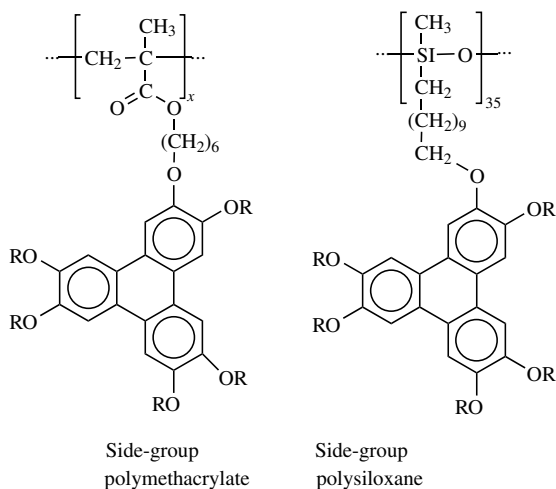
polysiloxanes

6.2.3 Side-Chain Liquid-Crystalline Polymers

These are polymers that have mesogenic moieties linked as side groups to the polymer:



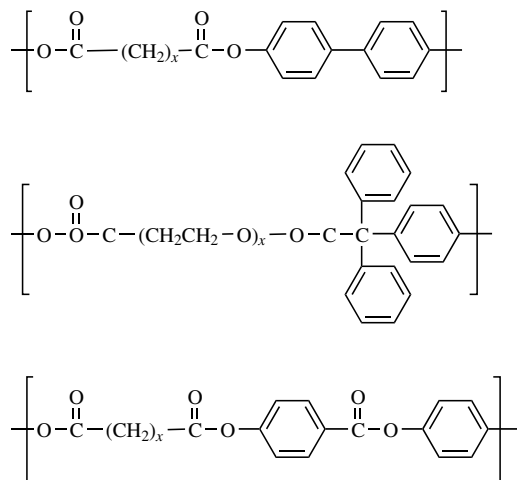
Examples are



6.2.4 Segmented-Chain Liquid-Crystalline Polymers

These are liquid-crystalline polymers consisting of an alternate sequence of rigid and flexible molecular sections. Virtually all segmented-chain liquid-crystalline polymers are polycondensated.

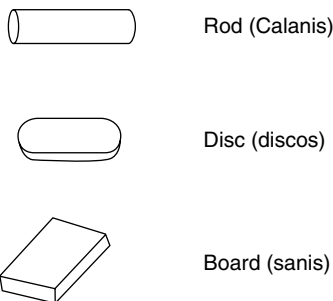
Examples are



6.3 SHAPES OF MESOGENS

The shapes of mesogens are classified into three types: rodlike, dislike, and boardlike. Among the three, the first two are more common than the third.

Diagrams of the three shapes are shown below:



The Greek expressions are given in parentheses.

Rodlike mesogenes have an elongated anisotropic geometry which allows for preferential alignment along one spatial direction. They are the core of liquid crystals. At either end are terminal groups, one of which is usually a long alkyl, acyl, or alkoxy chain.

Discotics are flat disclike mesogens consisting of a core of adjacent aromatic rings. This allows for mesophases based on columnar ordering (see next section).

Boardlike molecules do not show rotational symmetry about any axis at all, nor about the long axis as in rods or about the short axis as in discs.

6.4 LIQUID-CRYSTAL PHASES

6.4.1 Mesophases in General

Mesophases are related to the geometry and structure of the compound. The transitions from crystal to liquid may be classified into four different phases. They also represent four different stages, each of which is influenced by temperature. Figure 6.1 shows a diagram of these four phases.

The straight short lines represent the molecules. In terms of the two characteristic properties of liquid crystals, order and mobility, the two extremes among the four phases are the crystal phase and the liquid phase. The crystal phase is the one that is well ordered and the liquid phase is the one that is disordered. The two liquid-crystal phases, also known as mesophases, are ranked between the two extremes. The smectic phase is more ordered than the nematic phase. By contrast, increasing mobility runs in the opposite direction. A crystal has no mobility whereas a liquid has high mobility. Both mesophases are mobile, with nematic more so than smectic. Figure 6.1 also illustrates that crystal and liquid phases are isotropic, meaning that no direction is involved in the order and mobility. The two mesophases are anisotropic; that is, both have direction. This is particularly true in the nematic phase. The properties of the nematic phase are very sensitive to direction.

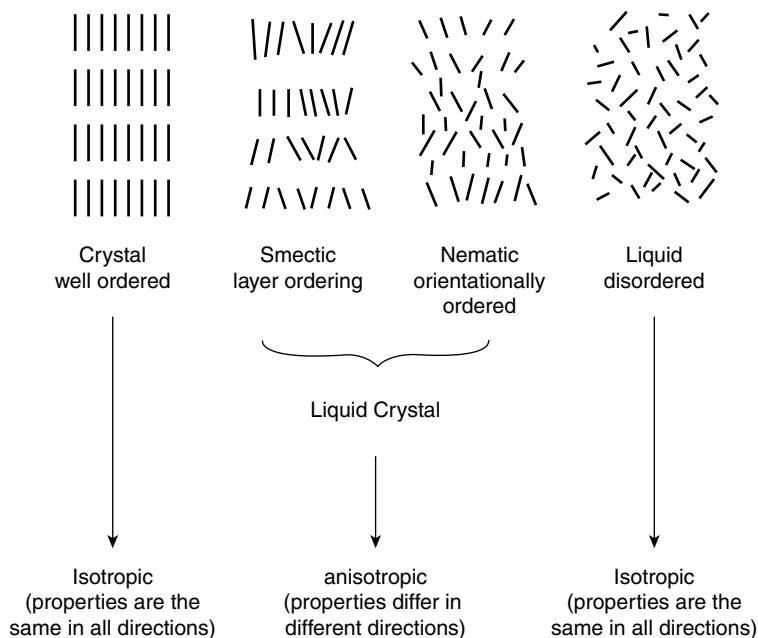


FIGURE 6.1 Diagram of phases.

6.4.2 Nematic Phase

The nematic phase is the simplest mesophase. It is described by the director n and the orientational order parameter S . In the nematic phase, the mesogens are arranged in such a way that their long axes lie preferentially in one direction (long-range orientational order). The long-range orientational order is responsible for the characteristic differences with respect to their isotropic melt. If the constituent compound is racemic, it is possible to form another phase from the enantiomerically pure compound. This is chiral nematic.

6.4.3 Smectic Phase

The smectic phase has at least two unique directions, the director and the layer normal. Eleven types of smectic mesophases have been identified, ranging from smectic A to smectic K. They differ in the arrangement of the mesogens within each individual layer. For example, in the smectic-A phase, these two directions are collinear (orientational order), whereas in the smectic-C phase the director could make an angle with the layer normal (positional order). In addition to orientational order and positional order which we have just mentioned, there is another order called bond orientation order. There are several smectic phases which contain this order and they are called hexatic smectics.

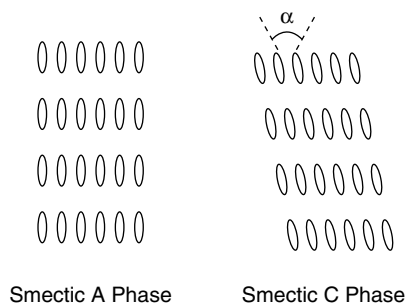


FIGURE 6.2 Rodlike molecules: (a) smectic-A phase, rods not tilted; (b) smectic-C phase, rods tilted, tilt angle α between long axis and layer normal.

6.4.3.1 Smectic A and Smectic C Smectic-A phase and smectic-C phase are of particular interest to us, for they have been thoroughly studied and well documented in the literature. Figure 6.2 shows a diagram of the structures of the two mesophases.

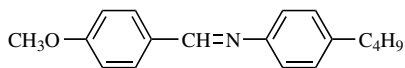
In the smectic-A phase the molecules are oriented on average in a direction perpendicular to the layers, whereas in the smectic-C phase the director is tilted with respect to the layer normal. The tilted smectic-C phase has been compared to superfluid helium, and the smectic A–smectic C transition is predicted to exhibit critical behavior similar to that of helium.

6.4.4 Compounds Representing Some Mesophases

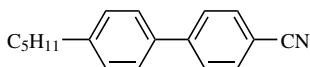
The following is a short list of some mesophases which are known in literature and commercially available:

- Single mesophase:

Nematic:

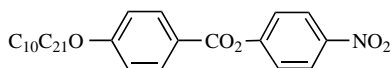


N-(4-Methoxybenzylidene)-4-butylaniline



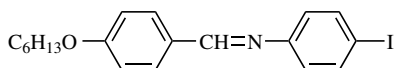
4'-Pentyl-4-biphenylcarbonitrile

Smectic A:

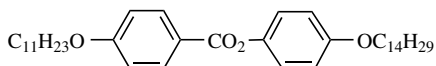


p-Nitrophenyl-*p*-decyloxybenzoate

Smectic B:

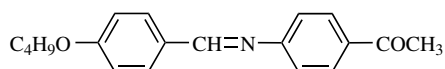


Smectic C:

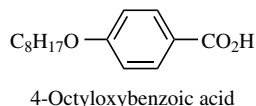
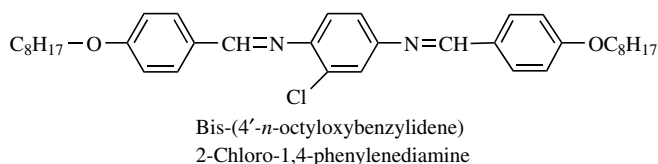


- Two mesophases:

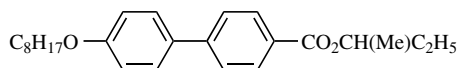
Nematic and smectic A:



Nematic and Smectic C:



Smectic A and smectic C:



6.4.5 Shape and Phase

The three different shapes (rodlike, disclike, boardlike) and two different mesophases (nematic and smectic) together form six different kinds of crystals. They are rodlike nematic, discotic nematic, boardlike nematic, rodlike smectic, discotic smectic, and boardlike smectic. Figure 6.3 shows these six combinations.

Among the six combinations, the discotic smectic deserves special attention. Besides being a smectic mesophase, it often forms columns and hence is also called columnar mesophase. Many of the columnar phases have symmetry resulting from ordered side-to-side packing with or without ordering in the column. In the discotic smectic hexagonal phase, the molecules define columns which are packed together in a hexagonal manner. This is also found in the discotic smectic rectangular and oblique phases where the columns are packed in a rectangular or oblique manner.

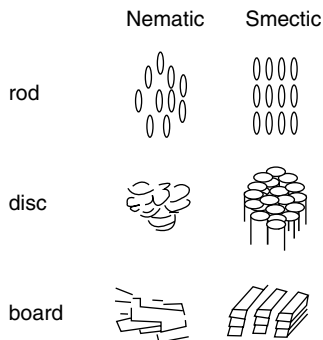


FIGURE 6.3 Combination of shape and phase.

The columnar mesophases possess the property of self-assembly of columns of indefinite length. Hence, they also belong to the class of supramolecules.

6.4.6 Decreasing Order and ΔH of Phase Transition

Decreasing order follows the sequence

Crystal > smectic C < smectic B < smectic A < nematic < I (isotropic liquid)

Correspondingly, ΔH , in kilojoules per mole of phase transition between two phases, is influenced as observed by the decreasing order:

Crystal-I	117.3
Smectic C-I	43.7
Nematic-I	9.64

The inter-mesophase transitions are

Smectic B-smectic C	10.5
Smectic C-nematic	9.64
Smectic A-nematic	4.61
Smectic B-smectic A	4.61

Experimental determinations of phase transition are based upon thermal analysis: classical adiabatic calorimetry (CAC), differential thermal analysis (DTA), and differential scanning calorimetry (DSC).

6.5 THERMOTROPIC AND LYOTROPIC LIQUID CRYSTALS

Polymers may exhibit the behavior of liquid-crystal order either in melt (thermotropic liquid crystals) or in solution (lyotropic liquid crystals). In thermotropic liquid crystals, the phases of the liquid crystals may be observed to change as temperature is increased. In lyotropic liquid crystals, the ordered crystalline state is

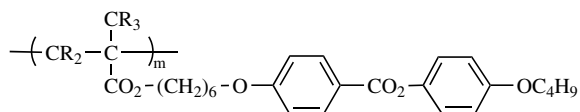
disrupted less by temperature than by the addition of the solvent, that is, changing concentrations.

Thermotropic liquid crystals are controlled by the melting temperature T_m and by the isotropic temperature T_i for the stability of mesophases. In certain cases, a glass temperature T_g rather than a melting temperature T_m may be observed before the isotropic temperature T_i . The mesophases of thermotropic liquid-crystalline polymers are formed in pure compounds or in polymer melt. Their properties are essentially based upon rodlike mesogenic moieties polymerized together with small flexible chains, that is, the main-chain or side-chain polymers.

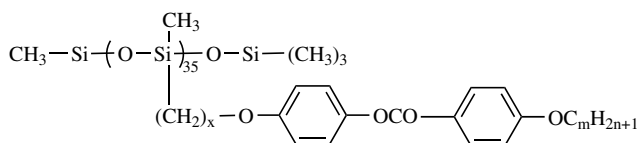
Lyotropic liquid crystals are formed by solutions. They undergo a spontaneous transformation from an isotropic to an anisotropic (nematic or smectic) ordered solution above certain threshold concentrations which are a function of their molecular axial ratio (length L to diameter D).

Surfactants (e.g., soaps and detergents) form micelles. If the concentration of a surfactant is increased above the micelle critical concentration, the density of the micelles becomes sufficiently large that they begin to form ordered arrays. These ordered arrays correspond to lyotropic liquid crystals. Different mesophases result from different micelle types. Spherical micelles in general give rise to cubic closed-packed phases. Rodlike micelles give rise to hexagonal mesophases and disc mesophases give rise to lamellar phases. A variety of additional phases are based on bilayer structures ranging from the flat lamellar phases to the highly convoluted bicontinuous phases; many are of cubic symmetry in which the interface is curved.

Examples of thermotropic liquid crystals are

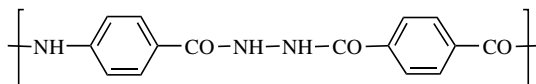


PMA (H,D) OC₄H₉

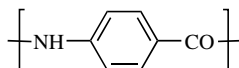


Polysiloxanes

Those of lyotropic liquid crystals are



Polyterephthalamide of *p*-aminobenzhydrazide



Poly(*p*-benzamide)

DNA, TMV (tobacco mosaic virus)

6.6 KERR EFFECT

In electric fields, liquid crystals react by reflecting light to display certain colors. This is the basis for the manufacturing of liquid-crystal display screens in the electronics industry. This phenomenon can be explained in terms of the Kerr effect.

In 1875, J. Kerr observed that if a transparent isotropic substance is placed in a stationary electric field, it becomes optically anisotropic and doubly reflecting because the electric field tends to bring about a definite orientation of the molecules.

The Kerr effect may be described as follows. Let b_1 , b_2 , and b_3 be the three imaginary principal axes at right angles. The mean molar polarizability of the molecule α is defined as

$$\alpha = \frac{1}{3}(b_1 + b_2 + b_3)$$

The anisotropy of liquid crystals is related to the constant K , now called the Kerr constant:

$$K = \frac{(n^2 - 1)(n^2 + 2)}{4n^2} \frac{\theta_1 + \theta_2}{2} \left(\frac{D + 2}{3} \right)^2$$

where n is the refractive index and D is the dielectric constant. The terms θ_1 and θ_2 are the anisotropy and dipole, respectively. The term θ_1 is given by the equation

$$\theta_1 = \frac{1}{2kT} \frac{(n_0 - 1)(n - 1)}{(\pi N_A \rho / m)^2} \frac{\Delta}{6 - 7\Delta}$$

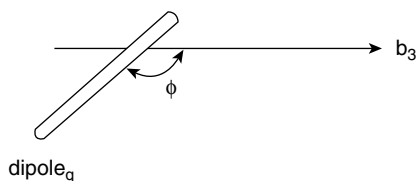
where k is the Boltzmann constant, ρ is the density of the liquid crystal, M is its molecular weight, N_A is Avogadro's number, n_0 is the refractive index for infinite wavelength, and Δ is the depolarization factor:

$$\Delta = \frac{I_{11}}{I_1}$$

where I_{11} is the intensity of the ray with vibration parallel to the incident light and I_1 with vibration perpendicular to that direction. The term θ_2 is expressed in another equation as

$$\theta_2 = \frac{1}{45k^2T^2} \mu^2 [(3 \cos^2 \phi - 1)(b_3 - b_1)]$$

where μ is the dipole moment and ϕ is the angle of μ with the axis b_3 :



In the current approach, the term $3 \cos^2 \phi - 1$ is called the nematic orientation parameter.

Although the Kerr effect is a classical subject well discussed in physics, its significance has gained importance in industry only recently. It is now used to assist in the understanding of the wide application of liquid crystals in modern devices such as computer screens and watch tops.

6.7 THEORIES OF LIQUID-CRYSTALLINE ORDERING

Most theories of the polymeric nematic phase are based upon the model in which the liquid crystal is considered as a packed system interacting through its hard-core diameters. Historically, attention was first focused on lyotropic liquid crystals. The binary collision or second virial approximation is taken into account at low volume fractions. A slightly different approach is to use a scaling law to describe the fluctuation of nematic order parameters. In this section we select three different methods to represent the three different treatments.

6.7.1 Rigid-Rod Model

The first molecular theory of liquid-crystalline ordering was proposed by Onsager on a solution of cylindrical, long, rigid rods. The theory may be described as follows. Let N_2 be the number of rods in a volume V . Each rod has length L and cross-sectional area d . The volume fraction of rods, v_2 , in the solution can be calculated as

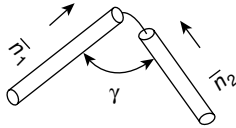
$$v_2 = \frac{1}{4}\pi c L d^2$$

where c is the concentration of the rods. Let $f(\mathbf{n})$ be the orientational distribution function for the rods, where \mathbf{n} is the direction vector; then $c f(\mathbf{n}) d\Omega_n$ is the number of rods per unit volume with direction lying within the bounds of the small solid angle $d\Omega_n$. In the isotropic state, all directions are identical and $f(\mathbf{n}) = \text{const} = 1/4\pi$. In a liquid-crystalline nematic phase, $f(\mathbf{n})$ is a function with a maximum along the free energy of the solution of rods. Onsager proposed a formula for the free energy of the solution of rods F in the following form:

$$G = N_2 T \left[\ln c + \int f(\mathbf{n}) \ln [4\pi f(\mathbf{n})] d\Omega_n \right. \\ \left. + \frac{c}{2} \int f(\mathbf{n}_1) f(\mathbf{n}_2) B(\gamma) d\Omega_{n_1} d\Omega_{n_2} \right]$$

The first term is the free energy of the translational motion of the rods; the second term is the loss of orientational entropy, and the last term the free energy of interaction of the rods in the second virial approximation. The term $B(\gamma)$ is the

second virial coefficient of interaction of rods and is the central focus of the theory. The long axes of the two interaction rods are specified by the unit vectors \mathbf{n}_1 and \mathbf{n}_2 which form an angle γ with each other:



When only steric interactions of the rods are present, the term $B(\gamma)$ is expressed as

$$B(\gamma) = 2L^2d \sin \gamma$$

The next step is to find the equilibrium distribution function of $f(\mathbf{n})$. Onsager used a standard approximation method, namely, the variation principle (well known in mathematical physics) to attack the problem. Taking h as a variational parameter, a new angle θ is defined between \mathbf{n} and the direction of the anisotropy axis. He then took as a trial function

$$f(\mathbf{n}) = F(h \cos \theta)$$

to study the transition between the isotropic phase and the nematic phase. All these lead to the equations of pressure π and chemical potential μ respectively:

$$\pi = \frac{(c^2/N_2) \partial F}{\partial c}$$

$$\mu = \frac{F + c \partial F / \partial c}{N_2}$$

The final purpose is to calculate the quantity of v_2 :

At $v_2 < v_2^i$ the solution is isotropic.

At $v_2 > v_2^a$ it is anisotropic.

At $v_2^i < v_2 < v_2^a$ the solution separates into isotropic and anisotropic phases, the values of v_2^i and v_2^a being

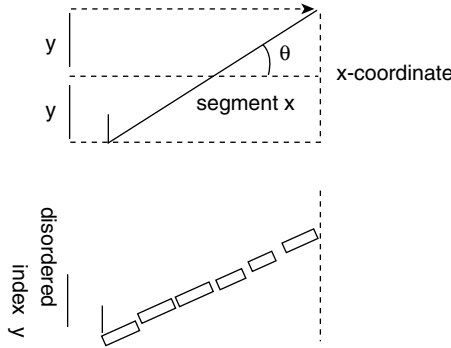
$$v_2^i = 3.34 \text{ d/L} \quad v_2^a = 4.49 \text{ d/L}$$

6.7.2 Lattice Model

This is Flory's approach to the problem of lyotropic liquid crystals. The ordering transition of a system of rodlike molecules from an isotropic state to an ordered nematic state is treated in terms of lattice models. Essentially, it is the evaluation of the partition function (see p. 215). As with Onsager's approach, in this model steric

repulsions between the anisotropic molecules are principally responsible for order in liquid-crystalline systems.

Consider a system of rods having an orientation with respect to a preferred axis measured by an angle of inclination θ . The rods are broken up into a sequence of y consecutive submolecules. The diagram of the model is as follows:



The relationship between the disordered index y and the number of segments x and angle θ is

$$y = x \sin \theta$$

Subdividing the molecule into a succession of structural entities, the segments each occupies one cell of the lattice.

The principal step for evaluating the partition function is in estimating the expectation v_{i+1} that a sequence of empty lattice sites is vacant when j molecules have already been inserted into the lattice containing n_0 sites. The molecules can be represented by hard bodies of appropriate size and shape whose only interactions with each other are repulsions. After i molecules have been assigned, the quantity v_{i+1} is found to be

$$v_{i+1} = (n_0 - ix) \left(\frac{n_0 - ix}{n_0} \right)^{y_{i+1}-1} \left(\frac{n_0 - ix}{n_0 - ix + \sum_{j=1}^i y_j} \right)^{x-y_{i+1}}$$

The partition function Z for a system consisting of n_2 molecules is

$$Z = \frac{Z_c}{n_2!} \prod_1^{n_2} v_j$$

where Z_c is the intramolecular chain configuration partition function. From the equation of v_{i+1} and Z , we can now obtain

$$\begin{aligned} -\ln Z &= n_s \ln v_s + n_x \ln \left(\frac{v_x}{x} \right) - n_s \ln \left[1 - v_x \left(1 - \frac{\bar{y}}{x} \right) \right] \\ &\quad + n_x (\bar{y} - 1) - n_x \ln (f_1 \sigma) \end{aligned}$$

where

$$v_s = \frac{n_s}{n_s + n_x x} \quad (\text{volume fraction of solvent})$$

$$v_x = \frac{n_x x}{n_s + n_x x} \quad (\text{volume fraction of segments})$$

The subscripts s and x being solvent and segment, respectively. The term f_1 is a normalization constant in the mathematical calculation and the term σ is an arbitrary constant.

The equation of $-\ln Z$ gives the free energy G of a system of n_x rigid rods immersed in a solvent containing n_s molecules at orientational, equilibrium, with the ordering being measured by the disordered index y . The term \bar{y} is the mean value of the disorder index y defined by

$$\bar{y} = \sum \frac{n_{xy} y}{n_x}$$

where n_{xy} is the orientational distribution specifying the fraction of the molecules with disorientation y . Partial differentiation of G with respect to n_s and n_x leads to the two important equations from which we can calculate the concentrations in terms of volume fractions: v_s^a , v_s^i , v_x^a , and v_x^i . The two equations are

$$\ln \left(\frac{v_s^a}{v_s^i} \right) = \left(1 - \frac{1}{x} \right) v_x^i - \frac{(\bar{y} - 1) v_x^a}{x} + \ln \left[1 - v_x^a \left(1 - \frac{\bar{y}}{x} \right) \right]$$

$$\ln \left(\frac{v_x^a}{v_x^i} \right) = (x - 1) v_x^i - (\bar{y} - 1) v_x^a + \ln f_1$$

The integral f_p may be evaluated according to the equation

$$f_p = \int_0^{\pi/2} \sin^p \Theta \exp(-\alpha \sin \Theta) d\Theta$$

with $p = 1, 2, 3$. Once f_1 (with $p = 1$) has been evaluated, the average value of y and the nematic order parameter S can be calculated using the equations

$$\bar{y} = \frac{(4/\pi) x f_2}{f_1} \quad \langle \sin^2 \Theta \rangle = \frac{f_3}{f_1} = \frac{2}{3} (1 - S)$$

On the basis of lattice theory, the results for the properties of nematic ordering in solutions of long rigid rods are found to be $v_x^i = 7.89$ d/L and $v_x^a = 11.57$ d/L.

6.7.3 De Genne's Fluctuation Theory

De Gennes explained the pretransitional orientation fluctuations in nematic systems in terms of a phenomenological treatment as far as thermodynamic and structural

properties were concerned. The state behavior of the pretransitional fluctuations in the isotropic phases is described by the free-energy density $G(T, S)$ in the vicinity of this transition, where $G(T, S)$ is a function of both temperature and the scalar nematic order parameter S , which is defined as (see Kerr effect)

$$S = \frac{1}{2}(3 \cos^2 \theta - 1)$$

The function $G(T, S)$ is expressed in the equation

$$G(T, S) = G_0(T) + \left[\frac{1}{2}a(T)\right]S^2 - \left[\frac{1}{3}b(T)\right]S^3 + \left[\frac{1}{4}c(T)\right]S^4$$

The terms a , b , and c are all coefficients. The coefficient c may be negligible, and the coefficient b is nonzero only for symmetry reasons. It is the coefficient $a(T)$ that is the most important in describing the phase transition. De Gennes adopted the Landau treatment and expressed it in a scaling law:

$$a(t) = a_0(T - T^*)^v$$

where T^* is the characteristic temperature at which the isotropic phase and nematic phase begin to separate. In the isotropic state, the exponent v is taken to be 1 and the mean value of the order parameter S is zero. The mean-square value of the order parameter fluctuations $\langle \Delta S^2 \rangle_{s=0}$ behaves as

$$\langle \Delta S^2 \rangle \sim \left(\frac{\partial G}{\partial S^2} \right) \sim [a_0(T - T^*)]^{-1}$$

That is, it diverges as T^* is approached.

De Gennes used a hydrodynamic approach to relate the Kerr relaxation time with the viscosity of the isotropic phase and with the thermodynamic driving force as follows:

$$\tau(T) = \frac{3\eta(T)}{2\alpha_0(T - T^*)}$$

where η is viscosity (see Chapter 8). The basic concepts are the comparison of the time-dependent fluctuations of the order parameter S and the spatial fluctuations of the velocity field. The former seems to be much faster than the latter.

6.8 CURRENT INDUSTRIAL APPLICATIONS OF LIQUID CRYSTALS

Here we discuss the two most hotly pursued areas in the liquid-crystal industry: crystal displays and electronic devices.

6.8.1 Liquid-Crystal Displays

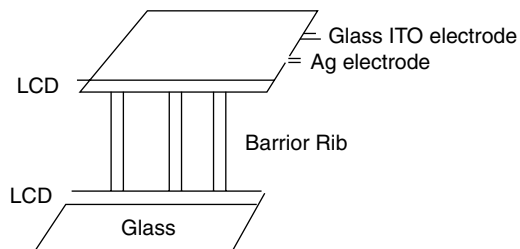
Liquid crystal displays (LCDs) are used in watches, calculators, mobile phones, computer monitors, and flat-screen televisions. Since 1995, plasma display panels (PDPs) had been big business for television manufacturers. Now LCDs are rapidly rising to be a major competitor. Both employ liquid crystals as an important ingredient; PDPs use them as auxiliary components, whereas in LCDs it is the main component.

An LCD consists of a glass sandwiched by two glass substrates each with conducting and alignment coatings and a 5- μm -thick layer of liquid-crystal material such as penty-cyano-biphenyls. This thin layer of liquid crystal is aligned in a particular way by a nematic device. Application of an electric field across a layer of liquid crystal changes the alignment of the liquid crystal and produces a switching effect on polarized light.

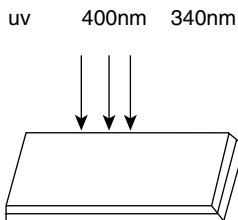
The sandwich construction could be changed into making a paint. This is done by making a mixture of liquid crystal, a polymer-forming monomer, an ultraviolet absorbing dye, and a photo initiator. The mixture is then painted onto the substrate (i.e., a panel). Two exposures to ultraviolet light are carried out, at 400 and 340 nm. The first exposure, at 400 nm, is to create a series of polymer walls and the second, at 340 nm, is to form polymer boxes containing the liquid crystals.

The layered construction and the painting construction are shown in the following diagrams:

(a) Layered construction:



(b) Painting construction:



Two layers form a 20- μm film consisting of a blend of isobornylmethacrylate, stilbene-dimethacrylate, and E7 by photopolymerization-induced

phase separation in the vertical direction. Several different kinds of displays can be made from liquid crystals: single-color passive matrix displays and multi- and full-color displays. The unit will make red-, green-, and blue-light-emitting polymers, enabling full-color displays.

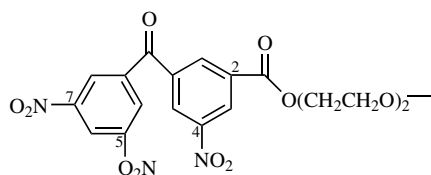
6.8.2 Electronic Devices

Liquid crystals are also used to create electronic devices. This is carried out by synthesizing molecular systems in the form of supramolecules. The synthesis follows designs suitable to meet certain purposes. There are certain mesogens which are supramolecular materials, possessing the property of self-assembling. As mentioned before, dislike mesogens (smectics) are particularly well known for self-organizing into stacks and columns.

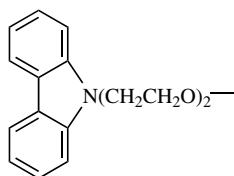
Simple strategies have been developed to program various electronically active molecules into liquid-crystalline columns containing cores with π -stack that display high electron and hole mobility. The technique is similar to that in synthesizing main-chain and side-chain polymers. First choose a suitable mesogen which has a precise ordering of thin crystalline layers and can support the high-charge-carrier (electron and hole) mobility essential for electronic performance. Second select appropriate monomers for the polymers. Third, fuse the mesogen and polymer into the desired liquid-crystalline materials. The electron properties are basically derived from the mesogen, but it is the polymer that makes the device easy to process. The last step is the assembly of all the materials into columns.

The following is an example of manufacturing such an electronic device: The materials are

A1: 4,5,4-Trinitrofluorenone-2-carboxylic acid (TNF)



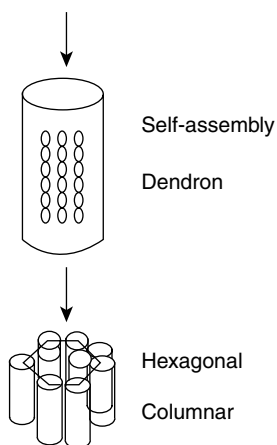
D1: Carbazole



A1 and D1 are self-assembled groups which form D1 + A1 discotic liquid crystals. They assemble into a hexagonal columnar mesophase.

Diagram of the process:

D + A + disordered amorphous polymer containing D and A side groups



Another interesting example in a recent publication [*Nation* **420**, 800 (2002)] is the fabrication of high-efficiency organic light-emitting diodes. Light-emitting centers are cadmium–selenium nanocrystals. The images are generated through fluorescence as electrons make transitions between orbital states of π -conjugated organic molecules. (*Note*: The π bond arises from the overlap of the $2p$ orbitals of electrons in the carbon atom.) The device is in the form of layered construction:



The liquid-crystal materials used are

N, N'-diphenyl-*N, N'*-bis(3methylphenyl)-(1,1'-biphenyl)-4,4'-diamine and 3-(4-biphenyl)-4-phenyl-5-*t*-butylphenyl-1,2,4-triazole.

We may mention a similar device, a multiple-color, tunable organic light-emitting construction. A 12-layer construction is assembled consisting of sequentially stacked layers of metal oxide, amorphous organic, crystalline organic, and metal thin films.

The organic crystalline materials used are

a 650 Å layer of hole-conducting 4,4'-bis[*N*-(1-naphthyl)-*N*-phenyl-amino] biphenyl,

- a 650 Å layer of blue fluorescent bis(8-hydroxy)-quinoline aluminum phenoxide and
- a 150 Å layer of electroconducting tris(8-hydroxy-2-quinoline aluminum).

REFERENCES

- Ciferri, A. (Ed.), *Liquid Crystallinity of Polymers*. New York: VCH Publishers, 1991.
- de Gennes, P. G., *The Physics of Liquid Crystals*, Oxford: Clarendon, 1975.
- Fisher, E. W., R. C. Schulz, and H. H. Sillescu (Eds.), *Chemistry and Physics of Macromolecules*. New York: VCH Publishers, 1991.
- Flory, P. J., *Proc. R. Soc. London A* **234**, 73 (1956).
- Flory, P. J., and Ronca, G., *Mol. Cryst. Liq. Cryst.* **54**, 311 (1979).
- Coe, S., W. K. Woo, M. Bawendi, and V. Bulovic, *Nature* **420**, 800 (2002).
- Kerr, J., *Philos. Mag.* **50**(4), 337, 446 (1875).
- Kumar, S. (Ed.), *Liquid Crystals*, Cambridge, U.K.: Cambridge University Press, 2001.
- Mingos, D. M. P. (Ed.), *Liquid Crystals*, Volumes I d II, Berlin: Springer-Verlag, 1999.
- Penterman, R., et al., *Nature* **417**, 55 (2002).
- Percec, V., et al., *Nature* **417**, 384 (2002).
- Onsager, L., *Ann. NY Acad. Sci.* **51**, 627 (1949).

7

RUBBER ELASTICITY

7.1 RUBBER AND RUBBERLIKE MATERIALS

As its temperature increases, a polymer chain may go through the three molecular states in the following order: first, the viscoelastic state, then the glassy state, and finally the crystalline state. It may stay in any of the above states when the temperature stops increasing. The change in state is the change in the internal mobility of polymer chains. At the viscoelastic state, the chain moves just like a liquid but also solidifies just like a solid (but not like a crystal). When the chain is completely solidified, it becomes a glass. The temperature at which the chain is turned into a glass is called the glass temperature or the freezing temperature. Above the glass temperature, the chain segment may change its arrangement from a random one to an ordered one. We now have the polymer in the crystalline state.

This book does not discuss the polymer in the glass state, which is a subject in a specialized area. However, it discusses the other two states in three different chapters: the crystalline state in the Chapter 6 and the viscoelastic state in the present chapter and in Chapter 8.

The viscoelastic state is also known as the rubber state. A piece of rubber under external force can be stretched. When the external force stops, the rubber recovers to its original position. Usually long-chain polymers can be induced to exhibit typical rubberlike behavior, for example, chains such as polyesters, polyamides, elastic sulfur (sulfur cooled from the liquid), and cellulose derivatives.

The phenomenon that a rubber or a rubberlike material can be stretched is termed *deformation* and the ability of it to recover and return to its original conformation is termed *recoverability*. Thus, the basic properties of rubber and rubberlike materials are deformation and recoverability, which are parallel to the properties of liquid crystals, namely, order and mobility.

7.2 NETWORK STRUCTURE

The unique feature of rubber is its network. It is the network that can sustain its stretching and its ability to recover. Once a linear polymer chain is stretched or deformed, it cannot recover. Natural rubber obtained from the rubber tree does not have practical uses because there are no cross-links in the molecules. Only when the cross-links between the chain segments are introduced to form a three-dimensional network do deformation and recoverability become intrinsic properties of the material. Figure 7.1 shows a statistical model of the network structure of rubber.

The junction arrangement (in the unstretched form) and the rearrangement (upon stretching) is controlled by the entanglement structure of the neighboring chains. The model is based on the structure of random walk (Gaussian distribution). There are no intermolecular or intramolecular potentials involved. The structure is described by two quantities: the density of the cross-linking and the proportion of free-chain ends. Here, elasticity refers to the mobility of the junctions, say A, from one position to another and then back to the original position. The network is composed of random-coil strands joined by a number of fixed points which move rigidly in response to any deformation. The junction points at which three or more

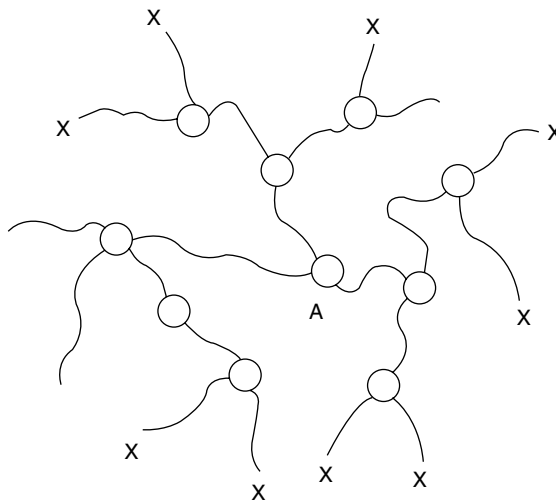


FIGURE 7.1 Statistical model of the network structure of rubber (after Grassley, 1975): ○, mobile junction; X, peripheral fixed point; A, junction under investigation.

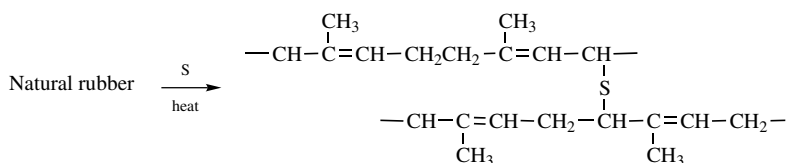
polymer chains are chemically bound fluctuate about a mean position. This is a well-known model upon which the statistical theory is based. There are, of course, several other models which we do not describe here.

Experimentally, the effects on elasticity and dimensions of networks are tested by varying the degree of cross-linking, the primary molecular weight, the amount of filler (the additive ingredients in rubber such as carbon black and various silicas to increase its hardness and change the tensile strength), and the temperature, particularly, T_g (the glass transition temperature). Notice that at T_g the network is no longer that of a rubber, but rather that of a glass.

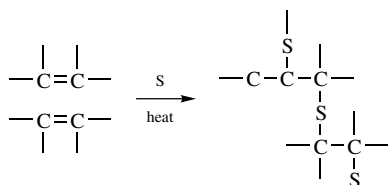
7.3 NATURAL RUBBER AND SYNTHETIC RUBBER

Cross-linking can be introduced not only between polymer molecules but also between certain segments and other segments of the same polymer chain. For this reason, a network can have many free ends.

In 1490, rubber materials from trees grown in Brazil (milk of the rubber tree, *Hevea brasiliensis*) were already known, but without cross-linking, they could be used only as wax or water-proof substances. It was not until 1830, when Charles Goodyear and Thomas Hancock accidentally mixed natural materials from the trees with sulfur and lead carbonate, that a hard, resilient, infusible solid was formed with the network of rubber. The process of heating rubber with sulfur to form cross-linking is called vulcanization. The process may be described as follows:



or in general form

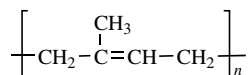


Vulcanization often requires 5–8% by weight of sulfur, and special hard rubbers require as much as 25–50% sulfur.

Today, the term vulcanization is used for all the reactions which lead to the cross-linking of elastic polymers (elastomers). Thus, one can vulcanize unsaturated elastomers (from isoprene or butadiene), not only with sulfur, but also with peroxide, trinitrobenzene, dinitrobenzene, and urea- and phenol-formaldehyde precondensates.

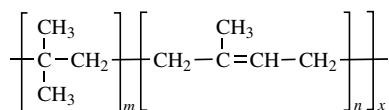
There are three types of rubbers which are in demand mostly by industry:

1. Natural rubber (poly-isoprene):

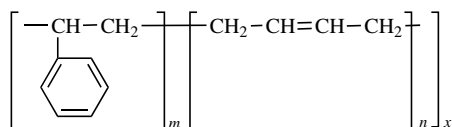


The monomer isoprene does not necessarily have to be supplied from rubber trees since it can be synthesized in the laboratory.

2. Butyl rubber (poly-isobutylene containing a small amount of isoprene):

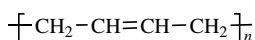


3. SBR (styrene-butadiene rubber)—a random copolymer of 30% styrene and 70% butadiene:

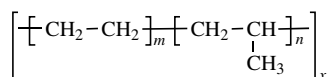


In contrast to natural rubber, butyl rubber and SBR are synthetic rubbers. Other synthetic rubbers which are produced in the factory include:

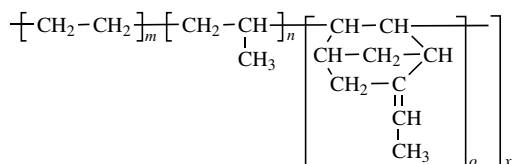
a. Poly-butadiene rubber:



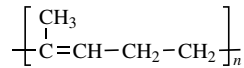
b. Ethylene-propylene copolymer:



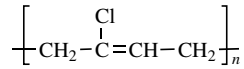
c. Ethylene-propylene-diene terpolymer:



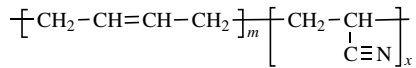
d. Poly-isoprene rubber:



e. Poly-chloroprene rubber:



f. Nitrile rubber:



In the 1990s, natural rubber consumption exceeded 4 million metric tons while synthetic rubber consumption exceeded 7 million metric tons. Among synthetic rubbers the largest production was of SBR, polybutadiene, and ethylene-propylene. Production has been continually increasing in the 2000s.

7.4 THERMODYNAMICS OF RUBBER

Rubber elasticity is strikingly similar to the behavior of a gas. A gas is characterized by three independent variables, P , V , and T , as has been discussed in Chapter 4. In addition to P , V , and T , rubber elasticity is characterized by two more independent variables: the stretching force f (also called the tensile force) and the length L . For a rubber, the volume is virtually constant during the deformation. A comparison can be made, therefore, between a gas and rubber in terms of three independent variables: PVT for gas and fLT for rubber. The similarity consists of the following: If V is kept constant, P is directly proportional to T for a gas, whereas if L is kept constant, f is directly proportional to T for rubber. For this reason, we can treat rubber in thermodynamics in a similar way that we treat gas. Our attention is consequently focused on the influence of temperature on the elasticity of rubber.

The first law and the second law remain the same:

$$dE = dQ - dw \quad dS = \frac{dQ_r}{T}$$

Here dw is no longer the same. We have to add the term $f dL$, that is,

$$dw = P dV - f dL$$

To derive measurable thermodynamic quantities such as $(\partial H/\partial L)_{T,P}$ and $(\partial f/\partial T)_{P,L}$, we need the four exact differentials together with the Maxwell

TABLE 7.1 Maxwell Relationships

Basic Equations (Exact Differentials)	Maxwell Relationships
a. $dE = T dS - P dV$	$\left(\frac{\partial T}{\partial V}\right)_S = -\left(\frac{\partial P}{\partial S}\right)_V$
b. $dA = S dT - P dV$	$\left(\frac{\partial S}{\partial V}\right)_T = -\left(\frac{\partial P}{\partial T}\right)_V$
c. $dH = T dS - V dP$	$\left(\frac{\partial T}{\partial P}\right)_S = -\left(\frac{\partial V}{\partial S}\right)_P$
d. $dG = S dT - V dP$	$\left(\frac{\partial S}{\partial P}\right)_T = -\left(\frac{\partial V}{\partial T}\right)_P$

relationships listed in Table 7.1. In all differential equations in the table, we have to add the term $f dL$. Now let us derive an expression of f . From the equation

$$dG = V dP - S dT + f dL$$

we obtain

$$\left(\frac{\partial G}{\partial L}\right)_{T,P} = f \quad \text{and} \quad \left(\frac{\partial G}{\partial T}\right)_{P,L} = -S$$

and from the equation $dH = T dS + V dP + f dL$, we obtain[†]

$$f = \left(\frac{\partial H}{\partial L}\right)_{T,P} - T \left(\frac{\partial S}{\partial L}\right)_{T,P} \quad (7.1)$$

Since (from the dG equation)

$$\left(\frac{\partial S}{\partial L}\right)_{T,P} = \left(\frac{\partial f}{\partial T}\right)_{P,L}$$

we get

$$f = \left(\frac{\partial H}{\partial L}\right)_{T,P} + T \left(\frac{\partial f}{\partial T}\right)_{P,L} \quad (7.2)$$

This is the equation of state for elasticity.

[†]Equation (7.1) means that in rubber elasticity the restoring force is derived from two factors: the enthalpy change $(\partial H/\partial L)_{T,P}$ and the entropy change. At high elongation, the enthalpy term vanishes so that the restoring force is entirely due to entropy change.

The term $(\partial H/\partial L)_{T,P}$ in Eq. (7.2) can be expressed in the form

$$\left(\frac{\partial H}{\partial L}\right)_{T,P} = \left(\frac{\partial E}{\partial L}\right)_{T,P} + P\left(\frac{\partial V}{\partial L}\right)_{T,P}$$

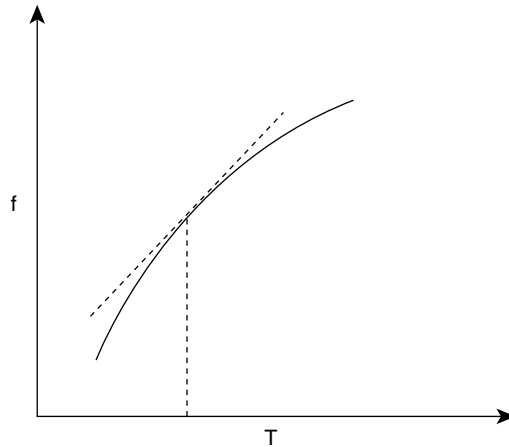
Since the quantity $(\partial V/\partial L)_{T,P}$ is negligible, V being nearly constant, we can write the equation of state for elasticity (or for rubber) as

$$f = \left(\frac{\partial E}{\partial L}\right)_{T,P} + T\left(\frac{\partial f}{\partial T}\right)_{P,L} \tag{7.3}$$

This is almost identical with the equation of state for gas,

$$P = -\left(\frac{\partial E}{\partial V}\right)_T + T\left(\frac{\partial P}{\partial T}\right)_V \tag{7.4}$$

The equation of elasticity, Eq. (7.3), can be used to determine the quantities $(\partial f/\partial T)_{P,L}$ or $(\partial S/\partial L)_{T,P}$. Experimentally, if we measure the stretching force as the function of temperature, we obtain the curve as



The slope at any time T will give the value of $-(\partial S/\partial L)_{T,P}$ and the intercept gives the value of $(\partial E/\partial L)_{T,P}$. By a standard manipulation, we can obtain the equation

$$\left(\frac{\partial E}{\partial L}\right)_{T,P} = \left(\frac{\partial E}{\partial L}\right)_{T,V} + \left(\frac{\partial E}{\partial V}\right)_{T,L}\left(\frac{\partial V}{\partial L}\right)_{T,P}$$

Here derived quantity is $(\partial E/\partial L)_{T,V}$, which is appropriately identical with the change in energy arising solely from orientation of the chain structure. Moreover,

we can proceed to investigate further the thermodynamic behavior of rubber. Consider the equation

$$\begin{aligned} dA &= dE - T dS - S dT \\ &= \underbrace{P dV - f dL}_{dE} - T dS - S dT \end{aligned}$$

and use its Maxwell relationship. We obtain

$$\begin{aligned} \left(\frac{\partial P}{\partial T}\right)_V &= \left(\frac{\partial S}{\partial V}\right)_T \\ \left(\frac{\partial f}{\partial T}\right)_{V,L} &= \left(\frac{\partial S}{\partial V}\right)_{V,T} \end{aligned}$$

Substituting into Eqs. (7.3) and (7.4), respectively, we now have

$$\begin{aligned} f &= \left(\frac{\partial E}{\partial V}\right)_{T,V} + T \left(\frac{\partial S}{\partial L}\right)_T \\ P &= -\left(\frac{\partial E}{\partial V}\right)_T + T \left(\frac{\partial S}{\partial V}\right)_T \end{aligned}$$

It is well known that for an ideal gas

$$\left(\frac{\partial E}{\partial V}\right)_T = 0$$

This is based upon the famous experiment by Joule. By analogy, we deduce that (which can also be experimentally confirmed)

$$\left(\frac{\partial E}{\partial L}\right)_{T,V} = 0$$

Thus we have two parallel equations: one describing the pressure P of ideal gas and the other one describing the stretching force of ideal rubber. They are

$$\begin{aligned} f &= -T \left(\frac{\partial S}{\partial L}\right)_{V,T} \\ P &= T \left(\frac{\partial p}{\partial T}\right)_V = T \left(\frac{\partial s}{\partial V}\right)_T \end{aligned}$$

This leads to the conclusion that “just as the pressure of an ideal gas may be attributed solely to the increase in its entropy with volume, the force of retraction in

an ideal rubber is due entirely to the decrease in entropy with increase in length” (Flory, 1953, p. 451).

7.5 STATISTICAL THEORY OF RUBBER ELASTICITY

Thermodynamics deals with macroscopic properties, the change in a system with respect to its surroundings. It has nothing to do with the geometry and structure of the molecules. Statistical mechanics considers the geometric and structural aspects.

We shall now develop a statistical theory of rubber elasticity using the Gaussian formula to represent the most probable distribution of molecular end-to-end distance. The mass of rubber is assumed to consist of N chains each end of which is joined to the ends of other chains. Suppose that the rubber is extended by a factor α .

Let x, y, z be the three coordinates of the unstretched rubber and

$$r^2 = x^2 + y^2 + z^2$$

Let L_0 be the length of the edge of an isotropic cube of rubber and α be the extent of stretching so that

$$\alpha_x = \frac{L_x}{L_0} \quad \alpha_y = \frac{L_y}{L_0} \quad \alpha_z = \frac{L_z}{L_0}$$

Then P_0 , the distribution of end-to-end lengths of r of the N chains in the undeformed network, is

$$P_0(x, y, z) \, dx \, dy \, dz = \frac{\beta^3}{\pi^{3/2}} e^{-\beta^2(x^2+y^2+z^2)} \, dx \, dy \, dz$$

where

$$\beta^2 = \frac{3}{2r^2}$$

The distribution of end-to-end lengths for the deformed network is

$$P(x, y, z) \, dx \, dy \, dz = \frac{\beta^3}{\alpha_x \alpha_y \alpha_z \pi^{3/2}} e^{-\beta^2[(x^2/\alpha_x^2)+(y^2/\alpha_y^2)+(z^2/\alpha_z^2)]} \, dx \, dy \, dz$$

Note that P_0 is Gaussian (the most probable distribution) while P is not.

Furthermore, the probability of a free chain having an end-to-end vector in $d\mathbf{r}_i$ is

$$P_i = P_0(\mathbf{r}_i) \, d\mathbf{r}_i$$

and the probability of the chain in a deformed state is

$$w_i = NP(\mathbf{r}_i) \mathbf{d}\mathbf{r}_i$$

What we want to calculate is the ratio of the probabilities of these two distributions, $\Omega(\alpha_x, \alpha_y, \alpha_z)/\Omega(x, y, z)$, which would lead to the calculation of ΔS . The quantity ΔS is directly related to the ratio Ω/Ω_0 :

$$\Delta S = k \ln \left(\frac{\Omega}{\Omega_0} \right)$$

For N chains, the most probable number of the specific chain n_i is

$$n_i = NP_i$$

In contrast, w_i is not the most probable number.

Now, if the probability that any specific chain in $\mathbf{d}\mathbf{r}_i$ is P_i , then the probability that the n_i specific chain is in $\mathbf{d}\mathbf{r}_i$ is $P_i^{n_i}$. Therefore, for the undeformed state, most probable distribution Ω_0 , we can write

$$\Omega_0 = \frac{N!}{\prod_i n_i!} \prod_i P_i^{n_i} \quad (7.5)$$

The combinatorial factor is inserted because it is immaterial which particular chains are in $\mathbf{d}\mathbf{r}$.

If we place the number w_i in each of $\mathbf{d}\mathbf{r}_i$, we have

$$\Omega = \frac{N!}{\prod_i w_i!} \prod_i P_i^{w_i}$$

Using the assumed conditions

$$\sum_i P_i = 1 \quad \sum_i w_i = \sum_i n_i = N$$

we find

$$\ln \frac{\Omega}{\Omega_0} = \sum_i w_i \ln \frac{n_i}{w_i}$$

But

$$\begin{aligned} \ln \frac{n_i}{w_i} &= \ln \frac{P_0}{P} \\ &= \ln \alpha_x \alpha_y \alpha_z - \beta^2 \left[x_i^2 \left(1 - \frac{1}{\alpha_x^2} \right) + y^2 \left(1 - \frac{1}{\alpha_y^2} \right) + z_i^2 \left(1 - \frac{1}{\alpha_z^2} \right) \right] \end{aligned}$$

so that

$$\ln \frac{\Omega}{\Omega_0} = N \ln \alpha_x \alpha_y \alpha_z - \beta^2 \left[\left(1 - \frac{1}{\alpha_x^2} \right) \left(\sum_i w_i x_i^2 + \sum_i w_i y_i^2 + \sum_i w_i z_i^2 \right) \right]$$

To evaluate the term $\sum w_i x_i^2$, we use the equation

$$\sum w_i x_i^2 = N \sum P x_i^2 dr_i$$

We replace the summation by integration and make use of the well-known mathematical formula[†]

$$\begin{aligned} \sum n_i x_i^2 &= N \iiint_{-\infty}^{\infty} x^2 p(x, y, z) dx dy dz \\ &= \frac{N \alpha_x^2}{2\beta^2} \end{aligned}$$

Similarly, we obtain

$$\sum w_i y_i^2 = \frac{N \alpha_y^2}{2\beta^2} \quad \sum w_i z_i^2 = \frac{N \alpha_z^2}{2\beta^2}$$

Therefore, we get

$$\begin{aligned} \Delta S &= S(\alpha_x \alpha_y \alpha_z) - S_0 = k \ln \frac{\Omega}{\Omega_0} \\ &= \frac{Nk}{2} \left[\ln \alpha_x \alpha_y \alpha_z - (\alpha_x^2 + \alpha_y^2 + \alpha_z^2 - 3) \right] \end{aligned} \quad (7.6)$$

We now consider the rubber elasticity for stretching in the x direction. This gives the conditions

$$\begin{aligned} V &= L_0^3 = \text{const} & \alpha_x \alpha_y \alpha_z &= 1 \\ L_x &= L & \alpha_x &= \alpha \\ L_y &= L_z & \alpha_y &= \alpha_z = \frac{1}{\alpha^{1/2}} \end{aligned}$$

[†]Mathematical formula:

$$\int_{-\infty}^{\infty} \exp(-\beta^2 x^2 / \alpha_x^2) dx = (\alpha_x / \beta) \sqrt{\pi}$$

Then we have

$$\Delta S = \frac{Nk}{2} \left(3 - \alpha^2 - \frac{2}{\alpha} \right)$$

Recall the equation

$$f = -T \left(\frac{\partial S}{\partial L} \right)_T$$

and redefine the parameter α as

$$\alpha = \frac{L}{L_0}$$

We now have the equation

$$\begin{aligned} f &= \frac{T}{L_0} \left(\frac{\partial S}{\partial \alpha} \right)_T \\ &= \frac{NkT}{L_0} \left(\alpha - \frac{1}{\alpha^2} \right) \end{aligned} \tag{7.7}$$

This is the equation of state for an ideal rubber obtained from the statistical mechanics derivation. It is consistent with the equation obtained from the thermodynamic relations. Consequently, for an ideal rubber, we have

$$Q = W = T \Delta S = -\frac{NkT}{2} \left(\alpha^2 - \frac{2}{\alpha} - 3 \right)$$

Equation (7.6) predicts that the elastic force is directly proportional to the temperature and the total number of chains in the network. Both of these have been experimentally observed.

Historic Note Equations (7.1) and (7.3) were known to Kelvin (1857) and Joule (1859), the two pioneers of thermodynamics. They firmly established that the stretching force of rubber is almost entirely entropic. All rubber and rubberlike materials behave as entropic springs. According to Eq. (7.1), the stretching force required to extend elastic materials serves in part to produce a change in internal energy and in part to produce a change in entropy. The first term is dominant and experimental study has shown that, for rubber, it is negligible. Kelvin and Joule's work was carried out on a macroscopic level. A microscopic explanation was not developed until the 1930s when Guth and Mark (1934) demonstrated that a macromolecule with an end-to-end distance L behaved as a molecular entropic

spring in tension. For a long linear chain of N freely jointed links, each of length a , the entropy is found to be

$$S = -\frac{3k_{\text{B}}L^2}{2Na^2} + C \quad (7.8)$$

where k_{B} is Boltzmann's constant and C is a constant. Using Eq. (7.1), we obtain

$$f = \frac{3k_{\text{B}}Tl}{Na^2} \quad (7.9)$$

Equations (7.8) and (7.9) may be compared with the Eqs. (7.5) and (7.6). The concept of a linear macromolecule as an entropic spring has since played a central role in polymer science (see Chapter 8, Sections 8.2.1 and 8.2.2).

7.6 GELS

Gels are similar to rubbers in that they both have long-chain polymers and the properties of elasticity. But rubbers are a one-component system, whereas gels are a two-component system (solute and solvent). In addition, rubbers are solids and gels are solutions.

Nevertheless, we discuss these two subjects (rubbers and gels) together because they have more similarities than differences.

In gels, concentration plays an important role. In the dilute solution, the long-chain polymer molecules are in the form of coils, each having a certain mobility. As the concentration increases, the mobility of the coils decreases. At a critical concentration, known as the gel point, the coils no longer move as units and can no longer interchange their places. Even though all of the polymerizing material still exists as monomers, dimers, trimers, and so forth, a three-dimensional network will appear. After the gel point is reached, more and more of these loose groups become attached to the network. The transition from a concentrated solution to a gel corresponds to the transition of a liquid to a solid.

The minimal concentration C_{g} required for gelation may be expressed by the equation

$$C_{\text{g}} = \frac{1}{\rho(m_{\text{w}} - 1)}$$

where ρ is the density of polymer and m_{w} is the weight of the average number of monomer units in a macromolecule. If the molecules are very long, so that $m_{\text{w}} \gg 1$, we can calculate the concentration of cross-links, C_{cr} , using the equation

$$C_{\text{cr}} = \frac{c}{2m_{\text{c}}}$$

where c is the concentration of polymer in grams per liter and m_c is the weight of the average molecular weight of a strand between cross-links. The minimum concentration of the polymer itself in terms of volume of fraction of space occupied by the strand is

$$(v_2)_{\min} = 1.02 \left(\frac{d}{L} \right)^2$$

where d is the diameter and L is the length of the strand.

A general characterization of gels can be based on the determination of rigidity and swelling.

- (a) *Rigidity* Gelation (the appearance of rigidity) occurs suddenly at a definite point, the gel point. As the reaction continues, the rigidity of the gel increases. Rigidity is determined by the measurement of modulus, which is the ratio of shearing stress (force per unit area) to shearing strain (angular deformation) and has the dimensions of force per area (see Chapter 8).
- (b) *Swelling* Swelling takes place due to the positive entropy of mixing. Flory and Rehner (1943) describe swelling by the equation

$$\mu v_2^2 + \ln(1 - v_2) + v_2 = - \frac{\rho v_1 v_2^{1/2}}{m_c}$$

where v_2 is the volume fraction of polymer at equilibrium, v_1 the molal volume of the solvent, and μ is a constant characterizing the degree of interaction.

REFERENCES

- Flory, P. J., and J. Rehner, *J. Chem. Phys.* **II**, 513 (1943).
 Flory, P. J., *Chem. Revs.*, **35**, 51 (1944).
 Grassley, W. W., *Macromolecules* **8**, 865 (1975).
 Guth, E., and H. Mark, *Monatsh* **65**, 93 (1934).
 Hill, T. L., *Introduction to Statistical Thermodynamics*, Reading, MA: Addison-Wesley, 1960.
 James, H. M., and E. Gutts, *J. Chem. Phys.* **11**, 455 (1943).
 James, H. M., and E. Gutts, *J. Chem. Phys.* **15**, 669 (1947).
 Joule, J. P., *Philos. Trans. R. Soc. London* **149**, 91 (1859).
 Kuhn, W., *Kolloid Z.* **76** 258 (1936).
 Thomson, W., *J. Pure Appl. Math.* **1**, 57 (1857).
 Wall, F. T., *Chemical Thermodynamics*, 3rd ed. San Francisco: W. H. Freeman, 1974.
 Wall, F. T., *J. Chem. Phys.* **10**, 132, 485 (1942).
 Wall, F. T., *J. Chem. Phys.*, **11**, 527 (1943).

PROBLEMS

- 7.1 Show that for rubber-like systems, the heat capacities at constant length and constant force are respectively

$$C_l = \left(\frac{\partial V}{\partial T} \right)_l$$

and

$$C_f = \left(\frac{\partial K}{\partial T} \right)_f$$

Note: $K = E - fl$

- 7.2 A 1-cm rubber band is stretched to 8 cm by the force of 700 g. The volume of the rubber band is 0.05 cm^3 , density 1 g/cm^3 , and specific heat $2 \text{ J K}^{-1} \text{ g}^{-1}$. Calculate ΔT of the rubber band.
- 7.3 The length of a rubber-band at constant force decreases as it is heated. Calculate the degree of shortening if the rubber-band stretches from 10 cm to 18 cm originally at $T = 300^\circ\text{K}$ with the temp now rises to 400°K .
- 7.4 The shear modulus (see Chapter 8, 8.2) of the rubber is described by the equation.

$$G_0 = \frac{dRT}{M_c} \left(\frac{\pi_0^2}{\pi_f^2} \right) \left(1 - \frac{2M_c}{M} \right)$$

where d is the density of rubber (in gm/ml), M_c is the molecular weight (in gm/mole) of each chain in the network, the parameter (π_0^2/π_f^2) is the average deviation of the network chains from the dimensions which they would assume if they were free of all constraints and M is the molecular weight of the linear polymer before cross linking. (See Flory 1944). Calculate the shear modulus of a piece of an ideal rubber whose density is 1 g/cm^3 . At room temperature M_c is 6,000 gm/mole and M is 120,000 gm/mole.

- 7.5 Show that ΔS has its maximum value when $\alpha_x = \alpha_y = \alpha_z = 1$. Hint: Eq. 7.6.

8

VISCOSITY AND VISCOELASTICITY

Consider the motion of a body in space against an external force. If the vector sum of all force components (translational and rotational motions) in all directions is not zero, then the body will accelerate in motion or change in state, that is, change in force components. If, on the other hand, the vector sum is zero, then the body will be stressed. If that body is not rigid, then it will undergo a deformation; it will be strained. We call this body a viscoelastic body. The mechanical properties of a polymer may be described by three quantities: stress σ , strain ϵ , and rigidity or modulus E . The units of both stress and modulus are dynes per centimeter squared (or grams per centimeter per second squared). Strain is dimensionless.

In this chapter we devote two-thirds of the space to viscosity and one-third to viscoelasticity of a polymer in solution. Viscosity is related to shear stress σ and shear strain ϵ , without reference to E . Viscoelasticity is related to all the three parameters, with E being of primary importance.

8.1 VISCOSITY

Imagine a fluid as a stack of parallel plates separated in coordinate x . The plates move in the same direction y but with different velocity, as seen in Figure 8.1. Each

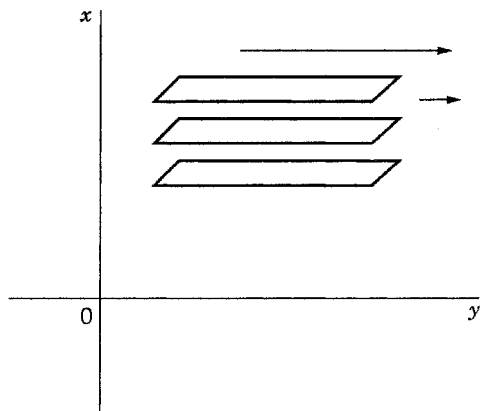


FIGURE 8.1 Fluid as a stack of parallel plates.

plate exerts force on the plate underneath. The shear stress σ is the force F per unit area A .

$$\sigma = \frac{F}{A} \quad \text{dyn/cm}^2 \quad (8.1)$$

and the shear strain ε is the derivative of coordinate y with respect to x ,

$$\varepsilon = \frac{dy}{dx} \quad (8.2)$$

The viscosity η is the ratio of shear stress over the rate of shear strain:

$$\eta = \frac{\sigma}{d\varepsilon/dt} \quad (8.3)$$

But notice the identities

$$\frac{d\varepsilon}{dt} = \frac{d}{dt} \left(\frac{dy}{dx} \right) = \frac{d}{dx} \left(\frac{dy}{dt} \right) = \frac{dv}{dx}$$

where v is velocity of the fluid. We thus have

$$\eta = \frac{\sigma}{dv/dx} \quad (8.4)$$

A fluid that obeys Eq. (8.4) is called a Newtonian fluid; a fluid that does not obey Eq. (8.4) is called a non-Newtonian fluid. The non-Newtonian behavior of a polymer solution is rarely investigated. It is the Newtonian behavior that is dealt with here.

8.1.1 Capillary Viscometers

The viscometers that are most commonly used for polymers in solution are the Oswald, Fenski, and Ubbelohde types. The devices are all based on the

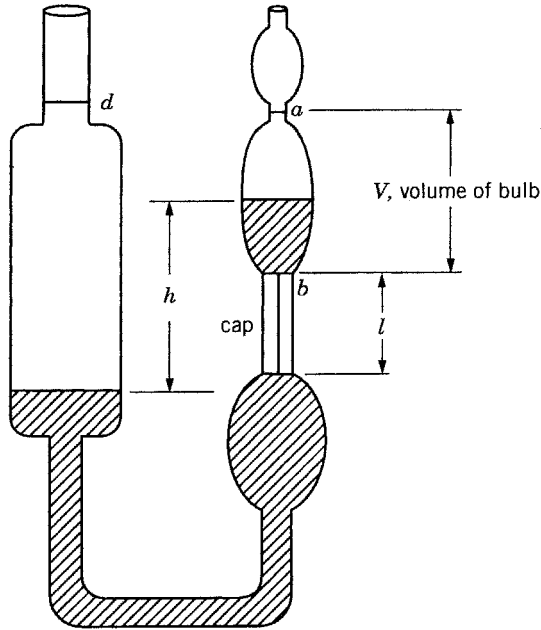


FIGURE 8.2 Oswald viscometer.

measurement of the flow of liquids through a tube. We describe the Oswald viscometer (Figure 8.2) as an example.

The flow time t of liquid through the capillary of length l is the time taken for the meniscus to fall from point a to point b , that is, the efflux of the bulb. The pressure head p is the difference of pressure at the two ends of the liquid, h . It is calculated from

$$p = h\rho_0g$$

where ρ_0 is the density of the liquid and g is the acceleration of gravity. Since h is variable as the liquid flows, p is likewise variable.

The viscosity η may be calculated according to Poiseuille's law:

$$\eta = \frac{\pi r^4 t p}{8 V l} \quad (8.5)$$

where r is the radius of the capillary in centimeters, p is the pressure head in dynes per centimeter squared, V is the volume of bulb, and V/t is the volume flow rate.

The unit of η is the poise, P (in honor of Poiseuille), of $\text{g cm}^{-1} \text{s}^{-1}$ (1 poise). For example, the viscosity of water at 20°C is 0.01 P, or 1 centipoise (cP). The dimensions of η are $ml^{-1} t^{-1}$ (m , mass; l , length; t , time); hence in the International System (SI) the units are kilograms per meter-second and in the centimeter-gram-second (cgs) system the units are grams per centimeter-second.

From Eq. (8.5), two quantities can be defined: the maximum shearing stress σ at the capillary wall,

$$\sigma = \frac{h\rho gr}{2l} \quad (8.6)$$

and the rate of shear D (i.e., velocity gradient)

$$D = \frac{4V}{r^3\pi t} \quad (8.7)$$

Then the viscosity η can be expressed in terms of σ and D :

$$\eta = \frac{\sigma}{D} \quad (8.8)$$

The plot of $\log D$ versus $\log \sigma$ will indicate whether the fluid is Newtonian or non-Newtonian (Figures 8.3*a,b*). The flow of fluid may depend on the force of shear in different regions, as shown in Figure 8.3*b*.

If a solution is known to be independent of the force of shear, then the measurement of η based on Poiseuille's law can be made easy by grouping all those terms related to a specific viscometer as a calibration constant A' . Hence, we have

$$\eta = A'h\rho_0 t \quad (8.9)$$

If the polymer solution is very dilute, ρ_0 may be used as the density of the solution without introducing a significant error. Since h and t are both variables, to use the Oswald viscometer, we must fill up the solution (or solvent) to the mark d to keep h constant for each measurement. Only by so doing is h incorporated into the constant A' , and we have

$$\eta = A\rho_0 t \quad (8.10)$$

Equation (8.9) can be applied to any solution (not necessarily dilute) in the form

$$\eta = A\rho t \quad (8.11)$$

where ρ is the density of solution. If we divide both sides by ρ , we have

$$\eta_k = \frac{\eta}{\rho} = At \quad (8.12)$$

The quantity η_k is called the kinematic viscosity and the viscosity is proportional to the flow time alone. The units of kinematic viscosity are the stoke (S) and centistoke (cS), or centimeters squared per second.

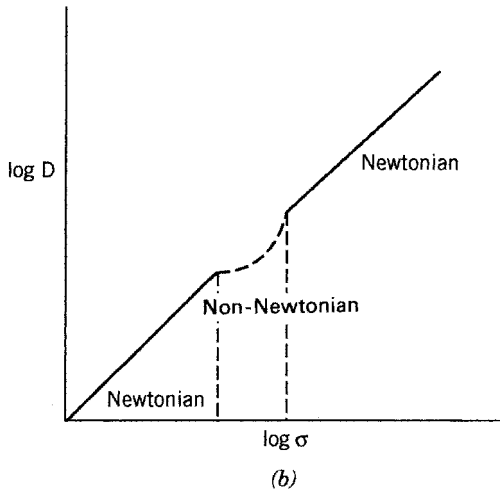
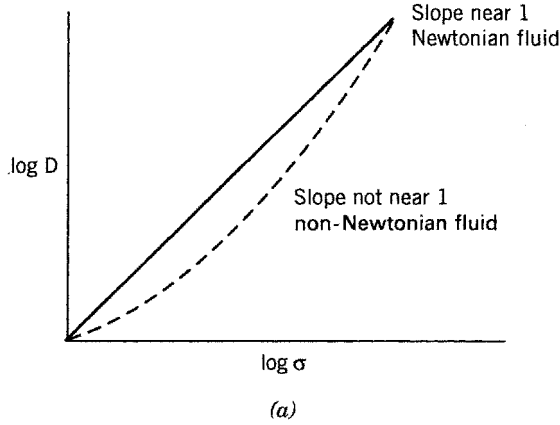


FIGURE 8.3 $\log D$ versus $\log \sigma$.

To avoid the tedious process of filling the solution to a certain mark d each time, Ubbelohde modified the Oswald viscometer to the form shown in Figure 8.4. The U-tube of the Ubbelohde viscometer eliminates the need to refill the solution each time.

For high-precision work, a small correction for kinetic energy may be considered:

$$\eta = A\rho_0 t - \frac{Y}{T} \tag{8.13}$$

where Y is another calibration constant and Y/t is the kinetic energy correction term. The values of A and Y can be determined by carrying out two experiments for

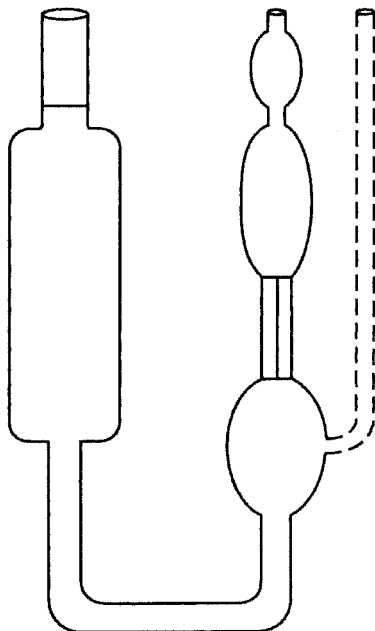


FIGURE 8.4 Ubbelohde viscometer.

two liquids (such as water and benzene) of known viscosity at the same temperature or the same liquid (such as water) as two different temperatures.

8.1.2 Intrinsic Viscosity

In macromolecular chemistry, the relative viscosity η_r is often measured. The relative viscosity is the ratio of the viscosity of the solution to that of the solvent:

$$\eta_r = \frac{\eta_{\text{solution}}}{\eta_{\text{solvent}}} = \frac{\eta}{\eta_0} = \frac{(\rho t)_{\text{solution}}}{(\rho t)_{\text{solvent}}} \cong \frac{t_{\text{solution}}}{t_{\text{solvent}}} \quad (8.14)$$

The specific viscosity η_{sp} is obtained from the relative viscosity by subtracting one unit from η_r :

$$\eta_{\text{sp}} = \eta_r - 1 \quad (8.15)$$

The intrinsic viscosity, denoted by $[\eta]$, is defined as

$$[\eta] = \lim_{c \rightarrow 0} \frac{\eta_{\text{sp}}}{c} = \lim_{c \rightarrow 0} \left(\frac{1}{c} \ln \frac{\eta}{\eta_0} \right) \quad (8.16)$$

where c is the concentration of the polymer in grams per 100 mL or grams per milliliter of the solution. The quantity η_{sp}/c is called the reduced viscosity. The unit of intrinsic viscosity is deciliters per gram (dL/g) or milliliters per gram (mL/g) depending on the concentration unit of the solution. The intrinsic viscosity is also called the limiting viscosity number.

The plot of η_{sp}/c versus c or $(1/c) \ln \eta_r$ versus c often gives a straight line, the intercept of which is $[\eta]$. Huggins (1942) showed that the slope is

$$\frac{d}{dc} \frac{\eta_{sp}}{c} = k[\eta]^2$$

or

$$\frac{1}{[\eta]^2} \frac{d}{dc} \frac{\eta_{sp}}{c} = k$$

In integrated form, the equation is

$$\frac{\eta_{sp}}{c} = [\eta] + k[\eta]^2 c \tag{8.17}$$

where k is a dimensionless constant, called the Huggins constant. The value of k is related to the structures of polymers. It enables an estimate of $[\eta]$ to be made from a single determination of η_{sp}/c . Table 8.1 gives some sample values of k .

Some other equations for the determination of $[\eta]$ are

$$\frac{\eta_{sp}}{c} = [\eta] + k'[\eta]\eta_{sp} \quad (\text{Schultz and Blaschke, 1941}) \tag{8.18}$$

$$\frac{1}{c} \log \eta_r = [\eta] + k''[\eta]^2 c \quad (\text{Kraemer, 1938}) \tag{8.19}$$

$$\frac{\eta_{sp}}{c} = [\eta] e^{k''[\eta]c} \quad (\text{Martin, 1942}) \tag{8.20}$$

For molecules of high intrinsic viscosity a correction must be made for the effect of the rate of shear strain. For relatively low intrinsic viscosity, the rate of shear strain does not have any appreciable effect.

TABLE 8.1 Some Sample Values of k

Polymer	Solvent	Temperature (°C)	Huggins k Value
Polystyrene	Toluene	30	0.38
	Methylethyl ketone	40	0.54
Polyisobutene	Benzene	24	0.94
	Cyclohexane	25	0.405
	Methylethyl ketone	25	1.598

8.1.3 Treatment of Intrinsic Viscosity Data

Mark–Houwink Equation Staudinger (1932) suggested that the molecular weight M of polymers is proportional to the reduced viscosity:

$$\frac{\eta_{sp}}{c} = k'M$$

where k' is a proportionality constant. Mark (1938) and Houwink (1940) independently correlated the intrinsic viscosity with molecular weight:

$$[\eta] = KM^a \quad (8.21)$$

where K and a both are constants. The Mark–Houwink equation is applicable to many polymers and is extensively used to determine molecular weight. The constants K and a both vary with polymers and solvents. Table 8.2 gives values of K and a for a number of polymer–solvent pairs.

Equation (8.21) describes the relationship between viscosity and molecular weight. Since molecular weight is related to the size of the polymer chain, Eq. (8.21) also describes the relationship between $[\eta]$ and N (the number of links in a polymer chain) or $[\eta]$ and $\langle R^2 \rangle$ (the mean-square end-to-end distance). This has stimulated a great deal of interest over the last 40 years as to how they are related. More specifically, what are the meaning of K and a ?

Flory–Fox Equation As mentioned earlier, at the θ temperature there are only short-range steric interactions between neighboring or near-neighboring polymer segments. The polymer molecule shrinks to a compact form. Flory and

TABLE 8.2 Viscosity and Molecular Weight, $[\eta] = KM^a$

Polymer	Solvent	Temperature (°C)	$K \times 10^4$ (dL/g)	a	$M \times 10^{-4}$
Polystyrene Atactic	Benzene	25	2.7	0.71	6–31
	Cyclohexane	25	1.6	0.80	6–31
		34(θ)	7.5	0.50	7
	1-Chloronaphthalene	74(θ)	18	0.50	4–33
Isotactic	Decalin	135	1.6	0.77	2.39
	Decalin	135	1.1	0.80	2.62
Poly(methyl methacrylate) Atactic	Benzene	20	0.84	0.73	7–700
	Chloroform	20	0.96	0.78	1.4–60
	3-Heptanone	34(θ)	6.3	0.50	6.6–171
Polyvinylacetate	Toluene	25	0.71	0.73	4–330
	Benzene	30	2.2	0.65	97–153
Nylon 6	<i>m</i> -Cresol	25	3.2	0.62	0.05–0.5

Source: Brandrup and Immergut (1975).

Fox (1951) suggested that the intrinsic viscosity at θ the condition may be regarded as measure of the ratio of the effective hydrodynamic volume of the polymer to its molecular weight M . They took the radius of hydrodynamic volume as the root-mean-square end-to-end distance $\langle R^2 \rangle^{1/2}$ in the random coil:

$$[\eta]_{\theta} \sim \frac{\langle R^2 \rangle^{1/2}}{M}$$

If the proportionality constant is taken as Φ , the equation becomes

$$[\eta]_{\theta} = \Phi \frac{\langle R^2 \rangle_0^{3/2}}{M} = \Phi \left(\frac{\langle R^2 \rangle_0}{M} \right)^{3/2} M^{1/2} = KM^{1/2} \quad (8.22)$$

where

$$K = \Phi \left(\frac{\langle R^2 \rangle_0}{M} \right)^{3/2} \quad (8.23)$$

The proportionality constant Φ is a universal constant, called the Flory viscosity constant. Thus, Flory and Fox provided, partially, the meanings of K and a in the Mark–Houwink equation. At the θ temperature, K is defined by Eq. (8.23) and $a = \frac{1}{2}$.

The exact value of Φ is very difficult to determine. Rearranging the equation in the form

$$\Phi = \frac{[\eta]_{\theta} M}{\langle R^2 \rangle_0^{3/2}} \quad (8.24)$$

we see that any uncertainty in experimental values of $[\eta]_{\theta}$ and $\langle R^2 \rangle_0$ would contribute to the error of Φ . Two different experimental methods are required to determine these two quantities: viscosity measurement for $[\eta]_{\theta}$ and light-scattering measurement for $\langle R^2 \rangle_0$. The sample solution must be identical and the experimental conditions must be the same. It is very difficult to minimize errors to the same extent simultaneously in two different experiments. In using Eq. (8.24), many investigators therefore rely on the theoretical value. But theoretical values vary with the model assumed (e.g., the pearl string model and the hydrodynamic equivalent sphere, which are discussed later). Flory and Fox estimated the value of Φ to be 2.1×10^{21} from a set of experimental data, whereas the Kirkwood–Riseman equation (to be discussed later) would give 3.6×10^{21} . The value of the exponent depends on the unit of $[\eta]_{\theta}$ and $\langle R^2 \rangle_0$. If $[\eta]_{\theta}$ is chosen in deciliters per gram and $\langle R^2 \rangle_0$ in centimeters squared, then Φ is 2.1×10^{21} . If, however, $[\eta]_{\theta}$ is in centimeters cubed per gram and $\langle R^2 \rangle_0$ is (usually) in centimeters squared, then Φ is 2.1×10^{23} . Table 8.3 gives the values of Φ to show the variations.

TABLE 8.3 Some Values of Φ

Polymer	Solvent	$M \times 10^{-6}$	$\Phi \times 10^{-21}^a$
Polystyrene	Cyclohexane	0.20–4.0	1.5–2.9
	Methylethyl ketone	0.20–1.8	2.0–2.5
	Dichloromethane	0.50–1.8	2.0–2.2
Poly(methyl methacrylate)	Chloroform	0.70–1.4	2.0–2.2
	Methylethyl ketone	0.70–1.4	2.0–2.2
Polyisobutylene	Cyclohexane	0.50–0.72	2.2
Poly(acrylic acid)	Dioxane	0.80–1.4	2.2

^a $[\eta]$ in dL/g.

In a good solvent (or in a poor solvent at a temperature other than θ), long-range interactions (or excluded volume effect) take place. The polymer molecule expands. The expansion factor α , which describes the excluded volume effect, can now be calculated from the intrinsic viscosity data:

$$\alpha^3 = \left(\frac{\langle R^2 \rangle}{\langle R^2 \rangle_0} \right)^{3/2} = \frac{[\eta]}{[\eta]_0} = (= \alpha_\eta^3)$$

Flory and Fox suggested that the Mark–Houwink equation (8.21) can be put in the form

$$[\eta] = KM^{1/2}\alpha^3 \quad (8.25)$$

where

$$K = \Phi \left(\frac{\langle R^2 \rangle}{M\alpha^2} \right)^{3/2} = \Phi \left(\frac{\langle R^2 \rangle_0}{M} \right)^{3/2} \quad (8.26)$$

Equation (8.26) provides new meanings for K and a if $[\eta]$ is not measured at the θ temperature. Flory and Fox further suggested that once the value of α^3 is obtained, we can calculate α^5 and use the equation

$$\alpha^5 - \alpha^3 = 2c_M \psi_1 \left(1 - \frac{\theta}{T} \right) M^{1/2} \quad (8.27)$$

to obtain thermodynamic parameters, ψ_1 , κ_1 , and θ . The quantity c_M can be calculated from

$$c_M = \left(\frac{27}{2^{5/2}\pi^{3/2}} \right) \left(\frac{\bar{v}^2}{N_A^2 V_0} \right) \left(\frac{\langle R^2 \rangle_0}{M} \right)^{-3/2} \quad (8.28)$$

TABLE 8.4 Thermodynamic Parameters Obtained from Intrinsic Viscosities

Solvent	θ (K)	ψ_1	κ_1 at 25°C
<i>Polystyrene</i>			
Cyclohexane	307	0.13	0.134
Benzene	100	0.09	0.03
Toluene	160	0.11	0.06
Dioxane	198	0.10	0.07
Ethyl acetate	222	0.03	0.02
Methylethyl ketone	0	0.006	0
<i>Polyisobutylene</i>			
Benzene	297	0.15	0.15
Toluene	261	0.14	0.12
Cyclohexane	126	0.14	0.059
<i>n</i> -Hexadecane	175	0.094	0.055
<i>n</i> -Heptane	0	0.035	0

Note: See Problem 8.4.

Source: Flory (1953).

where V_0 is the molar volume of the solvent and \bar{v} is the partial specific volume of the polymer and N_A is the Avogadro number. Thus, through the efforts of Mark, Houwink, Flory, and Fox, the measurement of intrinsic viscosities makes it possible to determine the molecular weight M , the unperturbed dimension of the polymer chain $\langle R^2 \rangle_0$, the extent of expansion α , and the thermodynamic parameters ψ_1 , κ_1 , and θ . Table 8.4 gives the values of thermodynamic parameters for polystyrene and polyisobutylene obtained by intrinsic viscosity measurements.

Stockmayer–Fixman Equation If several samples of the same polymer with different molecular weight are available, we can determine the structural parameter K and the interaction parameter χ_1 simultaneously by measuring the intrinsic viscosities. This was suggested by Stockmayer and Fixman (1963) in the equation

$$[\eta] = KM^{1/2} + 0.51\Phi BM \quad (8.29)$$

where

$$B = \frac{(1 - 2\chi_1)\bar{v}^2}{V_0N_A}$$

The equation is valid for polymer chains in all solvents (good or poor). It separates the effect of short-range interaction K from that of long-range interaction B . A plot of $[\eta]/M^{1/2}$ versus $M^{1/2}$ would give the intercept K , from which we can determine $\langle R^2 \rangle_0$, and the slope $0.51\Phi B$, from which we can determine χ_1 .

Among the three equations we have discussed, only the Mark–Houwink equation is exact; that is, no assumptions have been made. The Flory–Fox and Stockmayer–Fixman equations are both based on their models.

8.1.4 Stokes' Law

Let R be the radius of a large particle in the form of a sphere and \mathbf{v} be the velocity of the particle moving through a continuum fluid. Then the frictional force that the particle experiences may be expressed as

$$F = -f\mathbf{v} = -6\pi\eta R\mathbf{v}$$

where f is the frictional coefficient and η is the viscosity of the fluid medium. This equation is called Stokes' law. In polymer chemistry the law is more often expressed in the form

$$f = 6\pi\eta_0 R \quad (8.30)$$

where η_0 is the viscosity of solvent. Note that here the polymer molecule is assumed to be in the shape of a sphere; hence, its size is expressed in terms of radius.

The frictional force increases with velocity, because the moving object experiences more drag as it collides with more molecules. Several physical properties are directly related to the frictional coefficient f , for example, the diffusion coefficient and the sedimentation coefficient. For this reason, the intrinsic viscosity, diffusion coefficient, and sedimentation coefficient are often referred to as frictional properties. Stocks' law will be discussed in this chapter and in the chapters on the diffusion coefficient and sedimentation coefficient (Chapters 10 and 11).

8.1.5 Theories in Relation to Intrinsic Viscosity of Flexible Chains

Kirkwood–Riseman Theory (1948) This theory is based on a model in which the chain consists of a sequence of monomer units. When a polymer molecule is placed in a fluid of surrounding medium (solvent molecules), the flow is perturbed by the resistance offered by each polymer unit. This model is known as the pearl string (or pearl necklace) model, where each monomer unit is a bead (see Figure 8.5). The emphasis of the Kirkwood–Riseman theory is on the hydrodynamic resistance of the individual beads. When the individual resistance is summed, we obtain the resistance of the whole molecule.

According to Kirkwood and Riseman, the frictional force \mathbf{F}_l exerted on the surrounding medium by the bead l due to the motion of the chain in the medium may be expressed as

$$\mathbf{F}_l = f|\mathbf{v}_l - \mathbf{u}_s|$$

where f is the friction coefficient, \mathbf{v}_l is the velocity of the bead, and \mathbf{u}_s is the velocity of the solvent. The perturbation is calculated by a tensor formula advanced by Oseen (1927) which leads to

$$[\eta] = \left(\frac{N_A f b^2}{3600 \eta_0 M_0} \right) N F(\lambda_0 N^{1/2}) \quad (8.31)$$

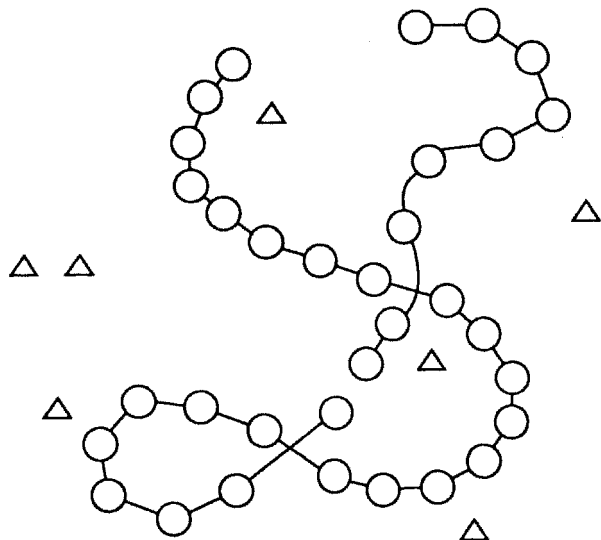


FIGURE 8.5 Pearl string model: Δ , solvent molecule; \circ , monomeric unit.

where

$$\lambda_0 = \frac{f}{(6\pi^3)^{1/2} \eta_0 b} \quad N = \frac{M}{M_0}$$

In these equations, N_A is the Avogadro number, b is the effective bond length of the chain, N is the number of links in the polymer molecule, M is the molecular weight of the polymer, and M_0 is the molecular weight of the monomer unit. The function $F(\lambda_0 N^{1/2})$ is theoretically tabulated. Its value is between 0 and 1.

Thus, according to this theory, at a given molecular weight, the intrinsic viscosity $[\eta]$ is related to N by the frictional coefficient f of a monomer unit and the effective bond length b of the chain. As N approaches infinity, $[\eta]$ becomes independent of f and the above equation may be simplified to

$$b^3 = \frac{2267M_0}{(6\pi^3)^{1/2} N_A} \lim_{N \rightarrow \infty} \frac{[\eta]}{N^{1/2}} \quad (8.32)$$

By plotting $[\eta]/N^{1/2}$ versus $N^{-1/2}$, the intercept leads to the determination of b . The frictional coefficient of the polymer may also be determined by plotting $\log\text{-}\log[\eta]$ versus N with the assistance of the theoretical table of $F(\lambda_0 N^{1/2})$ given by Kirkwood and Riseman in their original paper.

Debye–Bueche Theory Debye and Bueche (1948) criticize the theory of Kirkwood and Riseman as being unrealistic in assuming that the hydrodynamic

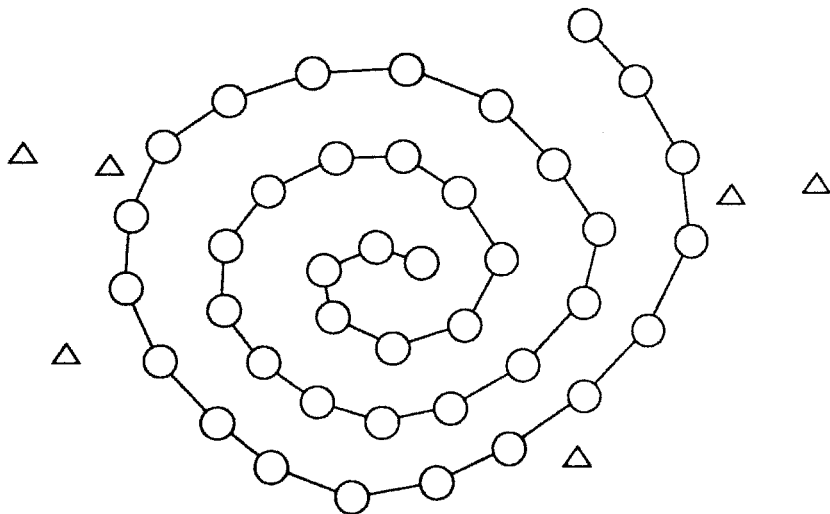


FIGURE 8.6 Equivalent hydrodynamic sphere model: Δ , solvent molecule; \circ , monomeric unit.

resistance of each individual bead is equal. They cannot accept the assumption that there is no mutual interaction among the beads. Instead, they argue that because of the superposition of the disturbances caused by all the other beads, an individual bead deviates from the original undisturbed velocity field during the motion. Following Einstein's method of calculating the effect of a number of immersed impermeable spheres on the overall viscosity (Einstein, 1911), Debye and Bueche considered the polymer molecule as a whole to be an equivalent hydrodynamic sphere of radius R_s , impenetrable to the solvent (Figure 8.6). Inside the sphere the bead density ρ' is constant everywhere; outside the sphere, $\rho' = 0$. The quantity of ρ' may be defined as

$$\rho' = \left(\frac{3}{4\pi}\right) \left(\frac{N}{R_s^3}\right)$$

where N is the number of beads in the string. This model is now called the equivalent sphere model.

The intrinsic viscosity based on this model is given by

$$[\eta] = \frac{(4\pi/3)R_s^3}{M} \phi(\gamma) \quad (8.33)$$

where the argument γ of the function ϕ is the shielding ratio defined as

$$\gamma = \frac{R_s}{L}$$

and L is the shielding length related to bead density:

$$\frac{1}{L^2} = \rho' \left(\frac{f}{\eta} \right)$$

The values of γ are in the range between zero and infinity. For small value of γ , ($\lim \gamma = 0$)

$$\phi(\gamma) = \frac{\gamma^2}{10(1 - \frac{2}{35}\gamma^2 + \dots)}$$

and we have

$$[\eta] = \left(\frac{1}{10} \right) \left(\frac{f}{\eta_0 m} \right) R_s^2 \quad (8.34)$$

where f is the friction coefficient of one bead, m is the mass of one bead, and η_0 is the viscosity of the solvent. For large values of γ , we have

$$\phi(\gamma) = \frac{5}{2} \left[1 - \left(\frac{3}{\gamma} \right) - \dots \right]$$

and

$$[\eta] = \frac{5}{2} \left(\frac{4\pi}{3} R_s^3 \right) \frac{1}{M} = \frac{5}{2} \left(\frac{4\pi}{3} R_s^3 \right) \frac{1}{Nm} \quad (8.35)$$

According to this model, intrinsic viscosity depends not only on the molecular weight but also on the specific volume of the macromolecule and the shielding ratio. de Gennes considered this a model of porous sponge with uniform density. The monomers inside the sponge are screened from the flow. Only those on the surface are subject to friction.

8.1.6 Chain Entanglement

Bueche (1952) studied the viscosity behavior of a polymer in concentrated solution, or rather Newtonian melt viscosity. He derived first an equation for unentangled chains:

$$\eta_0 = \left[\frac{N_A}{\sigma} \left(\frac{\langle R^2 \rangle_0}{M \bar{v}_2} \right) z_c \right] f$$

where N_A is Avogadro's number, σ is the tensile strength, \bar{v}_2 is the specific volume of the liquid, f is the friction factor, z is the chain length (or in a slightly different

sense the number of submolecules per polymer chain), and z_c is the critical chain length below which there are no entanglements. This equation predicts that

$$\eta_0 \sim z \quad \text{for unentangled chains}$$

Using the power law, we can express more specifically the intrinsic viscosity for unentangled chains as a function of the chain length:

$$\eta_0 \sim z^a$$

where a is between 1 and 2.5 for $z < z_c$.

If there are entanglements involved, as in a polymer melt, the equation of viscosity is modified to

$$\eta_0 = \frac{1}{8} \left(\frac{N_A^2}{6^{1/2}} \right) \left[\left(\frac{\langle R^2 \rangle_0}{M} \right)^{2.5} \left(\frac{z^{3.5} g(z)}{m_0^{1/2} v_2^2 z_2^2} \right) \right] f \quad \text{for } z \geq z_c$$

Here m_0 is the mass per chain atom and $g(z)$ is the slippage function. From asymptotic dimensional analysis, this equation may be expressed in the power law as

$$\eta \sim M^{3.4}$$

Experimental results confirm the power law in the form

$$\eta \sim M^{3.4}$$

Theoretical analyses (due to Freed, 1980) in terms of scaling theory describe the complexity of this equation in the following way:

$$\frac{\eta}{c} = \frac{\zeta l^2 N^2 N_A}{\eta_0 M} F \left(\frac{c N_A \alpha^3}{M}, \frac{\omega \zeta^2 l^2 N^2}{kT} \right)$$

where c is the concentration, ζ is the frictional coefficient of the monomer, l is the monomer length, N is the number of monomers, N_A is Avogadro's number, M is the molecular weight of the polymer, ω is the frequency, which corresponds to the elastic modulus of an entanglement network (see Section 8.10), α is the distance in space between entanglement functions, and kT is the absolute temperature in energy unit. The first argument of the scaling function F , $c N_A \alpha^3 / M$, is related to the probability of entanglements, and the second argument, $\omega \zeta^2 l^2 N^2 / kT$, is related to the shear modulus. The equation describes the complexity of the dependence of viscosity on the molecular weight in power law form and the justification of the exponent 3.4 in the empirical equation, but it is still impossible to reduce the equation to a simple form with which we can theoretically calculate the viscosity from molecular parameters.

8.1.7 Biological Polymers (Rigid Polymers, Inflexible Chains)

Most biological polymers, such as proteins and nucleic acids and some synthetic polymers, have relatively inflexible chains. For rigid particles, the size is no longer of predominant importance, because the polymer chain is no longer in the form of a flexible random coil; instead, shape becomes an important parameter. The shape factor ν may be expressed in terms of the axial ratio p , defined as

$$p = \frac{a}{b}$$

where a is the major semiaxis and b is the minor semiaxis. Following are some theoretical proposals for the estimation of the shape factor ν from the viscosity measurement.

Einstein (1911) Equations for Spherical Molecules Einstein, in a study of the viscosity of a solution of suspension of particles (colloids), suggested that the specific viscosity η_{sp} is related to a shape factor ν in the following way:

$$\eta_{sp} = \nu\phi \quad (8.36)$$

where ϕ is the volume fraction;

$$\phi = \frac{n\nu}{V}$$

where n is the number of noninteracting identical particles, ν is the volume of each particle, and V is the volume of the solution or suspension. Assume that the molecules are of a spherical shape, rigid and large relative to the size of the solvent molecules, and that the particles are small enough to exhibit Brownian motion but large enough to obey the laws of macroscopic hydrodynamics. Then

$$\nu = 2.5$$

The Einstein equation

$$\eta_{sp} = 2.5\phi \quad (8.37)$$

is now used as a reference to estimate the shape of macromolecules. Any deviation can be interpreted as the fact that the molecules are not a sphere.

Peterlin (1938) Equations for Ellipsoids of Revolution in General Under the influence of an applied shearing stress, a gradient of the distribution function $\partial F/\partial t$ may be defined to specify the orientation of the particle with respect to two axes (major and minor):

$$\frac{\partial F}{\partial t} = \psi \nabla^2 F - \nabla(F\omega) = 0 \quad (8.38)$$

where F is a function of (ψ, δ, R) , the quantity ψ is the rotational diffusion coefficient, δ is the ratio of the rate of shear to the rotational diffusion coefficient, and R is the ellipsoids of rotation. The Laplacian operator ∇^2 is given as

$$\nabla^2 = \frac{\partial^2}{\partial x^2} + \frac{\partial^2}{\partial y^2} + \frac{\partial^2}{\partial z^2}$$

and ω is the angular velocity of the rotating particles. On the basis of Eq. (8.38), Peterlin derived an equation of the ellipsoids of rotation R from which the shape factor v is determined as

$$v = \frac{p^2 - 1}{p^2 + 1}$$

Simha (1940) Equations for Prolate and Oblate Ellipsoids Simha solved Eq. (8.38) for the viscosities of solutions of ellipsoids of revolution for the limiting case $\delta \rightarrow 0$. For very dilute solution at $\delta \rightarrow 0$, Simha derived the following two equations of shape factors v :

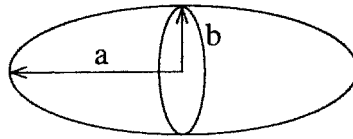
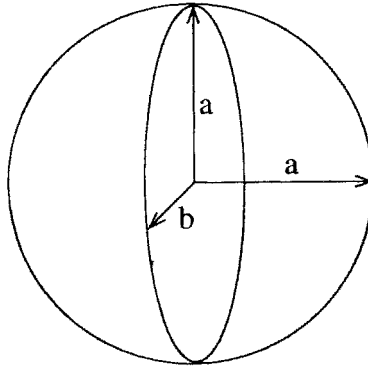
$$v = \begin{cases} \frac{p^2}{15(\ln 2p - 1.5)} & \text{for prolate ellipsoids} & (8.39a) \\ \frac{16p}{15 \arctan p} & \text{for obtate ellipsoids} & (8.39b) \end{cases}$$

Two ellipsoids are shown in Figure 8.7. Table 8.5 gives some of the numerical values of p and ellipsoids.

Kuhn–Kuhn (1945) Equations for Rigid Rods and Disks Kuhn and Kuhn derived equations for the shape factors of rigid rods and disks as follows:

$$v = \begin{cases} 0.4075(p - 1)^{1.508} + 2.5 & 1 < p < 15 & (8.40a) \\ \frac{p^2}{15(\ln 2p - 1.5)} + P^2 5(\ln 2p - 0.5) + 1.6 & l > 15 & (8.40b) \\ \left(\frac{32}{15\pi}\right)(q - 1) - \frac{0.628(q - 1)}{q - 0.075} + 2.5 & q = \frac{1}{p} > 1 & (8.40c) \end{cases}$$

Scheraga–Mandelkern (1953) Equations for Effective Hydrodynamic Ellipsoid Factor β Scheraga and mandelkern suggested that $[\eta]$ is the function of two independent variables: p , the axial ratio, which is a measure of shape, and V_e , the effective volume. To relate $[\eta]$ to p and V_e , Scheraga and Mandelkern introduced f ,


Prolate ellipsoid

Oblate ellipsoid
FIGURE 8.7 Shapes of macromolecules.

the frictional coefficient, which is known to be a direct function of p and V_e . Thus, for a sphere we have

$$\frac{\eta_{sp}}{c} \equiv [\eta] = \left(\frac{N_A}{100} \right) \left(\frac{V_e}{M} \right) v$$

$$f_0 = 6\pi\eta_0 \left(\frac{3V_e}{4\pi} \right)^{1/3}$$

where v is the shape factor (for a sphere, $v = 2.5$). The parameter V_e could be eliminated from the above two equations.

TABLE 8.5 Some Numerical Values of p

Axial Ratio	Prolate	Oblate
1	2.50	2.50
10	13.6	8.04
20	38.6	14.8
40	121	28.3
100	593	68.6
300	4278	204

Using the Einstein and Svedberg equations, which we discuss later,

$$D = \frac{kT}{f} \quad (\text{Einstein's equation of diffusion coefficient } D)$$

$$S = \frac{M(1 - \bar{v}\rho)}{Nf} \quad (\text{Svedberg's equation of sedimentation coefficient } S)$$

We obtain

$$\beta \equiv \frac{D[\eta]^{1/3}M^{1/3}\eta_0}{kT} \quad (8.41)$$

or

$$\beta \equiv \frac{NS[\eta]^{1/3}\eta_0}{M^{2/3}(1 - \bar{v}\rho)} \quad (8.42)$$

The value of β is a measure of the effective hydrodynamic ellipsoid.

8.2 VISCOELASTICITY

The term viscoelasticity is a combination of viscosity and elasticity. In the study of viscosity, we neglect the modulus; in the study of viscoelasticity, we attach great importance to the modulus. A mechanical body contains both elastic springs and viscous damping elements. On this basis several models were developed to describe viscoelastic behavior. Among them are Maxwell's model and the Kelvin–Voigt model. Here we discuss Maxwell's model of a mechanical body under one-dimensional deformation. The diagram of the model is shown in Figure 8.8.

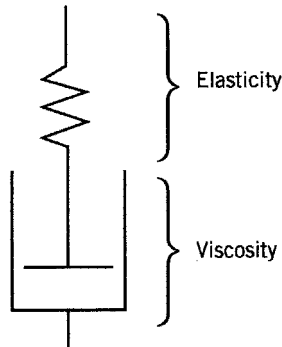


FIGURE 8.8 Maxwell's model of a mechanical body.

The elasticity is characterized by Hooke's law:

$$\sigma_0 = \varepsilon_0 E$$

where σ_0 is the instantaneous stress; E is Young's modulus, or the tensile modulus; and ε_0 is the instantaneous strain. The reciprocal of the tensile modulus is called the tensile compliance D :

$$D = \frac{1}{E}$$

In Maxwell's model the two parameters E and η are related by

$$\eta = \tau E \quad (8.43)$$

where τ is the relaxation time. Recalling Eq. (8.3), we can write the equation of motion of the Maxwell model as

$$\frac{d\varepsilon}{dt} = \underbrace{\frac{1}{E} \frac{d\sigma}{dt}}_{\text{Hooke's law}} + \underbrace{\frac{\sigma}{\eta}}_{\text{Newton's law}} \quad (8.44)$$

It is clear that viscoelasticity is basically a relaxation phenomenon. The relaxation time often characterizes the behavior of the material. In comparison to the time scale of measurement, if the relaxation time is long, the material behaves as an elastic solid. If the relaxation time is very short, the material behaves as a viscous liquid. Only when the relaxation time is comparable to the time scale of measurement is the material viscoelastic.

For one-dimensional deformation, the body undergoes uniaxial tension or compression. For a three-dimensional deformation, the body undergoes the shear force. That is, for a three-dimensional deformation, we have shear stress (labeled σ_s) and shear strain (labeled γ). The shear modulus G and the shear compliance J are defined and related by

$$G = \frac{\sigma_s}{\gamma} = \frac{1}{J}$$

The relationships between E and G and between D and J are given by

$$E = 2(1 + \mu)G \quad J = 2(1 + \mu)D$$

where μ is Poisson's ratio:

$$\mu = \frac{1}{2} \left[1 - \frac{1}{V} \frac{dV}{d\varepsilon} \right]$$

and V is the volume.

If a mechanical body is under a constant stress and if its strain is measured as a function of time, we can introduce two more quantities:

$$J(t) = \frac{\gamma(t)}{\sigma_{s0}} \quad D(t) = \frac{\varepsilon(t)}{\sigma_{t0}}$$

where σ_{s0} is the constant shear stress, ε is the tensile strain, and σ_{t0} is the constant tensile stress. The quantity $J(t)$ is called the shear creep and the quantity $D(t)$ is called the tensile creep. Both are measured by relaxation experiments and both are known as step functions. In a dynamic relaxation experiment, however, the stress or the strain is an oscillating function with an angular frequency ω . Our measurement of dynamic modulus values is often in terms of ω rather than time. The quantities $\sigma(t)$ and $\varepsilon(t)$ for one dimension are redefined:

$$\sigma(t) = \sigma_0 e^{i\omega t} \quad \varepsilon(t) = \varepsilon_0 e^{i(\omega t - \delta)} \tag{8.45}$$

where δ is the loss angle. Similarly, for three dimensions, we redefine

$$\sigma_s(t) = \sigma_0 \sin \omega t \quad \gamma(t) = \frac{\sigma_0}{G} \sin \omega t$$

The viscosity behavior measured by the relaxation experiment is now described by

$$\frac{d\gamma}{dt} = \frac{\sigma_0}{\eta} \sin \omega t$$

which can be integrated to give

$$\gamma(t) = \frac{\sigma_0}{\eta\omega} - \frac{\sigma_0}{\eta\omega} \cos \omega t$$

Substituting Eq. (8.45) into Eq. (8.44), we obtain

$$\frac{d\varepsilon(t)}{dt} = \frac{\sigma_0}{E} i\omega e^{i\omega t} + \frac{\sigma_0}{\eta} e^{i\omega t} \tag{8.46}$$

Solving this equation for a Maxwell body leads to the following equations of moduli, which include the parameter τ :

$$\begin{aligned} \tan \delta &= \frac{E_2}{E_1} = \frac{1}{\tau\omega} \\ E_1 &= E \frac{\tau^2\omega^2}{1 + \omega^2\tau^2} \quad E_2 = E \frac{\tau\omega}{1 + \omega^2\tau^2} \end{aligned} \tag{8.47}$$

where δ is the tangent of the phase angle between the stress and strain, that is, the loss angle, and E_1 and E_2 are real parts of the complex modulus E^* :

$$E^* = E_1 + iE_2 \quad (8.48)$$

Similar equations can be written for a complex shear modulus G^* (where j is an index of the element; $j = 1, 2, \dots, N$):

$$G^* = G_1 + iG_2 = \frac{i\omega\eta_j}{1 + i\omega\tau_j} \quad (8.49)$$

with

$$\begin{aligned} \tau_j &= \frac{\eta_j}{G_j} \\ G_1 &= G_j \frac{\omega^2\tau_j^2}{1 + \omega^2\tau_j^2} & G_2 &= G_j \frac{\omega\tau_j}{1 + \omega^2\tau_j^2} \\ \tan \delta &= \frac{1}{\omega\tau_j} \end{aligned} \quad (8.50)$$

8.2.1 Rouse Theory

In 1953 Rouse published a paper to describe theoretically the flow of polymers in dilute solutions. The polymer molecule is assumed to exist as a statistical coil and is subdivided into N submolecules. Each submolecule is thought of a solid bead. The beads behave as Gaussian chains and their entropy-elastic recovery can be described by a spring with a spring constant $3kT/a^2$, where a is the average end-to-end distance of a submolecule and k is the Boltzmann constant. The model is shown in Figure 8.9.

However, there is no interaction between beads other than the spring force. The restoring force on each of the beads is given by

$$f_{jx} = \frac{-3kT}{a^2} (-x_{j-1} + 2x_j - x_{j+1}) \quad (8.51)$$

When the polymer is emerged in a solvent medium, an additional force, frictional drag, acts on the bead:

$$f_{jx} = \zeta \frac{dx_j}{dt} = \zeta \dot{x}_j \quad (8.52)$$

where ζ is the segmental friction factor. Because the forces arising from the acceleration of the beads are small, the elastic force given in Eq. (8.51) and the

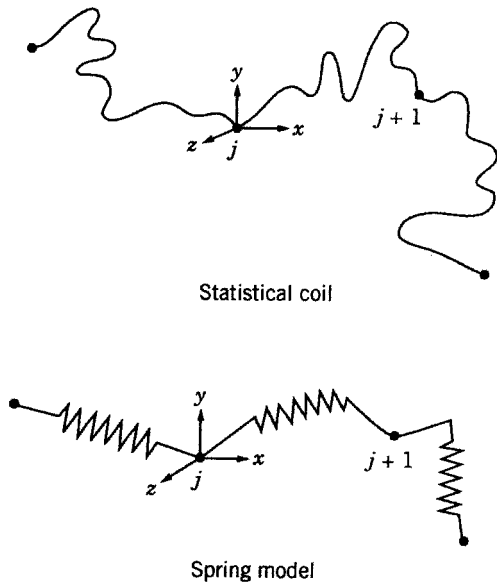


FIGURE 8.9 Spring-bead model.

viscous force given in Eq. (8.52) must be equal. Thus, we have

$$\zeta \dot{x}_j = \frac{-3kT}{a^2} (-x_{j-1} + 2x_j - x_{j+1}) \tag{8.53}$$

This set of linear first-order differential equations can be summarized in the form of a matrix equation

$$[\dot{X}] = -B[A][X] \tag{8.54}$$

where B represents the mobility of the end of a submolecule. To solve Eq. (8.54), an orthogonal transformation of coordinates was performed (see Yamakawa, 1971). By doing so, the coordination of all the motions of the path of a polymer is resolved into a series of modes. Each mode has a characteristic relaxation time τ_j .

Final results obtained for the viscoelastic properties of dilute solutions of coiling polymers are given in a series of equations. The real and imaginary components of a complex viscosity $\eta^* = \eta_1 - i\eta_2$ are

$$\begin{aligned} \eta_1 &= \eta_s + nkT \sum_{j=1}^N \frac{\tau_j}{1 + \omega^2 \tau_j^2} \\ \eta_2 &= nkT \sum_{j=1}^N \frac{\omega \tau_j^2}{1 + \omega^2 \tau_j^2} \end{aligned} \tag{8.55}$$

where η_s is the viscosity of the solvent and η is the number of links of a chain. The components for a complex shear modulus

$$G^* = G_1 + iG_2 = i\omega\eta^* \quad (8.56)$$

are

$$G_1 = nkT \sum_{j=1}^N \frac{\omega^2 \tau_j^2}{1 + \omega^2 \tau_j^2}$$

$$G_2 = \omega\eta_s + nkT \sum_{j=1}^N \frac{\omega \tau_j}{1 + \omega^2 \tau_j^2} \quad (8.57)$$

The relaxation times τ_j in these equations are

$$\tau_j = r^2 \left[24 BkT \sin^2 \frac{j\pi}{2(N+1)} \right]^{-1} \quad j = 1, 2, \dots, N \quad (8.58)$$

where r^2 is the mean-square end-to-end distance of the submolecule. In a steady flow, $\omega = 0$, we have $G_1 = 0$, $G_2 = 0$, and $\eta_2 = 0$. The real part of η^* is now the steady-flow viscosity η_0 :

$$\eta_0 = \eta_s + \frac{nr^2 N(N+2)}{36B} \quad (8.59)$$

Each relaxation time makes a contribution of $\eta kT \tau_j$ to η_0 . The subscript runs from 1 to N . The longer relaxation time, τ_1 , accounts for nearly all of the viscosity. The short relaxation time, τ_N accounts for only a small part of the viscosity. The two quantities may be expressed as

$$\tau_1 = nr^2 \left[24 B \sin^2 \frac{\pi}{2(N+1)} \right]^{-1}$$

$$\tau_N = \frac{r^2}{24 BkT} \quad \text{if } N \gg 1 \quad (8.60)$$

According to Eq. (8.58), the relaxation times are inversely proportional to temperature and to the mobility of the end of a submolecule. The mobility increases with the decrease in the viscous force that is exerted by the surrounding medium. The relaxation times are directly proportional to r^2 (the mean-square end-to-end distance of the submolecule) and consequently to $\langle R^2 \rangle$ (the mean-square end-to-end distance of the polymer molecule).

If $N \gg 2$, Eq. (8.59) can be rewritten

$$\eta_0 - \eta_s = \frac{\eta N \langle R^2 \rangle}{36B} \quad (8.61)$$

Note that $\langle R^2 \rangle = r^2 N$. This equation is similar to the one obtained by Debye in his hydrodynamic calculation of the viscosity of a solution of free-draining chains. However, N here is the number of submolecules rather than the number of atomic groups, and the frictional coefficient of an atomic group is replaced by B^{-1} , as Rouse pointed out. For experimental study, see Rouse's other two papers (1953, 1954).

8.2.2 Zimm Theory

Zimm's model (1956) is also a chain of beads connected by ideal springs. The chain consists of N identical segments joining $N + 1$ identical beads with complete flexibility at each bead. Each segment, which is similar to a submolecule, is supposed to have a Gaussian probability function. The major difference between the two models lies in the interaction between the individual beads. In the Rouse model, such interaction is ignored; in Zimm's model, such interaction is taken into consideration.

According to Zimm's model, if a chain is suspended in a viscous liquid, each bead j encounters three different forces: mechanical force, Brownian motion, and the motion of a fluid.

Mechanical Force Mechanical force can be expressed by

$$F_{xj} = \zeta(\dot{x}_j - v'_{xj}) \quad (8.62)$$

where ζ is a friction factor, $\dot{x}_j = dx_j/dt$, and v'_{xj} is the velocity component of the fluid if the j th bead were absent. Similar expressions are given for F_{yj} and F_{zj} .

Brownian Motion From the Brownian motion, the beads move, resulting in a force F that involves Hooke's law:

$$F_{xj} = -kT \frac{\partial \ln \psi}{\partial x_j} - \frac{3kT}{a^2} (-x_{j-1} + 2x_j - x_{j+1}) \quad (8.63)$$

where ψ is the probability of finding each bead j with coordinates between x_j and $x_j + dx_j$; the term $3kT/a^2$ is the Hooke's law spring force constant; the x 's are coordinates of the j th bead and its next neighbors. Similar equations are given for F_{yj} and F_{zj} .

Motion of a Fluid Zimm adopted the Kirkwood–Riseman approximate form of the Oseen interaction formula to describe the force on the motion of a fluid:

$$v'_{xj} = v_{xj} + \sum_{j \neq k} T_{jk} F_k \quad (j \text{ and } k \text{ both being index numbers}) \quad (8.64)$$

where v_{xj} is the x component of the velocity that the fluid would have in the absence of all forces from a chain and the interaction coefficients T_{jk} are given as

$$T_{jk} = \frac{1}{(6\pi^3)^{1/2} \eta a (|j-k|)^{1/2}} \quad (8.65)$$

with η the viscosity of the fluid. Similar equations are given for v'_{yj} and v'_{zj} .

The equation of motion is obtained by combining three equations representing three different forces:

$$\begin{aligned} \dot{x}_j = v_{xj} - D \frac{\partial \ln \psi}{\partial x_j} - \sigma(-x_{j-1} + 2x_j - x_{j+1}) \\ - \zeta \sum_{k \neq j} T_{jk} \left[D \frac{\partial \ln \psi}{\partial x_k} + \sigma(-x_{k-1} + 2x_k - x_{k+1}) \right] \quad (8.66) \\ 0 < j < N \end{aligned}$$

where $D = kT/\zeta$ and $\sigma = 3kT/a^2\zeta$. Similar expressions are given for \dot{y}_j and \dot{z}_j .

The solutions to the above differential equations are based on a method similar to the one used by Rouse. The equations are first put in the form of vector and matrix notations. Then the matrices are diagonalized by similarity transformation, congruent transformation, and so on, all of which are well-known techniques in matrix algebra. Finally, the matrices are separated by a linear transformation into normal coordinates with which direct integrations become possible.

Zimm's results are

$$\begin{aligned} [\eta] &= \frac{N_A a^2 \zeta}{6M\eta} \sum_{k=1}^N \frac{1}{\lambda_k (1 + i\omega\tau_k)} \\ \tan 2\chi &= \frac{\sum_{k=1}^N \tau_k / (1 + i\omega\tau_k)}{\kappa \sum_{k=1}^N \tau_k^2 / (k - 2\omega^2\tau_k^2 + 3i\omega\tau_k)} \quad (8.67) \\ \Delta n &= \frac{q'cNa^2[\eta]\kappa\eta}{MR'T} \left(1 + \frac{1}{4} \tan^2 2\chi \right)^{1/2} \end{aligned}$$

where χ is the angle between the principal axes of the polarizability tensor and the χ axis, q' is an optical constant, R' is the gas constant, c is the concentration, T is the temperature, and κ is the shear rate. The lost angle δ here is the phase angle between the stress and strain and

$$\tan \delta = \frac{E''}{E'} = \frac{1}{\tau\omega}$$

where E is the tensile modulus. The relaxation times τ_k are given by

$$\tau_k = \frac{1}{2\sigma\lambda_k} = \frac{M\eta[\eta]_0}{R'T\lambda_k \left(\sum_{k=1}^N 1/\lambda_k \right)} \quad (8.68)$$

where $[\eta]_0$ is the intrinsic viscosity at $\omega = 0$. For the free-draining case,

$$\lambda_k = \frac{\pi^2 k^2}{N^2}$$

and we get

$$\begin{aligned} [\eta]_0 &= \frac{N_A N^2 a^2 \zeta}{36 M \eta} \\ \tan 2\chi_0 &= \frac{5R'T}{2M[\eta]_0 \kappa \eta} \\ \tau_k &= \frac{6M\eta[\eta]_0}{\pi^2 R'T k^2} \end{aligned} \quad (8.69)$$

For the non-free-draining case, we have

$$\lambda_k = \left(\frac{4h}{N^2}\right) \lambda'_k$$

where h is a parameter and λ'_k can be tabulated. The intrinsic viscosity is

$$[\eta] = \frac{\pi^{3/2} N_A L^3}{4 \cdot 3^{1/2} M} \sum_{k=1}^N \frac{1}{\lambda'_k (1 + i\omega\tau_k)} \quad (8.70)$$

with

$$\begin{aligned} L &= N^{1/2} a \quad (a = \text{mean segment length}) \\ \tau_k &= \frac{M\eta[\eta]_0}{0.586 R'T \lambda'_k} \end{aligned} \quad (8.71)$$

REFERENCES

- Aklonis, J. J., W. J. MacKnight, and M. Shen, *Introduction to Polymer Viscoelasticity*. New York: Wiley, 1972.
- Baxendale, J. H., S. Bywater, and M. G. Evans, *J. Polym. Sci.* **1**, 237 (1946).
- Brandrup, J., and E. H. Immergut (Eds.), *Polymer Handbook*. New York: Wiley, 1975.
- Brant, D. A., and P. Flory, *J. Am. Chem. Soc.* **87**, 2788 (1965).
- Bueche, F., *J. Chem. Phys.* **20**, 1959 (1952).
- Bueche, F., *J. Chem. Phys.* **22**, 603 (1954).
- Bueche, F., *Physical Properties of Polymers*. New York: Wiley, 1962.
- Debye, P., and A. M. Bueche, *J. Chem. Phys.* **16**, 573 (1948).
- de Gennes, P. G., *Introduction to Polymer Physics*. Cambridge: Cambridge University Press, 1990.

- Einstein, A., *Ann. Phys.* **19**, 289 (1906).
- Einstein, A., *Ann. Phys.* **34**, 591 (1911).
- Eisele, U., *Introduction to Polymer Physics*, New York: Springer, 1990.
- Ferry, J. D., *Viscoelastic Properties of Polymers*, 3rd ed. New York: Wiley, 1980.
- Flory, P. J., *Principles of Polymer Chemistry*. Ithaca, NY: Cornell University Press, 1953.
- Flory, P. J., and T. G. Fox, Jr., *J. Am. Chem. Soc.* **73**, 1904 (1951).
- Fox, T. G., Jr., J. C. Fox, and P. J. Flory, *J. Am. Chem. Soc.* **73**, 1901 (1951).
- Freed, K. F., *Macromolecules* **13**, 623 (1980).
- Houwink, R., *J. Prakt. Chem.* **157**, 15 (1940).
- Huggins, M. L., *J. Am. Chem. Soc.* **64**, 2716 (1942).
- Kirkwood, J. G., and J. Riseman, *J. Chem. Phys.* **16**, 565 (1948).
- Kirkwood, J. G., and J. Riseman, *J. Chem. Phys.* **17**, 442 (1949).
- Kraemer, E. O., *Ind. Eng. Chem.* **30**, 1200 (1938).
- Kuhn, W., and H. Kuhn, *Helv. Chim. Acta* **28**, 97 (1945).
- Kurata, M., and W. H. Stockmayer, *Fortschr. Hochpolym. Forsch.* **3**, 196 (1963).
- Mark, H., *Der feste Körper*. Leipzig: Hirzel, 1938.
- Martin, A. F. *Abstr. 103rd Am. Chem. Soc. Meeting*, p. 1-c ACS (1942).
- Oseen, C. W., *Hydrodynamik*. Leipzig: Akademische Verlagsgesellschaft, 1927.
- Peterlin, A., *Z. Phys.* **111**, 232 (1938).
- Peterlin, A., *J. Polym. Sci.* **5**, 473 (1950).
- Rouse, P. E., Jr., *J. Chem. Phys.* **21**, 1272 (1953).
- Rouse, P. E., Jr., and K. Sittel, *J. Applied Phys.* **24**, 690 (1953).
- Scheraga, H. A., and L. Mandelkern, *J. Am. Chem. Soc.* **75**, 179 (1953).
- Schultz, G. W., and F. Blaschke, *J. Prakt. Chem.* **158**, 130 (1941).
- Simha, R., *J. Phys. Chem.* **44**, 25 (1940).
- Sittel, K., P. E. Rouse, Jr., and E. D. Bailey, *J. Appl. Phys.* **10**, 1312 (1954).
- Staudinger, H., *Die hochmolekularen organischen Verbindungen*. Berlin: Julius Springer, 1932.
- Stockmayer, W. H., and M. Fixman, *J. Polym. Sci. C* **1**, 137 (1963).
- Sun, S. F., *J. Phys. Chem.* **76**, 128 (1972).
- Sun, S. F., and N. del Rosario, *J. Am. Chem. Soc.* **92**, 1837 (1970).
- Yamakawa, H., *Modern Theory of Polymer Solutions*. New York: Harper & Row, 1971.
- Yang, J. T., *Adv. Protein Chem.* **16**, 323 (1961).
- Zimm, B. H., *J. Chem. Phys.* **24**, 269 (1956).

PROBLEMS

- 8.1** The following data were found using a Cannon–Ubbelohde viscometer N.50 to measure the flow time of bovine serum albumin in 25% dioxane–75% water (at ionic strength 0.03 and temperature 25°C) as a function of the concentration of protein:

c (g/100 mL)	t (s)
0.986	337.2
0.657	335.5
0.493	334.6
0.394	334.1
0.329	333.7
0	331.7

The density ρ of a solution may be estimated by

$$\rho = \rho_0 + \left(\frac{1 - \bar{v}\rho_0}{100} \right) c$$

where \bar{v} for BSA is 0.738 mL/g and ρ_0 for 25% dioxane–75% water is 1.0181 g/mL. Determine the intrinsic viscosity (Sun, 1972).

- 8.2** The following data were obtained in terms of degree of polymerization versus the intrinsic viscosity for poly(methyl methacrylate) in benzene at 25°C:

Degree of Polymerization	$[\eta]$ (dL/g)
700	0.334
1450	0.678
2230	0.929
3940	1.153
4080	1.305
9800	2.510

The molecular weight of the monomer is 100. Determine K and a (Baxendale et al., 1946).

- 8.3** The intrinsic viscosity of polystyrene in benzene (a good solvent) at 25°C is 5.27 dL/g, and in 27.2% methanol–72.8% toluene (a poor solvent) it is 1.39 dL/g. Calculate the molecular weight of polystyrene. Take $K = 9.71 \times 10^{-5}$ and $a = 0.74$ for benzene and $K = 8.81 \times 10^{-4}$ and $a = 0.5$ for 27.2% methanol–72.8% toluene.
- 8.4** The following data were obtained for the intrinsic viscosity of polystyrene in cyclohexane as a function of temperature:

Molecular Weight of Polymer	T (°C)	$[\eta]$ (dL/g)
1,270,000	34	0.89
	45	1.14
	55	1.43

Molecular Weight of Polymer	T ($^{\circ}\text{C}$)	$[\eta]$ (dL/g)
360,000	34	0.47
	45	0.56
	55	0.66
92,000	34	0.23
	45	0.25
	55	0.28

- (a) Evaluate K .
 (b) Assuming $\phi = 2.1 \times 10^{21}$, calculate $\langle R_0^2 \rangle / M$.
 (c) Calculate ψ_1 , c_m , and θ .
 (d) Estimate ψ_1 and κ_1 at 25°C .

For polystyrene at 25°C , \bar{v} is 0.92. *Hint:* $[\eta]_{\theta} = [\eta]_{34^{\circ}\text{C}}$ (Fox and Flory, 1951).

- 8.5** For a large value of the degree of polymerization N (where $N = M/M_0$), the Kirkwood–Riseman equation of the intrinsic viscosity is reduced to

$$b^3 = \frac{2267}{(6\pi^3)^{1/2}} \frac{M_0}{N_A} \lim_{n \rightarrow \infty} \frac{[\eta]}{\sqrt{N}}$$

where N_A is Avogadro's number. The following experimental data are given for the intrinsic viscosity of polystyrene in benzene as a function of the degree of polymerization:

$[\eta]$ (mL/g)	$N \times 10^3$
0.20	0.625
0.60	2.50
1.75	10.0
3.15	22.5

- (a) Plot $[\eta]/\sqrt{N}$ versus $1/\sqrt{N}$ and extrapolate the curve to obtain the intercept

$$\left(\frac{[\eta]}{\sqrt{N}} \right)_0 \left(= \lim_{\sqrt{N} \rightarrow 0} \frac{[\eta]}{\sqrt{N}} \right)$$

Then calculate the value of b , the effective bond length. Here $M_0 = 52$ for $-\text{C}_6\text{H}_5\text{CH}-\text{CH}_2-$.

- (b) Assume that $\lambda_0 = 1.9 \times 10^{-4}$ (see Kirkwood and Riseman, 1948). Calculate ζ , the frictional coefficient of a monomeric unit, from

$$\lambda_0 = \frac{\zeta}{(6\pi^3)^{1/2} \eta_0 b}$$

where η_0 is the viscosity of the solvent ($\eta_0 = 0.602$ cP for benzene).

- (c) Estimate the root-mean-square end-to-end distance of a polystyrene with molecular weight 10^6 using

$$R_0 = N^{1/2}b$$

(Kirkwood and Riseman, 1948).

- 8.6** Calculate the root-mean-square end-to-end distance for a polystyrene with molecular weight 2×10^5 in benzene with an intrinsic viscosity of 107 mL/g. According to Debye and Bueche's analysis, the shielding ratio is in the vicinity of 0.836 with $\sigma = 3.92$ (Debye and Bueche, 1948).
- 8.7** The following data were obtained in the measurement of intrinsic viscosities and sedimentation coefficients of bovine serum albumin in acidic water-dioxane mixtures at 25°C and ionic strength 0.03:

% Dioxane	$[\eta]$ (mL/g)	$S_{25, w}$	$100\eta_0$
0	0.170	2.25	0.893
15	0.198	2.09	1.190
30	0.231	1.98	1.502
40	0.253	2.06	1.705

- (a) Calculate the Scheraga–Mandelkern shape factor β .
- (b) Discuss the physical significance in the change of β (Sun and del Rosario, 1970).
- 8.8** The following experimental data were obtained for the study of molecular dimensions of polypeptides poly- β -benzyl-1-aspartate (PBLA) and poly- β -benzyl-1-glutamate (PBLG):

Polymer	M_0	Solvent	Temperature (°C)	$[\eta]$ (dL/g)	$M_n \times 10^{-3}$	$A_2 \times 10^4$ (cm ³ mol/g ²)	α
PBLA	205	<i>m</i> -Cresol	100	0.915	187	3.37	1.22
PBLG	219	Dichloro acetic acid	25	1.84	3.36	7.5	1.51

where M_0 is the molecular weight of an amino acid residue, $[\eta]$ is the intrinsic viscosity, M_n is the molecular weight obtained from the osmotic pressure measurements, A_2 is second virial coefficient, and α is the linear expansion factor. Assume that M_v (viscosity molecular weight) = M_n and $T = \theta$. Calculate the following:

- (a) $\langle R^2 \rangle_0 / M$, the ratio of the mean-square unperturbed distance $\langle R^2 \rangle_0$ between the polymer chain ends and the molecular weight of the chain
- (b) $\langle R^2 \rangle_0$, the unperturbed mean-square end-to-end distance

- (c) nl^2 , the theoretical mean-square end-to-end distance where n is the degree of polymerization and l is the fixed distance between the α carbon of the trans peptide repeating unit in the chain. Assume that $l = 3.80 \text{ \AA}$.
- (d) $\langle R^2 \rangle_0 / nl^2$, the characteristic ratio of the polypeptides (Brant and Flory, 1965).

8.9 The shear stress relaxation modulus for one element in the Maxwell model is given by

$$G(t) = Ge^{-t/\tau}$$

For the z element

$$G(t) = \sum_{i=1}^z G_i e^{-t/\tau_i}$$

show that the viscosity η , in terms of relaxation time, for this model is

$$\eta = \sum_{i=1}^z G_i \tau_i$$

The viscosity is related to $G(t)$ by

$$\eta = \int_0^{\infty} G(t) dt$$

(Aklonis et al., 1972).

9

OSMOTIC PRESSURE

Osmotic pressure is one of four well-known colligative properties of a non-electrolyte solution; the other three are lowering of vapor pressure, elevation of the boiling point, and depression of the freezing point. They are all expressed in terms of the change in the activity of the solvent a_1 when a solute is present. The activity a_1 is defined as

$$\mu_1 - \mu_1^\circ = RT \ln a_1 \quad (9.1)$$

where for a two-component system the subscript 1 refers to the solvent, the subscript 2 refers to the solute, and μ is the chemical potential. The Gibbs–Duhem equation (Gibbs, 1931; Duhem, 1896) relates the activity a_1 to mole fraction x_2 :

$$\left(\frac{\delta \ln a_1}{\delta \ln x_1} \right)_{T,P} = \left(\frac{\delta \ln a_2}{\delta \ln x_2} \right)_{T,P} \quad (9.2)$$

If the solution is very dilute, we can write

$$\frac{\ln a_1}{\ln x_1} \cong 1$$

That is, $a_1 \cong x_1$. Since $x_1 + x_2 = 1$, we can now express a_1 (the activity of the solvent) in terms of x_2 (the mole fraction of the solute) by

$$a_1 = 1 - x_2$$

By definition, the mole fraction is related to the concept of mole, which in turn is related to the molecular weight. We thus have the following correlation:

$$a_1 \Rightarrow x_2 \Rightarrow \text{molecular weight of solute}$$

The value of a_1 can be determined with any of the four colligative properties. We have already discussed vapor pressure measurement. In this chapter, we discuss the measurement of osmotic pressure, neglecting boiling point elevation and freezing point depression because they are less important.

The chemical potential, activity, and osmotic pressure are related by the following equation:

$$\mu_1 - \mu_1^\circ = R'T \ln a_1 = -\pi' \bar{v}_1 \quad (9.3)$$

where π' is the osmotic pressure (to be distinguished from $\pi = 3.1416$, an irrational number) and \bar{v}_1 is the partial specific volume of the solvent. Equation (9.3) states that because of the difference in chemical potential between the solvent in the solution (μ_1) and that in its pure phase (μ_1°), there is a driving force to push the solvent flow into the solution. This driving force is expressed by the quantity a_1 .

9.1 OSMOMETERS

There are various types of osmometers. In Figure 9.1 we show two examples. Some commonly used membranes are cellulose acetate, cellulose hydrate, cellulose nitrate, polyurethanes, gel cellophane membranes, and poly(chlorotrifluoroethylene).

The osmotic pressure is calculated using

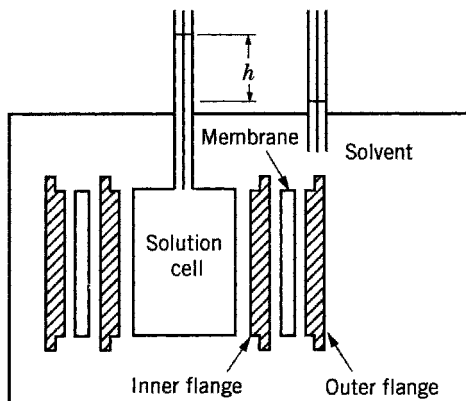
$$\pi' = \rho_1 g h \quad (9.4)$$

where ρ_1 is the density of the solvent (in grams per cubic centimeters or kilograms per cubic meters), g is the gravitational constant, 0.981 m s^{-2} , and h is the height expressed in centimeters. The unit of osmotic pressure is $\text{Pa M}^3 \text{ kg}^{-1}$ (SI system: $1 \text{ PA} = 1 \text{ N/m}^2$).

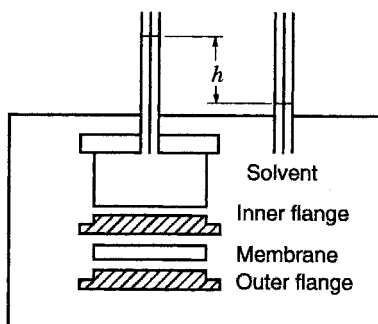
9.2 DETERMINATION OF MOLECULAR WEIGHT AND SECOND VIRIAL COEFFICIENT

For a thermodynamically ideal solution (e.g., a very dilute solution), the osmotic pressure obeys Van't Hoff's equation:

$$\frac{\pi'}{c} = \frac{R'T}{M} \quad (9.5)$$



(a)



(b)

FIGURE 9.1 Osmometers: (a) Helfritz type; (b) Schultz type.

where c is the concentration of the solute in g/100 mL, R' is the gas constant (8.314 Pa m³/(mol K)), T is the temperature in kelvin, and M is the number average molecular weight. The plot of π' versus c or π'/c versus c gives characteristic straight lines with slopes 1 and 0, respectively. In either case, Van't Hoff's equation is used to determine the molecular weight of the solute, that is, the y intercept of the linear plot. At higher concentrations, deviations from the ideal are usually pronounced and the plot of π'/c versus c , while still a straight line, gives different slopes, depending on the chemical system. Van't Hoff's equation must be modified to

$$\frac{\pi'}{c} = \frac{R'T}{M}(1 + \Gamma_2 c) \quad (9.6)$$

where Γ_2 is the second virial coefficient, which is a measure of the deviation from the ideal. In a complicated system the plot of π'/c versus c may not give a straight

line, in which case Van't Hoff's equation must be further modified. Parallel to the equation of state for real gases, the osmotic pressure may be expressed in terms of the virial equation:

$$\pi' = R'T(A_1c + A_2c^2 + A_3c^3 + \dots) \quad (9.7)$$

where $A_1 = 1/M$ and A_2 and A_3 are the second and third virial coefficients, respectively [cf. Eq. (4.16) in Chapter 4]. For the convenience of treating data, the virial equation may be expressed in a slightly different form:

$$\frac{\pi'}{c} = R'T(A_1 + A_2c + A_3c^2 + \dots) \quad (9.8)$$

$$\frac{\pi'}{c} = A_1(1 + \Gamma_2c + \Gamma_3c^2 + \dots) \quad (9.9)$$

where

$$\Gamma_2 = A_2M, \quad \Gamma_3 = A_3M, \dots$$

The coefficients A_2, A_3, \dots or $\Gamma_2, \Gamma_3, \dots$ are functions of the molecular weight distribution of solute, the solvent-solute system, and the temperature. Virial coefficients beyond A_3 or Γ_3 are usually of no physical interest and can be neglected.

There are several ways to treat the osmotic pressure data if the plot is not linear:

1. The curve-fitting method can be used to determine A_1, A_2 , and A_3 directly.
2. In the case where A_1 is known or can be reasonably estimated, Eq. (9.9) can be rearranged in the form

$$\left(\frac{\pi'/c - 1}{A_1}\right) \frac{1}{c} = \Gamma_2 + \Gamma_3c \quad (9.10)$$

and $[(\pi'/c - 1)/A_1](1/c)$ versus c can be plotted. A straight line may be obtained in which the intercept gives the value of Γ_2 and the slope gives the value of Γ_3 .

3. Flory (1953) suggested that data be treated in the following way:

$$\frac{\pi'}{c} = \frac{R'T}{M}(1 + \Gamma_2c + j\Gamma_2^2c^2)$$

The value of j depends on the polymer-solvent system. As a trial we may assume that $j \cong 0.25$ and take the square root on both sides. The equation becomes

$$\left(\frac{\pi'}{c}\right)^{1/2} = \left(\frac{\pi'}{c}\right)_0^{1/2} \left(1 + \frac{\Gamma_2}{2}c\right) \quad (9.11)$$

By plotting $(\pi'/c)^{1/2}$ versus c , a straight line may be expected and the values of M and Γ_2 may be determined.

4. The value of j in Eq. (9.11) may not be a constant and may depend on the molecular weight. To avoid complications, Bawn and co-workers (1950) suggested another method to treat data:

$$\left(\frac{\pi'}{cR'T}\right)_1 - \left(\frac{\pi'}{cR'T}\right)_2 = A_2(c_1 - c_2) + A_3(c_1^2 - c_2^2)$$

and hence

$$\frac{(\pi'/cR'T)_1 - (\pi'/cR'T)_2}{c_1 - c_2} = A_2 + A_3(c_1 + c_2) \quad (9.12)$$

The pairs of points (c_1, c_2) , $[(\pi'/c)_1, (\pi'/c)_2]$ are selected on the experimental curve. By plotting the term of the left side of the equation against $c_1 + c_2$, a straight line may be obtained, from which we get intercept A_2 and slope A_3 .

Summary The equation of osmotic pressure is usually expressed in one of the following three ways:

$$\frac{\pi'}{c} = \frac{R'T}{M} + Bc + Cc^2 \quad (9.13a)$$

$$\frac{\pi'}{c} = R'T \left(\frac{1}{M} + A_2c + A_3c^2 + \dots \right) \quad (9.13b)$$

$$\frac{\pi'}{c} = \frac{R'T}{M} (1 + \Gamma_2c + \Gamma_3c^2 + \dots) \quad (9.13c)$$

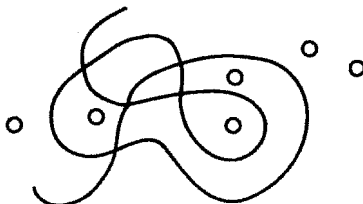
The quantity π'/c is called the reduced osmotic pressure and has the unit joules per kilogram and B , A , and Γ are different symbols for the same quantity, virial coefficient.

9.3 THEORIES OF OSMOTIC PRESSURE AND OSMOTIC SECOND VIRIAL COEFFICIENT

While the measurement of osmotic pressure π' and the calculation of the second virial coefficient A_2 are relatively simple, their theoretical interpretations are rather complicated. Throughout the past half century, many investigators have tried to set up a model and derive equations for π' and A_2 . Because of the unsymmetrical nature with respect to the sizes of solute (macromolecule) and solvent (small molecule), polymer solutions involve unusually large intermolecular interactions. Furthermore, since π' is directly related to μ_1 , any theoretical knowledge learned from the osmotic pressure and the second virial coefficient contributes to the knowledge of the general thermodynamic behavior of polymer solutions. For this reason, Chapter 4 and 9 are closely related in macromolecular chemistry.

9.3.1 McMillan–Mayer Theory

In the McMillan–Mayer theory of solutions, the macromolecule is considered as a small gel immersed in a solution. The gel is surrounded by the solvent, but inside the gel there are also solvent molecules (\circ), as shown in the diagram:



Macromolecule

The gel acts like a semipermeable membrane. Only the solvent molecule can pass through the gel. The temperature remains the same inside and outside. The outside system has a specified value of the chemical potential μ_1 , while the inside system has specified values of μ_1 for the solvent and μ_2 for the solute. If the solution is in osmotic equilibrium with pure solvent, the inside (solution) would have pressure $p + \pi'$ to balance the outside (pure solvent) pressure p . The osmotic pressure inside the system is the excess pressure created to give μ_1 the same value (which tends to be lowered in the presence of the solute) inside as outside.

The grand partition function (See Appendix C) for the inside solution (according to Hill, 1960) is

$$e^{(p+\pi')V/kT} = \sum Q(V, T) \lambda_1^{N_1} \lambda_2^{N_2} \quad (9.14)$$

where Q is the grand canonical ensemble partition function, N is the number of molecules, V is the volume of the solution, and λ is often called the absolute activity, which is defined as $\lambda = e^{kT}$. The expression on the left, $e^{(p+\pi')V/kT}$, is the Boltzmann distribution factor and k is the Boltzmann constant.

With a messy mathematical manipulation on the equation that is related to Q and μ_1 , one can reach the theoretical expressions for π' and A_2 :

$$\pi' = kT\rho_2 + \sum A_2\rho_2^n \quad (9.15)$$

$$A_2 = -\frac{1}{2} \int_0^\infty \left[\exp\left(-\frac{w}{kT}\right) - 1 \right] 4\pi r^2 dr \quad (9.16)$$

where ρ_2 is the density of the polymer molecule, n is the number of molecules involved in the interaction, and w is the reversible work that is needed to bring two solute molecules together from $r = \infty$ to r in the outside solution.

The value of A_2 depends on w . If the solute molecule is considered as a hard sphere of diameter a , then

$$w = \begin{cases} \infty & r < a \\ 0 & r \geq a \end{cases}$$

and

$$A_2 = \frac{2\pi a^3}{3} \quad (\text{here } \pi = 3.1416) \quad (9.17)$$

9.3.2 Flory Theory

Flory's theory concerns the distribution of excluded volume u between n_2 polymer molecules over a volume V of solution. If there is an independent volume exclusion on the part of the individual molecules, the partition function of the system is

$$Q = \text{const} \times \prod_{i=0}^{n_2-1} (V - iu) \quad (9.18)$$

and

$$\begin{aligned} \Delta G &= -kT \ln Q \\ &= -kT \sum_{i=0}^{n_2-1} \ln(V - iu) + \text{const} \\ &= -kT \left[n_2 \ln V + \sum_{i=1}^{n_2-1} \ln \left(1 - \frac{i u}{V} \right) \right] + \text{const} \end{aligned} \quad (9.19)$$

Expanding the logarithmic terms in series and manipulating for the purpose of simplification, we obtain

$$\begin{aligned} \pi' &= -\frac{\mu_1 - \mu_1^0}{V_1} \\ &= -N \frac{(\partial \Delta G / \partial n_1)_{T,P,n_2}}{V_2} \end{aligned}$$

That is,

$$\pi' \cong kT \left[\frac{n_2}{V} + \frac{u}{2} \left(\frac{n_2}{V} \right)^2 \right] \quad (9.20)$$

Note that $n_2/V = cN_A/M$, where c is the concentration in grams per unit volume, and N_A is Avogadro's number. Equation (9.20) can be rewritten as

$$\frac{\pi'}{c} \cong R'T \left[\frac{1}{M} + \left(\frac{N_A u}{2M^2} \right) c \right] \quad (9.21)$$

and is discussed further in a later section.

In comparison of Eq. (9.21) with the virial equation,

$$\frac{\pi'}{c} \cong R'T(A_1 + A_2c + A_3c^2 + \dots)$$

we find

$$A_1 \cong \frac{1}{M} \quad A_2 = \frac{N_A u}{2M^2} \quad (9.22)$$

While Eq. (9.22) clearly relates A_2 to u and M , it vaguely indicates that the value of A_2 for a polymer system in solution decreases with the increasing value of M . It is vague because the theory has not specified yet the significance of u . To interpret u , the model needs to be improved.

9.3.3 Flory–Krigbaum Theory

In the improved model offered by Flory and Krigbaum (1950) the very dilute polymer solution is considered a dispersion of clouds, or dilute clusters, of segments. The region between swamps contains pure solvent. Consider a pair of polymer molecules l and m separated by a distance A_{lm} . When they are brought together, the change in entropy $\partial(\Delta S)$ and the change in enthalpy $\partial(\Delta H)$ are given by

$$\begin{aligned} \partial(\Delta S) &= -2k\psi_1 \left(\frac{V^2}{V_1} \right) \rho_l \rho_m \partial V \\ \partial(\Delta H) &= -2kT\kappa_1 \left(\frac{V^2}{V_1} \right) \rho_l \rho_m \partial V \end{aligned} \quad (9.23)$$

where ψ_1 is the entropy parameter, κ_1 is the enthalpy parameter, V is the volume of the polymer molecule, V_1 is the volume of the solvent molecule, ∂V is the volume element in the vicinity of the pair of molecules, and ρ_l and ρ_m are the densities of segments in ∂V . The partition function Q is

$$\ln Q = -2 \int_0^\infty \int_0^\pi J V^2 \bar{v}^{-2} \rho_l \rho_m 2\pi r^2 \sin \theta \, dr \, d\theta \quad (9.24)$$

where $\pi = 3.1416$, r and θ represent cylindrical coordinates, \bar{v} is the partial specific volume, and J is defined as

$$J = \frac{(\psi_1 - \kappa_1) \bar{v}^2}{V_1} \quad (9.25)$$

The second virial coefficient for homogeneous polymers can now be expressed theoretically:

$$\Gamma_2 = M \left(\frac{\bar{v}^2}{V_1} \right) (\psi_1 - \kappa_1) F(x)$$

or

$$A_2 = \frac{\bar{v}^2}{V_1} (\psi_1 - \kappa_1) F(x) \quad (9.26)$$

where

$$F(x) = 1 - \frac{x}{2!} 2^{3/2} + \frac{x^2}{3!} 3^{3/2} - \dots \quad (9.27)$$

The quantity x is related to the expansion factor α by

$$x = 2(\alpha^2 - 1) \quad (9.28)$$

In relation to the dimensions of the molecule over those of its random-flight counterpart, we have, as we may recall from Chapter 5,

$$\alpha^5 - \alpha^3 = 2c_M(\psi_1 - \kappa_1)M^{1/2} \quad (9.29)$$

If polymer molecules are not homogeneous in size, we need to modify the second virial coefficient:

$$A_2 = \frac{\bar{v}^2}{V_1} (\psi_1 - \kappa_1) \gamma \quad (9.30)$$

where

$$\gamma = \sum_i \sum_j w_i w_j F(x_{ij}) \quad (9.31)$$

The terms w_i and w_j are weight fractions of polymer species i and j and are related to x_{ij} ,

$$\frac{x_{ij}}{M_i M_j} = \left[\frac{2(x_{ii}/M_i^2)^{2/3} (x_{jj}/M_j)^{2/3}}{(x_{ii}/M_i^2)^{2/3} (x_{jj}/M_j)^{2/3}} \right]^{2/3} \quad (9.32)$$

Note: Here we have variable x_{ij} instead of x .

The characteristic features of Flory's theory and Flory and Krigbaum's theory are summarized as follows:

1. These theories introduced the Gaussian approximation for a spatial distribution of segments around the center of the mass.
2. They showed further the dependence of A_2 on M . The relationship between the two parameters may be expressed as

$$A_2 \sim M^\nu \quad (9.33)$$

The value of the exponent ν is between -0.1 and -0.3 , which is of great current interest in polymer chemistry.

3. Since $\psi_1 - \kappa_1 = 1 - \theta/T$, Eqs (9.26) and (9.30) can be rewritten respectively as

$$A_2 = \left(\frac{\bar{v}^2}{V_1}\right) \left(1 - \frac{\theta}{T}\right) F(x) \quad (9.34)$$

$$A_2 = \left(\frac{\bar{v}^2}{V_1}\right) \left(1 - \frac{\theta}{T}\right) \gamma \quad (9.35)$$

At the θ temperature, $T = \theta$ and $A_2 = 0$. This is now used as a definition of the θ temperature. Experimentally, if A_2 of a polymer system vanishes, we say that the temperature at which the measurements (e.g., osmotic pressure and light scattering) are taken in the θ temperature.

9.3.4 Kurata–Yamakawa Theory

Kurata and Yamakawa (1958) criticized McMillan and Mayer's theory for lack of experimental support and Flory and Krigbaum's theory for their assumption of Gaussian distribution of polymer segments around the center of the mass. The introduction of the factorization approximation does not help much. As a result, Flory and Krigbaum's theory underestimates the molecular weight dependence of A_2 . For Kurata and Yamakawa, the excluded volume effect has a non-Gaussian character with respect to the chain configuration. Kurata and Yamakawa's approach, however, basically follows the same line as that of McMillan and Mayer.

Consider a polymer molecule that consists of $N + 1$ segments of diameter b . The length of each link between two segments is a constant a . Kurata and Yamakawa assume that the total potential energy of the solution is additive over segment pair i and j :

$$w_{ij} = w(R_{ij}) = \begin{cases} \infty & \text{if } 0 \leq R_{ij} \leq b \\ -w_0 \exp\left(-\frac{3R_{ij}^2}{2d^2}\right) & \text{if } R_{ij} > b \end{cases} \quad (9.36)$$

where R_{ij} represents the distance between the segment pair and w_0 and d are constants. Then a function $\chi(R_{ij})$ can be defined as

$$\chi_{ij} \equiv \chi(R_{ij}) = \exp\left(-\frac{w_{ij}}{kT}\right) - 1 \tag{9.37}$$

Let α and β refer to the configurations of the polymer molecule and let l and m be the specified segments (*Note: i and j are for general segments.*) Then A_2 can be theoretically expressed as

$$A_2 = -\left(\frac{N_A}{2VM^2}\right)(B_1 + B_2 + \dots) \tag{9.38}$$

with

$$B_1 = \sum_{l_\alpha l_\beta} \int \chi_{l_\alpha l_\beta} f_\alpha f_\beta \, d\alpha \, d\beta \tag{9.39a}$$

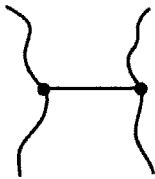
$$B_2 = \sum_{l_\alpha l_\beta m_\alpha m_\beta} \int \chi_{l_\alpha l_\beta} \chi_{m_\alpha m_\beta} f_\alpha f_\beta \, d\alpha \, d\beta \tag{9.39b}$$

The terms f_α and f_β are pairwise distribution functions and are defined as

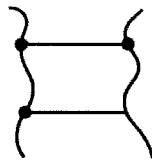
$$f_\alpha = \text{const} \times \exp\left(-\sum \frac{w_{i_\alpha j_\alpha}}{kT}\right) \tag{9.40a}$$

$$f_\beta = \text{const} \times \exp\left(-\sum \frac{w_{i_\beta j_\beta}}{kT}\right) \tag{9.40b}$$

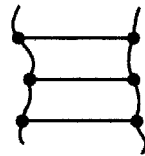
Here, B_1 is a single contact term, with one term of interaction function $\chi_{l_\alpha l_\beta}$; B_2 is a double intermolecular contact, with two terms of interaction function, $\chi_{l_\alpha l_\beta}$ and $\chi_{m_\alpha m_\beta}$. The following are diagrams of one-term contact, two-term contact, and three-term contact:



One term contact, B_1



Two term contact, B_2



Three term contact, B_3

The final results of these B terms are

$$B_1 = -VN_A^2 \left(\frac{4\pi b^3}{3}\right) \left(1 - \frac{\theta}{T}\right) \tag{9.41}$$

$$B_2 = B_{20} + B_{21} + B_{30} \tag{9.42}$$

In the expressions B_{20} , B_{21} , and B_{30} , the first subscript refers to the number of intermolecular contacts and the second refers to the number of intramolecular contacts. The numerical estimation of these three terms are

$$B_{20} = -2.865B_1z$$

$$B_{21} = 8.78B_1z^2$$

$$B_{30} = 9.73B_1z^2$$

where z , as defined in Chapter 5, is

$$z = \left(\frac{6}{\pi}\right)^{1/2} \left(\frac{b}{a}\right)^3 \left(1 - \frac{\theta}{T}\right) N_A^{1/2} \quad (\text{here } \pi = 3.1416) \quad (9.43)$$

By substituting these quantities into the equation of A_2 , we obtain

$$A_2 = \frac{2\pi Nb^3}{3M_0} \left(1 - \frac{\theta}{T}\right) h(z) \quad (\text{here } \pi = 3.1416) \quad (9.44)$$

$$h(z) = 1 - 2.865z + 18.51z^2 - \dots \quad (9.45)$$

Again, Eq. (9.44) defines the θ temperature as the temperature at which A_2 for the polymer system is zero.

9.3.5 des Cloizeaux–de Gennes Scaling Theory

A different approach to the interpretation of osmotic pressure and the second virial coefficient is an attempt to investigate the universal properties: scaling laws and characteristic exponents in polymer solutions. des Cloizeaux (1975) suggested that the properties of chain with excluded volume effect in a dilute solution can be deduced from Lagrangian theory (Appendix D) for a zero component field in the absence of an external field. If there are n components, the Green's functions (Appendix E) can be used to expand the Lagrangian theory in terms of interactions. In this way, the asymptotic behavior of the correlation function between the extremities of a single chain can be obtained, leading to the scaling law of universal properties.

Consider the polymer solution as a grand canonical ensemble which can be derived by using the Lagrangian theory. The averages of the total number of polymers and the total number of monomers are determined by two chemical potentials, H_0 and $s(= m_0^2 b^2)$, where m_0 is the normalized mass (a quantity used in the renormalization group theory) and b is the monomer length. The term H_0 is the magnetic field and is chosen because of the similarity between magnetic critical and tricritical phenomena and the behavior of flexible polymer solutions. The magnetic field H_0 is believed to be in correspondence with the chemical potential. The grand

partition function $Z(H_0)$ to be introduced to represent polymer solutions is expressed by des Cloizeaux as

$$Z(H_0) = 1 + \sum_{M=1}^{\infty} \frac{1}{2^M M!} [H_0 b^{(d/2)+1} (2\pi)^{d/2}]^{2M} \times \int_0^{\infty} \frac{dL_1}{b} \dots \int \frac{dL_M}{b} e^{-sLb^{-1}Z(L_1, \dots, L_M)} \quad (9.46)$$

where M is the index of a chain (not molecular weight), L is the length of the chain, d is the space dimension, and $\pi = 3.1416$. The expression $Z(L_1, \dots, L_M)$ refers to the number of polymer configurations in a box. Using the ordered Green's function, $Z(H_0)$ can be reduced to a simple expression:

$$Z(H_0) = \exp[V_w(H_0)] \quad (9.47)$$

where V is the volume of solution. The function $w(H_0)$ is directly related to the osmotic pressure π' :

$$\frac{\pi'}{kT} = w(H_0) \quad (9.48)$$

The concentration of polymers (chains) c_P and the concentration of monomers (links) c_M can also be expressed in terms of the function $w(H_0)$:

$$c_P = \frac{H_0}{2} \frac{\partial w(H_0)}{\partial H_0} \quad (9.49a)$$

$$c_M = -\frac{\partial}{\partial s} w(H_0) \quad (9.49b)$$

If there is no interaction, we have

$$w(H_0) = \frac{b^2 H_0^2}{2s} \quad (9.50)$$

and, therefore, we have

$$\pi' = kT c_P \quad (9.51)$$

Equation (9.51) is the classical Van't Hoff equation. To introduce the scaling law, we can define the average number of links per chain N as

$$N = \frac{c_M}{c_P} = \frac{1}{2s} \quad (9.52)$$

If there are interactions, we use Green's function, which is included in a term $\Gamma(M_0)$,

$$\Gamma(M_0) = \sum_{m=1}^{\infty} \frac{1}{2^m M!} [M_0 (2\pi)^{d/2}]^{2M} \Gamma^{(2m)}(0, \dots, 0) \quad (9.53)$$

the two concentration terms are now expressed as

$$c_P = \frac{M_0}{2} \frac{\partial \Gamma(M_0)}{\partial M_0} \quad (9.54a)$$

$$c_M = \frac{\partial \Gamma(M_0)}{\partial s} \quad (9.54b)$$

The derivation of the equation for osmotic pressure is more complicated. The final result is expressed in a parametric equation:

$$\frac{\pi'}{kT c_P} = F(c_P b^d N^{vd}) = F\left(\frac{b^d c_M^{vd}}{c_P^{vd-1}}\right) = F(\lambda) \quad (9.55)$$

where F is a scaling function and can be written in a power series

$$F(\lambda) = 1 + F_1 \lambda + F_2 \lambda^2 + \dots$$

des Cloizeaux' equation can be compared with Flory's equation [Eq. (9.20)]:

- Flory's equation:

$$\frac{\pi'}{kT} = \frac{n_2}{V} + \frac{u}{2} \left(\frac{n_2}{V}\right)^2$$

or

$$\frac{\pi'}{kT c_P} = 1 + \frac{1}{2} u c_P$$

where $c_P = n_2/V$.

- des Cloizeaux' equation:

$$\frac{\pi'}{kT c_P} = 1 + F_1 N^{vd} (b^d c_P) \quad (9.56)$$

or

$$\frac{\pi'}{kT c_M} = \frac{1}{N} + F_1 N^{vd-2} c_M$$

The interesting part is that des Cloizeaux' equation can be translated into the scaling law,

$$\frac{\pi'}{kTc_p} \sim N^{vd} \quad (9.57)$$

whereas Flory's equation cannot.

It was de Gennes (1972) who first introduced the Lagrangian theory to interpret the behavior of polymer solutions. Although des Cloizeaux showed the similarity between his and Flory's interpretations of the osmotic pressure, de Gennes pointed out that des Cloizeaux' interpretation is superior to Flory's. To compare the two theories, de Gennes first translated the Flory lattice theory into his language. Let Φ represent the fraction of lattice sites occupied by the monomers. Then $\Phi = ca^3$, where c is the concentration in terms of the number of monomers per cubic centimeters and a^3 is the volume of the unit needed in the cubic lattice. Flory's equation of osmotic pressure [Eq. (9.20)] can be expressed in the form

$$\frac{\pi'a^3}{kT} = \frac{\Phi}{N} + \frac{1}{2}(1 - 2\chi)\Phi^2 \cong \frac{1}{2}(1 - 2\chi)\Phi^2 \quad (9.58)$$

$$\left(\text{Note: } \frac{\Phi}{N} \cong 0 \quad \text{if } \frac{1}{N} \leq \Phi \leq 1 \right)$$

des Cloizeaux' equation [Eq. (9.56)] can be expressed in a similar form:

$$\begin{aligned} \frac{\pi'}{kT} &= \frac{c}{N} + \text{const} \left(\frac{c}{N} \right)^2 R^3 + \dots \\ &\cong \frac{c}{N} f_n \left(\frac{cR^3}{N} \right) = \frac{c}{N} f_n \left(\frac{c}{c^*} \right) \end{aligned} \quad (9.59)$$

In a semidilute solution, des Cloizeaux' equation can be further simplified by eliminating coefficients in the form

$$\frac{\pi'a^3}{kT} = \text{const} \times \Phi^{9/4} \quad (9.60)$$

which de Gennes called the des Cloizeaux law. Now the difference is clear:

- For Flory

$$\pi' \sim \Phi^2 \quad (9.61)$$

- For des Cloizeaux

$$\pi' \sim \Phi^{9/4} \quad (9.62)$$

Flory neglected certain correlations between adjacent and ever more distant monomers, as criticized by de Gennes.

de Gennes himself is more interested in the relationship between the correlation length ξ and the osmotic pressure, namely, in constructing the scaling form of ξ in the semidilute regime. The scaling relationship between the osmotic pressure and the correlation length, as he suggested, is

$$\pi' = \frac{kT}{\xi^3} \quad (\Phi^* \leq \Phi \leq 1) \quad (9.63)$$

9.3.6 Scatchard's Equation for Macro Ions

Scatchard's equation (1946) is derived to explain A_2 for proteins. The change in dimensions (e.g., mean-square end-to-end distance) is not of any concern in Scatchard's derivation. No model was assumed and no statistical mechanics[†] was used. Scatchard successfully correlated the osmotic pressure with the distribution of diffusible solutes across a semipermeable membrane by manipulating the terms of activities of the components (such as protein, salt, and water) with changing composition of the solutions. The mathematical detail is simple but messy. According to Scatchard, the interactions involved in protein solutions are not limited to the exclusion of volume between the segments of macromolecules but also includes the Donnan effect and the binding of small ions to macro ions in a given system. For simplicity, let us consider a three-component system, and let 1 represent the solvent (or buffer), 2 the macromolecule (such as protein), and 3 a salt (e.g., NaCl). Scatchard derived an equation of the second virial coefficient:

$$A_2 = \frac{1000\bar{v}_1}{M_2^2} \left(\frac{\varepsilon^2}{4m_3} + \frac{\beta_{22}}{2} - \frac{\beta_{23}^2 m_3}{4 + 2\beta_{33} m_3} \right) \quad (9.64)$$

where \bar{v}_1 is the partial specific volume of the solvent, ε is the net charge carried by the macro ion (which could be obtained from acid-base titration data), m is the molality of a component in solution, and the β 's are derivatives of activity coefficients γ :

$$\begin{aligned} \beta_{22} &= \frac{\delta \ln \gamma_2}{\delta m_2} && \text{(Donnan effect)} \\ \beta_{23} &= \frac{\delta \ln \gamma_2}{\delta m_3} && \text{(excluded volume effect including charge effect)} \\ \beta_{33} &= \frac{\delta \ln \gamma_3}{\delta m_3} && \text{(binding)} \end{aligned}$$

[†]Thermodynamics and statistical mechanics are closely related. They differ only in their approach to a system. Given a mole of gas, thermodynamics describes its behavior in terms of PVT and, later, in terms of $E, H, S, G,$ and A . Given the same mole of gas, statistical mechanics describes its behavior in terms of energy states. The statistical behavior is basically the fluctuations of a random variable which characterizes the system. Eventually, statistical mechanics also leads to the study of change in $E, H, S, G,$ and A .

Eq. (9.64) consists of three terms. The first describes the Donnan effect, which states that in osmosis the small ions are not distributed equally on the two sides of the membrane. The Donnan effect always causes an increase in osmotic pressure. To minimize this effect, the protein solution should have high ionic strength or should be near the isoelectric pH. The second term represents the excluded volume effect and the interaction between charges on different macro ions. It is basically similar to the parameter χ_1 in the properties of synthetic polymer solutions but is a little more complicated because of the charges involved. The third term involves the interaction between macro ions and the actual binding of small ions. This term is particularly important to the study of the behavior of proteins in dilute salt solutions.

Experimental values for all of the three parameters (β_{22} , β_{23} , β_{33}) and the molecular weight M_2 can be determined from osmotic pressure experiments as follows. The plot of π'/c_2 versus c_2 is expected to be a straight line from which the intercept A_1 and the slope A_2 are obtained. From the intercept we obtain M_2 using the relation

$$A_1 = \frac{R'T}{V_m^\circ M_2} \quad (9.65)$$

where V_m° is the volume of the solution which contains grams of macro ion in 1000 g of solvent, this is, $V_m^\circ = 1$; R' is the gas constant (0.082 atm L/mol K) if π' is in atm. The parameter β_{33} , itself not important, is calculated from the following empirical equation:

$$\frac{\beta_{33}}{2} = \ln \gamma_3 = \frac{-1.172\sqrt{m_3}}{1 + 1.55\sqrt{m_3}} + 0.0215m_3 + 0.0212m_3^2 \quad (9.66)$$

This is obtained from a separate and independent experiment (not included in the osmotic pressure measurement). The parameter β_{23} is calculated using

$$\beta_{23} = M_2 b_{23} (2 + \beta_{33} m_3^\circ) \quad (9.67)$$

where

$$b_{23} = \frac{1}{c_2} \ln \frac{m_3'}{m_3}$$

In the above equations m_3° is original concentration of the salt in the protein solution, m_3 is the concentration of the salt in the solution after diffusion, and m_3' is the concentration of salt diffused out through the membrane. The quantities m_3° , m_3 , and m_3' are all measured in the same osmotic pressure experiment. After all of the above parameters are calculated, the parameter β_{22} can be determined directly from the slope A_2 using Eq. (9.64).

APPENDIX A ENSEMBLES

An ensemble is a collection of systems each of which contains N particles, occupies a volume V , and possess energy E . Each system represents one of the possible microscopic states and each is represented by a distribution of points in phase space. A phase space is defined by $3n$ coordinates and $3n$ momenta for a dynamic system consisting of n particles. There are three types of ensembles:

1. *Microcanonical Ensemble* The microcanonical ensemble is the assembly of all states in which the total energy E , the number of molecules N , and the total volume V are all fixed. It is a closed and isolated system. In a microcanonical ensemble, there is no fluctuation of any of the three variables N , E , and V .
2. *Canonical Ensemble* In the canonical ensemble, all states have fixed V (volume) and N (the number of molecules), but the energy E fluctuates. The ensemble could be considered as a closed system in contact with a heat bath that has infinite heat capacity.
3. *Grand Canonical Ensemble* In a grand canonical ensemble, not only E fluctuates but also N . The grand canonical ensemble is an open isothermal system. Both heat (energy) and mass (particles) can be transported across the walls of the system.

APPENDIX B PARTITION FUNCTIONS

The partition function Q is defined as

$$Q = \sum_i g_i e^{-\mu \varepsilon_i}$$

where ε_i is the energy level and μ is identified as

$$\mu = \frac{1}{kT}$$

where k is the Boltzmann constant and T is the temperature. The term g_i refers to the degeneracy of energy levels. The partition function is the sum of the internal energy states of the entire system. The term $\sum_i e^{-\mu \varepsilon_i}$ is the Boltzmann-weighted sum over all possible fluctuations, that is, all microscopic states permitted by the constraints with which we control the system. The partition function can be used to describe the configuration of a polymer chain, for example,

$$Q = \sum \exp \left[\frac{-U(\{R_n\})}{kT} \right]$$

where U is the potential and $\{R_n\}$ is a set of elements R_n ,

$$\{R_n\} = (R_1, R_2, \dots, R_n) \quad (R = \text{coordinate})$$

The grand ensemble partition function is usually expressed as

$$\begin{aligned} \Xi &= \Xi(V, T, \mu) \\ &= \sum_{j,N} e^{-E_j/kT} e^{N\mu/kT} \end{aligned}$$

Partition functions are used to calculate thermodynamic functions. They are related as follow:

$$\begin{aligned} A(N, V, T) &= -kT \ln Q \\ p &= kT \left(\frac{\partial \ln Q}{\partial V} \right)_{T,N} \\ E &= kT^2 \left(\frac{\partial \ln Q}{\partial T} \right)_{V,N} \\ C_V &= \left(\frac{\partial E}{\partial T} \right)_{V,N} \\ S &= k \frac{\partial}{\partial T} (T \ln Q)_N \end{aligned}$$

APPENDIX C MEAN-FIELD THEORY AND RENORMALIZATION GROUP THEORY

Both of these theories are about the distribution of molecules, which involves interaction among molecules themselves. Both are proposals for solving the equation of the Ising (1925) model about electron spins in two or three dimensions. Both are highly mathematical in nature.

The idea of the mean-field theory is to focus on one particular particle in the system. The method singles out only those fluctuations that occur within the cell and neglects the effects of fluctuations beyond the cell. It reduces the many-body statistical mechanics problem into a one-body problem.

The renormalization group theory, proposed by Wilson in 1971, is about large-length-scale fluctuations. The method consists of two steps: (1) removing from the partition function a finite fraction of the degrees of freedom by averaging over them and (2) rescaling the resultant partition function by Kadanoff transformation. The transformations contain the group property and provide a renormalization scheme.

APPENDIX D LAGRANGIAN THEORY

Lagrangian theory is basically the variational principle. There are several forms to express this principle. The simplest one, also the earliest one, is the principle of action.

According to Hamilton's principle in mechanics, a dynamical system is characterized by a definite function L and an integral

$$\int_{t_1}^t L dt$$

which describes the motion of the system between two positions and which takes the least possible value or least action for its natural path. The product $L dt$ is called the action, and the variation of the action leading to its own vanishing is the least action:

$$\delta \int_{t_1}^t L dt = 0$$

The function L is called the Lagrangian and is defined as

$$L = T - U$$

where T is the kinetic energy term and U is the potential energy term. In polymer chemistry U refers to interactions and intra-actions between molecules.

APPENDIX E GREEN'S FUNCTION

Green's function is a powerful tool for the solution of second-order partial differential equations, satisfying boundary conditions. For example, given the differential equation

$$\frac{\partial^2 z}{\partial x \partial y} + \frac{2}{x+y} \left(\frac{\partial z}{\partial x} + \frac{\partial z}{\partial y} \right) = 0$$

we wish to find the solution that satisfies the boundary conditions

$$z = 0 \quad \frac{\partial z}{\partial x} = 3x^2$$

on $y = x$. Since the values of z and $\partial z / \partial x$ (or $\partial z / \partial y$) are prescribed along the line $y = x$, we first find the solution of the differential equation at a point $p(\xi, \eta)$. Then

Green's function is found to be

$$G(x, y; \xi, \eta) = \frac{(x + y)[2xy + (\xi - \eta)(x - y) + 2\xi\eta]}{(\xi + \eta)^3}$$

The term z can now be evaluated with the aid of Green's function, although the process is rather complicated.

REFERENCES

- Albrecht, A. C., *J. Chem. Phys.* **27**, 1002 (1957).
 Bawn, C. E. H., C. Freeman, and A. Kamaliddin, *Trans. Faraday Soc.* **46**, 862 (1950).
 Chandler, D., *Introduction to Modern Statistical Mechanics*. Oxford: Oxford University Press, 1987.
 de Gennes, P. G., *Phys. Lett.* **38A**, 339 (1972).
 de Gennes, P. G., *Scaling Concepts in Polymer Physics*. Ithaca, NY: Cornell University Press, 1979.
 des Cloizeaux, J., *J. Phys. (Paris)* **36**, 281 (1975).
 Duhem, P., *Compt. Rend.* **102**, 1449 (1896).
 Flory, P. J., *Principles of Polymer Chemistry*. Ithaca, NY: Cornell University Press, 1953.
 Flory, P. J., and W. R. Krigbaum, *J. Chem. Phys.* **18**, 1086 (1950).
 Freed, K. F., *Renormalization Group Theory of Macromolecules*. New York: Wiley, 1987.
 Gibbs, J. W., *Collected Works*. New York: Longmans, Green & Co., 1931.
 Hill, T. L., *Introduction to Statistical Thermodynamics*. Reading, MA: Addison-Wesley, 1960.
 Ising, E., *Z. Physik* **31**, 253 (1925).
 Krigbaum, W. R., and P. J. Flory, *J. Am. Chem. Soc.* **75**, 1775 (1953a).
 Krigbaum, W. R., and P. J. Flory, *J. Polym. Sci.* **11**, 37 (1953b).
 Kurata, M., and H. Yamakawa, *J. Chem. Phys.* **29**, 311 (1958).
 Ma. S. K., *Statistical Mechanics*. Philadelphia, PA: World Scientific, 1985.
 McMillan, W. G., and J. E. Mayer, *J. Chem. Phys.* **13**, 276 (1945).
 Orofino, T. A., and P. J. Flory, *J. Chem. Phys.* **26**, 1067 (1957).
 Orofino, T. A., and P. J. Flory, *J. Phys. Chem.* **63**, (1959).
 Scatchard, G., *J. Am. Chem. Soc.* **68**, 2315 (1946).
 Scatchard, G., A. C. Batchelder, and A. Brown, *J. Am. Chem. Soc.* **68**, 2320 (1946).
 Sneddon, I. N., *Elements of Partial Differential Equations*. New York: McGraw-Hill, 1957.
 Wilson, K. G., *Phys. Rev.* **B4**, 3174, 3184 (1971).
 Zimm, B. H., *J. Chem. Phys.* **14**, 164 (1946).

PROBLEMS

- 9.1** The osmotic pressures at a series of concentrations from 2 to 10 g of polymer per kilogram of solution of a fractionated vinyl chloride polymer in methyl

amyl ketone at 27°C have been determined. The experimental data are as follows:

π' (cm)	0.4	1.1	2	3	4
c (g solute/kg solution)	2	4	6	8	10

- (a) Plot π' versus c and π'/c versus c .
- (b) Determine the molecular weight of the polymer (using either plot).
Suggestion: Consider the empirical equation

$$\frac{\pi'}{c} = \left(\frac{1000R'T}{M} \right) + Ac$$

where R' is 0.0821 l atm per mole-degree, T is the absolute temperature, M is the molecular weight, and A is a constant. Which plot is good for the determination of molecular weight?

- 9.2 The osmotic pressures at a series of concentrations and temperatures of a polymer in water have been determined as follows:

c (kg/m ³)	t (°C)	π' (Pa)
10.00	25	855
	30	827
	35	755
	40	722
50.00	25	7,335
	30	6,360
	35	5,085
	40	3,965
100.0	25	22,340
	30	18,790
	35	14,300
	40	9,670
150.00	25	46,260
	30	38,595
	35	28,845
	40	18,675

Determine (a) the molecular weight and (b) the second and third virial coefficients.

- 9.3 According to the Flory-Krigbaum theory, the excluded volume for a pair of polymer molecules may be expressed in the form

$$u = \left(\frac{\bar{v}^2}{NV_1} \right) (\psi_1 - \kappa_1) M^2 F(x)$$

The function $F(x)$ is defined as

$$F(x) = \left(\frac{4}{\pi^{1/2}}\right)x^{-1} \int_0^\infty \{1 - \exp[-x \exp(-y^2)]\}y^2 dy$$

Show that

$$F(x) = \sum_{i=1}^\infty \frac{(-x)^{i-1}}{i^{3/2}i!}$$

Hence,

$$F(x) = 1 - \frac{x}{2!}2^{3/2} + \frac{x^3}{3!}2^{3/2} - \dots$$

Hint: The definite integrals

$$I_p = \int_0^\infty y^p \{1 - \exp[-x \exp(-y^2)]\} dy$$

have the series solutions

$$I_p = \frac{1}{2} \Gamma\left(\frac{p+1}{2}\right) \sum_{n=1}^\infty \frac{x^n (-1)^{n+1}}{n!n^{(p+2)/2}}$$

where $p = 0, 1, 2, \dots$ and Γ is the gamma function.

9.4 The following data were obtained by Flory and Krigbaum for polystyrene in toluene at 30°C:

\bar{M}_n	Γ_2	α^3
30,900	0.195	2.56
41,700	0.251	2.80
61,500	0.309	3.00
120,000	0.576	3.56
328,000	1.21	4.20
612,000	2.02	5.56

(a) Show that the second virial coefficient decreases with increasing molecular weight by plotting Γ_2 versus \bar{M}_n .

- (b) Calculate the theoretical values of A_2 as a function of molecular weight using

$$A_2 = \frac{\bar{v}^2}{V_1} (\psi_1 - \kappa_1) F(x)$$

Hint: $x = 2(\alpha^2 - 1)$.

- (c) Convert the experimental values of Γ_2 to A_2 and compare with the theoretical values A_2 by plotting A_2 observed versus \bar{M}_n and A_2 calculated versus \bar{M}_2 on the same graph.

Useful information: $\bar{v} = 0.93$ mL/g at 30°C and $\psi_1 - \kappa_1 = 0.058$ (Krigbaum and Flory, 1953a,b).

- 9.5 A theoretic equation was derived by Kurata and Yamakawa for the osmotic second virial coefficient of a flexible polymer chain which takes into account not only the intermolecular interaction but also the intramolecular interaction of segments (such as the excluded volume effect). The equation given by

$$A_2 = \frac{2}{3} \pi N b_0^3 \left(1 - \frac{\theta}{T} \right) (1 - 2.865z + 18.15z^2 - \dots)$$

Plot the theoretical curve of A_2 versus the temperature for polystyrene in cyclohexane. The conditions are specified as follows: Temperature (in kelvin): 308, 310, 315, 320, $\theta = 308$; molecular weight of the polymer: 3.20×10^6 , of the segment 104, $b_0 = 0.1178$, $z = 0.15$ (Kurata and Yamakawa, 1958).

- 9.6 Osmotic pressure measurements were carried out by Scatchard and co-workers (1946) for bovine serum albumin (BSA) in various NaCl solutions for the study of molecular interaction between the protein and the salt and for the determination of the molecular weight of BSA. The quantities that were measured are c_2 , the concentration of BSA in grams of isoelectric protein, inside the membrane; c'_2 , the concentration of BSA outside the membrane; m_3 , the average concentration of NaCl inside the membrane; m'_3 , the average concentration of NaCl outside the membrane; and π' , the osmotic pressure in millimeters of mercury. Also measured were the pH of the solution inside the membrane and z_2 , the net charge of the protein (i.e., the valence number). The experimental data are as follows:

c_2	c'_2	pH	z_2	m_3	m'_3	π'
57.42	0.06	4.98	5.3	0.1523	0.1488	18.93
27.28	0.00	5.28	1.2	0.1506	0.1489	8.35
56.20	0.04	5.29	1.0	0.1506	0.1477	19.33
8.95	0.00	5.30	1.0	0.1500	0.1488	2.51

c_2	c'_2	pH	z_2	m_3	m'_3	π'
75.03	0.16	5.35	0.3	0.1521	0.1482	28.52
17.69	0.15	5.42	-1.1	0.1498	0.1488	5.07

Calculate the following:

- (a) Molecular weight of BSA, M_2
- (b) Distribution of the salt, b_{23} , in each solution
- (c) Molecular interaction between the protein and the salt, β_{23} , in each solution
- (d) Molecular interaction between proteins, β_{22} , in each solution

10

DIFFUSION

Diffusion is a process that involves the random motion of particles and the concentration gradient dc/dx in the system. The diffusion coefficient, which is the major concern of this chapter, is a measure of the mass of solute transported in a given period of time under the influence of a known driving force. The driving force is essentially the concentration gradient caused by external forces, such as the gravitational field or centrifugal field. There are two kinds of diffusion: translational and rotational.

10.1 TRANSLATIONAL DIFFUSION

10.1.1 Fick's First and Second Laws

In 1822 Fourier derived an equation for heat conduction. Realizing that the process of transferring heat by induction is analogous to the process of diffusion and that both are due to random molecular motion, in 1855 Fick adapted the Fourier equation to describe diffusion.

Fick's first law is about the change of concentration (of solute) with respect to coordinates:

$$J = -D \frac{\delta c}{\delta x} \quad (10.1)$$

In Eq. (10.1), J is called the flux (or diffusion flux) or flow (in kilograms per square meter second) and is the rate of transfer per unit of section, c is the concentration of solute (or particles) (in grams per milliliter or grams per 100 mL), x is the space coordinate measured normal to the section where the particles cross, and D is the diffusion coefficient (in square centimeters per second). The direction of diffusion is opposite to that of increasing concentration; hence, a negative sign is given in the equation.

Fick's second law describes the change of concentration with time:

$$\frac{\delta c}{\delta t} = -\frac{\delta J}{\delta x} = \frac{\delta}{\delta x} \left(D \frac{\delta c}{\delta x} \right)$$

which leads to

$$\frac{\delta c}{\delta t} = D \frac{\delta^2 c}{\delta x^2} \quad (10.2)$$

if D is a constant. Notice that this is a well-known continuity equation.

10.1.2 Solution to Continuity Equation

The equation

$$\frac{\delta c}{\delta t} = D \frac{\delta^2 c}{\delta x^2}$$

is difficult to solve because three variables, c , x , and t , are involved. However, Boltzmann (1894) pointed out that in free diffusion the variables x and t always occur in the ratio x/\sqrt{t} . This is true whether or not D depends on the concentration. This suggests a solution:

$$\frac{\delta c}{\delta x} = -\frac{c_0}{\sqrt{4\pi Dt}} e^{-x^2/4Dt} \quad (10.3)$$

which satisfies the differential equation (10.2). That this is the solution can be verified by substituting Eq. (10.3) into Eq. (10.2). The great advantages of Eq. (10.3) are that it is identical to the Gaussian equation or error distribution equation, that it is closely related to experimental data of dc/dx and x , and that it is easy to evaluate it numerically to obtain D .

Figure 10.1 shows the graph of dc/dx versus x on the basis of Eq. (10.3). A plot of $(\text{area/height})^2$ versus t will give a straight line of slope $4\pi D$ (Figure 10.2). The curve of dc/dx versus x may also be treated in terms of the standard deviation σ (Figure 10.3). From σ we obtain

$$D = \frac{\sigma^2}{2t} \quad (10.4a)$$

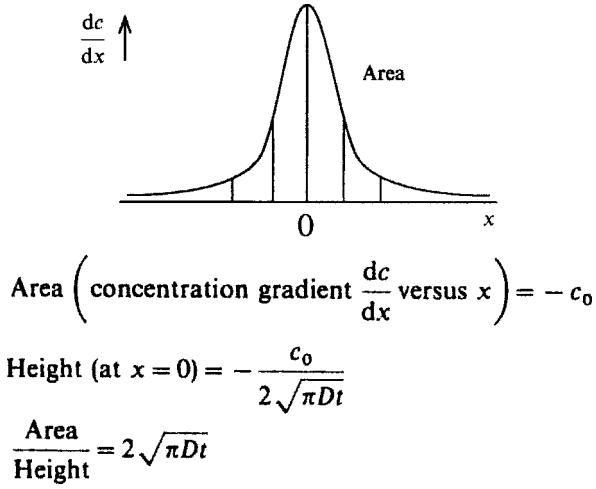


FIGURE 10.1 Diffusion profile.

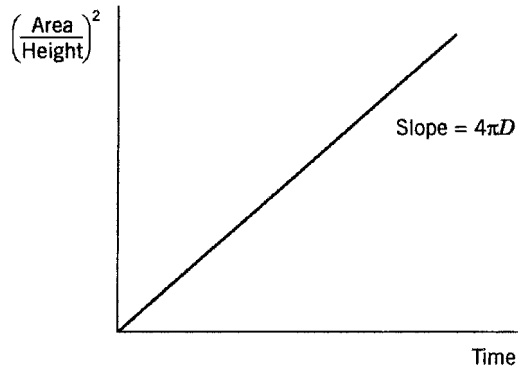


FIGURE 10.2 Evaluation of diffusion coefficient from area/height plot.

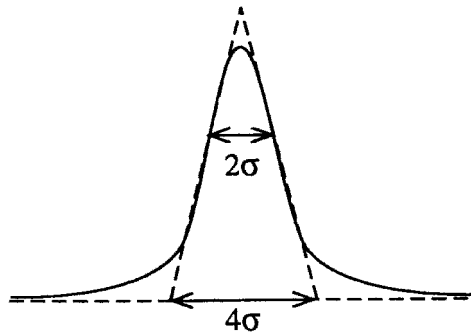


FIGURE 10.3 Evaluation of the diffusion coefficient from standard deviation.

or

$$D = \frac{\sigma_1^2 - \sigma_2^2}{2(t_1 - t_2)} \quad (10.4b)$$

where t_1 and t_2 refer to the two different times in which the experiment was carried out and σ_1 and σ_2 represent the standard deviations of the two curves recorded at the two different times. Integrating Eq. (10.3), we obtain

$$c = \frac{c_0}{2} \left(1 - \frac{2}{\sqrt{\pi}} \int_0^{x/2\sqrt{Dt}} e^{-z^2} dz \right) \quad (10.5)$$

with $z = x/\sqrt{4Dt}$. The integral term in Eq. (10.5) is the well-known error (or Gaussian) function:

$$\text{erf } z = \frac{2}{\sqrt{\pi}} \int_0^{x/\sqrt{4Dt}} e^{-z^2} dz$$

Values of the integral are tabulated in most mathematical function books, usually expressed in terms of z :

$$\begin{aligned} \text{erf } z &= \frac{1}{\sqrt{\pi}} \int_0^z e^{-t^2} dt \\ \text{erfc } z &= \frac{2}{\sqrt{\pi}} \int_z^\infty e^{-t^2} dt = 1 - \text{erf } z \end{aligned}$$

Both of these equations are called error functions.

10.2 PHYSICAL INTERPRETATION OF DIFFUSION: EINSTEIN'S EQUATION OF DIFFUSION

Einstein interpreted diffusion as being a result of the random thermal motion of molecules. Such a random motion is caused by fluctuations in pressure in a liquid. Thus, diffusion is closely related to Brownian motion. The Brownian motion consists of zigzag motion in all directions. It is a random walk, as discussed in Chapter 5, and is described by the parameter $\langle x^2 \rangle$, the square mean displacement. The equation of motion in one dimension for the Brownian motion of a particle in solution is given by

$$m \frac{d^2x}{dt^2} = -f \frac{dx}{dt} + F' \quad (10.6)$$

where m is the mass of the particle, f is the frictional coefficient, $f(dx/dt)$ is the viscous drag, and F' is a force component due to random motion. If we take the average over many particles, then $\langle F' \rangle = 0$. This is because F' , being a random force, is as likely to be positive as negative. It eventually vanishes. The equation then becomes

$$m \frac{d^2x}{dt^2} = -f \frac{dx}{dt} \quad (10.7)$$

Multiplying Eq. (10.7) by x , we obtain

$$mx \frac{d^2x}{dt^2} = -fx \frac{dx}{dt} \quad (10.8)$$

Notice the identities:

$$\begin{aligned} \frac{d(x^2)}{dt} &= 2x \frac{dx}{dt} \\ x \frac{dx}{dt} &= \frac{1}{2} \frac{d(x^2)}{dt} \end{aligned}$$

Differentiating $d(x^2)/dt$ with respect to t gives

$$\frac{d^2(x^2)}{dt^2} = 2 \left(\frac{dx}{dt} \right)^2 + 2x \frac{d^2x}{dt^2}$$

or

$$x \frac{d^2x}{dt^2} = \frac{1}{2} \frac{d^2(x^2)}{dt^2} - \left(\frac{dx}{dt} \right)^2$$

Equation (10.8) becomes

$$\frac{m}{2} \frac{d^2(x^2)}{dt^2} - m \left(\frac{dx}{dt} \right)^2 = -\frac{f}{2} \frac{d(x^2)}{dt}$$

Notice also that

$$m \left(\frac{dx}{dt} \right)^2 = mv^2$$

The thermal motion assumption provides a justification here to use the principle of equipartition of energy, which states that the kinetic energy of each particle on the

average is $\frac{3}{2}kT$; that is,

$$\begin{aligned}\frac{1}{2}mv^2 &= \text{kinetic energy of each particle} \\ &= \frac{3}{2}kT\end{aligned}$$

where k is the Boltzmann constant. For one degree of freedom $\frac{1}{2}mv^2 = \frac{1}{2}kT$. If we change the notation x^2 into $\langle x^2 \rangle$ and substitute it, we have

$$\frac{m}{2} \frac{d^2 \langle x^2 \rangle}{dt^2} - kT = -\frac{f}{2} \frac{d \langle x^2 \rangle}{dt} \quad (10.9)$$

To solve this differential equation, we let

$$y = \frac{d \langle x^2 \rangle}{dt}$$

Then, Eq. (10.9) is in the form

$$m \frac{dy}{dt} + fy = 2kT$$

This is in the standard form for a linear differential equation of first order:

$$\frac{dy}{dx} + Py = Q$$

where P and Q are functions of x . The standard solution is

$$y = \exp\left(-\int P dx\right) \left(\int e^{\int P dx} Q dx + c\right)$$

If the integral is from zero (the origin) to t , the integration constant in our case would be zero. Then

$$\begin{aligned}y &= \exp\left[-\int (f/m) dt\right] \left\{ \int_0^t \exp\left[\int (f/m) dt\right] \frac{2kT}{m} dt \right\} \\ &= \frac{2kT}{f}\end{aligned}$$

That is,

$$\frac{d \langle x^2 \rangle}{dt} = \frac{2kT}{f} \quad (10.10)$$

Again, if diffusion starts at $t = 0$, the integration constant obtained from integration of Eq. (10.10) is zero. Thus, we have

$$\frac{\langle x^2 \rangle}{2t} = \frac{kT}{f} \quad (10.11)$$

But the mean-square displacement is proportional to the time $2t$ with the proportionality constant equal to the diffusion coefficient D :

$$\langle x^2 \rangle = D(2t)$$

This leads to

$$D = \frac{\langle x^2 \rangle}{2t} = \frac{kT}{f} \quad (10.12)$$

The expression

$$D = \frac{kT}{f} \quad (10.13)$$

is called the Einstein equation of diffusion. Because of the correlation between D and f , as shown in Eq. (10.13), D becomes an important parameter characterizing macromolecules and relates to other hydrodynamic properties, such as η (viscosity) and S (sedimentation coefficient).

10.3 SIZE, SHAPE, AND MOLECULAR WEIGHT DETERMINATIONS

10.3.1 Size

Kirkwood derived an equation to correlate the diffusion coefficient D with the size of polymer molecule $\sum \langle R_{ij} \rangle$ in the form

$$D = \frac{kT}{N_A \rho} \left[1 + \frac{\rho}{6\pi\eta N_A} \sum_{i=0}^{N_A} \sum_{j=0}^{N_A} (1 - \delta_{ij}) \langle R_{ij}^{-1} \rangle \right] \quad (10.14)$$

where N_A is Avogadro's number, ρ is the density of the solution, $\delta_{ij} = 0$ if $i \neq j$, $\delta_{ij} = 1$ if $i = j$, and R_{ij} is the distance between the polymer segments i and j . The summation of R_{ij} gives the average dimension (size) of the polymer molecule in the solution. Since D is related to f according to the Einstein equation, Eq. (10.14) can

also be expressed in the form

$$f = n\zeta \left(1 + \frac{\zeta}{6\pi n\eta} \sum_{i,j=1, i \neq j}^n \left\langle \frac{1}{R_{ij}} \right\rangle \right)^{-1} \quad (10.15)$$

where n is the number of monomer units and ζ is the frictional coefficient of each individual monomer unit.

10.3.2 Shape

If a particle of a suspension (here, we mean a macromolecule) is spherical, then the following equation provides the relationship between the diffusion coefficient D and the radius of the sphere r :

$$D = \frac{kT}{6\pi\eta r} \quad (10.16)$$

where η is the viscosity of the solvent. Equation (10.16) is called the Stokes–Einstein equation. A modification of Eq. (10.16) was proposed by Sutherland in 1905 to take into consideration sliding friction. The diffusion coefficient D is then expressed as

$$D = \frac{kT}{(6\pi\eta r)(1 + 2\eta/\beta r)/(1 + 3\eta/\beta r)} \quad (10.17)$$

where β is the coefficient of sliding friction.

Perrin in 1936 derived equations that relate frictional coefficients to the shape of macromolecules formed as ellipsoids of revolution. The frictional coefficients (f) of prolate and oblate ellipsoids (see Chapter 8) are both greater than the frictional coefficients of spheres (f_s or f_0) of equal volume. The difference depends on the ratio of the major to the minor axis. Let $p = b/a$ be the axial ratio, where b is the equatorial radius and a is the semiaxis of revolution. For prolate ellipsoids or elongated ellipsoids ($a/b > 1$), we have

$$\frac{D}{D_s} = \frac{f}{f_s} = \frac{f}{f_0} = \frac{\sqrt{1-p^2}}{p^{2/3} \ln[(1 + \sqrt{1-p^2})/p]} \quad (10.18)$$

For oblate ellipsoids ($a/b < 1$), we have

$$\frac{D}{D_s} = \frac{f}{f_s} = \frac{f}{f_0} = \frac{(p^2 - 1)^{1/2}}{p^{2/3} \tan^{-1}(p^2 - 1)^{1/2}} \quad (10.19)$$

The frictional ratios of irregular shapes, that is, other than the sphere and the ellipsoid, have not yet been investigated.

10.3.3 Molecular Weight

Diffusion and molecular weight are related in three ways:

1. *Einstein–Stokes Relation* From

$$D = \frac{kT}{f}$$

$$f = 6\pi\eta r$$

$$\frac{4}{3}\pi r^3 = \frac{\bar{v}M}{N_A}$$

we obtain

$$M = \frac{4\pi r^3 N_A}{3\bar{v}} \quad (10.20)$$

where \bar{v} is the partial specific volume of the polymer molecule and M is its molecular weight. It should be noted that

$$D = \frac{kT}{f} = \frac{R'T}{N_A f} = \frac{R'T}{6\pi\eta N_A (3M\bar{v}/4\pi N_A)^{1/3}}$$

where R' is the gas constant. Hence, $D \sim 1/M^{1/3}$, that is, D is inversely proportional to the cubic root of molecular weight.

2. *Einstein–Svedberg Relation*

$$M = \frac{SR'T}{D(1 - \bar{v}\rho)} \quad (10.21)$$

where S is the sedimentation coefficient, which is discussed in Chapter 11, and ρ is the density of the solution.

3. *Empirical Relation* For homologous polymers, we have an equation relating D and M analogous to the Mark–Houwink equation for intrinsic viscosity:

$$D = K'M^{-a} \quad (10.22)$$

where K' and a are constants. For example, for polystyrene in 2-butanone at 25°C, we have

$$D = (3.1 \times 10^{-4})M^{0.53}$$

The physical meanings of K' and a are yet to be explored.

10.4 CONCENTRATION DEPENDENCE OF DIFFUSION COEFFICIENT

The translational diffusion coefficient is considered to be a constant only for particles in dilute solution. In general, if the solution is not dilute, D is dependent on

concentration. This dependence may be expressed as

$$D = D_0(1 + k_D c + \dots) \quad (10.23)$$

where

$$D_0 = \frac{kT}{f_0}$$

The parameter D_0 is the diffusion coefficient at infinite dilution. The term k_D is the hydrodynamic and thermodynamic combined factor and can be expressed in either of two different ways:

$$k_D = 2A_2M - f' - \frac{N_A V}{M} \quad (10.24)$$

or

$$k_D = \left(\frac{d \ln y}{dc} \right) (\bar{v}_1 \rho) \quad (10.25)$$

In Eqs. (10.24) and (10.25) f' is the first-order frictional coefficient, V is the polymer molecular volume, y is the activity coefficient of the polymer in solution, \bar{v}_1 is the partial specific volume of the solvent, and ρ is the density of the solution. Equation (10.24) fits the description for the behavior of synthetic polymers, while Eq. (10.25) fits that for biological polymers, particularly proteins. Substituting Eq. (10.24) into Eq. (10.23), we obtain

$$D = D_0[1 + (2A_2M - f')c + \dots] \quad (10.26)$$

The relative values of the two terms $2A_2M$ and f' provide a measure of the property of solvent in polymer solutions. For good solvents, the difference between $2A_2M$ and f' is large. For poor solvents, the difference between $2A_2M$ and f' is small.

Substituting Eq. (10.25) in Eq. (10.23), we obtain

$$D = D_0 \left(1 + \frac{d \ln y}{dc} c \right) (\bar{v}_1 \rho) \quad (10.27)$$

The quantity $(\bar{v}_1 \rho)$ is approximately equal to unity, except at very high concentrations of solution. This equation is suitable for systems of three or more components with interacting flows, as is the case with protein solutions.

There is a subtle difference in the two interpretations of k_D . In the first interpretation, Eq. (10.26), the driving force dc/dx is identical to a gradient of osmotic pressure; hence, the equation for D involves the second virial coefficient

A_2 . In the second interpretation, Eq. (10.27), the driving force dc/dx is identical to a gradient of chemical potential; hence, the equation for D involves the activity coefficient γ of the polymer. The equation fits into the analysis of an interacting multicomponent system. Of course, it must be remembered that osmotic pressure and chemical potential are closely related, as discussed in Chapter 9.

10.5 SCALING RELATION FOR TRANSLATIONAL DIFFUSION COEFFICIENT

Scaling relations for quantities that are time independent, for example, the osmotic pressure π' , the mean-square end-to-end distance $\langle R^2 \rangle$, and the screen length ξ , are known as static scaling relations. Those for time-dependent quantities, such as the translational diffusion coefficient, are called dynamic scaling relations.

The Rouse model considers the polymer chain as a succession of “beads,” $\mathbf{r}_1, \dots, \mathbf{r}_n, \mathbf{r}_{n+1}$, separated by “springs” along the vectors $\mathbf{a}_1, \dots, \mathbf{a}_n$ (see Chapter 8). If all the internal forces add up to zero, the equation is reduced to

$$\frac{\partial \mathbf{r}}{\partial t} = \frac{B}{N} \sum_n \mathbf{f}_n$$

where f_n is an external force. Since the overall mobility of a single chain is B/N (B is the mobility and N is the number of segments per chain), the corresponding diffusion coefficient can be derived, similarly to Einstein’s equation, as

$$D = BkTN^{-1}$$

In scaling relations, we can put the diffusion coefficient in the form (Adler and Freed, 1979)

$$D = \frac{kT}{\eta_0 b} N^{-1/2} f_D(\varepsilon) \quad (10.28)$$

where ε is the argument of the function f_D and is defined as

$$\varepsilon = ue^{-4} N^{(v-d)/2}$$

and b is the Kuhn length (the length of chain segment), u is the excluded volume strength, v is the critical exponent, and d is the dimensionality of the system under consideration.

In a θ solvent where the excluded volume effect vanishes, Eq. (10.28) reduces to Zimm’s extension of the Rouse treatment:

$$D = \frac{kT}{\eta_0 b} N^{-1/2} f_D(0) \quad (10.29)$$

where $f_D(0)$ is numerical factor. In a good solvent, the diffusion coefficient can be expressed in a simplified form:

$$D \sim N^{-\nu} \quad (10.30)$$

where $\nu = 0.6$.

10.6 MEASUREMENTS OF TRANSLATIONAL DIFFUSION COEFFICIENT

10.6.1 Measurement Based on Fick's First Law

A classical simple method used by Northrop and Anson (1929) is to measure the diffusion coefficient by a porous disk (not a semipermeable membrane, which was unavailable at that time). Figure 10.4 is a diagram of the experimental setup. Let c be the concentration of macromolecules, with c_{in} the concentration inside the cell, c_{out} the concentration outside the cell, V the volume of the cell, A the area of the disk, l the thickness of the disk, m the mass, and t the time of measurement. Fick's first law can be put into a practical form as

$$dm = -AD \frac{dc}{dx} dt$$

or

$$\Delta m = -AD \frac{\Delta c}{\Delta x} \Delta t \quad (10.31)$$

The explicit expression to determine D is then

$$D = \frac{-\Delta m}{A(\Delta c / \Delta x) \Delta t}$$

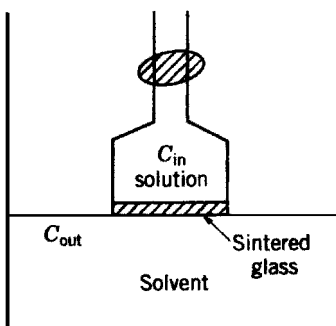


FIGURE 10.4 Northrop–Anson experiment for the determination of diffusion coefficient.

In terms of experimental quantities, we have

$$\begin{aligned}\Delta m &= V(C_{\text{in}} - c_{\text{in}}^0) \\ \Delta c &= c_{\text{in}}^0 - c_{\text{out}}^0 \\ \Delta x &= l\end{aligned}$$

where the zero superscript refers to the concentration in the reservoir when $t = 0$. We then have

$$D = \frac{V(c_{\text{in}} - c_{\text{in}}^0)}{K'(c_{\text{in}}^0 - c_{\text{out}}^0) \Delta t} \quad (10.32)$$

where $K' = A/l$, a constant known as the cell constant, which can be determined with a substance of known diffusion coefficient. Using a cell constant we can avoid determining A and l .

10.6.2 Measurement Based on Fick's Second Law

Several methods based on Fick's second law are available to measure the diffusion coefficient. Among these are the following three classical methods: the Schlieren method, the Gouy interference method, and the Rayleigh interference method. We describe here the Rayleigh interference method, for its application is also found in ultracentrifuge sedimentation. We use the classical Tiselius electrophoresis cells to illustrate (Figure 10.5).

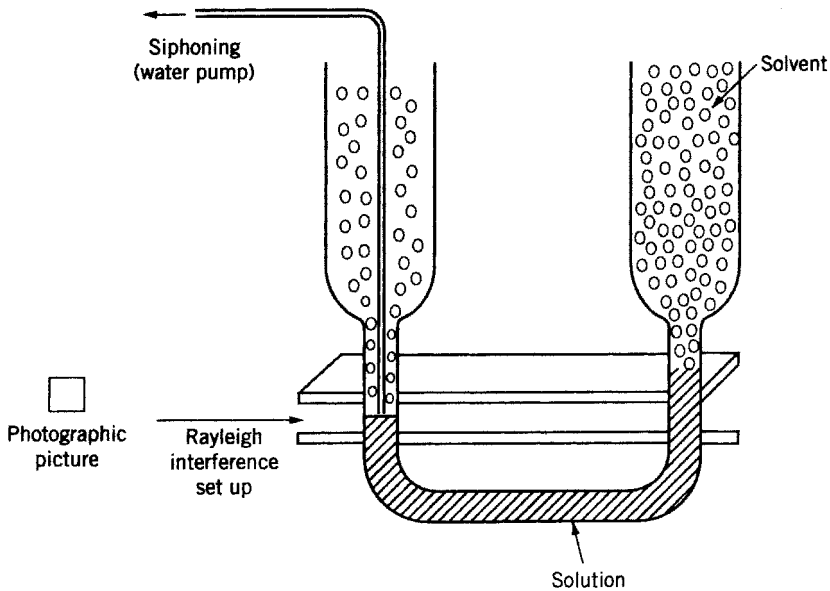
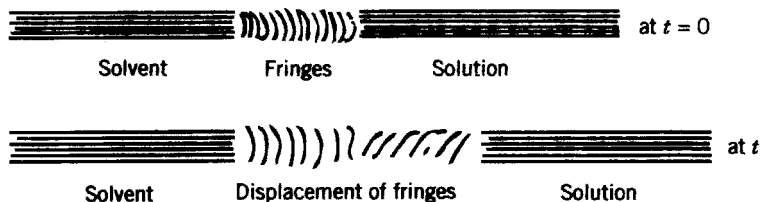
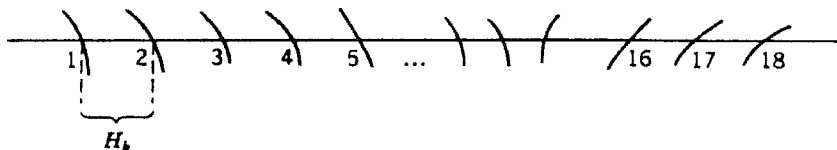


FIGURE 10.5 Rayleigh interference method for determination of diffusion coefficient.

Typical pictures found in a photographic plate are the displacements of fringes caused by differences in refractive indices in the diffusion region:



To aid in our discussion, we enlarge the fringes:



Let $j_k = 1, 2, 3, \dots$ be the fringe numbers. We then arbitrarily divide these numbers into two sets, j_k and j_l :

Fringes ($J = 18$)	
j_k	j_l
2	10
3	11
4	12
5	13
6	14
7	15
8	16
9	17
1(0)	18

Let J be the total number of fringes, for example, 18, and let H_k and H_l be the microcomparator reading for the distance of each j_k and j_l from the reference point, for example, $j_k = 1$. The value of j is related to Δn by[†]

$$J = \frac{a \Delta n}{\lambda}$$

[†] The cell constant a often refers to the cell thickness. It is on the order of 1.2 or 3.0 cm. In a 1.2-cm cell a displacement of one fringe ($j = 1$) corresponds to (assuming $\lambda = 5461 \times 10^{-8}$ cm),

$$\Delta n = \frac{(\lambda)(1)}{1.2} = \frac{5461 \times 10^{-8} \text{ cm}}{1.2 \text{ cm}} = 4.55 \times 10^{-5}$$

This corresponds to a concentration difference about 0.25 mg/mL. That is, 1 fringe \cong 0.25 mg/mL and 0.03 fringe (measurable) \cong (0.03)(0.25) = 0.0075 mg/mL.

where Δn is the difference in refractive index of the solution and the solvent, a is the cell constant, and λ is the wavelength of the light. Recalling the solution of Fick's second law,

$$\frac{dc}{dt} = D \frac{\delta^2 c}{\delta x^2}$$

which is in the form

$$c = \frac{c_0}{2} \left[1 - \frac{2}{\sqrt{\pi}} \underbrace{\int_0^{x/\sqrt{4Dt}} e^{-x^2/4Dt} d\left(\frac{x}{\sqrt{4Dt}}\right)}_{j_k^*} \right]$$

This can now be related to the interference fringes by

$$j_k^* = \frac{2j_k - J}{J} = \frac{2}{\sqrt{\pi}} \int_0^z e^{-z^2} dz$$

With the aid of a table from the *Tables of Probability Functions* (1941), the value of z may then be determined for each fringe. Thus, we have

$$\begin{aligned} H_k - H_l &= \Delta H \\ z_k &= \frac{h_k}{(4Dt)^{1/2}} & z_l &= \frac{h_l}{(4Dt)^{1/2}} \\ z_k + z_l &= \frac{h}{(4Dt)^{1/2}} \\ \frac{\Delta H}{h/(4Dt)^{1/2}} &= \text{known value } Q \end{aligned}$$

Here we change notation from x to h . The quantity $\Delta H/h$ is the magnification factor for the camera lens that relates distances in the diffusion cell to distances in the photographic plate. From Q , the value of D is determined.

10.7 ROTATIONAL DIFFUSION

A macromolecule may move, not in a transverse direction, but in a rotary motion under a torque, that is, oriented in an angle θ around a reference axis. Let $\rho(\theta) d\theta$ be

the number of particles per cubic center of solution, with an orientation between θ and $\theta + d\theta$. Then, the rotary concentration gradient $d\rho/d\theta$ is analogous to the transverse concentration gradient dc/dx and the laws governing translational diffusion apply equally to rotational diffusion. Fick's first law is

$$J(\theta) = -\Theta \frac{\delta\rho}{\delta\theta} \quad (10.33)$$

where Θ is the rotational diffusion coefficient. Fick's second law is

$$\frac{\delta\rho}{\delta t} = \Theta \frac{\delta^2\rho}{\delta\theta^2} \quad (10.34)$$

The rotational frictional coefficient ζ may be defined as

$$\zeta = \frac{T'}{\omega} \quad (10.35)$$

where T' is the torque and ω is the angular velocity. This may be compared to the definition for the translational frictional coefficient f :

$$f = \frac{F}{v}$$

Similar to translational diffusion D , we now have rotational diffusion Θ , which follows the Einstein equation:

$$\Theta = \frac{kT}{\zeta} \quad (10.36)$$

We also have Stokes' law for spherical macromolecules,

$$\zeta = 8\pi\eta r^3 \quad (10.37)$$

and Perrin's equation for ellipsoids of revolution,

$$\zeta = \frac{16\pi\eta a^3}{3[-1 + 2 \ln(2a/b)]} \quad (10.38)$$

with semiaxes of length a and b .

The rotary motion in three dimensions is related to the relaxation time τ :

$$\tau = \frac{1}{2\Theta} = \frac{\zeta}{2kT} \quad (10.39)$$

This equation is important to the design of the experiment to determine Θ . For a sphere, all three τ values in all three dimensions (τ_x , τ_y , and τ_z) are equal, whereas for an ellipsoid of revolution only two of the τ values are equal.

The most common methods for measuring the rotational diffusion coefficient Θ are non-Newtonian viscosity, flow birefringence, NMR, dielectric relaxation, fluorescence depolarization, electric birefringence, and polarized light scattering. Here, we describe the methods of flow birefringence and fluorescence depolarization. Currently, the most common and fruitful method is through laser light-scattering measurement, which is discussed in Chapter 16. The laser light-scattering method is used to measure both translational and rotational diffusion coefficients.

10.7.1 Flow Birefringence

The instrument used consists of two cylinders, one fixed and one moving, as shown in Figure 10.6. The sample is placed between these two cylinders. The extinct angle χ is measured where particles orient with respect to flow line. At the shaded part, no light is transmitted; at the empty part, light is transmitted.

The rotational diffusion coefficient Θ can be calculated using

$$\chi = a - \frac{B'}{120} + b \left(\frac{B'}{\Theta} \right)^3 + \dots \quad (10.40)$$

where a and b are constants and B' is the velocity gradient:

$$B' \frac{du}{dy}$$

10.7.2 Fluorescence Depolarization

Fluorescence spectroscopy is discussed in Chapter 17. Here we describe the experimental method for determining the rotational diffusion coefficient. The parameter we are interested in is ρ_h , which is the harmonic mean of the two

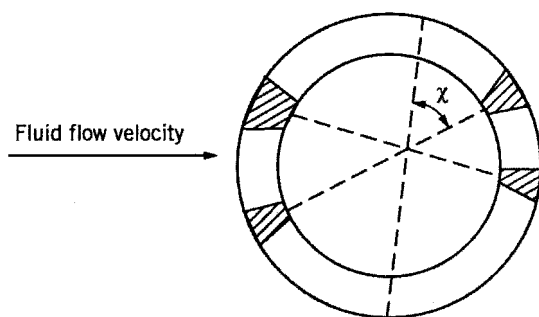


FIGURE 10.6 Flow birefringence.

principal relaxation times for the rotation of the ellipsoid. This is based on an equation derived by Perrin (1936):

$$\frac{1}{P} + \frac{1}{3} = \left(\frac{1}{P_0} + \frac{1}{3} \right) \left(1 + 3 \frac{\tau_0}{\rho_h} \right) \quad (10.41)$$

Here P is the degree of polarization of fluorescent light emitted at right angles to the direction of the incident light, τ_0 is the lifetime of the excited state of the fluorescence, and P_0 is an empirical constant. The rotational diffusion coefficient Θ_h is obtained from

$$\Theta_h = \frac{1}{2\rho_h} \quad (10.42)$$

REFERENCES

- Adler, R. S., and K. F. Freed, *J. Chem. Phys.* **70**, 3119 (1979).
 Boltzmann, L., *Ann. Phys. Chem. Wied.* **53**, 959 (1894).
 Crank, J., *Mathematics of Diffusion*, 2nd ed. Oxford: Oxford University Press, 1975.
 Einstein, A., *Ann. Phys.* **17**, 549 (1905).
 Fick, A., *Ann. Phys. Chem.* **170**, 59 (1855).
 Fourier, J. B. J., *Theorie Analytique de la Chaleur* (Paris, 1822), translated by A. Freeman, Cambridge, England, 1878, and New York, 1955. (See Grattan-Guinness, I., *Joseph Fourier 1768–1830*. Cambridge, MA: MIT Press, 1972.)
 Gosting, L. J., *Adv. Protein Chem.* **11**, 429 (1956).
 Kirkwood, J. G., *J. Polym. Sci.* **12**, 1 (1954).
 Lamm, O., and P. Polson, *Biochem. J.* **30**, 528 (1936).
 Northrop, J. H., and M. L. Anson, *J. Gen. Physiol.* **12**, 543 (1929).
 O’Konski, C. T., and A. J. Haltner, *J. Am. Chem. Soc.* **78**, 3604 (1956).
 Perrin, F., *J. Phys. Radium* **1**, 1 (1936).
 Schachman, H. K., *Methods Enzymol.* **4**, 78 (1957).
 Sutherland, W., *Philos. Mag.* **9**, 781 (1905).
Tables of Probability Functions, Vol. 1. Washington, DC: Government Printing Office, 1941.
 Tiselius, A., *Trans. Faraday Soc.* **33**, 524 (1937a).
 Tiselius, A., *Biochem. J.* **31**, 1464 (1937b).
 Weber, G., and L. B. Young, *J. Biol. Chem.* **239**, 1424 (1964).

PROBLEMS

10.1 Show that Fick’s second law (a) can be written in the form

$$\frac{dc}{dx} = \frac{D}{w} \frac{d^2c}{dx^2}$$

where w is the rate of vertical flow (i.e., $w = dx/dt$) and (b) has a solution

$$\frac{c - c_0}{c_{\max} - c_0} = \frac{e^{x/x^*} - 1}{e^{x_{\max}/x^*} - 1}$$

where c_0 is the concentration at $x = 0$, c_{\max} is the asymptotic concentration, x_{\max} is the asymptotic depth, and $x^* = D/w$.

10.2 A solution was suggested to the diffusion equation

$$c = \alpha t^{-1/2} e^{-x^2/4Dt}$$

where

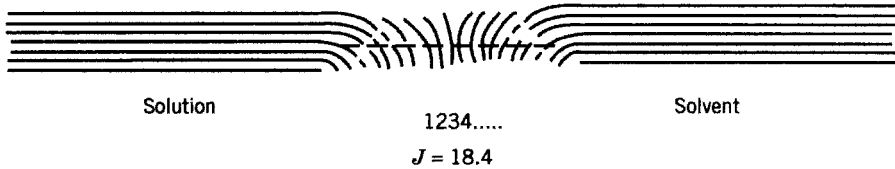
$$\alpha = \frac{n_0}{2(\pi D)^{1/2}}$$

and n_0 is the number of macromolecules initially present at $x = 0$. Show that this solution satisfies Fick's second law:

$$\frac{\partial c}{\partial t} = D \frac{\partial^2 c}{\partial x^2}$$

10.3 What is the probability that a macromolecule will diffuse a distance x in time t ?

10.4 The drawing is a representative Rayleigh pattern from a diffusion experiment on ribonuclease:



The total number of fringes J was found to be 18.4. The distance H_k between every two neighboring individual fringes j_k was measured on a photographic plate with a microcomparator. The graph was taken 2048 min after the boundary was sharpened. The camera lens magnification factor was $\Delta H/\Delta h = 1.00$. All the pertinent data of this particular graph are given in the following table:

j_k (mm)	j_l (mm)	H_k (mm)	H_1 (mm)
2	10	64.053	58.929
3	11	63.085	58.402
4	12	62.278	57.864
5	13	61.614	57.301
6	14	61.022	56.717

j_k (mm)	j_l (mm)	H_k (mm)	H_l (mm)
7	15	60.473	56.036
8	16	59.932	55.257
9	17	59.399	54.270

Calculate the apparent diffusion coefficient of ribonuclease (Schachman, 1957).

- 10.5** The diffusion coefficient of a polymer at infinite dilution is found to be $2.8 \times 10^{-7} \text{ cm}^2/\text{s}$. Estimate the hydrodynamic radius of this polymer. *Hint:* $D_0 = kT/f$.
- 10.6** The relaxation time τ_i can be determined from the slope of experimentally birefringent decay curves by constructing a tangent to the decay curve at the time t_i , where $i = 1, 2, 3, 4, \dots$ and t_i is the time required for the birefringence to decay to $\exp(-i)$ of its initial steady-state value. Relaxation times (in meters per second) for a tobacco mosaic virus were found to be $\tau_0 = 0.54$, $\tau_1 = 0.53$, $\tau_2 = 0.53$, $\tau_3 = 0.53$, and $\tau_4 = 0.54$. Calculate the rotational diffusion coefficient for this virus (O'Konski and Haltner, 1956).
- 10.7** The diffusion coefficient of bovine serum albumin at zero concentrations in water at 25°C is $6.75 \times 10^{-7} \text{ cm}^2/\text{s}$. The molecular weight is known to be 68,000.
- (a) Calculate the frictional factor f .
- (b) Calculate the frictional ratio f/f_0 .
- (c) Using a computer, construct a table for oblong ellipsoids ($p < 1$),

$$\frac{f}{f_0} = \frac{\sqrt{1-p^2}}{p^{2/3} \log(1 + \sqrt{1-p^2})/p}$$

and another table for oblate ellipsoids ($p > 1$),

$$\frac{f}{f_0} = \frac{\sqrt{p^2-1}}{p^{3/2} \arctan \sqrt{p^2-1}}$$

The values of $1/p$ or p may be selected from 1.0 to 25. Determine the axial ratio p for the bovine serum albumin and discuss the shape of the molecule.

- 10.8** At the θ temperature and infinite dilution, the diffusion coefficient D_0 of a polymer is found to be empirically related to its molecular weight:

$$D_0 = K'M^{-1/2}$$

where K' is a proportionality constant. Show that at the θ temperature the hydrodynamic volume is proportional to $M^{3/2}$.

11

SEDIMENTATION

Like intrinsic viscosity and diffusion, sedimentation is a frictional property. It is the transport of mass from the surface toward the bottom. In ultracentrifuge sedimentation, which is our major subject in this chapter, macromolecules in solution are forced to sediment by a centrifugal force that is 100,000 times greater than gravitational force. Sedimentation can be described by Fick's two laws with some modification, since sedimentation is often accompanied by diffusion. The modified equation of Fick's first law is

$$J = \underbrace{cS\omega^2 r}_{\text{Sedimentation}} \underbrace{-D(\partial c/\partial r)}_{\text{Diffusion}} \quad (11.1)$$

Flow of
solute

and that of the second law is

$$\frac{\partial c}{\partial t} = \frac{1}{r} \frac{\partial}{\partial c} \left[\left(cS\omega^2 r - D \frac{\partial c}{\partial r} \right) r \right] \quad (11.2)$$

where c is the concentration of the solute in solution, r is the distance from the axis of rotation, S is the sedimentation coefficient, ω is the number of rotations per minute (angular velocity), D is the diffusion coefficient, and t is time.

The first law is more important than the second law in treating sedimentation data. Using Eq. (11.1), two basic methods have been developed in ultracentrifuge sedimentation studies:

1. The sedimentation velocity method, in which diffusion is negligible. This is done by setting the rotor at a very high speed, for example, 60,000 rpm (rotations per minutes), which is equivalent to a pressure of 420 bars.
2. The sedimentation equilibrium method, in which diffusion plays an equally important role. This is done at a relatively low speed, for example, 12,000 rpm.

In between, there are two techniques that are extensively used to study biological polymers:

1. The approach to equilibrium method, in which sedimentation plays an important role but diffusion is not completely neglected. This method sets up a speed that is neither too fast nor too slow. During the run, macromolecules do not diffuse into the region of the meniscus or onto the bottom. Even at a relatively early stage of sedimentation, equilibrium reaches the regions of the meniscus and bottom, whereas the concentration in the region between the meniscus and bottom still changes with time. Thus, analysis need be focused only on the meniscus and bottom regions.
2. Density gradient at equilibrium, in which a density gradient is created by adding materials such as CsCl and CsBr to the system. The macromolecules float between the meniscus and the bottom and remain in a definite position when the force exerted on the macromolecules from the meniscus is balanced by that from the bottom.

11.1 APPARATUS

The ultracentrifuge apparatus comprises three major components: cell coordinates (Figure 11.1), rotor (Figure 11.2), and optical systems. There are three different optical systems: Schlieren, Rayleigh interferometric, and absorption. The Schlieren system is a basic unit of the ultracentrifuge instrument. It is commonly used in both sedimentation velocity and sedimentation equilibrium experiments. The system's only drawback is that the concentration of sample required is 5–50 mg/mL, which is too high and too costly for biological polymers (e.g., enzymes). The Rayleigh interferometric system measures the difference in refractive index Δn between the solution and a reference column of the solvent. This difference is measured through the displacement of interference fringes formed by slits placed behind the two columns. As mentioned before (Chapter 10), a displacement of one fringe ($j = 1$) corresponds to a concentration difference of about 0.25 mg/mL for most proteins and it is not difficult to measure displacement to about 0.02 fringe. The absorption

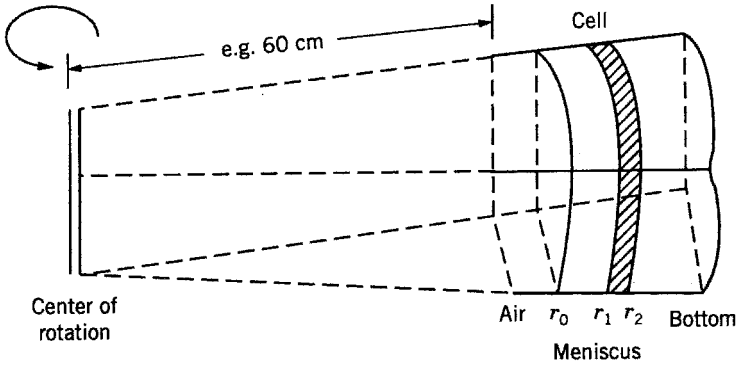


FIGURE 11.1 Coordinates of ultracentrifuge.

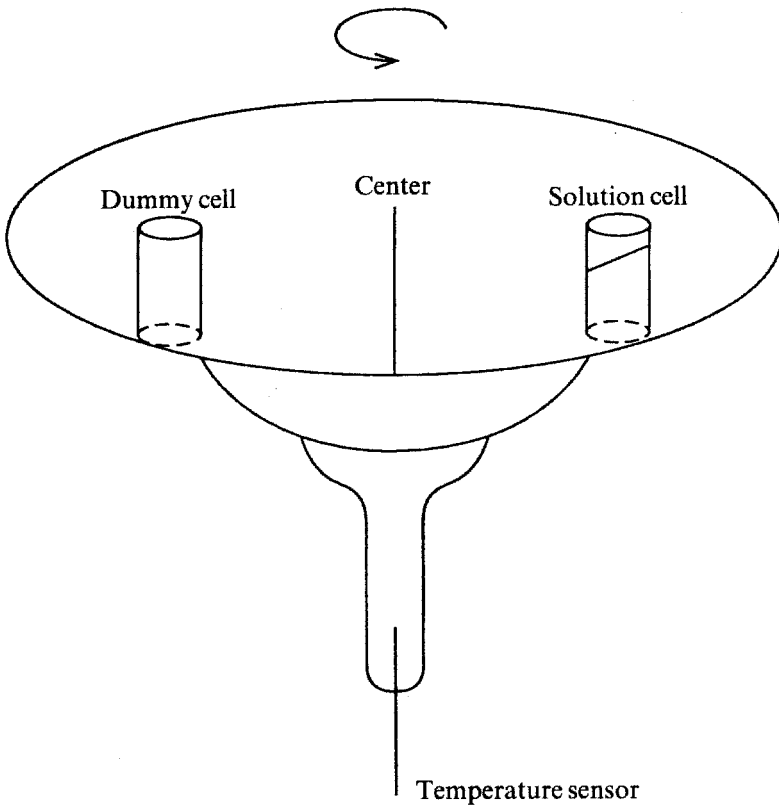


FIGURE 11.2 Rotor of the ultracentrifuge.

system needs a scanner and a monochromator light source as accessories. The advantage of the absorption system is its need for even smaller amounts of sample for measurement, that is, $20 \mu\text{g}$ ($20 \times 10^{-6} \text{ g}$).

11.2 SEDIMENTATION VELOCITY

Since it is usually included with the Spinco E analytical ultracentrifuge (a commercially available instrument), we will first analyze the graph obtained with the Schlieren system.

11.2.1 Measurement of Sedimentation Coefficients: Moving-Boundary Methods

Assuming that the boundary is sharp and no diffusion occurs (which is usually the case for a homogeneous system), we have

$$J = cS\omega^2 r$$

But at r ,

$$J = c \frac{dr}{dt}$$

We thus have

$$c \frac{dr}{dt} = cS\omega^2 r$$

and

$$S = \frac{1}{\omega^2 r} \frac{dr}{dt} = \frac{1}{\omega^2} \frac{d \ln r}{dt} \quad (11.3)$$

This is the equation used in the experimental determination of the sedimentation coefficient S . Figure 11.3 describes the experiment. Let R be the reference point, M the meniscus, and B the boundary. All of these points are measured from the center of rotation. Then we have

$$\Delta R = B - R$$

where ΔR is the distance of the boundary from the reference point that was read from the plate. The value of ΔR may be converted to that of Δr :

$$\Delta r = \Delta R \frac{1}{F} = (\Delta R) \quad \left(\frac{1}{F} = 0.462 \text{ cm} \right)$$

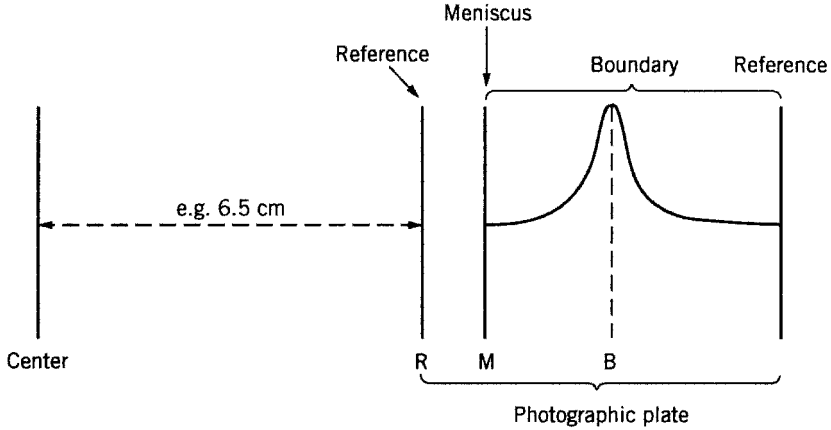


FIGURE 11.3 Sedimentation velocity experiment.

where Δr is the corrected distance of the boundary from the reference point and F is the magnification of the camera, which depends on the instrument. For example, $1/F = 0.462$ for a given instrument. The value of Δr is further converted to r_b ,

$$r_b = \Delta r + 6.5$$

where r_b is the distance of the boundary from the center of rotation. The value 6.5 cm is measured for a given rotor. It varies from rotor to rotor but usually is in the neighborhood of 6.5 cm.

Now we divide the values of r_b for the second, third, fourth, and fifth pictures (usually five pictures in a photographic plate taken at certain time intervals, e.g., 16 min) by the value of r_b for the first picture to obtain the values

$$\frac{r_b(2)}{r_b(1)} \quad \frac{r_b(3)}{r_b(1)} \quad \frac{r_b(4)}{r_b(1)} \quad \frac{r_b(5)}{r_b(1)}$$

If we set the time of the first picture at t_1 , then we have

$$\Delta t = t - t_1$$

where Δt is the time interval between the two pictures (e.g., 16, 32, 48, and 64 min). The rotor speed (rpm) is changed into the angular velocity ω :

$$\omega = \frac{\text{rpm}}{60} 2\pi$$

With all the pertinent values available we can now calculate the sedimentation velocity coefficient directly by using Eq. (11.3):

$$S = \ln \frac{r_b/r_b(1)}{\omega^2 \Delta t}$$

The unit of S is seconds or svedbergs (in honor of Theodor Svedberg, who was a pioneer in developing the ultracentrifuge). One svedberg equals 1×10^{-13} s.

To facilitate comparison with other biological polymers, the experimental value of the sedimentation coefficient is usually corrected to a standard basis corresponding to a reference solvent having the viscosity and density of water at 20°C. The equation for correction is

$$S_{20,w} = S_{t,b} \frac{(1 - \bar{v}\rho)_{20,w}}{(1 - \bar{v}\rho)_{t,b}} \frac{\eta_{t,b}}{\eta_{20,w}} \cong S_{t,b} \frac{\eta_t}{\eta_{20}}$$

where \bar{v} is the partial specific volume, ρ is the solution density, and η is the viscosity. The subscripts w and b refer to water and the buffer used (if any). Usually, the major effect is the change of water viscosity with temperature; data for making this correction are readily available in the literature.

Two important factors have to be considered to report accurate values of sedimentation coefficient. First is the possible dependence of the sedimentation coefficient on concentration. Although the sedimentation coefficient is supposed to be a constant under specified conditions, it may vary with concentration. A correction formula is given as follows:

$$S = \frac{S_0}{1 + kc}$$

where S_0 is the value of the sedimentation coefficient at infinite dilution, k is a constant that expresses the dependence of the sedimentation coefficient on concentration, and S is the sedimentation coefficient at the concentration c . A plot of $1/S$ versus c is expected to give a straight line, thereby enabling an extrapolation to infinite dilution. If k is small, that is, if the dependence of S on c is slight, then the equation is in the form

$$S = S_0(1 - kc)$$

Note:

$$\frac{1}{1 + kc} = 1 - kc + \dots$$

The second factor is the Johnston–Ogston effect, which is related to the multicomponent system. If a solution contains the fast and slow components and

if the mixture is diluted, the relative peak area of the fast components increases. Thus, in the region of the fast component boundary there is a decrease in the concentration of the slow component, which causes a decrease in the height of the Schlieren peak. The slow component often appears to be greater than its true concentration, whereas the faster component appears to be less than its true concentration. Consequently, there may be an error.

11.2.2 Svedberg Equation

If the rotor turns with an angular velocity ω (radians per second), n molecules suspended in a liquid will experience a centrifugal force F_c which is balanced by a frictional force F_f . The centrifugal force is expressed by

$$F_c = nv(\rho_m - \rho)\omega^2 r$$

where v is the volume of a single molecule, ρ_m is the density of the molecule, ρ is the density of the solution, ω is the angular velocity, and r is the distance from the center of rotation. If n is taken as Avogadro's number, then

$$F_c = M(1 - \bar{v}\rho)\omega^2 r$$

where \bar{v} is now the partial specific volume. The parameter $1 - \bar{v}\rho$ is a correction of the buoyancy factor. The frictional force may be expressed by

$$f_t = f \frac{dr}{dt}$$

If we equate the two forces

$$M(1 - \bar{v}\rho)\omega^2 r = f \frac{dr}{dt}$$

and rearrange the terms, we obtain

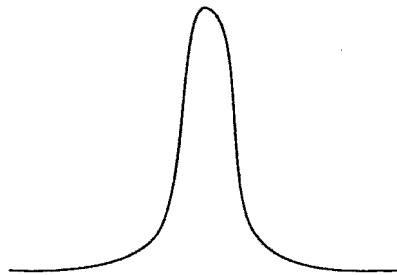
$$\frac{M(1 - \bar{v}\rho)}{f} = \frac{dr/dt}{\omega^2 r} = S$$

This is the Svedberg equation. It is also the definition of the sedimentation coefficient S .

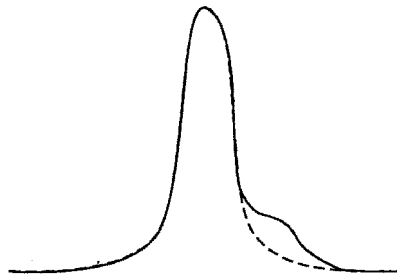
11.2.3 Application of Sedimentation Coefficient

Molecular Weight Determination See Eq. (10.21).

Characterization of Molecular Species The sedimentation coefficient can be used to evaluate the purity of a material. A sharp boundary is usually (though not always) an indication of the homogeneity of the particles. A broad boundary (asymmetrical) or more than one boundary grouped together is a clear indication that there is a heterogeneity of particles. The number of fast-moving molecules (e.g., dimers) can be estimated. Caution must be exercised, however, since the most serious consequence of the dependence of the sedimentation coefficient on concentration is a possible distortion of the boundary. Thus, before we draw any conclusions, the degree of dependence of S upon c must be assessed from a series of experiments performed at various concentrations.



Sharp and symmetrical—homogeneous



Broad and asymmetrical—heterogeneous

In biochemistry different species of the same kind of molecules are often labeled in terms of sedimentation coefficients. As an example, *Escherichia coli* ribosome has been separated into four different species, 30S, 50S, 70S, and 100S (see 18.6). The larger the number of S , the larger the size of the molecule.

11.3 SEDIMENTATION EQUILIBRIUM

Recall Eq. (11.1):

$$J = cS\omega^2 r - D \frac{dc}{dr}$$

When equilibrium is reached, the force of diffusion equals the force of sedimentation, that is, $J = 0$. We then have

$$0 = cS\omega^2 r - D \frac{dc}{dr}$$

Substituting Svedberg's equation for S ,

$$S = \frac{M(1 - \bar{v}\rho)}{f}$$

and Einstein's equation for D ,

$$D = \frac{R'T}{f}$$

we obtain

$$0 = \frac{M(1 - \bar{v}\rho)\omega^2 rc}{f} - \frac{R'T}{f} \frac{dc}{dr}$$

If we divide the equation by the factor c , we then have

$$M = \frac{2R'T}{(1 - \bar{v}\rho)\omega^2} \frac{d \ln c}{dr^2} \quad (11.4)$$

Equation (11.4) was first derived by Goldberg in 1953 on the assumption that the total potential of any component in the centrifugal solution is constant at equilibrium.

Three experimental methods are used to evaluate the term $d \ln c / dr^2$ in Eq. (11.4): the Archibald method, the van Holde and Baldwin method, and the Yphantis method. All are designed to determine the molecular weight of polymers (particularly biological polymers).

11.3.1 Archibald Method

At the beginning of the run, the material enters the column of solution at the meniscus and the bottom. It soon becomes saturated, so that the material can no longer transport to the meniscus and bottom. A simple criterion is the plot of the experimental data in the form of $(1/rc)(dc/dr)$ versus r . If the plot produces a horizontal line, then equilibrium is attained.

Archibald suggested that we need focus only on the top and the bottom of the cell during the process of equilibrium sedimentation to determine molecular weight; we do not have to wait for equilibrium to be reached. Hence, the method is also called approach to equilibrium. Equation (11.4) can be rearranged for

meniscus (m) and bottom (b) as follows:

$$M_m = \frac{R'T}{\omega^2(1 - \bar{v}\rho)} \frac{(\partial c/\partial r)_m}{c_m r_m}$$

$$M_b = \frac{R'T}{\omega^2(1 - \bar{v}\rho)} \frac{(\partial c/\partial r)_b}{c_b r_b}$$

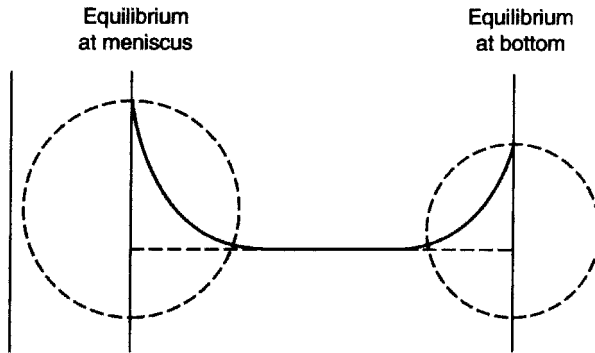
where

$$c_m = c_0 - \frac{1}{r_m^2} \int_{r_m}^{r_p} r^2 \frac{\partial c}{\partial r} dr$$

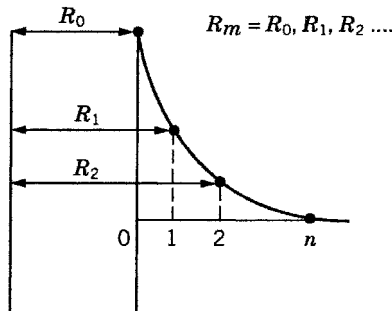
$$c_b = c_0 + \frac{1}{r_b^2} \int_{r_p}^{r_b} r^2 \frac{\partial c}{\partial r} dr$$

The value of c_0 is obtained from a synthetic boundary cell run, which we describe later. The term r_p refers to the position at the plateau region.

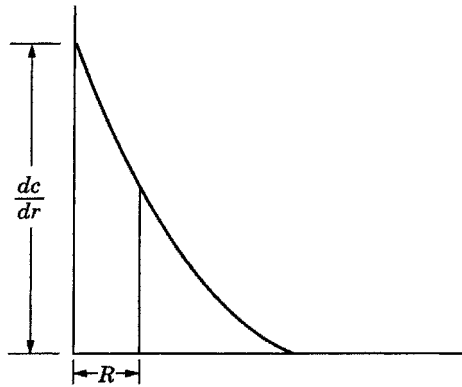
Let us consider the equilibrium at meniscus. To determine the value of M , we need the values of four parameters (in addition to other constants): $(\partial c/\partial r)_m$, r_m , c_m , and c_0 . Using the Schlieren system, a typical graph in the photographic plate is obtained in the following form:



The four parameters may then be evaluated by using data read from the plate:



The division from 0 to n is arbitrary. The length of the vertical line gives dc/dr , whereas the length of the division is R :

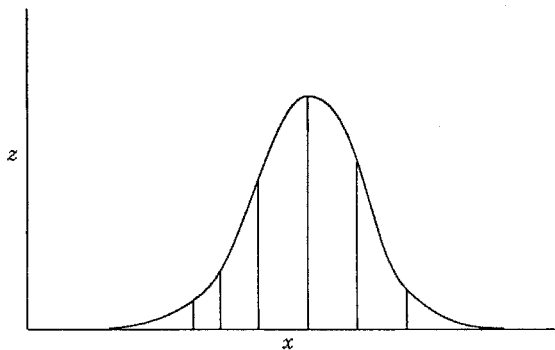


The values of R should be converted to r as follows:

$$r_m = \frac{R_m}{F} + k \quad m = 0, 1, 2, \dots$$

where F is the magnification factor (relating distances in the cell to distances on the enlargement) and the value k is the distance of the reference point in the plate from the center of rotation. The value of k is measured on the rotor and depends on the rotor used, e.g., 6.5 cm.

The value of c_0 is usually obtained from an independent synthetic boundary experiment that is relatively simple. A layer of pure solvent (e.g., 6.45 mL) is placed over a solution (e.g., 0.15 mL) of known concentration in a synthetic boundary cell, and a sedimentation velocity (8000 rpm) is run to obtain a graph:



The abscissa x is divided into intervals of 0.1. From the summation

$$\sum x_n z_n = (0.1) \sum z_n$$

we obtain

$$c_0 = \frac{0.1 \sum x_n}{F} = \text{area}$$

Note that the concentration unit is not grams per 100 mL; instead, it is in arbitrary units. The value of c_m can then be evaluated from the integral:

$$c_m = c_0 - \frac{1}{r_m^2} \sum_{n=0}^q r_n^2 \left(\frac{dc}{dr} \right)_n \frac{\Delta r}{F}$$

where Δr may be chosen to be 0.1 cm and q is the number of divisions in the horizontal coordinate. Since we have the values of c_0 , c_m , r_m , $(dc/dr)_m$, ω , T , \bar{v} , and ρ , we can calculate the molecular weight.

Sedimentation equilibrium experiments do not have to be run with the Schlieren system. They can also be run with the interference or absorption system. The only difference is in the expression of concentration in the photographic plate. The concentrations are expressed experimentally in terms of arbitrary units: square centimeters for Schlieren optics, number of fringes for interference optics, and optical density for absorption optics.

11.3.2 Van Holde–Baldwin (Low-Speed) Method (Rotor Velocity 10,000–14,000 rpm)

Equation (11.4) may be rewritten in the form

$$\frac{1}{c} \frac{dc}{dr} = \frac{M(1 - \bar{v}\rho)\omega^2 r}{R'T}$$

Multiplying both sides by the factor $c dr$ and integrating from the limit m (the meniscus) to the limit b (the bottom), we have

$$\int_{c_m}^{c_b} dc = \frac{M(1 - \bar{v}\rho)\omega^2}{R'T} \int_{r_m}^{r_b} rc dr$$

The two definite integrals may be evaluated as follows:

$$\int_{c_m}^{c_b} dc = c_b - c_m$$

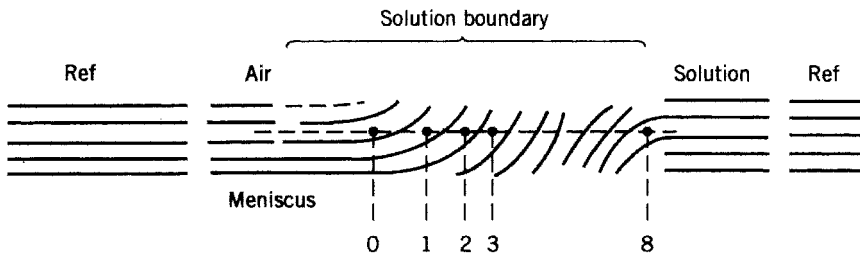
$$\int_{r_m}^{r_b} rc dr = c_0 \int_{r_m}^{r_b} r dr = c_0 \frac{r_b^2 - r_m^2}{2}$$

The equation of sedimentation equilibrium then becomes

$$\frac{c_b - c_m}{c_0} = \frac{M(1 - \bar{v}\rho)}{2R'T} (r_b^2 - r_m^2)$$

Both terms $(c_b - c_m)/c_0$ and $r_b^2 - r_m^2$ can be experimentally determined using either Schlieren optics or the Rayleigh interference system. Here, we illustrate with the Rayleigh interference system.

First, we run a synthetic boundary experiment to determine c_0 . The following drawing is an example:

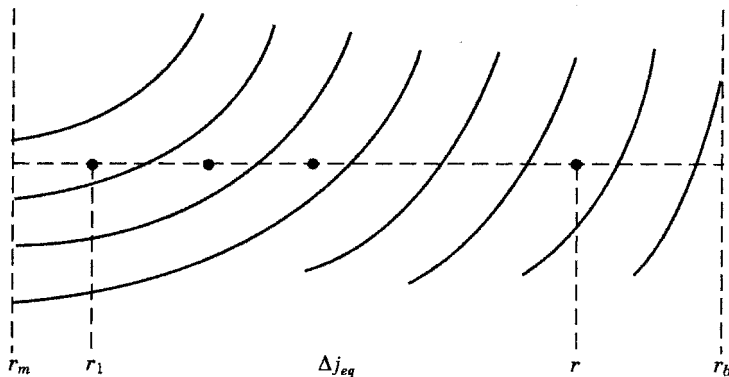


We count the number of fringes. Let Δj_{sb} be the total number of fringes crossed from the meniscus to the bottom, where the subscript sb denotes synthetic boundary. We then have

$$c_0 = k \Delta j_{sb}$$

where k is the proportionality constant which need not be evaluated, as we will see later.

Second, we run an equilibrium experiment for the sample. As an example of the moving boundary, consider the following drawing:

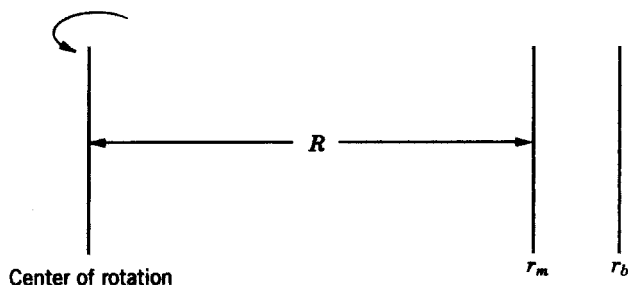


Δj_{eq} is the total number of fringes, where the subscript eq refers to the equilibrium. Then,

$$c_b - c_m = k \Delta j_{\text{eq}}$$

where k is the same constant that appeared in the evaluation of c_0 .

The values of r_m and r_b are measured by reading on the plate, while the value of the distance of the reference from the center is available as was described previously:



We thus can determine the molecular weight of the macromolecule:

$$M = \frac{2R'T}{\omega^2(1 - \bar{v}\rho)(r_b^2 - r_m^2)} \frac{\Delta j_{\text{eq}}}{\Delta j_{\text{sb}}}$$

The above equation is based on the assumption that the solution under study is an ideal solution, that is, there is no interaction between solute molecules. If it is not an ideal solution, the term of a second virial coefficient, A_2 , should be included in the equations:

$$\frac{M(1 - \bar{v}\rho)\omega^2}{(1 + 2A_2Mc)R'T} = \frac{(c_b - c_m)/2}{c_0(r_b^2 - r_m^2)}$$

or

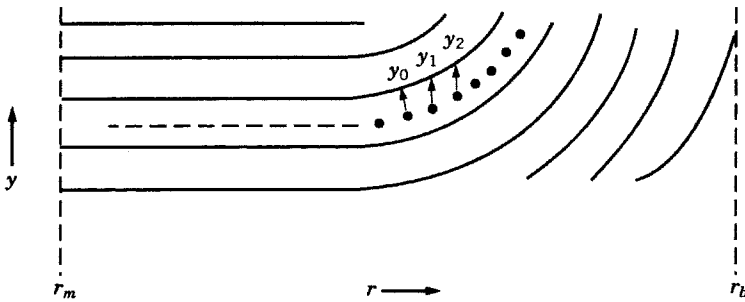
$$M = \frac{2R'T(1 + 2A_2Mc)}{\omega^2(1 - \bar{v}\rho)(r_b^2 - r_m^2)} \frac{\Delta j_{\text{eq}}}{\Delta j_{\text{sb}}}$$

11.3.3 Yphantis (High-Speed) Method (Rotor Velocity 28,000–32,000 rpm)

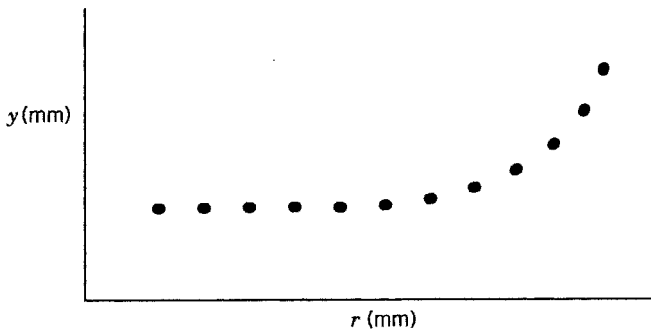
Equation (11.4) may be remodified as

$$\begin{aligned} M &= \frac{2R'T}{(1 - \bar{v}\rho)\omega^2} \frac{d \ln c}{dr^2} \\ &= \frac{2R'T}{(1 - \bar{v}\rho)\omega^2} \frac{d \ln(y - y_0)}{dr^2} \end{aligned}$$

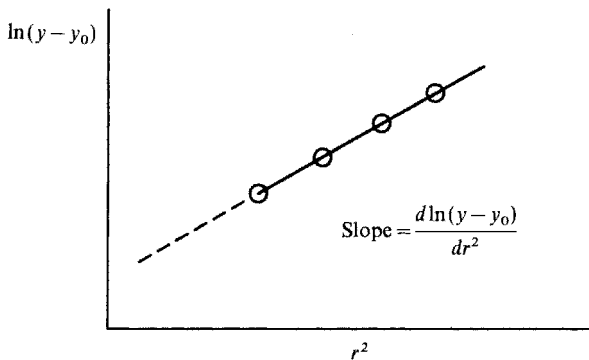
where y refers to the fringe displacement. The graph of a high-speed run is sketched as follows:



The crucial part in analyzing the data is the reading of r versus y of the curve in the photographic plate. The enlarged curve is in the following form:



With the data of y , y_0 , and r now available, we plot the final results:



The experimental points are expected to be on a straight line and the slope is equal to $[d \ln(y - y_0)]/dr^2$. From the slope of the plot we can thus calculate molecular weight.

The following table (van Holde, 1967) compares the low-speed method to the high-speed method:

Method	Approximate Concentration of Sample (mg/mL)	Approximate Solution Volume (mL)	Total Weight of Solute (mg)
Low speed	2	0.10 (for run), 0.15 (for synthetic boundary)	0.5
High speed	0.5	0.1	0.05

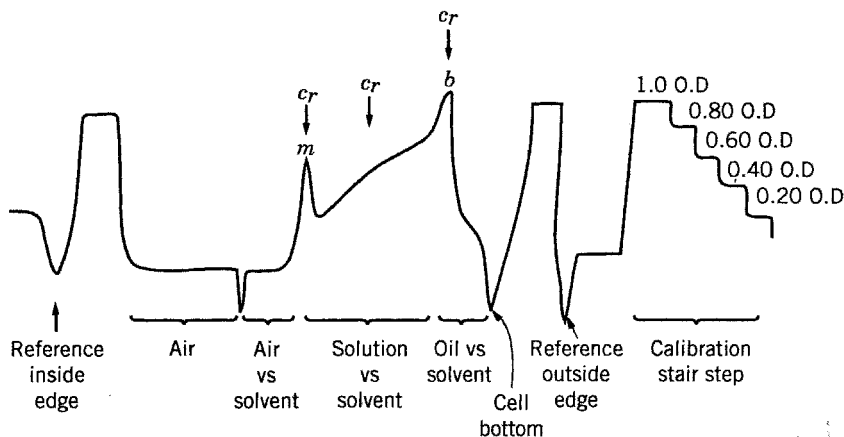
The high-speed method seems more economical and convenient than the low-speed method. The low-speed method requires an additional experiment, the synthetic boundary, whereas the high-speed method does not.

11.3.4 Absorption System

Equation (11.4) is rearranged in the form

$$\ln \frac{c_r}{c_m} = \frac{M(1 - \bar{v}\rho)\omega^2}{R'T} \frac{r^2 - r_m^2}{2}$$

In the absorption system, we measure c_r and c_m directly. The measurement is of the absorption of light and on the development of the scanner, which allows direct photoelectric recording of the optical density versus the r curve, as in the following sketch:



The coordinates are the absorption outside diameter (OD) and the distance r . Since the OD is directly proportional to the concentration (see Chapter 17), we can measure all four parameters used in the equation to calculate the molecular weight.

They are c_r , c_m , r^2 (the distance of the position from the center of rotation), and r_m^2 (the distance of the meniscus from the center of rotation).

11.4 DENSITY GRADIENT SEDIMENTATION EQUILIBRIUM

When materials with very high densities, such as CsCl and CsBr, are introduced into the macromolecular solution, a new density gradient is created. The centrifugal force sediments the macromolecules down to the bottom, but the heavy density from the sedimentation of CsCl or CsBr in the bottom forces the macromolecule to float in the region between the bottom and the meniscus. At equilibrium, the macromolecule rests at a definite position in the density gradient. The position that represents this density is called the buoyancy density, ρ_0 , of the macromolecule. The main purpose of the experiment for density gradient sedimentation equilibrium is to obtain the value of ρ_0 . Important information in characterizing a macromolecule may be obtained by analyzing ρ_0 and the gradient density $d\rho/dr$, where r is the distance of the point in a gradient from the center of rotation. Most density gradient experiments so far have been carried out with nucleic acids and proteins. Our discussion is therefore focused on biological polymers.

The buoyancy density of a protein, ρ_0 , is related to the net hydration of the protein salt complex and the net hydration of the salt-free protein. Let the number 1 represent water, 2 the protein, and 3 the salt. Then

$$\rho_0 = \frac{1 + \Gamma'_1}{\bar{v}_3 + \Gamma'_1 \bar{v}_1}$$

where Γ'_1 is the net hydration and \bar{v} the partial specific volume. The concentration gradient $d\rho/dr$ is related to rotor speed and the physical properties of CsCl. If we use the activity of the solute a (here, protein) instead of the concentration of the solute c , Eq. (11.4) could be put in the form

$$\frac{da}{dr} = \frac{M(1 - \bar{v}\rho)\omega^2 r}{R'T} a$$

We now relate the gradient density to the above equation by a simple manipulation:

$$\begin{aligned} \frac{d\rho}{dr} &= \frac{d\rho}{da} \frac{da}{dr} = \frac{d\rho}{da} \frac{M(1 - \bar{v}\rho)\omega^2 r}{R'T} a \\ &= \frac{d\rho}{d \ln a} \frac{M(1 - \bar{v}\rho)\omega^2 r}{R'T} \end{aligned}$$

We define a parameter β by

$$\beta = \frac{R'T}{(1 - \bar{v}\rho)M} \frac{d \ln a}{d\rho}$$

Then the density gradient is related to β in the form

$$\frac{d\rho}{dr} = \frac{\omega^2 r}{\beta}$$

From the photograph of the experiment for gradient density in equilibrium we can locate not only ρ_0 but also the values for r_m , r_b , and r_0 , where r_0 is the radial position of the center of band or bands. Let us define a new term r_e , the isoconcentration point in the cell:

$$r_e = \sqrt{\frac{r_b^2 + r_m^2}{2}}$$

At position r_e , the density of the solution is the same as that of the initial solution, ρ_e . The isoconcentration is the same as the isodensity.

If the photographic image of the macromolecular band is a Gaussian distribution curve, then we have

$$c = c_0 e^{-(r-r_s)^2/2\sigma^2}$$

and

$$\sigma^2 = \frac{R'T}{M\bar{v}(d\rho/dr)_r \omega^2 r_s}$$

Thus, the graphic determination of the standard deviation σ enables us to calculate the molecular weight of the sample.

The density gradient in equilibrium is an elegant method for determining molecular weight and for binding salt and water to the proteins. However, the experimental run is complicated and the analysis of data is tedious. For these reasons, this method is never extensively used in macromolecular chemistry, except for proteins and some nucleic acids.

11.5 SCALING THEORY

Except for water-soluble polymers, most synthetic polymers dissolve only in organic solvents, which are usually volatile and thus more difficult to deal with in the ultracentrifuge. Furthermore, unlike proteins whose polydispersity is near unity, polymer (synthetic) solutions are often heterogeneous. For this reason, sedimentation experiments are used less frequently in (synthetic) polymer chemistry. Investigators usually avoid using the ultracentrifuge for the determination of molecular weight.

However, while the ultracentrifuge is no longer heavily used in biochemistry (because of the development of sodium dodecyl sulfate (SDS)–polyacrylamide gel electrophoresis for the estimation of molecular weight, see Chapter 13), it has become an important tool for the study of dimensions of synthetic polymers in solution.

In the semidilute range, we may imagine the solution as a continuum formed by entangled macromolecules which can be divided into spheres (or blobs) of radius equal to the screen length ζ . If we write the Svedberg equation in its approximate form,

$$S \sim \frac{M}{f}$$

and make use of two other approximations

$$M \sim c\zeta^3 \quad f \sim \zeta$$

we can then obtain the approximate relation

$$S \sim c\zeta^2$$

In good solvents, it can be shown that

$$\zeta^2 \sim c^{-3/2}$$

Hence

$$S \sim c^{-1/2} \tag{11.5}$$

Equation (11.5) predicts that in the semidilute range of concentration ($c \sim c^*$) the sedimentation coefficient should be independent of the molecular weight of the polymer and the plot of $\log S$ versus $\log c$ should give the slope -0.50 .

This theory has been partially confirmed by sedimentation experiment (Langevin and Rondelez, 1978). The value of the slope so far found was -0.50 ± 0.10 . We now have some evidence to believe that in the semidilute range of polymer solution the solvent is forced through in orderly fashion around the blob of radius ζ but still cannot penetrate the interior of the blob. Note that this theory is reminiscent of the pearl necklace model and the hydrodynamic equivalent sphere.

Sedimentation experiments may also be used to test the scaling theory in another way. A small number of inert spheres with diameters of $2R \sim 100\text{--}200 \text{ \AA}$ (e.g., bovine serum albumin) is added to an aqueous solution of synthetic polymer (such as polyethylene oxide). If $2R > \zeta$, the spheres should move easily and f (the frictional coefficient) is related to η_0 (the viscosity of solvent). If $2R < \zeta$, the spheres will be trapped and f is related to η (the viscosity of entangled solution). To

measure η (the absolute viscosity) as a function of concentration is relatively difficult. It is much more convenient to test through the sedimentation experiment since the sedimentation coefficient, as shown in Svedberg's equation, is also closely related to f . The equation to be used is

$$\frac{f}{f_0} = \frac{S_0 - S_p}{S - S_p}$$

where S_0 is the sedimentation coefficient of the inert sphere alone, S_p that of the polymer alone, and S that of the inert sphere in the polymer solution. According to a scaling law

$$\frac{f}{f_0} = \psi\left(\frac{R}{\xi}\right)$$

we have

$$\psi\left(\frac{R}{\xi}\right) \sim \begin{cases} 1 & \text{for } R < \xi \\ \frac{f_0}{f} & \text{for } R \gg \xi \end{cases}$$

Thus, we can have

$$\frac{S}{S_0} \sim \exp(-c^{0.50})$$

By plotting $\ln(S/S_0)$ versus c , we can test whether the exponent is close to 0.50.

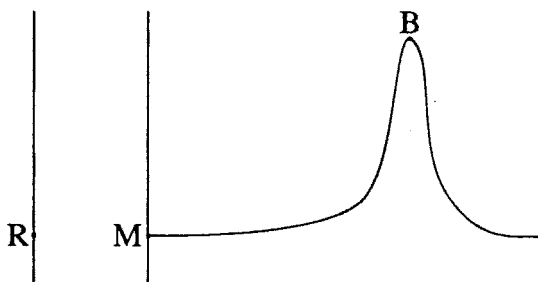
REFERENCES

- Archibald, W. J., *J. Phys. Colloid Chem.* **51**, 1204 (1947).
 Baldwin, R. L., *Biochem. J.* **65**, 503 (1957).
 Chervenka, C. H., *A Manual of Methods for the Analytical Ultracentrifuge*. Palo Alto, CA: Spinco Division of Beckman Instruments, 1969.
 Goldberg, R. J., *J. Phys. Chem.* **57**, 194 (1953).
 Johnston, J. P., and A. G. Ogston, *Trans. Faraday Soc.* **42**, 789 (1946).
 Langevin, D., and F. Rondelez, *Polymer* **19**, 875 (1978).
 Meselson, M., F. W. Stahl, and J. Vinograd, *Proc. Natl. Acad. Sci. USA* **43**, 581 (1957).
 Schachman, H. K., in S. P. Colowick and N. O. Kaplan (Eds.), *Methods in Enzymology*, Vol. 4. New York: Academic, 1957.
 Studier, F. W., *J. Mol. Biol.* **11**, 373 (1965).
 Svedberg, T., and K. O. Pedersen, *The Ultracentrifuge*. Oxford: Clarendon Press, 1940.
 van Holde, K. E., *Fractions* (Spinco Division), **1**, 1 (1967).

- van Holde, K. E., and R. L. Baldwin, *J. Phys. Chem.* **62**, 734 (1958).
 Vinograd, J., and J. E. Hearst, *Fortschr. Chem. Org. Naturstoffe* **20**, 372 (1962).
 Vinograd, J., *Methods Enzymol.* **6**, 854 (1963).
 Williams, J. W., K. E. van Holde, R. L. Baldwin, and H. Fujita, *Chem. Rev.* **58**, 715 (1958).
 Yphantis, D. A., *Biochemistry*, **3**, 297 (1964).

PROBLEMS

- 11.1** The speed of the ultracentrifuge (rpm) is often expressed in terms of g , the gravitational constant; for example, 45,000 rpm = 100,000 g . Express the following in terms of g : 12,000, 18,000, 24,000, 57,890, 60,000 rpm.
- 11.2** A protein was dissolved in buffer at pH 3.2 and was studied in the ultracentrifuge sedimentation velocity experiment. After the boundary was developed, five pictures were taken at intervals of 16 min. A typical picture with labels in a photographic plate is shown in the following sketch:



where R is the reference point, M is the meniscus, and B is the boundary. The plate was measured with a comparator and data are given as follows ($\Delta t = 16$ min, $1/F = 0.428$, $R = 5.765$ cm, $T = 298$ K, rpm = 59,780):

R (in.)	M (in.)	B (in.)
9.000	9.037	11.076
48.958	55.321	59.203
9.859	16.213	21.96
57.099	63.466	71.12
46.88	40.49	30.91

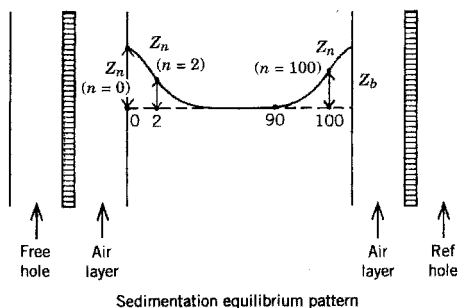
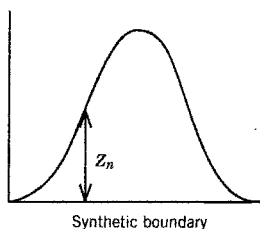
Calculate the sedimentation coefficient of the protein.

- 11.3** In a study of the sedimentation of bovine serum albumin, S was determined at a number of concentrations. When corrected to 25.0°C, the data are as

follows:

c_0	$S_{25}(10^{-13} \text{ s})$
0.29	4.927
0.59	4.839
0.87	4.772
1.17	4.663
1.17	4.662
1.76	4.475

- (a) From these data determine the value of S at $c_0 = 0$.
- (b) Using this value and the current best value for D_0 at 25°C ($6.97 \times 10^{-7} \text{ cm}^2/\text{s}$) and \bar{v} (0.734 mL/g), calculate the molecular weight.
- 11.4** Two ultracentrifuge sedimentation equilibrium experiments were carried out with ribonuclease in aqueous solution. The first was run in a conventional 12-mm cell and the second was performed in a synthetic boundary cell. The schematic diagrams of the ultracentrifuge patterns are shown in the following two figures:

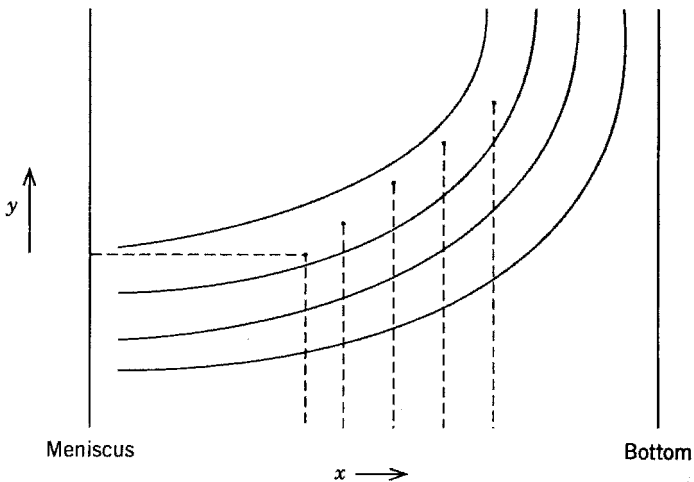


All the pertinent data are given in the following table for the sedimentation equilibrium of ribonuclease calculation at the meniscus (time 38 min, $F = 12.19$, $\bar{v} = 0.709 \text{ mL/g}$, $T = 298.9 \text{ K}$, $\omega^2 = 1.3633 \times 10^6$):

m	R_n (cm)	z_n (cm)
0	2.2	1.41
1	2.3	1.30
2	2.4	1.20
3	2.5	1.08
4	2.6	0.99
5	2.7	0.88
6	2.8	0.77
7	2.9	0.66
8	3.0	0.57
9	3.1	0.50
10	3.2	0.42
11	3.3	0.35
12	3.4	0.25
13	3.5	0.19
14	3.6	0.13
15	3.7	0.10
16	3.8	0.08
17	3.9	0.04
18	4.0	0.02

The value of c_0 was found from the synthetic boundary measurement to be 1.2167. Calculate the molecular weight of ribonuclease.

11.5 Following is a diagram of the fringe displacements as a function of the radial distance from the center of rotation typically found on a photographic plate:



Experimental data actually recorded on the sedimentation equilibrium run for a protein, sodium dioxidase, in an acetate buffer solution at pH 5, 25°C, and rotor speed 2.42×10^3 rpm are given as follows:

Plot $\log(y - y_0)$ versus r^2 and determine the molecular weight of the protein. The values of r may be calculated from the following practical equation:

$$r = 5.64 + \frac{x - 10.00}{(2.15)(10)}$$

where 5.64 cm is the distance of the center of rotation of a rotor, the value 10.00 in the numerator refers to an arbitrary setup in the comparator which was used for reading the plate, and the 10 in the denominator refers to the conversion factor 10 mm/cm.

- 11.6** To illustrate the scaling law, sedimentation coefficients were determined for poly(ethylene oxide) (molecular weight 3×10^5) in aqueous solution as a function of the concentration. Data are as follows:

Sedimentation Coefficient S (10^{-13} s)	Concentration c (g/cm ³)
1.24	0.99
0.82	2.98
0.56	4.78
0.41	6.62

Show that $S \sim c^{-\alpha}$. Determine α (Langevin and Rondelez, 1978).

12

OPTICAL ROTATORY DISPERSION AND CIRCULAR DICHROISM

Optical rotatory dispersion (ORD) and circular dichroism (CD) are useful for the study of the molecular structure, particularly the secondary structure, (helices), of biological polymers. The instrument used is called a spectropolarimeter and is easy to operate. Information is abundant in the literature for comparison and interpretation of new experimental results.

12.1 POLARIZED LIGHT

A light that oscillates in a single plane is called plane-polarized light, as shown in Figure 12.1. The magnetic field M is perpendicular to the electric field E . The direction is from left to right. It is the electric field that is related to ORD and CD. Plane-polarized light can be decomposed into circularly polarized components: right-handed E_R and left-handed E_L . Conversely, the two circularly polarized components may combine to form plane-polarized light. If the two components, E_R and E_L , are not equal in amplitude, then we have elliptically polarized light (Figure 12.2).

12.2 OPTICAL ROTATORY DISPERSION

As plane-polarized light passes through a substance, the velocities of the two circularly polarized components are reduced. If they are reduced to the same extent,

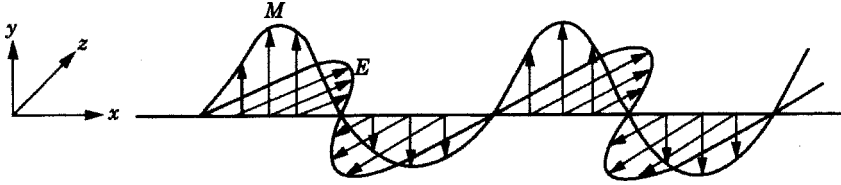


FIGURE 12.1 Plane-polarized propagation in the x direction.

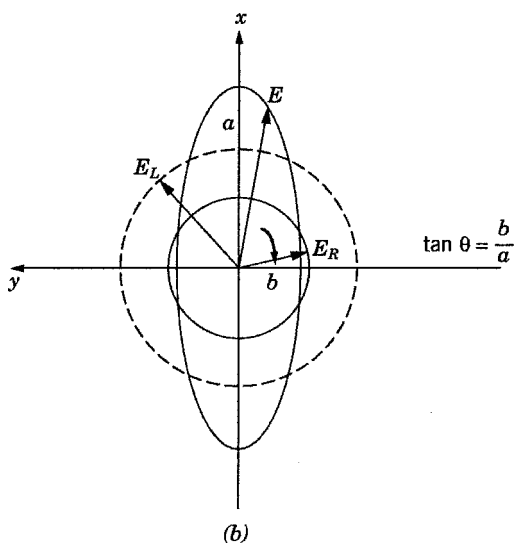


FIGURE 12.2 (a) Polarized light and (b) elliptically polarized light.

the substance is optically inactive; if not, the substance is optically active. After passing through an optically inactive substance, recombination of the two circularly polarized components does not create a phase difference; it emerges as an outgoing plane-polarized wave. On the other hand, after passing through an optically active substance, there is a phase difference and there will be a rotation of the plane of polarization, designated α .

Experimentally, the velocity of light in a medium is characterized by the refractive index of the medium. The different velocities of the two circularly polarized components are thus expressed in terms of their different refractive indices. An optically active substance is one that has different refractive indices for its left and right circularly polarized lights, n_L and n_R . The optical rotation α at a given wavelength of incident light λ is directly proportional to the difference between the refractive indices of the two circularly polarized components:

$$\alpha = k(n_L - n_R)$$

where k is the proportionality constant

$$k = \frac{180l}{\lambda}$$

and l is the path length in the medium.

Customarily, the optical rotation of an optically active substance is expressed in terms of the specific rotation $[\alpha]_\lambda$ and the molar rotation $[M]_\lambda$:

$$[\alpha]_\lambda = \frac{\alpha}{l'c} \quad [M]_\lambda = \alpha \frac{M}{100l'c}$$

where α (in degrees) is the observed rotation, λ (in centimeter) is the wavelength of incident light, l' (in decimeters) is the light path, c (in grams per milliliter) is the concentration of the optically active substance, and M (in grams per mole) is its molecular weight. Molar rotation is used to compare substance of different molecular weight.

In the study of macromolecules, such as proteins and nucleic acids, optical rotation is expressed in mean residual rotation $[M]_\lambda$:

$$[m]_\lambda = \alpha \frac{M_0}{100lc}$$

where M_0 is the mean residual molecular weight (e.g., for most globular proteins, M_0 is 117 or 115), and c is the concentration of the sample in grams per 100 mL.

If the refractive index of solvent n is included for correction, the equation of $[m]_\lambda$ is

$$[m]_\lambda = \frac{3}{n^2 + 2} \frac{\alpha M_0}{100lc}$$

where $n^2 = 1 + a\lambda^2/(\lambda^2 - \lambda_0^2)$ and a and λ_0 are both constants.

Optical rotatory dispersion is the change of optical rotation with wavelength. The data for optical rotatory dispersion are often analyzed in terms of the Drude (1900) equation:

$$[\alpha'] = \sum_i \frac{K_i}{\lambda^2 - \lambda_i^2}$$

where $[\alpha']$ is the observed rotation corrected for the refractive index of the solvent, K_i is a constant, and λ_i is the wavelength of the i th transition. It has been suggested that K_i is not really a constant. It is related to λ_i by another constant A_i such that

$$K_i = A_i \lambda_i^2$$

where A_i is related to the rotational strength of the i th transition R_i :

$$R_i = \frac{hc}{96\pi n} A_i$$

The rotational strength is the dot product of vectors $\boldsymbol{\mu}$ and \mathbf{m} :

$$R_i = \boldsymbol{\mu}_i \cdot \mathbf{m}_i$$

where $\boldsymbol{\mu}$ is the charge transition and \mathbf{m} is the magnetic transition. Both $\boldsymbol{\mu}$ and \mathbf{m} result from the interaction of electromagnetic radiation (light) with an optically active matter.

In many cases (such as protein) the Drude equation is used with only one term:

$$[\alpha'] = \frac{A_0 \lambda^2}{\lambda^2 - \lambda_0^2}$$

However, the one-term Drude equation has three drawbacks: (1) The equation is valid only at wavelengths far from the absorption band, (2) the analysis is informative only when the molecule has low α -helix content, and (3) the constants A_0 and λ_0 do not provide physical meaning.

Multiterm Drude equations are an improvement on the one-term Drude equation. There is no a priori way to demonstrate which multiterm Drude equation is best for analysis of any particular experimental data; whichever fits the data is the best.

The Moffit–Yang (1956) equation provides a different way to analyze experimental data and is given in the form

$$[m']_{\lambda} = \frac{a_0 \lambda_0^2}{\lambda^2 - \lambda_0^2} + \frac{b_0 \lambda_0^4}{(\lambda^2 - \lambda_0^2)^2}$$

where $[m']$ is called the effective residue rotation and a_0 and b_0 are constants. The parameter a_0 seems to have no physical meaning, but b_0 does. The plot of $[m']$ ($\lambda^2 - \lambda_0^2$) or $[\alpha](\lambda^2 - \lambda_0^2)$ versus $1/(\lambda^2 - \lambda_0^2)$ is expected to give a straight line from which b_0 can be determined. The terms b_0 and λ_0 are principally functions of the helical backbone, independent of side chains and environment. The value of λ_0 is assumed to be 212 nm for the wavelength range between 600 and 350 nm and 216 nm for the wavelength range between 280 and 240 nm. The value of b_0 , which is of primary importance in ORD measurements, is a measure of the helical content of a macromolecule. On the basis of experimental studies of some polypeptides, the maximum value for b_0 is 630. The sign of the value for b_0 indicates the direction of the helix: minus for a right-handed helix and plus for a left-handed helix. Thus, there are three extreme values for b_0 : -630 for a 100% right-handed helix; 0 for no helix at all; $+630$ for a 100% left-handed helix. In between these three values, the molecule is supposed to have a partial helix in its secondary structure. The Moffitt–Yang equation has been used extensively in the literature for the estimation of the α -helix content of polypeptides and proteins.

Figure 12.3 shows a typical rotatory dispersion curve, where there is no maximum or minimum. Figure 12.4 shows a plot of $[m']$ versus λ , in which a protein in denatured form is compared with the same protein in native form. The plot of the Moffitt–Yang equation is shown in Figure 12.5. If a synthetic polypeptide is in a random conformation, the rotatory dispersion, which is simple, may be adequately expressed by a one-term Drude equation. If a synthetic polypeptide is in an α -helical conformation, the Moffitt–Yang plot may be employed to describe the rotatory dispersion.

In assessing the optical rotatory change of proteins, the sequence and molecular weight are unimportant. The important parameters are the composition and conformation, particularly the latter. Any change in environment (such as pH or

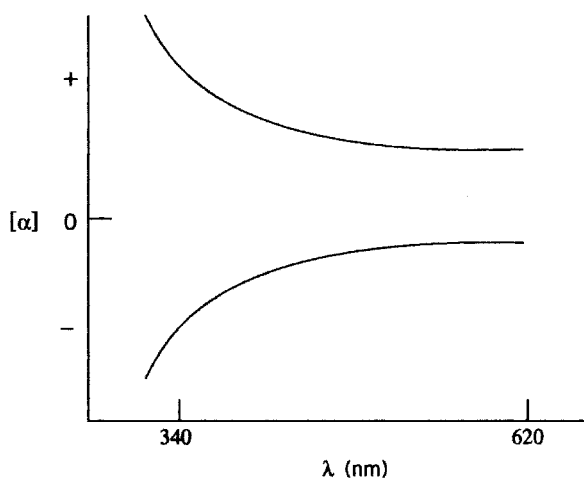


FIGURE 12.3 $[\alpha]$ versus λ .

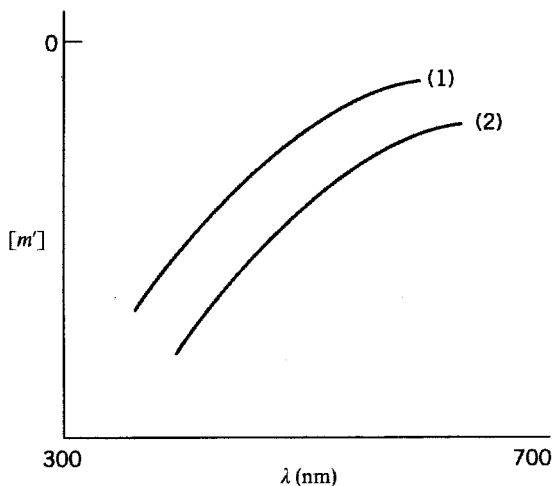


FIGURE 12.4 $[m']$ versus λ in (1) native form and (2) denatured form.

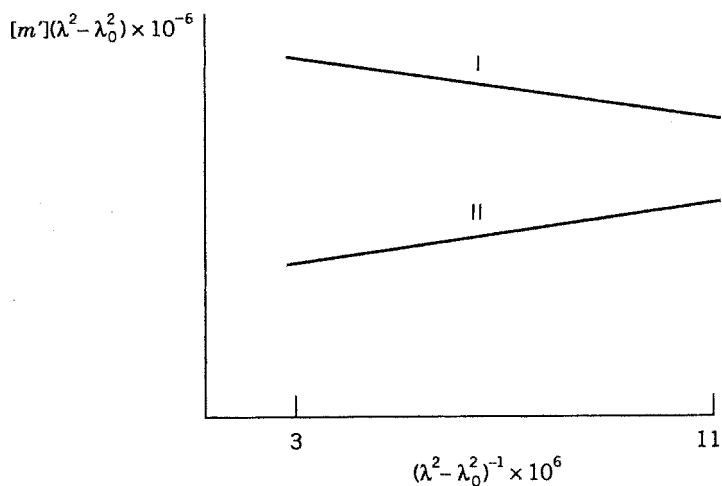


FIGURE 12.5 Plot of the Moffit-Yang equation.

salt concentration) could cause a change in conformation. Quantitatively, the numerical values of $[\alpha]$ or $[m']$, λ_0 , and b_0 provide information on the extent of change.

12.3 CIRCULAR DICHROISM

If the intensity of absorption (not the refractive index n) is used as a function of the orientation of the plane of polarization, we have a phenomenon called circular

dichroism. As in the case of refractive indices, for an optically inactive substance, the intensities of the left and right circularly polarized components are equal. For an optically active substance, they are not equal. The difference $\Delta\varepsilon$ is expressed in the equation

$$\Delta\varepsilon = \varepsilon_L - \varepsilon_R$$

where ε is the molar absorptivity and L and R refer to the left and right circularly polarized components, respectively. The value of $\Delta\varepsilon$ varies with wavelength and can be positive or negative. The values of ε_L , ε_R , and $\Delta\varepsilon$ are in a narrow region in the absorption maximum of the compound. The plot of $\Delta\varepsilon$ versus λ for a simple optical transition is bell shaped, similar to the ordinary absorption curve in spectroscopy.

Circular dichroism is usually measured as a dichroic ratio, which is the ratio of the optical densities of an absorption band in the direction of the polarized light (parallel over perpendicular) to a specified direction in the sample. More specifically, dichroic ratios depend on the angle θ , as shown in Figure 12.2*b*. The tangent of θ is the ratio of the minor axis b to the major axis a of the ellipse that is defined as

$$\theta = \tan^{-1} \frac{b}{a}$$

The angle θ , written as $[\theta]$, is called the molar ellipticity. The relationship between $\Delta\varepsilon$ and $[\theta]$ is expressed in the equation

$$[\theta] = (3300^\circ)(\Delta\varepsilon)$$

The dimension of $\Delta\varepsilon$ is in $(\text{L}/\text{cm}) \text{mol}^{-1}$, while that of $[\theta]$ is in $\text{deg} \cdot \text{cm}^2/\text{d mol}$. The molar ellipticity $[\theta]$ is often considered to consist of possible electronic transitions in the molecules:

$$[\theta] = \sum_i [\theta_i]$$

where $[\theta_i]$, the ellipticity for the i th transition, is characterized by three parameters:

- λ_i^0 The wavelength at which the maximum ellipticity is located
- Δ_i^0 The half width of the dichroism band
- R_i The rotational strength of the i th transition

All three parameters could easily be evaluated, as shown in Figure 12.6. The parameter R_i can be calculated using the following equation:

$$R_i = \frac{3hc'}{8\pi^3 N_1} \int_0^\infty \frac{\theta_k(\lambda)}{\lambda} d\lambda$$

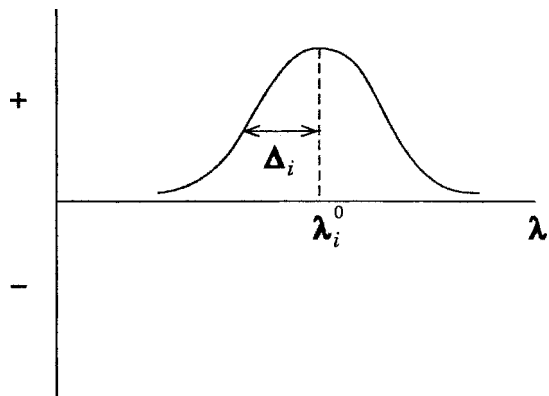


FIGURE 12.6 A dichroic band.

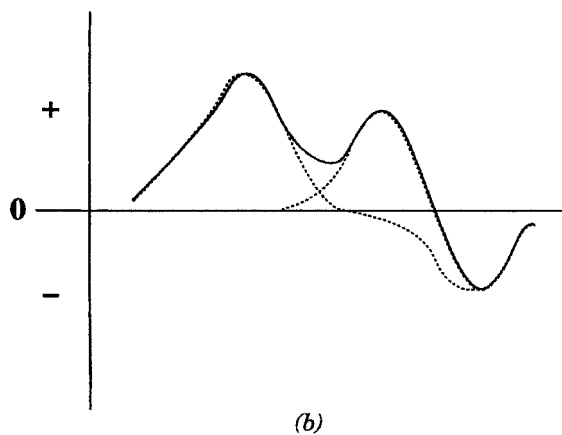
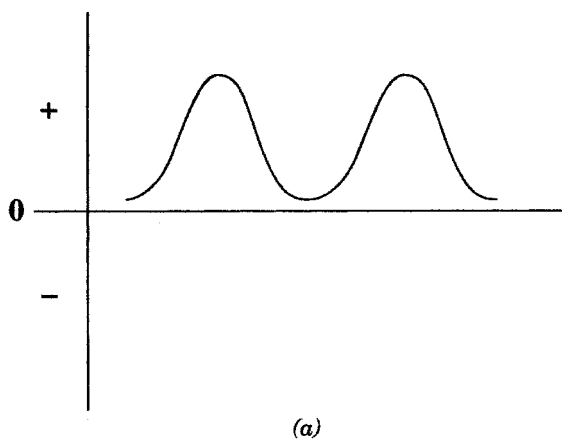


FIGURE 12.7 Dichroic bands.

where $\theta_k(\lambda)$ is the partial ellipticity for the k th transition, h is Planck's constant, c' is the velocity of light, and N_1 is the number of absorbing molecules per cubic centimeter. The integral is the area under the dichroic band. The rotational strength is related to the induced electric and magnetic dipole moments by $R_i = \mu_i^e \mu_m^i$, as mentioned before.

The dichroic bands are not always neatly separated as in Figure 12.7a; they may overlap and be located in positive and negative directions as in Figure 12.7b. When they overlap, each band should be resolved. Provided that the dichroic bands are Gaussian, the three parameters λ_i^0 , Δ_i^0 , and R_i can be evaluated as a single separate dichroic band.

Circular dichroism is extensively employed in the structural study of biological polymers, but not in the study of synthetic polymers. This is because most biological polymers are optically active, whereas most synthetic polymers are not. However, if the optically active vinyl or vinylidene monomers are incorporated in a synthetic polymer, the synthetic polymer could become optically active.

12.4 COTTON EFFECT

An anomalous curve may appear within the optical rotatory spectrum, showing one or more maxima or minima in the neighborhood of the absorption band. Such an anomalous curve is attributed to a special combination of unequal refractive indices known as the Cotton effect. The maxima are called peaks and the minima are called troughs (Figure 12.8). If the peak is at the longest wavelength (i.e., right of the trough), there is a positive Cotton effect. Otherwise, the Cotton effect is negative.

The Cotton effect can also appear in CD, but there is only a positive or a negative maximum, not peaks and troughs. The positive maximum in CD corresponds to the inflection of the positive Cotton effect and the negative maximum corresponds to the negative Cotton effect (see Figure 12.9). Since the two extremes, peak and trough, are so obvious, the Cotton effect is more easily visualized in ORD than in

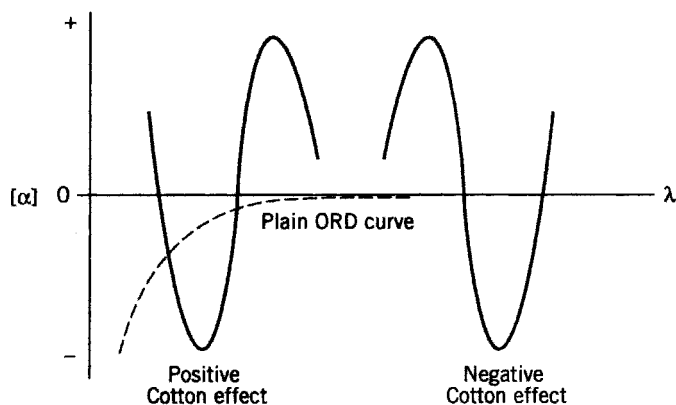


FIGURE 12.8 ORD Cotton effect.

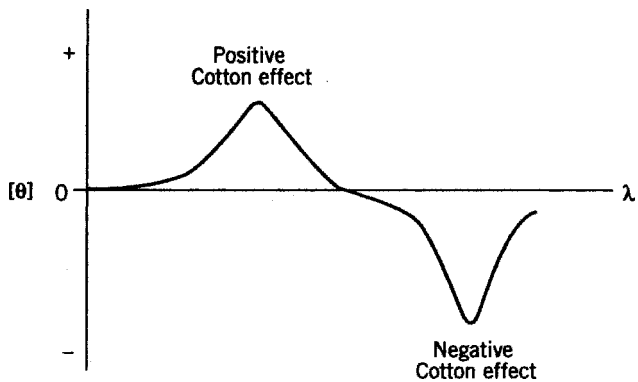


FIGURE 12.9 CD Cotton effect.

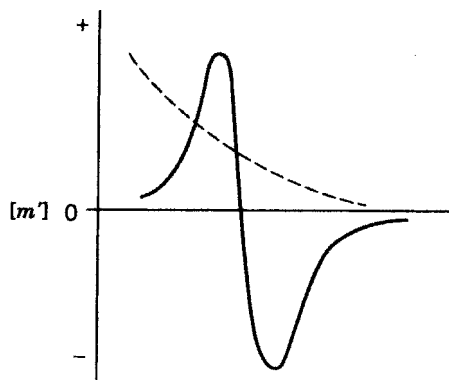


FIGURE 12.10 Loss of Cotton effect: —, Cotton effect; - - -, loss of Cotton effect.

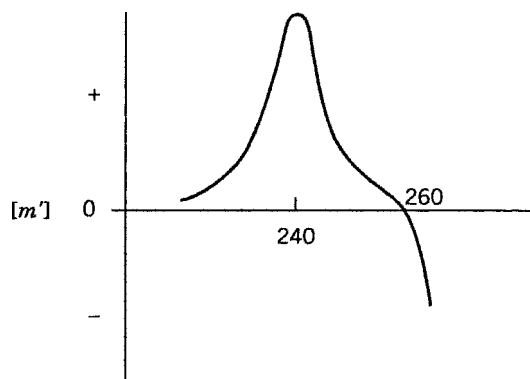


FIGURE 12.11 Cotton effect of mononucleosides and mononucleotides

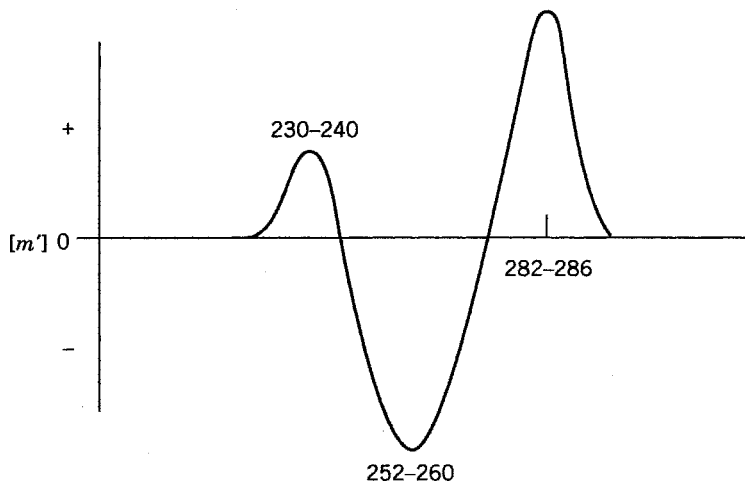


FIGURE 12.12 Cotton effect of synthetic polynucleotides.

CD; but CD is much more sensitive than ORD because the trailing parts of the ORD curves representing Cotton effects often overlap.

The Cotton effect curve is very sensitive to conformational alterations of proteins and polypeptides. It is a method that can also be used to assess α -helical content. In a dissymmetric environment, the α -helical conformation is characterized in ORD by a large negative Cotton effect with a trough at 233 nm and an inflection at about 225 nm. Quantitatively, the magnitude of the trough at 233 nm provides an estimation of the α -helix content. When the helix is destroyed, the Cotton effect is lost (Figure 12.10). For mononucleosides and mononucleotides, a single Cotton effect appears above 220–240 nm and a crossover appears near 260 nm (Figure 12.11). For synthetic polynucleotides, such as poly A and poly U, the multiple Cotton effects all have a large peak at 282–286 nm and a trough at 252–260 nm, followed by a small peak near 230–240 nm (Figure 12.12).

12.5 CORRELATION BETWEEN ORD AND CD

Both ORD and CD are sensitive to conformational changes and chemical transformation. ORD has the following advantages over CD: (1) It is easier to visualize the Cotton effect with ORD because of the three distinct points in the ORD curve: the peak, the crossover, and the trough (in that order or in reverse order). (2) An optically active compound that does not show the band in the wavelength range of interest in the absorption spectrum will not show a CD curve but will show a plain ORD curve. CD, on the other hand, possesses an intrinsic discreteness and is a more sensitive tool in examining the environmental effect on the conformation of macromolecules.

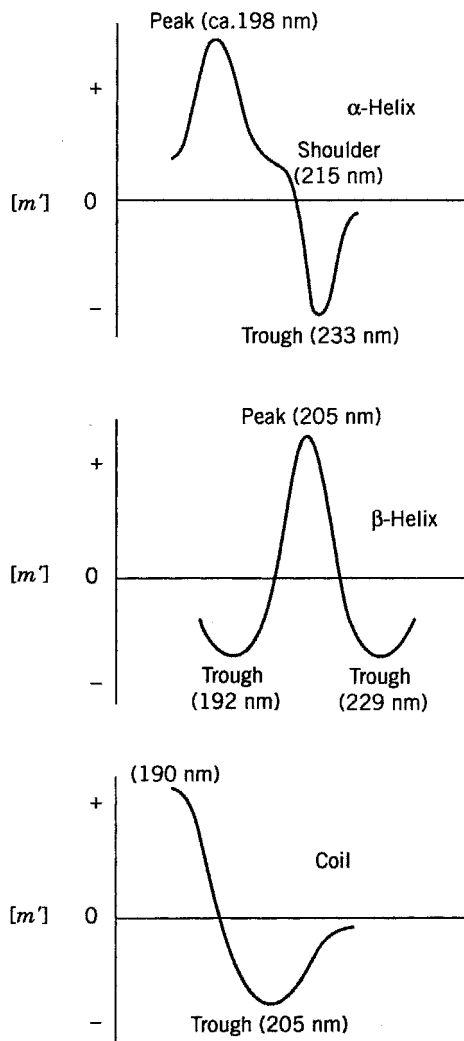


FIGURE 12.13 Optical rotatory dispersion.

A reciprocal relationship exists between ORD and CD using the Kronig–Kramers (Kronig, 1926; Kramers, 1927) transform:

$$[m_i(\lambda)] = \frac{2}{\pi} \int_0^{\infty} [\theta_i(\lambda')] \frac{\lambda'}{\lambda^2 - \lambda'^2} d\lambda'$$

$$[\theta(\lambda)] = -\frac{2}{\pi\lambda} \int_0^{\infty} [m(\lambda')] \frac{\lambda'^2}{\lambda^2 - \lambda'^2} d\lambda'$$

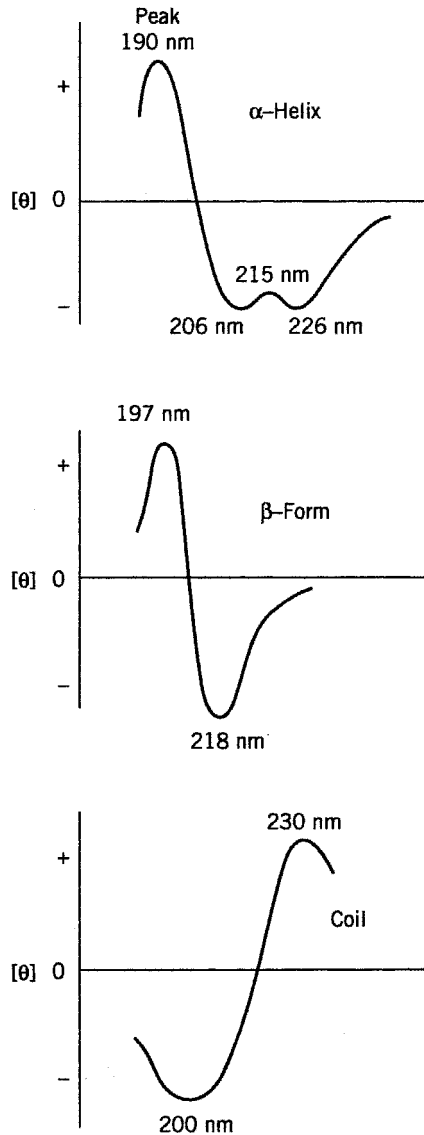


FIGURE 12.14 Circular dichroism.

The prime (′) represents the assigned vacuum values (see Moscovitz, 1960). The condition attached to this transform is that the rotatory dispersion curve must be Gaussian. Thus, from the CD curves, we can calculate the rotatory dispersion and vice versa.

12.6 COMPARISON OF ORD AND CD

In what follows, we compare ORD and CD by sketching the typical curves for proteins and polypeptides in α -helical, β -helical, and random coil forms. We first give a few theoretical remarks to provide background. It is now well known that the spectral region of the amide involves $\pi^0-\pi^-$ and $n_1-\pi^-$ transitions. According to Moffit, the electronic dipole transition moments and the optical activity of helical molecules are coupled. The electronic transition $\pi^0-\pi^-$ occurs at around 190 nm, while that of $n_1-\pi^-$ occurs at around 225 nm. The actual values, of course, depend on the structure of the molecules at specific conditions. They are not exactly at 190 and 225 nm, respectively. Still, it is worthwhile to focus on the curve near these two wavelengths.

In general, an ORD curve of α -helical polypeptides or proteins shows a trough at ~ 233 nm, a crossover at ~ 225 nm, a shoulder at ~ 215 , and a peak at 198 nm. At random conformation, the Cotton effect at ~ 225 is lost (Figure 12.13). In the study of synthetic polypeptides and proteins, CD is found in the region between 190 and 250 nm, where absorption is basically due to peptide linkage. The value of molar ellipticity has been suggested to the estimate of α -helical content (Figure 12.14).

Figure 12.15 shows CD of a typical polypeptide. There are three bands in the accessible region: 191, 206 (or 209), and 227 nm. The two dichroic peaks (222 and 209) are negative; they are clearly separated by a distinct notch at 215 nm. The dichroic band at 191 nm is positive. Whenever there is a conformational change, for example, from α -helical to disordered, there is a change in the three bands. In certain cases the change is strong; in others it is weak.

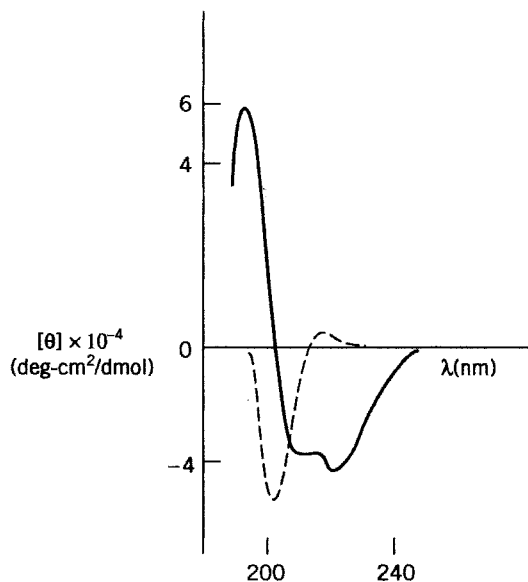


FIGURE 12.15 CD of a polypeptide: —, helical structure; ---, disordered state.

REFERENCES

- Blout, E. R. I. Schnier, and N. S. Simmons, *J. Am. Chem. Soc.* **84**, 3193 (1962).
 Brahms, J., *J. Am. Chem. Soc.* **85**, 3298 (1963).
 Chen, Y. H., and J. T. Yang, *Biochem. Biophys. Res. Commun.* **44**, 1285 (1971).
 Cotton, A., *Ann. Chim. Phys.* **8**, 347 (1896).
 Djerassi, C., *Optical rotatory Dispersion*. New York: McGraw-Hill, 1960.
 Doty, P., A. Wada, J. T. Yang, and E. R. Blout, *J. Polym. Sci.* **23**, 831 (1957).
 Drude, P., *Lehrbuch der Optik*. Leipzig: Hirzel, 1900.
 Greenfield, N., and G. D. Fasman, *Biochemistry* **8**, 4108 (1969).
 Holzwarth, G., and P. Doty, *J. Am. Chem. Soc.* **87**, 218 (1965).
 Holzwarth, G., W. B. Gratzer, and P. Doty, *J. Am. Chem. Soc.* **84**, 3194 (1962).
 Iizuka, E., and J. T. Yang, *Proc. Natl. Acad. Sci. USA* **55**, 1175 (1966).
 Kramers, H. A., *Atticongr. Intern. fisici, como* **2**, 545 (1927).
 Kronig, R. de. L., *J. Opt. Soc. Am.* **12**, 547 (1926).
 Moffitt, W., and J. T. Yang, *Proc. Natl. Acad. Sci. USA* **42**, 596 (1956).
 Moscowitz, A., in C. Djerassi (Ed.), *Optical Rotatory Dispersion*. New York: McGraw-Hill, 1960.
 Shechter, E., and E. R. Blout, *Proc. Natl. Acad. Sci. USA* **51**, 695 (1964).
 Simmons, N. S., C. Cohen, A. G. Szent-Gyorgyi, D. B. Wetlaufer, and E. R. Blout, *J. Am. Chem. Soc.* **83**, 4766 (1961).
 Tinoco, I., and C. Cantor, *Methods Biochem. Anal.* **18**, 81–203 (1970).
 Yang, J. T., and T. Sameijima, *Progr. Nucl. Acids Res.* **9**, 223 (1969).

PROBLEMS

- 12.1** In a certain environment, the residual rotation value $[R']_{233}$ band was found to be $-12,600$ for poly-L-glutamic acid, $-10,400$ for poly-L-methionine, and $-12,800$ for poly- γ -benzyl-L-glutamate. Calculate the percentage helix of each of the polypeptides, assuming a mean value of $[R']_{233} = 12,700$ for 100% helix and $[R']_{233} = 1800$ for 0% helix (Simmons et al., 1961).
- 12.2** The ORD of poly- γ -benzyl-L-glutamate in chloroform does not fit a simple Drude equation. Such dispersion results may be plotted in the general form proposed by Moffit. The data are as follows:

λ (nm)	$[a]$ (deg-cm ² /dg)
340	-40
420	9
500	12
580	8
600	10

- (a) Give a Moffit plot ($[\alpha](\lambda^2 - \lambda_0^2)$ versus $1/(\lambda^2 - \lambda_0^2)$) assuming that $\lambda_0 = 212 \pm 5 \mu\text{m}$.
- (b) Determine the value of b_0 .
- (c) Interpret the results. (See Doty et al., 1957).

12.3 The following are the experimental data for CD of poly-uridylic acid in 0.01 M MgCl_2 , pH 6.8, at 1°C . Concentrations ranged from 0.008 to 0.0013%.

λ (nm)	$\varepsilon_L - \varepsilon_R$ (cm^2/mol)
230	-3
240	-5
243	-6
250	-2
255	6
260	14
265	17
270	14
275	10
280	7
290	2
295	0

- (a) Plot $\varepsilon_L - \varepsilon_R$ versus λ .
- (b) Determine λ_m , λ_c , and $\Delta\nu$ (in reciprocal centimeters), respectively, where λ is the wavelength where the maximum occurs, λ_c is the wavelength at which the curve is crossing, and $\Delta\nu$ is the half width of the band.
- (c) Calculate the rotational strength R_{ba} using

$$R_{ba} = \frac{3hc \times 10^8 \ln 10}{32\pi^3 N} \int \left| \frac{\varepsilon_L - \varepsilon_R}{\nu} \right| d\nu$$

(See Brahms, 1963.)

12.4 Circular dichroism possesses the advantage of intrinsic discreteness and can be transformed to rotatory dispersion. Holzwarth et al., (1962) measured the CD of poly-L-glutamic acid in 0.1 M NaF at concentrations from 0.03 to 0.4%. At pH 4.3, poly-L-glutamic acid exists in the helical form, whereas at pH 7.3, it is in the disordered form. The data are as follows:

pH 4.3		pH 7.3	
λ (nm)	$[\theta] \times 10^{-4}$	λ (nm)	$[\theta] \times 10^{-4}$
185	4.8	198	-2.0
190	7.5	200	-4.0
192	8.0	205	-4.5

pH 4.3		pH 7.3	
λ (nm)	$[\theta] \times 10^{-4}$	λ (nm)	$[\theta] \times 10^{-4}$
195	7.3	210	0.01
200	2.0	215	0
205	0.2	220	0
210	0.4		
215	-4.4		
220	-4.2		
225	-3.0		
230	-2.0		
240	-0.2		

- (a) Plot the CD of poly-L-glutamic acid in 0.1 M NaF.
 (b) Express each curve in Gaussian form.
 (c) Calculate the rotational strength of each solution.
 (d) Calculate the rotational dispersion curves (as $[m]$, the mean residue rotation) from the CD data using the Kronig–Kramers transformation:

$$[m_K] = \frac{2[\theta_K^\circ]}{\sqrt{\pi}} \left(\int_0^{\lambda - \lambda_K / \Delta_K} e^{x^2} dx - \frac{\Delta_K}{\lambda + \lambda_K} \right)$$

(See Holzwarth et al., 1962).

13

HIGH-PERFORMANCE LIQUID CHROMATOGRAPHY AND ELECTROPHORESIS

13.1 HIGH-PERFORMANCE LIQUID CHROMATOGRAPHY

A chromatograph is a device in which sample components are differentiated into various zones, depending on their velocity of migration through a medium. Control of the migration rates is largely dependent on the device constructed. High-performance liquid chromatography (HPLC), which was first introduced around 1969, utilizes pressure (from 100 to 6000 psi) to push sample mixtures through a column of specific packing materials that are designed to differentiate migration rates. The pressure on the sample is generated by a pumping system. The essential components of a HPLC system are shown in Figure 13.1. The detectors most frequently used in HPLC systems are UV-visible photometric detectors, fluorescence detectors, refractive index detectors, and differential refractometers. Almost all instruments that are capable of identifying a compound can be used as detectors, for example, conductance meter, mass spectrometer, light-scattering apparatus, viscosity apparatus, and even molecular beam devices.

13.1.1 Chromatographic Terms and Parameters

Mobile Phase and Stationary Phase *Mobile phase* and *stationary phase* are standard terms used in chromatography, including HPLC. The mobile phase is the

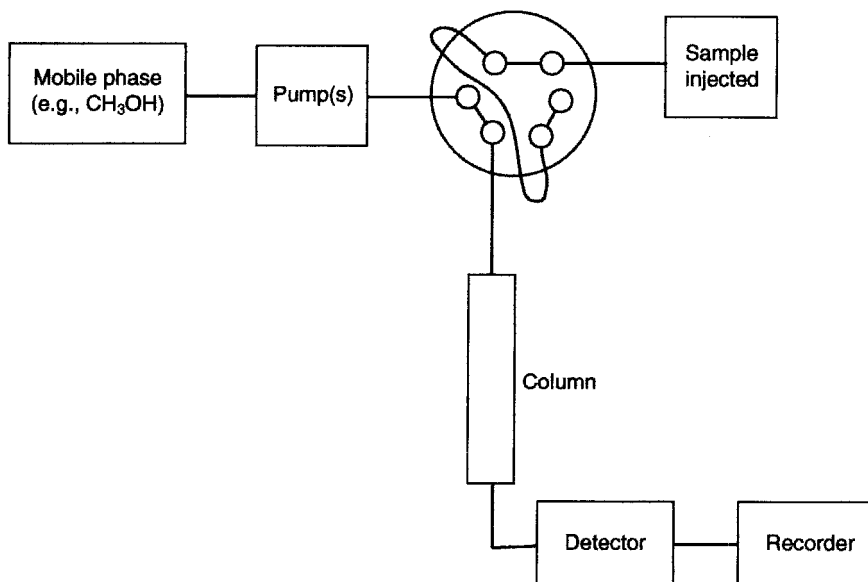


FIGURE 13.1 Diagram of an HPLC system.

solvent, and the stationary phase is the sorbent. The stationary phase, which can be a liquid too, may or may not be supported by a solid. The solid, if used, is called the matrix. The separation of molecular species in HPLC is related to the equilibrium distribution of different compounds between the stationary phase and the mobile phase, while the spreading of the resulting chromatogram is related to the migration rate of the molecules. The various types of HPLC systems are based on the different substances that are used to construct the stationary phase and the mobile phase.

Retention Retention R is defined as the equilibrium fraction of the sample in the mobile phase; hence, $1 - R$ is the sample equilibrium fraction in the stationary phase. The ratio of R over $1 - R$ is expressed by

$$\frac{R}{1 - R} = \frac{c_m V_m}{c_s V_s} \quad (13.1)$$

where c_m (in moles per liter) is the concentration of the sample in the mobile phase that is contained in volume V_m (in liters); c_s (in moles per liter) is the concentration of the sample in the stationary phase that is contained in volume V_s (in liters). The product $c_m V_m$ is the number of moles of the sample in the mobile phase, and product $c_s V_s$ is the number of moles of the sample in the stationary phase. If we

divide the right-hand expression of Eq. (13.1), both numerator and denominator, by the term c_m , we obtain

$$\frac{R}{1-R} = \frac{V_m}{KV_s} \quad (13.2)$$

where $K = c_s/c_m$ is the well-known constant called the partition or distribution coefficient. On solving Eq. (13.2) for R , we have

$$R = \frac{V_m}{V_m + KV_s} \quad (13.3)$$

This is the classical equation derived by Martin and Synge (1941). Equation (13.3) can be extended to the form

$$R = \frac{V_m}{V_m + \sum K_i V_i}$$

where the retention involves i , the number of mechanisms. Dividing both the numerator and the denominator of the right-hand expression of Eq. (13.3) by the term V_m leads to

$$R = \frac{1}{1 + K(V_s/V_m)} = \frac{1}{1 + k'} \quad (13.4)$$

where $k' = K(V_s/V_m)$ is another constant called the capacity factor. In practice, k' is the key parameter in describing a given chromatographic system. More specifically, it depends on the chemical nature and temperature of the liquid phases that form the system. It also depends on the surface area of the chromatographic support. Let us rewrite k' in the form

$$k' = \frac{c_s V_s}{c_m V_m}$$

If we let $V_R = c_m V_m$ and $V_R - V_0 = c_s V_s$, the equation of k' is then in the form

$$k' = \frac{V_R - V_0}{V_R}$$

where V_R is the retention volume and V_0 is the unretained volume, also called the void volume. In practice, both the retention R and the capacity factor k' can also be expressed in terms of time t . The retention R in terms of time t is given by

$$R = \frac{t_m}{t_m + t_s}$$

where t_m is the average time that the sample molecules stay in the mobile phase and t_s is the average time that the molecules stay in the stationary phase before they are absorbed. The capacity factor k' in terms of t is given by

$$k' = \frac{t_R - t_0}{t_0}$$

where t_R is the retention time, namely, the time required for a peak to elute from the time of injection and t_0 is the time for unretained molecules in the mobile phase to move from one end of the column to the other.

Among the parameters described, the most frequently used in HPLC are V_R , t_R , and k' . The parameters V_R and t_R are further related by a factor F , the flow rate in milliliters per second of the mobile phase through the column:

$$V_R = t_R F$$

Note that we can also have

$$V_m = t_0 F$$

Here, V_R and V_m are related in the following way:

$$V_R = V_m \frac{t_R}{t_0} = V_m(1 + k') = V_m + K V_s$$

The determination of these parameters is shown in Figure 13.2. We see that the chromatogram is a bell-shaped band or Gaussian curve, which is characterized by

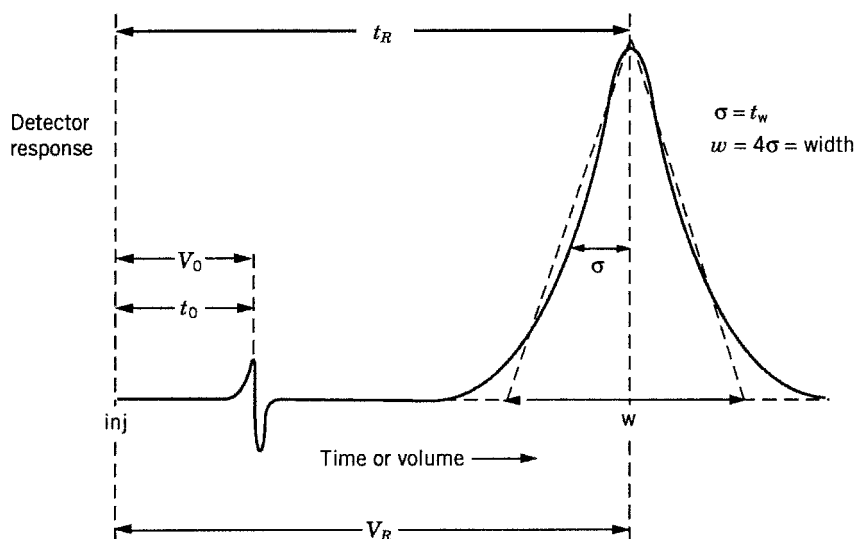


FIGURE 13.2 A typical chromatogram.

the parameter w (in terms of volume) or t_w (in terms of time). Both w and t_w refer to the bandwidth and both can be expressed in terms of the standard deviation σ :

$$\sigma = \frac{1}{4}w$$

or

$$\sigma = t_w$$

Resolution The capacity factor k' and retention volume V_R are characteristics of individual chemical species in a given chromatographic system. For two components in the mixture, a and b, in a given chromatographic system, each has its own capacity factor and retention volume, that is, k'_a , k'_b and V_{Ra} , V_{Rb} , as shown in Figure 13.3. The resolution R_s can be expressed by

$$R_s = \frac{2(V_{Rb} + V_{Ra})}{w_a + w_b} = \frac{V_{Ra} - V_{Rb}}{2(\sigma_a + \sigma_b)} \quad (13.5)$$

We can now define a parameter α by

$$\alpha = \frac{k'_b}{k'_a}$$

which is called the selectivity. A separation between a and b in a mixture is possible only if $\alpha \neq 1$. That is, for any separation to be possible, each component must have a different value for the capacity factor and each must be retained to a different degree. The value of the selectivity can be controlled by changing the composition

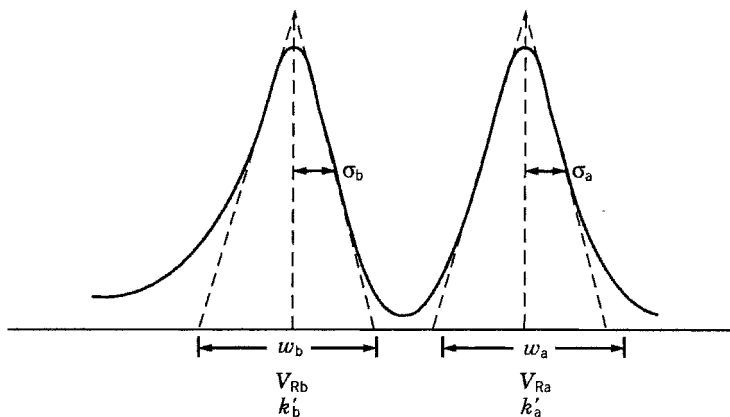


FIGURE 13.3 Resolution of a two-component system.

of the mobile and stationary phases, for example, by changing the mobile phase solvent, pH, temperature, and chemical shift.

In addition, the separation depends on the efficiency of a column, N . The term N , which was originally obtained from the efficiency of the column in a fractional distillation, refers to the number of theoretical plates in an HPLC column. Therefore, N is also called the theoretic plate number. In a chromatogram, the narrower the width of an eluting peak, the greater is the efficiency of separating a multi-component mixture in a column, that is, the greater the value of N . An equation of N is given by

$$N = 16 \left(\frac{t_R}{t_w} \right)^2 = \frac{16}{L} \left(\frac{V_R}{w} \right)^2 = \frac{1}{L} \left(\frac{V_R}{\sigma} \right)^2 \quad (13.6)$$

where L is the column length. The three factors (α , N , and k') can be incorporated into one equation:

$$R_s = \frac{1}{4}(\alpha - 1)\sqrt{N} \left(\frac{k'}{k' + 1} \right)$$

13.1.2 Theory of Chromatography

The theory of chromatography is basically concerned with zone spreading. The dispersion of sample zones, which results in chromatographic peaks, causes a distribution of the sample concentration. For a good separation, zones should not overlap. Often a separation is not totally effective because the zones spread into one another.

In 1940, Wilson singled out the nonequilibrium in the local concentration as a major cause of zone spreading. In the following year, Martin and Synge proposed the theory of spreading in terms of flow velocity and the square of the particle diameter. In 1956 Van Deemter et al. related zone spreading to the sorption-desorption kinetics of solute molecules in the column. Giddings in 1958 suggested the random-walk model to describe the physical processes involved in zone spreading.

If the eluted chromatographic peak follows a Gaussian distribution, the zone spreading σ^2 is related to the height of the chromatographic curve H , which is equivalent to a theoretical plate (or plate height), in the form

$$H = \frac{\sigma^2}{L}$$

Here σ^2 is the variance in statistics. The quantity H can also be calculated from

$$H = \frac{L}{N}$$

In general, H measures the specific column frequency and N measures the system efficiency.

According to the current chromatography theory, the flow of solute through a column in the presence of a stationary phase and a mobile phase undergoes three processes, which correspond to the three components of H or σ^2 . Following are the three physical processes that determine zone spreading (the volume of σ^2) or H :

1. *Translation diffusion* (assuming the random-walk model):

$$\sigma_D^2 = 2Dt \quad t = \frac{L'}{v}$$

where L' is the distance of zone migration and v is the solvent velocity.

2. *Eddy diffusion* (due to the inhomogeneity of packing materials):

$$\sigma_E^2 = L'd$$

where d is the diameter of a zone displaced from the channel.

3. *Sorption and desorption* (due to a local nonequilibrium condition created by the process of sorption and desorption):

$$\sigma_{k_1}^2 = \frac{2R(1-R)vL'}{k_2}$$

where k_1 is the rate constant of sorption and k_2 is the rate constant of desorption.

The sum of the three processes constitutes the total zone spreading:

$$\sigma^2 = L' \left(\frac{2D}{v} + d + \frac{2R(1-R)v}{k_2} \right) \quad (13.7a)$$

or

$$H = \frac{2D}{v} + d + \frac{2R(1-R)v}{k_2} \quad (13.7b)$$

Equations (13.7a) and (13.7b) are different forms of the Van Deemter equation:

$$H = A + \frac{B}{v} + Cv \quad (13.8)$$

where

$$A = d \quad B = 2D \quad C = \frac{2R(1-R)v}{k_2}$$

13.1.3 Types of HPLC

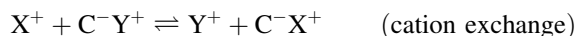
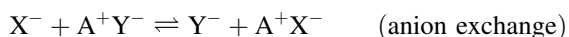
The four major types of HPLC are as follows:

1. Ion-exchange chromatography
2. Liquid–solid (adsorption) chromatography
3. Liquid–liquid chromatography
 - a. Normal phase
 - b. Reversed phase
4. Size-exclusion chromatography

They represent four separate mechanisms for the interaction of sample molecules with the stationary phase. Size-exclusion chromatography is used for sample molecular weight over 2000, whereas the other types do not have this limit. Usually these other types are used for sample molecular weights below 2000.

The differences between the types of chromatography lie basically, among others, in the different columns that are used.

Ion-Exchange Chromatography This is a type of chromatography in which the active surface of the column packing carries a charge: An anion exchanger carries a positive charge (e.g., quaternary ammonium groups) and a cation exchanger carries a negative charge (e.g., sulfonate groups). The retention of a sample occurs when the ionic sample carries the counterions:



Ion-exchange chromatography is used for amino acid analysis; separations of nucleic acids, nucleosides, nucleotides; identification of sulfa drugs (such as sulfaquandine, sulfadiazine, sulfasoxazole, sulfamethizide); and food compounds (e.g., caffeine, ascorbic acid, vanillin). The mobile phase usually contains water or water–organic solvent mixtures. The peak retention can be controlled by pH and ionic strength (salt, concentration). Column packings are made of a polystyrene backbone cross-linked with divinylbenzene attached with ionic functional groups such as $-\text{SO}_3^- \text{H}^+$ (cation exchanger) and $-\text{N}(\text{CH}_3)_3^+ \text{OH}^-$, NH_2^- (anion exchanger).

Liquid–Solid (Adsorption) Chromatography This type of chromatography is based on the competition between the molecules of the sample and the molecules of the mobile phase for adsorbent sites on the active adsorbent surface of the stationary phase. To alter adsorptive activity, two solvents are used in the mobile phase: the principal solvent and the modifying solvent. In most cases, the principal solvent is hexane or dichloromethane and the modifying solvent is water, alcohol, or dimethyl sulfoxide. A modifying solvent is added to the principal solvent to control the absorptive activity of the samples.

Two kinds of adsorbents are used for column packings: polar adsorbents and nonpolar adsorbents. The acidic polar adsorbents, such as silica, are used for aliphatic nitrocompounds or aromatic amines. The basic adsorbents, such as alumina, are used for pyrrole derivatives, phenols, and carboxylic acids. The nonpolar adsorbents, such as charcoal, are used for high-molecular-weight homologs and aromatic compounds.

Liquid–Liquid (Partition) Chromatography If a third component is dissolved in the immiscible layers of the solvents, there is a distribution of the third component between the two layers. Liquid–liquid (partition) chromatography is based on a multistage distribution of a sample between two solvents within a column. The mobile phase is a liquid. The stationary phase is also a liquid (another liquid), which may be dispersed onto a finely divided inert support. The separation is attributed to the different distribution of the sample compounds between the two liquid phases. There are two kinds of partition chromatography: normal systems in which the mobile phase is less polar than the stationary phase and reversed-phase systems in which the mobile phase is the more polar liquid. Table 13.1 compares the two different types of partition chromatography.

Reversed-phase chromatography is perhaps the most widely used chromatographic method. It was first developed by Howard and Martin (1950) to separate fatty acids by using a polar eluent (mobile phase) and a nonpolar stationary phase that consisted of paraffin oil and octane. Today the stationary phase consists of a liquid that is chemically bonded to a support. For example, the column packings contain octadecylsilyl (C_{18}), octylsilyl (C_8), butylsilyl (C_4), or propylsilyl (C_3), which are bonded to silica supports having various pore sizes (e.g., 100, 300, and 500 Å) and particle sizes (e.g., 5 and 10 μm). The extent of retention of a molecule depends on the number, size, and stereochemistry of its hydrophobic (e.g., alkyl) and hydrophilic (e.g., ionic) groups.

Reversed-phase chromatography is currently used for the separation as well as identification of substances having a wide range of polarity and molecular weight. It is now an indispensable tool in biotechnology. For example, it can be used to separate homologous proteins from different species and synthetic diastereoisomeric peptides. Retention in reversed-phase chromatography has nothing to do with molecular weight, nor does it have anything to do with acidity or basicity. In other chromatographic methods, an isocratic solvent (with a mobile phase of constant

TABLE 13.1 Comparison of the Two Types of Chromatography

Type of Chromatography	Mobile Phase	Stationary Phase
Normal partition	Pentane, hexane, heptane, chloroform, dichloromethane	Water, ethylene glycol, polyethylene glycol, trimethylene glycol, acetonitrile
Reversed phase	Methanol–water, acetonitrile–water	Squalane

composition, such as a single solvent) is usually used. In reversed-phase chromatography gradient elutions (with a mobile phase of different compositions, two or three solvents mixed) are used. Typical examples in reversed-phase chromatography of the mobile phase used in the separation of proteins are acetonitrile for solvent A and aqueous 0.1% trifluoroacetic acid for solvent B. By controlling the percentage of the two or three solvents in the mixture eluted at different time intervals, the sample components (proteins) are separated.

Size-Exclusion Chromatography

General Principle Size-exclusion chromatography relies on the different rates of diffusion or permeation of molecules of different sizes through the pores of packing materials and not on the rates of adsorption and desorption. Size-exclusion chromatography functions as a molecular sieve. The distribution coefficient of molecules in different sizes of pores, K , is defined as

$$K = \frac{V_i}{V_{i0}}$$

where V_i is the pore volume accessible to a molecular species and V_{i0} is the total pore volume. The retention volume V_R is given in the form

$$V_R = V_0 + KV_{i0}$$

where V_0 is the void of interstitial volume.

Since both the size of the pores and the interstitial volume are fixed, the flow of the sample molecules is limited by their size. The largest molecules that can pass through the column are limited by the size of V_0 , while the smallest molecules are limited by the size $V_0 + V_{i0}$. The sample molecule whose size is within the given limit of a column can pass between V_0 and $V_0 + V_{i0}$. Hence, the retention volume V_R for sample molecules is also between V_0 and $V_0 + V_{i0}$.

Two Types of Size-Exclusion Chromatography When an organic solvent is used as the mobile phase, the separation is called gel permeation chromatography (GPC), which is used extensively in polymer chemistry to characterize organic polymers, for example, in the determination of molecular weight. Some of the most commonly used columns are the μ -styragels of Waters and the Micro Pak TSK type H columns in the GPC mode with a mobile phase such as tetrahydrofuran (THF).

If an aqueous mobile phase is used, the separation is called gel filtration chromatography (GFC). GFC is mainly used to separate and characterize biological polymers such as proteins. Some of the most commonly used columns are Water's I-125 and Varian's Micro Pak TSK type SW columns.

Applications of Size-Exclusion Chromatography If a perfect size-exclusion column were available, chromatography could be used for preparative purposes, that is, to separate materials in quantity according to their size. Such an exclusion column is still in development. At present two important applications are used:

- (1) the determination of molecular weight and molecular weight distribution and
- (2) the study of the binding of small molecules to macromolecules.

DETERMINATION OF MOLECULAR WEIGHT AND MOLECULAR WEIGHT DISTRIBUTION A universal calibration curve by GPC has been suggested in which the logarithm of hydrodynamic volume $[\eta]M$ is plotted against the retention volume V_R . The term $[\eta]$ refers to the intrinsic viscosity and M the molecular weight. Such a plot is shown in Figure 13.4. If the retention volume of a polymer is known, one can read

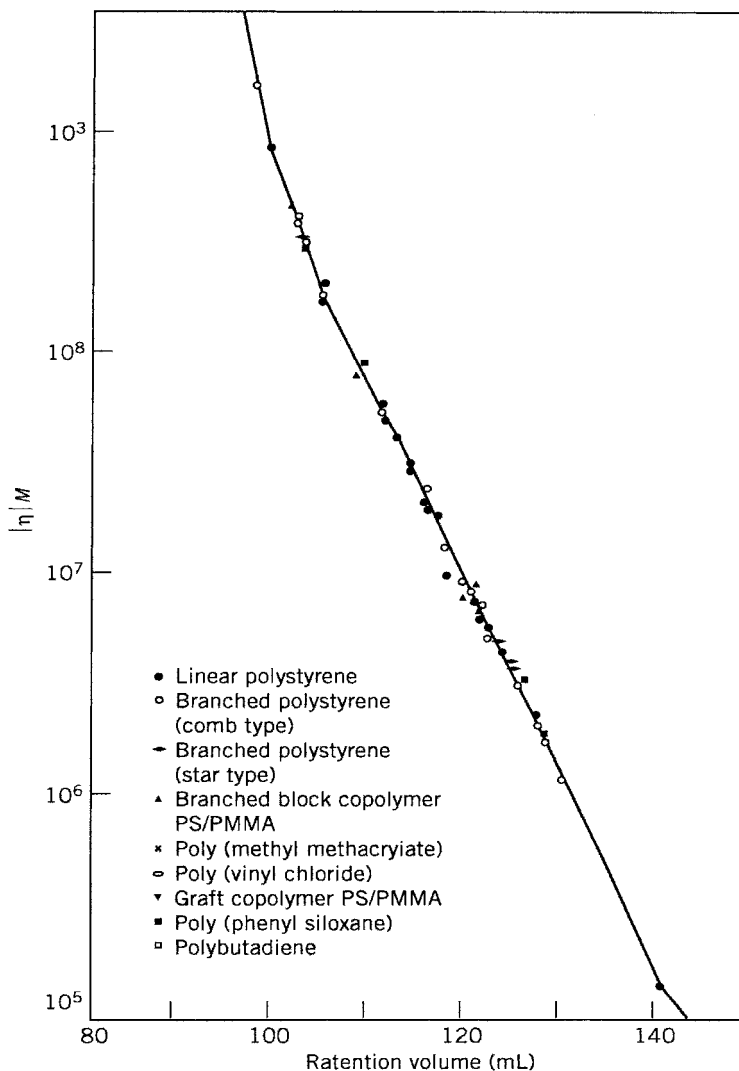


FIGURE 13.4 Calibration curve for GPC. [Source: Grubistic et al. (1967). Reproduced by permission of John Wiley & Sons.]

the value of $[\eta]M$ directly from the calibration curve. The value of M can then be determined if $[\eta]$ is also known. This method suffers from two drawbacks: (1) The calibration curve is almost linear but not really linear and (2) one still has to determine the value of $[\eta]$ in addition to V_R .

A modified method has been proposed in an attempt to improve the universal calibration approach. At a given elution volume, two polymers, 1 and 2, are assumed to have the same hydrodynamic volumes $[\eta]M$:

$$[\eta]_1 M_1 = [\eta]_2 M_2$$

Recall the equation

$$[\eta] = KM^a$$

From the above two equations, we obtain

$$\begin{aligned} \log M_2 &= \underbrace{\frac{1}{1+a_2} \log \frac{K_1}{K_2}}_A + \underbrace{\frac{1+a_1}{1+a_2}}_B \log M_1 \\ &= A + B \log M_1 = A + BCV_R \end{aligned}$$

where C is the slope of the calibration curve. Let 1 represent polystyrene standard and 2 any sample. Since K_1 and a_1 are known in the literature, and since K_2 and a_2 either are known in the literature [e.g., poly(methyl methacrylate)] or are obtainable by carrying out a few measurements through intrinsic viscosity and osmotic pressure (or light-scattering) techniques, M_2 can be easily determined for any sample of the same species from GPC data V_R . The calibration curve is shown in Figure 13.5, where the slope C can be determined.

The above method still requires viscosity measurement in addition to GPC work. Another method, originally suggested by Waters Associates, enables calculation of molecular weight and molecular weight distribution directly from GPC chromatograms provided that Figure 13.5 is available.

Consider the chromatograms of poly(methyl methacrylate) shown in Figure 13.6. We arbitrarily divide the abscissa of the chromatogram units into s parts and measure either the height of the curve h_i or the area of the curve A_i . There is a one-to-one correspondence between the h_i (or A_i) coordinate and the V_{Ri} coordinate. The value of V_{Ri} can be converted to M_i by reading the calibration curve in Figure 13.5. Hence, we obtain a table in the form h_i versus M_i . The values of \bar{M}_n and \bar{M}_w can now be calculated from the following two sets of equations:

$$\begin{aligned} \bar{M}_n &= \frac{\sum h_i}{\sum (h_i/M_i)} & \bar{M}_w &= \frac{\sum h_i M_i}{\sum h_i} \\ \bar{M}_n &= \frac{\sum A_i}{\sum (A_i/M_i)} & \bar{M}_w &= \frac{\sum A_i M_i}{\sum A_i} \end{aligned}$$

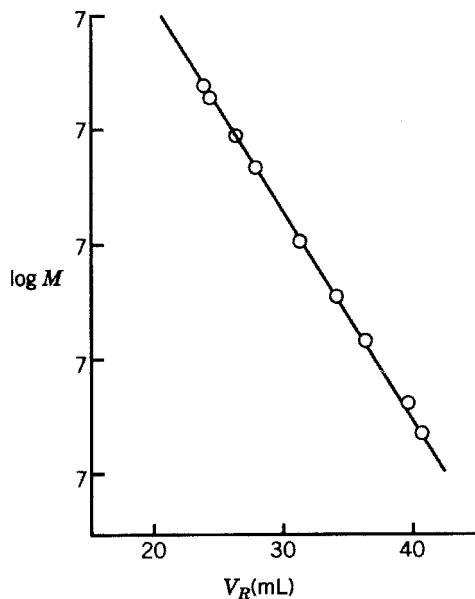


FIGURE 13.5 GPC calibration plot: polystyrene standard in THF at 25°C. The values of viscosity constants used were $K_1 = 1.41 \times 10^{-4}$ dL/g; $a_1 = 0.70$. [Source: Sun and Wong (1981). Reproduced by permission of Elsevier Science Publishers BV.]

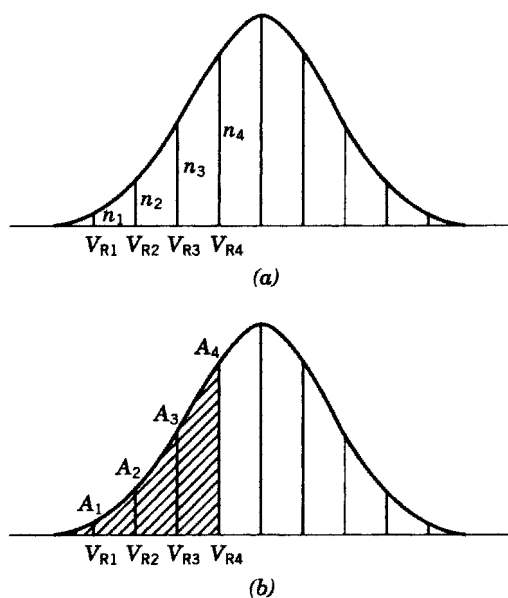


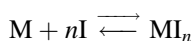
FIGURE 13.6 Analysis of the chromatogram: (a) h_i versus V_{Ri} ; (b) A_i versus V_{Ri} . [Source: Sun and Wong (1981). Reproduced by permission of Elsevier Science Publishers BV.]

Once \bar{M}_n and \bar{M}_w values are determined, we can calculate the polydispersity \bar{M}_w/\bar{M}_n and the mean average molecular weight \bar{M}_m , which is calculated with the following equation:

$$\bar{M}_m = (\bar{M}_n \bar{M}_w)^{1/2}$$

Similar attempts have been made to construct a universal calibration plot for determining the molecular weight of protein polypeptides in GFC. A straight line of logarithm molecular weight versus retention volume V_R or the capacity factor k' has been reported in the literature. Its application, however, is difficult because (1) protein polypeptides carry charges (positive or negative), while the packing materials for most commonly used columns also carry charges on the surface, making ionic interaction almost unavoidable, and the column cannot function by size exclusion; and (2) since protein polypeptides carry charges, they cannot be viewed as completely random as in the case of most synthetic polypeptides. Thus, in addition to size, we have to consider the shape of the protein polypeptides, particularly under certain environments (pressure and temperature).

STUDY OF THE BINDING OF SMALL MOLECULES TO MACROMOLECULES Consider the binding of a ligand, I, to a macromolecule, M. A mobile phase that contains a buffer and the ligand is suddenly disturbed in the column by injection into the flow system of a small amount of the sample solution (5–100 μL) that contains macromolecules (macromolecules are dissolved in the same buffer or in the mobile phase). Due to the size differences, the macromolecules (M) move faster, leaving the small molecules (I) behind. After a short time an equilibrium is reached:



As the macromolecule–ligand complex leaves the column, a void of ligand is created until a new equilibrium is reached. This phenomenon was first observed by Hummel and Dreyer in 1962. In the chromatogram, as shown in Figure 13.7, the peak represents the excess of I (i.e., the amount of I in equilibrium with MI_n) whereas the trough represents the deficiency of I (the concentration of I that binds to the macromolecule). The mean number of moles of bound ligands per mole of macromolecules \bar{r} can be evaluated directly from the chromatogram. There are two techniques for the evaluation of \bar{r} : external calibration and internal calibration (Sun et al., 1984, 1985, 1993).

External Calibration A set of experiments is carried out in which a series of mobile phases with known concentrations of ligand are chosen. To each mobile phase two samples are injected one after the other. The first sample contains solvent alone and the second contains the macromolecule in solvent (e.g., protein in buffer). The first chromatogram will give one, and only one, peak (negative), the area of which is equivalent to the concentration of ligand in the given mobile phase. Since a

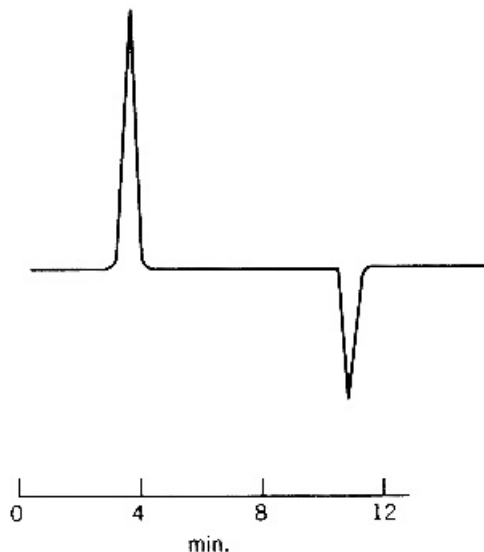


FIGURE 13.7 A Hummel–Dreyer chromatogram: L-tryptophan–BSA binding.

series of mobile phases with different concentrations will be used, a calibration curve (a straight line) can be established, as shown in Figure 13.8, in the form of area versus the concentration of ligand.

The second chromatogram will give two peaks, positive and negative, as shown in Figure 13.7. The area of negative peak is equivalent to the concentration of bound ligand, which can directly be read on the calibration curve, that is, area of the negative peak = $[L]_b$. Since the concentration of macromolecules $[M]$ is known at the time the second sample is prepared, we can easily calculate

$$\bar{r} = \frac{[L]_b}{[M]}$$

Internal Calibration Given the same mobile phase (same concentration of ligand in the solution), several samples that contain a known amount of macromolecules and ligand are run. In the samples, the concentration of macromolecules is kept constant, while the amount of the ligand is varied. By plotting the area of the trough (negative peak) versus the amount of ligand in the sample (in moles); the interpolated amount of ligand L_b (where area is equal to zero in Figure 13.9) is the exact amount of ligand bound to the macromolecules. We can thus calculate the value \bar{r} :

$$\bar{r} = \frac{L_b}{M}$$

Both the quantities of L_b and M are in moles.

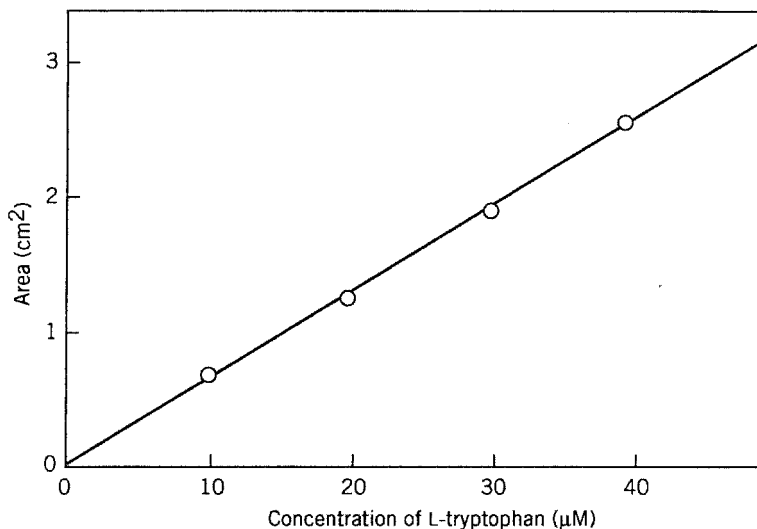


FIGURE 13.8 Correlation of area of negative peak with concentration of L-tryptophan for external calibration method. [Adapted from Sun and Wong (1985).]

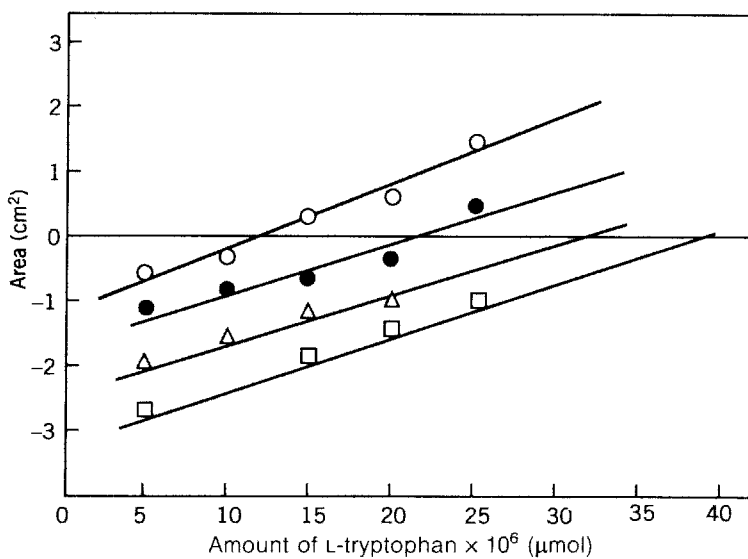


FIGURE 13.9 Internal calibration for determination of amount of L-tryptophan that binds to BSA. [Adapted from Sun and Wong (1985). Reproduction by permission of Friedr. Vieweg & Sohn.]

13.2 ELECTROPHORESIS

13.2.1 Basic Theory

The movement of charged particles (ions) in an electric field is called electrophoresis. The basic theory of electrophoresis is related to ionic mobility u , which is also called electrophoretic mobility. When an ion in solution is moving in the direction of a field E , its velocity v depends on three factors: the charge z carried by the ion, the frictional coefficient f arising from the resistance of the solution, and the strength of the field E . The quantity E is defined as

$$E = \frac{d\phi}{dx} = \frac{I}{A\kappa}$$

where ϕ is the potential difference (in volts) of the two electrodes, x is the coordinate, I is the current (in amperes), A is the cross-sectional area (in centimeters squared) through which the solution passes, and κ is the ionic conductance of the solution (in reciprocal ohm-centimeters or siemens per meter). The product of velocity v and the frictional coefficient f is equal to the force of the field on the charge of the ion:

$$fv = zeE \quad (13.9)$$

where e is the electrostatic charge in coulombs ($e = 1.602 \times 10^{-19}$ C). Ionic mobility u is defined by Eq. (13.9) as follows:

$$u = \frac{v}{E} = \frac{ze}{f}$$

Its units are in $(\text{m s}^{-1})/(\text{V m}^{-1})$ or $\text{m}^2 \text{V}^{-1} \text{s}^{-1}$. Thus, the mobilities u_+ , u_- and the velocities v_+ , v_- of ions (+, -) are related by

$$v_+ = Eu_+ \quad v_- = Eu_-$$

A classical example is the electrophoresis of 0.02 M NaCl. When a current of 1.60 mA was used, the boundary moved 0.020 m in 689 s. The cell is a tube with an inner radius of 0.188 cm. The specific conductance of the solution was $\kappa = 1.26 \text{ S m}^{-1}$ at 25°C. The electric field strength and the mobility of an ion can then be calculated as follows:

$$\begin{aligned} \frac{d\phi}{dx} &= \frac{1.60 \times 10^{-3} \text{ A}}{[\pi(0.188 \times 10^{-2} \text{ m})^2](1.26 \text{ S m}^{-1})} = 114 \text{ V m}^{-1} \\ u_{\text{Na}^+} &= \frac{0.020 \text{ m}}{(689 \text{ s})(114 \text{ V m}^{-1})} = 2.50 \times 10^{-7} \text{ m}^2 \text{ V}^{-1} \text{ s}^{-1} \end{aligned}$$

Historically, ionic mobility is measured in terms of conductance because there is a linear relationship between the conductance Λ and the ionic mobility u in a dilute solution:

$$\Lambda = \mathcal{F}(u^+ + u^-)$$

where \mathcal{F} is the Faraday constant ($1\mathcal{F} = 96487 \text{ C mol}^{-1}$). Therefore, behind the method of electrophoresis there is a rich theory of conductance which has been developed for more than a century. Here we describe three well-known subjects that provide the theoretical background of electrophoresis: ionic atmosphere and mobility, the relaxation time effect, and the zeta potential.

Ionic Atmosphere and Mobility Due to electrostatic forces, an ion is always surrounded by many other ions of opposite charge which form an ionic atmosphere. The ionic atmosphere can affect the conductance and mobility of the central ion in three ways:

1. *Viscous Effect* Opposing the electrical force that exists between the ion and the field is a frictional viscous drag of the solvent, which, in many cases lowers the conductance and the mobility of the ion. The frictional drag is usually expressed by Stokes' law:

$$f = 6\pi a\eta v$$

where a is the radius of the ion, η is the viscosity coefficient of the solvent, and v is the velocity of the ion.

2. *Electrophoretic Effect* While the central ion moves in one direction, the ionic atmosphere which consists of ions of opposite charge move in the opposite direction. Thus, the central ions are forced to move against a stream of solvent. Their velocities are consequently reduced.
3. *Relaxation Time Effect* On the way to the electrode, the central ion leaves the ionic atmosphere behind. As a result, the originally symmetric atmosphere becomes asymmetric. It exerts an electrostatic drag on the ion, thereby reducing its velocity in the direction of the field.

The ionic atmosphere depends on the concentration of both positive and negative ions. On this basis, Onsager derived an equation for the concentration dependence of the equivalent conductance in which all three aforementioned effects are incorporated. The equation is given in the form

$$\Lambda_c = \Lambda_\infty - \left[\frac{29.142(z_+ + |z_-|)}{(\epsilon T)^{1/2} \eta} + \frac{9.903 \times 10^5}{(\epsilon T)^{3/2}} \Lambda_\infty \omega \right] 2I^{1/2} \quad (13.10)$$

where I is the ionic strength

$$I = \frac{1}{2}(c_+z_+^2 + c_-z_-^2)^{1/2}$$

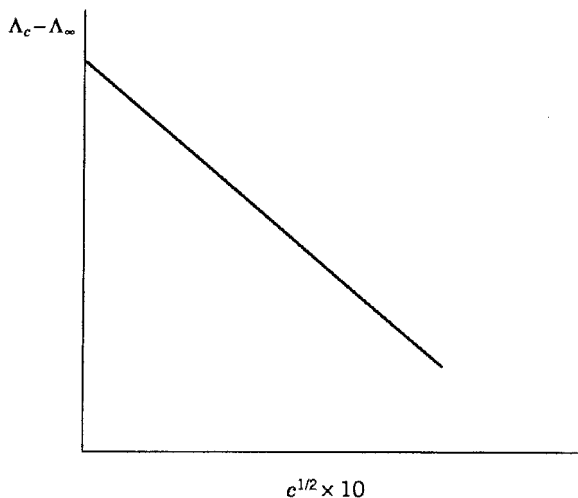
z_+ and z_- are the valence numbers of the cation and anion, respectively, ϵ is the dielectric constant of the bulk solvent, Λ_∞ is the equivalent conductance at infinite dilution, T is the absolute temperature, and ω is defined as

$$\omega = (z_+|z_-|) \frac{2q}{1 + q^{1/2}}$$

in which

$$q = \frac{(z_+|z_-|)}{z_+ + |z_-|} \times \frac{\lambda_\infty^+ + \lambda_\infty^-}{z_+\lambda_\infty^- + |z_-|\lambda_\infty^+}$$

In a uni-uni valent electrolyte, $q = 0.5$. According to Eq. (13.10), the plot of $\Lambda_c - \Lambda_\infty$ versus \sqrt{I} or \sqrt{c} should be linear: Eq. (13.10) is valid only for dilute solutions, $c < 0.01$.



Zeta Potential Zeta (ζ) potential is a parameter used to describe the electrophoretic mobility of colloidal particles. Charged colloidal particles are slightly different from ions in that colloidal particles are surrounded by an electric double layer which is similar but not identical to the ionic atmosphere. The inner part of the double layer moves as a unit in transport experiments. The ζ potential is the surface potential of the inner part of the double layer, as shown in Figure 13.10. It is defined as

$$\zeta = \phi_{r=a}$$

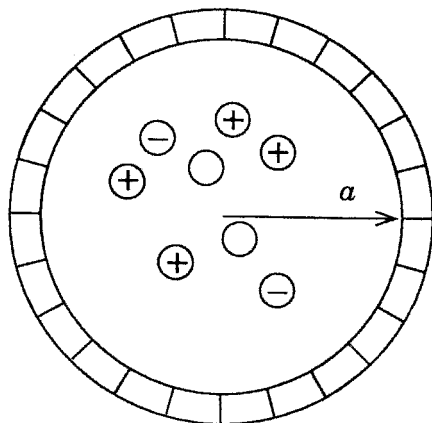


FIGURE 13.10 Zeta potential.

Von Smoluchowski derived an equation to describe the electrophoretic mobility of charged colloidal particles u' :

$$u' = \frac{\epsilon\zeta}{\eta} E$$

This equation is valid for relatively thin double layers, $\kappa'a \gg 1$ (κ' being the Debye–Huckel parameter). For high potentials an additional correction is required for the relaxation effect, which is similar to the situation described above.

Moving Boundary Moving-boundary electrophoresis is performed with the substance in free solution. Historically, this was the first form of electrophoresis. Although it is no longer as widely used as before, it does illustrate the important role that diffusion plays in electrophoresis. The diffusion phenomenon is shown in Figure 13.11.

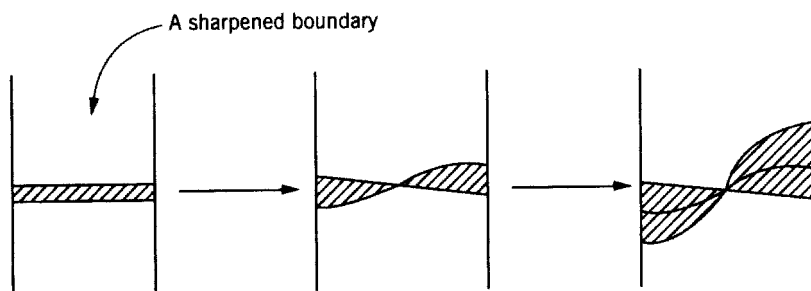
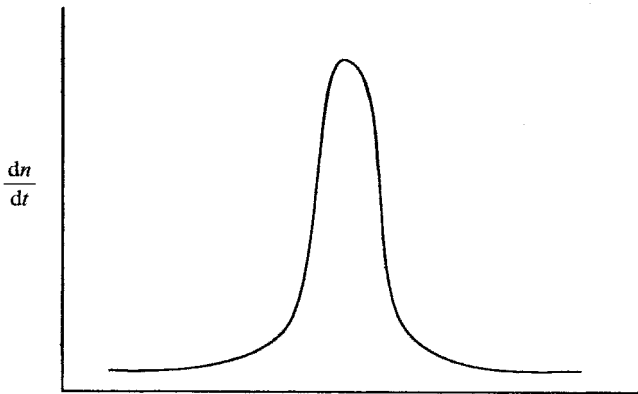


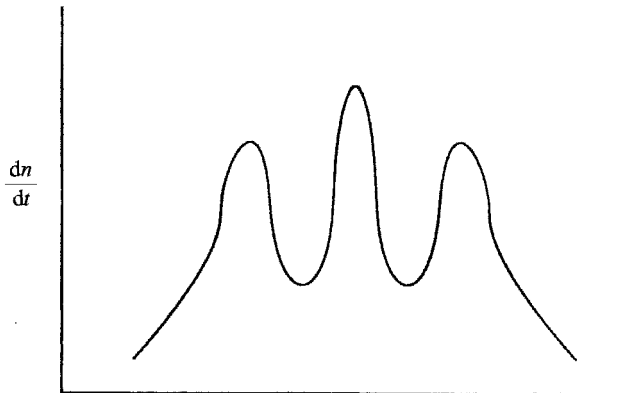
FIGURE 13.11 Diffusion phenomena. One may use a capillary tube to siphon a sharpened boundary.

The moving boundary spreading in the electrophoresis of protein is usually measured in terms of the refractive index gradient dn/dx , where n is the refractive index. The results are often recorded as shown in Figure 13.12. The formation of the boundary, its spreading, and its separation (if any) are functions of diffusion. The equation of the moving boundary is given in the form

$$\frac{\partial n}{\partial x} = \frac{\Delta n}{2\sqrt{\pi Dt_D}} \int_{-\infty}^{\infty} q(u) \exp\left[\frac{-(x - uEt_E)^2}{4Dt_D}\right] du \quad (13.11)$$



(a)



(b)

FIGURE 13.12 Moving-boundary spreading: (a) one component in the system (sample); (b) three components in the system (sample).

where t_D is the time recorded after the formation of the boundary, t_E is the time after application of the electric field, $q(u)$ is the distribution of mobilities, D is the diffusion coefficient, which is assumed to be a constant for all the proteins, and $\Delta n = n_1 - n_2$ is the difference in the refractive index of the solution and the solvent.

For a first approximation let $q(u)$ be a Gaussian distribution:

$$q(u) = \frac{1}{h\sqrt{2\pi}} e^{-u^2/(2h^2)}$$

where h is the standard deviation of the mobility distribution. Then

$$\frac{\partial n}{\partial x} = \frac{\Delta n}{\sqrt{2\pi}\sigma} e^{-x^2/(2\sigma^2)}$$

where

$$\sigma = \sqrt{E^2 h^2 t_E^2 + 2Dt_D}$$

The apparent diffusion coefficient(s) can now be calculated from the gradient curves by standard methods, including the measurement of the ratio of height versus area from the Gaussian graph.

13.2.2 General Techniques of Modern Electrophoresis

Techniques of modern electrophoresis applied to biological polymers are similar to those of modern liquid chromatography. An apparatus of modern liquid chromatography consists of three basic parts: the eluent (mobile phase), the column (stationary phase), and the detector. Likewise, an apparatus of electrophoresis consists of three basic parts: the electrolyte buffer, the supporting medium, and the mode of detectors. The classification of electrophoresis is in general based on the choice of the three fundamental parts, particularly the supporting medium.

Electrolyte Buffer The selection of a proper electrolyte buffer is an important step in the successful run of an electrophoresis. The two major factors in the selection of a proper electrolyte buffer are pH and ionic strength. The pH directly influences the mobility of the molecule, and the ionic strength affects the electrokinetic potential, which in turn affects the rate of migration. Low ionic strengths increase the rate of migration and high ionic strengths decrease the rate of migration. As shown in the Onsager equation, if the ionic strength of the buffer is increased, the conductivity increases. The greater conductivity generates a great amount of heat, which often poses a serious problem in the formation of a temperature gradient. The Onsager equation also indicates that the temperature increase

affects the viscosity of the medium, which in turn affects the frictional coefficient, and so forth. All these factors suggest that ionic strength should not be kept high. On the other hand, high ionic strength sharpens the boundary, which is desirable in obtaining good resolution. Thus, the ionic strength of the system should be neither too high nor too low.

Detectors As in HPLC, almost all physical or chemical methods that can be used for the identification of chemical compounds can be used as detectors. The following are among the most popular:

UV Absorption This is often used for monitoring the migration of ionic species.

Autoradiography If the compound initially in a mixture is labeled with radioactive elements, such as ^{14}C , ^3H , ^{35}S , or ^{131}I , the separated compound can be detected by radioactive measurements, such as autoradiography.

Staining and Destaining This is used in gel electrophoresis where the separation can be visibly detected by dyes such as coomassie blue and bromophenol blue.

Immunodiffusion When a sliced gel that contains the chemical species of interest is separated from the mixture and placed in a medium near another chemical compound, the interaction causes the migration of the chemical species. This is particularly useful for the study of immunomaterials in relation to antigens. Hence, this process has a special name: immunoelectrophoresis.

The Supporting Media The supporting media can be paper, cellulose acetate membranes, agarose, starch, polyacrylamide gels, or nothing, that is, free solutions. Running electrophoresis in free solutions has a serious drawback, however, because the resulting sample components not only will move in the direction of the electric field but also will diffuse in various directions, as has been discussed in the previous section on the moving boundary. This would make data analysis unnecessarily complicated. Today electrophoresis is often run in supporting medium. In the literature, the apparatus is frequently named after the supporting medium used, for example, paper electrophoresis and starch gel electrophoresis. This supporting media are usually cast in glass tubes or plates (except paper), as shown in Figure 13.13.

There are many types of electrophoresis, such as

microgel electrophoresis,
two-dimensional macromolecular maps,
thin-layer electrophoresis,
affinity electrophoresis,
paper electrophoresis,

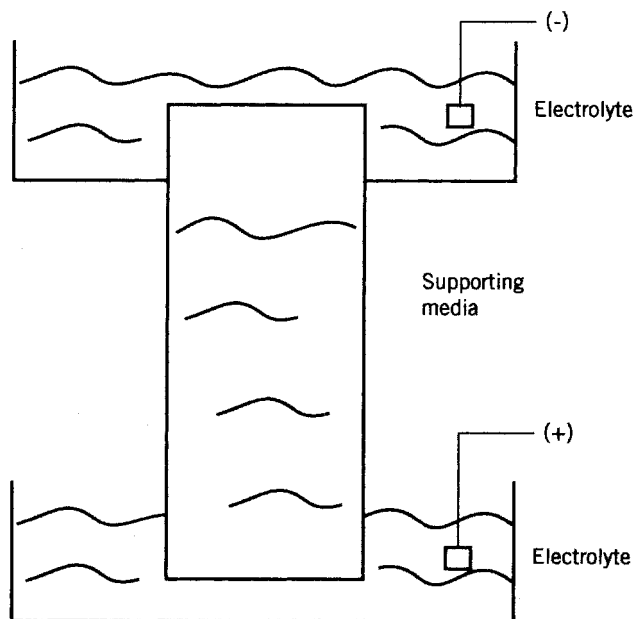


FIGURE 13.13 Typical analytical apparatus for electrophoresis.

starch electrophoresis,
 agarose gel electrophoresis,
 polyacrylamide gel electrophoresis,
 isofocusing and isotachopheresis, and
 SDS-protein capillary electrophoresis.

Paper electrophoresis and starch gel electrophoresis were commonly used 15 years ago. Now, they are seldom used. Agarose gel electrophoresis and polyacrylamide gel electrophoresis, particularly the latter, continue to be widely used, and it seems that they are becoming even more important in studies of proteins and nucleic acids. In what follows we describe (1) agarose gel electrophoresis and polyacrylamide gel electrophoresis, (2) isofocusing and isotachopheresis, and (3) DNA sequencing (which, of course, can apply equally well to RNA sequencing).

13.2.3 Agarose Gel Electrophoresis and Polyacrylamide Gel Electrophoresis

Agarose Gel Electrophoresis Agarose is a polysaccharide of galactose and 3,6-anhydrogalactose. It dissolves in boiling water, and when it is cooled to room temperature, it forms a gel. The pore size of agarose gel is relatively large (500 Å in a 2.5% gel). The separation of the macromolecules, however, is basically due to the

gel's charge density and not its pore size. The higher the charge, the faster the macromolecule moves. Agarose gel is widely used in immunoelectrophoretic procedures where immunodiffusion is a major step in the separation of the largest molecules and supramolecular complexes, such as viruses, enzyme complexes, lipoproteins, and nucleic acids.

Polyacrylamide Gel Electrophoresis Polyacrylamide gels are prepared by the radical polymerization of acrylamide monomers ($\text{CH}_2=\text{CH}-\text{CO}-\text{NH}_2$) with the cross-linking comonomer *N,N'*-methylbisacrylamide ($\text{CH}=\text{CH}-\text{CO}-\text{NH}-\text{CH}_2-\text{NH}-\text{CO}-\text{CH}=\text{CH}_2$). The pore size is controlled by the concentration of monomers and cross-linking reagents. It is possible to prepare gels with a variety of pore sizes, and separation is basically due to the size of the macromolecules. Hence, polyacrylamide gel electrophoresis is a molecular sieving apparatus. The largest pores of the polyacrylamide gel, however, are still smaller than those of agarose gel.

Polyacrylamide gels are used for separating and identifying small fragments of DNA and RNA molecules. They are also used for monitoring the process of a preparative scheme by identifying the presence of impurities. In many instances, polyacrylamide gel is joined with agarose gel to form composite polyacrylamide–agarose gel, which is used to separate larger segments. However, for separating intact DNA molecules, agarose gels alone must be used.

SDS–Polyacrylamide Gel Electrophoresis Polyacrylamide gel electrophoresis is often used simultaneously for both separating and estimating the molecular weight of proteins that are solubilized with the detergent sodium dodecyl sulfate (SDS). This special kind of electrophoresis is called SDS–polyacrylamide gel electrophoresis or SDS–PAGE.

SDS binds to proteins to form complexes that carry negative charges in the form of rods. When subjected to PAGE, the molecules migrate at different rates. Larger molecules migrate slowly, whereas small molecules migrate quickly. There is a correlation between migration rate and molecular weight (molecular size). Recall the definition of mobility:

$$u = \frac{d}{vt}$$

where d is the distance of migration, t is the time, and v is the voltage difference. If two compounds are migrating in the gel with the same v and t , then the mobility of the two compounds have a ratio equal to the ratio of distance (migration):

$$\frac{u_1}{u_2} = \frac{d_1/vt}{d_2/vt} = \frac{d_1}{d_2}$$

If d_2 is chosen as a standard, for example, a marker dye, then

$$u_1 = \frac{d_1}{d_2} u_2$$

Arbitrarily we set $u_2 = 1$ mobility unit. Then, we have $u_1 = d_1/d_2$. For the correction of gel length before and after staining due to possible further swelling, we introduce the term l/l' :

$$u_1 = \left(\frac{d_1}{d_2}\right) \left(\frac{l}{l'}\right)$$

where l is the length of gel before staining and l' is the length after staining of the chemical compound of interest (e.g., protein polypeptide). Since the separation of the mixture is basically due to the sieve effect, the mobility of a compound is proportional to its size, which in turn is proportional to its molecular weight. It was empirically found that the plot of $\ln(\text{molecular weight})$ versus mobility is linear. Thus, a universal calibration plot can be constructed so that for any unknown compound, if its mobility in electrophoresis is determined, its molecular weight can be estimated.

13.2.4 Southern Blot, Northern Blot, and Western Blot

Blotting analysis is a technique in which the resolved DNA, RNA, or protein on the gel electrophoresis is extracted from the gel matrix to a blotting membrane (or filter) such as nitrocellulose. The DNA, RNA, or protein fragments that stick to the blotting membrane (or filter) are then further isolated, purified, and analyzed. These techniques are extensively used in molecular biology to study gene structure, particularly to define the presence of a gene-related sequence in a genome.

Southern Blot Southern blot is a technique used on a fractionation of DNA fragments. The technique used primarily is agarose gel electrophoresis and the nitrocellulose filter is the major apparatus used. DNA from a tissue or cell is isolated, purified, and cleaved with a specific restriction endonuclease into defined fragments. The fragments are separated through agarose gel electrophoresis. After fractionation, they are transferred from the gel to a nitrocellulose filter which is called a blot. The blot is hybridized with a probe that is specific for the gene under study. Autoradiography of the blot enables us to identify the restriction fragments which form complementary base pairs.

Northern Blot Northern blot is used to separate single-stranded RNA. Formaldehyde/agarose gel is used for the electrophoresis. The fragments of RNA are then transferred to a cellulose filter from the gel and are hybridized with a specific radiolabeled probe as in the case of the Southern blot.

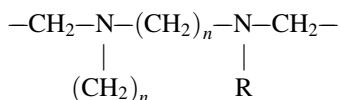
Western Blot Western blot is a technique used to investigate proteins. Here PAGE is used in conjunction with a nitrocellulose filter. Protein products are fractionated by size using PAGE and then are transferred to nitrocellulose for identification with a primary antibody. The bound primary antibody may be further detected with a second species, such as ^{125}I -protein A or biotinylated goat anti-Ig G.

13.2.5 Sequencing DNA Fragments

Gel electrophoresis can be used to sequence DNA (or RNA) fragments, that is, to identify the sequence of bases in DNA molecules. The process involves chemical modification and cleavage of specific nucleotides followed by electrophoresis on high-resolution denaturing acrylamide gels. In the first step, a base is chemically modified (e.g., methylation of guanine) and then is removed from its sugar by cleaving the DNA strand at its sugar. The cleavage is accomplished by a restriction endonuclease. Each base cleaved is contingent on the one that precedes it. DNA is cleaved only at the sugar attached to the modified base. The second step is to end label the fragments and to extract DNA from PAGE. Sequencing DNA fragments is one of the most important techniques in modern biotechnology.

13.2.6 Isoelectric Focusing and Isotachopheresis

Isoelectric Focusing Isoelectric focusing electrophoresis is based on a pH gradient from anode to cathode. Such a gradient, however, is not created by the buffers of different pH. It is produced and maintained by the electric field on the synthesized materials, known as *carrier ampholytes*, such as Ampholines (a commercial product of LKB) or Biolytes (Bio-Rad Laboratories). Ampholine has the following structure:



where $n = 2, 3$ and R is H or $\text{---(CH}_2\text{)}_x\text{---COOH}$. Its molecular weight is in the range 300–1000. It is water soluble and can produce a pH range of 3.9–9.5 when an electric field is applied. During the electrophoretic process protein molecules migrate anodically (from a basic region) or cationically (from an acidic region) until they lose their net electrical charge and cease to migrate. That particular pH region in which they cease to migrate is the region of an isoelectric point. There are two types of stabilizing media for isoelectric focusing: a density gradient of sucrose or a gel of polyacrylamide. The separation by any of the two types is based on composition rather than size of the protein molecules.

Density Gradient Isoelectric Focusing As an illustration of the general principle of density gradient isoelectric focusing, we chose a U-tube apparatus (Figure 13.14). After the U-tube is filled halfway with a 1% ethanolamine solution containing 40% sucrose (base), nine or more layers are added one by one to form the density gradient. The volume of each layer is approximately 1 mL. Layer 1 contains 1.5% carrier ampholytes in 30% sucrose, layer 2 contains 1.2% carrier ampholytes in 37% sucrose, and so on. The last layer contains 0.5% carrier ampholytes in 5% sucrose. On top of the density gradient is placed 1 or 2 mL of sulfuric acid. The protein sample (1–3 mg) is dissolved in an intermediate solution(s). The anode is

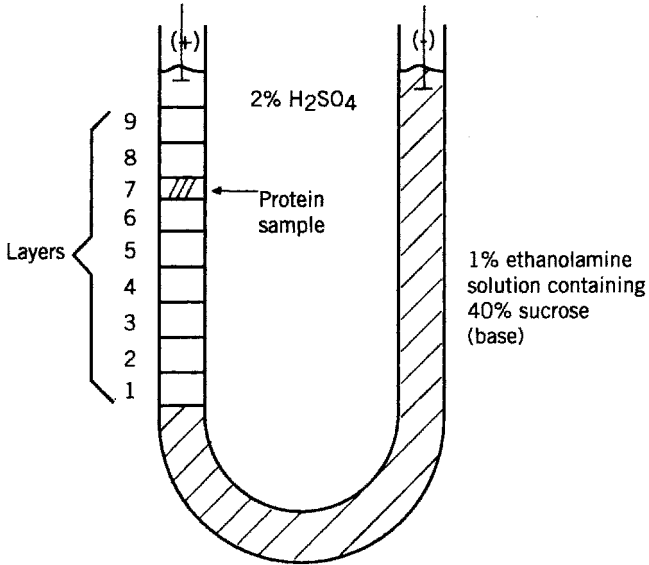


FIGURE 13.14 U-tube apparatus for density isoelectric focusing.

inserted into the sulfuric acid solution and the cathode into the ethanolamine solution. The voltage increases gradually to 500 V. Focusing should be complete in 4–10 h.

Polyacrylamide Gel Isoelectric Focusing Two well-established techniques that use polyacrylamide are the gel cylinder and the thin layer. Here we discuss only the gel cylinder technique because it is simpler and easier to understand. Figure 13.15

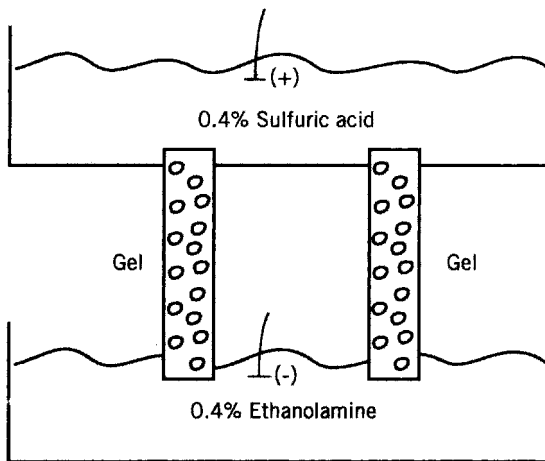


FIGURE 13.15 Disk electrophoresis apparatus for gel isoelectric focusing. ○, sample.

shows a disk electrophoresis apparatus for gel isoelectric focusing. The protein sample (approximately 30 μm per component) may be incorporated into the gel, which contains polyacrylamide and carrier ampholytes, or layered on top of the gel under a protecting layer of 2% carrier ampholytes and 5% sucrose. The voltage is raised gradually to 400 V for 60-mm gels and to 700 V for double-length gels. The following equation should be kept in mind:

$$\begin{array}{rcccl} v & \times & ma & = & \text{Watt} \\ \text{Voltage} & & \text{Current} & & \text{Power} \end{array}$$

For protein, v should be high, while milliamperes should be low. If v is high, the velocity (mobility) is high. If milliamperes are low, the temperature is low, and the protein will not be denatured (at 35°C, proteins are usually denatured). For nucleic acid, milliamperes should be high. At high temperatures, the strains of nucleic acid are kept separated.

Two-Dimensional Electrophoresis Two-dimensional electrophoresis is a combination of two different electrophoretic separation procedures. The use of two separation techniques is based on the principle that they have independent parameters; that is, they separate chemical species according to different properties.

Usually isoelectric focusing on a thin gel is chosen for the first dimension separation. Once the ionic species (protein) are focused into narrow bands, they serve as zones for the second-dimension analysis. The second dimension can be any of the following: immunoelectrophoresis, a discontinuous SDS–polyacrylamide gel system, or gradient electrophoresis.

Isotachophoresis Isotachophoresis is a steady-state stacking electrophoresis and can be used in capillary tubes, thin-layer equipment, gel rods, slabs, or columns. It consists of a leading ion with high mobility, such as chloride, sulfate, phosphate, or cacodylate, and a trailing ion with low mobility, such as ϵ -amino-caproic acid, β -alanine, or glycine. In between the leading and trailing ions, sample constituents continue to migrate on the basis of their mobilities. The leading ion and the trailing ion carry the same charge. Once the sample zones in between the leading stack zone and the trailing stack zone are separated, a steady state is reached. According to Kohlrausch's law,

$$\Lambda_0 = \Lambda_0^+ + \Lambda_0^-$$

where the conductivity Λ (hence, the mobility u) of an ion is independent of the compound from which it is electrolyzed. On this basis, the concentration of each separated sample zone can be calculated by the concentration of the leading ion zone, which is known by the solution preparation.

Capillary Electrophoresis Because of its remarkable separation capabilities, capillary electrophoresis has been rapidly developed for use in biotechnology, particularly in gene splicing. In this technique a capillary tube of glass is used. The capillary is immersed in electrolyte-filled reservoirs containing electrodes

connected to a high-voltage power supply. A protein sample is introduced at one end of the capillary (the inlet) and analytes are separated as they migrate through the capillary toward the outlet end. As separated components migrate through a section at the far end of the capillary, they are sensed by a detector and an electronic signal is sent to a recording device. The capillary electrophoresis can be used as isotachopheresis, isoelectric focusing as well as nongel sieving size-based electrophoresis by adding spacers. Figure 13.16 shows a sample of protein analysis by capillary electrophoresis.

Since 1994 gel electrophoresis is used to determine the order of bases on a strand in both the clone-by-clone approach and the whole genome short run method. DNA molecules are labeled with nucleotide-specified fluorescent dye and loaded into a slab of acrylamide gel and a voltage is applied. The DNA fragments are separated by size as they migrate through the gel. The apparatus includes a detector or photomultiplier to read the color of the fluorescent dye at the end of each DNA fragment.

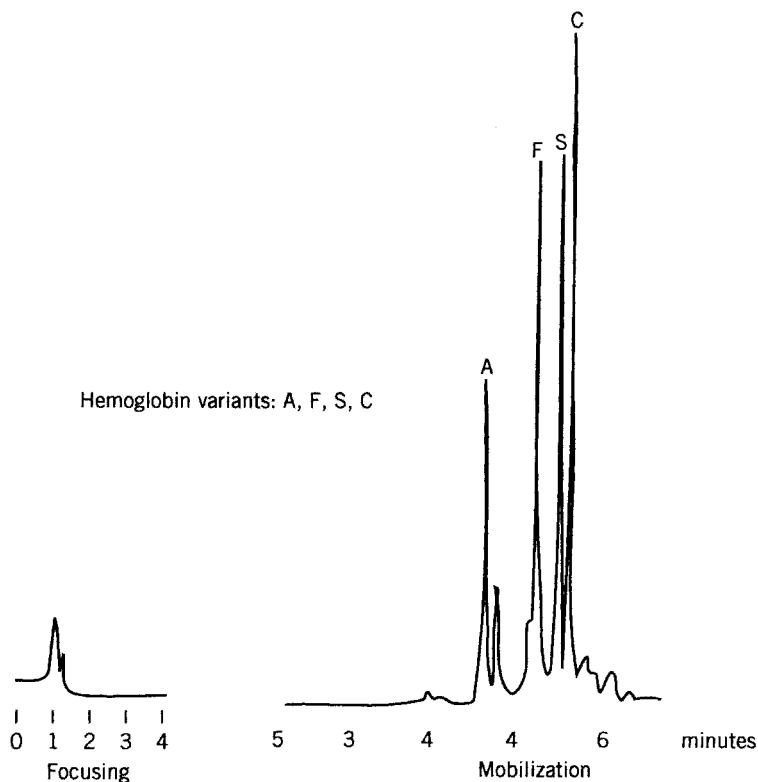


FIGURE 13.16 Separation by capillary electrophoresis. (Source: Bio-Rad HPE 100 capillary electrophoresis system, Application note 2, 1992. Reproduced by permission of Bio-Rad Laboratories, Hercules, California.)

To separate proteins, a two-dimensional gel electrophoresis is usually employed. A mixture of proteins is placed in a gel. They are separated in one direction by their charges and in the perpendicular direction by their molecular weight. The separated proteins are cut from the gels, purified, and broken into fragments. These fragments are sent to a mass spectrometer which measures their atomic masses. These masses are used to identify the protein of interest.

Today's instruments of electrophoresis often incorporate capillary tubes to hold the sequence gel, automatic sample loading, separation matrix loading and removal, data collection and analysis, and provide significant improvement over the manual gel preparation and lane tracking required in slab-gel sequencers.

13.3 FIELD-FLOW FRACTIONATION

Field-flow fractionation is a separation method that is similar to both liquid chromatography and electrophoresis. It has only one phase, the mobile phase. It can use an electric field to separate molecules as in electrophoresis, but it is not limited to an electric field and it does not need gels. The method was developed by Giddings (1966, 1970, 1993) and is based on the concept of coupling concentration and flow nonuniformities. Separation occurs when an electric field is applied on the channel in which the sample flows. The molecules near the center of the channel have a higher velocity than those near the walls, thereby creating a concentration gradient. Meanwhile, diffusion works in the opposite direction to the driving forces. At equilibrium, the two opposite forces are balanced and the concentrating molecules stay around the equilibrium position. Thus, zones of molecules of different sizes are formed. Figure 13.17 illustrates this concept. The applied field can be centrifugal, gravitational, magnetic, or electric; it can also be a concentration gradient, a temperature gradient, or a chemical potential gradient. Detectors that can be used are similar to those used in liquid chromatography, namely, UV, visible, IR, fluorescence, refractive index, viscosity, density, and osmotic pressure.

The fractionation diagram is similar to a chromatographic design (Figure 13.18). According to Giddings (1970), the retention R can be expressed by

$$R = 6\lambda[\coth(2\lambda)^{-1} - 2\lambda]$$

where $\lambda = l/w$, with l as the ratio of diffusion coefficient D and the vector induced by the applied field V ($l = D/V$) and w as the thickness of the fractionation channel.

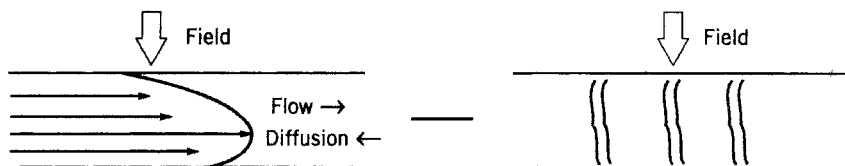


FIGURE 13.17 Field-flow fractionation.

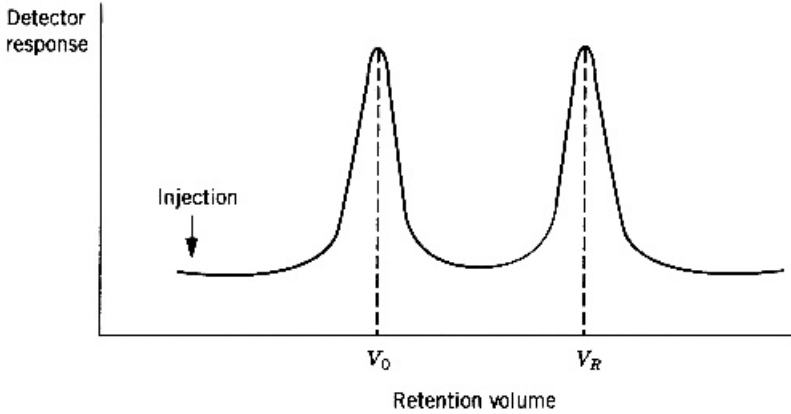


FIGURE 13.18 Fractionation diagram.

The value of λ depends on V , which in turn depends on the type of the applied field. The following are some common field-flow fractionation methods:

Thermal Field-Flow Fractionation This method is based on the principle of thermal diffusion D_T (Figure 13.19). The value of λ may be evaluated by using

$$\lambda = w \frac{D_T}{D} \frac{dT}{dx}$$

where D is the diffusion of the solution and D_T is the thermal diffusion coefficient.

Electric Field-Flow Fractionation This method is similar to electrophoresis. The electric field is induced by charging the two parallel plates, as in Figure 13.20. The channel between the two plates is filled with buffer as in the case of electrophoresis. The value of λ is calculated by using

$$\lambda = \frac{D}{uEw}$$

where u is the electrophoretic mobility and E is the electric field strength.

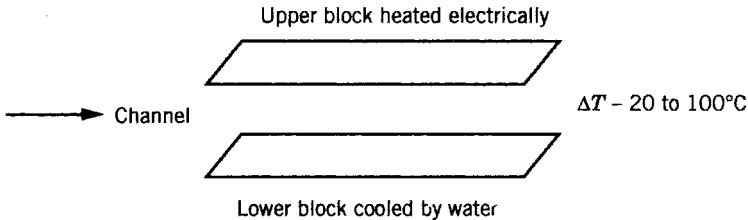


FIGURE 13.19 Thermal field-flow fractionation.

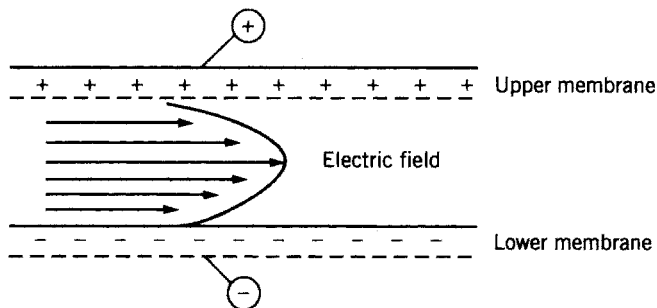


FIGURE 13.20 Electric field-flow fractionation.

Sedimentation Field-Flow Fractionation This method uses the centrifugal field to separate molecules. The value of λ is calculated by using

$$\lambda = \frac{6kT}{\pi a^3 g w \Delta \rho}$$

where k is the Boltzmann constant, a is the particle diameter, g is the gravitational constant, and $\Delta \rho$ is the difference in the densities of the solute and solvent.

Flow Field-Flow Fractionation This method is similar to dialysis or ultrafiltration, with the solvent acting uniformly on all the solutes. The field is generated by the flow of the solvent. The separation is mainly determined by the diffusion coefficient or frictional coefficient. The value of λ is calculated using

$$\lambda = \frac{R' T V_0}{3 \pi N_A \eta V_c w^2 a}$$

where R' is the universal gas constant, V_0 is the void volume, V_c is the flow rate of the solvent, η is the viscosity of the solvent, a is the diameter of the

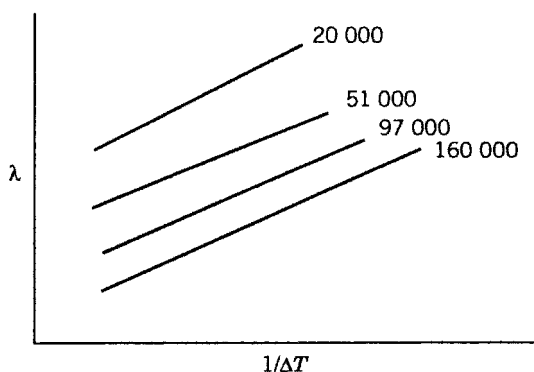


FIGURE 13.21 Separation of polystyrene sample in terms of λ . [Adapted from Giddings (1974).]

particle, and N_A is Avogadro's number. Figure 13.21 shows the separation of polystyrene sample in terms of λ .

REFERENCES

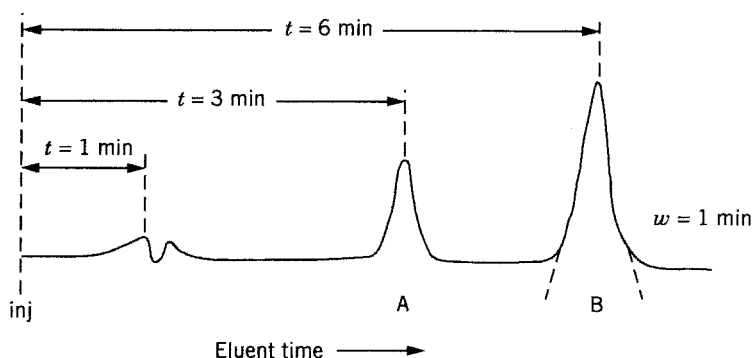
- Andrews, A. T., *Electrophoresis: Theory, Techniques, and Biochemical and Clinical Applications*. Oxford: Clarendon, 1986.
- Clin. Chem.* **28**, 737 (1982). The entire issue is devoted to two-dimensional electrophoresis.
- Davis, L. G., M. D. Dibner, and J. F. Batley, *Basic Methods in Molecular Biology*. New York: Elsevier Science, 1986.
- Deyl, Z. (Ed.), *Electrophoresis: A Survey of Techniques and Applications*; Part A, *Techniques*. Amsterdam: Elsevier, 1979.
- Giddings, J. C., *Dynamics of Chromatography*, Part 1. New York: Dekker, 1965.
- Giddings, J. C., *Sep. Sci.* **1**, 123 (1966).
- Giddings, J. C., *Anal. Chem.* **42**, 195 (1970).
- Giddings, J. C., *Science* **260**, 1456 (1993).
- Giddings, J. C., and K. D. Caldwell, in B. W. Rossiten and B. W. Hamiton (Eds.), *Physical Methods of Chemistry*. New York: Wiley, 1989.
- Giddings, J. C., and H. Eyring, *J. Phys. Chem.* **59**, 416 (1955).
- Grubistic, Z., R. Rempp, and H. Benoit, *J. Polym. Sci. B* **5**, 753 (1967).
- Hummel, J. P., and W. J. Dreyer, *Biochim. Biophys. Acta*, **63**, 530 (1962).
- Heftmann, E. (Ed.), *Chromatography: A Laboratory Handbook of Chromatographic and Electrophoretic Methods*, 3rd ed. New York: Van Nostrand Reinhold, 1975.
- Howard, G. A., and A. J. P. Martin, *Biochem. J.* **46**, 532 (1950).
- James, A. T., and A. J. P. Martin, *Analyst (London)* **77**, 915 (1952a).
- James, A. T., and A. J. P. Martin, *Biochem. J.* **50**, 679 (1952b).
- Janca, J., *Field-Flow Fractionation*. New York: Dekker, 1988.
- Martin, A. J. P., and R. L. M. Synge, *Biochem. J.* **35**, 1358 (1941).
- Maxam, A. M., and W. Gilbert, *Methods Enzymol.* **65**, 499 (1980).
- Ravindranath, B., *Principles and Practice of Chromatography*. Chichester, UK: Ellis Horwood, 1989.
- Sun, S. F., and C. L. Hsiao, *Chromatographia* **37**, 329 (1993a).
- Sun, S. F., and F. Wong, *J. Chromatogr.* **648**, 325 (1993b).
- Sun, S. F., S. W. Kuo, and R. A. Nash, *J. Chromatogr.* **288**, 377 (1984).
- Sun, S. F., and E. Wong, *J. Chromatogr.* **208**, 253 (1981).
- Sun, S. F., and F. Wong, *Chromatographia* **20**, 445 (1985).
- Tung, L. H., *J. Appl. Polym. Sci.* **10**, 375 (1966).
- Van Deemter, J. J., F. J. Zuiderwig, and A. Klinkenberg, *Chem. Eng. Sci.* **5**, 271 (1956).
- Wilson, J. N., *J. Am. Chem. Soc.* **62**, 1583 (1940).
- Yau, W. W., J. J. Kirkland, and D. D. Bly, *Modern Size-Exclusion Chromatography*. New York: Wiley, 1979.

PROBLEMS

13.1 Derive the equation for calculating the theoretical plates:

$$N = 16 \left(\frac{t_R}{t_w} \right)^2 = \frac{16}{L} \left(\frac{V_R}{w} \right)^2 = \frac{1}{L} \left(\frac{V_R}{\sigma} \right)^2$$

13.2 Following is a chromatogram of the mixture of sample A and sample B:



(a) Calculate N , α , k'_a , k'_b , N_s (resolution).

(b) If the column length is 12 cm, what is the plate height?

13.3 The values of elution volume for some proteins using the same column and mobile phase and under the same conditions are as follows:

Protein	Molecular Weight	V_l (mL)
Sucrose		210
Ribonuclease	13,700	138
Chymotrypsinogen	25,000	135
Ovalbumin	45,000	110
Serum albumin	67,000	98
Thyroglobulin	670,000	68

Sucrose and thyroglobulin are used for references on both ends. For sucrose, $K_d = 1$ and $V_l = V_0 + V_i$, while for thyroglobulin, $K_d = 0$ and $V_l = V_0$. Plot:

(a) Molecular weight versus V_l

(b) Molecular weight versus K_d

(c) Molecular weight versus k'

- 13.4** Because of electroosmosis, the observed mobility u should be corrected by including the gel length l :

$$u = \frac{d}{tv/l} = \frac{dl}{tv}$$

Show that if the actual migration length is d' and the gel length after staining is l' , then

(a) $u_{\text{act}} = u \left(\frac{l'}{l}\right)^2$

(b) $d' = d \frac{l'}{l}$

- 13.5** In the isotachopheresis, the concentrations of separated sample fragments can be calculated once the concentration of the leading zone is known. This can be done by using Kohlrausch's equation. Show how this can be done.

14

LIGHT SCATTERING

In 1869 Tyndall studied the phenomenon of the scattering by particles in colloidal solution and he demonstrated that if the incident light is polarized, scattering is visible in only plane. In 1871 and 1881 Rayleigh derived an equation that showed the scattering to be inversely proportional to the fourth power of the wavelength of the incident light. Then in 1944 and 1947 Debye suggested that the measurement of light-scattering intensity could be used to determine the molecular weight of a macromolecule in dilute solutions and possibly to determine its size and shape. Since then light scattering has become an important tool in the study of polymer behavior in solutions.

14.1 RAYLEIGH SCATTERING

Light is a form of electromagnetic radiation. The properties of an electromagnetic field may be expressed by two vector quantities: the electric field strength \mathbf{E} and the magnetic field strength \mathbf{H} . The two field strengths are related by four differential equations according to Maxwell:

$$\begin{aligned}\nabla \times \mathbf{E} &= \frac{1}{c'} \frac{\partial \mathbf{H}}{\partial t} & \nabla \cdot \mathbf{H} &= 0 \\ \nabla \times \mathbf{H} &= \frac{1}{c'} \frac{\partial \mathbf{E}}{\partial t} + 4\pi \mathbf{g} & \nabla \cdot \mathbf{E} &= 4\pi \rho\end{aligned}$$

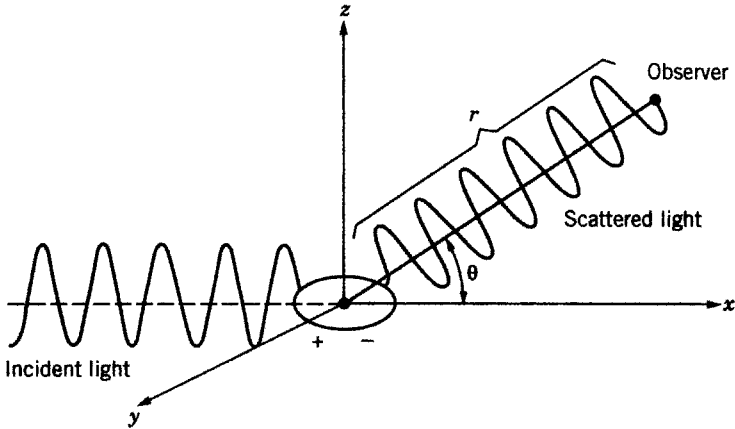


FIGURE 14.1 Rayleigh scattering model.

where \mathbf{g} is the current density, ρ is the charge density, c' is the velocity of light, and ∇ is the mathematical operator:

$$\nabla = \frac{\partial}{\partial x} \mathbf{i} + \frac{\partial}{\partial y} \mathbf{j} + \frac{\partial}{\partial z} \mathbf{k}$$

Rayleigh scattering is best described in terms of three factors: the incident light, the particle (e.g., a macromolecule), which serves as an oscillating dipole, and the scattered light. The model is shown in Figure 14.1. The incident light may be expressed by the following well-known equation:

$$E = E_0 \cos 2\pi \left(vt - \frac{x}{\lambda} \right)$$

where E is the electric field or electric intensity, E_0 is the amplitude of the incident wave, v is the frequency of the light in the solution, and t is the propagation time. The frequency v is related to the wavelength λ by

$$v = \frac{c'}{\lambda}$$

The wavelength of the light in the solution is

$$\lambda = \frac{\lambda_0}{n}$$

where λ_0 is the wavelength of the light in vacuum and n is the refractive index of the medium.

As the incident light hits the molecule, the distribution of electrons in the molecule is distorted, resulting in the polarization of the molecule, which now acts as an oscillating dipole p . The dipole is related to the electric field E_0 by

$$p = \alpha E = \alpha E_0 \cos 2\pi \left(vt - \frac{x}{\lambda} \right)$$

Here α is the polarizability of the molecule. The second derivative of the oscillating dipole with respect of time d^2p/dt^2 describes the electric strength of the scattered light:

$$\frac{d^2p}{dt^2} = \alpha E_0 \cos 2\pi \left(vt - \frac{x}{\lambda} \right) (4\pi^2 v^2)$$

The negative sign in the above equation is dropped because we are interested only in its absolute value.

If the incident light is plane polarized, the scattered light can then be expressed:

$$E_s = \frac{(d^2p/dt^2)(\sin \theta/r)}{c^2}$$

where r is the distance of the dipole from the observer and θ is the angle between the dipole axis and the line r . The division by the square of the velocity of light, c^2 , is a dimensional correction.

Substituting d^2p/dt^2 in the above equation, we obtain

$$E_s = \frac{4\pi^2 v^2 \alpha E_0 \sin \theta}{c^2 r} \cos 2\pi \left(vt - \frac{x}{\lambda} \right)$$

Since the measurable quantity in a light wave is the intensity I , we convert E to I . The intensity of the light is the amount of energy that falls on a unit area per unit time:

$$I = \epsilon_0 c' \langle E^2 \rangle$$

In the SI system E is in newtons per coulomb, $\epsilon_0 = 8.85418 \times 10^{-12} \text{ C}^2 \text{ N}^{-1} \text{ m}^{-2}$. The intensity I is also expressed in joules per square meter per second ($\text{J m}^{-2} \text{ s}^{-1}$). Here $\langle E \rangle$ is the field averaged over a period of vibration from $t = 0$ to $t = 1/v$.

In measurement we are concerned with the ratio of the intensity of scattered light I over the intensity of the incident light I_0 :

$$\begin{aligned} \frac{I}{I_0} &= \frac{E_s^2}{E^2} = \frac{\{[(4\pi^2 v^2 \alpha E_0 \sin \theta)/c^2 r] \cos 2\pi(vt - x/\lambda)\}^2}{[E_0 \cos 2\pi(vt - x/\lambda)]^2} \\ &= \frac{16\pi^4 \alpha^2 \sin^2 \theta}{\lambda^4 r^2} \end{aligned}$$

The equation

$$\frac{I}{I_0} = \frac{16\pi^4 \alpha^2 \sin^2 \theta}{\lambda^4 r^2} \quad (14.1)$$

is called the Rayleigh equation for plane-polarized light. If the incident beam is unpolarized, the equation is slightly modified:

$$\frac{I}{I_0} = \frac{16\pi^4 \alpha^2}{\lambda^4 r^2} (1 + \cos^2 \theta)$$

The correction term is based on the consideration of the total intensity:

$$\begin{aligned} I(\text{total}) &= I(\text{y component}) + I(\text{z component}) \\ &\rightarrow \sin^2 \phi_y + \sin^2 \phi_z = 1 + \cos^2 \theta \end{aligned}$$

The ratio $(I r^2 / I_0)_\theta$ is called the Rayleigh ratio and is often designated as R_θ :

$$R_\theta = \left(\frac{I r^2}{I_0} \right)_\theta$$

Its unit is reciprocal centimeters (path length, 1 cm). Thus, in light-scattering experiments, the three quantities R_θ , λ , and θ are the major parameters that we measure.

The physical meaning of the Rayleigh ratio is the attenuation of the incident beam by the loss of intensity after passage through a medium. Although intensity lost here is due to scattering, not absorption, we can still use Lambert's law to describe the phenomenon. Lambert's law states that

$$\frac{I}{I_0} = e^{-\tau l}$$

where τ is the turbidity, which is a measure of the loss of intensity of the incident beam, and l is the path length of the cell. For $l = 1$ (cm), $\tau = -\ln(I/I_0)$. The relationship between the Rayleigh ratio and the turbidity is given by

$$\tau = 2\pi \int_0^\pi \left(\frac{I r^2}{I_0} \right)_\theta \sin \theta \, d\theta$$

For special scattering angles 90° and 0° , we have

$$\tau = \frac{16\pi}{3} R_{90^\circ} = \frac{8\pi}{3} R_{0^\circ}$$

14.2 FLUCTUATION THEORY (DEBYE)

In 1947 Debye suggested that the amount of light scattered by a solution of high-molecular-weight polymers is related to the mass of the solute molecules. Hence, the measurement of the intensity of scattered light enables us to determine the molecular weight of polymers. The difficulty is in how to utilize the Rayleigh equation for that purpose. Debye proposed the following theory.

The Rayleigh scattering equation is applicable to gases where molecules move at random and in near chaos. In a liquid solution the molecules are far from being independent of one another, but unlike crystals, liquids, are not well ordered either. Instead, there is a fluctuation in the concentration of a volume element. The fluctuation of the concentration $\langle \Delta c \rangle$ results in the fluctuation of polarizability α . Therefore, to apply the Rayleigh scattering equation to the liquid state, we need only to modify the parameter α . For gases, we have $p = \alpha E$; for solutions, we should have $p = \langle \Delta \alpha^2 \rangle E$. The quantity $\langle \Delta \alpha^2 \rangle$ is the fluctuation of the polarizability.

Since $\alpha = \alpha(c, \rho)$, the differential $d\alpha$ is given by

$$d\alpha = \frac{\partial \alpha}{\partial c} dc + \frac{\partial \alpha}{\partial \rho} d\rho$$

where c is the concentration of the solution and ρ is the density. For the first approximation the density term may be ignored because we are more interested in the composition of solutions, not the physical state (liquid) of the solution. Furthermore, we should change notation from $d\alpha$ and dc to $\Delta\alpha$ and Δc :

$$\Delta\alpha = \frac{\partial \alpha}{\partial c} \Delta c$$

Polarizability α is usually measured in terms of refractive index n or dielectric constant ϵ and the light-scattering apparatus can be designed in relation to the measurement of refractive index. (*Note:* $\epsilon^2 = n^2$ according to Maxwell's theory.) For that reason, we utilize the relation

$$\alpha = \frac{n^2 - 1}{4\pi}$$

and convert $\partial\alpha$ to ∂n by

$$\frac{\partial \alpha}{\partial c} = \frac{n}{2\pi} \frac{\partial n}{\partial c}$$

and hence

$$\langle \Delta \alpha^2 \rangle = \frac{n^2}{4\pi^2} \left(\frac{\partial n}{\partial c} \right)^2 \langle \Delta c^2 \rangle$$

We may change δ into d , since there is only one independent variable involved now:

$$\langle \Delta \alpha^2 \rangle = \frac{n^2}{4\pi^2} \left(\frac{dn}{dc} \right)^2 \langle \Delta c^2 \rangle$$

where dn/dc is called the differential refractive index and is an experimentally measurable quantity. Our attention now is focused on $\langle \Delta c^2 \rangle$.

The fluctuation of concentrations is always accompanied by a change in free energy, ΔG . We now expand ΔG in terms of Δc around the equilibrium concentration $\langle c \rangle$ using Taylor's series:

$$\Delta G = \frac{\partial G}{\partial c} \Delta c + \frac{1}{2!} \left(\frac{\partial^2 G}{\partial c^2} \right) (\Delta c)^2 + \dots$$

The first term is zero for a closed term at constant temperature, whereas the higher terms, including $(\Delta c)^3$, may be neglected since the fluctuations are rather small. Thus, only the second term is physically meaningful:

$$\Delta G = \frac{1}{2!} \left(\frac{\partial^2 G}{\partial c^2} \right) (\Delta c)^2$$

Using the Boltzmann expression, we obtain a distribution function of concentration:

$$\exp\left(-\frac{\Delta G}{kT}\right) = \exp\left[-\frac{1}{kT} \frac{1}{2!} \left(\frac{\partial^2 G}{\partial c^2} \right) (\Delta c)^2\right]$$

The fluctuation of concentration, $\langle \Delta c^2 \rangle$, can then be evaluated as follows:

$$\langle \Delta c^2 \rangle = \frac{\int_0^\infty (\Delta c)^2 \exp[-(\partial^2 G/\partial c^2)(\Delta c)^2/2kT] dc}{\int_0^\infty \exp[-(\partial^2 G/\partial c^2)(\Delta c)^2/2kT] dc} = \frac{kT}{(\partial^2 G/\partial c^2)_{T,P}}$$

Note:

$$\int_0^\infty e^{-ax^2} dx = \frac{1}{2} \left(\frac{\pi}{a} \right)^{1/2}$$

$$\int_0^\infty x^2 e^{-ax^2} dx = \frac{1}{4a} \left(\frac{\pi}{a} \right)^{1/2}$$

The two integrals in the equation of $\langle \Delta c^2 \rangle$ can be evaluated by using the two formulas and we obtain

$$\int_0^\infty (\Delta c)^2 \exp\left[-\left(\frac{\partial^2 G/\partial c^2}{2kT}\right) (\Delta c)^2\right] dc = \frac{1}{4a} \left(\frac{\pi}{a} \right)^{1/2}$$

$$\int_0^\infty \exp\left[-\left(\frac{\partial^2 G/\partial c^2}{2kT}\right) (\Delta c)^2\right] dc = \frac{1}{2} \left(\frac{\pi}{a} \right)^{1/2}$$

Hence

$$\langle \Delta c^2 \rangle = \frac{(1/4a)(\pi/a)^{1/2}}{(1/2)(\pi/a)^{1/2}} = \frac{1}{2a} = \frac{1}{(\partial^2 G / \partial c^2) / kT}$$

It remains to calculate $(\partial^2 G / \partial c^2)_{T,P}$. We utilize the following three equations at constant T and P :

(i) $dG = \mu_1 dn_1 + \mu_2 dn_2$. *Note:* From $G = G(T, p, n_1, n_2)$

$$dG = \left(\frac{\partial G}{\partial T} \right)_{P, n_i} dT + \left(\frac{\partial G}{\partial P} \right)_{T, n_i} dP + \left(\frac{\partial G}{\partial n_1} \right)_{T, P, n_2} dn_1 \\ + \left(\frac{\partial G}{\partial n_2} \right)_{T, P, n_1} dn_2 \quad n_i = n_1, n_2 \dots$$

(ii) $dn_1 = (\bar{V}_2 / \bar{V}_1) dn_2$. *Note:* From $V = n_1 \bar{V}_1 + n_2 \bar{V}_2$, where μ_1, μ_2 are chemical potentials, n_1, n_2 are the number of moles, and \bar{V}_1, \bar{V}_2 are partial molar volumes of 1 and 2, respectively.

(iii) $dn_2 = (V/M) dc$. *Note:* From $n_2/V = c/M$, where V is the volume of solution in milliliters, c is in grams per milliliter and M is in grams per mole and then with a simple manipulation, we obtain

$$dG = \left(\frac{-\bar{V}_2}{\bar{V}_1} \mu_1 + \mu_2 \right) \left(\frac{V}{M} \right) dc$$

and

$$\frac{dG}{dc} = \left(-\frac{\bar{V}_2}{\bar{V}_1} \mu_1 + \mu_2 \right) \left(\frac{V}{M} \right)$$

Differentiating this equation with respect to c then gives

$$\left(\frac{\partial^2 G}{\partial c^2} \right)_{T,P} = \frac{V}{M} \left(\frac{\partial \mu_2}{\partial c} - \frac{\bar{V}_2}{\bar{V}_1} \frac{\partial \mu_1}{\partial c} \right)$$

According to the Gibbs–Duhem equation, μ_1 and μ_2 are related in the form

$$n_1 d\mu_1 + n_2 d\mu_2 = 0$$

from which we obtain

$$d\mu_2 = -\frac{n_1 d\mu_1}{n_2}$$

and

$$\frac{\partial \mu_2}{\partial c} = -\frac{n_1}{n_2} \frac{\partial \mu_1}{\partial c}$$

Substituting into $(\partial^2 G / \partial c^2)_{T,P}$, we now have

$$\begin{aligned} \left(\frac{\partial^2 G}{\partial c^2}\right)_{T,P} &= \frac{V}{M} \left(-\frac{n_1}{n_2} - \frac{\bar{V}_2}{\bar{V}_1}\right) \left(\frac{\partial \mu_1}{\partial c}\right) \\ &= \frac{-V}{M} \left(\frac{n_1 \bar{V}_1 + n_2 \bar{V}_2}{n_2 \bar{V}_1}\right) \left(\frac{\partial \mu_1}{\partial c}\right) \end{aligned}$$

Since

$$\frac{n_2 M}{n_1 \bar{V}_1 + n_2 \bar{V}_2} = c$$

we have

$$\left(\frac{\partial^2 G}{\partial c^2}\right)_{T,P} = -\frac{V}{c \bar{V}_1} \left(\frac{\partial \mu_1}{\partial c}\right)_{T,P}$$

Recall van't Hoff's equation:

$$\mu_1 - \mu_1^\circ = -\bar{V}_1 \frac{R'T}{M} c$$

This gives us

$$-\frac{\partial \mu_1}{\partial c} = \frac{\bar{V}_1 R'T}{M}$$

Our equation of $(\partial^2 G / \partial c^2)_{T,P}$ then becomes

$$\left(\frac{\partial^2 G}{\partial c^2}\right)_{T,P} = \frac{V}{c \bar{V}_1} \frac{\bar{V}_1 R'T}{M} = \frac{VR'T}{cM}$$

and

$$\langle \Delta c^2 \rangle = \frac{kT}{(\partial^2 G / \partial c^2)_{T,P}} = \frac{kT}{VR'T/cM} = \frac{N_A kTcM}{N_A VR'T} = \frac{cM}{N_A V}$$

where N_A is Avogadro's number. In comparison, we now have

$$\frac{I}{I_0} = \frac{16\pi^4 \alpha^2 \sin^2 \theta}{\lambda^4 r^2} \quad \text{for gases}$$

and

$$\frac{I}{I_0} = \frac{16\pi^4 \langle \Delta \alpha^2 \rangle \sin^2 \theta V}{\lambda^4 r^2} \quad \text{for solutions} \quad (14.2)$$

Here again V is the volume of solution in which n scatterers are contained. Since we have already derived the equation for $\langle \Delta \alpha^2 \rangle$, Eq. (14.2) can now be put in the form

$$\frac{I}{I_0} = \frac{16\pi^4 \sin^2 \theta n^2}{\lambda^4 r^2} \left(\frac{dn}{dc} \right)^2 \frac{cM}{N_A V}$$

Simplifying and rearranging the terms, we get

$$\frac{Ir^2}{I_0} = \frac{4\pi^2 n^2 (dn/dc)^2 \sin^2 \theta Mc}{\lambda^4 N_A} \quad (14.3)$$

This equation is for plane-polarized incident light. If the incident light is not polarized, we have

$$\frac{Ir^2}{I_0} = \frac{2\pi^2 n^2 (dn/dc)^2 \sin^2 \theta}{\lambda^4 N_A} Mc(1 + \cos^2 \theta) \quad (14.4)$$

If the incident light is not polarized and if $\theta = 90^\circ$, we have

$$\frac{Ir^2}{I_0} = \frac{2\pi^2 n^2 (dn/dc)^2 MC}{\lambda^4 N_A} \quad (14.5)$$

Let

$$K = \frac{2\pi^2 n^2 (dn/dc)^2}{\lambda^4 N_A}$$

Then the light-scattering equation becomes

$$\frac{Kc}{R_\theta} = \frac{1}{M} \quad (14.6)$$

(cf. the equation for osmotic pressure: $\pi'/R'Tc = 1/M$).

The Rayleigh ratio R_θ may be converted to the turbidity τ using the conversion factors

$$H = \frac{16\pi K}{3} \quad (14.7)$$

$$\tau = \frac{16\pi}{3} R_\theta \quad (14.8)$$

Then we have another form of the light-scattering equation:

$$\frac{HC}{\tau} = \frac{1}{M} \quad (14.9)$$

Both Eqs. (14.6) and (14.8) are very similar to the osmotic pressure equation of van't Hoff.

14.3 DETERMINATION OF MOLECULAR WEIGHT AND MOLECULAR INTERACTION

14.3.1 Two-Component Systems

If the behavior of the solution is not ideal, we have the light-scattering equation in the following forms:

$$\frac{Kc}{R_\theta} = \frac{1}{M} + 2A_2c + 3A_3c^2 + \dots \quad (14.10)$$

$$\frac{Hc}{\tau} = \frac{1}{M} + 2A_2c + 3A_3c^2 + \dots \quad (14.11)$$

In comparison with the osmotic pressure equation,

$$\frac{\pi'}{c} = \frac{1}{M} + A_2c + A_3c^2 + \dots$$

we notice that the slope of the plot in the case of straight lines gives the second virial coefficient directly to the osmotic pressure data, whereas it gives a half value of the second virial coefficient to the light-scattering data. That is,

$$\begin{aligned} \text{Second virial coefficient} &= A_2 \\ &= \text{slope of osmotic pressure linear plot} \\ &= \text{twice slope of light-scattered linear plot} \end{aligned}$$

14.3.2 Multicomponent Systems

In multicomponent systems (i.e., more than two components in the solution), there is in addition preferential binding (or preferential adsorption) of the solvent

components on the polymer chain segment. To obtain accurate molecular weight, a correction term of preferential binding must be included in the light-scattering equation. The correction term basically involves dn/dc . If we let component 1 be the solvent, component 2 be the polymer, and component 3 be another solvent (or salt in the case of biological polymers such as protein), we have two slightly different ways to express the light-scattering equation:

$$\left[\frac{K'c}{R_{90}} \left(\frac{dn}{dc} \right)^2 \right]_{c=0} = \left(\frac{1}{M_2} \right)_{\text{two}} \quad \text{for two-component system}$$

$$\left[\frac{K'c}{R_{90}} \left(\frac{dn}{dc} + D' \frac{dn}{d\phi_1} \right)^2 \right]_{c=0} = \left(\frac{1}{M_2} \right)_{\text{three}} \quad \text{for three-component system}$$

where $K' = 2\pi^2 n^2 / \lambda^4 N_A$, ϕ_1 is the volume fraction of the solvent, and

$$D' = - \frac{d\phi_1}{dc}$$

If we take the ratio of the two equations, we obtain

$$D' = \frac{(dn/dc)[(M_2)_{\text{three}}/(M_2)_{\text{two}} - 1]}{dn/d\phi_1} \quad (14.12)$$

Thus, D' , which is the preferential adsorption or preferential binding, can be obtained from the two light-scattering measurements of the same macromolecule, one in a single solvent and the other in a solvent mixture.

In biochemistry there is another method to determine the true molecular weight M_2 and the preferential binding D' . This can be done by carrying out two light-scattering experiments both for the same polymer (e.g., a protein) in a solvent mixture. One of them is dialyzed against the solvent system (solvent mixture) prior to the measurement and the other is not. The dialysis is to establish the equilibrium between the solute and solvents. We now have

$$\left(\frac{Kc}{R_{90}} \right)_{c=0} = \frac{1}{M_{\text{app},2}} \quad (\text{undialyzed solution})$$

$$\left(\frac{Kc}{R_{90}} \right)_{c=0} = \frac{1}{M_2} \quad (\text{dialyzed solution})$$

and

$$M_{\text{app},2} = M_2(1 + D)^2$$

where

$$D = \frac{(\partial n / \partial g_3)_{T,P,g_2}}{(\partial n / \partial g_2)_{T,P,g_3}} \left(\frac{\partial g_3}{\partial g_2} \right)_{T,\mu_1,\mu_3} \quad (14.13)$$

The symbol g refers to the gram and the term $\partial g_3 / \partial g_2$ refers to the preferential binding of component 3 (a solvent) to component 2 (polymer segment). The term $M_{\text{app},2}$ is the apparent molecular weight of the macromolecule and M_2 is its true molecular weight. The parameter D may also be expressed in the equation

$$D = \frac{(1 - c_2 \bar{v}_3)(\partial n / \partial c_3)_{m_2} M_3}{(1 - c_2 \bar{v}_2)(\partial n / \partial c_3)_{m_3} M_2} \left(\frac{\partial m_3}{\partial m_2} \right)_{T,\mu_1,\mu_3} \quad (14.14)$$

where

$$\frac{M_3}{M_2} \left(\frac{\partial m_3}{\partial m_2} \right)_{T,\mu_1,\mu_3} = \left(\frac{\partial g_3}{\partial g_2} \right)_{T,\mu_1,\mu_3}$$

m being the molal concentration (moles of solute per kilogram of the solvent) and the \bar{v} the partial specific volume. The parameters D and D' are related in the following way:

$$D = D' \frac{\partial n / \partial c_2}{\partial n / \partial \phi_1}$$

and

$$D' = \frac{(\partial n / \partial c_2)_\mu - \partial n / \partial c_2}{\partial n / \partial \phi_1} \quad (14.15)$$

where $(\partial n / \partial c_2)_\mu$ is the refractive index of the polymer solution dialyzed against the solvent mixture and $\partial n / \partial c_2$ is not dialyzed.

14.3.3 Copolymers

The problem with copolymers is also caused by the complexity of the dn/dc values. There are three factors to be considered:

1. The interference in the differential refractive index of one homopolymer by that of the other.
2. The low dn/dc value in certain solvents, which is difficult to measure.
3. The fluctuation in chain composition. The value of molecular weight of the same copolymer often varies with the dn/dc of the solvent.

Assuming that the refractive index increments of a copolymer chain are proportional to their composition, Stockmayer et al. (1955) suggested the following equation:

$$\left(\frac{I}{K'c}\right)_{c \rightarrow 0} = \left(\frac{dn}{dc}\right)_0^2 \bar{M}_w + 2b \left(\frac{dn}{dc}\right)_0 \langle M \Delta x \rangle + b^2 \langle M(\Delta x)^2 \rangle \quad (14.16)$$

where

$$b = \left(\frac{dn}{dc}\right)_A - \left(\frac{dn}{dc}\right)_B$$

A, B being monomers of two different types. The other two terms are defined as

$$\begin{aligned} \langle M \Delta x \rangle &= \sum w_i M_i(\Delta x)_i \\ \langle M(\Delta x)^2 \rangle &= \sum w_i M_i(\Delta x)_i^2 \end{aligned}$$

where x_i is the composition of the copolymer sample (i.e., a volume fraction of monomer i), w is the weight fraction, and M is the molecular weight. In the above equation there are three unknowns: \bar{M}_w , $\langle M \Delta x \rangle$, and $\langle M(\Delta x)^2 \rangle$. If the light-scattering experiment is carried out for the copolymer in three different solvents, we can solve for three unknowns in three linear equations and thereby get an accurate value of \bar{M}_w .

Another proposal was made by Bushuk and Benoit (1958):

$$\bar{M}_{ap} = \bar{M}_w + 2P \frac{v_A - v_B}{v_0} + Q \left(\frac{v_A - v_B}{v_0}\right)^2 \quad (14.17)$$

where

$$\begin{aligned} P &= \frac{1}{2}(1 - x_0)(\bar{M}_w - \bar{M}_B) - x_0(\bar{M}_w - \bar{M}_A) \\ Q &= x_0(1 - x_0)(\bar{M}_A + \bar{M}_B - \bar{M}_w) \\ v_A &= \left(\frac{dn}{dc}\right)_A \\ v_B &= \left(\frac{dn}{dc}\right)_B \\ v_0 &= \left(\frac{dn}{dc}\right)_{\text{copolymer of uniform composition}} \end{aligned}$$

In the above equations, x_0 is the average composition of the copolymer and A and B are two different homopolymers. The equation also contains three parameters to be

determined: M_w , P , and Q . Likewise, if we measure the light-scattering intensities from the polymeric solutions in three different solvent, the three parameters could be determined by solving the three equations simultaneously.

14.3.4 Correction of Anisotropy and Depolarization of Scattered Light

If the scattering molecules are not isotropic, we must make corrections. The correction factor for anisotropy involves the depolarization ratio P_u , which is defined as the ratio of the horizontal to the vertical components of the scattered light at a 90° angle when the incident light is unpolarized. The correction factor is $(6 - 7P_u)/(6 + 6P_u)$ for R_{90° and $(3 - 7P_u)/(6 + 7P_u)$ for τ_{90° .

14.4 INTERNAL INTERFERENCE

For a macromolecule with molecular weight greater than 300,000, the molecule does not act as a single dipole; that is, there is no longer one scattering point. Instead, there may be more than one scattering point. Consider the two-scattering-point system shown in Figure 14.2. When the phase differences between rays that are scattered at two points, P_i and P_j , in a molecule are more than $\lambda/20$ apart, nonspherical scattering envelopes form (Figure 14.3). Mathematical analysis of the situation may be described as follows. Consider the two scattering points O and B in Figure 14.4. The vectors \mathbf{s}_0 (incident) and \mathbf{s} (scattered) are unit vectors ($|\mathbf{s}_0| = |\mathbf{s}| = 1$) that define the propagation directions of the incident and scattered rays. The angles F and G specify the orientation of the vector \mathbf{r} relative to the vector $\mathbf{s} - \mathbf{s}_0$. The probability that \mathbf{r} simultaneously points between the angles F and $F + dF$ and G and $G + dG$ is

$$\frac{\sin F dF dG}{4\pi}$$

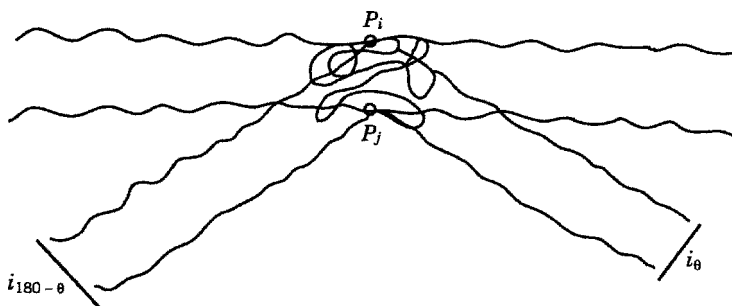


FIGURE 14.2 Model of internal interference.

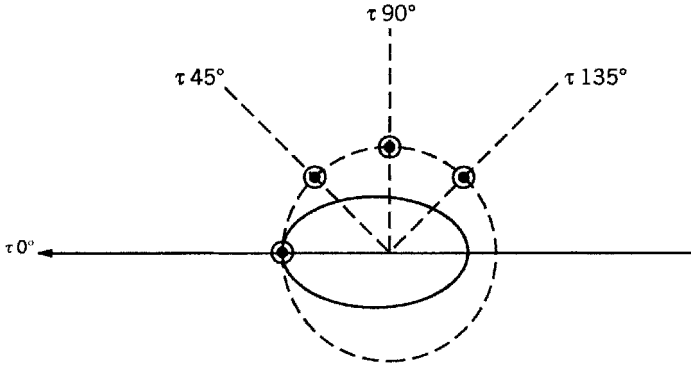


FIGURE 14.3 Scattering envelopes: ---, symmetrical, no destructive interference; —, scattering envelope, nonsymmetrical, with destructive interference.

The term 4π is the sum of all possible orientations that can be obtained from

$$\int_0^{2\pi} \int_0^\pi \sin F \, dF \, dG = 4\pi$$

The amplitude A (i.e., OA) is related to the phase shift ϕ' , our major interest here, between scattered points (O and B). Their average values are related in the form

$$\langle A \rangle \sim \langle \cos \phi' \rangle$$

On a geometric basis, the phase shift ϕ' can be expressed as

$$\phi' = gr \cos F$$

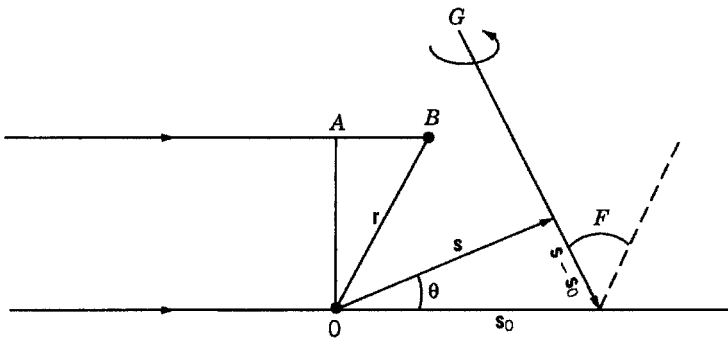


FIGURE 14.4 Coordinates of internal interference.

where

$$g = \frac{4\pi}{\lambda} \sin \frac{\theta}{2}$$

The average phase shift can thus be calculated:

$$\langle \cos \phi' \rangle = \int_0^{2\pi} \int_0^\pi \cos(gr \cos F) \frac{\sin F \, dF \, dG}{4\pi}$$

Note: $(\sin F \, dF \, dG)/4\pi$ is a distribution or probability function.

To carry out the integration, we change the variable to $x = gr \cos F$; hence,

$$dx = -gr \sin F \, dF$$

and the integration limits change from $F = 0$ to $x = -gr$ and from $F = \pi$ to $x = gr$. Then

$$\langle \cos \phi' \rangle = \frac{1}{4\pi} \frac{2\pi}{gr} \int_{-gr}^{gr} \cos x \, dx = \frac{\sin gr}{gr}$$

This result shows that the average amplitude scattered by a rotating molecule exhibits g - (or θ) and r -dependent minima and maxima which could possibly be used to determine the internuclear distance r .

Debye suggested the use of $\langle \cos \phi' \rangle$ as a correction factor for the (internal) interference. It is expressed in the form of $1/P(\theta)$ or $1/P(g)$:

$$P(\theta) = P(g) = \sum_i \sum_j \frac{\sin gr_{ij}}{gr_{ij}} \quad (14.18)$$

where r_{ij} is the distance between two elements i and j and the double summation is performed over all pairs of scattering elements.

The light-scattering equation is now written as

$$\begin{aligned} \frac{Kc}{R_\theta} &= \frac{1}{MP(\theta)} + 2A_2c && \text{(with interference)} \\ \frac{Kc}{R_\theta} &= \frac{1}{M} + 2A_2c && \text{(without interference)} \end{aligned} \quad (14.19)$$

The interference factor $P(\theta)$ depends on the shape of the molecules:

- For spheres

$$P(\theta) = \left[\frac{3}{x^3} (\sin x - x \cos x) \right]^2$$

where

$$x = 2\pi \frac{d}{\lambda} \sin \frac{\theta}{2}$$

If the values of x are small, we have

$$\frac{1}{P(\theta)} = 1 + \frac{4\pi^2}{5} \left(\frac{d}{\lambda}\right)^2 \sin^2 \frac{\theta}{2} + \dots \quad (14.20)$$

- For coils

$$P(\theta) = \frac{2}{x^2} [e^{-x} - (1-x)]$$

$$x = \frac{8}{3} \pi^2 \sin^2 \frac{\theta}{2} \frac{\langle R^2 \rangle}{\lambda^2}$$

If the values of x are small, we have

$$\frac{1}{P(\theta)} = 1 + \frac{8\pi^2 \langle R^2 \rangle}{9 \lambda^2} \sin^2 \frac{\theta}{2} + \dots \quad (14.21)$$

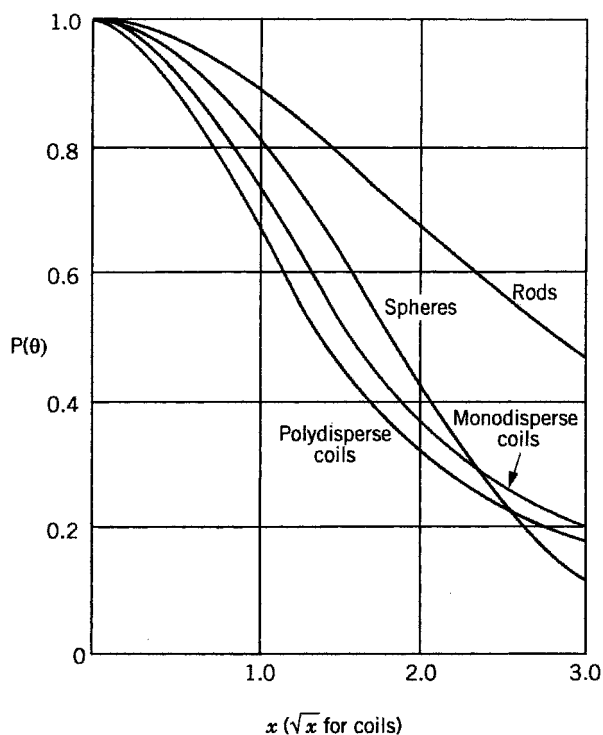


FIGURE 14.5 Theoretical curves for spheres, rods, and coils. [Source: Doty and Steiner (1950) with permission of Dr. Doty and American Institute of Physics].

- For rods

$$P(\theta) = \frac{1}{x} \int_0^{2x} \frac{\sin x}{x} dx - \left(\frac{\sin x}{x} \right)^2$$

$$x = 2\pi \frac{l}{\lambda} \sin \frac{\theta}{2}$$

If the values of x are small, we have

$$\frac{1}{P(\theta)} = 1 + \frac{4\pi^2}{9} \left(\frac{1}{\lambda} \right)^2 \sin^2 \frac{\theta}{2} + \dots \quad (14.22)$$

Thus, from the interference factor $P(\theta)$ we can obtain the values for d , the diameter if the molecule is in the shape of a sphere; $\langle R^2 \rangle^{1/2}$, the root-mean-square end-to-end distance if the molecule is in the shape of coils; and l , the length of the molecule if the molecule is in the shape of a rod. Figure 14.5 shows the theoretical curves for spheres, rods, and coils.

We may also take the ratio $P_{45}/P_{135} = z$, that is, through substitution of $\theta = 45^\circ$ and $\theta = 135^\circ$ in the above equations, and plot $1/P_{90}$ versus z or P_{90} versus z . The quantity z is called the dissymmetry ratio. If $z = 1$, the particles are small compared to the wavelength of light. If $z > 1$, we can use it to evaluate d , $\langle R^2 \rangle^{1/2}$, or l . In practice, one fits the data by trial and error to the theoretical curves (coils, spheres, or rods) and then determines the dimensions of the macromolecules under study (d , $\langle R^2 \rangle^{1/2}$, l).

14.5 DETERMINATION OF MOLECULAR WEIGHT AND RADIUS OF GYRATION BY THE ZIMM PLOT

The Zimm plot is used to determine the molecular weight and radius of gyration of a macromolecule simultaneously regardless of its shape. There is no trial-and-error method or any information about the shape. Expanding each term under the summation sign in terms of a power series,

$$\sin x = x - \frac{x^3}{3!} + \frac{x^5}{5!} - \dots$$

we have

$$P(\theta) = P(g) = \sum_i \sum_j \frac{\sin gr_{ij}}{gr_{ij}}$$

$$= \sum_i \sum_j \left(1 - \frac{g^2 r_{ij}^2}{3!} + \frac{g^4 r_{ij}^4}{5!} - \dots \right)$$

where

$$g = \frac{4\pi}{\lambda} \sin \frac{\theta}{2}$$

Neglecting the higher terms, we have

$$P(\theta) = 1 - \frac{g^2}{3!} \sum_i \sum_j r_{ij}^2$$

But

$$\sum_i \sum_j r_{ij}^2 = 2R_g^2 = 2S^2$$

where $R_g = S$ is the radius of gyration. Hence

$$\begin{aligned} P(\theta) &= 1 - \frac{16\pi^2}{3 \cdot 2\lambda^2} \sin^2 \frac{\theta}{2} (2S^2) \\ &= 1 - \frac{16\pi^2}{3\lambda^2} S^2 \sin^2 \frac{\theta}{2} \end{aligned}$$

Notice that

$$\frac{1}{1-x} = 1 + x + \dots$$

So

$$\frac{1}{P(\theta)} = 1 + \frac{16\pi^2}{3\lambda^2} S^2 \sin^2 \frac{\theta}{2} \quad (14.23)$$

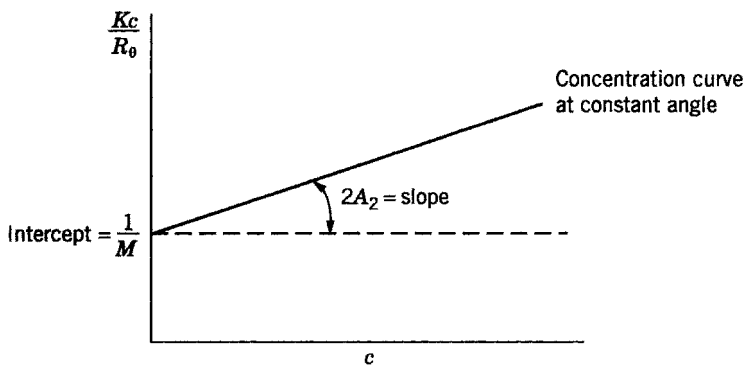


FIGURE 14.6 Determination of molecular weight and second virial coefficient.

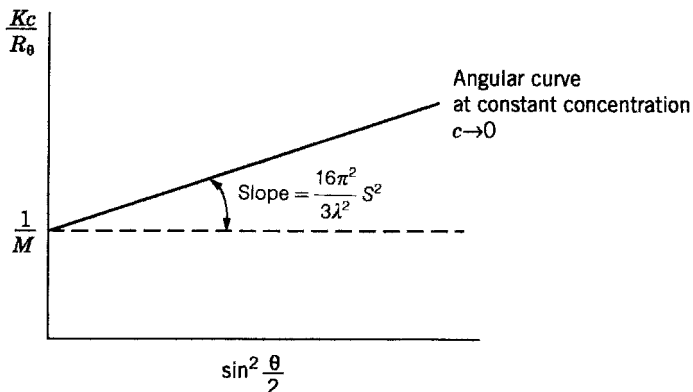


FIGURE 14.7 Determination of radius of gyration.

We thus have the following expressions, all about the light scattering:

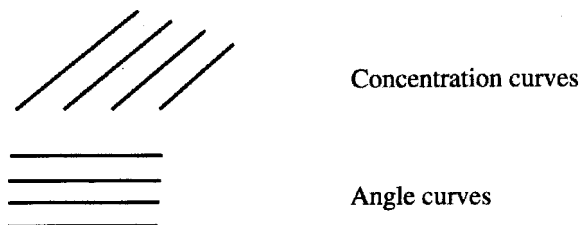
$$\frac{Kc}{R_\theta} = \frac{1}{MP(\theta)} + 2A_2c + \dots \quad (\text{general})$$

$$\lim_{\theta \rightarrow 0} \frac{Kc}{R_\theta} = \frac{1}{M} + 2A_2c + \dots \quad (\text{no internal interference})$$

Equation (14.25) is plotted in Figure 14.6. Equation (14.24) is rewritten as

$$\lim_{c \rightarrow 0} \frac{Kc}{R_\theta} = \frac{1}{MP(\theta)} = \frac{1}{M} \left(1 + \frac{16\pi^2}{3\lambda^2} S^2 \sin^2 \frac{\theta}{2} + \dots \right) \quad (\text{with internal interference})$$

and is plotted in Figure 14.7. The combination of the two plots in Figures 14.6 and 14.7 gives the Zimm plot of Figure 14.8 (see the Appendix). In the Zimm plot k is an arbitrary constant to adjust the size of the plot. The lines are defined as follows:



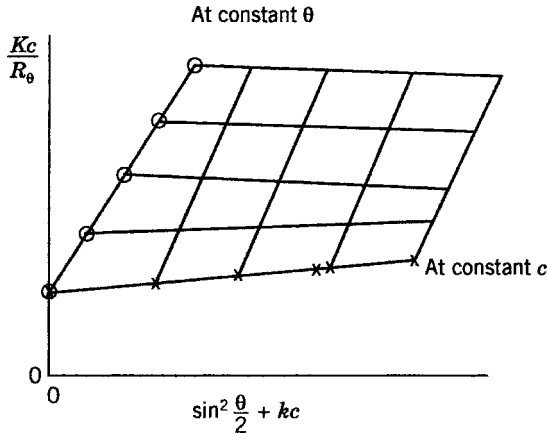


FIGURE 14.8 Zimm plot.

From the plot we obtain

$$\text{Intercept} = \lim_{\substack{c \rightarrow 0 \\ \theta \rightarrow 0}} = \frac{1}{M}$$

$$\frac{\text{Limiting slope of } c \text{ curve, } c \rightarrow 0}{\text{Intercept}} = \frac{16\pi^2}{3\lambda^2} S^2$$

$$\frac{\text{Limiting slope of } \theta \text{ curve, } \theta \rightarrow 0}{\text{Intercept}} = 2A_2$$

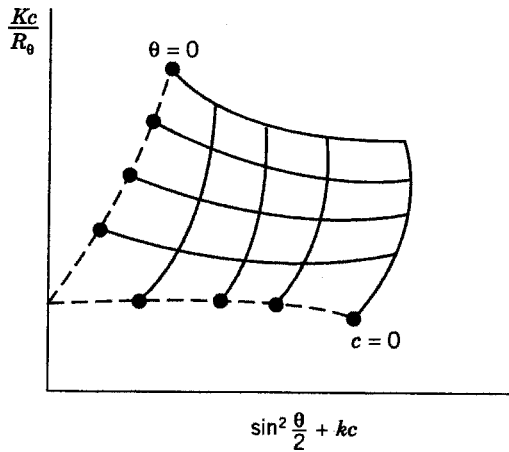


FIGURE 14.9 External interference as shown in the Zimm plot. In these cases, there is not only internal interference but also external interference in light scattering. So far there is no simple theory to treat external interference in light scattering.

The radius of gyration, S^2 , gives an indication as to whether a chain is compact or extended. If additional information, such as shape, is available, we may estimate the size:

$$S^2 = \frac{3d^2}{20} \quad \text{for a sphere}$$

$$S^2 = \frac{l^2}{12} \quad \text{for a rod}$$

$$S^2 = \frac{\langle R^2 \rangle}{6} \quad \text{for a coil}$$

Sometimes, the Zimm plot is shown in a distorted form, as in Figure 14.9.

APPENDIX EXPERIMENTAL TECHNIQUES OF THE ZIMM PLOT

Measurement

First a stock solution is prepared, for example, 5.2153×10^{-3} g/mL, and, labeled as 1 unit. The dilution is labeled as $\frac{1}{4}$, $\frac{2}{4}$, and $\frac{3}{4}$ units. Thus, the concentrations are always 1, 2, 3, and 4 (unit: $\frac{1}{4}$ stock concentration, e.g., $\frac{1}{4}(5.2153 \times 10^{-3}$ g/mL) or $\frac{1}{4}$, $\frac{2}{4}$, $\frac{3}{4}$, 1 (unit: stock concentration).

Light scattering is then measured: I , the intensity of scattered light. Note that

$$I = R_\theta$$

Recall that

$$K \left(\frac{c}{I} \right) = \frac{1}{M} P^{-1}(\theta) + 2A_2c$$

where

$$K = \frac{2\pi^2}{\lambda^4 N_A} n^2 \left(\frac{dn}{dc} \right)^2 k'$$

where k' is the instrument constant. For example,

$$k' = \frac{I_B}{R_B}$$

where B is benzene, used as a standard. The term I_B is the intensity of benzene selected (e.g., 0.100, 0.200, 1.00) related to the sensitivity. The values of R_B may be

determined experimentally:

$$R_B = \frac{I_{90^\circ}}{I_{0^\circ}} = 16.3 \times 10^{-6} \quad \lambda = 546 \text{ nm}$$

$$K = \frac{2\pi^2}{\lambda^4 N_A} n^2 \left(\frac{dn}{dc}\right)^2 \frac{I_B}{R_B}$$

$$\left(\frac{2\pi^2}{\lambda^4 N R_B} = 0.2249 \text{ for } \lambda = 546 \text{ nm}\right)$$

The dn/dc values are obtained from the measurement of the solutions (same solutions as for light-scattering apparatus) with a differential refractometer (a separate instrument).

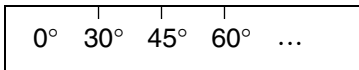
Treatment of Data

Data are presented in the following form:

<i>c</i>	<i>c/I</i>			
	30°	45°	60°	...
1/4	
1/2	
3/4				
1				

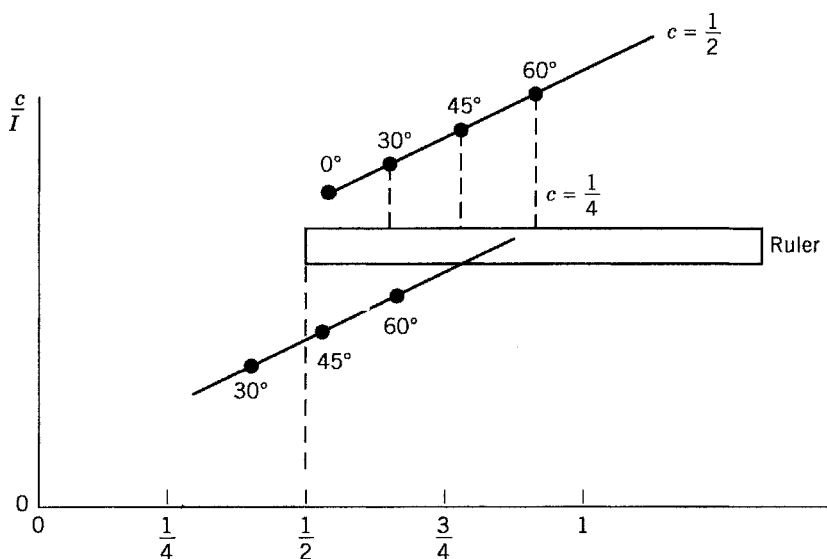
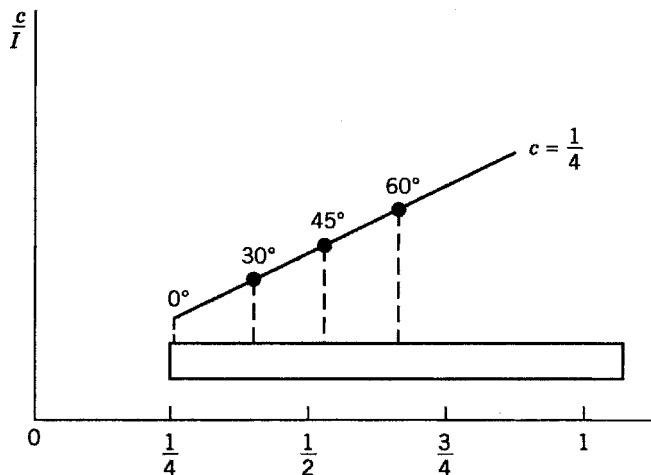
Draw a ruler on graph paper:

θ	$\sin^2 \theta/2$
30°	0.067
37.5°	0.101
45°	0.146
...	

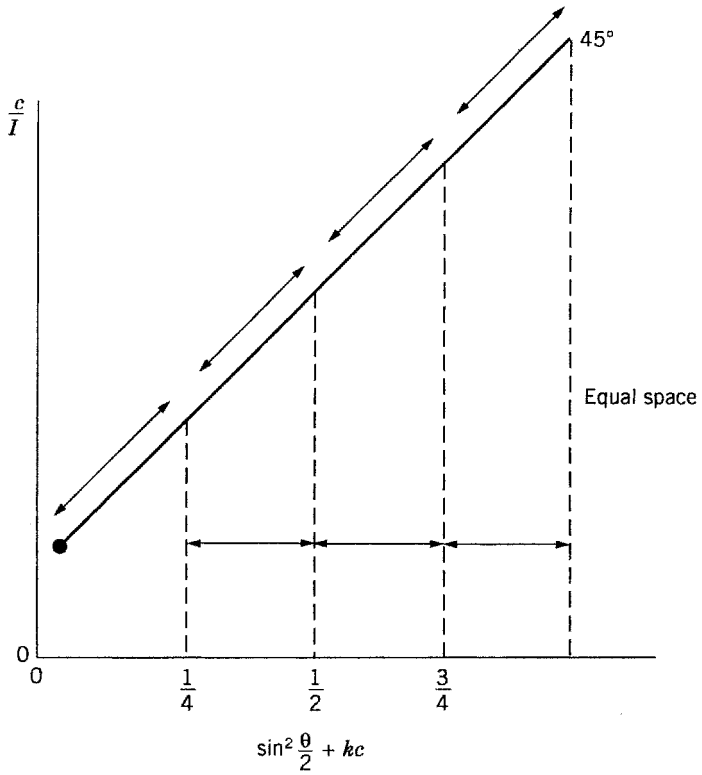


$$\sin^2 \frac{\theta}{2}$$

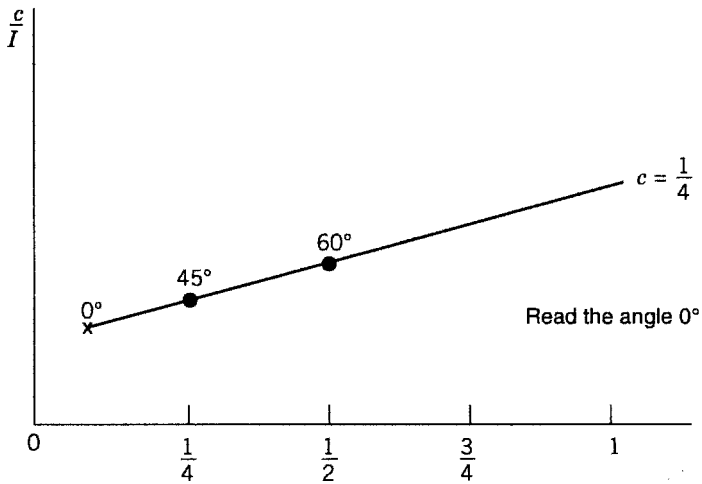
Arbitrarily select $0, \frac{1}{4}, \frac{1}{2}, \frac{3}{4}, 1$ units for the abscissa: For the $c = \frac{1}{4}$ line, we line up the 0 point of the ruler to the point $\frac{1}{4}$ on the abscissa. Plot and then proceed to $c = \frac{1}{2}$, and so forth.



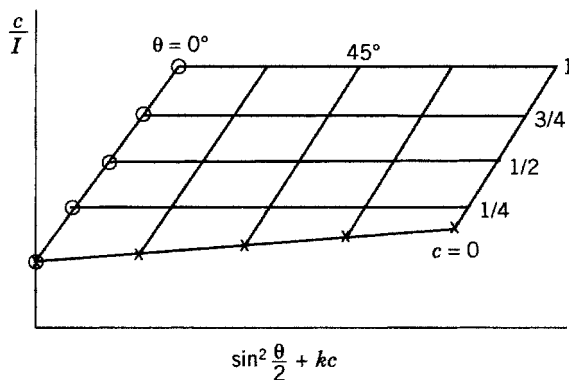
To extrapolate to 45° , for example, we first connect the four points at 45° from the four lines of $c(\frac{1}{4}, \frac{1}{2}, \frac{1}{3}, 1)$ and extend to $c = 0$.



Then extrapolate $c = \frac{1}{4}$. We connect the points at different angles and extend to zero angle.



Combining yields



REFERENCES

- Bushuk, W., and H. Benoit, *Can. J. Chem.* **36**, 1616 (1958).
- Casassa, E. F., and H. Eisenberg, *J. Phys. Chem.* **64**, 753 (1960).
- Cassada, E. F., and H. Eisenberg, *J. Phys. Chem.* **65**, 427 (1961).
- Debye, P., *J. Appl. Phys.* **15**, 338 (1944).
- Debye, P., *J. Phys. Coll. Chem.* **51**, 18 (1947).
- Del Rosario, N. O., and S. F. Sun, *Can. J. Chem.* **51**, 3781 (1973).
- Doty, P., and R. F. Steiner, *J. Chem. Phys.* **18**, 1211 (1950).
- Edsall, J. T., H. Edelhoeh, R. Lontre, and P. R. Morrison, *J. Am. Chem. Soc.* **72**, 4641 (1950).
- Eisenberg, H., *J. Chem. Phys.* **36**, 1837 (1962).
- Eisenberg, H., and E. F. Cassassa, *J. Polym. Sci.* **47**, 29 (1960).
- Inoue, H., and S. N. Timasheff, *J. Am. Chem. Soc.* **90**, 1890 (1968).
- Kerker, M., *The Scattering of Light and Other Electromagnetic Radiation*. New York: Academic, 1969.
- Krause, S., *J. Phys. Chem.* **65**, 1618 (1961).
- Rayleigh, Lord, *Philos. Mag.* **41**, 447 (1871).
- Rayleigh, Lord, *Philos. Mag.* **12**, 81 (1881).
- Read, B. E., *J. Chem. Soc.* 382 (1960).
- Stacey, K. A., *Light Scattering in Physical Chemistry*. London: Butterworths Scientific, 1956.
- Stockmayer, W. H., L. D. Moore, Jr., M. Fixman, and B. N. Epstein, *J. Polym. Sci.* **16**, 517 (1955).
- Tanford, C., *Physical Chemistry of Macromolecules*. New York: Wiley, 1961.
- Tyndall, J., *Philos. Mag.* **37**, 384 (1869).
- Tyndall, J., *Proc. Roy. Soc. (London)* **17**, 223 (1869).
- Vollmert, B., *Polymer Chemistry*. New York: Springer, 1973.
- Zimm, B. H., *J. Chem. Phys.* **16**, 1093 (1948a).
- Zimm, B. H., *J. Chem. Phys.* **16**, 1099 (1948b).

PROBLEMS

- 14.1** The refractive index of dioxane at 25°C is 1.4232 and the refractive index increment of the system poly(methyl methacrylate) in dioxane is $0.065 \text{ cm}^3 \text{ g}^{-1}$. Given the following turbidities of the solutions of poly(methyl methacrylate) in dioxane with benzene as reference, determined at $\lambda = 5461 \text{ \AA}$, calculate (a) the molecular weight and (b) the radius of gyration of the polymer.

Concentration	C/I										
	30°	37.5°	45°	60°	75°	90°	105°	120°	135°	142.5°	150°
$\frac{1}{4}$	2.37	2.34	2.35	2.46	2.59	2.74	2.89	3.00	3.12	3.18	3.16
$\frac{1}{2}$	3.53	3.52	3.51	3.62	3.79	3.97	4.12	4.20	4.35	4.41	4.35
$\frac{3}{4}$	4.59	4.55	4.55	4.67	4.85	5.05	5.21	5.32	5.46	5.49	5.35
1	5.49	5.43	5.46	5.56	5.68	6.21	6.41	6.58	6.76	6.80	6.71

$$\text{Stock solution} = 5.315 \times 10^{-3} \text{ g/cm}^3$$

$$I_B = 0.100$$

$$R_B = I_{90}/I_0 = 16.3 \times 10^{-6} \text{ for } \lambda_0 = 5461 \text{ \AA}$$

- 14.2** Light-scattering measurements were carried out for bovine serum albumin in 0.1 M KI solution at the isoelectric point ($\text{pH} = 5.17, z_2 = 0$). The wavelength was set at 546 nm and the experiment was performed at room temperature. The following turbidity data were obtained:

Concentration (g/mL) $\times 10^3$	$\tau \times 10^4$
0	0.213
0.936	2.88
1.902	5.75
2.801	8.18
3.701	10.59
5.590	15.37

Separate experiments were carried out for the determination of the refractive index and differential refractive increment. The value of dn/dc_2 was found to be 0.168 and that of n was 1.3342.

- (a) Calculate the Debye factor H .
 (b) Plot $HC_2/\Delta\tau$ versus C_2 to determine the molecular weight and the second virial coefficient B .
 (c) Suggest a method by which the values of β_{23} and β_{22} could be determined (Edsall et al., 1950; Inoue and Timasheff, 1968; Del Rosario and Sun, 1973).

- 14.3** A protein dissolved in water ($n_2 = 1.33$) is known to be 1200 Å in diameter. Calculate the degree of dissymmetry in light scattering at $\lambda = 5461$ Å.
- 14.4** The angular dissymmetry of tobacco mosaic virus is 1.90 with light of $\lambda = 5461$ Å, its density is 2 g/cm³, and its molecular weight is 4.45×10^7 . Decide whether the molecule is in the shape of a rod or a sphere.
- 14.5** Light-scattering measurements at 436 nm of a polystyrene–poly(methyl methacrylate) copolymer in the three different solvents give the following data:

	$\left(\frac{dn}{dc}\right)_0$	$M_{\text{app}} \times 10^{-6}$
Butanone	0.184	1.05
1,2-Dichloroethane	0.135	0.97
Toluene	0.075	1.11

The quantity $b = (dn/dc)_A - (dn/dc)_B$ was found to be 0.117 at 436 nm. Calculate the \bar{M}_w of the copolymer. *Hint:*

$$\left(\frac{I_\theta}{K'c}\right)_{\substack{c \rightarrow 0 \\ \theta \rightarrow 0}} = \left(\frac{dn}{dc}\right)_0^2 M_{\text{app}}$$

$$\left(\frac{I_\theta}{K'c}\right)_{\substack{c \rightarrow 0 \\ \theta \rightarrow 0}} = \left(\frac{dn}{dc}\right)_0^2 \bar{M}_w + 2b \left(\frac{dn}{dc}\right)_0 \langle M \Delta X \rangle + b^2 \langle M(\Delta X)^2 \rangle$$

(Krause, 1961).

15

FOURIER SERIES

This chapter gathers the important formulas of the Fourier series and related mathematical subjects. Most of these formulas have rigorous proofs. Some of the proofs are attributed to great mathematicians and often bear the mathematician's name, which is a common practice in naming the laws of physics and chemical reactions in organic chemistry. Although the purpose of this chapter is to provide a background for Chapters 16, 17, 19, and 20, the way we present the material here is more than just as background. The mathematics here is an independent topic in itself, except that we have omitted the proofs in order to remain within the scope of this book.

15.1 PRELIMINARIES

Definition 1 A function $f(x)$ is called periodic if it follows the condition

$$f(x) = f(x + kp)$$

where p is the period and k is an integer (positive or negative).

Examples:

$$f(x) = \cos x$$

or

$$f(x) = \sin x$$

and

$$\cos x = \cos(x + 2\pi) \quad \sin x = \sin(x + 2\pi)$$

Here $p = 2\pi$.

Definition 2 If $f(x)$ and $g(x)$ are two periodic functions, their inner product (fg) is defined as

$$(f, g) = \int_{-\pi}^{\pi} f(x)g(x) \, dx \quad \text{or} \quad (f, g) = \int_{-\infty}^{\infty} f(x)g(x) \, dx$$

Definition 3 Two functions $f(x)$ and $g(x)$ are orthogonal if and only if

$$\int_{-\infty}^{\infty} f(x)g(x) \, dx = 0$$

Definition 4 A function $f(x)$ is said to be odd if and only if the quantity $f(-x) = -f(x)$ holds for all x 's in the given domain; $f(x)$ is an even function if and only if $f(-x) = f(x)$.

Following are some examples. The terms $\cos nx$ and $\sin mx$ form orthogonal functions as seen in their inner product:

$$\begin{aligned} \int_{-\pi}^{\pi} \cos mx \cos nx \, dx &= \pi \delta_{nm} \\ \int_{-\pi}^{\pi} \sin mx \sin nx \, dx &= \pi \delta_{nm} \\ \int_{-\pi}^{\pi} \sin mx \cos nx \, dx &= 0 \end{aligned}$$

where δ_{mn} is the Kronecker delta, defined as

$$\delta_{mn} = \begin{cases} 0 & \text{if } m \neq n \\ 1 & \text{if } m = n \end{cases}$$

Note that $\sin mx$ are odd functions and $\cos mx$ are even functions. The functions e^x and $\log x$ are neither odd nor even. It can be shown that for an odd function

$$\int_{-\infty}^{\infty} f(x) \, dx = 0$$

15.2 FOURIER SERIES

15.2.1 Basic Fourier Series

The basic Fourier series is the trigonometric series

$$f(x) = \frac{1}{2}a_0 + \sum_{n=1}^{\infty} (a_n \cos nx + b_n \sin nx)$$

in which

$$a_n = \frac{1}{\pi} \int_{-\pi}^{\pi} f(x) \cos nx \, dx \quad n = 0, 1, 2, \dots$$

$$b_n = \frac{1}{\pi} \int_{-\pi}^{\pi} f(x) \sin nx \, dx \quad n = 1, 2, \dots$$

where f is defined on the interval $(-\pi, \pi)$.

Example 1 Fourier Series of $f(x)$ Let

$$f(x) = \begin{cases} 0 & -\pi < x < 0 \\ \pi & 0 < x < \pi \end{cases}$$

and $f(x)$ is defined by periodicity outside the basic interval. Then the Fourier series of $f(x)$ is

$$f(x) = \frac{1}{2}\pi + 2\left[\sin x + \frac{1}{3}\sin 3x + \frac{1}{5}\sin 5x + \dots\right]$$

This converges to $f(x)$ for $x \neq n\pi$ and to $\pi/2$ for $x = n\pi$.

Figure 15.1 illustrates the behavior of the partial sums.

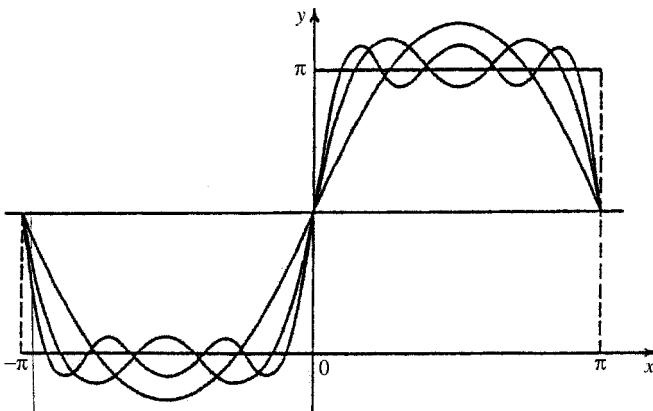


FIGURE 15.1 Representation of $f(x) = 0 < |x| < \pi$ by Fourier series.

Example 2 Fourier Series of x Since $x \cos nx$ is an odd function,

$$a_n = \frac{1}{\pi} \int_{-\pi}^{\pi} x \cos nx \, dx = 0$$

and since $x \sin nx$ is even,

$$b_n = \frac{1}{\pi} \int_{-\pi}^{\pi} x \sin nx \, dx = \frac{2}{\pi} \int_{-\pi}^{\pi} x \sin nx \, dx$$

Thus we have

$$\begin{aligned} b_n &= \frac{2}{\pi} \int_0^{\pi} x \sin nx \, dx = -\frac{2}{n\pi} x \cos nx \Big|_0^{\pi} + \frac{1}{n\pi} \int_0^{\pi} \cos nx \, dx \\ &= -\frac{2}{n} \cos n\pi = (-1)^{n+1} \frac{2}{n} \end{aligned}$$

and the Fourier series of x is

$$x = \sum_1^{\infty} \frac{2}{n} (-1)^{n+1} \sin nx$$

Note: The series

$$2 \left[\sin x - \frac{1}{2} \sin 2x + \frac{1}{3} \sin 3x - \frac{1}{4} \sin 4x + \dots - \dots \right]$$

converges to x in $\{-\pi < x < \pi\}$ and to 0 at π and $-\pi$.

Example 3 The Fourier series of f is defined by

$$f(x) = \begin{cases} 0 & -\pi < x < 0 \\ 1 & 0 \leq x \leq \pi \end{cases}$$

Here we can calculate

$$a_0 = \frac{1}{\pi} \int_{-\pi}^{\pi} f(x) \, dx = \frac{1}{\pi} \int_0^{\pi} 1 \, dx = 1$$

For $n \geq 1$,

$$\begin{aligned} a_n &= \frac{1}{\pi} \int_0^{\pi} \cos nx \, dx = \frac{1}{n\pi} \sin nx \Big|_0^{\pi} = 0 \\ b_n &= \frac{1}{\pi} \int_0^{\pi} \sin nx \, dx = -\frac{1}{n\pi} \cos nx \Big|_0^{\pi} \\ &= -\frac{1}{n\pi} [\cos n\pi - \cos 0] = -\frac{1}{n\pi} [(-1)^n - 1] \\ &= \begin{cases} 0 & \text{if } n \text{ is even} \\ \frac{1}{n\pi} & \text{if } n \text{ is odd} \end{cases} \end{aligned}$$

Thus the Fourier series defined above is

$$f(x) \sim \frac{1}{2} + \frac{1}{\pi} \sum_0^{\infty} \frac{\sin(2k+1)x}{2k+1}$$

15.2.2 Fourier Sine Series

If f is an odd function, $a_n = 0$, and

$$b_n = \frac{2}{\pi} \int_0^{\pi} f(x) \sin nx \, dx$$

Then

$$f(x) = \frac{2}{\pi} \sum_{n=1}^{\infty} \sin nx \int_0^{\pi} f(y) \sin ny \, dy$$

This Fourier sine series will serve to represent odd functions on the interval $(-\pi, \pi)$ or odd periodic functions of period 2π for all x .

Example: The complete Fourier series for x is a sine series since x is odd.

15.2.3 Fourier Cosine Series

If f is an even function on the interval $(-\pi, \pi)$ its Fourier coefficients have the values

$$a_n = \frac{2}{\pi} \int_0^{\pi} f(x) \cos nx \, dx \quad n = 0, 1, 2, \dots$$

and $b_n = 0$ ($n = 1, 2, \dots$). Thus its Fourier series reduces to

$$f(x) = \frac{1}{\pi} \int_0^{\pi} f(y) \, dy + \frac{2}{\pi} \sum_{n=1}^{\infty} \cos nx \int_0^{\pi} f(y) \cos ny \, dy$$

This is the *Fourier cosine series* corresponding to f on the interval $(0, \pi)$ with respect to the orthogonal set $\{\cos nx\}$, $n = 0, 1, 2, \dots$.

Example: The cosine series of $|x|$ —Here

$$a_0 = \frac{2}{\pi} \int_0^{\pi} x \, dx = \frac{2}{\pi} \frac{\pi^2}{2} = \pi$$

and for $n > 0$

$$a_n = \frac{2}{\pi} \int_0^{\pi} x \cos nx \, dx = \frac{2}{\pi n^2} [(-1)^n - 1] = \begin{cases} 0 & n \text{ even} \\ \frac{-4}{\pi n^2} & n \text{ odd} \end{cases}$$

Thus

$$|x| = \pi - \frac{4}{\pi} \sum_1^{\infty} \frac{\cos(2k+1)x}{(2k+1)^2}$$

15.2.4 Complex Fouries Series

A complex number is defined as $z = a + ib$, where a and b are real numbers and $i = \sqrt{-1}$; a complex variable is defined as $z = x + iy$. When complex numbers are involved,

$$f(x) = \sum_{-\infty}^{\infty} \alpha_n e^{inx}$$

and

$$\alpha_n = \frac{1}{2\pi} \int_a^{a+2\pi} f(y) e^{-iny} dy$$

Example: The Fourier spectrum is a complex Fourier series:

$$f(t) = \sum_{-\infty}^{\infty} \alpha_n e^{in\omega t}$$

with

$$\alpha_n = \frac{\omega}{2\pi} \int_{-\pi/\omega}^{\pi/\omega} f(t) e^{-in\omega t} dt$$

where ω is frequency and t is time; $f(t)$ is in the time domain and α_n is in the frequency domain.

15.2.5 Other Forms of Fourier Series

If we introduce a new independent variable t ,

$$t = \frac{\pi}{c} x$$

such that $-\pi < t < \pi$ when $-c < x < c$, then $f(x) = f(ct/\pi)$. The Fourier series is now in the form

$$f(x) = \frac{1}{2} a_0 + \sum_{n=1}^{\infty} \left(a_n \cos \frac{n\pi x}{c} + b_n \sin \frac{n\pi x}{c} \right)$$

where

$$a_n = \frac{1}{c} \int_{-c}^c f(x) \cos \frac{n\pi x}{c} dx \quad n = 0, 1, 2, \dots$$

$$b_n = \frac{1}{c} \int_{-c}^c f(x) \sin \frac{n\pi x}{c} dx \quad n = 1, 2, \dots$$

This is the form of the Fourier series with functions of period $2c$, an extension of Definition 1.

15.3 CONVERSION OF INFINITE SERIES INTO INTEGRALS

If $a = x_0 < x_1 < x_2 \cdots$ forms an unbounded sequence of points and the term

$$\sum_{j=1}^{\infty} c_j f(x_j)$$

is a convergent series, then the series can be converted into an integral:

$$\int_a^{\infty} f(x) d(hx) = \sum_{j=1}^{\infty} c_j f(x_j)$$

This theorem has been rigorously proved by Riemann and Stieltjes. The integral is called the Riemann–Stieltjes integral. The term h itself is also a function of x . If $f(x)$ and $h(x)$ are both bounded on a closed interval $[a, b]$, the Riemann–Stieltjes integral is then in the form $\int_a^b f(x) dh(x)$.

15.4 FOURIER INTEGRALS

Using the Riemann–Stieltjes theorem, we can convert the Fourier series into Fourier integrals. Fourier integrals express $f(x)$ in terms of sine and cosine functions of x in the form

$$f(x) = \int_0^{\infty} [A(\alpha) \cos \alpha x + B(\alpha) \sin \alpha x] d\alpha$$

where

$$A(\alpha) = \frac{1}{\pi} \int_{-\infty}^{\infty} f(y) \cos \alpha y dy$$

$$B(\alpha) = \frac{1}{\pi} \int_{-\infty}^{\infty} f(y) \sin \alpha y dy$$

They are similar to Fourier series, but instead of summation as an operation, we have integration as an operation.

Corresponding to the sine Fourier series and cosine Fourier series, we have sine and cosine Fourier integrals.

The Fourier sine integral is

$$f(x) = \frac{2}{\pi} \int_0^{\infty} \sin \alpha x \int_0^{\infty} f(y) \sin \alpha y \, dy \, d\alpha$$

The Fourier cosine integral is

$$f(x) = \frac{2}{\pi} \int_0^{\infty} \cos \alpha x \int_0^{\infty} f(y) \cos \alpha y \, dy \, d\alpha$$

Similarly, we have the Fourier exponential formula

$$f(x) = \frac{1}{2\pi} \lim_{\beta \rightarrow \infty} \int_{-\infty}^{\infty} e^{-i\alpha x} \int_{-\infty}^{\infty} f(y) e^{i\alpha y} \, dy \, d\alpha \quad -\infty < x < \infty$$

Note: Here we use two well-known formulas:

$$\cos[\alpha(y-x)] = \int_{-\infty}^{\infty} f(y) e^{i\alpha y} \, dy$$

$$\cos[\alpha(y-x)] = \int_{-\infty}^{\infty} f(y) e^{-i\alpha y} \, dy$$

which we have rearranged to write the Fourier integral formula in the form

$$f(x) = \frac{1}{2\pi} \lim_{\beta \rightarrow \infty} \int_0^{\beta} \int_{-\infty}^{\infty} 2f(y) \cos[2(y-x)] \, dy \, d\alpha$$

The following table compares the Fourier series with Fourier integrals.

Fourier Series	Fourier Integrals
$f(x) = \frac{a_0}{2} + \sum_{n=1}^{\infty} (a_n \cos nx + b_n \sin nx)$ $= \frac{a_0}{2} + \sum_{n=1}^{\infty} \frac{1}{\pi} \int_{-\pi}^{\pi} \beta(y) \cos n(x-y) \, dy$ $= \sum_{-\infty}^{\infty} c_n e^{inx}$ $= \frac{1}{2\pi} \sum_{-\infty}^{\infty} \int_{-\pi}^{\pi} \beta(y) e^{in(x-y)} \, dy$	$f(x) = \int_0^{\infty} (a(t) \cos tx + b(t) \sin tx) \, dt$ $= \frac{1}{\pi} \int_0^{\infty} \int_{-\infty}^{\infty} \beta(y) \cos t(x-y) \, dy \, dt$ $= \int_{-\infty}^{\infty} c(t) e^{itx} \, dt$ $= \frac{1}{2\pi} \int_{-\infty}^{\infty} \int_{-\infty}^{\infty} \beta(y) e^{it(x-y)} \, dy \, dt,$

where

$$a_n = \frac{1}{\pi} \int_{-\pi}^{\pi} \beta(y) \cos ny \, dy,$$

$$b_n = \frac{1}{\pi} \int_{-\pi}^{\pi} \beta(y) \sin ny \, dy,$$

$$c_n = \frac{1}{2\pi} \int_{-\pi}^{\pi} \beta(y) e^{-iny} \, dy,$$

$$c_n = \frac{a_n - ib_n}{2}, \text{ when}$$

$$a_{-n} = a_n, \quad b_{-n} = -b_n.$$

where

$$a(t) = \frac{1}{\pi} \int_{-\infty}^{\infty} \beta(y) \cos ty \, dy,$$

$$b(t) = \frac{1}{\pi} \int_{-\infty}^{\infty} \beta(y) \sin ty \, dy,$$

$$c(t) = \frac{1}{2\pi} \int_{-\infty}^{\infty} \beta(y) e^{-ity} \, dy,$$

$$c(t) = \frac{a(t) - ib(t)}{2}.$$

15.5 FOURIER TRANSFORMS

The Fourier sine integral formula can be written in the form

$$f(x) = \frac{2}{\pi} \int_0^{\infty} F_s(\alpha) \sin \alpha x \, d\alpha \quad x > 0 \quad (15.1)$$

where

$$F_s(\alpha) = \int_0^{\infty} f(y) \sin \alpha y \, dy \quad \alpha > 0 \quad (15.2)$$

If f is a given function, then Eq. (15.1) is an integral equation in the function F_s , an equation containing the unknown function in the integrand. The function F_s defined by Eq. (15.2) is the Fourier sine transform of the function f . The transformation Eq. (15.2), which we may abbreviate as $F_s \alpha = S_\alpha \{f\}$, sets up a correspondence between functions f and F_s . The Fourier cosine transform $F_c(\alpha)$ of a function f is

$$F_c(\alpha) = \int_0^{\infty} f(y) \cos \alpha y \, dy = C_\alpha \{f\} \quad \alpha > 0$$

The inverse of the transformation $C_\alpha \{f\}$ is given by the Fourier cosine integral formula

$$f(x) = \frac{2}{\pi} \int_0^{\infty} F_c(\alpha) \cos \alpha x \, d\alpha \quad x > 0$$

Other Fourier transformations include the exponential form

$$\int_{-\infty}^{\infty} f(y) e^{i\alpha y} \, dy = F(\alpha) \quad -\infty < \alpha < \infty$$

15.5.1 Fourier Transform Pairs

These transform equations may be written more symmetrically by putting $c(k) = (1/\sqrt{2\pi})g(k)$. Then we have

$$f(x) = \frac{1}{\sqrt{2\pi}} \int_{-\infty}^{\infty} g(k) e^{ikx} \, dk$$

$$g(k) = \frac{1}{\sqrt{2\pi}} \int_{-\infty}^{\infty} f(t) e^{-ikt} \, dt$$

Two functions f and g related in the above way are called a pair of Fourier transforms; that is, g is the Fourier transform of f and vice versa. The simplest

Fourier transform pairs in mathematics are the sine transforms

$$F(n) = \int_0^{\infty} f(t) \sin nt \, dt \quad 0 < n < \infty$$

$$f(t) = \int_0^{\infty} F(n) \sin nt \, dn \quad 0 < t < \infty$$

and the cosine transforms

$$F(n) = \int_0^{\infty} f(t) \cos nt \, dt \quad 0 < n < \infty$$

$$f(t) = \int_0^{\infty} F(n) \cos nt \, dn \quad 0 < t < \infty$$

The Fourier transform pairs that we used in Chapters 16, 17, 19, and 20 may be summarized as follows.

Spectroscopy The Fourier transform pairs in spectroscopy are

$$A(\nu) = \frac{1}{\pi} \int_{-\infty}^{\infty} f(t) \cos(\nu t) \, dt \quad (\text{absorption spectrum})$$

$$D(\nu) = \frac{1}{\pi} \int_{-\infty}^{\infty} f(t) \sin(\nu t) \, dt \quad (\text{dispersion spectrum})$$

$$F(\nu) = \frac{1}{2\pi} \int_{-\infty}^{\infty} f(t) e^{-i\nu t} \, dt \quad (\text{complex spectrum})$$

$$M(\nu) = \sqrt{[A(\nu)]^2 + [D(\nu)]^2} \quad (\text{magnitude spectrum})$$

$$2|F(\nu)|^2 = \frac{1}{2}[A(\nu)]^2 + [D(\nu)]^2 = P(\nu) \quad (\text{power spectrum})$$

The inverse transform for connecting the frequency domain amplitude to the time domain signal is very similar:

$$f(t) = \int_{-\infty}^{\infty} [A(\nu) \cos(\nu t) + D(\nu) \sin(\nu t)] \, d\nu$$

$$= \int_{-\infty}^{\infty} F(\nu) e^{+i\nu t} \, d\nu$$

For FTIR, we have the pairs

$$F(x) = \int_0^{\infty} A(\nu) \cos(2\pi\nu x) \, dx$$

$$A(\nu) = 2 \int_0^{\infty} F(x) \cos(2\pi\nu x) \, dx$$

where $A(v)$ is the interferogram for a polychromatic source while $F(x)$ is the actual interferogram.

NMR All the information of an NMR spectrum is contained in the frequency domain, $F(\omega)$. The Fourier transform relates the time domain $f(t)$ to the frequency domain $F(\omega)$ by the equation

$$F(\omega) = \int_{-\infty}^{\infty} f(t)e^{-i\omega t} dt$$

Since there is an identity

$$e^{-ix} = \cos x - i \sin x$$

we can decompose $F(\omega)$ into sine $S(\omega)$ and cosine transforms $C(\omega)$:

$$S(\omega) = 2 \int_0^{\infty} f(t) \sin \omega t dt$$

$$C(\omega) = 2 \int_0^{\infty} f(t) \cos \omega t dt$$

The time domain function, which is the time decay of signal intensity, can be expressed as

$$f(t) = Ae^{-t/\tau} \cos(\omega - \omega_i)t \quad t > 0$$

where A is the coefficient and τ is the relaxation time. The coefficient A itself is given by

$$A_f = \sum_{t=0}^{N-1} x_t \exp\left(-\frac{2\pi vt}{N}\right) \quad f = 0, 1, 2, \dots, N - 1$$

where x_t is the value of the time decay at time t . The equation of A_f is a discrete Fourier transform, which will be discussed later.

X-Ray Crystallography (See Chapter 20)

$$F_{hkl} = \int_V \rho(x, y, z) \exp\left[2\pi i\left(\frac{hx}{a} + \frac{ky}{b} + \frac{lz}{c}\right) dv\right]$$

$$\rho(x, y, z) = \frac{1}{V} \sum_h \sum_k \sum_l F_{hkl} \exp\left[-2\pi i\left(\frac{hx}{a} + \frac{ky}{b} + \frac{lz}{c}\right)\right]$$

where h, k, l are Miller indices. The values of structure factor F_{hkl} were obtained for all the reflections when an x-ray hits a molecule. They become the coefficients of a

Fourier series for the electron density function $\rho(x, y, z)$, from which an electron density distribution can be constructed.

15.6 CONVOLUTION

15.6.1 Definition

Convolution is an operation by which two individual transforms $f_1(t)$ and $f_2(t)$ are combined to form a third transform $f(t) = f_1(t) * f_2(t)$. The process of convolution may be described as follows: Let

$$f_1(t) = \int_{-\infty}^{\infty} g_1(\mu) d\mu e^{i\mu t}$$

and

$$f_2(t) = \int_{-\infty}^{\infty} g_2(\nu) d\nu e^{i\nu t}$$

Then

$$f(t) = \int_{-\infty}^{\infty} \int_{-\infty}^{\infty} g_1(\mu) g_2(\nu) e^{i(\mu+\nu)t} d\mu d\nu \quad (15.1)$$

Since μ and ν are completely independent variables, we can let

$$\mu + \nu = \omega$$

Then $\nu = \omega - \mu$ and $d\nu = d\omega$.

Equation (15.1) can now be written

$$\begin{aligned} f(t) &= \int_{-\infty}^{\infty} d\omega \underbrace{\int_{-\infty}^{\infty} g_1(\mu) g_2(\omega - \mu) d\mu}_{g(\omega)} e^{i\omega t} \\ &= \int_{-\infty}^{\infty} g(\omega) d\omega e^{i\omega t} \end{aligned}$$

Our next step is to change variable: $g_1(\mu)$ to $g_1(\omega)$ and $g_2(\nu)$ to $g_2(\omega)$. We have

$$g_1(\omega) = \frac{1}{2\pi} \int_{-\infty}^{\infty} f_1(\theta) d\theta e^{-i\omega\theta}$$

and

$$g_2(\omega) = \frac{1}{2\pi} \int_{-\infty}^{\infty} f_2(\tau) d\tau e^{-i\omega\tau}$$

Then the inverse transform of the function in Eq. (15.1),

$$g(\omega) = g_1(\omega)g_2(\omega) = \frac{1}{2\pi} \int_{-\infty}^{\infty} f(t) dt e^{-i\omega t}$$

is given by

$$f(t) = \frac{1}{2\pi} \int_{-\infty}^{\infty} f_1(\theta)f_2(t - \theta) d\theta = f_1 * f_2$$

Note: This mathematical process is called convolution and the notation of convolution is $f_1 * f_2$. Convolution is an integral. When we say “the convolution of α and β ,” we mean

$$\alpha * \beta = \frac{1}{\sqrt{2\pi}} \int_{-\infty}^{\infty} \alpha(x - t)\beta(t) dt = \alpha(x)$$

By the change of variable, $y = x - t$, we write

$$(\alpha * \beta)(x) = \frac{1}{\sqrt{2\pi}} \int_{-\infty}^{\infty} \alpha(y)\beta(x - y) dy = (\beta * \alpha)(x)$$

That is, the convolution product is commutative.

Convolution is a linear operator because it has the following properties:

$$\begin{aligned} [(f + g) * h](x) &= (f * h)(x) + (g * h)(x) \\ [(\lambda f) * g](x) &= \lambda(f * g)(x) \\ [f * (g + h)](x) &= (f * g)(x) + (f * h)(x) \\ [f * (\lambda g)](x) &= \lambda(f * g)(x) \end{aligned}$$

Example: Let

$$f(x) = e^{-ax}x_{(0, \infty)} \quad g(x) = e^{-bx}x_{(0, \infty)}$$

Calculate $(f * g)(x)$. We have

$$\begin{aligned} (f * g)(x) &= \int_{-\infty}^{\infty} f(x - y)g(y) dy \\ &= \begin{cases} \int_0^x e^{-a(x-y)}e^{-by} dy & x \geq 0 \\ 0 & x < 0 \end{cases} \\ &= e^{-ax}x_{(0, \infty)}(x) \int_0^x e^{(a-b)y} dy \end{aligned}$$

If $a \neq b$, then

$$\begin{aligned} (f * g)(x) &= \frac{1}{b-a} e^{-ax} x_{(0,\infty)}(x) (1 - e^{(a-b)x}) \\ &= \frac{1}{b-a} (e^{-ax} - e^{-bx}) x_{(0,x)}(x) \end{aligned}$$

If $a = b$, then

$$\begin{aligned} (f * g)(x) &= e^{-ax} x_{(0,\infty)}(x) \int_0^x 1 \, dy \\ &= x e^{-ax} x_{(0,\infty)}(x) \end{aligned}$$

15.6.2 Convolution Theorem

$$\begin{aligned} T(\alpha * \beta) &= \frac{1}{2\pi} \int_{-\infty}^{\infty} \beta(t) e^{-itx} \int_{-\infty}^{\infty} \alpha(y-t) e^{-i(y-t)x} \, dy \, dt \\ &= \frac{1}{2\pi} \int_{-\infty}^{\infty} \beta(t) e^{-itx} \int_{-\infty}^{\infty} \alpha(\omega) e^{-i\omega x} \, d\omega \, dt \\ &= \frac{T\alpha}{\sqrt{2\pi}} \int_{-\infty}^{\infty} \beta(t) e^{-itx} \, dt = T\alpha \cdot T\beta \end{aligned}$$

Here we are in the area of advanced mechanics. All the equations must fulfill boundary conditions, for example, convergence of sequence. For the simple operations to be valid, they must be understood to satisfy all conditions by limiting the domains in which the variables x, y, t, \dots belong.

15.6.3 Convolution and Fourier Theory: Power Theorem

The power theorem is based upon Presvel's equality:

$$(\alpha, \beta) = \sum_{i=1}^{\infty} (\alpha, \alpha_i) (\alpha_i, \beta) \quad \text{for } \beta \text{ in } \sum$$

or

$$|\alpha|^2 = \sum_{i=1}^{\infty} |(\alpha, \alpha_i)|^2$$

where \sum means infinite dimension and α is a member of an orthonormal sequence $\{\alpha_i\}$. The equality also extends to

$$\alpha = \sum_{i=1}^{\infty} |(\alpha, \alpha_i)| \alpha_i$$

The terms (α, α_i) are called the generalized Fourier coefficients of α relative to $\{\alpha_i\}$. Parseval's equality says that for any signal the total power contained in a spectrum is the sum of the squared magnitude of all the frequency components:

$$P_n = \text{total power} = \sum_{n=0}^{n-1} |f_n|^2$$

where

$$|f_n|^2 = f_n f_n^*$$

15.7 EXTENSION OF FOURIER SERIES AND FOURIER TRANSFORM

The two extensions of the Fourier series and Fourier transform are the Lorentz line shape and the autocorrelation function.

15.7.1 Lorentz Line Shape

In optics, the general solution of the differential equation of oscillators is given in terms of the Fourier series,

$$x(t) = e^{-(1/2)\Gamma t} (A \sin \omega t + B \cos \omega t)$$

where Γ is a damping constant and ω is the angular frequency (Crawford, 1968). Using the formulas of definite integrals,

$$\int_0^\infty e^{-ax} \sin bx = \frac{b}{b^2 + a^2}$$

$$\int_0^\infty e^{-ax} \cos bx = \frac{a}{b^2 + a^2}$$

the Fourier coefficients are given as

$$A \sim \frac{(\frac{1}{2}\Gamma)^2}{(\omega_0 - \omega)^2 + (\frac{1}{2}\Gamma^2)} \qquad B \sim \frac{(\omega_0 - \omega)^2}{(\omega_0 - \omega)^2 + (\frac{1}{2}\Gamma)^2}$$

where A is the absolute amplitude, B is the elastic amplitude, and the term on the right,

$$L \sim \frac{(\frac{1}{2}\Gamma)^2}{(\omega_0 - \omega)^2 + (\frac{1}{2}\Gamma^2)}$$

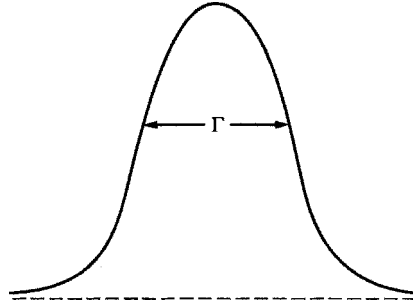


FIGURE 15.2 Lorentz line shape.

is the Lorentz function L which describes the Lorentz line shape curve as in Figure 15.2. The quantity $\Gamma = \Delta\omega$ is called the linewidth of the frequency spectrum of the Fourier superposition. The Lorentz line shape is the basis of the photon beat technique for the determination of translational and rotational diffusion coefficients.

15.7.2 Correlation Function

The inner product of the two functions of time $f(t)$ and $f(t + \tau)$ form a correlation function (see Chapter 16) $\langle f(t)f(t + \tau) \rangle$ defined as

$$\langle f(t)f(t + \tau) \rangle = \lim_{T \rightarrow \infty} \frac{1}{2T} \int_{-T}^T f(t)f(t + \tau) dt$$

where T is the period of length. This is the Fourier integral in a slightly different form. The Fourier transform pairs are

$$\begin{aligned} \langle f(t)f(t + \tau) \rangle &= \int_{-\infty}^{\infty} s(\omega)e^{-i\omega t} d\omega \\ s(\omega) &= \frac{1}{2\pi} \int_{-\infty}^{\infty} \langle f(t)f(t + \tau) \rangle e^{i\omega t} dt \end{aligned}$$

where $\langle f(t)f(t + \tau) \rangle$ is the correlation function and $s(\omega)$ is the power special density. Either equation of the pair is called the Wiener–Khinechine theory. Experimentally, $s(\omega)$ is the photocurrent density and $\langle f(t)f(t + \tau) \rangle$ is the current–density correlation function.

A typical example is the rectangular pulse shown in Figure 15.3. The auto-correlation function in the diagram is

$$A(\tau) = \langle f(t)f(t + \tau) \rangle = x_0^2 \left(1 - \frac{\pi}{2t_0} \right)$$

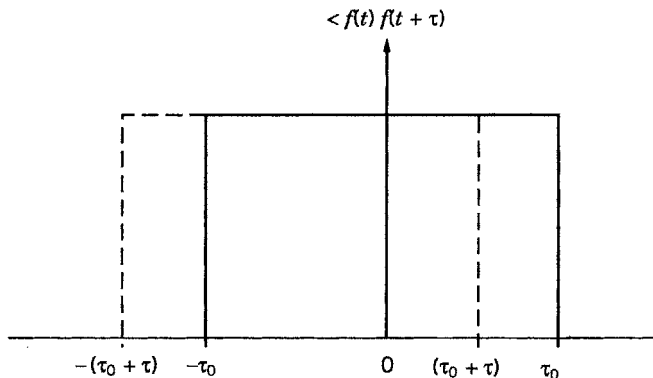


FIGURE 15.3 A rectangular pulse.

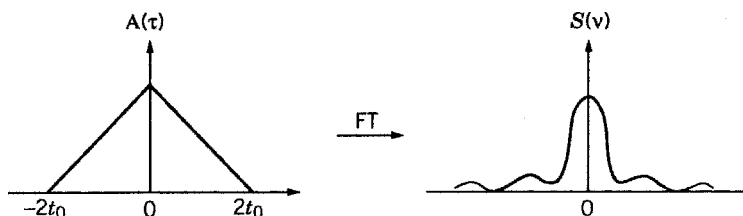


FIGURE 15.4 Graphical representation of an autocorrelation function to a spectral density function.

The spectral density function $s(\nu)$ is the Fourier transform of $A(\tau)$:

$$S(\nu) = 4 \int_0^{\infty} A(\tau) \cos 2\pi\nu t \, d\tau = 4x_0^2 t_0 \frac{\sin 2\pi\nu t_0}{2\pi\nu t_0}$$

In graphical representation, we see the transformation shown in Figure 15.4.

15.8 DISCRETE FOURIER TRANSFORM

15.8.1 Discrete and Inverse Discrete Fourier Transform

In NMR calculations, we may consider the x domain as the data series and the n domain as the calculated experimental data series. More specifically, x refers to the time when the measurement is taken and n refers to the spectrum (or frequency) for presentation. For that reason, we change our notation slightly to fit the actual work in science.

Let d_k designate the k th data in the d sequence $d_0, d_1, d_2, \dots, d_{N-1}$ and f_n designate the n th spectrum point in the f sequence $f_0, f_1, f_2, \dots, f_{N-1}$. Here N is the total number of frequency components in the spectrum estimate.

Then, instead of the continuous Fourier transform

$$F(n) = \int_{-\infty}^{\infty} f(x)e^{-i2\pi nx} dx$$

we have the discrete Fourier transform (DFT),

$$F(n) = \frac{1}{n} \sum_{x=0}^{n-1} f(x)e^{-i2\pi nx/n}$$

For convenience in writing a Fourier transform pair, we rewrite DFT in the form

$$f_n = \frac{1}{\sqrt{N}} \sum_{k=0}^{N-1} d_k e^{-2\pi i kn/N}$$

Then the inverse discrete Fourier transform is

$$d_k = \frac{1}{\sqrt{N}} \sum_{n=0}^{N-1} f_n e^{2\pi i kn/N}$$

Thus, we can also calculate the time series d from the frequency series of f .

15.8.2 Application of DFT

Discrete Fourier transform inherits important properties of continuous Fourier transform. In addition, we can add data point by point and results point by point. Thus, we can use another simple mathematical function to modify the data series as well as the results series independently.

Time Shifting and Frequency Shifting If we multiply the DFT of the original signal by the function $e^{-2\pi i nj/N}$, we can shift the time domain signal by j points:

$$\begin{aligned} d_k &= \frac{1}{\sqrt{N}} \sum_{n=0}^{N-1} f_n e^{2\pi i kn/N} \\ &= \frac{1}{\sqrt{N}} \sum_{n=0}^{N-1} (f_n e^{-2\pi i nj/N}) e^{2\pi i kn/N} \end{aligned}$$

Likewise, we can shift the DFT spectrum to the left by an integral number of points j . This would affect the shift of the time series:

$$\begin{aligned} f_{n+1} &= \frac{1}{\sqrt{N}} \sum_{k=0}^{N-1} d_k e^{-2\pi i n k (n+y)/N} \\ &= \frac{1}{\sqrt{N}} \sum_{k=0}^{N-1} (d_k e^{-2\pi i k j / N}) e^{-2\pi i k n / N} \end{aligned}$$

Apodization: Minimizing Leakage Apodization is the process of modifying data by multiplying the data element by element using a vector \mathbf{a} ,

$$d'_k = a_k d_k$$

An important concept in signal processing is that of the matched filter, with an apodization function that matches the envelope of the signal.

For a Lorentzian line where the envelope decays as $e^{-\pi L t}$, we use it as the match filter (the apodization function),

$$(e^{2\pi i \omega t} e^{-\pi L t})(e^{-\pi L t}) = e^{2\pi i \omega t} \underbrace{e^{-2\pi L t}}_{\uparrow \text{Lorentzian}}$$

This results in a Lorentzian line shape that is broadened by a factor of 2.

Similarly, for Gaussian lines, applying the match filter

$$(e^{2\pi i \omega t} e^{-G t^2})(e^{-G t^2}) = e^{2\pi i \omega t} \underbrace{e^{-2G t^2}}_{\uparrow \text{Gaussian}}$$

results in broadening by a factor of $\sqrt{2}$ since the linewidth is proportional to \sqrt{G} .

15.8.3 Fast Fourier Transform

The discrete Fourier transform

$$f_n = \frac{1}{\sqrt{N}} \sum_{k=0}^{N-1} d_k e^{-2\pi i k n / N}$$

yields an N -point spectrum \bar{f} from an N -point time series \mathbf{d} .

In 1965, Cooley and Tukey proposed an algorithm in which N is factored to some power $N = 2^p$ or $N = 4^q$, p and q being the powers or exponents. This

algorithm not only simplifies the number of computer calculations required but also saves money. It became the basis of what is now called the fast Fourier transform (FFT), which is available in numerous software packages.

APPENDIX

In addition to the Fourier transform, there are the Laplace transform and the Mellin transform. They are all called integral transforms. The general formula is

$$\tilde{f}(\xi) = \int_I f(x)T(x, \xi) dx$$

where $T(x, \xi)$ represents the transform function, which is a two-variable function:

$$a < x < b \quad a < \xi < b$$

The three transforms are

$$\tilde{f}(\rho) = \int_a^\infty f(x) \underbrace{e^{-\rho x}}_T dx \quad (\text{Laplace transform})$$

$$f^*(s) = \int_a^\infty f(x) \underbrace{x^{s-1}}_T dx \quad (\text{Mellin transform})$$

$$\hat{f}(\xi) = \frac{1}{\sqrt{2\pi}} \int_{-\infty}^\infty f(x) \underbrace{e^{-i\xi x}}_T dx \quad (\text{Fourier transform})$$

Notice the three T's: $e^{-\rho x}$, x^{s-1} , $e^{-i\xi x}$.

Historic Note

Given a second-order differential equation $(d^2y/dx^2) + ay = 0$, a suitably restricted solution may be found in the form of a power series $f(x) = \sum_{n=0}^\infty \alpha_n \phi_n(x)$, where a and α are both coefficients. In 1807, Fourier proposed a theorem that the power series $\sum_{n=0}^\infty \alpha_n \phi_n(x)$ can be expressed as a combination of $\sum a_n \cos nx$ and $\sum b_n \sin x$,

$$f(x) = \sum_{n=0}^\infty (a_n \cos nx + b_n \sin nx)$$

He presented a paper to the French Academy and expanded it further by saying that the function $f(x)$ can be expressed in terms of sines and cosines. The Academy

meeting was attended by such great mathematicians as Lagrange, Legendre, and Laplace. Fourier's theorem was unanimously rejected on the basis that it lacked a rigorous proof. To a mathematician, a theorem without a rigorous proof is equivalent to a theory in science without experimental support. It is considered sheer nonsense. Lagrange told Fourier that the same idea had occurred to him as well but he had not claimed it because he found it difficult to prove.

Fifteen years later (1822), Fourier published a book, *The Theory of Heat Conduction*, in which he again proposed this theorem. His enthusiasm about a function $f(x)$ as expressed in terms of sines and cosines was not in any way diminished. He reiterated his theory, disregarding the early objections of Lagrange and other mathematicians. Unfortunately, he again did not provide any rigorous proof. Eight years later (1830), Fourier died. He must have died a sad man, having never earned distinction in his lifetime among his peers in mathematics.

However, Fourier's position in the history of mathematics was gradually recognized. Not only was his theorem partially proved but he also served to stimulate a great interest in such mathematicians of the nineteenth century as Riemann, Presnel, and Weierstrass in the field of analysis. Today, the Fourier series is developed in modern analysis alongside the rapid growth of automatic computing. Fourier integral and Fourier transform, which are derived directly from the Fourier series, are involved in all technical fields, such as engineering, physics, chemistry, biology, and medicine.

REFERENCES

- Bell, E. T., *The Development of Mathematics*, New York: McGraw-Hill Book Co., 1945.
- Bracewell, R. N., *Science* **248**, 697 (1990).
- Brand, L., *Advanced Calculus*. New York: Wiley, 1960.
- Cartwright, M., *Fourier Methods for Mathematicians, Scientists and Engineers*. New York: Ellis Horwood, 1990.
- Churchil, R. V., *Fourier Series and Boundary Value Problems*, 2nd ed. New York: McGraw-Hill, 1963.
- Cooley, J. W., and J. W. Tukey, *Math. Comput.* **19**, 297 (1965).
- Crawford, F. S. Jr., *Waves*, Berkeley Physical Course, Vol. 3, New York: McGraw-Hill, 1968.
- Fulks, W., *Advanced Calculus*. New York: Wiley, 1961.
- Guillemin, E. A., *The Mathematics of Circuit Analysis*. Cambridge, MA: MIT Press, 1949.
- Hoch, J. C., and A. S. Stern, *MMR Data Processing*. New York: Wiley-Liss, 1996.
- Indrity, J., *Methods in Analysis*. New York: McMillan Company, 1963.
- Lederman, W., *Handbook of Applicable Mathematics*, Vol. IV: *Analysis*. New York: Wiley, 1982.
- Rao, S. S. *Mechanical Vibrations*, Reading, Mass: Addison-Wesley Publishing Co., 1986.

PROBLEMS

15.1 Expand the function $(\sin hr)/hr$ in a power series.

15.2 The time correlation function is defined as

$$\langle x(t + \tau)x(t) \rangle = \langle x(\tau)x(0) \rangle$$

and the Fourier transform pairs are

$$\begin{aligned} x_{2T}(t) &= \int_{-\infty}^{\infty} \hat{x}_{2T}(\omega) \exp(-i\omega t) d\omega \\ \hat{x}_{2T}(\omega) &= \frac{1}{2\pi} \int_{-\infty}^{\infty} x_{2T}(t) \exp(-i\omega t) dt \\ 2\pi\delta(\omega - \omega') &= \int_{-\infty}^{\infty} \exp[i(\omega - \omega')t] dt \end{aligned}$$

Show that

$$\begin{aligned} \langle x(t + \tau)x(t) \rangle &= \int_{-\infty}^{\infty} S_x(\omega) \exp(-i\omega\tau) d\omega \\ S_x(\omega) &= \frac{1}{2\pi} \int_{-\infty}^{\infty} \langle x(t + \tau)x(t) \rangle \exp(i\omega\tau) d\tau \end{aligned}$$

where $S_x(\omega)$ is the power spectral density. *Note:* These two equations comprise the Wiener–Khinchine theorem.

15.3 Let τ be the correlation time beyond which intensity fluctuations at t are uncorrelated with those at $t + \tau$. The time correlation function of $x(t)$ can be defined as

$$\langle x(t)x(t + \tau) \rangle = \lim_{T \rightarrow \infty} \frac{1}{2T} \int_{-\infty}^{\infty} x(t)x(t + \tau) dt$$

where T is the length of the time. The power spectral density $S_x(\omega)$ is the time Fourier transform of the correlation function:

$$\begin{aligned} S(\omega) &= \frac{1}{2\pi} \int_{-\infty}^{\infty} \langle x(t + \tau)x(t) \rangle \exp(i\omega\tau) d\tau \\ \langle x(t + \tau)x(t) \rangle &= \int_{-\infty}^{\infty} S_x(\omega) \exp(i\omega t) d\omega \end{aligned}$$

Show that the real part of the Fourier transform of the time correlation function is Lorentzian:

$$\int_{-\infty}^{\infty} \exp(i\omega\tau) \exp(-\Gamma\tau) d\tau = 2 \frac{\Gamma}{\Gamma^2 + \omega^2}$$

15.4 Show that the Fourier transform of an exponential $e^{-a|t|}$ is

$$\pi^{-1} \operatorname{Re} \exp \frac{1}{i\omega + \alpha} = \pi^{-1} \left(\frac{\alpha}{\omega^2 + \alpha^2} \right)$$

15.5 Show that the equilibrium mean-square value of the property A as involved in the time correlation function

$$\langle A(0)A(t) \rangle = \int_{-\infty}^{\infty} d\omega e^{i\omega t} I(\omega)$$

is

$$\langle |A|^2 \rangle = \int_{-\infty}^{\infty} d\omega I(\omega)$$

15.6 Show that DFT and IDFT are orthogonal. (I stands for inverse).

16

SMALL-ANGLE X-RAY SCATTERING, NEUTRON SCATTERING, AND LASER LIGHT SCATTERING

16.1 SMALL-ANGLE X-RAY SCATTERING

Light-scattering apparatus is good for measuring the angle dependence of intensity in the range between 30° and 135° . Below 30° the measurement is usually unreliable. However, by taking extreme precautions and with a special device, the measurement may be carried out down to 10° , which is near the limit. X-ray scattering apparatus, on the other hand, is good for measurements at a very small angle, near 0° . While small-angle x-ray scattering is not as convenient (e.g., it is not readily available) as light scattering in determining molecular weight, it is superior for the determination of size ($\sum r_{ij}$) and shape (sphere, rod, and coil) of macromolecules. This is because the particle size is related inversely to the scattering angle. For macromolecule, with dimensions in the neighborhood of 100 \AA , the strong scattering with wavelength of 1.54 \AA will be chiefly at angles of about 1° .

Originally, small-angle x-ray scattering was a nuisance to investigators of x-ray diffraction pattern (which is described in Chapter 20). In the region of small angles the diffraction pattern was completely black due to parasitic scattering. By the early 1930s the use of a crystal monochromator filtered out parasitic scattering, making it possible to resolve the diffraction pattern close to the primary beam. At the same time it also became clear that the parasitic scattering itself, rather than being a nuisance, could actually yield important information on the conformation of macromolecules. Although the work of parasitic scattering (now called small-angle

x-ray scattering) is still x-ray diffraction, the laws governing scattering are basically similar to those governing light scattering. For this reason, small-angle x-ray scattering is discussed in this book after light scattering, instead of being included with our discussion of x-ray diffraction.

To demonstrate their similarity, small-angle x-ray scattering data may be treated as light-scattering data. In parallel to light scattering, we have

$$\frac{Kc}{I} = \frac{1}{MI_n(h)} + 2A_2T(h)c + \dots \quad (16.1)$$

where the only two different parameters are $I_n(h)$, which is the single-particle scattering function, and $T(h)$, which is a spatial arrangement of two polymer particles during their mutual approach. The independent variable h is related to the angle θ which we define later. Of course, the constant K is no longer defined in terms of n (the refractive index) and dn/dc (the differential refractive index). Instead, K is defined in terms of other parameters:

$$K = \frac{e^4}{m^2c'^4} \frac{P(\Delta z)^2 N_A d}{a^2} \quad (16.2)$$

where e is the electrostatic charge, m is the mass of the particle, c' is the velocity of light, P is the total energy per unit time irradiating the sample, Δz is the number of effective moles of electrons per gram, d is the thickness of the sample, N_A is Avogadro's number, and a is the distance between the sample and the plane registration.

16.1.1 Apparatus

A diagram of the small-angle x-ray scattering apparatus is shown in Figure 16.1. The x-ray source is a tube with a water-cooled copper anode, usually using a Kratky camera for measurement. The tube is operated at, for example, 30 kV direct current (dc) and a current of, for example, 80 mA. The total flux incident on the sample is approximately 10^8 photons/s. Monochromatization was achieved with balanced filter of nickel and cobalt foil which isolate the $\text{CuK}\alpha$ line. The x-ray wavelength (the most frequently used $\text{CuK}\alpha$ line) is 1.54 \AA .

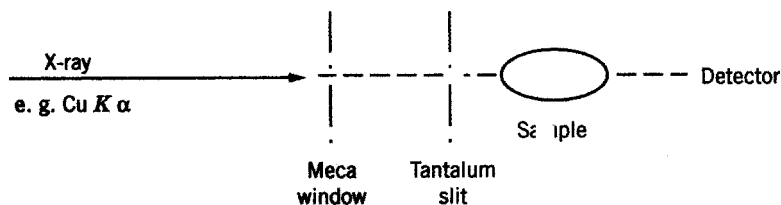


FIGURE 16.1 Diagram of small-angle x-ray scattering apparatus.

There are two types of detectors: film (which normally anticipates a long exposure time) and counter (e.g., Geiger–Muller, scintillation counters, and position-sensitive detector systems). Samples can take the forms of films, fibers, plates, disks, or solutions.

16.1.2 Guinier Plot

In spite of its similarity to light scattering, small-angle x-ray scattering is not usually used to determine M and A_2 as mentioned before; it is used mainly in the determination of the size and shape. The versatility of the experiment for the measurement of size and shape lies in the interpretation of the designated output, $I(h)$.

Intensity $I(h)$ The scattering intensity $I(h)$ is expressed as a function of the scattering angle θ . A scattering curve is shown in Figure 16.2. The variable h can be expressed in terms of magnitude,

$$h = \frac{4\pi}{\lambda} \sin \theta$$

or in terms of vectors,

$$\mathbf{h} = \frac{2\pi}{\lambda} (\mathbf{s} - \mathbf{s}_0)$$

In either expression, λ is the wavelength. In the magnitude expressions the angle θ is the scattering angle and h is almost identical to Q :

$$Q = \frac{4\pi}{\lambda} \sin \frac{\theta}{2}$$

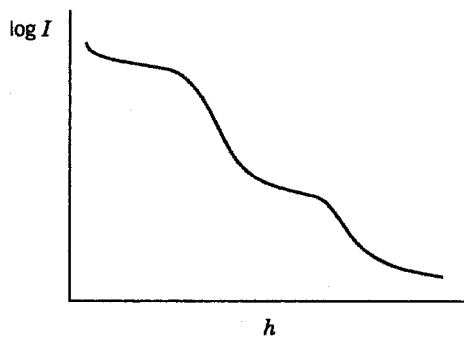


FIGURE 16.2 Scattering curve.

In the vector expression, the vector is normal to the plane of the atom (see Figure 20.11). If the intensity of scattering $I(\mathbf{h})$ is multiplied by the structure factor $\langle F^2(\mathbf{h}) \rangle$, we obtain the observed average intensity $\langle I(\mathbf{h}) \rangle$:

$$\langle I(\mathbf{h}) \rangle = I(\mathbf{h})\langle F^2(\mathbf{h}) \rangle$$

It is the structure factor $\langle F^2(\mathbf{h}) \rangle$ that correlates the scattering intensity and the configuration of the molecule; it is the center of the study of x-ray scattering. The structure factor can be expressed in the well-known Debye formula (1915)

$$\langle F^2(\mathbf{h}) \rangle = \sum_i \sum_j f_i f_j \frac{\sin hr_{ij}}{hr_{ij}}$$

where f is the individual scattering factor of electrons (e.g., the i th and j th electrons) and r_{ij} is the distance between the two atoms. The sine function can be expanded in the series

$$\langle F^2(\mathbf{h}) \rangle = \sum_i \sum_j f_i f_j - \frac{h^2}{6} \sum_i \sum_j f_i f_j \langle r_{ij} \rangle^2 + \dots$$

At the limit $h \rightarrow 0$

$$\sum_i \sum_j f_i f_j = F^2(0)$$

and

$$\langle F^2(h) \rangle = n^2 e^{-h^2 R_0^2/3} \quad (16.3)$$

where $n = \sum_i f_i$ is the total number of electrons in the particle and $R_0^2 = \sum \langle r_{ij} \rangle^2$. This is the Guinier equation (1939). The plot of $\ln I$ versus $(2\theta)^2$ is called the Guinier plot. (Note: 2θ is the scattering angle. In the small-angle region, $h \sim 2\theta$.)

Analysis of Data Depending on the way it is plotted, the Guinier equation can provide information about the size of macromolecules in various shapes:

Radius of Gyration of the Whole Particle R Here the equation is

$$I(h) = I(0)e^{-h^2 R^2/3}$$

If the particle is in the shape of a sphere, the linear plot of the experimental data $\ln I(h)$ versus h^2 [or $(2\theta)^2$] will yield the value of R , the radius of gyration of the whole particle. Here R is proportional to the square root of the slope of the tangent in the limit $2\theta \rightarrow 0$.

Radius of Gyration of the Cross Section R_c Here the equation is

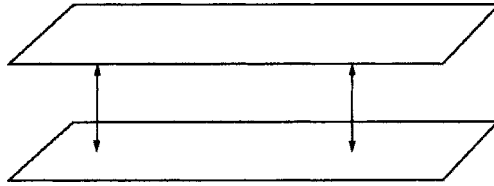
$$I_c(h) = I_c(0)e^{-h^2 R_c^2/2}$$

If the particle is rodlike, the linear plot of $I(h)h$ [or $I(h)2\theta$] versus h^2 [or $(2\theta)^2$] will yield the value of R_c , the radius of gyration of the cross section.

Radius of Gyration of the Thickness R_t Here the equation is

$$I_t(h) = I_t(0)e^{-h^2 R_t^2}$$

If the particle is lamellar (flatlike particles), as in the drawing,



the plot of $I(h)h^2$ [or $I(h)(2\theta)^2$] versus h^2 [or $(2\theta)^2$] will yield the information about R_t , the radius of gyration of the thickness of the particle. For particles with uniform electron density distribution, the thickness can be calculated from R_t according to

$$t = R_t \sqrt{12}$$

16.1.3 Correlation Function

In Guinier's approach, the key term is the scattering factor, which can be analyzed in terms of Debye's formula (the sine function in a power series). The same set of experimental data $I(h)$ can also be analyzed by a different approach. Here, we discuss the correlation function (see the Appendix to Chapter 5). Since the evaluation of $\langle r_{ij} \rangle$ is related to statistics, we can define a correlation function $\gamma(r)$ as the average of the product of two fluctuations at a distance r :

$$\gamma(r) = \langle \eta(r_1)\eta(r_2) \rangle$$

where

$$\begin{aligned} r &= \langle r_1 - r_2 \rangle \\ \eta &= \rho - \langle \rho \rangle \quad \rho \text{ is the density} \end{aligned}$$

Then the average square of $\langle \eta^2 \rangle$ may be expressed as

$$\langle \eta^2 \rangle = \langle \rho^2 - V \langle \rho \rangle^2 = V \gamma(r)$$

where V is the volume of the particle. At the limit $r \rightarrow 0$, that is, the two fluctuation points being at the same position, we have

$$V \gamma(0) = \frac{1}{2\pi^2} \int_0^\infty h^2 dh I(h)$$

The integral is known as invariant Q' (due to Porod, 1951); that is,

$$Q' = \int_0^\infty I(h) h^2 dh \quad (16.4)$$

Thus, if the scattering intensity at zero angle is available, Q' can be used to determine the volume of the particle:

$$V = \frac{I(0)}{Q'} 2\pi^2$$

The value of the invariant Q' can be obtained by the evaluation of the integration in Eq. (16.4). The integration is usually carried out numerically with the Simpson formula after the intensity data are plotted in the form of $I(h)h^2$ versus h . The invariant Q' is equal to the area under the curve. If the particle is in rodlike form, Q' can also be used to determine the cross-sectional area A :

$$A = \frac{I(h)h}{Q'} 2\pi \quad \text{at } h \rightarrow 0$$

It is interesting to note that the correlation function originally was also suggested by Debye and Buche (1949). The correlation function of the particle $\gamma(r)$ represents the probability of a point at a distance r in an arbitrary direction from a given point in the same particle. It can be related to the distance distribution function $p(r)$ by

$$p(r) = \gamma(r)r^2 \quad (16.5)$$

The distribution function itself is related to the shape of the macromolecules:

For spheres

$$p(r) = \frac{1}{2\pi^2} \int_0^\infty I(h)hr \sin hr dh \quad (16.6)$$

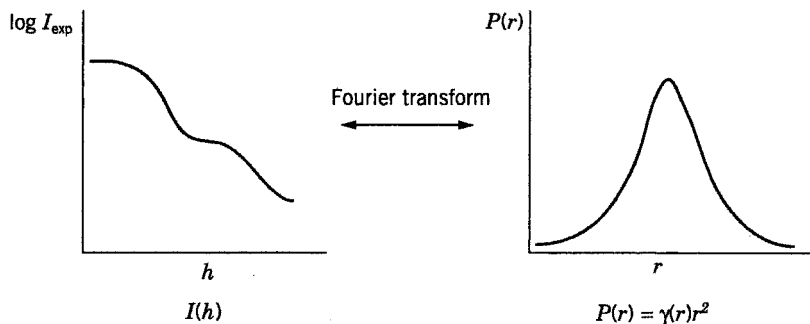


FIGURE 16.3 Fourier transform of $I(h)$ into $P(r)$.

For rodlike shapes

$$p_c(r) = \frac{1}{2\pi} \int_0^\infty I_c(h)(hr)J_0(hr) dh \quad (16.7)$$

where $J_0(hr)$ is the zero-order Bessel function. For lamella

$$p_t(r) = \frac{1}{\pi} \int_0^\infty I_t(h) \cos hr dh \quad (16.8)$$

All of the above distribution functions, $p(r)$, $p_c(r)$, and $p_t(r)$, are Fourier inversions of $I(h)$, $I_c(h)$, and $I_t(h)$, respectively. Modern experimental techniques can easily transform $I(h)$ into $p(r)$ (Figure 16.3).

Thus, by transforming the intensity data to the distance distribution function, we are able to estimate the shape of a macromolecule, particularly a biological polymer.

16.1.4 On Size and Shape of Proteins

With a small modification of Guinier's equation, Luzzati (1960) and with coworkers (1961a,b) suggested that the plot of \log (intensity) data versus scattering angle data, as shown in Figure 16.4 enables one to determine the radius of gyration R of protein molecules in solution:

$$\ln j_n(s) = \ln j_n(0) - \frac{4}{3}\pi^2 R s^2$$

Here the scattering angle parameter s is slightly different from that of h :

$$s = \frac{2 \sin \theta}{\lambda}$$

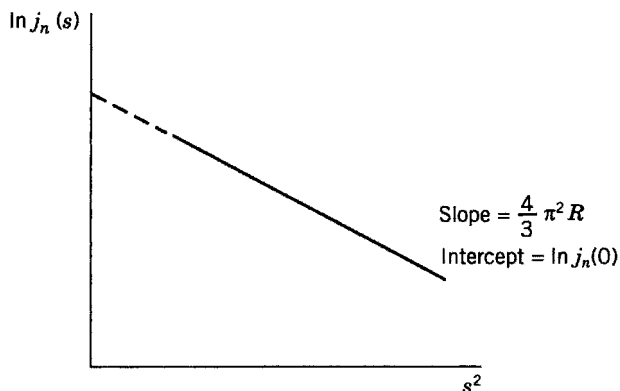


FIGURE 16.4 Modified Guinier plot.

Compare

$$h = \frac{4\pi \sin \theta}{\lambda}$$

The scattered light intensity parameter $j_n(s)$ is calculated from

$$j_n(s) = \left[\frac{I(s)}{nm \int i_0(s) ds} \right]_{\text{solution}} - \left[\frac{I(s)}{nm \int i_0(s) ds} \right]_{\text{solvent}}$$

where $I(s)$ is the scattered light intensity measured at s , the integral is the energy of the stack of incident beams i_0 , n is the number of electrons per square centimeter, and m is a constant.

If the internal structure of the protein molecules is stressed, we can plot the experimental results in a slightly different way (Figure 16.5). The equation that represents Figure 16.5 is

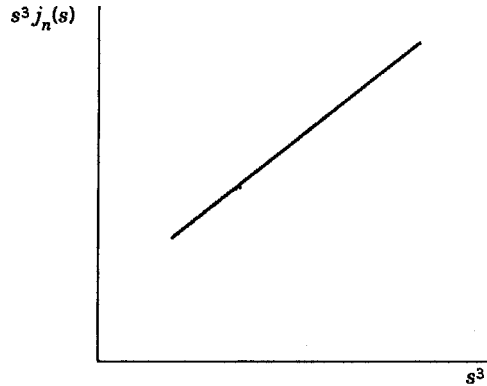
$$\lim_{s \rightarrow \infty} s^3 j_n(s) = \frac{1}{16\pi^2} \frac{S_1}{v_1} (\rho_1 - \rho_0) c_e (1 - \rho_0 \bar{v}) + \delta^* s^3$$

where the subscript 0 refers to the solvent and 1 refers to the solute. The slope δ^* is close to the term $j_n(0)$, with, of course, some deviation. The intercept contains two terms related to the internal structures:

$\rho_1 - \rho_0$ = distribution of electron density in molecule

$\frac{S_1}{v_1}$ = surface dimension of protein molecule in \AA^{-1}
which is a characteristic parameter

The symbol ρ refers to the density, S_1 is the surface dimension, V is the volume of the molecule, \bar{v} is the partial specific volume, and c_e is the concentration



Slope = δ^*

$$\text{Intercept} = \frac{1}{16\pi^2} \frac{S_1}{v_1} (\rho_1 - \rho_0) c_e (1 - \rho_0 \bar{v})$$

FIGURE 16.5 Guinier plot for determination of internal structure of protein molecule.

of electrons. For lysozyme, $c_e = 0.957c (1 - 0.55c)^{-1}$; for BSA, $c_e = 0.960c (1 - 0.042c)^{-1}$, c being the concentration in grams per milliliter.

From S_1/v_1 , the surface-to-volume ratio, one can calculate the dimension (i.e., the length of the molecule L) using the equation derived by Porod,

$$L_1 = n \frac{v_1}{S_1} \phi_1$$

where ϕ is the volume fraction.

However, the two parameters $\rho_1 - \rho_0$ and S_1/v_1 may also be evaluated independently by

$$\rho_1 - \rho_0 \cong \frac{\int_0^\infty 2\pi s j_n^*(s) ds}{c_e (1 - \rho_0 \bar{v})} + \rho_0 c_e (1 - \rho_0 \bar{v})$$

$$\frac{S_1}{v_1} \cong \frac{16\pi^2 \lim_{s \rightarrow \infty} s^3 j_n^*(s)}{\int_0^\infty 2\pi s j_n^*(s) ds} \left[\rho_1 - \frac{\rho_0 c_e (1 - \rho_0 \bar{v})}{\rho_1 - \rho_0} \right]$$

where $j_n^*(s)$ is calculated from

$$J_n^*(s) = j_n(s) - \delta^*$$

The shape of a protein molecule, whether spherical or not, can be determined by plotting $s^4 I(s)$ (called the Porod term) versus s , as shown in Figure 16.6.

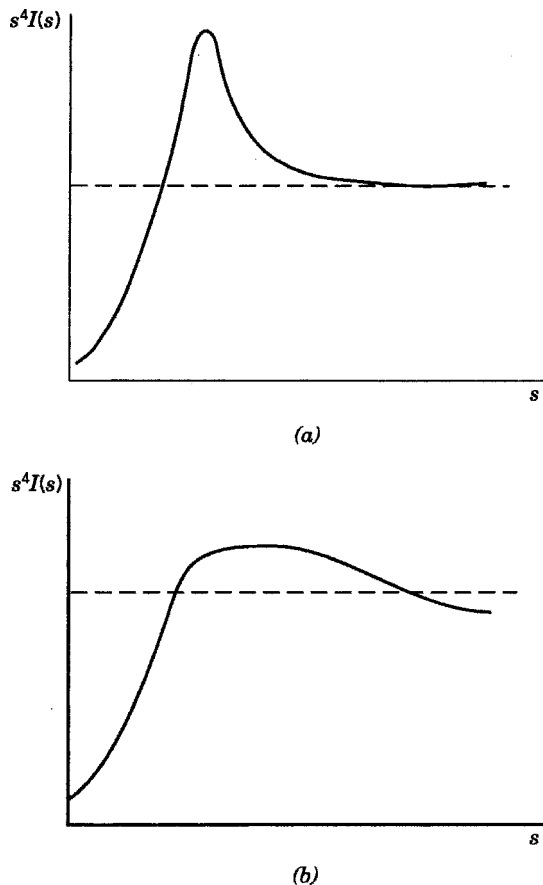


FIGURE 16.6 Determination of shape of protein molecule: (a) spherical—a curve that oscillates before setting toward the asymptote; (b) nonspherical—a curve that shows little oscillation in the asymptotic approach.

Luzzati et al. (1961) further suggested a set of theoretical equations for estimating the dimension of the equivalent ellipsoid of revolution on the basis of experimental values such as v_1 and S_1 :

$$v_1 = \frac{4\pi}{3}pb^3$$

$$S_1 = 2\pi b^2 \left(1 + \frac{p^2}{\sqrt{p^2 - 1}} \arcsin \frac{\sqrt{p^2 - 1}}{p} \right) \quad p > 1$$

$$= 2\pi b^2 \left(1 + \frac{p^2}{\sqrt{1 - p^2}} \arctan \sqrt{1 - p^2} \right) \quad p < 1$$

where $p = a/b$, the axial ration.

TABLE 16.1 Comparison of X-rays with Neutron Beams

	X-rays	Neutrons
Source	Energetic electron beam	Nuclear reactor of pulsed reaction
Wavelength	1.54 Å	2.0–10 Å
Kinetic energy	25–5 keV	0.3–0.0051 eV
Detection	Fluorescence, scintillation counter	Reaction with ^6Li or ^{10}Be

16.2 SMALL-ANGLE NEUTRON SCATTERING

Light scattering and small-angle x-ray scattering are based on electromagnetic radiation, while small-angle neutron scattering is based on particle radiation. The interaction between light and the collective electrical charges of a molecule produces the electric field. Neutron beams, on the other hand, interact with the nuclei of atoms via a strong nuclear force (called nuclear scattering). They also interact with unpaired electron spins of a molecule, if any, via the magnetic dipole (called magnetic scattering). Table 16.1 gives a brief comparison of x-rays with neutron beams.

16.2.1 Six Types of Neutron Scattering

The type of neutron scattering depends on the incident wave frequency ν_0 and the scattered wave frequency ν . If ν_0 is equal to ν , we have coherently scattered radiation; if not, we have incoherently scattered radiation. In coherently scattered radiation, phases of the electric and magnetic fields of incident radiation and those of scattered radiation are in a definite relation to each other.

The scattering events may or may not involve an energy change. If no energy change takes place, the scattering is elastic; if an energy change takes place, the scattering is inelastic. If an energy change is very small and if there is a Doppler shift (i.e., a frequency shift), then the scattering is quasielastic. Thus, there are six different types of scatterings: coherently elastic scattering, incoherently elastic scattering, coherently inelastic scattering, incoherently inelastic scattering, coherently quasielastic scattering, and incoherently quasielastic scattering.

Among the six types of scattering, only incoherently elastic scattering seems to have no application in polymer studies. Coherently elastic scattering of neutrons measures the correlations between scattering centers and hence is useful to the study of the conformation of polymers. The coherently inelastic scattering experiment is useful for obtaining information on photon dispersion curves, whereas the incoherently inelastic scattering is useful for determining the vibrational behavior of side groups of the polymer chain (i.e., molecular spectroscopy). Neutron quasielastic scattering studies, whether coherent or incoherent, of polymers in bulk and in solution have given much new information on the dynamics of a polymer chain in solution.

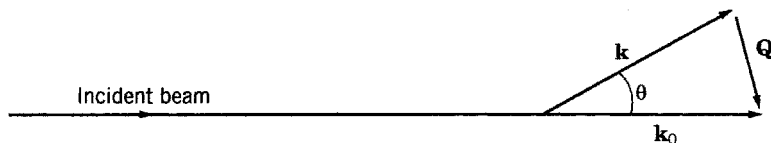


FIGURE 16.7 Neutron scattering phenomenon.

Small-angle neutron scattering, like small-angle x-ray scattering, is used to study the size, shape, and conformation of polymer molecules in bulk and in solution. It is particularly useful to investigate orientation of long polymer chains in solid states. In general, the laws that govern light scattering and small-angle x-ray scattering also govern small-angle neutron scattering. We will compare small-angle neutron scattering with light scattering in detail after we briefly describe the theory.

16.2.2 Theory

The scattering phenomenon is shown in Figure 16.7, where \mathbf{k}_0 is the incident wave vector, \mathbf{k} is the scattered wave vector, \mathbf{Q} is the resultant vector in the direction from the scattered beam to the incident beam, that is, $\mathbf{Q} = \mathbf{k} - \mathbf{k}_0$, and θ is the scattering angle. In any neutron scattering event energy and momentum transfers are always involved. The energy transfer from the incident neutron to the scattered neutron is given by

$$\Delta E = E - E_0 = \hbar\omega = \frac{1}{2}m(v^2 - v_0^2) = \frac{\hbar^2}{m}(k^2 - k_0^2)$$

where v is the frequency, \hbar is Planck's constant ($\hbar = h/2\pi$), m is mass, and the momentum transfer is given by

$$\hbar\mathbf{Q} = \hbar(k^2 + k_0^2 - 2kk_0 \cos \theta)^{1/2}$$

For elastic scattering, $\mathbf{k} = \mathbf{k}_0$ and

$$Q = |\mathbf{Q}| = \frac{4\pi}{\lambda} \sin \frac{\theta}{2}$$

where $|k_0| = 2\pi/\lambda$. (Notice the similarities between Q and h .) Scattered intensity is measured as a function of energy and of angle of scatterer. It is expressed in terms of the differential cross section $d^2\delta/d\Omega dE$, where δ is the cross section in barns and Ω is the solid angle including θ , which is related to Q . The differential cross section is the probability that neutrons will be scattered by an array of atoms in the sample with energy change dE . It may be used to define a function $S(\mathbf{Q}, \omega)$:

$$S(\mathbf{Q}, \omega) = \frac{k_0}{k} \frac{1}{Nb^2} \frac{d^2\delta}{d\Omega dE} \quad (16.9)$$

where b is the scattering length, which is a complex number, and N is the number of incident electrons. The imaginary part of b (in centimeters) is a measure of the neutron absorption, if any. The function $S(\mathbf{Q}, \omega)$ is called the scattering law by Van Hove.

The differential cross section is a measurable quantity, for example, from the sample count rate f . It can be calculated using

$$f = nN \frac{d^2\delta}{d\Omega d\tau'} \Delta\Omega \tau \varepsilon_{\tau'}$$

where n is the number of atoms per square centimeters in the sample, $\Delta\Omega$ the solid angle subtended by the detector at the sample, $\Delta\tau$ the channel width, and $\varepsilon_{\tau'}$ the efficiency of the detector to neutrons of time flight τ' .

The scattering law $S(\mathbf{Q}, \omega)$ is the double Fourier transform $G(r, t)$ of the space-time correlation function:

$$S(\mathbf{Q}, \omega) = \frac{1}{2\pi\hbar N} \iint \exp[-i(\omega t - \mathbf{Q}\mathbf{r})] G(\mathbf{r}, t) \, d\mathbf{r} \, dt \quad (16.10)$$

The quantity $S(\mathbf{Q}, \omega)$ is usually measured over a limited range of $\hbar\mathbf{Q}$ and $\hbar\omega$. A model correlation function $G(\mathbf{r}, t)$ is then predicted to fit the experimental data.

16.2.3 Dynamics of a Polymer Solution

Dynamics refers to the property that involves the time t . The scattering law $S(\mathbf{Q}, \omega)$ and the intensity $I(\mathbf{Q}, t)$ are related to the correlation function $G(\mathbf{r}, t)$ in the following equations (a Fourier transform pair):

$$I(\mathbf{Q}, t) = \int \exp(i\mathbf{Q} \cdot \mathbf{r}) G(\mathbf{r}, t) \, d\mathbf{r}$$

and

$$S(\mathbf{Q}, \omega) = \int \exp(i\omega t) I(\mathbf{Q}, t) \, dt$$

For a simple liquid, the intensity $I(\mathbf{Q}, t)$ can be described in terms of a self-diffusion coefficient D (see Chapter 11) by

$$I(\mathbf{Q}, t) = \exp(-Q^2 D t)$$

The self-diffusion coefficient is used to describe the center-of-mass motion for a simple liquid. It can also be used in connection with the Rouse–Zimm model to describe the behavior of a long chain. The determination of diffusion coefficient D

by the small-angle neutron scattering experiment will be further discussed in a slightly different way in Section 16.2.7.

16.2.4 Coherently Elastic Neutron Scattering

In the study of chain dimensions, we are interested in coherently elastic neutron scattering only, that is, $dE = 0$ and $k = k_0$. The experimental data needed are $d\sigma/d\Omega$ and $S(\mathbf{Q})$, not $d^2\sigma/d\Omega dE$ and $S(\mathbf{Q}, \omega)$. The differential cross section $d\sigma/d\Omega$ and the scattering law $S_{\text{coh}}(\mathbf{Q})$ are related in a very simplified form:

$$\frac{d\sigma}{d\Omega} = k' S_{\text{coh}}(\mathbf{Q})$$

where k' is called the contrast factor (which is discussed further in a later section) and is defined as

$$k' = \left(b_{1\text{coh}} - b_{2\text{coh}} \frac{\bar{V}_1}{\bar{V}_2} \right)^2$$

The subscripts 1 and 2 refer to one substance dissolved in another substance (including one solid sample mixed with another solid sample) coh refers to the coherent scattering, and \bar{V} is the partial molar volume. The scattering law $S(\mathbf{Q})$ here is the Fourier transform of the density fluctuation correlation function [instead of $G(\mathbf{r}, t)$] of the scattering centers:

$$S(\mathbf{Q}) = \sum_{ij} \langle [\exp i(\mathbf{Q}(\mathbf{r}_i - \mathbf{r}_j))]^2 \rangle$$

where \mathbf{r}_i and \mathbf{r}_j are the centers of mass of the scattering points i and j , which correspond to chain segments in a polymer molecule.

16.2.5 Comparison of Small-Angle Neutron Scattering with Light Scattering

The scattering intensity per unit volume $I(\mathbf{Q})$ of a polymer of molecular weight M and concentration c (weight per volume) is

$$\begin{aligned} I(\mathbf{Q}) &= \frac{d\sigma}{d\Omega} \frac{c}{M} N_A \\ &= k' S_{\text{coh}} \frac{c}{M} N_A \\ &= \frac{k' c}{M} N_A S_{\text{coh}} \end{aligned}$$

where N_A is Avogadro's number. With some manipulation, we can approximate $S_{\text{coh}}(\mathbf{Q})$ to the form

$$S_{\text{coh}}(\mathbf{Q}) = \frac{2(M/m)^2}{x - 1 + e^{-x^2}}$$

where M is the molecular weight of the polymer, m is the molecular weight of a segment unit, and

$$x = Q^2 \langle R^2 \rangle$$

$\langle R^2 \rangle$ being the mean square of the radius of gyration.

If we let $K = k'N_A/m^2$, then we have

$$I(Q) = KCM \frac{2}{x^2} (x - 1 + e^{-x})$$

or

$$\frac{KC}{I} = \frac{1}{M} \left(1 + \frac{\langle R^2 \rangle Q^2}{3} + \dots \right)$$

Thus, the governing equations of small neutron scattering are also almost identical to those of conventional light scattering. In the analysis of experimental data, we can use the Zimm plot (among others) to obtain the molecular weight and the radius of gyrations of the polymer molecules.

There are, however, some important differences. Because of the involvement of the contrast factor k' , in the K term, small-angle neutron scattering can observe the Gaussian behavior of polymer chains in their own bulk, whereas conventional light scattering cannot. The different ranges of Q in small-angle neutron scattering provide more ways than conventional light scattering to obtain the molecular parameter of a polymer chain. The four different ranges of Q , as Kratky pointed out, are

1. $Q < (R^2)^{1/2}$ The Guinier domains,

$$\frac{K^*C}{I(Q)} = M^{-1} \left(1 + \frac{Q^2 R^2}{3} \right)$$

2. $(R^2)^{1/2} \leq Q \leq a^{-1}$ The Debye domain where a is the persistent length of the polymer chain,

$$\frac{K^*C}{I(Q)} = \frac{M^{-1} Q^2 R^2}{2}$$

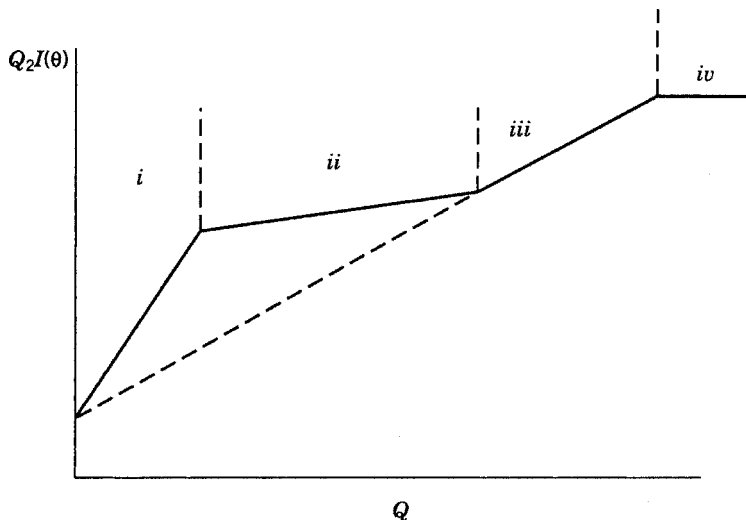


FIGURE 16.8 Kratky plot of Q ranges.

3. $a^{-1} < Q < l^{-1}$ The rod shape domain where l is the step length of the polymer chain and n is the number of statistical units in the chain,

$$\frac{K^* C}{I(Q)} = \frac{M^{-1} n l Q}{\pi}$$

4. $l^{-1} < Q$ The internal structure domain where no equation similar to that of light scattering can yet be formulated in this range.

Figure 16.8 shows that Kratky plot in an idealized form. Furthermore, small-angle neutron scattering experiments can be carried out on solid solutions, whereas light scattering cannot.

16.2.6 Contrast Factor

The contrast factor k' may be written in a slightly different form:

$$k = |a_D - a_H|^2$$

where a is the coherent scattering length of an atom for the i th nucleus. The values of a for the H atom and the D (deuterium) atom individually as well as in protonated polystyrene and deuterated polystyrene are given in Table 16.2. Because of the large difference in coherent scattering lengths between protonated and deuterated monomers, the contrast term $|a_D - a_H|^2$ is ideal for the study of an

TABLE 16.2 Values of a for H and D

Nucleus	$a(10^{-12} \text{ cm})$
H	-0.374
D	0.667
Polystyrene (C_8H_8)	2.328
d -Polystyrene (C_8D_8)	10.656

Source: Bacon, 1975.

isolated chain embedded in its environment. The data for a deuterated polymer and a deuterated matrix containing a small percentage of protonated polymer are sketched in Figure 16.9.

Techniques using the contrast factor have been applied to test the theoretical prediction of the behavior of a polymer in solutions (see Chapter 5):

$$\langle R^2 \rangle = \text{const} \times M^{2\nu}$$

where ν is a critical exponent for determining the excluded volume in solutions of nonintersecting chain segments. Experiments of small-angle neutron scattering were carried out, for example, on deuterated polystyrene in cyclohexane at 36°C (θ temperature) as well as CS_2 (good solvent) at temperatures not equal to θ . It was found that $\nu = 0.5$, as expected, only for chains in a θ condition. The value of k' is the same for the bulk as for a polymer in the θ solvent.

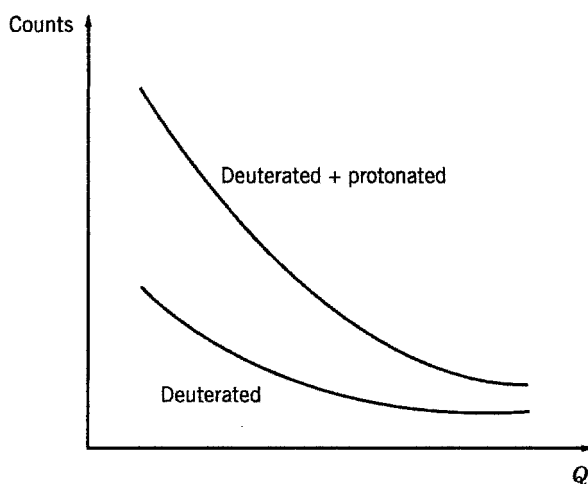


FIGURE 16.9 Effect of contrast factor.

16.2.7 Lorentzian Shape

The equation

$$I(Q) = KCM \frac{2}{x^2} (x - 1 + e^{-x})$$

can be modified for the intermediate momentum range to a Lorentzian form:

$$\frac{I(Q)}{KCM} = \frac{1}{Q^2 + \xi^{-2}}$$

where

$$\xi^{-2} = \frac{12cN_A}{M_0b^2} \phi$$

In the above equations the parameter ξ , as described before, is the screen length, ϕ is the excluded volume per statistical segment, c is the weight fraction concentration of tagged chain (e.g., a deuterated polymer embedded in a protonated polymer), and M_0 is the molecular weight of a monomer. Experimentally, ξ^{-2} is equal to a half width in the plot of the Lorentzian curve (similar to the Gaussian distribution curve).

Thus, the small-angle neutron scattering experiment can be used to determine the screen length ξ . With a small modification the scattering law $S(\mathbf{Q}, \omega)$ can be put in a different form of Lorentzian equation:

$$S(\mathbf{Q}, \omega) = \frac{\pi}{2} \frac{DQ^2}{\omega^2 + (DQ^2)^2}$$

where D is the diffusion coefficient and a half width $\propto DQ^2$. These kinds of experiments have been used to study the dynamics of polymer solutions.

16.2.8 Neutron Spectroscopy

Inelastic neutron scattering is used for the study of transmission or absorption neutron energy spectra, particularly the side-group motion in polymers. All data reported so far for polymers have been concerned with symmetric top molecules. Three spectrometries are available at present: (1) slow neutron spectrometry, which studies slow neutron excitation functions with continuous-energy neutron sources; (2) fast neutron spectrometry, which studies the spectra of neutrons produced in nuclear reaction; and (3) monoenergetic slow neutron spectrometry, which studies the spectra of neutrons corresponding to the inelastic scattering from atoms in solids or fluids.

16.3 LASER LIGHT SCATTERING

So far we have discussed light scattering, small-angle x-ray scattering, and small-angle neutron scattering. In this section we discuss laser light scattering, also known as dynamic light scattering. All these types of scattering are basically governed by the same or similar laws. The differences lie in the radiation sources and the techniques used to handle these sources. For light scattering (often called conventional light scattering), the source is light (wavelength 436–546 nm); for small-angle x-ray scattering, the source is x-rays (wavelength 0.05–0.25 nm); for small-angle neutron scattering, the source is neutrons (wavelength 0.05–0.4 nm); and for laser light scattering, the source is lasers (wavelength 488–635 nm). The spectrometer for light scattering is relatively simple, while those for the other three are rather complicated.

Laser light scattering is characterized by three aspects:

1. The high intensity of the laser source makes it possible to measure weakly scattered light and to observe very small frequency shifts.
2. Time t becomes an important variable in the measurement. The quantity we are interested in, $S(q, t)$, is a function of both the angle θ (included in q) and time t .
3. The correlation function as an experimental device and as a technique in the mathematical analysis of the phenomena is extensively employed.

Like conventional light scattering, laser light scattering can be used successfully to determine the molecular weight, size, and shape of macromolecules. But more important, laser light scattering is a powerful tool that can measure the diffusion coefficient in a more elegant manner than many other classical tools. For that reason, we place the topic in this chapter after Chapter 10 on diffusion. The extensive use of correlation function techniques in laser light scattering also provides methods for studying polymer chain statistics. The serious problem of dust, which causes many spurious signals in light scattering, is greatly minimized in the technique of laser scattering.

16.3.1 Laser Light-Scattering Experiment

Several well-known experimental techniques are employed in laser light scattering. Here we describe the homodyne and heterodyne methods. Both methods use a laser source for incident radiation. Both use a photomultiplier as a detector followed by an autocorrelator for computer analysis. The autocorrelator is defined as

$$\langle i(t)i(0) \rangle = B \langle |E(0)|^2 |E(t)|^2 \rangle \quad (16.11)$$

where i is the intensity of scattered light, t is the time, E is the scattered electric field, and B is a proportionality constant. The difference between the two methods lies in the substance (scattered light) for analysis. In the homodyne method, we

analyze only the scattered light that impinges on the photocathode. The amplitude of the scattered field is proportional to the instantaneous dielectric constant fluctuations. In the heterodyne method, we analyze a small amount of unscattered laser light that is mixed with the scattered light on the photocathode. The heterodyne method, therefore, is also called optical mixing or photon beating method.

16.3.2 Autocorrelation and Power Spectrum

If two dynamic properties are correlated over a period of time, the function that describes such a correlation is called the correlation function (Chapter 5, Appendix B). Let the dynamic property be $P(t)$. The value of $P(t)$ at t fluctuates about the value at t_0 . The average value of $\langle P \rangle$ at average time T is defined as

$$\langle P(t_0, T) \rangle = \frac{1}{T} \int_{t_0}^{t_0+T} P(t) dt \quad (16.12)$$

The measured bulk property P is simply a time average property $\langle P(t_0, T) \rangle$. At two different times, t and $t + \tau$, the property can have different values:

$$P(t + \tau) \neq P(t)$$

If τ is very small, $P(t + \tau) \equiv P(t)$. If τ is very large, there can be no correlation. Only within a certain range of τ can there be a correlation between $P(t)$ and $P(t + \tau)$. A measure of this correlation is called the autocorrelation function of P and is defined

$$\langle P(0)P(\tau) \rangle = \lim_{T \rightarrow \infty} \int_0^T dt P(t)P(t + \tau) \quad (16.13)$$

The time τ usually represents the relaxation time.

Experimentally, the autocorrelation function is a measure of the similarity between two noise signals, $P(t)$ and $P(t + \tau)$. If the two signals are completely in phase with each other, then $\langle P(0)P(\tau) \rangle$ is large. If they are out of phase with each other, then the autocorrelation function $\langle P(0)P(\tau) \rangle$ is small (see Berne and Pecora, 1976).

The intermediate scattering function $S(g, t)$ is the autocorrelation of density $\rho(t)$, defined as

$$S(g, t) = \langle \rho^*(0)\rho(t) \rangle \quad (16.14)$$

where ρ^* is the complex conjugate of ρ . The density $\rho(t)$ is itself defined as

$$\rho(t) = \sum_j \exp i\mathbf{q}\mathbf{R}_j(t) \quad (16.15)$$

where j sums over all scattering elements \mathbf{R} from an arbitrary origin and \mathbf{q} is the scattering wave function:

$$\mathbf{q} = \frac{4\pi}{\lambda} \sin \frac{\theta}{2} \quad (16.16)$$

The scattering function $S(q, t)$ and the spectra density $I(\omega)$ form a Fourier transform pair:

$$\langle \rho^*(0)\rho(t) \rangle = \int_{-\infty}^{\infty} d\omega e^{i\omega t} I(\omega) \quad (16.17)$$

$$I(\omega) = \frac{1}{2\pi} \int_{-\infty}^{\infty} dt e^{-i\omega t} \langle \rho^*(0)\rho(t) \rangle \quad (16.18)$$

where ω is the angular frequency. In the literature $I(\omega)$ is also called the power spectrum, which is the experimental result we are looking for.

16.3.3 Measurement of Diffusion Coefficient in General

Consider a time-dependent correlation function $\langle G(0, 0)g(\mathbf{r}, t) \rangle$ (first introduced by Van Hove, 1954):

$$S(\mathbf{q}, \omega) = \frac{1}{2\pi} \int_{-\infty}^{\infty} dt \exp(i\omega t) \int d\mathbf{r} \exp(i\mathbf{q}\mathbf{r}) \langle G(0, 0)G(\mathbf{r}, t) \rangle \quad (16.19)$$

By applying the Wiener–Khinchine theorem (Wiener, 1930; Khinchine, 1934; see Chapter 15), the scattering can be transformed into the power spectrum just like the pair $S(\mathbf{q}, t)$ and $I(\omega)$:

$$I(\omega) = N \frac{1}{2\pi} \int_{-\infty}^{\infty} e^{i(\omega - \omega_0)t} [G_A(\tau)][G_\phi(\tau)] d\tau \quad (16.20)$$

where N is the number of scatterers in a system, ω_0 is the undamped natural angular frequency, $G_A(\tau)$ is the orientation autocorrelation function, and $G_\phi(\tau)$ is the position autocorrelation function. The two autocorrelation functions are defined as

$$\begin{aligned} G_A(\tau) &= \langle A^*(t)A(t - \tau) \rangle \\ G_\phi(\tau) &= \langle e^{-i\mathbf{q}\mathbf{r}(t)} e^{-i\mathbf{q}\mathbf{r}(t - \tau)} \rangle \end{aligned} \quad (16.21)$$

If the scatterers are spherical, the orientation autocorrelation function is simplified to

$$G_A(\tau) = |A|^2 \quad (16.22)$$

where A is the amplitude of the wave. The position autocorrelation function, on the other hand, is related to the translational diffusion coefficient D :

$$G_\phi(\tau) = e^{-Dq^2\tau} \tag{16.23}$$

We now have the scattering intensity expressed more simply as

$$I(\omega) = N|A|^2 \frac{1}{2\pi} \int_{-\infty}^{\infty} e^{i(\omega-\omega_0)t} e^{-Dq^2t} dt \tag{16.24}$$

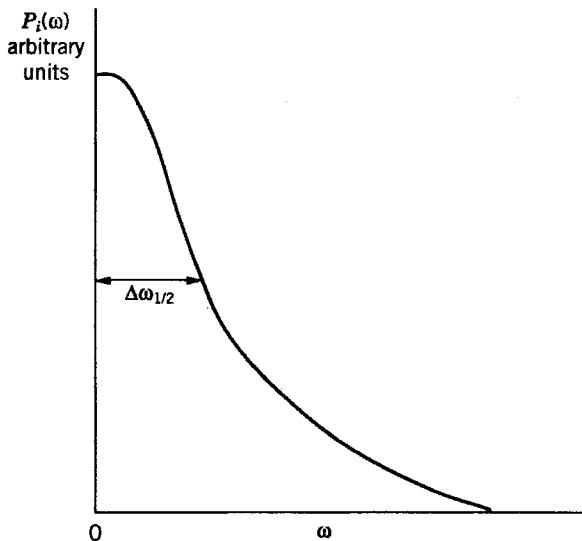
This equation can be further transformed into a Lorentzian equation:

$$I(\omega) = N|A|^2 \left[\frac{Dq^2/\pi}{(\omega - \omega_0)^2 + (Dq^2)^2} \right] \tag{16.25}$$

The quantity in brackets is a normalized Lorentzian centered at $\omega = \omega_0$. Thus, the Rayleigh scattered light has a Lorentzian frequency distribution with a half width:

$$\Delta\omega_{1/2} = Dq^2 = \frac{1}{\tau_0} \tag{16.26}$$

where τ_0 is the correlation time beyond which intensity fluctuations at t are uncorrelated with those at $t + \tau$. The value of D can be determined from $\Delta\omega_{1/2}$ of a plot of experimental data. In experiments, photocurrent $P_i(\omega)$ is usually plotted versus frequency, as shown in the following diagram:



If the macromolecule takes the form of rigid rods, the equation of $\{G_A(\tau)\}$ is more complicated. The power spectrum is now expressed (Wada et al., 1969) as

$$I(\omega) = \frac{N|A|^2\omega_0^4}{60\pi T^4 R_0^2} (\alpha_z^0 - \alpha_x^0) L(6\theta) \quad (16.27)$$

where T is a parameter related to a diffusion tensor, R is the distance observed from the spectral power density, α is the polarizability, x and z are two Cartesian coordinates, and $L(6\theta)$ is the normalized Lorentzian of half width $\Delta\omega_{1/2}$. Again, we can determine the value of Θ (the rotational diffusion coefficient) from the graph of $P(\omega)$ versus ω as shown in the determination of D . The equation to be used is now

$$\text{Full width at half height} = \frac{6\Theta}{\pi} \quad (\pi = 3.1416) \quad (16.28)$$

16.3.4 Application to Study of Polymers in Semidilute Solutions

In the previous section, we describe the general method for measuring diffusion coefficients of a polymer solution by laser light scattering. We now list three techniques for measuring diffusion coefficient specifically for polymers in semidilute solutions.

16.3.4.1 Measurement of Lag Times According to the reptation theory (Chapter 5), there are two kinds of diffusion of the polymer molecule in the entanglement: the diffusion of individual segments in the tube confined by other chains and the diffusion of the whole molecule (the polymer chain) out of the tube to assume a new configuration. The former is represented by D_c , the cooperative diffusion coefficient, and the latter is represented by D_s , the self-diffusion coefficient. In the laser light-scattering experiment, if the intensity autocorrelation of the scattered light is measured with two widely different sample times, then the accumulated autocorrelation displays a reasonable portion of two decay times, or e-folds, of an apparent exponential decay. The sample times are now separated into short sample times and long sample times (Amis and Han, 1982). The scattering functions for the two different times can be expressed as follows:

$$S(q, t) = Ae^{-\tau_c t} + S_c(q) \quad (\text{short time}) \quad (16.29)$$

$$S(q, t) = Ae^{-\tau_s t} + S_s(q) \quad (\text{long time}) \quad (16.30)$$

By curve fitting an exponential function to $S(q, t)$ data, we can obtain the decay constant τ_c or τ_s either from the slope if the plot is linear or from a second-order cumulant fit (which is discussed later in this section) if the plot is not linear. The diffusion coefficient is obtained by

$$\tau = q^2 D \quad (\tau = \tau_c \text{ or } \tau_s)$$

From short-time data we obtain D_c and from long-time data we obtain D_s .

16.3.4.2 Forced Rayleigh Scattering Forced Rayleigh scattering provides another effective method for measuring D_s . The method makes use of tracer techniques and two laser sources (Leger et al., 1981). A portion of the sample polymer is labeled with a photochromic probe, such as 1'-(4-iodobutyl)-3',3'-dimethylindolino-6-nitrobenzospiropyran. The mixture of labeled and nonlabeled chains is dissolved in a solvent. The exciting laser beam (351 nm) is mechanically chopped to give a light pulse of 1 ms–1 s duration. It passes through another laser light source (633 nm) for scattering measurement. The relaxation of the diffracted intensity is recorded.

For data analysis, the following empirical equation is employed:

$$n(t) = (Ae^{-t/\tau} + B)^2 + I^2 \quad (16.31)$$

where $n(t)$ is the number of pulses in the pulse-counting mode, $Ae^{-t/\tau}$ represents the amplitudes of the diffracted fields, and B and I are the amplitudes of the scattered fields, which are coherent and incoherent with the signal, respectively. By least-squares curves fitting, with A , B , I , and t as adjustable, the quantity τ is determined, from which we calculated D_s .

16.3.4.3 Linewidth Analysis From the power spectrum, we can obtain the linewidth $\Gamma = \Delta\omega_{1/2} = q^2D$ (Chu and Nose, 1980). If the measurement is carried out for a polymer in a semidilute solution, we can relate asymptotically Γ to D and c (concentration) following the scaling law

$$\langle \Gamma \rangle \sim D \sim c^\alpha \quad (16.32)$$

where

$$D = \frac{kT}{6\pi\eta_0\xi} \quad (16.33)$$

and $D \sim c^\alpha$ represents the scaling law. In Eq. (16.23), k is the Boltzmann constant, T is temperature, and η_0 is the viscosity of the solvent. The quantity ξ is the hydrodynamic length of a polymer in the semidilute solution. The exponent α is a measure of the excluded volume effect v :

$$\alpha = \frac{v}{3v - 1} \quad (16.34)$$

It is the determination of an accurate value of $\langle \Gamma \rangle$ from experimental data that matters. One method to achieve this is first to define a normalized distribution function $G(\Gamma)$:

$$G(\Gamma) = e^{-q^2Dt} = e^{-\Gamma t} \quad (16.35)$$

Then we calculate

$$\langle \Gamma \rangle = \int_0^{\infty} \Gamma G(\Gamma) d\Gamma \quad (16.36)$$

The evaluation of $G(\Gamma)$ can be performed with the cumulant analysis as follows (Koppel, 1972). We take the logarithm of the normalized correlation function:

$$\ln G(\Gamma) = \ln e^{-q^2 D t} \quad (16.37)$$

Then we expand the natural log term in series:

$$\ln(1+x) = x - \frac{1}{2}x^2 + \dots$$

Thus, we have

$$\ln G(\Gamma) = 1 - K_1 t + \frac{1}{2} K_2 t^2 - \frac{1}{3!} K_3 t^3 \dots \quad (16.38)$$

where

$$K_n = \left[(-1)^n \frac{d^n}{dt^n} \ln G(\Gamma) \right]_{t=0} \quad (16.39)$$

The quantity K_n is the n th cumulant of $G(\Gamma)$. The first few cumulants are

$$\begin{aligned} K_1 &= \langle q^2 D \rangle \equiv q^2 \langle D \rangle_z \quad (= \langle \Gamma \rangle) \\ K_2 &= \langle (q^2 D - \langle q^2 D \rangle)^2 \rangle \\ K_3 &= \langle (q^2 D - \langle q^2 D \rangle)^3 \rangle \\ K_4 &= \langle (q^2 D - \langle q^2 D \rangle)^4 \rangle - 3K_2^2 \end{aligned} \quad (16.40)$$

Here D_z is the z average diffusion coefficient.

REFERENCES

- Akcasu, A. Z., M. Benmouna, and C. C. Han. *Polymer* **21**, 866 (1980).
 Amis, E. J., and C. C. Han, *Polymer* **23**, 1403 (1982).
 Berne, B. J., and R. Pecora, *Dynamic Light Scattering*. New York: Wiley, 1976.
 Chu, B., *Laser Light Scattering Basic Principles and Practice*, 2nd ed. New York: Academic, 1991.
 Chu, B., and T. Nose, *Macromolecules* **13**, 122 (1980).
 Cotton, J. P., D. Decker, H. Benoit, B. Farnoux, J. Higgins, G. Jannink, R. Ober, C. Picot, and J. Des Cloizeaux, *Macromolecules* **7**, 863 (1974).
 Cummins, H. Z., F. D. Carlson. T. J. Herbert, and G. Woods, *Biophys. J.* **9**, 518 (1969).

- Daoud, M., J. P. Cotton, B. Farnoux, G. Jannink, G. Sarma, H. Benoit, R. Duplessix, C. Picot, and P. G. De Gennes, *Macromolecules* **8**, 804 (1975).
- Debye, P., and A. M. Buche, *J. Appl. Phys.* **20**, 518 (1949).
- Debye, P., *Ann. Physik* **46**, 809 (1915).
- de Gennes, P. G., *Macromolecules* **9**, 587, 594 (1976).
- Dubin, S. B., J. H. Lunacek, and G. B. Benedek, *Proc. Natl. Acad. Sci. U.S.A.* **57**, 1164 (1967).
- Glatter, O., and O. Kratky (Ed.), *Small-Angle X-Ray Scattering*, New York: Academic, 1982.
- Guinier, A. *Ann. Phys.* **12**, 161 (1939).
- Guinier, A. And G. Fournet, *Small Angle Scattering of X-Rays*, New York: John Wiley 1953.
- Gupta, A. K., J. P. cotton, E. Marchal, W. Burchard, and H. Benoit, *Polymer* **17**, 363 (1976).
- Khinchine, A., *Math. Ann.* **109**, 604 (1934).
- King, J. K., *Methods Exp. Phys.* **16A**, 480 (1980).
- Koppel, D. E., *J. Chem. Phys.* **57**, 4814 (1972).
- Kratky, O., *J. Polym. Sci.* **3**, 195 (1948).
- Kratky, O., *Angew. Chem.* **72**, 467 (1960).
- Kratky, O., *Pure Appl. Chem.* **12**, 483 (1966).
- Kratky, O., and W. Kreutz, *Z. Elektrochem.* **64**, 880 (1960).
- Leger, L., H. Hervet, and F. Rondelez, *Macromolecules* **14**, 1732 (1981).
- Luzzati, V., *Acta Crystallogr.* **13**, 939 (1960).
- Luzzati, V., A. Nicolaieff, and F. Masson, *J. Mol. Biol.* **3**, 185 (1961a).
- Luzzati, V., J. Witz, and A. Nicolaieff *J. Mol. Biol.* **3**, 367, 379 (1961b).
- Maconachie, A., and R. W. Richards, *Polymer* **19**, 739 (1978).
- Mashall, W., and S. W. Lovessey, *Theory of Thermal Neutron Scattering*. Oxford: Clarendon, 1971.
- Ober, R., J. P. Cotton, B. Farnoux, and J. S. Higgins, *Macromolecules* **7**, 634 (1974).
- Porod, G., *Kolloid-Z.* **124**, 83 (1951).
- Ritland, M. N., P. Kaesberg, and W. W. Beeman, *J. Chem. Phys.* **18**, 1237 (1950).
- Safford, G. J., and A. W. Naumann, *Macromol. Rev.* **2**, 1 (1967).
- Van Hove, L., *Phys. Rev.* **95**, 249 (1954).
- Vonk, C. G., and G. Kortleve, *Kolloid-Z. Polym.* **220**, 19 (1967).
- Wada, A., N. Suda, T. Tsuda, and K. Soda, *J. chem. Phys.* **50**, 31 (1969).
- Wiener, N., *Acta Math.* **55**, 117 (1930).

PROBLEMS

- 16.1** The following experimental data of small-angle x-ray scattering were obtained for lysozyme and bovine serum albumin:

h^2 (rad ²)	$\ln I$ (arbitrary units)	
	Lysozyme	BSA
1×10^{-4}	10.0	4.9
2×10^{-4}	9.6	3.9

h^2 (rad ²)	$\ln I$ (arbitrary units)	
	Lysozyme	BSA
3×10^{-4}	9.3	3.0
4×10^{-4}	8.9	1.8

Determine the radius of gyration of each of the proteins (Ritland et al., 1950).

- 16.2** Persistence length a is a measure of the rigidity of the conformation of cellulose tricarbilate in dioxane, which can be determined by a Kratky plot of small-angle neutron scattering. Plot the following data in the Kratky form and determine the persistence length a of the polymer under study:

Iq^2 (arbitrary units)	q (Å ⁻¹)
0.65	0.046
0.55	0.04
0.40	0.03
0.30	0.02
0.22	0.015
0.19	0.01
0.08	0.005

The equation to be used is in the form $a = A/q^*$, where $A = 1.91$ is a constant and q^* is the point at which the wave vector enters a different domain (Gupta et al., 1976).

- 16.3** The scattering law $s(q)$ may be expressed as

$$s(q) = \frac{12}{(ql)^{1/\nu} + O(1/N)}$$

where l is the polymer step length, N is the number of links, O refers to the “other” terms, and q is the momentum transfer, which is related to the scattering angle θ and wavelength λ of the neutrons:

$$q = \frac{4\pi}{\lambda} \sin \theta$$

This law can be used experimentally to determine the excluded volume exponent ν . The following data were obtained from the low-angle neutron scattering data for a polystyrene dissolved in CS₂ (good solvent) and cyclohexane (poor solvent), respectively:

Good Solvent		Poor Solvent	
$\log s^{-1}$	$\log q$	$\log s^{-1}$	$\log q$
1.95	6.05	2.60	6.40
2.45	4.65	2.65	5.31
2.65	4.20	3.60	4.20
3.10	2.70	4.15	3.21

The values for s are in arbitrary units and those for q are 10^{-1} Å. Determine graphically the value of ν for the polymer in (a) good solvent and (b) poor solvent and compare the experimental value with that predicted by the scaling law (Cotton et al., 1974).

- 16.4** The radii of gyration as a function of concentration in the semidilute regime for a polystyrene with molecular weight 1.14×10^5 in CS_2 were found from small-angle neutron scattering measurements as follows:

c (g/cm ³)	R (Å)
0.00	137
0.03	120
0.06	117
0.10	111
0.15	104
0.20	101
0.33	95
0.50	91
1.06	82

Plot $\log R^2/M$ versus $\log c$ and determine the value of the slope. Show that this experiment confirms the scaling law at the semidilute solution $R^2 \sim Mc^\nu$ (Daoud et al., 1975).

- 16.5** The following data of the self-beating experiment were obtained for a protein at $\theta = 90^\circ$, $T = 25^\circ\text{C}$, and concentration 40 mg/mL:

$s(\omega)$ (arbitrary units)	ω ($\times 10^{-3}$, s ⁻¹)
69	0
59	10
44	20
31	30
24	40
18	50
14	60

The wavelength of the photons is 6328 Å and the refractive index of the solution is 1.453. Calculate the diffusion coefficient of the protein.

17

ELECTRONIC AND INFRARED SPECTROSCOPY

Spectra are observed as the result of the interchange of energy between a substance and electromagnetic radiation. If the energy is absorbed by a substance from the radiation field, we have absorption spectra; if the energy is added to the radiation field, we have emission spectra. An electromagnetic radiation may be characterized by the frequency ν , the wavelength λ , or the wave number $\bar{\nu}$. They are all related as shown in the following equations:

$$\nu\lambda = c' \qquad \frac{1}{\lambda} = \bar{\nu}$$

where c' is the velocity of light. The units are hertz (or reciprocal seconds) for frequency, reciprocal meters or reciprocal centimeters for wave number, and meters or centimeters for wavelength. Table 17.1 shows the relationship between some of these units. Table 17.2 shows the wavelength of spectroscopic regions of the electromagnetic spectrum.

In this chapter we describe the three most important types of optical spectroscopy: ultraviolet (UV) and visible, fluorescence, and infrared. UV and visible spectra can be obtained through the same spectrometer. They differ only in the selection of the wavelength of the incident light: UV at 180–400 nm and visible at 400–760 nm. Both UV (and visible) and fluorescence spectra describe the phenomenon of electron excitation; namely, a valence electron of a molecule is

TABLE 17.1 Examples of Relationship between Frequency, Wave Number, and Wavelength

Frequency (s^{-1})	Wave Number (m^{-1})	Wavelength
3×10^8 (300 MHz)	1	1 m
4.3×10^{14} (blue)	1.4×10^8	700 nm
7.5×10^{14}	2.5×10^6	400 nm (red)
3×10^{18}	1.0×10^{10}	0.1 nm (γ)

TABLE 17.2 Wavelength of Spectroscopic Regions of Electromagnetic Spectrum

X-rays	Vacuum UV	UV	Visible	Near Infrared	Far Infrared	Microwave	Radio Frequency
		1.0 200 400	750	1.0 50		1.0 30 100	
		nm		μm		mm	cm

excited upon absorbing energy from the electromagnetic radiation and is thereby transferred from one energy level to another energy level. The spectra are electronic.

By contrast, infrared spectra describe the vibration of the atoms (not electrons) around a chemical bond. When the frequency of the incident light (radiation) coincides with the characteristic frequency of the vibration of a chemical bond, a band (or peak) appears. Infrared spectra are not electronic spectra.

17.1 ULTRAVIOLET (AND VISIBLE) ABSORPTION SPECTRA

When a valence s electron of one atom moves into the same orbital as a valence s electron of another atom, the two atoms may form either a bond or an antibond, depending on whether the resultant bond energy is stable. The antibond is also called an excited state. The bond, which is stable, is designated as a σ bond; the antibond, which is not stable, is designated as a σ^* bond. If a valence s electron of one atom shares its orbital with a valence p electron of another atom or if a valence p electron of an atom shares its orbital with another valence p electron of another atom, then we have either a π bond or a π^* antibond, which again depends on whether the resultant bond energy is stable. In some atoms, such as N, O, and S, or

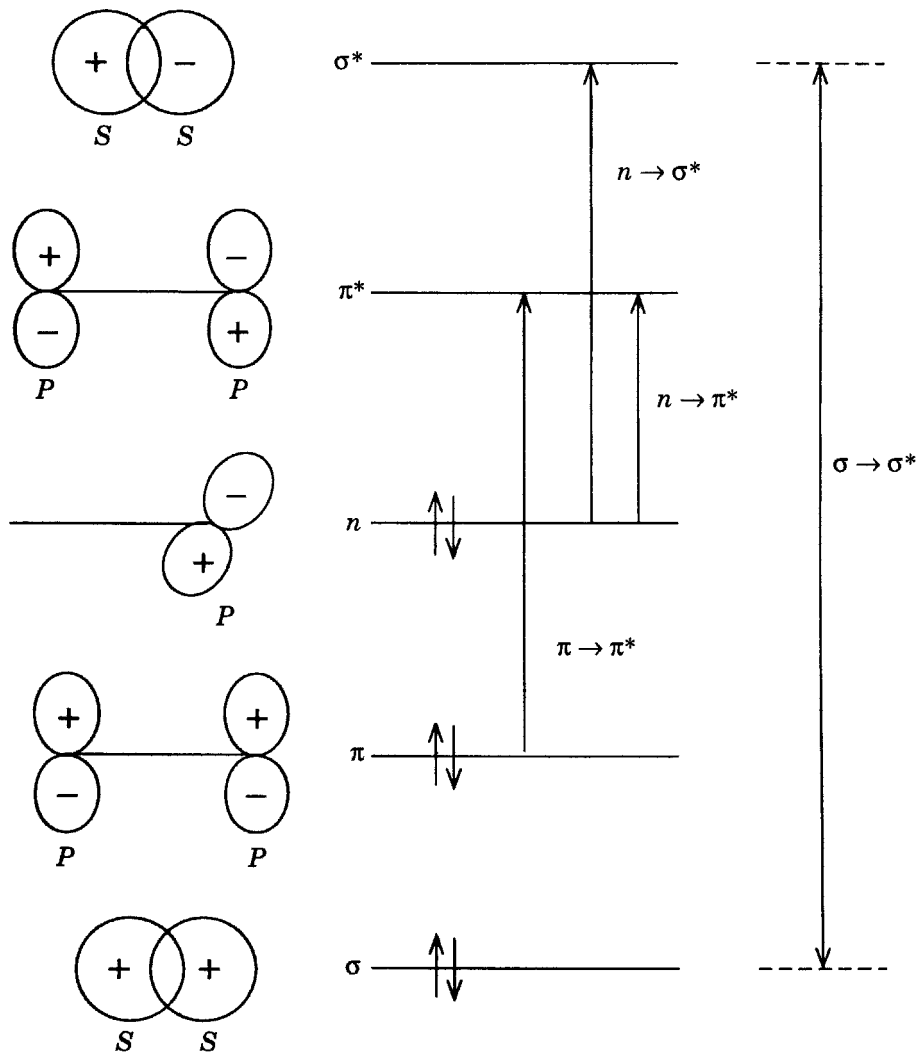


FIGURE 17.1 Four types of electron transitions.

molecules, such as >C=O and -ONO , there are lone-pair electrons. In Lewis dot symbols, for example, $\text{>C::}\ddot{\text{O}}$, two lone-pair electrons of the oxygen atom do not form bonds. These electrons are designated as n (nonbonding) electrons.

Figure 17.1 shows four types of electronic transition, $n \rightarrow \sigma^*$, $n \rightarrow \pi^*$, $\pi \rightarrow \pi^*$, and $\sigma \rightarrow \sigma^*$. Among the four types of electronic transitions in the UV (and visible) regions, the $\sigma \rightarrow \sigma^*$ transition requires the highest input of energy. For this reason, compounds where all the valence shell electrons are involved in single-bond (σ -bond) formations, such as saturated hydrocarbons (C_nH_{n+2}), do not show

absorption in the UV region. Most $\sigma \rightarrow \sigma^*$ transitions for individual bonds take place below 200 nm and a compound containing only σ bonds is transparent (i.e., near-zero absorptions) in the near-UV/visible region. The energy required for an $n \rightarrow \sigma^*$ transition is much lower than that required for a $\sigma \rightarrow \sigma^*$ transition. As a result, molecules containing a nonbonding electron, such as oxygen, nitrogen, sulfur, or the halogens, often exhibit absorption in the UV region. The $n \rightarrow \pi^*$ and $\pi \rightarrow \pi^*$ transitions require even lower inputs of energy. These are the two most important types of transitions for organic molecules and are commonly found in aldehydes and ketones. For an aldehyde or a ketone, two peaks often appear: one at 285 nm, which is attributed to an $n \rightarrow \pi^*$ transition, and the other at 180 nm, which is attributed to a $\pi \rightarrow \pi^*$ transition.

17.1.1 Lambert–Beer Law

In UV absorption spectroscopy, one important law frequently used is the Lambert–Beer law, which is a combination of Lambert’s law and Beer’s law. Lambert’s law states that as radiation of a given frequency passes through a medium (which contains the sample molecules), its intensity is reduced exponentially in the form

$$I = I_0 e^{-\alpha x}$$

or

$$\ln \frac{I_0}{I} = \alpha x$$

where I_0 is the intensity of the incident light, I is the intensity after passing through a medium of thickness x , and α is a constant known as the absorption coefficient. If we use common logarithms (base 10), the equation is converted to

$$I = I_0 \times 10^{-Kx}$$

or

$$\log \frac{I_0}{I} = Kx$$

where $K = \alpha/2.303$ is the extinction coefficient. Beer’s law states that the absorption is proportional to the concentration of the substance, that is, $K = \epsilon c$, where ϵ is a constant equal to the extinction coefficient for unit concentration. The combination of these two laws gives

$$\log \frac{I_0}{I} = \epsilon c x \quad \text{or} \quad \log \frac{I_0}{I} = \epsilon c b \quad (17.1)$$

which is the well-known Lambert–Beer law. If c is in moles per liter, ϵ is called the molar extinction coefficient. Customarily, x is kept constant and is renamed b , which is identical to the cell path length (e.g., 1 cm) of the spectrometer. The logarithm term,

$$\log \frac{I}{I_0} \equiv A$$

is called the absorbance or optical density. Its range is often recorded between 0 and 2. In the UV spectrum, absorbance is plotted versus the wavelength λ , or more commonly as ϵ versus λ or $\log \epsilon$ versus λ .

17.1.2 Terminology

Chromophores Electronic transitions in complex molecules, such as in polymer molecules, are regarded as being localized around certain chemical groups or bonds that are present in the molecule. It has been observed that certain series of related molecules that all contain a particular chemical group often produce absorption spectra of similar appearance. Such groups are called chromophores. If the chromophore contains π electrons, the absorption band appears in both the visible and the UV regions; if it contains σ electrons, the band will appear only in the far-UV region. Table 17.3 gives the absorptions of chromophores for some well-known compounds.

TABLE 17.3 Some Characteristic Chromophores^a

Chromophore	λ_{\max} (nm)	ϵ
>C=C<	171–177	15,530–12,600
$\text{—C}\equiv\text{C—}$	178–223	10,000–160
>C=O	160–279	16,000–15
$\begin{array}{c} \text{O} \\ \parallel \\ \text{—C—CH} \end{array}$	208	32
$\begin{array}{c} \text{O} \\ \parallel \\ \text{—C—Cl} \end{array}$	220	100
$\begin{array}{c} \text{O} \\ \parallel \\ \text{—C—NH}_2 \end{array}$	178–220	9500–63
>C=C—C=C<	217	20,900
$\text{C=C—C}\equiv\text{C}$	219	6500

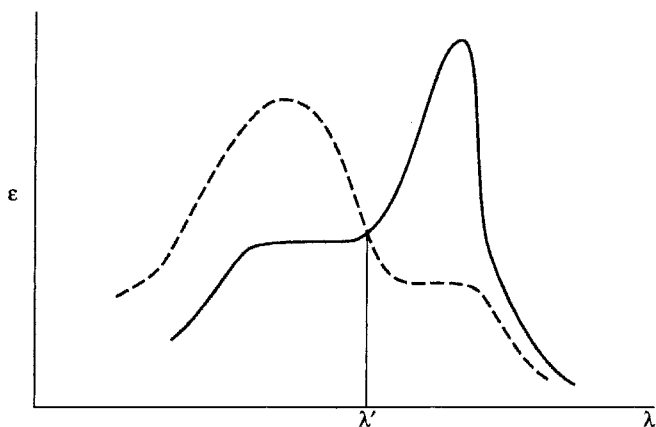
^aAll chromophores have $\pi \rightarrow \pi^*$ electronic transitions. The chromophore >C=O may also have a $n \rightarrow \pi^*$ transition.

TABLE 17.4 Auxochromes of Some Monosubstituted Benzenes

Auxochrome	λ_{\max} (nm)	ϵ
-H	203.5	7,400
-CH ₃	206.5	7,000
-I	207	7,000
-Cl	209.5	7,400
-Br	210	7,900
-OH	210.5	6,200
-CN	224	8,700
-COOH	230	11,600
-NH ₂	230	8,600
-NO ₂	268.5	7,800

Auxochromes Groups such as -OH, -NH₂, and the halogens, which all possess n electrons, are not chromophores themselves. But they can cause normal chromophoric absorptions to occur at longer wavelengths and with an increase in the value of molar absorptivity. These groups are called auxochromes. Auxochromes are responsible for the electronic transitions $n \rightarrow \sigma^*$ and $n \rightarrow \pi^*$. Table 17.4 shows the effect of auxochromes on the absorption of benzene.

Isobestic Point In the plot of ϵ versus λ , the absorbance curve generally shifts when the concentration of the solution is changed, as shown in Figure 17.2. At one particular wavelength, λ' , however, the concentration does not affect the extinction coefficient. This wavelength is called the isobestic point. When experiments are run at λ' , the interference caused by the concentration in the spectrum is avoided.

**FIGURE 17.2** Isobestic point λ' .

Red Shift and Blue Shift The shift of an absorption maximum toward a longer wavelength is called a red shift; that toward a shorter wavelength is called a blue shift. The shift of an absorption maximum is caused by either the change of the medium or the presence of an auxochrome. For example, in an aniline molecule the conjugation of the lone pair of electrons on the nitrogen atom gives an absorption at 230 nm ($\epsilon = 8600$), but when the molecule is placed in an acid solution, the occurrence of the main peak is almost identical to that of benzene, that is, at 203 nm ($\epsilon = 7500$). In this example a blue shift has occurred.

Hypochromism Hypochromism H is defined as

$$H \equiv 1 - \frac{A_p}{A_m}$$

where the subscripts p and m indicate polymer and monomer, respectively, and A refers to area. The values of A_p or A_m are obtained by computing the area under the curve of the polymer or monomer extinction coefficient ϵ versus frequency ν :

$$A \equiv \int \epsilon d\nu$$

Hypochromism is a measure of the decrease in absorption intensity due to the mixture of a monomer with a polymer. It is often an indication of a change in the geometry of the polymer segments due to their interaction with other segments (or with the free monomers, if present).

17.1.3 Synthetic Polymers

Aromatic polymers, such as polystyrene, and nonaromatic polymers with certain functional groups, such as C–N, can have their basic units excited to produce spectra in the UV region. Following are some of the UV absorption ranges for the major groups of polymers:

Group (Bond)	Absorption Range (nm)
C–N (amide)	250–310
C=O	187; 280–320
C–C	195; 230–250
O–H	230
C=C	180

Figure 17.3 shows the UV absorption spectrum of polystyrene. In the spectrum, absorption peaks for polystyrene are found at 260, 215, 194, and 80 nm. The first three peaks are the result of the transition of π electrons, whereas the 80-nm peak involves σ electrons.

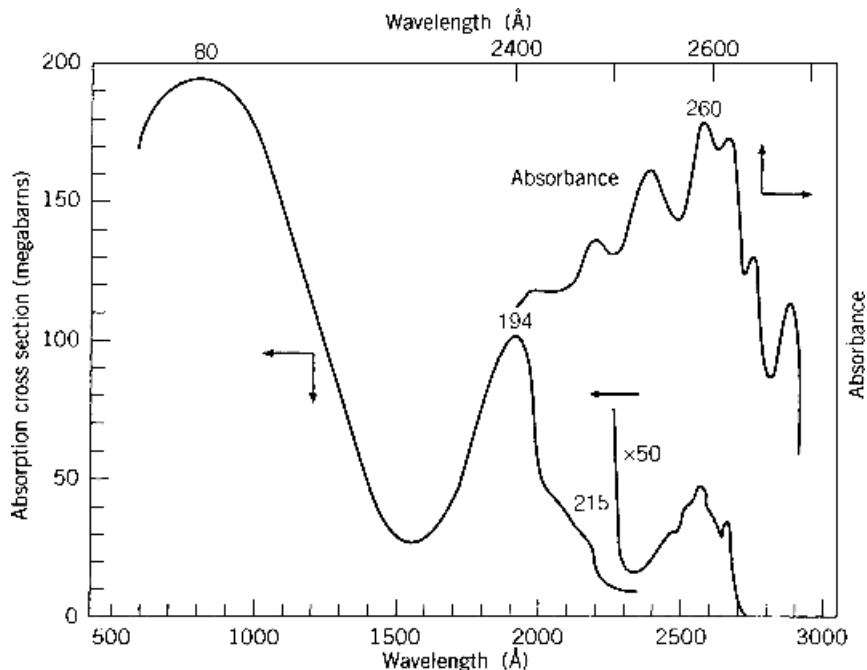


FIGURE 17.3 UV absorption spectrum of polystyrene. [Adapted from *Encyclopedia of Polymer Science and Technology*, Vol. 13 (1970) with permission from John Wiley.]

17.1.4 Proteins

UV spectroscopy plays a very important role in the study of biological polymers both as an analytical tool and as a probe to determine their structural properties. In the spectroscopy of biological polymers an absorption band at about 190 nm is attributed to the amides. This band is less intense for the helical polypeptides and helical proteins than for the same polymers in the random-coil conformation. For this reason the measurement of the extinct coefficient for a biological polymer near 190 nm can be used to estimate the helical content of the biological polymer sample in much the same way that optical activity was used in Chapter 12. The measurement of this band also reflects the hypochromism of the biological compound. Another important band occurs near 280 nm and is generally attributed to the presence of tyrosine, tryptophan, phenylalanine, or even arginine. The band at 280 nm is so strong that it often obscures the band at 190 nm.

Figure 17.4 shows the UV absorption spectra for the three amino acids: tyrosine, tryptophan, and phenylalanine. It is clear that near 280 nm tyrosine and tryptophan are stronger absorbers than phenylalanine. The UV absorption of tyrosine is often used to characterize the structure of the whole protein, as we discuss further. The following is a description of some of the applications of UV absorption spectroscopy in protein chemistry.

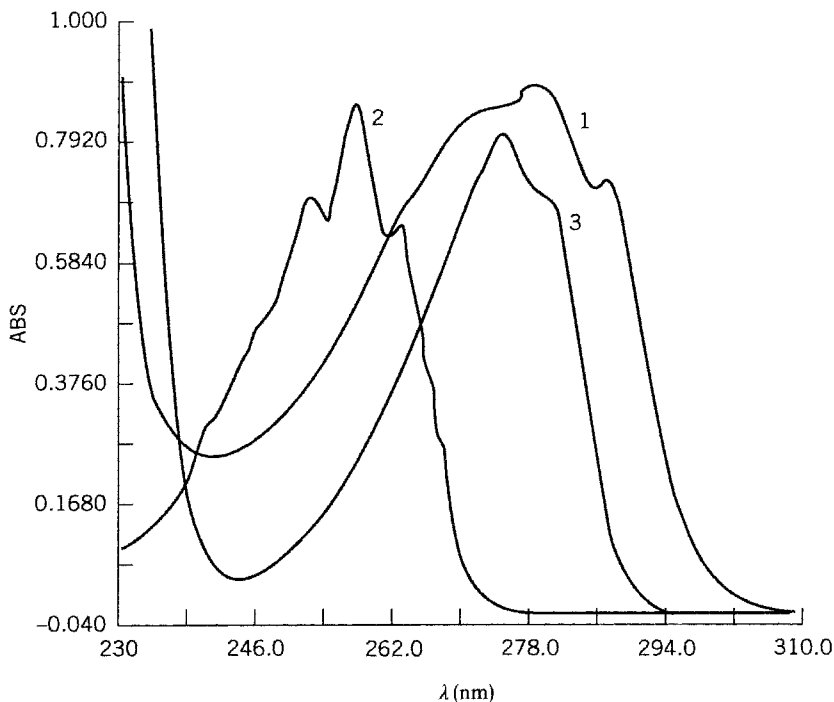


FIGURE 17.4 UV absorption spectra of amino acids: 1, L-tryptophan; 2, L-phenylalanine; 3, D-tyrosine.

Elucidation of Protein Structure UV absorption has been used to study the intra- and intermolecular interactions of biological chromophores in different environments. These interactions are often manifested in the shapes of macromolecules. For example, poly-L-lysine hydrochloride exists in three different forms in aqueous solution, depending on the pH and temperature of the solution: random coil, pH 6.0, 25°C; helix, pH 10.8, 25°C; and β -form, pH 10.8, 52°C. The UV absorption spectra of poly-L-lysine hydrochloride for these three forms are shown in Figure 17.5.

Determination of the Concentration Equation (17.1) can be expressed in the form

$$\varepsilon = \frac{A}{bC}$$

Let $E_{1\text{cm}}^{1\%}$ or $A_{1\text{cm}}^{1\%}$ be defined as the absorbance of a 1% solution of the substance in a 1-cm cell. Then $E_{1\text{cm}}^{1\%}$ is related to ε by

$$10\varepsilon = (E_{1\text{cm}}^{1\%})(M)$$

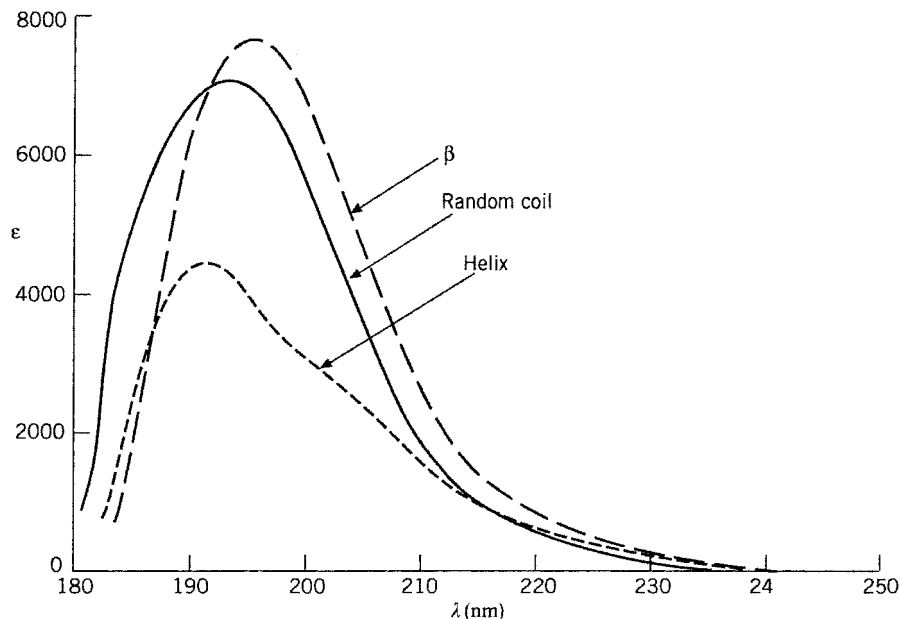


FIGURE 17.5 UV absorption spectra of poly-L-lysine hydrochloride in aqueous solution. [Source: Rosenbeck and Doty (1961) with permission of Dr. Doty.]

where M is the molecular weight of the substance. The concentration c (in grams per 100 mL) can now be determined by the measurement of its absorbance A :

$$c = \frac{A}{E_{1\text{cm}}^{1\%}}$$

Both A and E must be measured at the same wavelength λ , which is usually in the region of 210–290 nm. For example, the $E_{1\text{cm}}^{1\%}$ values are 6.67 for bovine serum albumin and 12.5 for trypsin when both are measured at 279 nm.

Spectrophotometric Titrations Spectrophotometric titrations are based on the ionization of the phenolic chromophore of tyrosyl groups which occurs in the pH range of 9 and above. When a protein is titrated with alkali, the tyrosyl residues are ionized, which results in a new stronger absorption peak at about 293–295 nm. The change in the absorption intensity at 293–295 nm can be used to estimate the tyrosine (and also the tryptophan) content as well as the acid strength of these groups in proteins. Figure 17.6 shows the spectrophotometric titration of bovine serum albumin at ionic strength 0.03 and temperature 25°C, measured at 295 nm.

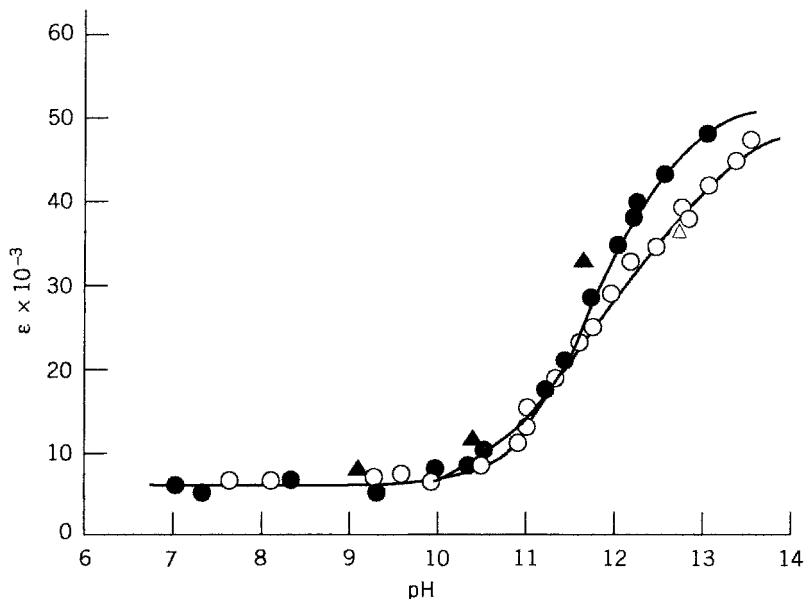


FIGURE 17.6 Spectrophotometric titration data for bovine serum albumin at ionic strength 0.03 and 25°C. ○, in dioxane–water (1 : 3, v/v); ●, in water; △, in dioxane–water (1 : 3, v/v) reserved; ▲, in water reversed. [Source: Sun (1970). Reproduced with permission of Elsevier Science Publishers B.V.]

Difference Spectra When the unperturbed material is taken as the reference and the perturbed material is taken as the sample, the shift in the absorption spectrum as observed along the wavelength axis produces the difference spectrum. Perturbation can be produced by adding a different compound (such as LiCl) or an organic solvent (such as alcohol) to the aqueous protein solution to affect the environment of the tyrosyl residues. The effect of these perturbation materials is not strong enough to change the conformation of the native protein but is large enough to cause measurable shifts in the spectrum. The purpose of using difference spectra is to study the location of the tyrosyl and tryptophyl residues and their environment in a protein. For example, difference spectra can be used to determine how many tyrosyl or tryptophyl residues lie in the surface of the protein molecule and how many are buried in the protein molecule. Difference spectra can also be used for the titration of protein samples to investigate the change in pK values of the aromatic groups. Figure 17.7 shows the difference spectra of bovine serum albumin produced by ethanol, *n*-propanol, and dioxane, respectively.

17.1.5 Nucleic Acids

The absorption spectra produced by nucleic acids are due to their individual bases. The spectra can be obtained either for the whole molecule or for the individual

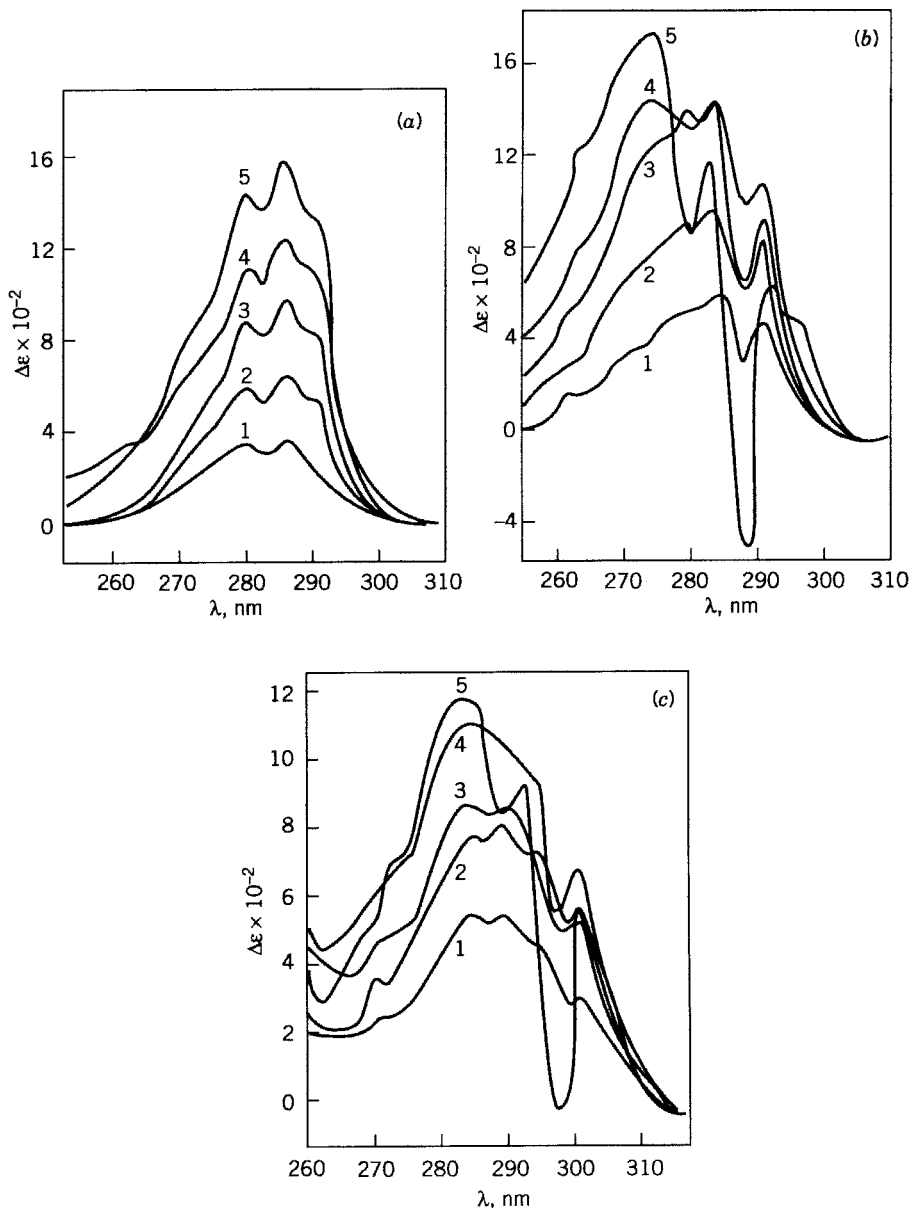


FIGURE 17.7 (a) Difference spectra of bovine serum albumin at pH 5.2–5.4, ionic strength 0.03, and 25°C produced by ethanol. Concentrations of ethanol (v/v): 1, 5%; 2, 10%; 3, 15%; 4, 20%; 5, 25%. (b) Difference spectra of bovine serum albumin at pH 5.2–5.4, ionic strength 0.03, and 25°C produced by *n*-propanol. Concentrations of *n*-propanol (v/v): 1, 5%; 2, 10%; 3, 15%; 4, 20%; 5, 25%. (c) Difference spectra of bovine serum albumin at pH 5.2–5.4, ionic strength 0.03, and 25°C produced by dioxane. Concentrations of dioxane (v/v): 1, 5%; 2, 10%; 3, 15%; 4, 20%; 5, 25%. [Source: Sun et al. (1983).]

bases. The absorption peaks for the four bases occur at the following frequencies: adenine, 260.5 nm; thymine, 264.5 nm; guanine, 275.0 nm; and cytosine, 267.0 nm. The ratio A_{250}/A_{280} for the four bases are often used to characterize DNA molecules under particular conditions. The values of these ratios are adenine, 2.00; thymine, 1.26; guanine, 1.63; and cytosine, 0.31. As in protein chemistry, the UV absorption spectra for nucleic acids can be used to determine their concentration. In addition, UV absorption can be used to study denaturation and renaturation of DNA molecules.

Determination of Concentration The amount of any base in a nucleic acid can be determined by measuring its optical density. The $E_{1\text{cm}}^{1\%}$ values for the four bases are adenine, 13.4×10^3 ; thymine, 7.9×10^3 ; guanine, 8.1×10^3 ; and cytosine, 6.1×10^3 ; all at 260 nm. For example, if the optical density (OD) at 260 nm of adenine were 0.80, the molar concentration would be $0.80/(1.34 \times 10^3) = 6.0 \times 10^{-5}$ M. As in the case of proteins, the value of OD_{260} is often used for estimating the concentration of DNA or RNA; for example, $OD_{260} = 1$ corresponds to 50 $\mu\text{g/mL}$.

Denaturation and Renaturation When DNA molecules are heated to certain temperature (e.g., 100°C), the two polynucleotide strands separate. The transition from the double strand (original form) to the single strand (denatured form) can be observed by the change in optical density at 260 nm. The plot of the optical density versus temperature gives a sinusoidal curve that is similar to an acid–base titration curve. In Figure 17.8 the point T_m , which corresponds to the equivalence point in an acid–base titration, is the hypochromic point and denotes where a mixture of the native and denatured strands occurs.

In contrast to denaturation, renaturation is the process by which the separated DNA strands are brought back together. If the denatured sample is reheated from 0°C to $T_m - 25^\circ\text{C}$ and maintained at $T_m - 25^\circ\text{C}$, then renaturation can be determined

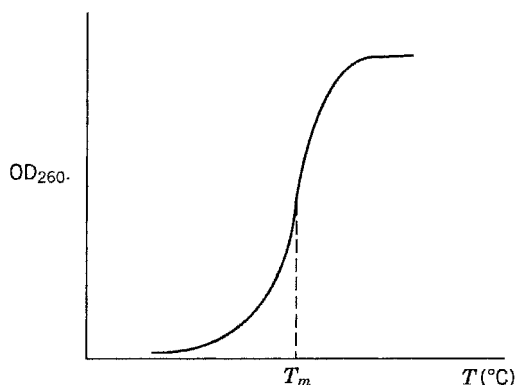


FIGURE 17.8 DNA denaturation process.

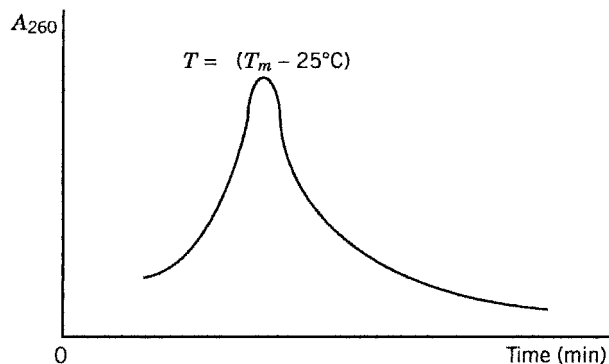


FIGURE 17.9 DNA renaturation process.

by measuring the absorbance at 260 nm as a function of time (Figure 17.9). Both denaturation and renaturation can be caused not only by heat but also by ionic strength and certain chemicals (e.g., alkali salts).

17.2 FLUORESCENCE SPECTROSCOPY

17.2.1 Fluorescence Phenomena

The absorption of radiation energy by a molecule causes an electron to be excited, whereby it jumps from the ground state to a higher energy state. The excited molecule, however, can return to the ground state by emitting photons of the same wavelength as the exciting radiation. The phenomenon is called resonance fluorescence. The excited molecule may also drop to various lower states by emitting photons with wavelengths different from that of the exciting radiation. This is known as fluorescence.

Most molecules have electrons that are spin paired in the ground state, namely $\uparrow\downarrow$. The \uparrow represents spin up and the \downarrow represents spin down. If one of the two electrons is excited to a higher energy state, we say that the electron is in a singlet excited state. There are also molecules that have unpaired electrons, namely $\uparrow\uparrow$ or $\downarrow\downarrow$ or a lone electron \uparrow or \downarrow . When an electron in these molecules is excited, we say that the electron is in a triplet state. Fluorescence is the emission that results from the return of the paired electron to the lower orbital. The return of the unpaired electron to the lower orbital emits radiation, called phosphorescence. Figure 17.10 shows the energy levels of a molecule that produce both fluorescence and phosphorescence. Since fluorescence consists of both an absorptive excitation and its subsequent emission, a fluorimeter is constructed with two sets of manometers, one to record the excitation and the other to record the emission. Because of their high sensitivity and high specificity, fluorescence measurements have long been used in biological studies of macromolecules. Phosphorescence measurements of biological macromolecules have yet to be explored.

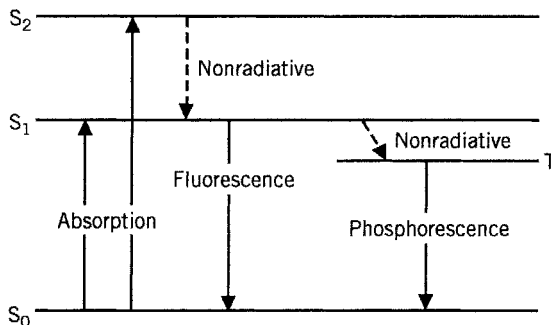


FIGURE 17.10 Fluorescence and phosphorescence: S, singlet; T, triplet.

Macromolecules may or may not fluoresce. Those that do are considered to contain intrinsic fluor. The common intrinsic fluor for proteins are tryptophan, tyrosine, and phenylalanine (the same three groups that absorb UV radiation). Macromolecules that have no intrinsic fluor can be made fluorescent by adding an extrinsic fluor to them. This is done by the process of chemical coupling or sample binding. The most common extrinsic fluor for proteins are 1-aniline-8-naphthalene sulfonate, 1-dimethylaminonaphthalene-5-sulfonate, dansyl chloride, 2-*p*-toluidyl-1-naphthalene-6-sulfonate, rhodamine, and fluorescein. The most common extrinsic fluor for nucleic acids are various acridienes (acridine orange, proflavin, acriflavin) and ethidium bromide.

17.2.2 Emission and Excitation Spectra

A fluorescence emission spectrum is a plot of fluorescence intensity versus wavelength (or wave number). It is a description of the distribution of photons in the fluorescence of a molecule excited by radiation. There is another type of spectrum, called the fluorescence excitation spectrum, which is also a plot of fluorescence intensity versus wavelength and which is also a description of the photon distribution. The difference lies in the method of obtaining the spectrum. For a fluorescence emission spectrum, it is a straightforward measurement of the intensity as a function of wavelength. For a fluorescence excitation spectrum, the measurement is carried out by varying the wavelength during the excitation, but the intensity of the emission is recorded at a constant wavelength. The fluorescence excitation spectrum is more similar to an absorption spectrum. Figure 17.11 shows the three spectra. In a UV difference spectrum the tyrosyl groups of a protein are the primary concern as to whether the tyrosyl groups are buried or on the surface of the molecule; in a fluorescence difference spectrum, it is the tryptophyl groups.

17.2.3 Quenching

In a collision with another molecule, Q, or with a surface, an excited molecule, M^* , may lose part or all of its excitation energy without any emission or radiation. Such

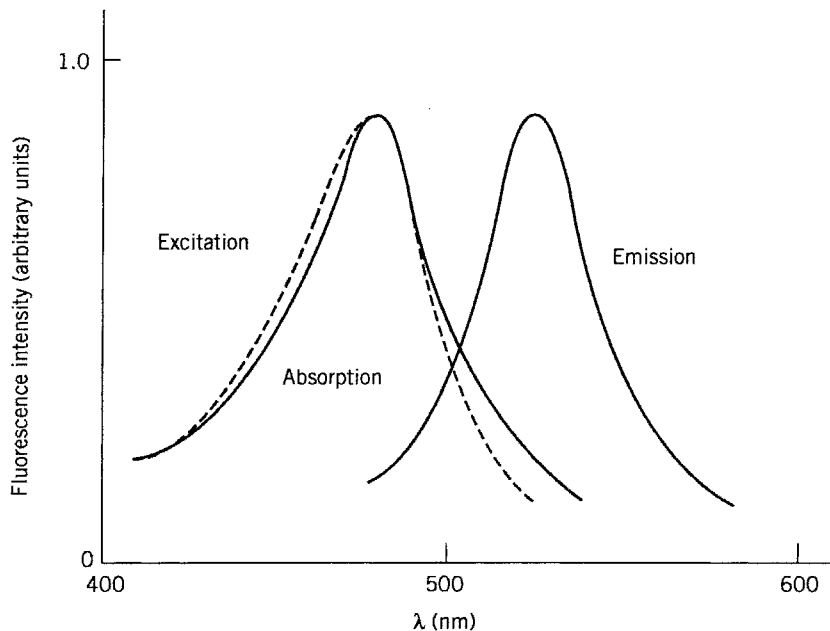
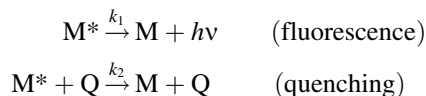


FIGURE 17.11 Fluorescence emission, fluorescence excitation, and visible absorption spectra of a fluorophore such as anthracene. The emission spectrum is obtained by irradiating the sample at one wavelength λ_{\max} (absorption) and recording the intensity as a function of wavelength. The excitation spectrum is obtained by plotting the intensity of the fluorescence emission at different wavelengths, but the recording is at one wavelength. Note that the excitation spectrum is virtually identical with the visible absorption spectrum.

a process is called quenching, and Q, with which the excited molecule M^* collides, is called the quencher. Moreover, the excited molecule M^* may encounter two competing parallel reactions:



The efficiency of fluorescence ϕ_F , which is also called the fluorescence quantum yield, or, simply, quantum yield, can be calculated based on the above two equations:

$$\phi_F = \frac{\text{number of photons emitted}}{\text{number of photons absorbed}}$$

$$= \frac{k_1 [M^*]}{k_1 [M^*] + k_2 [M^*][Q]}$$

The concentration term of $[M^*]$ can be eliminated by reversing the equation:

$$\frac{1}{\phi_F} = \frac{k_1[M^*] + k_2[M^*][Q]}{k_1[M^*]} = 1 + \frac{k_2}{k_1}[Q]$$

The resulting equation is called the Stern–Volmer equation, which is often used to obtain information about the nature of the local environment around a fluorescence molecule. The equation can be put into a slightly different form which is more easily appreciated from the experimental point of view:

$$\frac{F_0}{F} = 1 + k\tau_0[Q] = 1 + k_D[Q]$$

where F is the fluorescence intensity, the subscript 0 refers to the absence of the quencher, k is the bimolecular quenching constant, τ is the lifetime of the fluorescence, and k_D is the Stern–Volmer constant, defined as $k_D = k\tau_0$. The lifetime τ usually means the lifetime of the excited state. It is the average time the molecule spends in the excited state prior to its return to the ground state. The reciprocal of the fluorescence lifetime τ^{-1} is the fluorescence decay rate. Both F and τ are measurable quantities. They are related by

$$\frac{F_0}{F} = \frac{\tau_0}{\tau}$$

Figure 17.12 shows oxygen quenching of tryptophan as observed by fluorescence lifetimes and yields and is plotted according to the Stern–Volmer equation.

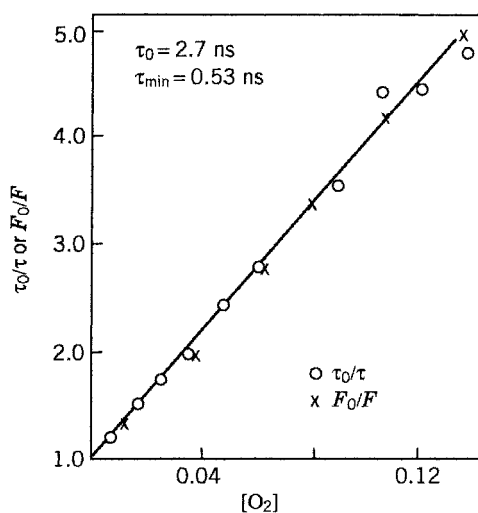


FIGURE 17.12 Oxygen quenching of tryptophan. [Source: Lakowicz and Weber (1973) with permission of Dr. Weber.]

Common quenchers are oxygen, xenon, hydrogen peroxide, iodide, and amines. The constant k is a second-order rate constant for a diffusion-controlled process. It is related to the translation diffusion coefficients of the fluorescence molecule and the quencher and hence is related to the radius of encounter.

17.2.4 Energy Transfer

Instead of the usual decay by a radiative or nonradiative process, an excited molecule may decay by another process, energy transfer. The excited molecule, which is called the donor, may transfer the excitation energy to another molecule, called the acceptor. The transfer is primarily a phenomenon of dipole-dipole interactions between the donor and the acceptor. The rate of energy transfer depends on several factors: the overlap of the emission spectrum of the donor with the absorption spectrum of the acceptor (J), the orientation of the donor and the acceptor transition dipoles (κ), and the distance between the donor and the acceptor (r). The overlap J is described by the integral

$$J = \int_0^{\infty} F_d(\lambda)\epsilon_a(\lambda)\lambda^4 d\lambda$$

where F_d is the fluorescence intensity of the donor and ϵ_a is the extinction coefficient of the acceptor. Both depend on wavelength λ . The orientation factor κ^2 is given by

$$\kappa^2 = (\cos \theta_T - 3 \cos \theta_d \cos \theta_a)^2$$

where θ 's are the angles, as shown in Figure 17.13.

The distance between the donor and the acceptor r is described by Forster's theory. Forster derived an equation for the rate of energy transfer from a specific donor to a specific acceptor k_T :

$$k_T = \frac{1}{\tau_d} \left(\frac{R_0}{r} \right)^{-6}$$

where τ_d is the lifetime of the donor in the absence of the acceptor and R_0 , which is now called the Forster distance, is defined as the characterized distance at which the

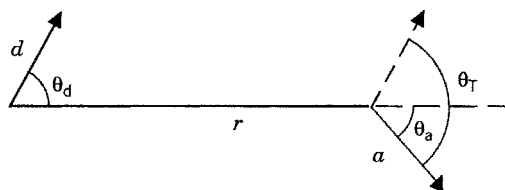


FIGURE 17.13 Orientation factor κ^2 .

transfer rate is equal to the decay rate of the donor, that is,

$$k_T = \tau_d^{-1}$$

At R_0 the efficiency of transfer is 50%. The donor fluorescence quantum yield in the absence of transfer ϕ_d and the overlap integral J are both incorporated in the equation of R_0 :

$$R_0 = [(8.8 \times 10^{-25})(\kappa^2 n^{-4} \phi_d J)]^{1/6}$$

where n is the refractive index of the medium (e.g., water). In experiments, the efficiency of energy transfer (E) can be directly related to the distance r using

$$E = \frac{R_0^6}{R_0^6 + r^6}$$

Figure 17.14 shows energy transfer in 1-anilinonaphthalene-8-sulfonic acid (ANS) and bovine serum albumin (BSA) complex. In this system, r is less than $\frac{3}{2}R_0$, $\tau = 8$ ns, $J = 2.0 \times 10^{10} \text{ cm}^3/\text{mM}^2$, and $R_0 = 24 \text{ \AA}$.

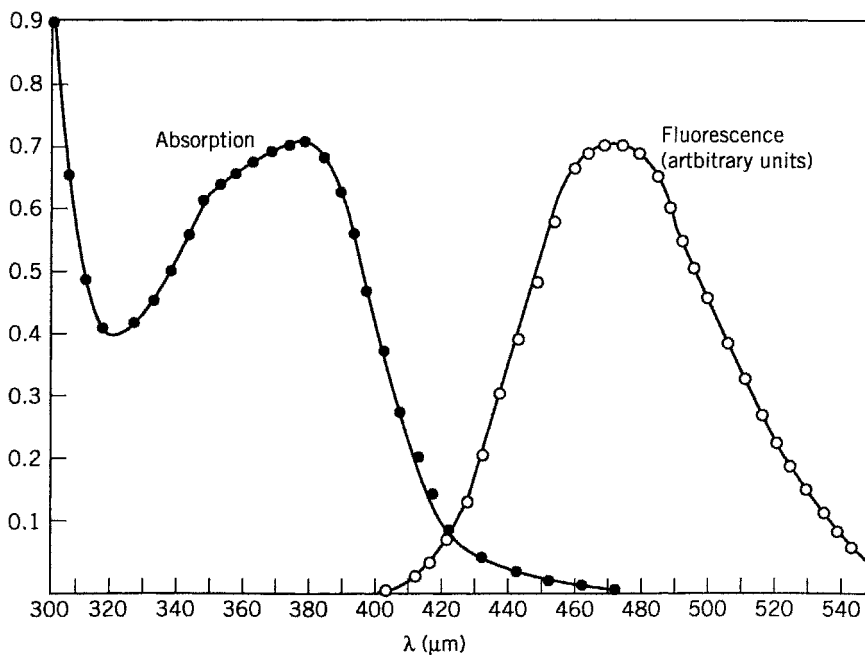


FIGURE 17.14 Energy transfer in ANS and BSA complex. [Source: Weber and Young (1964). With permission from Dr. Webber and the American Society for Biochemistry and Molecular Biology.]

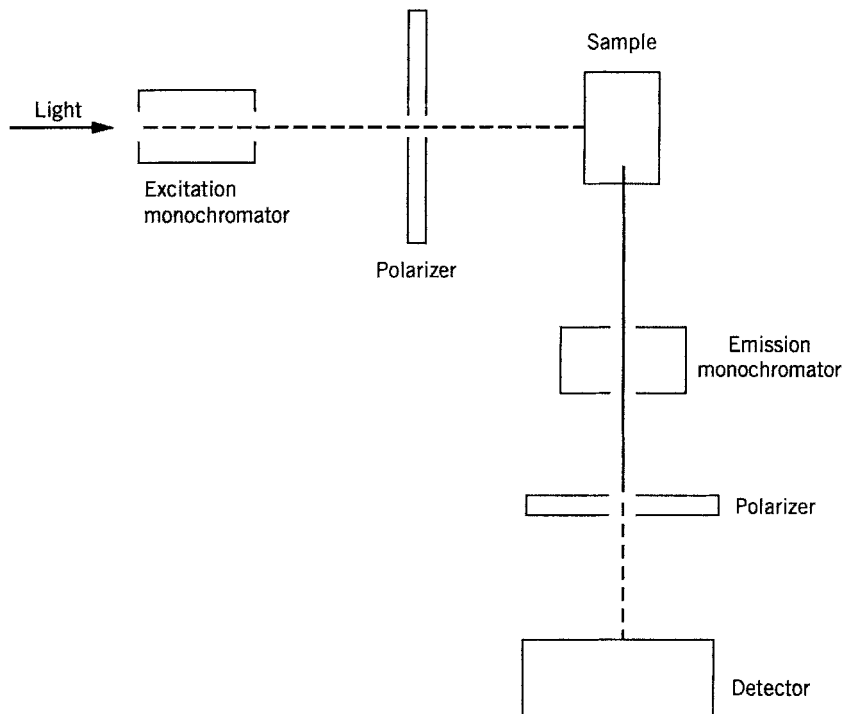


FIGURE 17.15 Diagram for polarization and depolarization measurements.

17.2.5 Polarization and Depolarization

Polarization of fluorescence is the result of the relative orientations of the absorption and emission oscillators. Consider Figure 17.15. By manipulating the two polarizers, we can measure the fluorescence intensities I_{\parallel} and I_{\perp} , respectively, where I_{\parallel} is obtained when the electric vector of the linearly polarized light is parallel to an arbitrary axis (such as z) while I_{\perp} is perpendicular to the arbitrary axis (z), as shown in Figure 17.16. The degree of polarization p is defined as

$$p = \frac{I_{\parallel} - I_{\perp}}{I_{\parallel} + I_{\perp}} = \frac{I_{zz} - I_{zy}}{I_{zz} + I_{zy}}$$

If all the molecules are oriented in the same direction, for example, parallel to the z axis, then p is clearly equal to unity. If the molecules are partially oriented, $p \neq 1$. For $p < 1$, we call p fluorescence depolarization.

Depolarization is a manifestation of the intrinsic properties of the macromolecule. It is the result of Brownian motion and it involves the translation of molecules and their rotational movements. Since Brownian motion is affected by temperature, solvent viscosity, and the size and shape of the molecule, these factors also affect the value of p . The angle θ between the original direction of the molecules in a

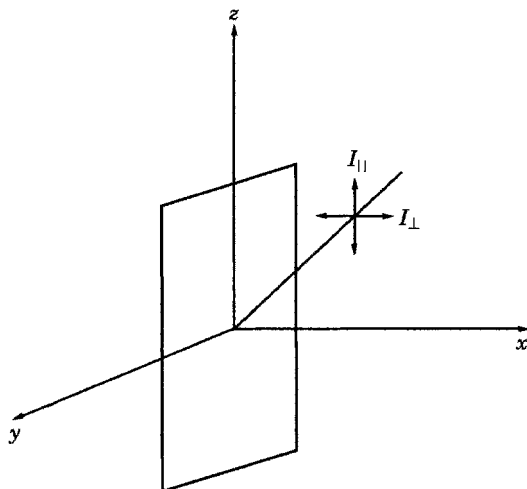


FIGURE 17.16 Coordinates of I_{\parallel} and I_{\perp} .

solvent system and their new direction due to some external force is called the orientation angle. The mean value of its cosine, $\overline{\cos \theta}$, is a measure of its orientation. Perrin (1926) derived an equation for p that takes all these factors into consideration:

$$\frac{1}{p} - \frac{1}{3} = \frac{8}{3} \frac{\overline{\cos^2 \theta}}{2\overline{\cos^4 \theta} - \overline{\cos^2 \theta}} \left(\frac{\tau}{\tau_R + 1} \right) (3 \overline{\cos^2 \delta} - 1)^{-1}$$

where τ_R is the rotational relaxation time of the fluorescent molecule, τ is the lifetime of excitation, and δ is the intramolecular vector angle. For molecules in random orientation, the equation becomes

$$\frac{1}{p} - \frac{1}{3} = \left(\frac{1}{p_0} - \frac{1}{3} \right) \left(1 + \frac{\tau}{\tau_R} \right)$$

where p_0 is the limiting polarization at infinite viscosity. In addition, if the molecules are spherical, then the frictional coefficient can be expressed in terms of Stokes' law for rotation:

$$\zeta = 8\pi\eta a^3$$

and

$$\tau_R^{-1} = \frac{kT}{V\eta}$$

where V is the molecular volume. The Perrin equation is now in the form

$$\frac{1}{p} - \frac{1}{3} = \left(\frac{1}{p_0} - \frac{1}{3} \right) \left(1 + \frac{kT}{V\eta} \tau \right)$$

By plotting $1/p$ or $(1/p_0 - \frac{1}{3})$ versus T/η , we can obtain information about V if τ is known or about τ if V is known from other sources.

17.3 INFRARED SPECTROSCOPY

Infrared (IR) spectroscopy has long been used to determine molecular structure and to identify unknown compounds. IR data have been used to obtain information about the chemical composition, configuration, and crystallinity of polymeric materials. Recently, IR spectroscopy has encountered competition from other techniques, such as NMR and x-ray diffraction. Nevertheless, IR spectroscopy's importance as an experimental technique continues largely because of the rapid development of Fourier transform infrared (FTIR) spectroscopy, which is sensitive to the detailed structure of a molecule.

17.3.1 Basic Theory

Assuming that atoms vibrate in a harmonic potential, the equation of motion that describes IR spectroscopy is the Lagrange equation:

$$Fr + K\ddot{r} = 0$$

where F involves force constants, K involves reduced mass of the molecule, r is the internal coordinate that describes changes in the bond lengths and bond angles, and \ddot{r} is the second derivative of r with respect to time. This equation can be reduced to the well-known eigenvalue equation:

$$GFL = L$$

where $G = K^{-1}$ is the matrix that contains the mass of the atoms and information on the geometry of the molecule and L is the matrix of elements l . The element l is the vibrational displacement and is defined as

$$r = l_j \cos(\omega_j t + \phi)$$

In the above equation ω is equal to $v/2\pi$, t is the time, and ϕ is the phase shift. The solution of the above eigenvalue equation is the secular determinant

$$|GF - E\Lambda| = 0$$

where E is a matrix of electric vectors, which is related to the dipole moment, and Λ is a diagonal matrix, with the vibrational frequency defined as

$$\nu_k = \left(\frac{\lambda_k}{4\pi^2 c'^2} \right)^{1/2}$$

where λ_k is the wavelength and c' is the velocity of light.

This theoretical calculation is used to idealize a macromolecule and to calculate the fundamental frequency ν_k , which is then compared to the experimental frequency. In the calculation of molecular symmetry, periodicity of potential functions and force constants were introduced. If the results of these calculations are in agreement with those from experiment, then the assumed parameters (symmetry, potential function, and force constant) contain information about the actual macromolecule. A detailed calculation is illustrated by the study of polyethylene (see Bower and Maddams, 1989).

17.3.2 Absorption Bands: Stretching and Bending

From the basic theory it is easy to understand that an absorption band appears only when the frequency of the radiation incident upon a compound is the same as the vibrational frequency of that compound. This phenomenon is related to the change of the dipole moment or to the change in polarizability. If it is related to the change of the dipole moment, we observe an IR band. If it is related to the change in polarizability, we observe a Raman band. Since dipole moment and polarizability are closely related, so are IR spectroscopy and Raman spectroscopy. These two spectroscopies can supplement the information of each other. The general principles that apply to IR spectroscopy can also be extended to Raman spectroscopy. In this section we describe IR spectroscopy only. The absorption range of IR spectroscopy is sketched in Figure 17.17. The term micro (μ) refers to the wavelength λ and $1\mu = 10^{-4}$ cm. In the older literature, prism instruments were used in IR spectroscopy and the IR spectra were presented in wavelengths. Today, grating instruments are used in most laboratories and the IR spectra are presented in wave numbers.

Two kinds of fundamental vibration bands are used to describe the vibrational behavior of polymers: stretching and bending. These bands may be further divided into different modes. The six typical modes are shown in Figure 17.18. The terms

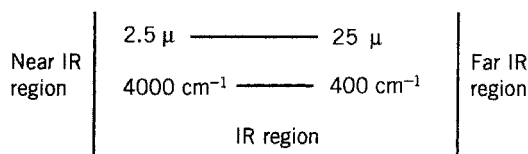


FIGURE 17.17 Absorption range of IR.

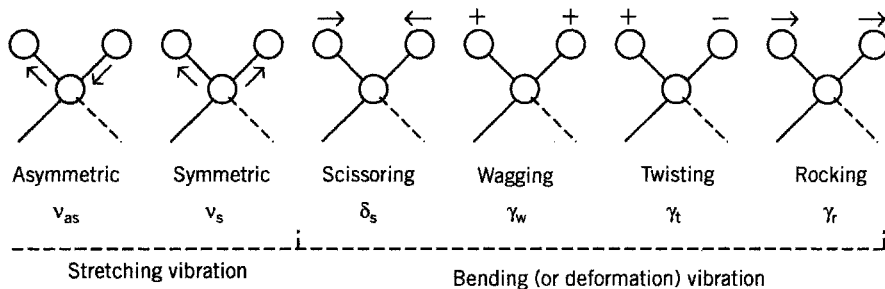


FIGURE 17.18 Six typical modes of vibration.

ν_{as} , ν_s , δ_s , γ_w , γ_t , and γ_r are given under each mode. The arrows show the direction of the vibration, while the plus and minus signs denote the vibrations that are in a direction perpendicular to the page.

In an IR spectrum, there often appear overtones, which have twice the frequency of the normal vibration (e.g., the carbonyl group has its fundamental vibration band at 1715 cm^{-1} and an overtone at 3430 cm^{-1}), and combination overtones, which are at frequencies equal to the sum or difference of two or more fundamental bands. Both overtones and combination overtones appear in the IR spectra as weak bands. They arise from small anharmonicities which tend to couple with the normal vibrations. Detailed information on the structure of the investigated macromolecule can be gained by correlating characteristic bands and band combinations with the aid of knowledge learned from small molecules. The mode of the alcohol group is shown in Figure 17.19 and the well-known IR spectrum of SO_2 is shown in Figure 17.20. In Figure 17.20 we observe fundamentals ν_1 1146 , ν_2 519 , and ν_3 1360 , overtones $2\nu_1$ 2322 , and combination bands $\nu_1 + \nu_3$ 2562 . The three fundamentals are sketched in Figure 17.21.

The factor that determines the position of the absorption bands is the potential energy of the molecule. For SO_2 , the potential energy V can be expressed as

$$V = \frac{1}{2} [k_1(Q_1^2 + Q_2^2) + k_8\delta^2]$$

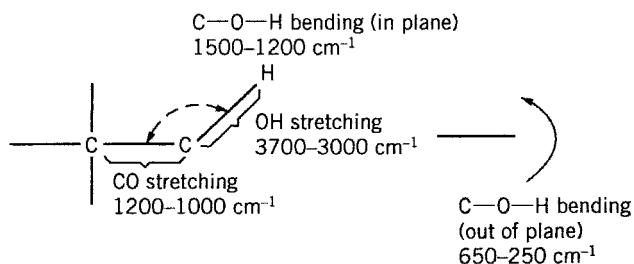


FIGURE 17.19 Mode of alcohol group.

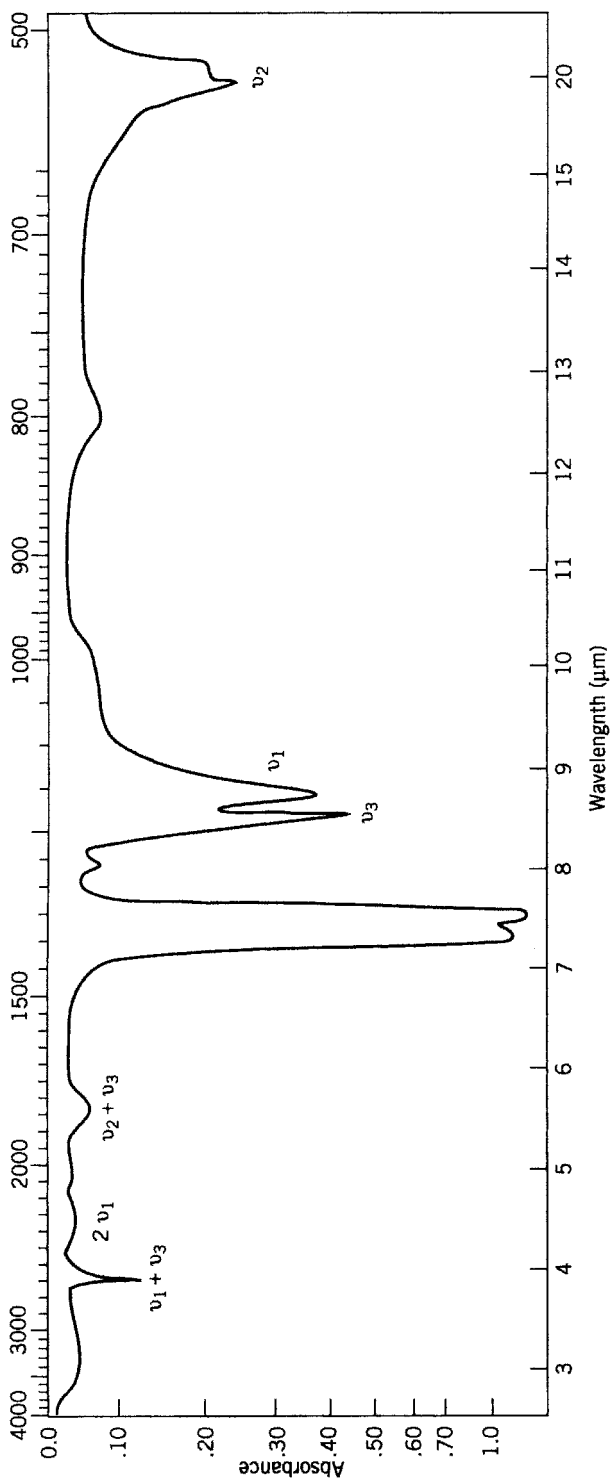


FIGURE 17.20 IR spectrum of SO₂.

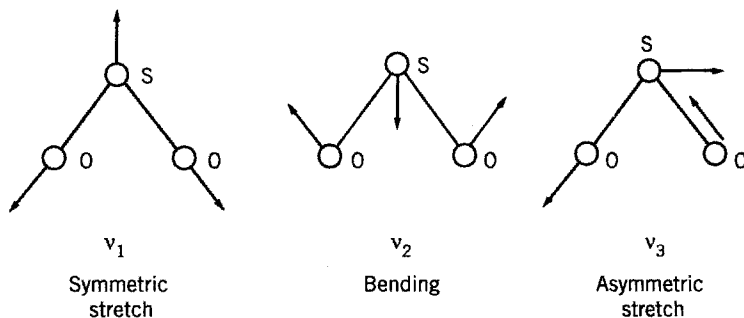


FIGURE 17.21 Three fundamentals of SO_2 .

where Q_1 and Q_2 are changes in S—O distance (whose equilibrium value is denoted by l) and δ is the change in the bond angle $2\alpha(\text{O—S—O})$. The quantities k_1 and k_δ/l^2 are force constants (usually in dynes per centimeter) for stretching and bending motions, respectively.

The stretching frequency ν of a diatomic molecule is, in general, based on the classical mechanics of a harmonic oscillator:

$$\nu = \frac{1}{2\pi c'} \sqrt{\frac{f(m_1 + m_2)}{m_1 m_2}}$$

where c' is the velocity of light and f is the force constant (bond strength or bond order). Thus, the absorption frequency depends on the bond strength f and the masses of atoms m . As the bond strengths increase from single to double to triple bonds, the stretching frequencies also increase from $700\text{--}1500\text{ cm}^{-1}$ to $1600\text{--}1800\text{ cm}^{-1}$ and to $2000\text{--}2500\text{ cm}^{-1}$. Also, the heavier the atoms are, the lower their frequency. For example, vibration of the O—H bond is at 3600 cm^{-1} but is lowered to 2630 cm^{-1} in the O—D bond.

17.3.3 Infrared Spectroscopy of Synthetic Polymers

The IR absorption spectrum of synthetic polymers is generally simple. In Figure 17.22 we illustrate the polystyrene spectrum, which is fairly representative of aromatic hydrogen polymers. The polystyrene spectrum's three IR bands appear sharply in the spectrum without ambiguity at 2850 , 1603 , and 906 cm^{-1} . The bands above 3000 cm^{-1} are due to unsaturated C—H stretching vibrations. The stretching vibration of conjugated C=C appears around 1600 cm^{-1} . The presence of the 760-- and 700--cm^{-1} bands are attributed to C—H deformations. Monosubstitution is confirmed by the pattern of weak bands from 2000 to 1600 cm^{-1} . Atactic polystyrene has bands at $670, 620, 565$ (shoulder), and 536 cm^{-1} . Isotactic polystyrene does not have any absorption from 550 to 500 cm^{-1} or at 670 cm^{-1} . The

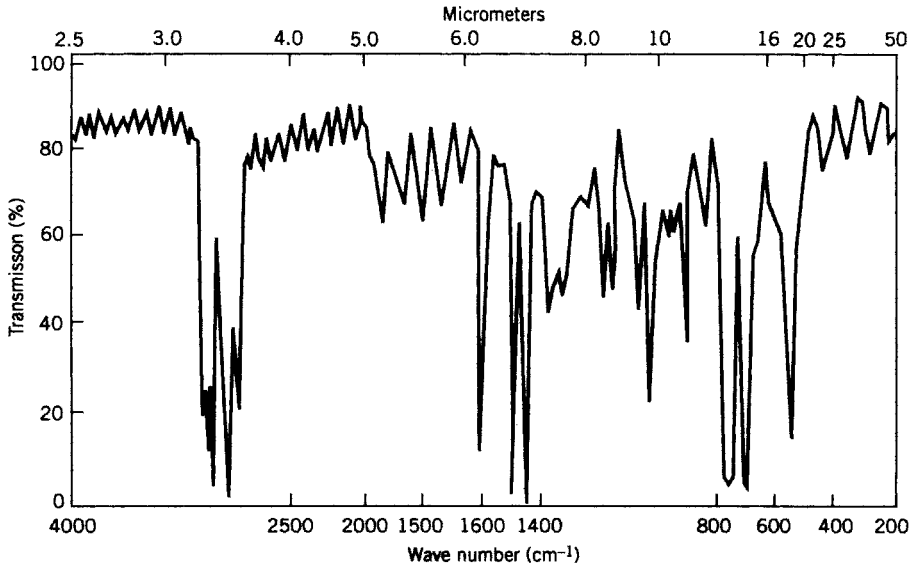


FIGURE 17.22 IR spectrum of polystyrene.

interference fringes between 4000 and 3200 cm^{-1} and between 2700 and 2000 cm^{-1} are used to determine the film thickness.

Characteristic Frequency of Functional Groups A large number of characteristic band tables are available. Here, we list the characteristic frequencies for functional groups that are frequently encountered in polymer spectroscopy:

Alkanes	
ν -CH	$2950\text{--}2850\text{ cm}^{-1}$
δ -CH	$1465\text{--}1380\text{ cm}^{-1}$
Alkene	
ν -CH	$>3000\text{ cm}^{-1}$
Aromatics	
In-plane bending	$1225\text{--}950\text{ cm}^{-1}$
Out-of-plane bending and ring puckering	Below 900 cm^{-1}
Hydroxyl	
ν -OH	3300 cm^{-1}
Ether	1250 cm^{-1}
Carbonyl	$1900\text{--}1600\text{ cm}^{-1}$
Triple bond	$2300\text{--}2000\text{ cm}^{-1}$
Double bond	$1900\text{--}1500\text{ cm}^{-1}$
Single bond	$1300\text{--}800\text{ cm}^{-1}$

Typical triple bonds:	
C≡C stretching	2140–2100 cm ⁻¹
C≡N Stretching	2260–2200 cm ⁻¹
Double bonds of unsaturated polymer chains:	
Vinyl, R ₁ CH=CH ₂	990–909 cm ⁻¹
<i>trans</i> -R ₁ CH=CH R ₂	962 cm ⁻¹
Vinylidene, R ₁ R ₂ C=CH ₂	885 cm ⁻¹
R ₁ R ₂ C=CHR ₃	833 cm ⁻¹
<i>cis</i> -R ₁ CH=CHR ₂	704 cm ⁻¹
Amides	
Primary –CONH ₂	1690 cm ⁻¹
Secondary –CONH	1700 cm ⁻¹

Stereoregularity We have already discussed the stereoregularity of the IR spectrum of polystyrene. Figure 17.23 shows three IR spectra of polypropene. The spectra of atactic, syndiotactic, and isotactic polypropene are virtually the same at wave numbers of 1000 cm⁻¹ and above. Remarkable spectral differences are observed, however, in the spectra at wave numbers below 1000 cm⁻¹. This is consistent with our observations on the IR spectra of atactic, syndiotactic, and isotactic polystyrene as mentioned previously.

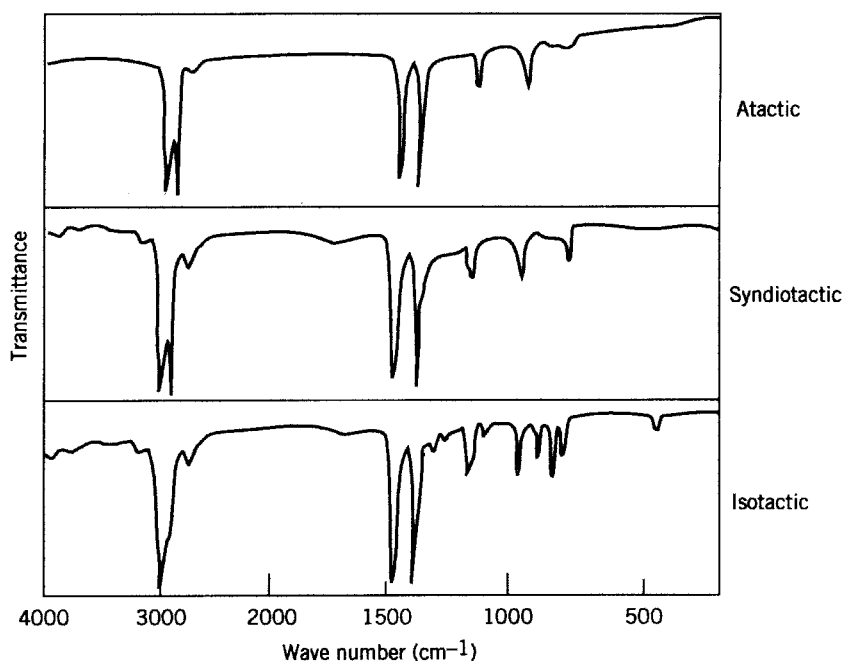


FIGURE 17.23 IR spectra of atactic, syndiotactic, and isotactic polypropene. [Source: Siesler and Holland-Mortiz (1980). By permission of Marcel Dekker, Inc.]

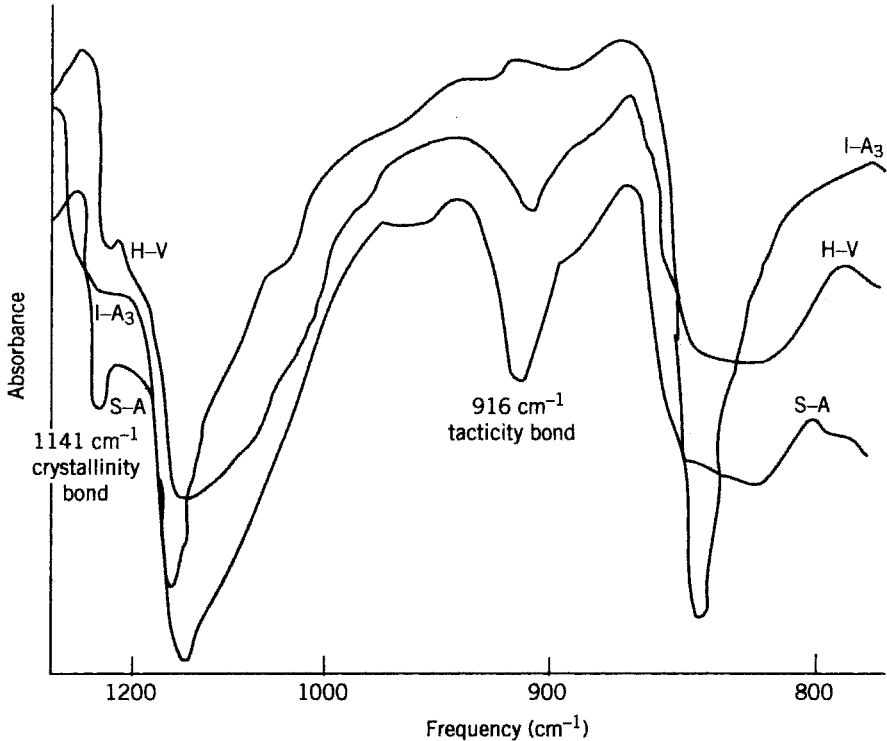


FIGURE 17.24 Crystallinity band of poly(vinyl alcohol). H-V, IA₃, and S-A are three different samples [Source: Kennedy and Willcockson (1966). By permission of John Wiley & Sons.]

Crystallinity Crystallinity bands are often assigned for polymer molecules in conjunction with the parameters of other techniques, such as density and x-ray diffraction. They describe the state of order in an investigated polymer molecule. In the spectrum of poly(vinyl alcohol), for example, the absorption band at 1141 cm^{-1} is assigned to the crystallinity of the molecule. The degree of crystallinity is measured by the intensity of the band at 1141 cm^{-1} , which matches the density of the molecule. Figure 17.24 shows this phenomenon.

17.3.4 Biological Polymers

Because of the complexity of biological polymers, their IR spectra are generally more difficult to analyze than the IR spectra of synthetic polymers. At present, IR spectra have been used basically as an analytic tool to identify certain functional groups of biological polymers. For proteins, the amide I and II bands appear in the region $1700\text{--}1500\text{ cm}^{-1}$ and are localized in the --CO--NH-- group. The frequencies of these bands are not dependent on the neighboring amino acid residue side

chains. Three important bands are related to the conformation of proteins: the amide bands at 1650 cm^{-1} for the α -helix, at 1685 cm^{-1} for the antiparallel, and at 1637 cm^{-1} for random structures. The appearance of a carbonyl band in a spectrum for a molecule that contains a hydroxyl group is an indication of its tautomerization. Identification of the number of hydrogen bonds can be determined by dissolving the polymer in D_2O and observing the bands due to the corresponding deuterium. For nucleic acids, since base pairs give bands at different frequencies, the ratio of the base pairs can be determined from the spectrum.

17.3.5 Fourier Transform Infrared Spectroscopy

The revival of interest in a very old instrument, the interferometer (for the study of light beams), together with the development of computer techniques has given IR spectroscopy new momentum and sophistication as a probe for investigating the structure of molecules, particularly macromolecules. Before FTIR was available, most spectroscopy instruments used prisms or gratings that could detect only the beams that passed through the slit. Much of the information about the molecular structure that could be obtained from beams other than those that could pass through the slit was completely wasted. The new FTIR device, along with the assistance of a rapid computer program (the Fourier transform algorithm), allows the study of all of the transmitted energy at one time.

Interferometer The interferometer was originally designed by Michelson in 1891. His idea was to divide a beam of light into two paths. The two beams were then recombined after a path difference had been introduced. The device is shown in Figure 17.25. The intensity of the beam can be measured as a function of the path difference by a detector. This optical path difference between the two beams traveling to the fixed and moving mirrors is called retardation and is designated by the symbol δ . When the two beams are in phase, they interfere with each other constructively; when the two beams are not in phase, they interfere with each other

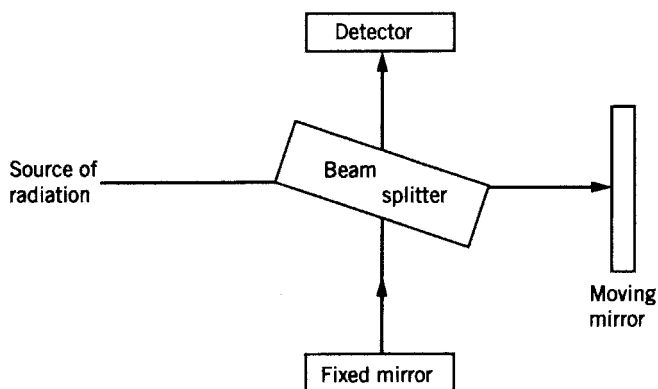


FIGURE 17.25 Diagram of an interferometer.

destructively. The intensity at any point is equal to the intensity of the source. The quantity measured by the interferometer is called the interferogram and is designated as $I(\delta)$, which is related to the true spectrum $\beta(\bar{\nu})$ by

$$I(\delta) = \beta(\bar{\nu}) \cos 2\pi\nu\delta$$

Fourier Transform The interferogram $I(\delta)$ is the Fourier transform of spectrum $\beta(\bar{\nu})$:

$$I(\delta) = \int_{-\infty}^{\infty} \beta(\bar{\nu}) e^{i\pi\nu\delta} d\bar{\nu}$$

$$\beta(\bar{\nu}) = \int_{-\infty}^{\infty} I(\delta) e^{-i2\pi\nu\delta} d\delta$$

For numerical computations the spectrum $\beta(\bar{\nu})$ should be changed into the form of a summation instead of an integration:

$$\beta(\bar{\nu}) = \sum_{j=0}^{(N/2)-1} A_j I_j(\delta) \exp(-ij2\pi\nu\delta)$$

where N is the number of spectrum points. Note that here $i = \sqrt{-1}$ and j is the index of a spectrum point. The values of $I_j(\delta)$ are obtained from the experiment. The symbol A_j is a mathematical function called the apodizing function, which is a corrective procedure for modifying the basic Fourier transform integral. The term $\exp(-ij2\pi\nu\delta)$ is usually transformed into sine and cosine functions. One can make a table of cosines or sines and then reduce the argument $2\pi j\nu\delta$ to the first period. For each $\beta(\bar{\nu})$, we carry out N multiplications for $A_j I_j \cos 2\pi j\nu\delta$ and N multiplications for $A_j I_j \sin 2\pi j\nu\delta$. This results in a total of $2N$ multiplications. The adoption of the Cooley–Tukey algorithm in which $N = 2^n$ for some integer n not only makes the computation fast but also saves computer time and hence cost. (See Chapter 15.)

FTIR Studies of Polymers For the most part, the techniques used in the measurement of FTIR are the same as those applied to conventional samples. Spectral features of a component in a polymer are isolated from the solvent bands and from all other compounds present in the system. Analysis is carried out by computer programs. Figure 17.26 shows the spectrum of polystyrene with an IR microscope through a 10- μm aperture. We see that the baseline is flat even below 1000 cm^{-1} . This is very important because the frequency range of the IR spectrum below 1300 cm^{-1} , especially that below 1000 cm^{-1} , is known as the fingerprint region. Changes in frequency and intensity may be used to determine the microscopic characterization of the polymer to see if there exists any defect due to stress or the environment.

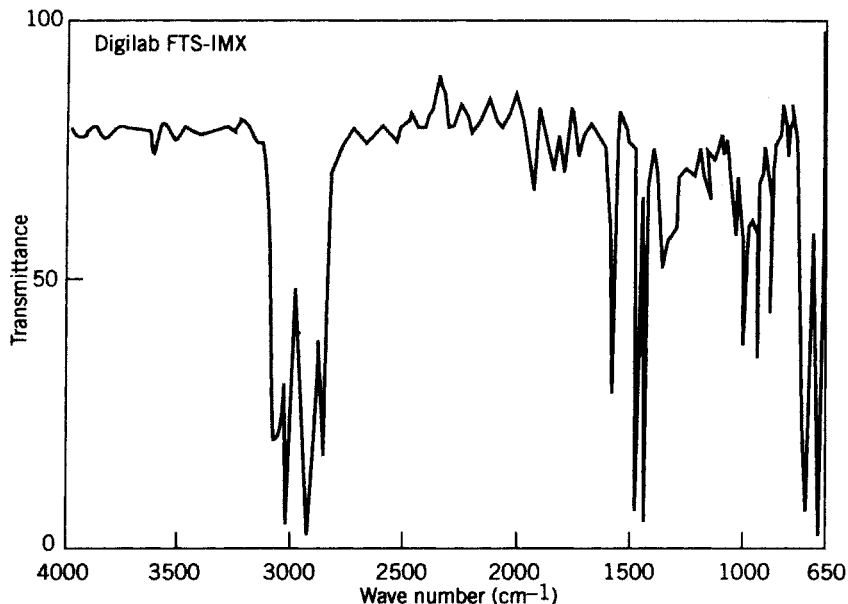


FIGURE 17.26 FTIR spectrum of polystyrene. [Source: Ferraro and Krishnan (1990). By permission of Dr. Krishnan and Academic Press, Inc.]

REFERENCES

- Alben, J. O., and L. Y. Fager, *Biochemistry* **11**, 842 (1972).
- Blout, E., *J. Am. Chem. Soc.* **83**, 712 (1961).
- Boaz, H., and G. K. Rollefson, *J. Am. Chem. Soc.* **72**, 3425 (1950).
- Bower, D. I., and W. F. Maddams, *The Vibrational Spectroscopy of Polymers*. New York: Cambridge University Press, 1989.
- Brand, E. A., *J. Chem. Soc.* 379 (1950).
- Briggs, D., *Polymer* 1379, (1984).
- Chapoy, L. L., and D. B. DuPré, *Methods Exp. Phys.* **16A**, 404 (1980).
- Chen, R. F., and R. L. Bowman, *Science* **147**, 729 (1965).
- Cooley, J. W., and J. W. Tukey, *Math. Comput.* **19**, 297 (1965).
- Duportail, G., D. Froelich, and G. Weil, *Eur. Polym. J.* **7**, 977, 1023 (1971).
- Encyclopedia of Polymer Science and Technology*, Vol. 13. New York: Wiley, 1970.
- Ferraro, J. R. and K. Krishnan (Eds.), *Practical Fourier Transform Spectroscopy*. New York: Academic, 1990, p. 112.
- Forster, T., *Ann. Phys. (Leipzig)* **2**, 55 (1948).
- Forster, T., *Naturforscher* **4**, 321 (1949).
- Freifelder, D., *Physical Biochemistry*. San Francisco: Freeman, 1976.
- Griffiths, P. R., and J. A. de Haseth, *Fourier Transform Infrared Spectrometry*. New York: Wiley, 1986.

- Harrington, W. F., P. Johnson, and R. H. Ottewill, *Biochem. J.* **62**, 569 (1956).
- Herskovits, T. T., and M. Laskowski, Jr., *J. Biol. Chem.* **235**, 57 (1960).
- Herzberg, G., *Molecular Spectra and Molecular Structure*, Vol. II: *Infrared and Raman Spectra of Polyatomic Molecules*. Princeton, NJ: Van Nostrand, 1945.
- Kämpf, G., *Characterization of Plastics by Physical Methods: Experimental Techniques and Practical Application*. Munich: Hauser, 1986.
- Kennedy, J. F., and G. W. Willcockson, *J. Polym. Sci. A* **4**, 679 (1966).
- Koenig, J. L., *Adv. Polym. Sci.* **54**, 89 (1984).
- Koenig, J. L., *Spectroscopy of Polymers*. Washington, DC: American Chemical Society, 1992.
- Krimm, S., *Fortschr. Hoch-Polym-Forschg.* **2**, 51 (1960).
- Krimm, S., in E. B. Mano, (Ed.), *Proceedings of the International Symposium on Macromolecules*. Amsterdam: Elsevier, 1975.
- Lakowicz, J. R., *Principles of Fluorescence Spectroscopy*. New York: Plenum, 1983.
- Lakowicz, J. R., and G. Weber, *Biochemistry* **12**, 4161 (1973).
- Marmur, J., and P. Doty, *J. Mol. Biol.* **5**, 109 (1962).
- McClure, W. O., and G. M. Edelman, *Biochemistry* **6**, 559, 567 (1964).
- McGovern, J. J., J. M. Grim, and W. C. Teach, *Anal. Chem.* **20**, 312 (1948).
- Nakanishi, K., and P. H. Solomon, *Infrared Absorption Spectroscopy*, 2nd ed. San Francisco: Holden-Day, 1977.
- Nishijima, Y., *J. Polym. Sci. C* **31**, 353 (1970).
- Nishijima, Y., A. Teramoto, M. Yamamoto, and S. Hiratsuda, *J. Polym. Sci. A2* **5**, 23 (1967).
- Perrin, F., *J. Phys.* **7**, 390 (1926).
- Rao, C. N. R., *Ultra-Violet and Visible Spectroscopy: Chemical Applications*, 3rd ed. London: Butterworth, 1975.
- Reddi, K. K., *Biochim. Biophys. Acta* **24**, 238 (1957).
- Rosenbeck, K., and P. Doty, *Proc. Natl. Acad. Sci. U.S.A.* **47**, 1775 (1961).
- Schiller, P. W., *Int. J. Peptide Protein Res.* **15**, 259 (1980).
- Siesler, H. W., and U. K. Holland-Mortiz, *Infrared and Raman Spectroscopy of Polymers*. New York: Dekker, 1980.
- Snyder, R. G., *J. Chem. Phys.* **47**, 1316 (1967).
- Stern, O., and M. Volmer, *Physics* **2** **20**, 183 (1919).
- Sun, S. F., *Biochim. Biophys. Acta* **200**, 433 (1970).
- Sun, S. F., T. S. Chang, and G. M. Lam, *Can. J. Chem.* **61**, 356 (1983).
- Thompson, H. W., *Proc. R. London Ser. A* **21** (1945).
- Weber, G., *Biochem. J.* **51**, 145, 155 (1952).
- Weber G., *Adv. Protein Chem.* **8**, 415 (1953).
- Weber, G., and D. J. R. Lawrence, *Biochem. J.* **56**, 31 (1954).
- Weber, G., and L. B. Young, *J. Biol. Chem.* **239**, 1415 (1964).
- Wetlaufer, D. B., *Adv. Protein Chem.*, Vol. 17. New York: Academic, 1961.
- Wetmur, J. G., and N. Davidson, *J. Mol. Biol.* **31**, 349 (1968).
- Yguerabide, J., H. F. Epstein, and L. Stryer, *J. Mol. Biol.* **51**, 573 (1970).
- Zerbi, G., L. Piseri, and F. Cabasi, *Mol. Phys.* **22**, 241 (1971).

PROBLEMS

- 17.1 The UV absorption extinction coefficient ϵ for a protein or a nucleic acid often does not represent the true value because of the partial scattering of light. This can be corrected by the equation

$$\epsilon_{\text{observed}} - \epsilon_{\text{scattered}} = \epsilon_{\text{true value}}$$

However, for correction, the extinction coefficient due to scattering, $\epsilon_{\text{scattered}}$, can be calculated with

$$\epsilon_{\text{scattered}} = \frac{c}{\lambda^4}$$

where c is the scattering constant, which can be determined by measuring absorption at wavelengths 350 and 400 nm where the protein and nucleic acid have no absorption. Plot the observed and corrected UV absorption spectra for tobacco mosaic virus on the basis of the following experimental data:

λ (nm)	ϵ
235	19,100
250	15,000
262	16,300
282	14,000
310	3,000
350	0.360
400	0.210

$$\begin{aligned} C &= 5.34 \times 10^{-19} \text{ cm}^{3/12} \\ &= 0.45 \times 10^{-19} \text{ cm}^3 \end{aligned}$$

(Reddi, 1957).

- 17.2 The molar extinction coefficient for acetyl esters of tyrosine is 1340 at 282 nm. If absorption was found to be 0.185 at 282 nm for a sample of aqueous solution of acetyl esters of tyrosine, find the concentration of the solution.
- 17.3 Helical contents of polypeptides can be estimated from UV absorption data at 190 nm ($\pi-\pi^*$ transition, which is characteristic of amide) by using the following equation:

$$\left(\frac{\epsilon_{\text{coil}} - \epsilon_{\text{peptide}}}{\epsilon_{\text{coil}} - \epsilon_{\text{helix}}} \right) (100) = \% \text{ helicity}$$

where ϵ is the molar extinction coefficient per residue. The values of ϵ_{coil} and ϵ_{helix} can be obtained from the model compounds (i.e., a compound assumed

to be 100% helical and one assumed to be 100% coil). For a series of oligopeptides of aspartate derivatives, if we take $\epsilon_{\text{coil}} = 7.2 \times 10^3$ and $\epsilon_{\text{helix}} = 3.2 \times 10^3$, what is the helical content in terms of percentage for polypeptides with $\epsilon_r = 2.5 \times 10^3$ and $\epsilon_r = 1.8 \times 10^3$, respectively?

- 17.4** The following data are given for iodide quenching of acridone:

KI (molar)	F_0/F
0.04	4.64
0.10	10.59
0.20	23.0
0.30	37.2
0.50	68.6
0.80	13.7

Construct a Stern–Volmer plot and determine the dynamic (k_D) and static (k_s) quenching constants. Assuming that $\tau_0 = 17.6$ ns, calculate the bimolecular quenching constant kq , (Lakowicz, 1983; Boaz and Rollefson, 1950).

- 17.5** The following experimental data are given for the reciprocal polarization ($1/p$) as a function of T/η for adsorbates of 1-anilino-naphthalene-8-sulfonic acid on BSA at 25°C in solutions of sucrose in water:

$1/p$	$T/\eta \times 10^{-4}$
3.00	1.23
3.07	1.75
3.16	2.29
3.22	2.75
3.29	3.31

Plot $1/p$ versus T/η to determine $1/p$ and calculate τ , the lifetime of the excited state of the fluorescence of the adsorbate. Assume that ρ_h , the mean harmonic rotational relaxation time, is 118 ns (Weber and Young, 1964).

- 17.6** A Perrin plot ($1/p$ vs. T/η) for fluorescense polarization of β -anthryl conjugate of BSA gave $p_0 = 0.267$ and $t_0 = 4.4 \times 10^{-8}$ s at 25°C. Calculate the rotational relaxation time ρ_h (Chen and Bowman, 1965; Harrington et al., 1956).
- 17.7** The intramolecular distance r can be estimated by measuring singlet–singlet energy transfer using the Förster equation:

$$E = \frac{R_0^6}{r^6 + R_0^6}$$

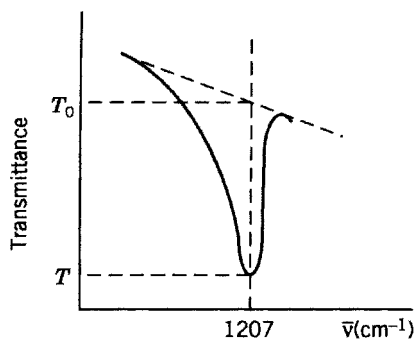
where E is the transfer efficiency and R_0 is defined as that donor–acceptor separation. For the angiotensin II analogs H·Tyr–Arg–Val–Phe–Val–His–Pro–Trp·OH in aqueous solution, pH 1.5, the values of Förster parameters were $E = 0.10$ and $R_0 = 11.6 \text{ \AA}$. Calculate the intramolecular Tyr–Trp distance (Schiller, 1980).

- 17.8** The oscillator strength f is defined as the number of oscillating units per molecule and, according to the classical theory, f is given by

$$f = 4.32 \times 10^{-9} \int \epsilon \, d\nu$$

where ϵ is the extinction coefficient and ν is the frequency of the light. Translating into experimental language, the integral $\int \epsilon \, d\nu$ is the integrated band area. Approximately, $\int \epsilon \, d\nu = \epsilon_{\max} \Delta\nu$, where $\Delta\nu$ is the half width (the width of the bands at point where $\epsilon = \frac{1}{2} \epsilon_{\max}$). Calculate f for proteins with ϵ_{\max} values of 1.5×10^3 and 135×10^3 and $\Delta\nu$ of 4500 and 5000 cm^{-1} , respectively (Brand, 1950).

- 17.9** A characteristic band at 1207 cm^{-1} of a polymer and its analysis is shown in the following hypothetical spectrum:



If a set of standard solutions of the monomer that contains the given polymer were available, a calibration curve could be constructed for the transmittance T as a function of the concentration of monomers. Assume that such data are given:

Concentration (% by volume)	10	20	40	60
Transmittance	80	68	45	30

Determine the concentration of a polymer in solution if its IR spectrum gives $T = 54$ and $T_0 = 86$.

17.10 A ligand in aqueous solution shows a characteristic band at 2048 cm^{-1} in an IR spectrum when a protein is present in the ligand solution. The spectrum consists of two bands: one at 2023 cm^{-1} , which is believed to be the ligand covalently bound to the protein, and the other at 2046 cm^{-1} , which is believed to be the ligand in ionic form. The equilibrium constant can be obtained from $(\text{area})_{2023}/(\text{area})_{2046}$ or A_{2023}/A_{2046} . Calculate thermodynamic constants ΔH° , ΔS , and ΔG on the basis of the following set of data:

A_{2046}	0.019	0.048	0.046	0.044
A_{2023}	0.094	0.084	0.080	0.070
$T(^{\circ}\text{C})$	-7	12	25	40

(Alben and Fager, 1972).

18

PROTEIN MOLECULES

After completion of the human genome sequences in the year 2000, the challenge was immediately redirected to using these data to interpret the function of proteins. Nucleic acids and proteins are inseparable components of the process of life. Nucleic acids direct the production of proteins, but it is the proteins that carry out the body's functions. Today, research in nucleic acids is always deeply intertwined with research of proteins and vice versa.

In Chapter 1, we introduced the concept of the protein. This chapter describes proteins in greater detail, including the fundamental principles that are emerging from post-human genome studies. The emphasis here is given to the sequence-structure relationship and how the protein is folded.

The classical way to describe a protein is in terms of its primary structure, secondary structure, tertiary structure, and quaternary structure. All four types of structure are closely related. They are only four different ways to characterize the same protein. We begin with the classical way to describe a protein, starting with its primary structure.

18.1 PROTEIN SEQUENCE AND STRUCTURE

18.1.1 Sequence

The sequence of the amino acid residues in a protein is called the primary structure. Two well-known examples are insulin and ribonuclease, as described in Chapter 2.

Among others, they are of historical importance, particularly insulin. The decade of work by Sanger and co-workers on the amino acid sequence of insulin represents pioneering research into the primary structure of a protein.

Insulin consists of two different polypeptide chains held together by —S—S— bridges. They can be separated by oxidation with performic acid. Similarly, ribonuclease consists of 124 amino acids and —S—S— bridges which can also be separated.

In the past, determination of the sequence of a protein was tedious and laborious work. For many years, only a very small number of well-known proteins had their sequence determined and reported in the research literature. Today, we have machines that do this painstaking work. As of the year 2000, The Protein Information Resource, a scientific organization, has catalogued the sequence of amino acids of at least 200,000 proteins and new data are accumulated every day.

18.1.2 Secondary Structure

The regular geometry of the segments is called the secondary structure. The secondary structure of a protein depends upon four factors: (1) the bond length and bond angles of the peptide bond, (2) the coplanar arrangement of the atoms involved in the amide groups, (3) the hydrogen bonds between N—H... and C=O... to maintain the maximum stability, and (4) the range of the distance in the hydrogen bonds.

Pioneering work was carried out by Pauling and Corey (1951, 1953). From x-ray diffraction studies on crystalline amino acids and small peptides, they drew a diagram of the spatial configurations of the polypeptide chains in which the covalent interatomic distances and bond angles were indicated. Figure 18.1 shows the diagram. Although such a diagram does not apply to all protein molecules, it does provide a general idea of the linkage of one amino acid to another. Figure 18.1 also demonstrates that the atoms involved in the amide group must remain coplanar, and, for maximum stability, each N—H group must be hydrogen bonded to a C=O and each C=O to a N—H.

18.1.2.1 α -Helix and β -Sheet Segments of the peptide chains are likely to be held in their coiled form because of intramolecular forces. The two best-known coils are the α -helix and β -sheet.

α -Helix Figure 18.2 shows Pauling and Corey's drawings of α -helices. The directions of the hydrogen bonds are nearly, though not quite, parallel to the axis of the helix. The left- and right-handed α -helices correspond to the turns of a left-handed screw and a right-handed screw.

The helices do not have to have an integral number of residues per turn. In many proteins, the α -helix repeats after exactly 18 residues, which amounts to five turns. It has, therefore, 3.6 residues per turn. Also, each carbonyl oxygen is hydrogen bonded to the amide proton on the fourth residue up the helix.

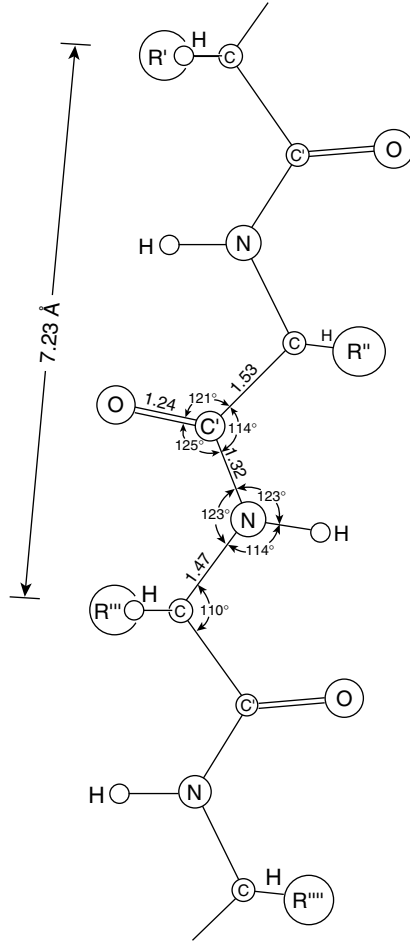


FIGURE 18.1 Dimensions and bond angles of a fully extended trans polypeptide chain.

β-Sheet A β -sheet (β -structure or pleated sheet) has a twist and the whole structure follows this twist, resulting in a staggered arrangement for the structural elements in the outer layers. Sheets can also curl and form a complete hydrogen-bonded cylinder (referred to as a “barrel”). All these parameters (twist, curl, stagger) might vary with different numbers of layers (of different compositions). Figure 18.3 shows the β -sheets in which all possible hydrogen bonds are formed between the segments of peptide backbone that are stretched out to nearly the maximum extension. They lay side by side. A sheet may be antiparallel, with chains that run in the opposite direction, as if the same chain were folded back and forth upon itself, or it may be made from segments of a chain that are looped back to run in the same direction, creating a parallel sheet.

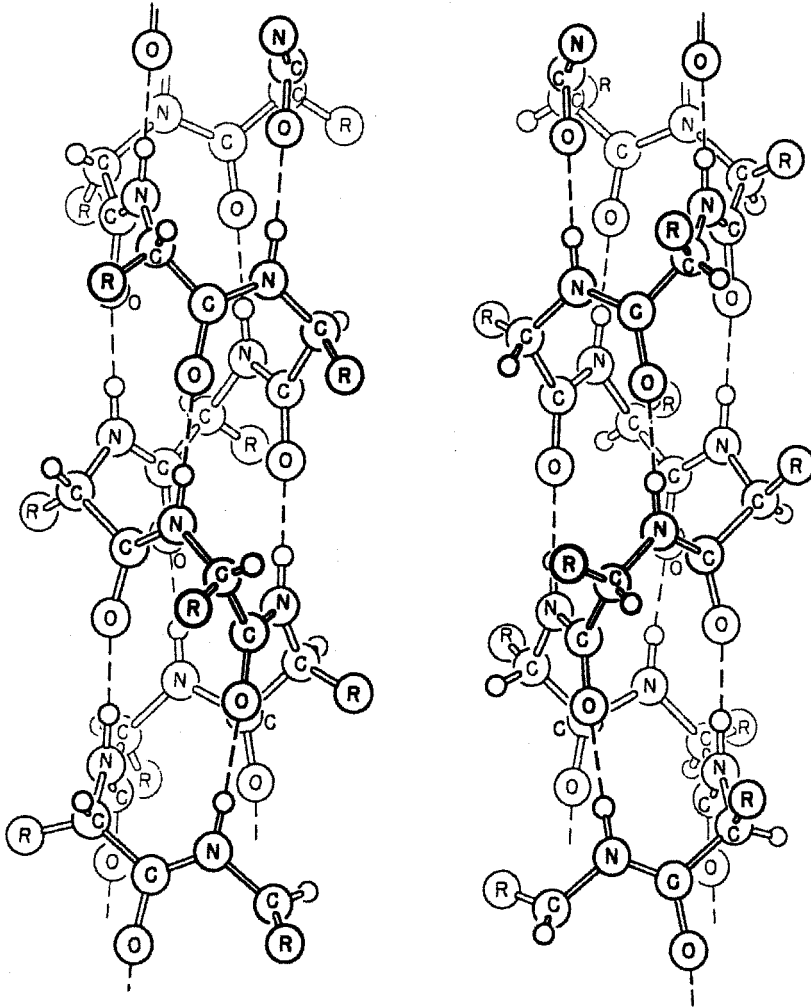


FIGURE 18.2 Drawings of the left- and right-handed α -helices.

18.1.2.2 Classification of Proteins Classification of proteins in terms of the secondary structure may be expressed as follows:

Protein	Examples
α -Proteins	Hemoglobin, myoglobin, myogen
β -Proteins	Immunoglobulin, concanavalin, chymotrypsin
$(\alpha + \beta)$ -Proteins (with both α and β)	Insulin, ribonuclease A, hen egg-white lysozyme
(α/β) -Protein (alternating α and β)	Alcohol dehydrogenase, subtilisin, hexokinase

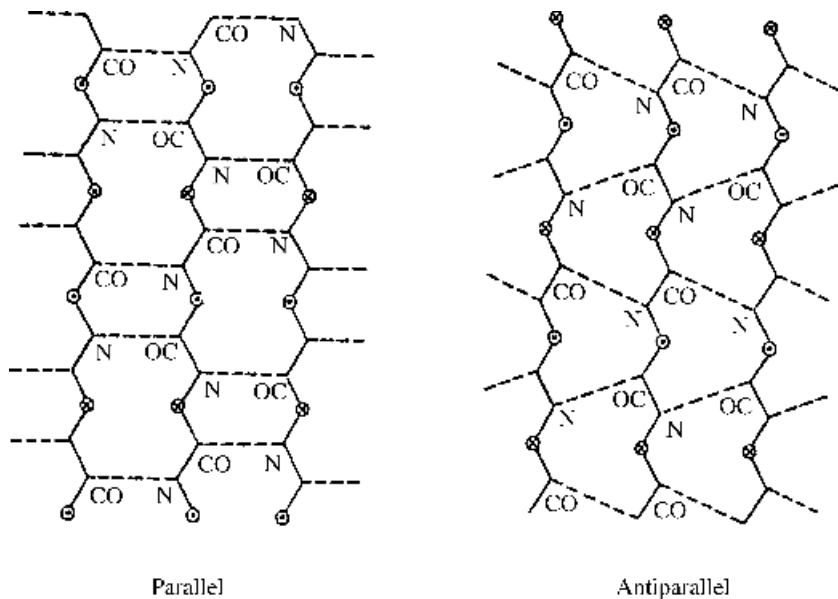


FIGURE 18.3 β -sheets.

Currently, classifications tend to have numerous small clusters, all roughly grouped into just a few categories which are still based on the overall secondary structure content and arrangements, such as $\alpha\beta\alpha$ layers, $\alpha\beta\alpha$ layers, $\alpha\beta$ barrel. This new classification is quite different from what we have described in Chapter 1.

18.1.2.3 Torsion Angles There are three types of two-backbone bonds about which rotation is permitted: (1) the bond between nitrogen and the α carbon, (2) the bond between nitrogen and carbon, and (3) the bond between the α carbon and carbonyl oxygen. The angles of rotation about these bonds are defined as Φ , ω , and ψ , respectively, and may be adjusted to form different structures (Figure 18.4).

Using the coordinates Φ and ψ alone, a map called a Ramachandran plot can be drawn. For α -helices, all residues are in equivalent conformations and have equivalent Φ and ψ angles; the points for all the residues would be superimposed. The plot would indicate the allowed Φ and ψ pairs within which conformations are actually possible.

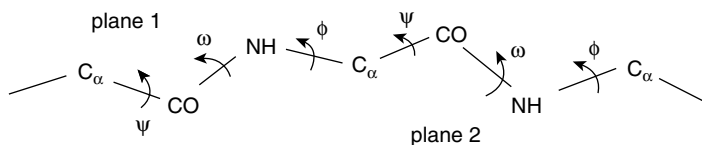


FIGURE 18.4 The three torsion angles.

18.1.3 Tertiary Structure

Tertiary structure is the overall folding of the protein molecules, in contrast to the secondary structure, which is the local folding (e.g., α -helix, β -sheets). Tertiary structure makes the protein compact and globular in shape. It may be divided into units called domains. A simple domain contains 100–150 amino acid residues and is about 25 Å in diameter. The light chain of IgG1, immunoglobulin, for example, consists of two domains and its heavy chain consists of four domains. In the same molecule, the domains may or may not have the same functions.

A domain can sometimes be isolated as a fragment by limited proteolysis under appropriate conditions. Each fragment has the same conformation in the native protein molecule. A fragment is also stable and can be refolded spontaneously from the unfolded state under native conditions.

18.1.4 Quaternary Structure

While tertiary structure refers to the topology of one polypeptide chain of a protein, the quaternary structure refers to the topology of several polypeptide chains aggregated together. The aggregation can easily be separated by using an external force such as ultracentrifuge. This indicates that the interpeptide chain attraction is neither strong nor weak. It is not strong because it can be easily separated and it is not weak because it sticks together to form an assembly.

In conclusion, a protein may be characterized by its structure in four different aspects:

Primary structure	The amino acid sequence
Secondary structure	The α -helices and β -sheets (motifs)
Tertiary structure	Domains
Quaternary structure	The entire protein assembly

18.2 PROTEIN STRUCTURE REPRESENTATIONS

Graphic representations of protein structures are carried out using computer programs and have become an essential part of understanding the molecule. They are often printed in several colors such as red, blue, green, yellow, and purple to indicate different parts of the molecule for clarity. They have become part of the protein language for show and discussion.

18.2.1 Representation Symbols

Figure 18.5 shows the symbols for α , β , and their combinations. The α -helices are drawn in the form of curls or cylinders and β -sheets (or β -strands) are drawn in the form of flat arrows. The arrows are pointing toward the C-terminus. The turn (hairpins, loops) indicates changes in the overall direction of the polypeptide chain.

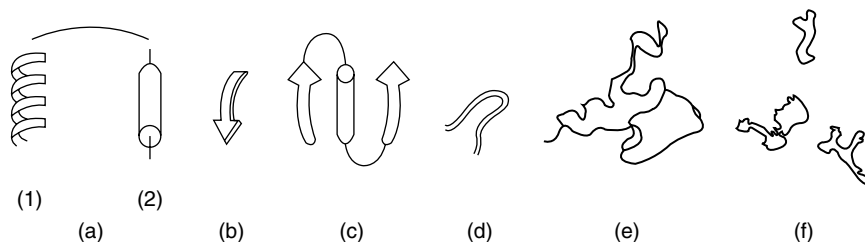


FIGURE 18.5 (a) α -Helix (1) or (2); (b) β -sheet; (c) $\beta\alpha\beta$ (a super secondary structure); (d) a twin; (e) a helix-loop-helix binding; (f) a catalytic triad.

The $\beta\alpha\beta$ which is found in most proteins consists of two β -sheets connected by an α -helix such that the helix axis is parallel to the β -sheets. Figure 18.5 also shows the symbols for protein functions (e and f).

18.2.2 Representations of Whole Molecule

Figure 18.6 shows some sample protein structures including their details.

Ribbon Diagrams of Three Proteins In protein 1, the binding occurs at a site on the β -barrel nested against the helix. In Figure 18.6 N and C refer to protein sequence terminals.

In protein 2, the two component structures, one red and the other yellow, forming two domains, are packed to form a V shape. The intradomain disulfide bonds are in cyan.

In protein 3, the numbers 142–177 and 198–431 indicate amino acid residues. The α -helices are in red and β -strands are in green, including the two novel β -strands, β_1 and β_1' , that complete the five-stranded antiparallel β -sheet.

Space-Filling Assembly This is another kind of representation of protein structure of the same three proteins in Figure 18.6. The subunits are assembled looking down the cleft into the active site. The distribution of positive charge and negative charge are often expressed on the surface. Figure 18.7 shows the assemblies of these three proteins.

Protein 1 shows the binding in a cavity of positive charge. The charge distribution is color coded with blue for positive, red for negative, and white for neutral.

Protein 2 shows the surface features of the interface area of two domains in cyan and yellow. The shape of the interface of one molecule complements that of the other.

Protein 3 shows electrostatic surface potentials. A cutaway view of the binding cavity, including electrostatic surface potentials (positive in blue, negative in red), reveals a relatively smooth, uncharged surface. The cavity is enclosed by portions of five α -helices, three β -strands, and three loops.

Publisher's Note:
Permission to reproduce this image
online was not granted by the
copyright holder. Readers are kindly
requested to refer to the printed version
of this article.

FIGURE 18.6 See color insert. Ribbon diagrams of three proteins. [Source: (1) Santagata, et al., *Science* **292**, 2041 (2001); (2) Szakonyi, et al., *Science* **292**, 1725 (2001); (3) Watkins, et al., *Science* **292**, 2329 (2001). With permissions from AAAS. Original in color.]



FIGURE 18.7 See color insert. Protein assemblies. [Source: (1) Santagata, et al., *Science* **292**, 2041 (2001); (2) Szakonyi, et al., *Science* **292**, 1725 (2001); (3) Watkins, et al., *Science* **292**, 2329 (2001). With permissions from AAAS. Original in color.]

18.3 PROTEIN FOLDING AND REFOLDING

This section covers how the primary structure of a protein develops into the secondary, tertiary, and quaternary structures. The primary structure is usually referred to as the sequence, and the secondary, tertiary, and quaternary structures together are referred to as the structure. The subject of protein folding and refolding deals with the relationship between the sequence and the structure. By the term “structure,” we mean the three-dimensional structure. The goal is to be able to determine the three-dimensional structure of a protein solely from knowing its sequence, but there still seems to be a long way to go.

In 1961, Anfinsen and co-workers demonstrated that the protein ribonuclease A molecule, after denaturation, undergoes complete refolding once the condition causing denaturation is removed. That is, the three-dimensional structure of a

protein is automatically or spontaneously formed from the amino acid sequence. Today, we know this is an oversimplification. First, the passage of newly synthesized polypeptide chains from the poorly defined conformation on the ribosome to the fully native functional state is turning out to be a complex multistep process. Second, the transmission into native states may pass through a series of partially folded intermediates: *in vitro* aggregation and *in vivo* inclusion body formation.

Currently, there are three different approaches to the problem: one is theoretical and the other two are experimental. The three approaches are computer simulation (theoretical), homolog modeling, and *de novo* prediction (experimental).

The underlying principles that characterize the theoretical approach are twofold:

- (a) Conformation reaches its native state only when the molecule is in a minimum energy.
- (b) The protein sequence goes through many pathways to the three-dimensional structure which corresponds to many energy states.

The basic concepts which characterize the experimental approach are correct atomic positions, correct topology (connectivity of secondary structures), correct architecture (gross arrangement of secondary structure), and correct structural class (mainly α , mainly β , etc.).

18.3.1 Computer Simulation

The two models that are frequently used are the thermodynamic-kinetics model and the statistical mechanics model. The thermodynamic-kinetics model assumes that the protein folding goes through numerous pathways, each of which is characterized by an energy state, ΔG , and a free-energy landscape is constructed. The statistical mechanics model is based on the theory of phase transition. Among the many routes leading to phase transition, the fastest one would be for the protein to collapse rapidly into a conformation that roughly approximates the native state. Attention is focused on how the collapsed stage emerges from the numerous random configurations. The collapsed state is the precursor to the native state of the macromolecule. A protein reaches its native state through a series of extremely rapid folds. This approach is also related to the well-known theory of chaos and randomness.

Thermodynamic-Kinetics Approach This model suggests that folding occurs through the progressive organization of ensembles of structures. The geometry of these ensembles changes from time to time and from place to place due to Brownian motions, and hence there is a change of entropy and free energy that occurs from time to time and from place to place. A free-energy landscape is proposed as a low-dimensional free-energy surface with two axes: the energy–entropy balance associated with competing physical processes and a ruggedness denoting the presence of frustration that leads to specific kinetics.

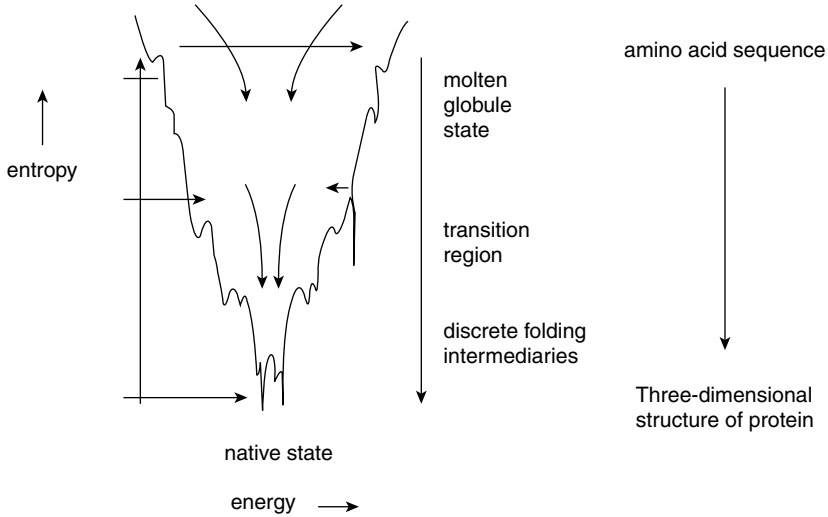


FIGURE 18.8 Free-energy landscape.

Figure 18.8 shows a diagram of the free-energy landscape.

The sequence of amino acids begins folding at the top of a funnel. It goes through the midpoint where the polypeptide attains a molten globule state. More than one-quarter of the amino acids have contact with each other. It then passes through an energy bottleneck, corresponding to the transition state for folding. Finally, it achieves its native state as a three-dimensional structure.

Computer programs have been written for simulations from one stage to another in comparison with experimental data.

Statistical Mechanics Approach In this approach, free energy is considered relatively as a constant. By using Monte Carlo simulation on model proteins, a random-number generator is employed to move molecules at random. Monte Carlo simulation aims at the calculation of the critical point at which the protein molecule collapses. This is basically the study of phase transition.

Folding starts by a rapid collapse from a random-coil state to a random semicompact globule. A rate-determining search is then carried out through semicompact states to reach a transition state from which the chain folds into its native state. In addition to the Monte Carlo calculation, there is also a renormalization group theory calculation.

In renormalization group theory, the short-range interactions are taken successively into account, leading eventually to a coarse-grained description. The aim here is also to reach the critical point.

At the critical point, there are two characteristic temperatures: T_f , the folding temperature, and T_g , the glass transition temperature. They correspond to two aspects of the energy landscape. Using computer simulations plus some experimental data, the renormalization values of the funnel parameters can be estimated.

Publisher's Note:
 Permission to reproduce this image
 online was not granted by the
 copyright holder. Readers are kindly
 requested to refer to the printed version
 of this article.

FIGURE 18.9 See color insert. Protein structure models: (a) a model of a complex between a fatty acid and a brain protein; (b) a model colored by the surface electrostatic potential. [Source: Baker, et al., *Science* **294**, 93 (2001). With permissions from AAAS. Original in color.]

18.3.2 Homolog Modeling

Homolog modeling is a knowledge-based method that uses information from the structure database to build models. It uses the evolutionary knowledge about a protein family with advanced computer sorting. To begin with, a known three-dimensional structure is adopted as a template from which a three-dimensional model of a novel sequence is calculated. The critical steps are the location of an appropriate homologous structure and the correct mapping of the novel sequence onto the known structure. This involves inference as to whether the structure is indeed homologous based on a sequence or structure-based comparison.

Homolog modeling requires knowledge of a common ancestor and common structural or functional features of proteins. It is not a measure of similarity; rather, it is a measure of divergent relationships among the sequences. Figure 18.9 shows two homolog models: (a) to rank binding facilities and (b) to facilitate identification of the structure of a protein molecule.

18.3.3 De Novo Prediction

The de novo prediction is to construct specific protein structures at will, more or less, from scratch. The design is not limited by any prior model. Once a design is constructed, the details of the protein process in its folding and refolding can then be followed.

Figure 18.10 shows the de novo predicted structure of a protein. Two cases are involved. Case 1 involves similar structures but not similar sequences, and case 2 involves a comparison of the de novo predicted structure with its experimentally determined structure. Case 1 indicates that the de novo approach provides clues about protein function in the absence of strong sequence homology. Even if we are not entirely sure about the three-dimensional structure, the de novo approach allows us to detect the protein function as long as we know the correct sequence. Case 2 aims at determining that the predicted structure is identical to the experimental structure.

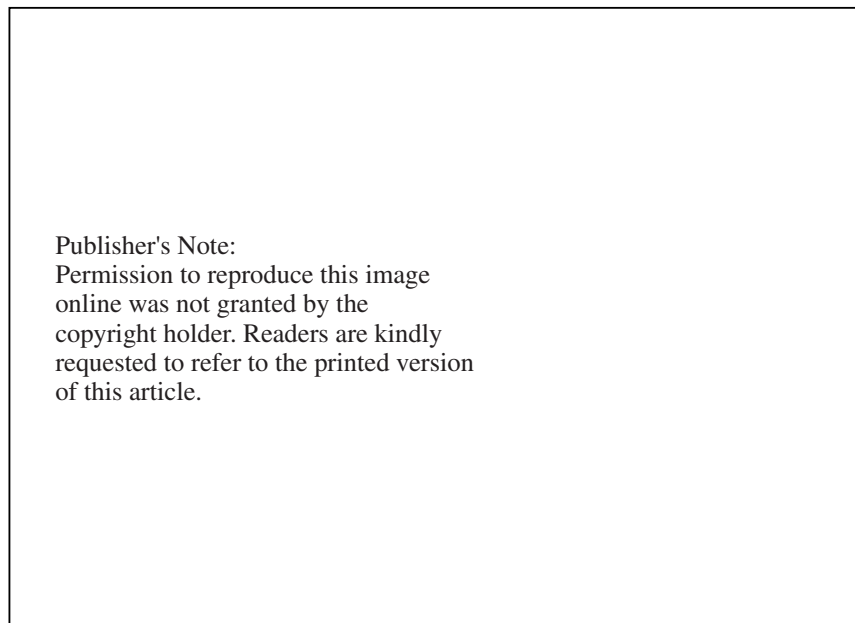


FIGURE 18.10 See color insert. Case 1: Sequence not indentified, function similar. Case 2: Sequence and function predicted (left) and experimentally confirmed (right). [Source: Baker, et al., *Science* **294**, 93 (2001). With permissions from AAAS. Original in color.]

18.4 PROTEIN MISFOLDING

Protein folding and refolding are virtually the same subject. Whatever we have learned from protein folding can be applied to protein refolding and vice versa. The subtle difference is that protein folding deals with the amino acid sequence which is directly synthesized in the cell, whereas protein refolding deals with the amino acid sequence from the denatured or unfolded protein. There is a third kind of protein folding, namely, protein misfolding. This is also a kind of folding, but it is unexpected in its structure on the basis of our current knowledge of folding and refolding. It is not a normal folding and it is usually biologically malfunctioning.

Protein folding and refolding have been investigated for a long time. Protein misfolding has attracted attention only in the last four or five years, yet it is of serious concern to all protein chemists. Protein misfolding is now known to cause much human suffering. The general idea at this time is that protein misfoldings are dependent on two kinds of factors: biological causes and chemical causes.

18.4.1 Biological Factor: Chaperones

In the process of protein folding from the initial sequence to its three-dimensional structure, the cell needs protective molecules called chaperones. Protein misfolding is due to the malfunctioning of chaperones in biological systems.

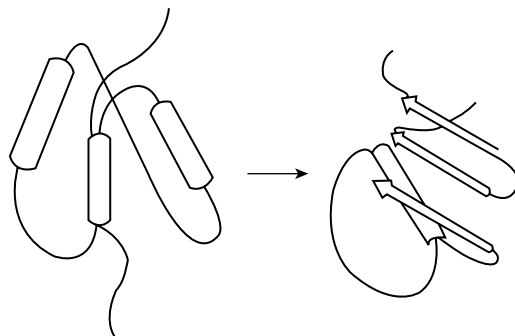


FIGURE 18.11 Conversion from α -helices to β -sheets.

In the crowded cell, chaperones help prevent partly folded proteins from interfering with proper folding. Once a protein is folded and ready to go to work, the chaperone leaves and finds another unfolded protein to protect. Chaperones can also react with misfolded intermediates and restart their folding process from the beginning. It is the chaperone that guides the sequence of amino acids to develop into the three-dimensional structure characteristic of normal biological functions.

Chaperones are a class of unrelated families of cellular proteins. They are not themselves components of the final functional structure. Chaperones have been experimentally observed in cellular action. A well-known example is a pair of bacterial proteins, GroEl and its cofactor GroEs. They belong to a class of chaperones called chaperonins. GroEl is believed to assist folding by repeatedly binding and releasing an unfolded or partially folded polypeptide. During each binding interval, GroEl sequesters the polypeptide and prevents the formation of nonnative conformations. When chaperones lose control, the polypeptide chains crowd into deformed assemblies called inclusion bodies or aggregates, depending upon the size and the degree of deformation. Diseases occur because of these misfolded chains since they cannot perform their normal functions. Inclusion bodies or aggregates are also involved in cellular reactions.

18.4.2 Chemical Factor: Intra- and Intermolecular Interactions

Protein misfolding can also happen because of chemical factors, intra- and intermolecular interactions. In the case of intramolecular interaction, the most famous example is the change in part of a protein molecule from an α -helix into a β -sheet. The α -helices are first untwisted and unfolded, then refolded into β -sheets. Figure 18.11 shows the diagram of such an intramolecular interaction.

An intramolecular interaction usually occurs when a third body binds on the surface of a domain. This causes changes in the secondary and tertiary structures. As a result, the protein molecule, originally correctly formed, is now misfolded. It can no longer carry out its proper biological functions. In addition, upon colliding with a misfolded protein molecule, even a normal protein molecule can become misfolded on contact. (See the case of a prion described in Chapter 19.)

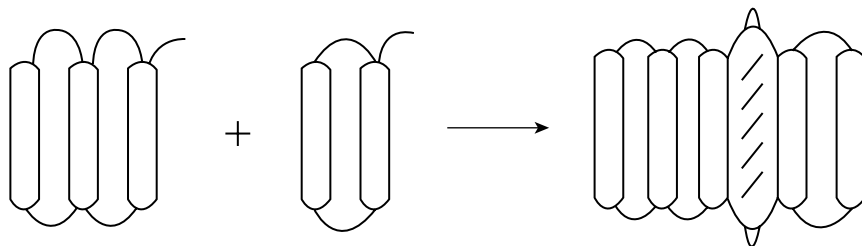


FIGURE 18.12 Aggregation of polypeptide chains.

Intermolecular interactions usually involve partly folded polypeptide chains that have been released from ribosomes (the protein-synthesizing machines of a cell). These partly folded polypeptide chains associate with similar chains to form aggregates (due to intermolecular forces). Aggregates vary in size from soluble dimers and trimers to insoluble fibrillar structures. Figure 18.12 shows the diagram of such an aggregation. (For example, see the reference to amyloid fibrils in the next section.)

18.4.3 Brain Diseases

Some brain diseases are caused by misfolded proteins. Examples of two kinds of brain diseases are (1) prion diseases (such as mad cow disease in cattle, scrapie in sheep, and Crutzfeldt-Jacob disease in humans) and (2) Alzheimer's and Huntington's disease. Both kinds have some features in common: the increase of β -sheets in the protein molecule and the aggregation to form amyloid fibrils. There is some evidence to relate these two kinds of brain disease to chaperones, but there seems to be more evidence to relate them to intra- and intermolecular reactions. Prion diseases are believed to have been caused by intramolecular interactions and Alzheimer's and Huntington's diseases seem to result from intermolecular interactions. From the chemical point of view, intra- and intermolecular interactions are two different kinds of reactions. In brain diseases, the difference is only a matter of degree. Prion diseases may be attributed to the change in conformation from α -helices to β -sheets, but in many cases the misfolded molecules Pr^{sc} can also aggregate. Similarly, Alzheimer's and Huntington's diseases are known to be the result of an accumulation of amyloid fibrils, but their aggregates contain β -sheets called $\text{A}\beta$ amyloids. The rich content of $\text{A}\beta$ is particularly well known in Alzheimer's disease.

The process of structural change with respect to brain diseases seems to go through a sequence: After the protein (normal as well as nonnormal) unfolds, its α -helices are untwisted and are consequently rearranged into β -sheets. Thermodynamical energy is more favorable for β -sheets to aggregate. Their accumulation results in the formation of amyloid fibrils.

18.5 GENOMICS, PROTEOMICS, AND BIOINFORMATICS

The triumphant success of the Human Genome Project has created, almost instantly, three new fields devoted to the study of proteins. They are genomics (here, we particularly refer to structural genomics), proteomics, and bioinformatics.

1. The goal of structural genomics is to obtain three-dimensional protein structures on an equivalent scale to the genome-sequencing projects. The emerging field of structural genomics is at the intersection of many disciplines. In addition to experts in the areas of protein expression, protein engineering, protein purification, and structure determination and analysis, this new field recruits engineers to develop robotics, high-throughput systems, and information-technology specialists to manage the laboratory systems. The traditional academic approach to determining protein structures—that is, having a graduate student do all the work from start to finish—is no longer appropriate.

2. Proteomics deals with the identity, function, and structure of each known protein and elucidates the protein–protein interactions. This is carried out by mass spectrometry along with x-ray crystallography and NMR spectroscopy. The project is formulated in an automated, large-scale manner. It attempts to catalog and characterize the proteins and to compare the variations in their expression levels under different conditions (notably sickness vs. health) and in their functional roles. While this research continues in the academic area, proteomics is of great interest to industry, particularly to pharmaceutical companies. These companies now hire a wide variety of scientists, including biologists, chemists, and software engineers, to do the job.

3. Bioinformatics handles the overwhelming amount of data generated by genomics and proteomics. Originally, it was established for gathering, archiving, ordering, and classifying the data as library work. Gradually, it has developed into a new field in its own right. It enhances the ability of researchers to manipulate, collect, and analyze data more quickly and in new ways. It is needed at nearly all levels involved with biological, medical, or pharmaceutical discovery. However, at its core, the field is the complex interaction of biology, chemistry, physics, and the computational sciences, which include mathematics and statistics.

These three fields, while independent, are overlapping. Genomics has enabled the progress of work in proteomics. There is a continuum of knowledge and techniques from genomics to proteomics. Vendors are adapting several approaches originally developed for genomics research to help do proteomics. Bioinformatics, which is the application of computational and mathematical methods to biological data, is of particular value to research involved in genomics and proteomics. It can reveal unsuspected relationships between different DNA and protein sequences.

Publisher's Note:
 Permission to reproduce this image
 online was not granted by the
 copyright holder. Readers are kindly
 requested to refer to the printed version
 of this article.

FIGURE 18.13 See color insert. Structure of a ribosome. [*Source*: Yusupov, et al., *Science* **292**, 883 (2001). With permissions from AAAS. Original in color.]

18.6 RIBOSOMES: SITE AND FUNCTION OF PROTEIN SYNTHESIS

At the conclusion of this chapter, we describe the source of proteins: ribosomes. Ribosomes in the cell are the site and function of protein synthesis. Ribosomes (molecular weight 2×10^6 – 6×10^6) are ribonuclear protein complexes responsible for protein synthesis in all cells. A single cell contains 20,000 ribosomes. From studies using x-ray crystallography, we know that each ribosome consists of two major subunits, called the 30s and 50s units (s, sedimentation constant; see Chapter 11). The whole ribosome is 70s, not 80s, because there are intermolecular and intramolecular force involved. The two subunits, when put together, result in either an expansion or shrinkage in size.

The large (50s) subunit contains 23s rRNA, 5s rRNA, and over 30 proteins, and the small (30s) subunit contains 16s rRNA and about 20 proteins. The complete 70s ribosome is formed by association of the 30s and 50s subunits through a networks of bridges. The 30s subunit mediates the interaction between mRNA codons and tRNA anticodons on which the fidelity of protein translation depends. The 50s subunit includes the activity that catalyzes peptide bond formation—peptide transferase and the binding site for GTP—which are the binding protein factors that assist in the initiative elongation and termination phases of protein synthesis.

Bridges are found not only between the two subunits but also between the subunits and tRNAs. The tRNAs function is to orient the subunits and facilitate movement. They also may function in signaling between the subunits and coordinating the multiple steps in the cycle of peptide elongation.

Figure 18.13 shows the complete structure of the *Thermus thermophilus* 70s ribosome at 5.5 Å resolution in the presence of mRNA and cognate tRNAs bound in the A (aminoacyl), P (peptidyl), and E (exit) sites. Viewed from the top, with the

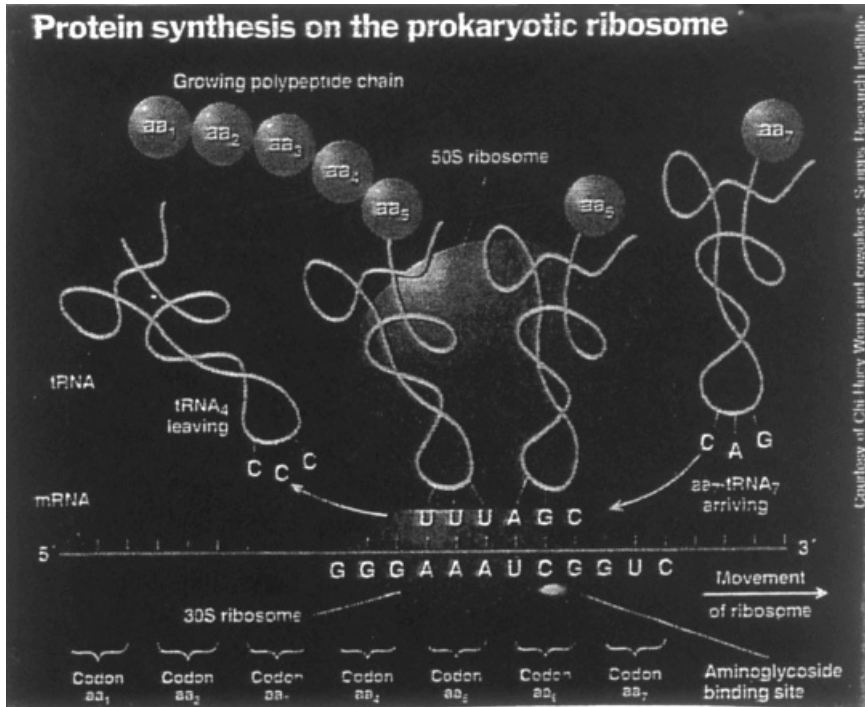


FIGURE 18.14 See color insert. Protein synthesis on the prokaryotic ribosome. [Source: Borman, S., *C & EN (ACS)* 54, October 2 (2000). Original in color.]

50s subunit above, the 30s subunit below, the E- (red), P- (orange), and A- (gold) tRNAs are visible in the interface cavity with their anticodon arms pointed downward into the 30s subunit.

Figure 18.14 shows the diagram of protein synthesis on the ribosome. As illustrated in the diagram, incoming tRNAs, each carrying a specific amino acid, shuttle through a series of three docking sites along the interface of the ribosome's two subunits. As the tRNAs move across these sites, they release their amino acids and make way for the addition of the next amino acid in the growing protein chain.

The distances the tRNAs have to move during translocation are about 20–50 Å. To make these moves, the tRNAs have to wriggle through quite a few obstacles. Figure 18.14 also shows that ribosomal proteins, and not just ribosomal RNA, are involved.

The diagram in Figure 18.14 was drawn on the basis of the classical point of view, which held that in the synthesis of proteins in a cell RNA played an auxiliary role by acting as a messenger to ferry the genetic code from the nucleus to the ribosome. In the years between 2000 and 2003, information has been accumulated about the existence of a class of RNA molecules, called small RNAs, which operate to control many of the cells.

RNAs usually are single strands as opposed to DNAs, which are double strands. When a familiar single strand kinks back in a hairpin bend, putting two complementary sequences alongside each other, a double-stranded RNA forms. Thus we have double-stranded RNAs which include micro-RNAs (miRNAs) and small interfering RNAs (siRNAs). Some of them inhibit genes that help generate the messenger RNA that transports a DNA sequence to the ribosome. They also shape genomics, carving out chunks to keep and discarding others. They might also help chart a cell's destiny by directing genes to turn on or off during development.

REFERENCES

- Anfinson, C. B., *Science* **181**, 22e (1973).
Baker et al., *Science* **294**, 93 (2001).
Borman, S., Chemistry and Engineering News, October 2, 2000.
Pauling, L., and R. B. Corey, *Proc. Natl. Acad. Sci. (US)* **37**, 205, 729 (1951).
Pauling, L., and R. B. Corey, *Proc. Natl. Acad. Sci. (US)*, **37**, 253 (1953).
Sanger, F., et al., *Biochem. J.* **49**, 463, 481 (1951).
Sanger, F., et al., *Biochem. J.* **53**, 353, 366 (1953).
Sanger, F., et al., *Biochem. J.* **59**, 569 (1954).
Sanger, F., et al., *Biochem. J.* **60**, 535, 541, 565 (1955).
Santagata, S., et al., *Science* **292**, 2041 (2001).
Szakonyi, et al., *Science* **292**, 1725 (2001).
Watkins, et al., *Science* **292**, 2329 (2001).

19

NUCLEAR MAGNETIC RESONANCE

Nuclear magnetic resonance (NMR) is an absorption phenomenon, similar to ultraviolet (UV) and infrared (IR), but the energy of NMR is from radio-frequency radiation by nuclei exposed to a magnetic field. Since Purcell and Bloch in 1946 announced the observation of the phenomenon in bulk matter, NMR has become an indispensable tool in chemistry for the study of molecular structure and behavior. In this chapter, first we describe the basic theory that underlies the NMR phenomenon. Then we discuss the techniques involved in its spectroscopy. Finally, we illustrate the spectra of some well-known synthetic and biological polymers. We also discuss the advances in this field since 1994.

19.1 GENERAL PRINCIPLES

19.1.1 Magnetic Field and Magnetic Moment

A magnetic field is produced by the motion of electric charge. It is characterized by two vectors: **B**, the magnetic induction or magnetic flux density, and **H**, the magnetic field strength (also called intensity).

The SI unit of **B** is the tesla (T), also called Wb/m^2 (webers per square meter). In the meter-kilogram-second (mks) system,

$$1 \text{ T} = 1 \text{ N C}^{-1} \text{ m}^{-1} \text{ s} = 1 \text{ kg s}^{-1} \text{ C}^{-1}$$

where N is newton, C is coulomb, m is meter, s is second, and kg is kilogram.

The unit of \mathbf{H} is in amperes per meter, where one ampere equals one coulomb per second. The equation to describe the magnetic field as the product of electric current is expressed as

$$\mathbf{B} = \frac{k'A}{r}$$

where A is the current in amperes, r is the distance of the force from the magnetic field, and k' is a constant; its value is

$$k' = 2 \times 10^{-7} \quad TA^{-1} = \frac{\mu_0}{2\pi}$$

where μ_0 is called the permeability of vacuum and $\pi = 3.1416$ and is an irrational number,

$$\begin{aligned} \mu_0 &= 4\pi \times 10^{-7} \text{ T m A}^{-1} = 4\pi \times 10^{-7} \text{ N C}^{-2} \text{ s}^2 \\ &= \text{W/A-m} \end{aligned}$$

Another quantity of magnetic field being used is G, gauss, and

$$\begin{aligned} 1 \text{ G} &= 1 \text{ dyne Stat C}^{-1} = 1 \text{ g}^{1/2} \text{ s}^{-1} \text{ cm}^{-1/2} \\ 1 \text{ T} &= 10,000 \text{ G} \end{aligned}$$

The vectors \mathbf{B} and \mathbf{H} are related by the equation

$$\mathbf{H} = \frac{\mathbf{B}}{\mu_0}$$

The magnetic moment μ is produced by the spin of the electron (spin magnetic moment) or the orbital motion (orbital magnetic moment). Its unit is Bohr magneton μ_s and

$$1\mu_s = \frac{eh}{4\pi mc'}$$

where e is the electric charge, h is Planck's constant, m is the electron mass, and c' is the velocity of light.

19.1.2 Magnetic Properties of Nuclei

The spin of a nucleus may be described in terms of two quantum numbers: the spin quantum number, or spin I , and the spin magnetic quantum number, or projection m_I . The two numbers are related as shown in the equation

$$m_I = 0, \pm 1, \pm 2, \dots, \pm I$$

Since, for a nucleus, the number I can take only two values, 1 or $\frac{1}{2}$, the number m_I can take only values 0, $\pm\frac{1}{2}$, and ± 1 .^{*} From I and m_I , two quantities, I and I_z , are defined:

$$I = \sqrt{I(I+1)}\hbar$$

and

$$I_z = m_I\hbar$$

where $\hbar = h/2\pi$. The quantity I is called the nuclear spin momentum and the quantity I_z is called the z component of the nuclear spin momentum.

The nuclear magnetic moment μ is expressed in terms of the nuclear g factor, g_I , and the nuclear magneton, μ_n , by using equations

$$\mu = g_I\mu_n$$

and

$$\mu_n = \frac{e\hbar}{2m}$$

where m is the mass of the nuclei. The g factor varies with the nucleus.

The following are some examples of g values:

Nucleus	^1H	^2H	^{13}C
I	$\frac{1}{2}$	1	$\frac{1}{2}$
g	5.5854	0.85738	1.4043

The component of μ on the z axis, μ_z , is proportional to the quantity $\hbar m_I$,

$$\mu_z \propto \hbar m_I$$

The proportionality constant is expressed as γ and is called the magnetogyric ratio of the nucleus,

$$\mu_z = \gamma\hbar m_I$$

γ is an experimentally determined quantity. It can be shown that

$$\gamma\beta = 2\mu\text{H}$$

^{*}There is, however, a slight difference in the values of the quantum numbers between the electron and the nuclei. The electron spin can only have two possible projections $\pm\frac{1}{2}$ in a given direction. The spin quantum number I for a nucleus can have a value different from $\frac{1}{2}$ (i.e., 1).

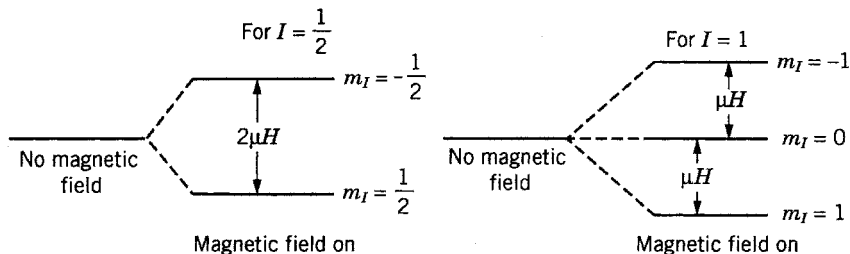


FIGURE 19.1 The effect of values of I on the splits of nuclear energy levels.

In a magnetic field \mathbf{H} , the energy of a nucleus in one state with a spin quantum number I is

$$Em_I = -g\mu m_I H$$

When it splits into different states, called Zeeman splitting, the energy of separation becomes

$$\Delta E = E_2 - E_1 = \mu \mathbf{H} m_I - (-\mu \mathbf{H} m_I) = 2\mu \mathbf{H} m_I = h\nu$$

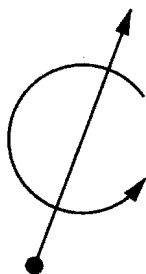
or

$$\nu = \frac{2\mu \mathbf{H} m_I}{h}$$

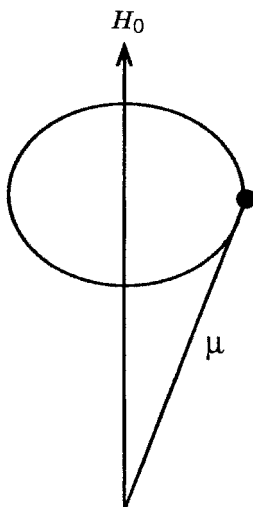
The splitting of nuclear energy with the same g factor depends on the value of I and is shown in Figure 19.1. The state $m_I = +\frac{1}{2}$ (sometimes with symbol \uparrow) is denoted α , and the state $m_I = -\frac{1}{2}$ (symbol \downarrow) is denoted β .

19.1.3 Resonance

Let a vector represent the spin of a nucleus with μ as the magnetic moment:



If a magnetic field H_0 is applied to the spin system, we observe a phenomenon known as the Larmor precession:



The Larmor precession frequency ω_0 is given by

$$\omega_0 = \gamma H_0$$

or

$$\nu = \frac{\gamma H_0}{2\pi}$$

The quantity γ is related to μ by

$$\gamma = \frac{2\pi\mu}{Ih}$$

If the Larmor precession frequency induced by the magnetic field matches the natural frequency of the spin system, then resonance occurs. Thus, the signal of resonance to be observed depends on the values of two factors, γ and H_0 , which are related by μ and γ . The NMR spectrometer is also specified by these two parameters.

Table 19.1 gives the values of μ and γ for some important nuclei that are currently used in NMR spectroscopy.

TABLE 19.1 Nuclei Magnetic Constants

Isotopes	Spin	μ (Nuclear Magnetron)	$\gamma \times 10^{-8}$	Natural Abundance (%)
^1H	$\frac{1}{2}$	2.7927	2.6752	99.98
^2H	1	0.8574	0.4107	0.0016
^{13}C	$\frac{1}{2}$	0.7022	0.6726	1.1
^{14}N	1	0.4036	0.1933	99.6
^{15}N	$\frac{1}{2}$	-0.2830	-0.2711	0.37
^{19}F	$\frac{1}{2}$	2.6273	2.5167	100.0
^{31}P	$\frac{1}{2}$	1.1305	1.0829	100.0

From these values, we can easily calculate \mathbf{H}_0 and γ for some well-known NMR spectrometers. For example, for protons, we have

γ (MHz)	\mathbf{H}_0 (T)
60	1.41
100	2.34
200	4.70
220	5.16
500	11.75
750	17.60
900	21.00

For ^{13}C , we have

γ (MHz)	\mathbf{H}_0 (T)
25.2	2.35
45	4.20
50	4.70

Notice that for the same strength magnetic field, 4.7 T, the resonance signal (Larmor frequency) occurs at 200 MHz for a proton but at 50 MHz for ^{13}C .

19.1.4 Nuclear Magnetic Resonance

According to the classical view, when a nucleus with spin I is placed in a magnetic field with strength \mathbf{H} (the external magnetic field), the magnetic moment μ precesses about the field direction. If the nucleus is placed in the second magnetic field (the radio-frequency magnetic field), the phenomenon of resonance occurs at a certain condition, as shown in Figure 19.2.

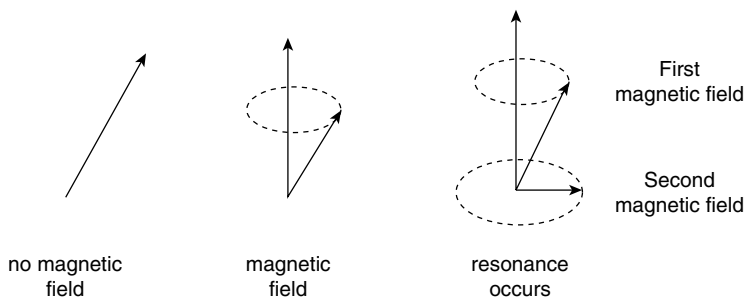
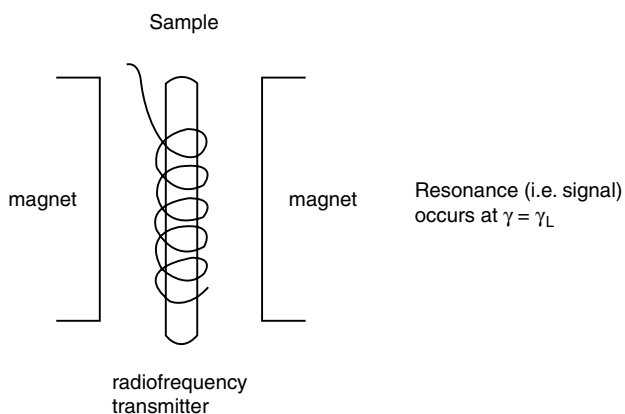


FIGURE 19.2 Phenomenon of resonance.

The condition of resonance is that

$$\Delta E = h\nu = h\omega_0 = h\nu_L$$

where ν_L is the Larmor frequency. An NMR instrument consists of a permanent magnet or superconducting magnet that produces a uniform, intense field (the external magnetic field) and appropriate sources of radio-frequency electromagnetic radiation (the second magnetic field). The sample is placed in the cylindrically wound magnet:



The technique applies a magnetic field on the sample and observes the frequency of the resonant electromagnetic field. When the resonant condition is reached, the frequency of the transmitter just matches the Larmor frequency of the magnetic field.

19.2 CHEMICAL SHIFT (δ) AND SPIN-SPIN COUPLING CONSTANT (J)

When a molecule is placed in a magnetic field H , orbital currents are induced in the electron clouds which create a small local magnetic field, H_{loc} . Each nucleus is

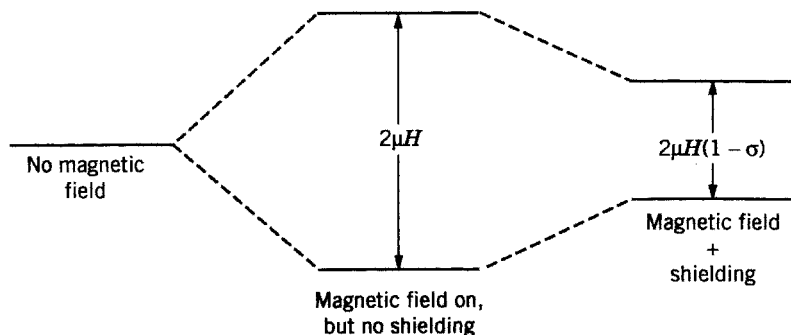


FIGURE 19.3 The effect of shielding on a magnetic field.

shielded by its surrounding electrons. The effective magnetic field felt by the nucleus is not the same as the applied field. The nucleus now requires slightly higher values of H to achieve resonance:

$$H = H_{\text{loc}} + \sigma H$$

or

$$H_{\text{loc}} = H(1 - \sigma)$$

where σ is the screening constant. The parameter σ is independent of H but dependent on the chemical (electronic) environment. The effect of shielding is shown in Figure 19.3.

The term $H\sigma$, which is called the chemical shift, is the displacement of a signal in different chemical environments due to variations in screening constants. The shielding constant is on the order of 10^{-5} – 10^{-6} . An external field of 1 T stirs up an extra local field of about 1 μT . This means that the screen constant is also on the order of 10^{-5} – 10^{-6} . Hence, the chemical shift is expressed in parts per million (ppm).

Another way to express chemical shift is the use of the parameter δ . The parameter δ is defined in several different ways:

$$\begin{aligned}\delta &= (\sigma_{\text{ref}} - \sigma_s) \times 10^6 \\ \delta &= \frac{H_r - H_s}{H_r} \times 10^6 \\ \delta &= \frac{\Delta\nu}{\text{oscillator frequency (cps)}} \times 10^6\end{aligned}$$

where $\Delta\nu = \nu_s - \nu_r$. The subscript r refers to the reference and s refers to the sample. Oscillator frequency refers to the characteristic frequency of the instrument. For example, a 60-MHz instrument for protons has an oscillator frequency

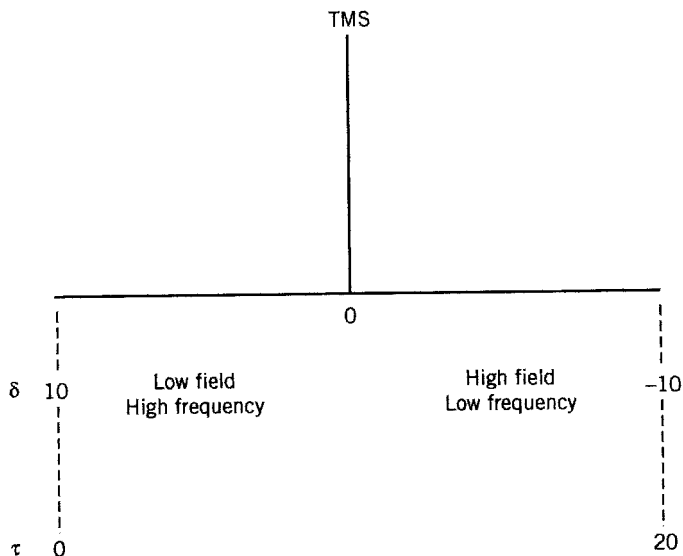


FIGURE 19.4 Two scales of a chemical shift.

of 60×10^6 cps. The standard reference chosen for proton NMR is usually TMS [$\text{Si}(\text{CH}_3)_4$, tetramethylsilane]. It is chemically inert and magnetically isotropic, and it gives a single sharp line.

Chemical shift (cps) when expressed as a δ value is said to be on the δ scale. The value of δ could be positive or negative with respect to TMS (the δ value for TMS being arbitrarily chosen as 0). To avoid a negative value for δ , another scale is often used, which is called the τ scale. The relationship between δ and τ is expressed by

$$\tau = 10 - \delta$$

The value of τ is always positive. The larger the value of τ , the greater is the magnetic shielding of the nucleus. Figure 19.4 shows the relationship between the two scales.

The resolution of NMR depends on both the magnetic field strength and the resonance frequency of the instrument. In the early years (ca. 1953), for example, NMR instruments could resolve only three proton resonances pertaining to ethyl alcohol. Modern instruments can show the multiplicity of the line shape, revealing more details of the nuclear environment. This multiplicity arises due to spin-spin coupling, another important NMR spectrum parameter.

Spin-spin coupling is the result of three types of interactions: (1) interactions of the electrons as moving charged particles in a magnetic field of nuclei; (2) dipole-dipole interactions between nuclear magnetic moments and electron magnetic moments, and (3) contact potential interactions. Spin-spin coupling in the NMR spectrum is often expressed as a numerical value, called the spin-spin coupling constant J , whose unit is the hertz. The values of J vary from 0.05 to 6000 Hz.

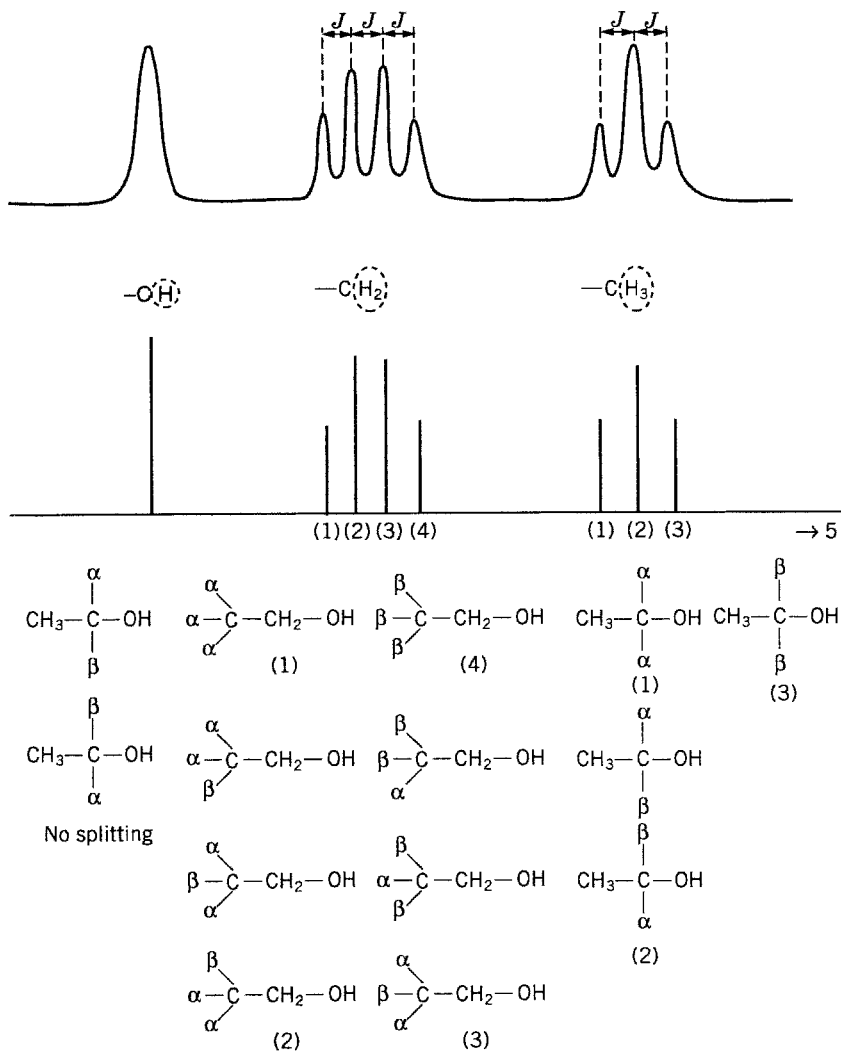


FIGURE 19.5 NMR spectrum of ethyl alcohol.

A classical example of chemical shifts and spin-spin coupling is the NMR spectrum of ethyl alcohol, which is shown in Figure 19.5. Often an NMR spectrum is displayed in terms of intensity in arbitrary units versus chemical shifts in parts per million or hertz. The two quantities, ppm and Hz, are interchangeable:

$$\text{ppm} = \frac{\nu_{\text{sample}} - \nu_{\text{reference}}}{\nu_{\text{reference}}} \times 10^6$$

For example, $\nu_{\text{reference}} = 60 \times 10^6$ cps for a 60-Mhz instrument.

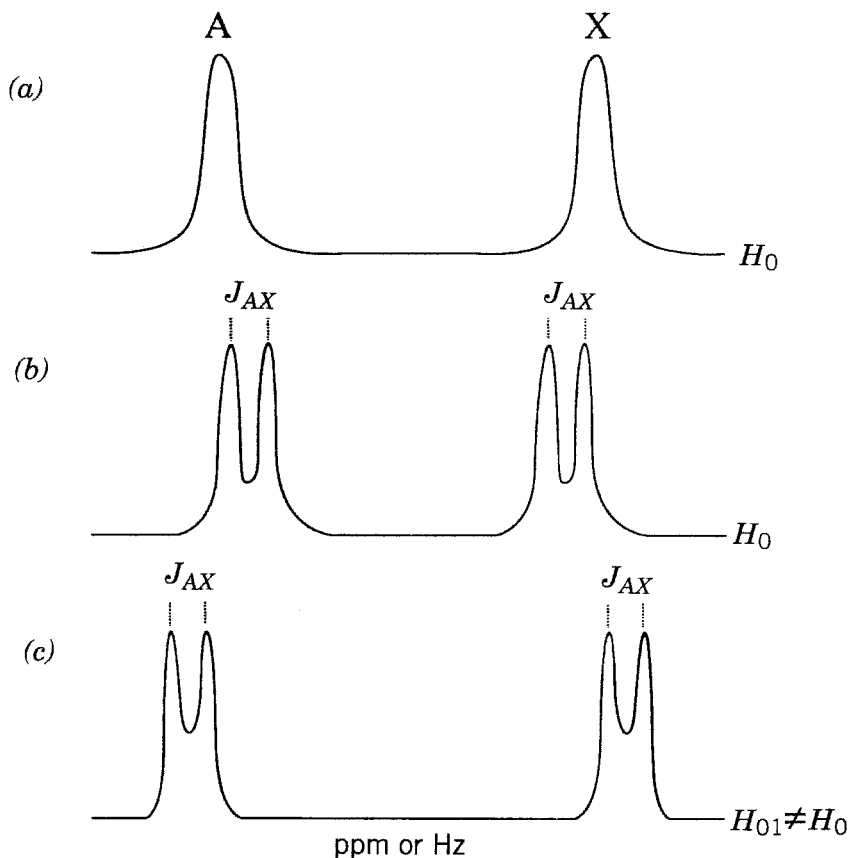


FIGURE 19.6 Schematic diagram of the spin resonances of two nuclei, A and X: (a) spin A and spin X without coupling; (b) spin A and spin X with coupling J_{AX} , split of spin A as well as of spin X; (c) an applied magnetic field H_{01} different from that in (a) and (b).

The chemical shift values depend on its applied field, but the value of the spin-spin coupling constant is independent of its applied field. Figure 19.6 is a schematic diagram of the spin resonances of two nuclei, A and X, of the same type (e.g., both are protons) in different positions with or without coupling. It also shows the change in J_{AX} values in a different field ($H_0 + H_{01}$).

In NMR, letters A and X represent two nuclei with very different chemical shifts; for those with smaller shifts, letters AB, AC, AD, ... are used.

The two effects, chemical shift and spin-spin coupling, can be separated by running spectra at two different magnetic fields. The peaks (or group of peaks) that arise from chemical shifts change their positions in the two spectra since the chemical shift is proportional to the applied magnetic field. The peaks arising from spin-spin interaction keep the same relative spacing in the two spectra since these splittings are independent of the applied field.

The value of the spin-spin coupling constant in proton NMR also varies according to the number of intervening bonds (i.e., geometry). For geminal protons, $(\overset{\curvearrowright}{\text{H}})-\text{C}-\overset{\curvearrowright}{\text{H}}$, $J = 12$ Hz in saturated systems; for vicinal protons, $(\overset{\curvearrowright}{\text{H}})-\text{C}-\text{C}-\overset{\curvearrowright}{\text{H}}$, J is 7 or 8 Hz. If the two protons are separated by four or more single bonds, $J = 0$. Because of the σ - π configuration interaction, the J value can be increased if there is an unsaturated bond in the coupling path. Furthermore, Karplus (1959) found that the values of the vicinal interproton coupling constants depend on the dihedral angle ϕ between the carbon-hydrogen bonds:



This relationship may be expressed by

$$J_{\text{vic}} = 4.22 - 0.5 \cos \phi + 4.5 \cos^2 \phi$$

19.3 RELAXATION PROCESSES

Relaxation processes reflect molecular vibrations, rotations, and spatial translations. These phenomena are well known for macromolecules because they involve not only the polymer as a whole but also the penetrating or diluting molecules within polymers. The key concepts for relaxation processes are diffusive motions, distribution of energies, and equilibrium.

In the absence of magnetic field, the populations of the two nuclear spin states (n_+ , the spin-up number and n_- , the spin-down number per unit volume) are equal. When a magnetic field is applied, there is a slight excess of nuclei in the lower spin state. The populations follow the Boltzmann distribution law:

$$\frac{n_+}{n_-} = \exp\left(\frac{2\mu H}{kT}\right)$$

where k is the Boltzmann constant. For protons at 300 K in a field of 10,000 G (60 MHz),

$$\exp\left(\frac{2\mu H}{kT}\right) \cong 1 + 6.0 \times 10^{-6}$$

As the nuclei continually absorb electromagnetic radiation, this small excess soon diminishes. Fortunately, for molecules that are undergoing Brownian motion, neighboring spins directly influence each molecule's magnetic field. This causes fluctuating magnetic fields, thereby inducing transition between energy states. This

radiationless transition, that is, the relaxation process, means that the induced population difference will soon return to equilibrium.

The relaxation rate can be described in terms of characteristic time T . If T is small, relaxation is fast; if T is large, relaxation is slow. There are two types of relaxation: spin–lattice and spin–spin. The latter is unrelated to the spin–spin coupling constant: spin–spin relaxation is a kinetic concept, while the spin–spin coupling constant is a thermodynamic constant.

19.3.1 Spin–Lattice Relaxation and Spin–Spin Relaxation

Spin–lattice relaxation is also called longitudinal relaxation and is designated by relaxation time T_1 . The term lattice refers to the framework of molecules that includes the sample and its medium (the neighboring nuclei) with the same meaning as in Chapter 4. Spin–lattice relaxation has a component of random intensity and phase at the nuclear resonant frequency. This involves interchange of nuclear energy with the rest of the system (the surroundings).

In solids, there is no Brownian motion and no random relaxing field; T_1 is very long. In both solids and liquids, the magnitude of T_1 is determined by the concentration of paramagnetic impurities in the lattice. The uncertainty principle,

$$\Delta E \Delta t \cong \hbar$$

dictates that

$$\Delta\nu \cong \frac{1}{2\pi \Delta t} \sim \frac{1}{\Delta t} \quad \Delta E = h \Delta\nu$$

Thus, the linewidth measured on a frequency scale ($\Delta\nu$) is roughly equal to $1/T_1$ ($\sim 1/\Delta t$). That is, T_1 broadens the peak in the spectrum. In terms of the transition of a spin from one energy state to another, the quantity $1/T_1$ may be defined as

$$\frac{1}{T_1} = p_{\uparrow} + p_{\downarrow}$$

where p_{\downarrow} is the probability of a downward transition per unit time of a spin from the higher to the lower magnetic level and p_{\uparrow} is the probability of an upward transition per unit time of a spin from the lower to the higher magnetic level.

Spin–spin relaxation is also called the transverse relaxation and is designated by a relaxation time T_2 . It occurs when there is an exchange of spins by two precessing nuclei in close proximity to one another. Here, T_2 may be defined as

$$\frac{1}{T_2} = \pi \delta\nu$$

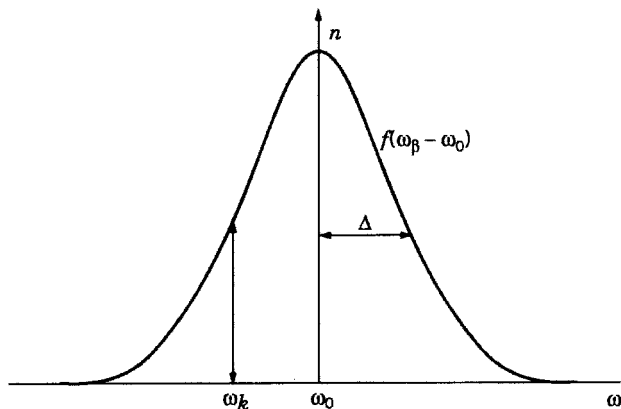


FIGURE 19.7 Distribution of frequency of resonance.

where δ is Dirac delta (here, δ is not chemical shift), which possesses the following property:

$$\delta(E_{\downarrow} - E_{\uparrow} - hv) = \begin{cases} 1 & \text{if } hv = E_{\downarrow} - E_{\uparrow} \\ 0 & \text{if } hv \neq E_{\downarrow} - E_{\uparrow} \end{cases}$$

While T_2 is short in solids (often in the range of microseconds), it is about equal to T_1 in liquids.

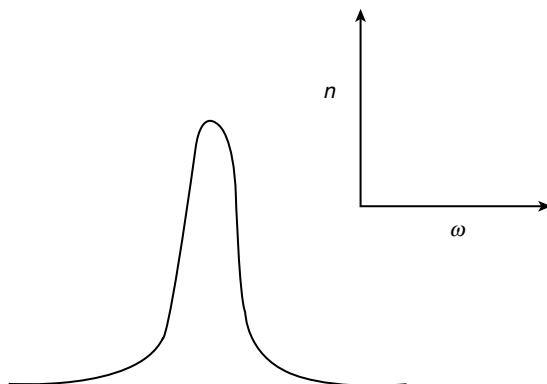
Both T_1 and T_2 are responsible for resonance signal shapes and intensities. There is a relationship between the linewidth Δ and T_2 . The linewidth Δ is shown in Figure 19.7 [the distribution of frequency $f(\omega)$ around its resonance ω_0]. Note that $\omega = 2\pi\nu$. The equation that relates T_2 and ω is

$$\int_0^{\infty} \nu(\omega_k - \omega_0) \cos(\omega_k - \omega_0)t \, d\omega = \frac{-t}{T_2}$$

The solution to this integral is

$$\nu = \frac{T_2}{1 + \tau_2^2(\omega_k - \omega_0)^2}$$

where ν is the absorption mode of the Lorentzian line shape. (Note that the Lorentzian line shape is similar to Gaussian distribution but less symmetrical.)



The quantity $(\omega_k - \omega_0)^2$ gives the value of linewidth Δ .

In addition to the two major relaxation processes, T_1 and T_2 , two other processes important to the study of nuclear properties are nuclear quadrupole relaxation and the Overhauser effect.

19.3.2 Nuclear Quadrupole Relaxation and Overhauser Effect

Nuclear quadrupole relaxation occurs only during nuclear spins with $I = 1$, not with $I = \frac{1}{2}$. For nuclei with $I = \frac{1}{2}$, there is a spherical distribution of the nuclear charge that is unaffected by the electric environment. For nuclei with $I > \frac{1}{2}$, the charge distribution in the nucleus is not spherical but ellipsoidal in revolution (prolate or oblate), which gives the nucleus a quadrupole moment Q . The relationship between I and Q may be expressed by

$$\frac{1}{T_1} = \frac{1}{T_2} \sim \frac{(2I + 3)Q^2}{I^2(2I - 1)} \left(\frac{d^2H}{dz^2} \right)^2 T_c$$

where H is the field, $-d^2H/dz^2$ is the maximum field gradient in the z direction, and T_c is the correlation time (the average time for a molecule to diffuse a distance equal to its own dimension or to rotate through 1 rad.)

The nuclear Overhauser effect (NOE) refers to the transfer of magnetization between spins coupled by the dipole–dipole interaction in a molecule. The dipole–dipole coupling is related to internuclear distance and it undergoes Brownian motion in a liquid. In the process of equilibrium, the population (α -spins and β -spins) transfers from one species to another species. For that reason, the NOE is a nuclear relaxation. It is a change in the intensity of one response to the other under perturbation.

Consider the nuclear spins i and s . The intensity I_n of the NOE may be expressed as

$$I_n \propto \langle r^{-6} \rangle f(T_c)$$

where r is the distance between the two interacting spins. The average of $\langle r^{-6} \rangle$ refers to the situation where the distance r may vary and thus has to be averaged appropriately. The inverse of r to -6 is the well-known quantity from the theory of polar molecules. In other words the NOE is proportional to the inverse of the distance between nuclei raised to the sixth power. (In physical chemistry terms, this is related to the London force, a weak intermolecular attractive force.) The term T_c characterizes the range of times between random translations and rotations of Brownian motion. Experimentally, it is a function of molecular weight, solution viscosity, temperature, and hydrogen bonding.

The NOE is observed in the interaction between H—H neighbors, H— ^{13}C neighbors and also unpaired electrons, that is, in the presence of paramagnetic materials such as oxygen atoms.

We can now summarize the basic NMR parameters as follows:

1. *The chemical shift*—for functional groups and the nuclei environment
2. *The J couplings*—for the torsion angles to obtain information about the molecular backbone and side chains if any
3. *Relaxations times*— T_1 , the spin–lattice or longitudinal relaxation time which is a measure of efficiency, with which excited nuclear spins return to their ground state by exchanging energy with their surroundings; T_2 , the spin–spin or transverse relaxation time that measures the efficiency of exchange energy
4. *Nuclear quadrupole relaxation*—the dipole–dipole interaction between spin $>1/2$
5. *Nuclear Overhauser effect*—for the distance between the two nuclei and important for the determination of molecular structure
6. *Correlation time*—related to NMR resonance linewidths which involve molecular size and tumbling time

19.4 NMR SPECTROSCOPY

For many years the continuous-wave (CW) method was used to detect resonance, but now most measurements of resonance rely on the pulsed Fourier transform (FT) method. In the CW method, only a single frequency which is attributed to a magnetically equivalent group (e.g., a methyl group) is excited and detected at any one moment. This is accomplished by monitoring the disturbance of the magnetization of a spin system with either the radio frequency (RF) varied or the applied field swept. In the FT method, the entire spectrum of frequencies is stimulated by a pulse of RF energy and the response of the system is observed as a function of time. Using the Fourier transform method, the time domain data are then transformed into the classical frequency domain spectrum.

The CW method was very popular in the 1960s and 1970s, but it takes time to scan. Fourier transform NMR obtains data hundreds of times faster than CW. The technique FT-NMR has also improved the signal-to-noise ratio for data obtained.

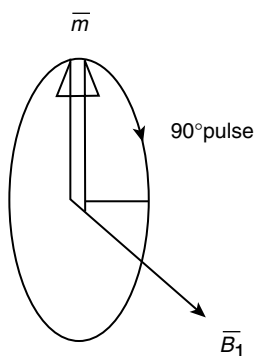
In this section, we will discuss the FT-NMR method only.

19.4.1 Pulsed Fourier Transform Method

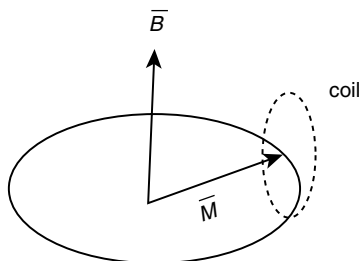
19.4.1.1 Rotating Frame of Reference Nuclear magnetization can be visualized by vectors x , y , and z . At various times during an NMR experiment, these vectors can be set in various orientations, depending on how we disturb them from equilibrium. At equilibrium, they are aligned along the z axis. In a rotating frame of reference, if we suddenly turn on another magnetic field along some direction in the xy plane, the nuclear spin responds by precessing about that direction. This is a way to induce an xy component of magnetization. In other words, the new magnetic field in the xy plane is the field forced upon it by an externally applied RF field.

The RF field can be turned on and off in much less than a microsecond. The rate of precession of the spin vectors is proportional to the strength of the RF field, just as the normal NMR frequency is proportional to the strength of the applied magnetic field. To the nucleus, the applied magnetic field is the first magnetic field and the RF field is the second magnetic field. The RF field can be tipped to different degrees in order to produce different final spin orientations: 180° to invert the magnetization, 270° to align it along the y axis, and 360° to return the magnetization to its original position. The most important angle is 90° , in which the RF field is long enough to tip the spin vector through exactly the proper angle.

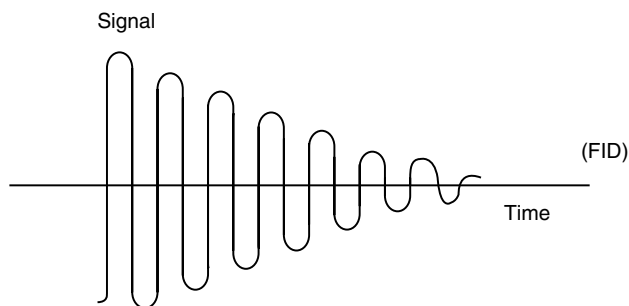
19.4.1.2 The 90° Pulse In a 90° pulse,



the magnetization vector is rotating in the xy plane at the Larmor frequency in an external field:



The signal is in the form of a simple free induction decay (FID) of a sample of spins, with a single resonance frequency.



As time passes, the individual spins move out of step, so the magnetization vector \bar{M} shrinks exponentially with a time constant T_c and induces an even weaker signal in the detector coil.

After a 90° pulse, the number of α -spins equals the number of β -spins. The populations revert to their thermal equilibrium values. But, as described earlier, at thermal equilibrium the spins have a Boltzmann distribution, with more α -spins than β -spins. By giving up energy to the surrounding area (the lattice), the β -spins again revert to α -spins. The time required for this reversion is T_1 , the spin-lattice relaxation time.

A 90° pulse is defined as that length of time necessary to rotate the magnetization through 90° . The transmitter is turned off at that point. The relaxation times T_1 and T_2 of different orientations are recorded. The resonance data obtained by the pulse method is the collection of signals expressed in time sequence, $X(t)$, which is now ready for Fourier analysis.

19.4.2 One-Dimensional NMR

The NMR data $X(t)$ can be treated in terms of the response theory, which is well-known in electrical engineering. The theory deals with the time domain (data collection) and the frequency domain (data exhibition).

Both time and frequency domains can carry the same information, although in different forms. This is accomplished by the Fourier transformation. Let $s(t)$ be the functions in the time domain and $S(\omega)$ or $S(\nu)$ be functions in the frequency

domain. The Fourier transformation provides a unique correspondence between the two functions in two different domains:

$$\begin{aligned} S(\omega) &= \int_{-\infty}^{\infty} s(t) e^{-i\omega t} dt \\ S(\nu) &= \int_{-\infty}^{\infty} s(t) e^{-i2\pi\nu t} dt \\ s(t) &= \frac{1}{2\pi} \int_{-\infty}^{\infty} S(\omega) e^{i\omega t} d\omega \\ &= \int_{-\infty}^{\infty} S(\nu) e^{i2\pi\nu t} d\nu \end{aligned}$$

while the frequency variable $\omega = 2\pi\nu$ (in units of radians per second) is convenient for formal calculations, the frequency variable ν (in hertz) is often more suitable to represent spectroscopic data.

The FID obtained from the pulse method contains all the NMR data of a sample. Fourier transformation not only enables the transformation from the time domain, $s(t)$, to the frequency domain, $S(\omega)$ or $S(\nu)$ but can also pretreat the time domain. The unnecessary data in the time sequence, such as noise, can be eliminated or trimmed before the transformation process. This would provide greater clarity of presentation and economy in labor. The pretreatment is carried out mathematically by the convolution theorem as follows: Let $r(t)$ be the function to pretreat the data function $s(t)$. The convolution integral of the two functions is defined by

$$r(t) * s(t) = \int_{-\infty}^{\infty} r(\tau) s(t - \tau) dt$$

Any pretreatment and filtering process in the NMR (such as apodization) can be expressed as

$$\begin{aligned} F\{r(t) * s(t)\} &= R(\omega) \cdot S(\omega) = R(\nu) \cdot S(\nu) \\ F^{-1}\{R(\omega) * S(\omega)\} &= \frac{1}{2\pi} r(t) \cdot s(t) \\ F^{-1}\{R(\nu) * S(\nu)\} &= r(t) \cdot s(t) \end{aligned}$$

19.4.3 Two-Dimensional NMR

The two-dimensional Fourier transformation is a straightforward generalization of the one-dimensional Fourier transformation. The complex two-dimensional Fourier transformation of the time domain signal $s(t_1, t_2)$ is defined by

$$s(t_1, t_2) = \frac{1}{4\pi^2} \int_{-\infty}^{\infty} dv_1 \exp(iv_1 t_1) \int_{-\infty}^{\infty} dv_2 \exp(iv_2 t_2) S(v_2, v_2)$$

with the inversion relation

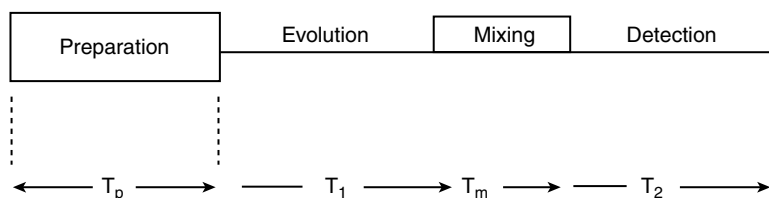
$$S(\nu_1, \nu_2) = \int_{-\infty}^{\infty} dt_1 \exp(-i\nu_1 t_1) \int_{-\infty}^{\infty} dt_2 \exp(-i\nu_2 t_2) s(t_1, t_2)$$

The process may be described as follows:

$$s(t_1, t_2) \xrightarrow[\text{FID}]{\text{FT over } t_2} S(t_1, \nu_2) \xrightarrow{\text{FT over } t_1} S(\nu_1, \nu_2)$$

time domain mixed domain frequency domain

where S refers to a time domain signal, FT refers to Fourier transformation, FID refers to the process of FID, t_1 is the first time variable in the pulse sequences, t_2 is the elapsed time of recording, ν_1 is the frequency expected in the first time period, and ν_2 is the frequency that is produced in a series of spectra manipulated by a variety of techniques. The first time variable t_1 is related to the evolution period, whereas the second time variable is related to the detection period:



where T_p and T_m are relaxation times known to the operator of the spectrometer.

A two-dimensional NMR spectrum is often displayed in the form of a map. One axis, ν_2 , contains the conventional chemical shifts. The other axis, ν_1 or t_1 , may contain chemical shift or J -coupling information or both. The position of a signal on the map tells us the chemical shift of that signal and the effect on that signal due to the presence of other nuclei.

There are two types of two-dimensional (2D) NMR spectra: a J -resolved spectrum and a chemical shift correlated spectrum. In a J -resolved spectrum the complex and overlapping NMR signals are resolved into individual shifts and coupling patterns. This is obtained by J couplings that modulate the nuclear signal during t_1 operation. The spectrum is displaced as depicted in the form of J versus σ , shown in Figure 19.8. In a correlated spectrum, one dimension is the chemical shift of any type of spin nuclei, such as ^{13}C , ^{15}N , ^{31}P , and the other dimension is usually the chemical shift of the coupled spin proton. Each peak on a contour map gives the shifts of a carbon and its coupled counterpart proton. The correlated spectrum identifies spin-coupled pairs of nuclei in a molecule. An example is discussed in the next section about the polypeptide polybenzyl- γ -glutamate.

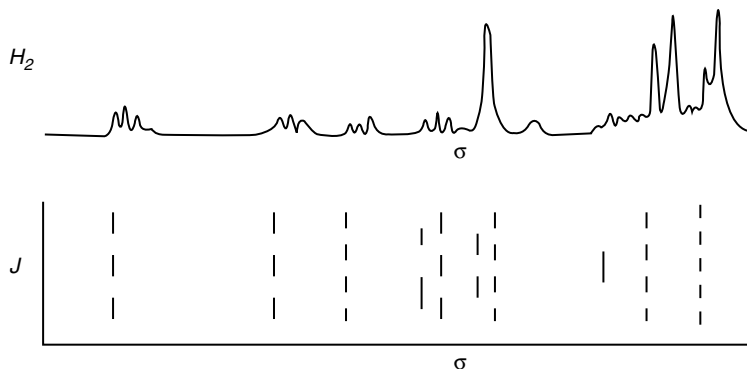


FIGURE 19.8 A 2D J spectrum. The 1D proton spectrum is overlaid on a 2D J spectrum.

Some of the most extensively used two-dimensional NMR are as follows:

- The J -resolved experiments, both homonuclear, ^1H - ^1H , and heteronuclear, ^{13}C - ^1H , sort couplings in F_1 from chemical shifts in F_2 .
- Homonuclear J -correlated ^1H experiments identify pairs of coupled spins (COSY), larger groups of coupled spins (RELAY), or whole spin systems (TOCSY).
- Heteronuclear J -correlated ^1H - ^{13}C (or ^1H - ^{15}N) experiments identify bonded ^1H - ^{13}C (or ^1H - ^{15}N) pairs or heteronuclear pairs connected by a long-range J coupling. Heteronuclear correlation may be accomplished by detecting the heteronucleus (HETCOR) or detecting ^1H (HMQC, HMBC).
- A homonuclear J -correlated ^{13}C experiment (INADEQUATE) detects directly bonded pairs of ^{13}C 's and can be used to determine the entire carbon skeleton of a molecule.
- Homonuclear dipolar-correlated ^1H experiments (NOESY and ROESY) identify pairs of protons close enough together to interact magnetically through space.
- A heteronuclear chemical shift correlation experiment, ^{15}N - ^1H , reduces line broadening with increasing molecular size (TROSY).

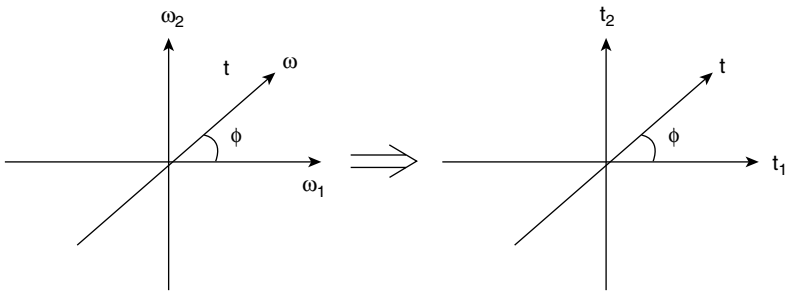
Three and four-dimensional NMRs are also available. They are more complicated than one- and two-dimensional NMR, but the underlying general principles are about the same. The three- and four-dimensional NMRs are useful for the determination of structures of larger proteins and protein complexes.

19.5 MAGNETIC RESONANCE IMAGING

Magnetic resonance imaging (MRI) is the NMR used for diagnosing certain diseases such as those in the brain and spinal cord. A patient is placed inside the

bore of a powerful magnet. A second oscillating magnetic field is then applied to the patient. This second field causes the hydrogen nuclei to move out of alignment with the first, thereby generating signals that are influenced by the chemical and physical environments of the nuclei which can be mathematically transformed into images of the body.

If a magnetic field gradient is applied to an object, the frequency of response of a given type of nucleus will also depend on its position in space. MRI utilizes a magnetic field gradient to disperse the NMR resonance frequencies of the various volume elements. It is a one-dimensional projection of the three-dimensional proton density in the direction of the field gradient. All nuclei in a plane perpendicular to the field gradient will experience the same field and contribute to the signal amplitude at the same frequency. The idea, proposed by Lauterbur, is to utilize a magnetic field gradient to disperse the NMR resonance frequencies of the various volume elements. In a sense, it is a special kind of two-dimensional NMR. Consider the diagram of the transformation of the skew coordinates:



Let $S(\omega_1, \omega_2)$ be the desired image of the object and $P(\omega, \varphi)$ be a projection obtained by applying a gradient in the direction φ . In correspondence with the projection $P(\omega, \varphi)$ there is a one-dimensional Fourier transformation to $C(t, \varphi)$. That is, there are relations

$$P(\omega, \varphi) = F\{C(t, \varphi)\}$$

$$C(t, \varphi) = F^{-1}\{P(\omega, \varphi)\}$$

where

$$C(t, \varphi) = s(t \cos \varphi, t \sin \varphi)$$

The one-dimensional Fourier transformation $C(t, \varphi)$ represents a central cross section. Applying two-dimensional transformations, we can obtain $s(t_1, t_2)$ in the time domain, which in turn can be transformed to $S(\omega_1, \omega_2)$ in the frequency

domain. The measured frequencies ω_1 and ω_2 are related to the spatial coordinates x_1 and x_2 through the relation

$$x_i = \frac{\omega_i}{\gamma g} \quad i = 1, 2, \dots$$

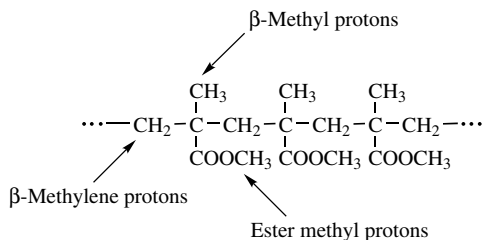
where g is the magnetic field gradient applied to obtain the projection.

19.6 NMR SPECTRA OF MACROMOLECULES

In this section we first discuss two synthetic polymers, poly(methyl methacrylate) and polypropylene, to illustrate the proton and ^{13}C NMR spectroscopy of macromolecules. The spectra of protein molecules will be discussed in later sections. We then describe deuterium NMR spectroscopy by illustrating the characteristic features of the motion in the polyethylene molecule. The motion is caused by a change in thermal energy. Finally, we describe polybenzyl- γ -glutamate as an example of two-dimensional NMR spectroscopy.

19.6.1 Poly(methyl methacrylate)

Below is the formula of the polymer molecule:



Since there is no J coupling between the CH_2 and $\alpha\text{-CH}_3$ protons, the NMR phenomenon for poly(methyl methacrylate) is relatively simple. In the proton NMR spectrum, the ester methyl protons appear near 6.5τ , the β -methylene protons appear near 8.0τ , and the β -methyl protons appear between 8.5 and 9.0τ . Figure 19.9 shows the β -methylene proton spectrum; Figure 19.10 shows the β -methyl proton spectrum. Both were observed at 220 MHz. In both spectra, the ester methyl protons appear near 6.5τ , but, in order to show the details of β -methylene protons and β -methyl protons, they were not shown in the two figures. In both cases, the sample was prepared by dissolving poly(methyl methacrylate) in 10–15% chlorobenzene, with the temperature of the NMR measurement at 135°C .

The methylene spectrum of the syndiotactic isomer (Figure 19.9a) shows three peaks in the range between 7.5 and 8.5τ (only one being shown in the 60-MHz spectrum). The isotactic isomer (Figure 19.9b) in the same range shows five distinct

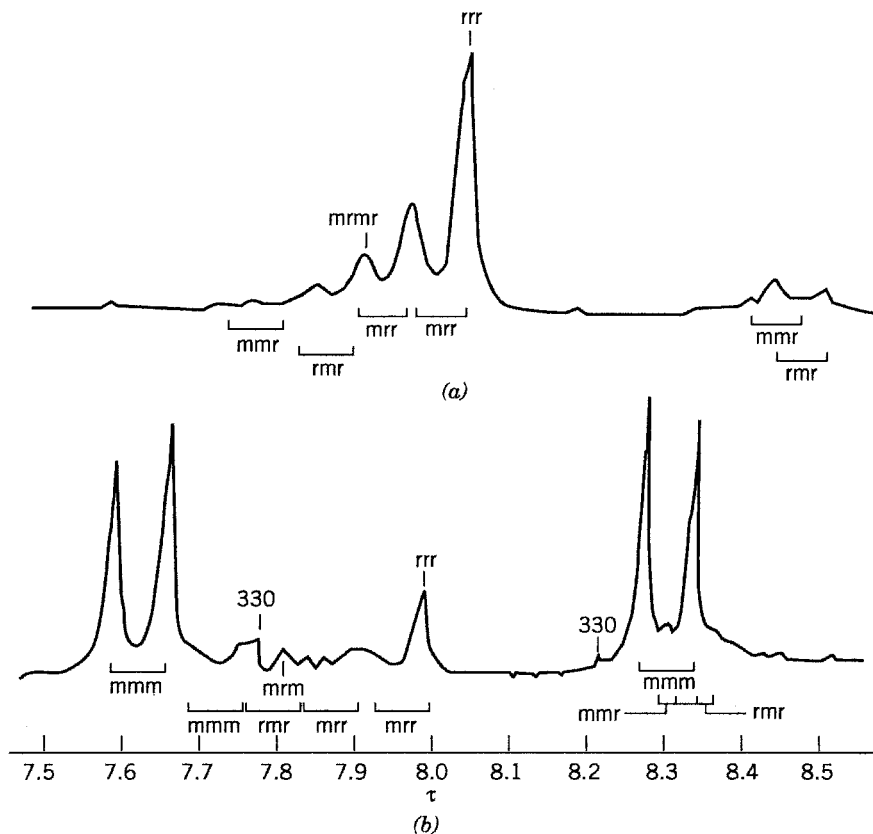


FIGURE 19.9 The 220-MHz β -methylene proton spectra of poly(methyl methacrylate) in chlorobenzene at 135°C: (a) syndiotactic; (b) isotactic. [Source: Bovey (1972). By permission of Dr. Bovey and Academic Press.]

peaks. The three peaks of the syndiotactic isomer are concentrated at 7.8–8.1 τ ; there are no signals between 7.5 and 7.8 τ or between 8.1 and 8.5 τ . The five distinct peaks of isotactic isomer spread from 7.5 to 8.5 τ .

By comparison, the spectrum of β -methyl proton (Figure 19.10) spreads wider for the syndiotactic isomer than for the isotactic isomer. In the range between 8.7 and 9.0 τ , the syndiotactic isomer shows two gigantic peaks, whereas the isotactic isomer shows only two baby peaks. These comparisons clearly show the structural differences between the two isomers. The symbols m and r, which refer to the meso mixture and the racemic mixture, are indicated on each peak in the graphs. A mixture of isomers is said to be racemic if one form is indistinguishable from the other by NMR alone. Their enantiomers are dissymmetric and magnetic equivalent. If the macromolecule involves symmetry and their enantiomers are magnetically nonequivalent, the mixture of isomers is said to be meso. The nuclei of meso

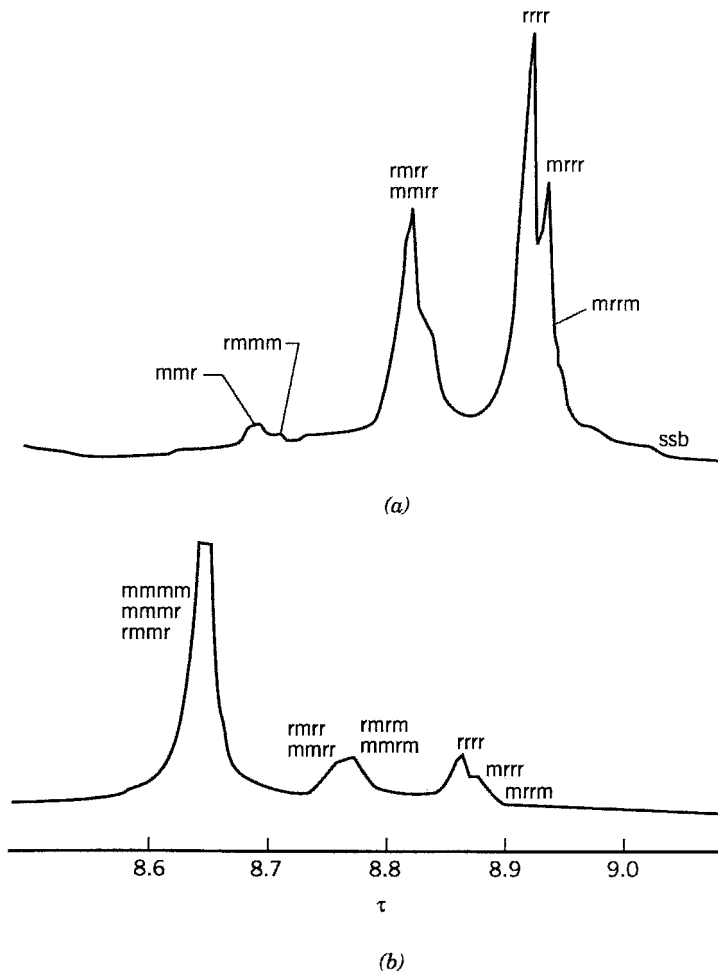
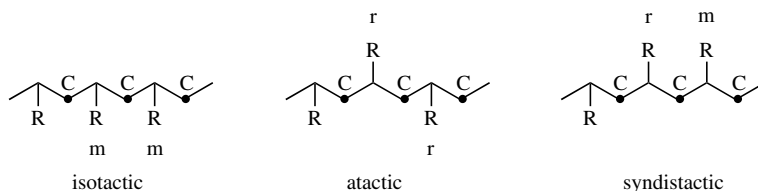


FIGURE 19.10 The 220-MHz ester methyl proton spectra of poly(methyl methacrylate) in chlorobenzene at 135°C: (a) syndiotactic; (b) isotactic. [Source: Bovey (1972). By permission of Dr. Bovey and Academic Press.]

polymers have different chemical shifts and couplings, while the nuclei of the racemic isomers have identical chemical shifts and couplings.

The following is an example of the meso and racemic mixture of a triad:



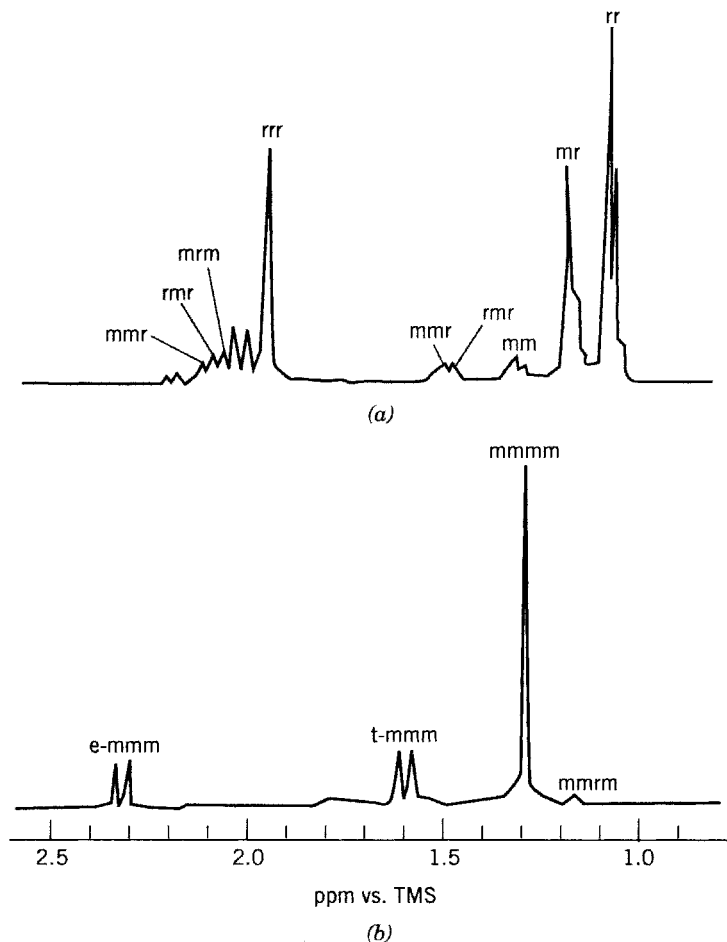


FIGURE 19.11 The 500-MHz proton spectra of poly(methyl methacrylate) in chlorobenzene at 100°C: (a) syndiotactic; (b) isotactic. [Source: Bovey (1988). By permission of Dr. Bovey and Academic Press.]

Figure 19.11 is similar to Figures 19.9 and 19.10 except that a more powerful magnetic field has been applied and the resonance frequency changes from 220 to 500 MHz. The scales are also different. As expected, the basic spectrum is the same but more structural details are displayed.

Figure 19.12 shows the ^{13}C NMR spectrum of poly(methyl methacrylate) in 1,2,4-trichlorobenzene at 25.2 MHz and 120°C. Here the signals are of C instead of protons. The spectrum shows the stereochemistry of the main-chain carbons (CH_2 and $\text{—}\overset{\text{O}}{\underset{\text{O}}{\text{C}}}\text{—}$) and the chain C—CH_3 and OCH_3 . The signal of >C=O is off the scale and is shown in the left corner of Fig. 19.12.

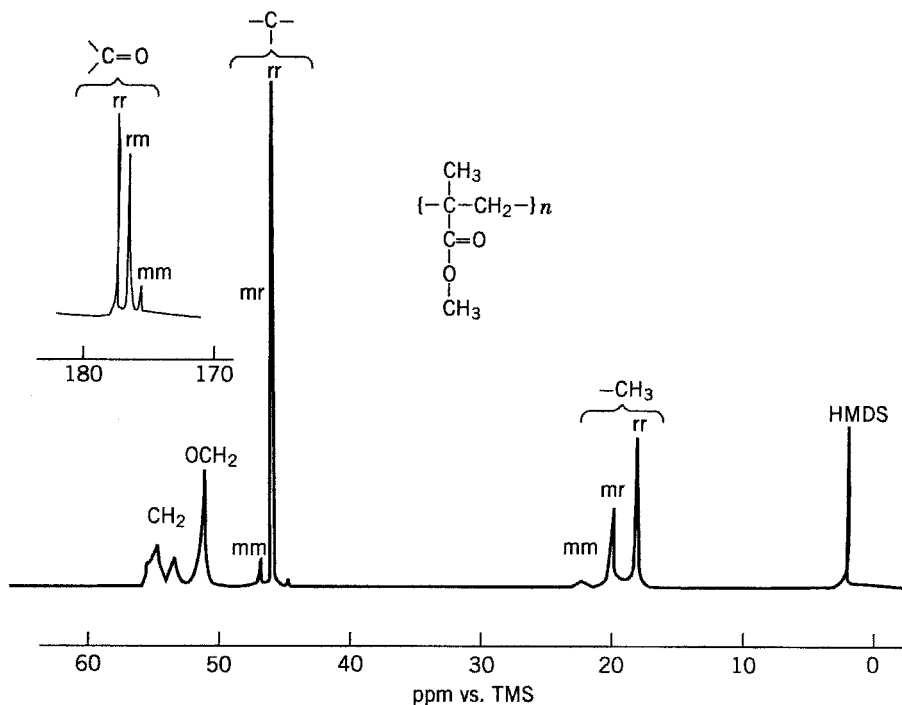
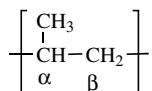


FIGURE 19.12 The 25.2-MHz ^{13}C spectrum of poly(methyl methacrylate) in 1,2,4-trichlorobenzene at 120°C . [Source: Randall (1977). By permission of Academic Press.]

19.6.2 Polypropylene

As seen in the formula of polypropylene,



the proton spectrum is complicated due to the vicinal coupling between α and β protons and between α and methyl protons, together with the geminal methyl proton coupling in the case of the isotactic polymer. Figure 19.13 shows the 220-MHz proton spectra of isotactic and syndiotactic polypropylene in *o*-dichlorobenzene at 165°C . The β protons of the isotactic polymer are more widely spread than those of the syndiotactic polymer. The proton spectrum of atactic polypropylene is not shown, because of a complex of overlapping multiplets. The situation is different in the case of ^{13}C spectra, where we can have three distinct spectra of all three forms

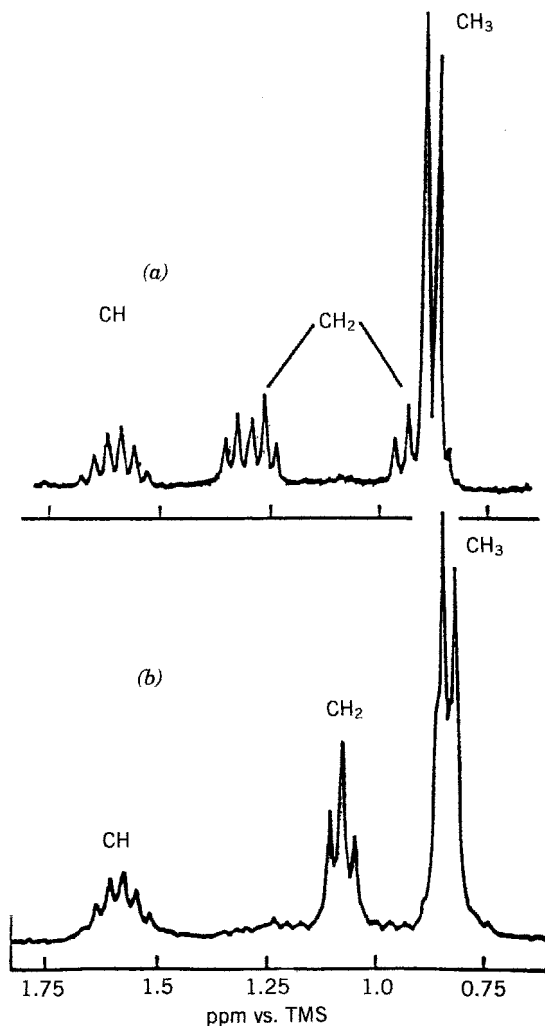


FIGURE 19.13 The 220-MHz proton spectra of polypropylene in *o*-dichlorobenzene at 165°C: (a) isotactic; (b) syndiotactic. [Source: Ferguson (1967). By permission of the New York Academy of Science.]

of the polymer. Figure 19.14 shows 25-MHz ^{13}C NMR spectra for comparing the structural differences. The ^{13}C NMR spectra can also show the difference between crystalline polypropylene from the amorphous polypropylene, as in Figure 19.15.

19.6.3 Deuterium NMR Spectra of Chain Mobility in Polyethylene

The deuterium NMR spectrum is basically the observation of the quadrupole coupling, $e^2q_{\alpha\beta}Q/h$, where e is the electric charge, $q_{\alpha\beta}$ is the electric field gradient

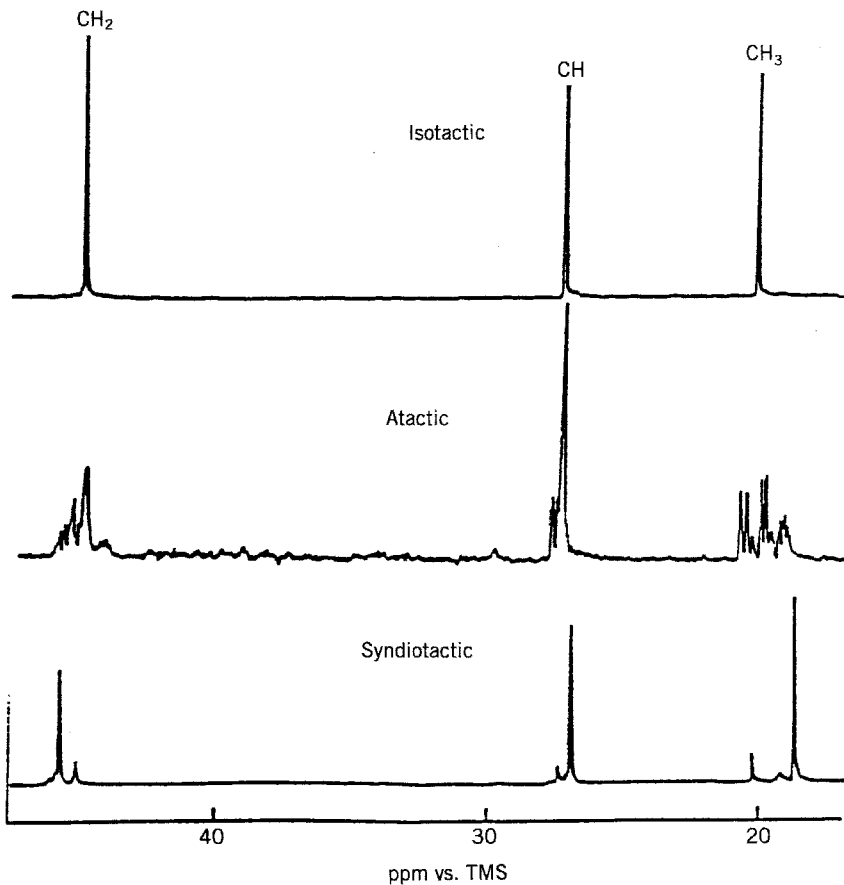


FIGURE 19.14 The 25-MHz ^{13}C spectra of polypropylene in 1,2,4-trichlorobenzene at 140°C . [Source: Bovey (1988). By permission of Dr. Bovey and Academic Press.]

tensor defined as

$$q_{\alpha\beta} = \left(\frac{\partial^2 v}{\partial r_\alpha \partial r_\beta} \right)_{r=0}$$

Q is the quadrupole moment, and h is Planck's constant. The magnitude of the splitting may be described by

$$\delta\nu = \frac{3}{2} \left(\frac{e^2 q_{\alpha\beta} Q}{h} \right) \left(C_1 S + \frac{3}{2} C_2 K \right)$$

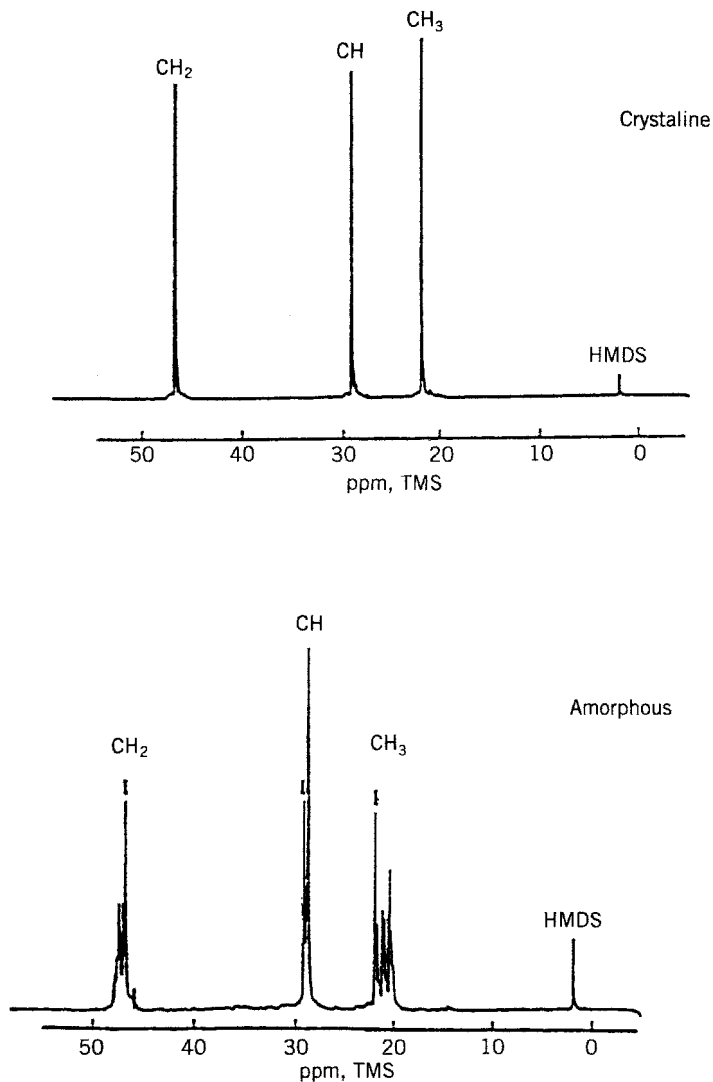


FIGURE 19.15 The 25.2-MHz ^{13}C spectra of polypropylene in 1,2,4-trichlorobenzene at 120°C . [Source: Randall (1977). By permission of Academic Press.]

where C_1 and C_2 are related coordinates and S and K are ordering parameters which give the orientation of the molecules in the magnetic field. The nucleus ^2H is well suited for studying molecular order and mobility in polymers. The intermolecular interaction is usually measured in terms of the spin-lattice relaxation time T_1 , whereas the mobility is measured through the change of line shapes. Figure 19.16

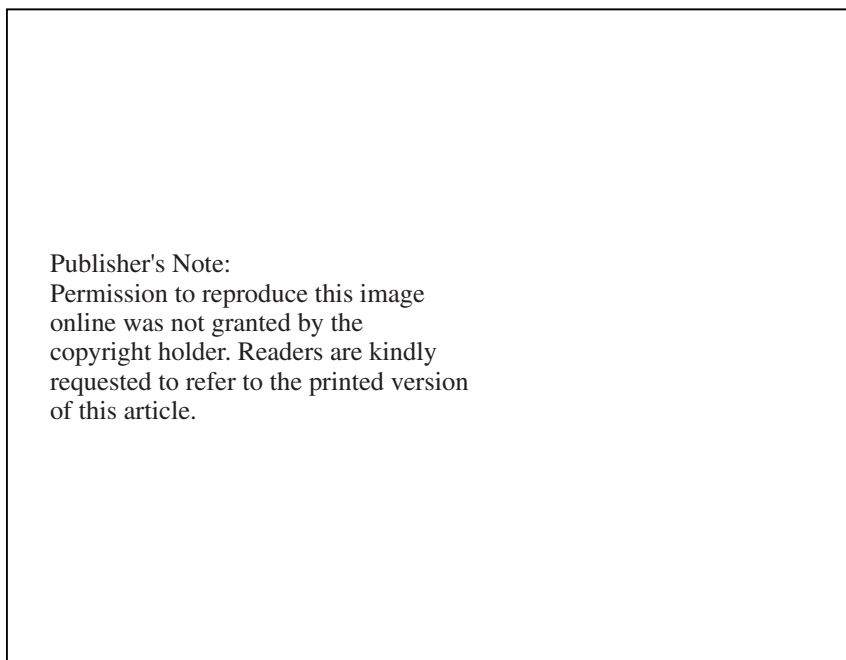


FIGURE 19.16 Chain mobility as shown in the deuterium spectra of amorphous regions of linear polyethylene at various temperatures. [Source: Speiss (1985). By permission of Springer-Verlag.]

shows the chain mobility in the amorphous regions of linear polyethylene, which is compared to the chain motion of polystyrene in the vicinity of the glass transition.

19.6.4 Two-Dimensional NMR Spectra of Poly- γ -benzyl-L-glutamate

The polypeptide poly- γ -benzyl-L-glutamate may be labeled as follows:

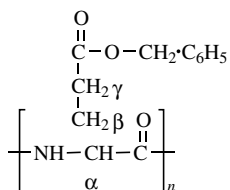


Figure 19.17 shows a one- and a two-dimensional NMR spectrum of a polypeptide.

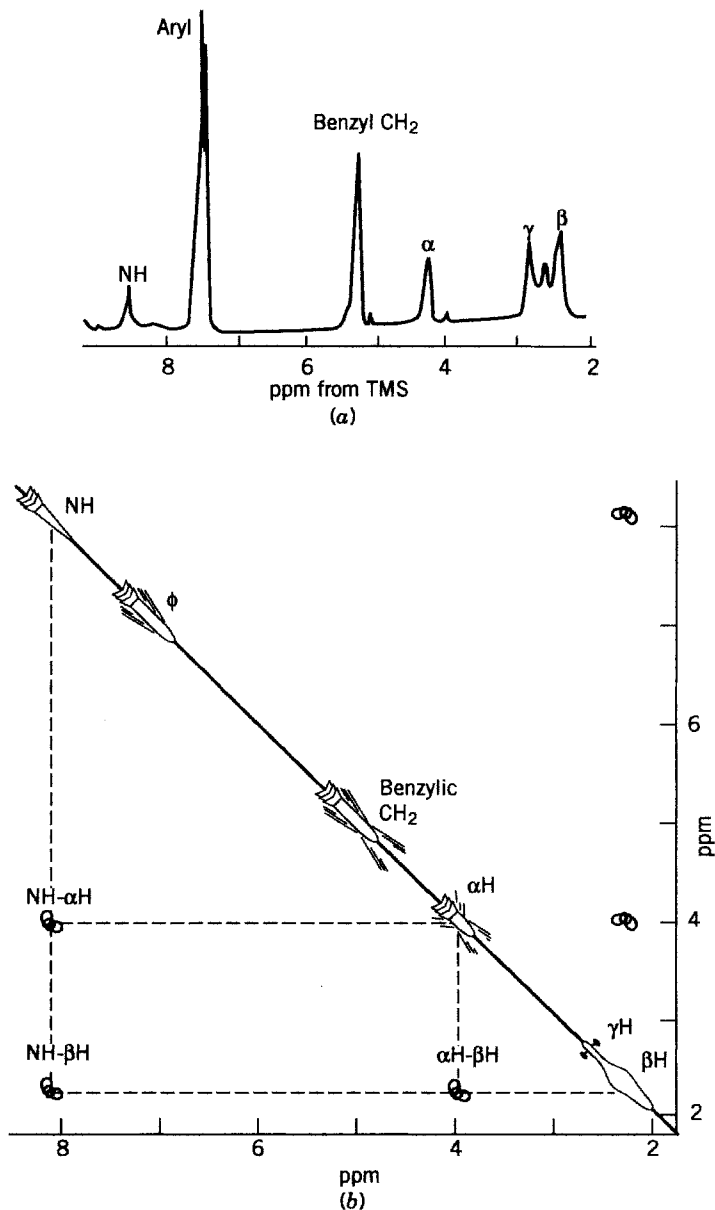


FIGURE 19.17 The 500-MHz proton spectra of poly- γ -benzyl-L-glutamate 20-mer in α -helical form in 95.5 chloroform trifluoroacetic acid at 120°C : (a) one dimensional; (b) two dimensional. [Source: Mirau and Bovey (1986) and Bovey (1988). By permission of Dr. Bovey and the American Chemical Society as well as Academic Press.]

19.7 ADVANCES IN NMR SINCE 1994

19.7.1 Apparatus

In the 1960s, the magnet for most available NMR spectrometers was first at 60 MHz, then at 100 MHz; in the 1970s, it became 250 MHz, then 300 MHz; in the 1980s, 400 and 500 MHz were reached. Since 1994, the most powerful magnet has jumped from 600 and 750 MHz to 900 MHz. A 900 MHz NMR spectrometer stands 7 m high, is surrounded by a shield made of 113 tons of iron, and holds some 240 km of superconducting wire. In terms of magnets, 750-MHz machines are fitted with 17.6-T magnets and the 900-MHz machines with 21-T magnets. A new 1000-MHz (1-GHz) machine is under planning and would require fields of more than 23.5 T.

The evolution of the NMR machine is very similar to that of the x-ray crystallography machine. Most individual laboratories can no longer afford such a gigantic machine. Cooperation must be arranged for researchers so that they conduct their preliminary work on smaller NMR spectrometers in their own institutions and then proceed to use bigger machines when available in other laboratories to complete their study. This is also similar to working with x-ray crystallography today.

The bigger the NMR machine, the more sensitive it is to detecting faint signals from smaller samples and the better its resolution or the better its ability to sort out one nuclear signal from another. This is particularly important in the investigation of three-dimensional structures of proteins.

19.7.2 Techniques

The advancement of techniques in NMR measurements is parallel to the advancement of the NMR apparatus itself. The apparatus is heavy equipment, and it is not easy for an individual to modify it except in very small ways. Improvements in techniques are proceeding all the time by individuals at different laboratories. This section lists a few of the common features under current development.

19.7.2.1 Computer-Aided Experiments Computers have become common tools for the analysis of NMR data as Fourier transform spectrometers have replaced CW instruments. These computers perform the basic processing of data, including digital filtering, Fourier transformation, and phase correction.

Time domain filtering is based upon a simple mathematical manipulation. FID are multiplied by the term C_1 ,

$$C_1 = \frac{D_1}{2 \Delta t_1}$$

where D_1 is the smallest time t_1 variable delay and Δt_1 is the sampling interval. The first column of the time domain data matrix is multiplied by the term C_2 ,

$$C_2 = \frac{D_2}{\Delta t_2}$$

where D_2 is the delay between the last pulse and the start of acquisition and Δt_2 is the sampling interval in t_2 .

Frequency domain filtering is carried out by using the polynomial filters where each point x_i is replaced by x_i^1 :

$$x_i^1 = \sum_{n=-1}^N a_n x_{i+n}$$

The term a_n ($n = -N, \dots, N$) is a series of coefficients defining the filter. The most common of these filters is the moving-average filter defined by

$$a_n = 1/(2N + 1)$$

which leads to a smoothing of the spectrum.

Linear prediction is a method to directly obtain the resonance frequencies and relaxation rates from time domain signals, which are a superposition of exponents, by solving the characteristic polynomials. Phases and intensities are calculated interactively using a least-squares procedure. The correlation spectroscopy of a two-dimensional NMR spectrometer employs several specific programs such as RELAY and TOCSY. The recognition of response peaks, the isolations of signals from noise and artifacts, and the spectral position (e.g., chemical shift) are all carried out by computers.

The following is a description of a typical run reported in scientific journals with computer-assisted NMR research (attention should be paid to the language of description): NMR experiments are carried out at 35°C on 600, 750, 800, and 900-MHz spectrometers, respectively. Proton, ^{15}N , and, ^{13}C backbone and side-chain resonances of proteins are assigned by three-dimensional (3D) double- and triple-resonance NMR experiments; ^1H resonance for a protein by two-dimensional (2D) ^{13}C -filtered experiments; and ^{31}P resonance of a protein from a 2D ^1H - ^{31}P correlation spectrum.

The observation of a strong $^{31}\text{P}(i)$ - $\text{H}4^1(i)$ correlation and the absence of $^{31}\text{P}(i)$ - $\text{H}5^1/\text{H}5^{11}(i)$ correlation indicates that the β and γ sugar-phosphate torsion angles are in the t and g^+ conformations, respectively.

Interpolation distance restraints within the protein are derived from 3D and four-dimensional (4D) ^{15}N - and ^{13}C -separated NOE experiments; within the protein from 2D ^{12}C -filtered NOE experiments; and between the protein and DNA from 3D ^{13}C -separated/ ^{12}C -filtered and ^{15}N -separated/ ^{12}C -filtered NOE experiments.

Backbone ϕ/ψ torsion angle restraints are derived from backbone chemical shift using the program TALOS.

Heteronuclear 3J couplings were measured by quantitative J correlation spectroscopy.

19.7.2.2 Modeling of Chemical Shift Modeling NMR spectroscopy chemical shifts is a theoretical subject aimed at the quantum mechanical links between the

tiny magnetic and electronic environments of nuclei and the external magnetic fields. It is useful for interpreting experimental work and for providing confidence in proposed conclusions. On the other hand, results obtained from experiments help to judge whether a model is adequate or not. Both the experiments and modeling enhance the ability to predict complex structures.

The mathematical framework for modeling a system is to solve the Schrödinger equation, which describes the energies of system, here, a spin system. Consider the Hamiltonian operator H_0 of the Schrödinger equation:

$$H_0 = H_Z + H_D + H_\delta + H_E + H_Q + H_R$$

where the Z, D, δ , E, Q, and R refer to the Zeeman interaction, dipolar interaction, chemical shift interaction, induced electron-coupled nuclear spin interaction, quadrupolar interaction for nuclei with $I > 1/2$, the interaction with the applied electromagnetic radiation, respectively. In a nonviscous liquid, H_D and H_Q average out to zero. Only the four terms, H_Z , H_δ , H_E , and H_R , are relevant. The terms H_Z and H_δ are related to chemical shift, and H_E and H_R are related to J coupling. The effects of the external NMR magnetic field, which does not belong to H_0 , on the nucleus of interest is added into the equation as perturbation. Fast computers are needed to solve the Schrödinger equation in order to gain accuracy and reliability. Various well-known ab initio methods using first principles make use of the modifications of theoretical standbys: Hartree–Fox or density function theory.

Chemical shifts are frequently expressed in terms of a tensor, which describes the magnitude of the field felt at the site of the nucleus along the α direction, induced by electronic currents brought about by an applied magnetic field along the β direction. A chemical shift tensor, often represented by a 3×3 matrix, describes all the directional aspects of shielding and deshielding at a nucleus.

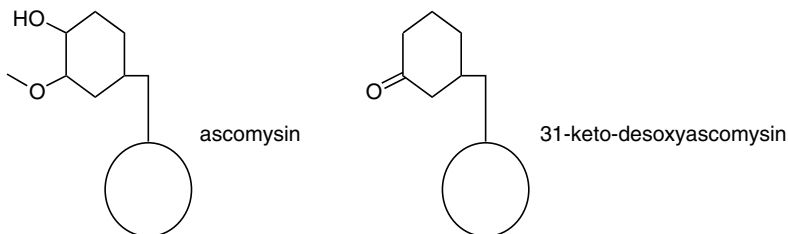
In actual experiments, techniques of heavy isotope tags and rapid pulses of radio waves, highly resolved, can generate multidimensional spectra. Correspondingly, theoretical calculations can use a relativistic effect to obtain results for comparison as well as for confirming the model proposed.

19.7.2.3 Protein Structure Determination NMR is an important tool to determine the three-dimensional structure of protein molecules and adds to or equals the knowledge obtained through the method of x-ray crystallography. It is hard to imagine how our knowledge of structural biology could have advanced to current levels if there had been no advanced NMR and x-ray crystallography. In this section, we describe three techniques relevant to NMR.

Chemical Shifts for Binding Study In this technique, we compare the chemical shifts of the free protein with those of the protein bound to a ligand. Those portions of the protein that show changes in chemical shifts in the bound form are likely to be near or in the binding pocket. And, by comparing the chemical shifts of the protein bound to one ligand with those of the same protein bound to a slightly different ligand, the perceived alteration provides an indication about the site of the

protein–ligand complex. With a series of structurally related ligands, an approximate mapping of the ligand in the binding site is reasonably established.

In parallel with the differential UV absorption method mentioned previously, a differential chemical shift method had been designed and employed experimentally. For example, to find the binding site of a compound—ascomysin, a slightly modified compound—31-keto-32-desoxyascomysin is synthesized. Comparison between the chemical shifts of the two compounds clearly indicates that the cyclohexyl ring is the binding site:



Hydrogen Bond J Coupling J couplings are related to the torsional angle of chemical bonding. The study of J couplings can provide information on the geometry of the structure of a molecule. Hydrogen bonding is a weak covalent bond, which, according to quantum theory, is the orbital overlap between atoms. J couplings make it possible to measure the orbital overlap of the nuclear state of a hydrogen bond donor atom and that of the acceptor atom. Since hydrogen bonds usually occur among certain atoms, such as N, O, and F, the technique is to use the isotope labeled materials with ^{15}N on both the donor and acceptor sides of the hydrogen bond. The magnitude of the observed nitrogen-to-nitrogen J coupling interaction across hydrogen bonds is in the range of 7 Hz. For accurate measurement, the spectra must have high resolution.

NOE Measurement of the NOE between the α protons of residue i and the amide protons of residue $i + 1$ provides NMR information about the protein sequence. The correct experimental path can be selected by comparing the NMR results with known amino acid sequences. However, NOEs arise from residues that are close together only in space, not in the chain sequence. For correct information about the geometry, there must be some way to distinguish between what is in the sequence and what is in the space. Several special programs are available to solve the problem, such as multidimensional NMR of NOESY (nuclear Overhauser and exchange spectroscopy) and ROESY (rotatory-frame Overhauser spectroscopy). Both offer some means to obtain the same Overhauser effect information for all nuclei in a molecule by a single experiment.

Overall Mapping The final step in the NMR measurement of protein structure is overall mapping. It begins with changes in the backbone amide ^1H and ^{15}N chemical

shifts of the protein domain. By NMR analysis, the sites of most perturbed residues are localized, including the NH₂ terminal unstructured region, the solvent-exposed surface of the first helix, and the regions around the loops. Then the electrostatic surface potential of the domain is calculated. In displaying the electrostatic potential surface, colors are used for clarity. Positive, negative, and neutral electrostatic potentials are shown in blue, red, and white, respectively. The calculation and drawing are both carried out by computer programs.

Some of these programs are commercially available, such as Delphi for calculations and Insight 98 for drawings. The final step is the construction of the space-filling model, which is also produced by computer programs such as Insight 98.

All the spectra and all the analyses can be processed with programs such as NMR Pipe (2) and NMR View software.

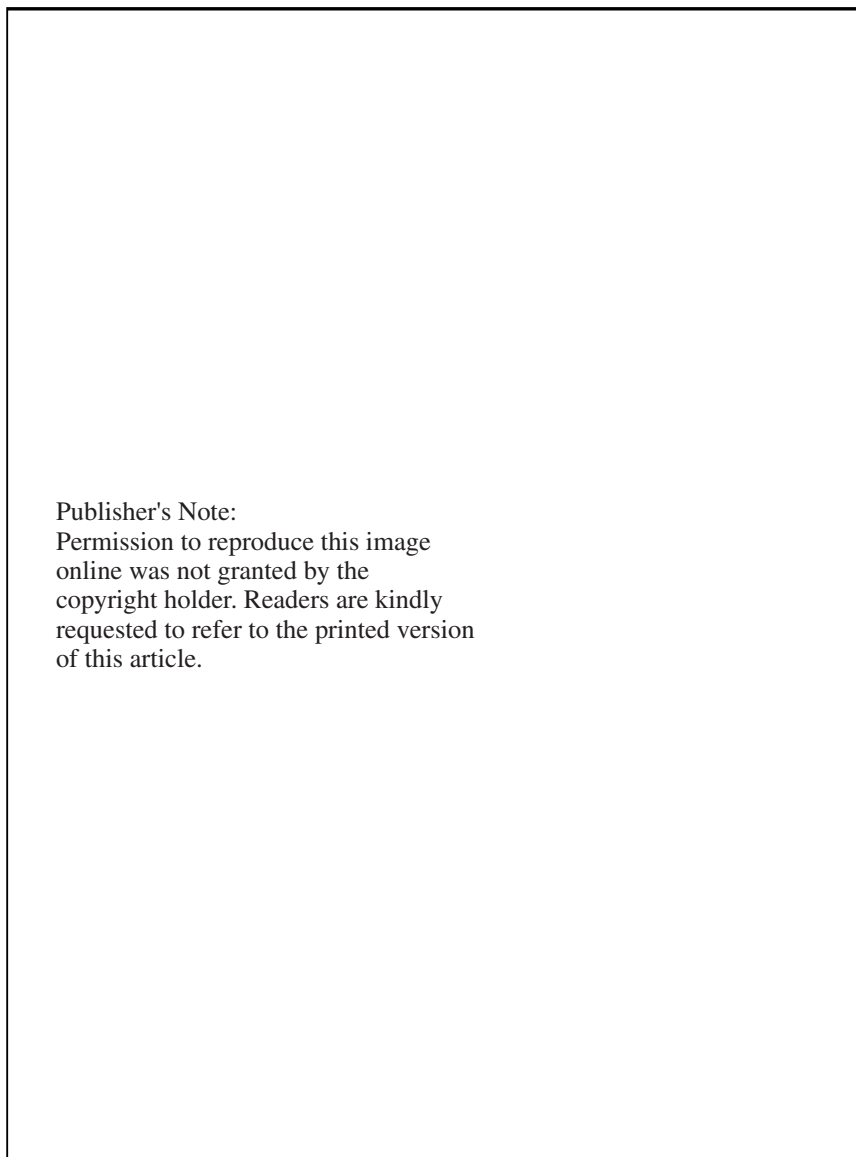
19.7.2.4 Increasing Molecular Weight of Proteins for NMR Study NMR spectroscopy is comparable to x-ray crystallography in the determination of the three-dimensional structures of DNA and proteins. However, for years there was a serious limitation to NMR in that the sample used could not be too big; molecular weight was limited to 30,000. Only recently, this limit has been lifted by using different experimental strategies.

In correlation spectroscopy, a two-spin system in a molecule, such as ¹⁵N-¹H or ¹³C-¹H, gives rise to a four-component fine-structure spectrum in which the individual component lines are well separated from each other. The strategy is that, instead of decoupling some component lines, the technique focuses on one of the four component lines (the sharpest one), using it as the correlation peak, while suppressing the other three fine-structure lines. By throwing away 50–75% of the intensity, one gains up to a factor of 10 in intensity and resolution for certain targeted spin systems. A successful example of this is the study of the conformational change and the binding site of the complex GroEl–GroEs with molecular weight 900,000.

The complex consists of GroEs (homo-tetradameric chaperonin) and GroEl (homoheptameric co-chaperonin) (see Chapter 18). Most amino acids of GroEs show the same resonances whether free in solution or in complex with chaperonin. It is residues 17–32 that show large chemical shift changes on binding. These amino acids belong to a mobile loop region of GroEs that forms contacts with GroEl. It was observed that the mobile loop of GroEs undergoes a large conformational change. This provides a binding mode in which some of the mobile loop residues are immobilized in the complex whereas others retain a relatively high degree of mobility.

19.8 TWO EXAMPLES OF PROTEIN NMR

Since 1994, there has been an avalanche of new three-dimensional protein structure determinations, currently at a rate of about 55 per week. Here, we illustrate two



Publisher's Note:
Permission to reproduce this image
online was not granted by the
copyright holder. Readers are kindly
requested to refer to the printed version
of this article.

FIGURE 19.18 See color insert. A membrane protein: (a) ribbon diagram; (b) recognition; (c) interaction. [Source: Kuteteladze, et al., *Science* **291**, 1793 (2001). With permission from AAAS. Original in color.

Publisher's Note:
 Permission to reproduce this image
 online was not granted by the
 copyright holder. Readers are kindly
 requested to refer to the printed version
 of this article.

FIGURE 19.19 See color insert. NMR molecular modeling of prions: (a) NMR structure of PrP^C; (b) binding of protein x to PrP^C; (c) plausible model for the tertiary structure of PrP^{Sc}. Color codes are: red, S₁; green, S₂; gray, α -helices H₃ and H₄; yellow, loop. Four residues implicated in the species barrier (Asn¹⁸⁸, Met¹¹², Met¹²⁹, and Ala¹³⁴) are shown in ball-and-stick form. [Source: Prusiner, S. B., *Science* **278**, 245 (1997). With permission from AAAS. Original in color.]

examples using NMR as a probe: one is a membrane protein and the other is a brain protein. The selection of these examples is arbitrary but highly informative.

19.8.1 Membrane Protein

Membrane proteins are attached to oily membrane bilayers. They are difficult to purify. Delicate detergents are required to suspend them in solution. It is important to realize that half of the proteins that are of biological and pharmaceutical interest are membrane proteins.

Here, our membrane protein is the FYVE domain (which is named for its identification with four proteins (Fablip, YOTB, Vac1p, EEAI) and the ligand is PtdIns(3)P, an abbreviation for phosphatidylinositol-3-phosphate.

Figure 19.18 shows (a) the structure of the protein of EEAI in the FYVE domain, (b) the phosphate group in PtdIns(3)P recognition by arginines, and (c) interactions in the PtdIns(3)P pocket.

The NMR spectrometers used include 400, 500, and 600 MHz. Structures were calculated using software X-PLOR 3.84.

19.8.2 A Brain Protein: Prion

The normal, cellular prion protein (PrP^c) is converted into disease-causing prion (PrP^{sc}) proteins through a posttranslational process. After conversion, PrP^c loses some α -helical content, while PrP^{sc} acquires a high β -sheet content.

PrP^c contains four regions of α -helices, denoted H1, H2, H3, and H4. Figure 19.19a shows molecular modeling NMR structure of PrP^c based on molecular modeling studies and its binding to an unknown protein x (Figure 19.19b). It also shows the plausible model for the tertiary structure of PrP^{sc} . Here, the NMR study draws the following conclusions: (1) the process of transmission involves unfolding of the PrP^c and refolding into PrP^{sc} ; (2) while PrP^c is converted into PrP^{sc} , PrP^{sc} acts as a template for further conversion (Figure 19.19c). Thus the conformational template provides a mechanism for both the generation and propagation of prion stains. If there is any effective therapeutic method to thwart prion alteration, it would be to modify the action of protein x.

REFERENCES

- Bloch, F. W. W. Hansen, and M. E. Packard, *Phys. Rev.* **69**, 127 (1946).
- Bloch, F., *Phys. Rev.* **70**, 460 (1946).
- Bovey, F. A., *Nuclear Magnetic Resonance Spectroscopy*, 2nd ed. New York: Academic, 1988.
- Croasmun, W. R., and R. M. K. Carlson (Eds.), *Two-Dimensional NMR Spectroscopy: Application for Chemists and Biochemists*. New York: VCH, 1987.
- Ernst, R. R., G. Bodenhausen, and A. Wokaun, *Principles of Nuclear Magnetic Resonance in One and Two Dimensions*. Oxford: Clarendon, 1991.
- Ferguson, R. C., *Trans. N. Y. Acad. Sci.* **29**, 495 (1967).
- Harris, R. K., *Nuclear Magnetic Resonance Spectroscopy*. London: Pitman, 1983.
- Karplus, M., *J. Chem. Phys.* **30**, 11 (1959).
- Kuteteladze, et al., *Science* **291**, 1793 (2001).
- lauterbur, P. C., *Nature* **242**, 190 (1973).
- Levy, G. C., *NMR Spectroscopy: New Methods and Applications*, ACS Symposium Series 191. Washington, DC: American Chemical Society, 1982.
- Levy, G. C., R. L. Lichter, and G. L. Nelson, *Carbon-13 Nuclear Magnetic Resonance Spectroscopy*. New York: Wiley, 1980.

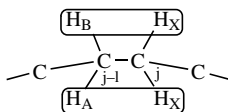
- Lyerla, J. R. *Methods Exp. Phys.* **16A**, 241 (1980).
 Overhauser, A. W., *Phys. Rev.* **91**, 476 (1953).
 Prusiner, S. B., *Science* **278**, 245 (1997).
 Purcell, E. M., H. C. Torrey, and R. V. Pound, *Phys. Rev.* **69**, 37 (1946).
 Purcell, E. M., R. V. Pound, and N. Bloembergen, *Phys. Rev.* **70**, 986 (1946).
 Sanders, J. K. M., and B. K. Hunter, *Modern NMR Spectroscopy: A Guide for Chemists*.
 Oxford: Oxford University Press, 1987.
 Spiess, H. W., *Adv. Polym. Sci.* **66**, 23 (1985).
 Wuthrich, K., *NMR of Protein and Nucleic Acids* New York: Wiley, 1986.
 Wuthrich, K., et al., *Nature* **418**, 207 (2002).

PROBLEMS

- 19.1** Polymer chain conformation can often be deduced from the coupling constant ΔJ , which is defined as

$$\Delta J = J_{AX} - J_{BX}$$

where J_{AX} and J_{BX} are vicinal ^1H - ^1H coupling constants, as shown in the diagram:



For a two-state conformational system (t , *trans*; g , *gauche*) we have the following equations to calculate:

$$J_{AX} = P_{t,j}(J_{AX,t} - J_{AX,g}) + J_{AX,g}$$

$$J_{BX} = P_{t,j}(\Delta J_t - \Delta J_g) + \Delta J_g$$

where

$$\Delta J_t = J_{AX,t} - J_{BX,t}$$

$$\Delta J_g = J_{AX,g} - J_{BX,g}$$

Assume that

$$J_{\text{vic}} = 4.22 - 0.5 \cos \phi + 4.5 \cos^2 \phi \quad (0 \leq \phi \leq 180^\circ)$$

Show that $\Delta J = 2\Delta J_t(2P_{t,j} - 1)$ and calculate ΔJ for isotactic poly(methyl acrylate). (Source: Lyerla (1980).)

- 19.2** The Fourier pair relationship between the time (t) and frequency (ω) is expressed in the form

$$F(\omega) = \int_{-\infty}^{\infty} f(t)e^{-i\omega t} dt$$

The shape of a spectral line $J(\omega)$, which is essentially the time dependence of the oscillations responsible for absorption, is the real part of the integral:

$$J(\omega) \sim \int_0^{\infty} f(t)e^{i\omega t} dt$$

Let $f(t)$ be the oscillating, decaying function:

$$f(t) = \cos \omega_0 t e^{-t/\tau}$$

where τ is the time constant for the decay. Plot the line shape for different values of τ . (*Source*: Atkins (1986).

- 19.3** The pulsed field gradient NMR method can be used to determine the diffusion coefficients D for protein by

$$\ln R = -\gamma^2 \delta G^2 \left(\Delta - \frac{\delta}{3} \right) D$$

where R is the ratio of the amplitude of the spin echo in the presence of the gradient pulses to the amplitude in the absence of the gradient pulses, γ is the gyromagnetic ratio of the proton nuclei, and G is the amplitude of the field gradient pulse (G/cm). Experimental data were obtained for hemoglobin in buffer at 25°C as follows:

R	G^2
1.31	0.775
1.29	0.866
1.28	0.938
1.26	1.00
1.24	1.14

Experimental parameters are $\delta = 1.75$ m/s, $\Delta = 8.10$ m/s, $\tau = 6.0$ m/s.

- (a) Plot $\ln R$ versus G^2 .
 (b) Determine the translation diffusion coefficient D for the protein.
 (*Source*: Everhart and Johnson (1982).

20

X-RAY CRYSTALLOGRAPHY

20.1 X-RAY DIFFRACTION

X-rays are produced by bombarding a metal with high-energy electrons. They can be diffracted when passed through a crystal (first suggested by von Laue in 1912). X-ray diffraction depends on the range of the incident beam, as shown in Figure 20.1. This observation was described in the Bragg equation, in the form

$$n\lambda = 2d \sin \theta \quad (20.1)$$

where λ is the wavelength of the incident x-ray (in the range between 0.001 and 50 Å), d is the interplanar spacing of the crystal, and $n (= 1, 2, \dots)$ is an integer and is associated with a given interference fringe of a diffraction pattern. If $n = 1$, there is a path difference of one wavelength. If $n = n$, there is a path difference of n wavelengths.

Analysis of x-ray diffraction gives numerical values of two important parameters: the interplanar spacing and the intensity of diffraction. Interplanar spacing is characteristic of the pattern of the crystal from which one learns the packing of the repeating units, while the intensities of a certain number of diffractions can provide information on the structure of a crystal.

For the past several decades x-ray studies have provided a genuine elegance to macromolecular chemistry. Investigators have relied much on x-ray crystallography

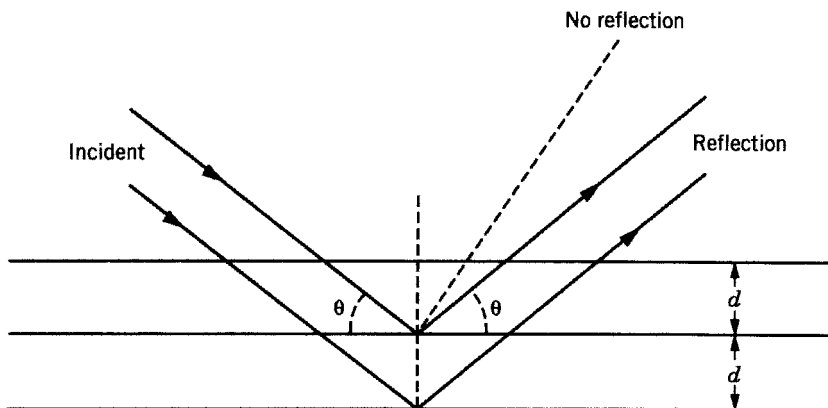


FIGURE 20.1 X-ray diffraction.

to develop a sense of how synthetic and biological polymers are shaped. Since the molecule under study must be crystallized, we begin our description with crystals. The structure of a crystal is the symmetrical arrangement of one or more species of atoms in three directions at certain angles, including right angles. A modern x-ray analysis of a crystal involves the determination of the quantity $F(hkl)$, which is a measure of the intensity of the x-beam, for each order (hkl) , scattered by the whole unit of a pattern. The final result is the detailed information about the geometry of a macromolecule, including the specific places where the atoms or the groups of atoms (e.g., amino acids in protein) are packed.

20.2 CRYSTALS

A crystal consists of periodic repetitions of some molecular arrangement, known as a “unit cell,” throughout space. The array of points that constitutes the regular arrangement is represented by lattices.

20.2.1 Miller Indices, hkl

Consider two-dimensional lattices (the array of points in Figure 20.2). The four lattices in two dimensions can be represented by four sets of numbers (x, y) :

$$(1, 1) \quad (-1, 1) \quad (3, 2) \quad (\infty, 1)$$

For three dimensions we just add another number to each set (x, y, z) . If the plane cuts through the z axis, as in Figure 20.3 (or parallel to z), that is, if z intercepts at ∞ , then we have four sets of trios:

$$(1, 1, \infty) \quad (-1, 1, \infty) \quad (3, 2, \infty) \quad (\infty, 1, \infty)$$

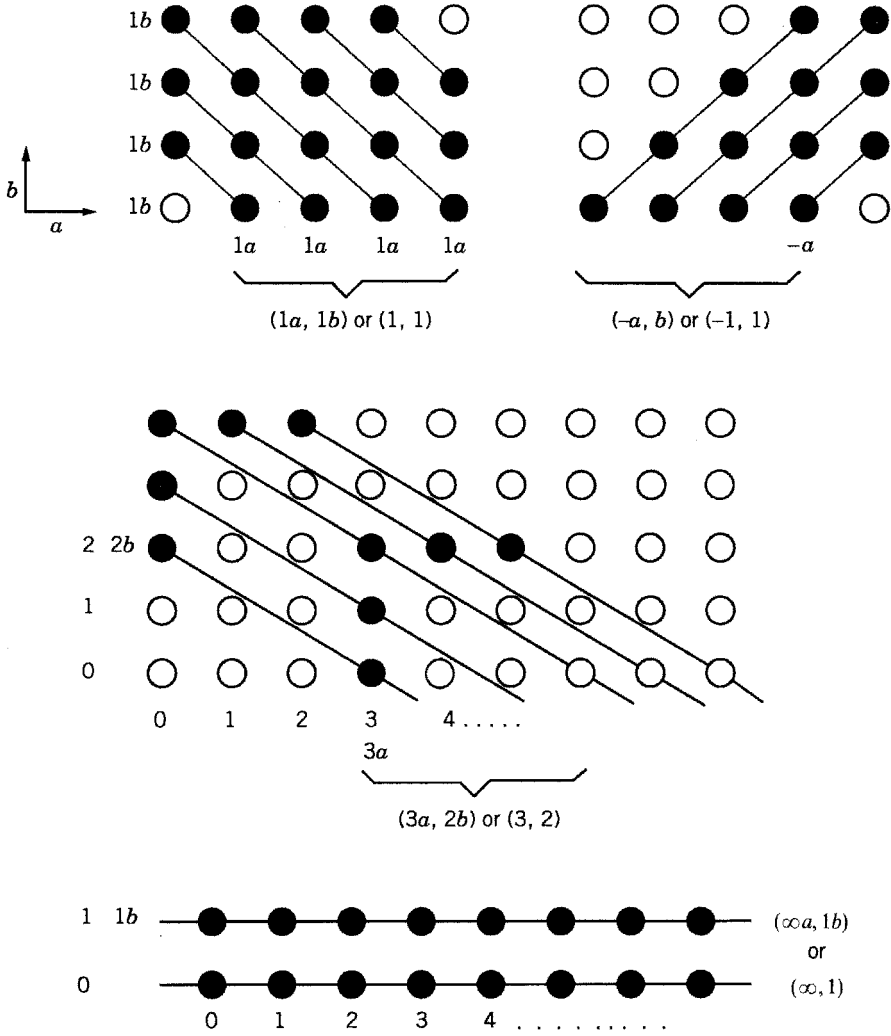


FIGURE 20.2 Space lattices.

These trios are expressed in what is known as the Weiss system. Miller indices are formed by taking two additional steps. First, the reciprocal of the three numbers in parentheses is taken:

$$\left(\frac{1}{1}, \frac{1}{1}, \frac{1}{\infty}\right) \quad \left(\frac{1}{-1}, \frac{1}{1}, \frac{1}{\infty}\right) \quad \left(\frac{1}{3}, \frac{1}{2}, \frac{1}{\infty}\right) \quad \left(\frac{1}{\infty}, \frac{1}{1}, \frac{1}{\infty}\right)$$

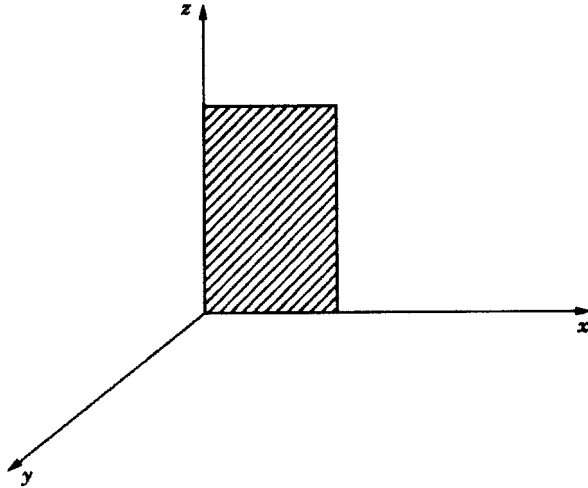


FIGURE 20.3 Representative plane cutting through the z axis.

Second, the denominator is removed by multiplying each numbers with the least common factor so that the trios are made of integers:

$$(1, 1, 0) \quad (\bar{1}, 1, 0) \quad (2, 3, 0) \quad (0, 1, 0)$$

The integers in each trio are called Miller indices and are expressed in terms of (hkl) .

Figure 20.4 illustrates four of the simplest planes expressed in terms of Miller indices hkl . Planes with indices, for example, (200) in dash lines have half the

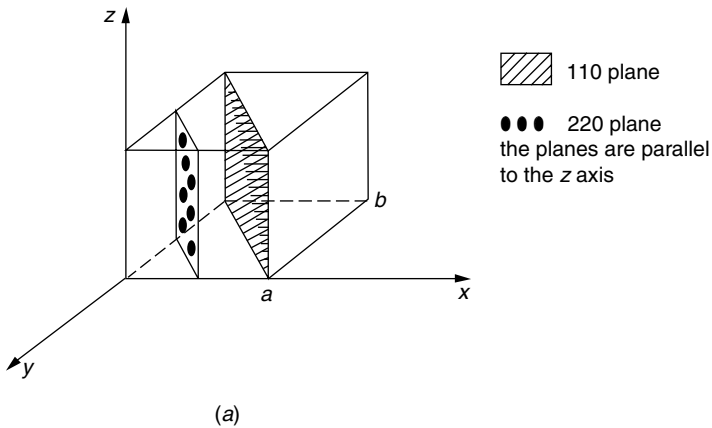


FIGURE 20.4 Four representative planes and Miller indices: hatchmark, 110 plane; circles, 220 plane. The planes are parallel to (a) z axis; (b) y and z axes; (c) x and z axes; (d) x and y axes.

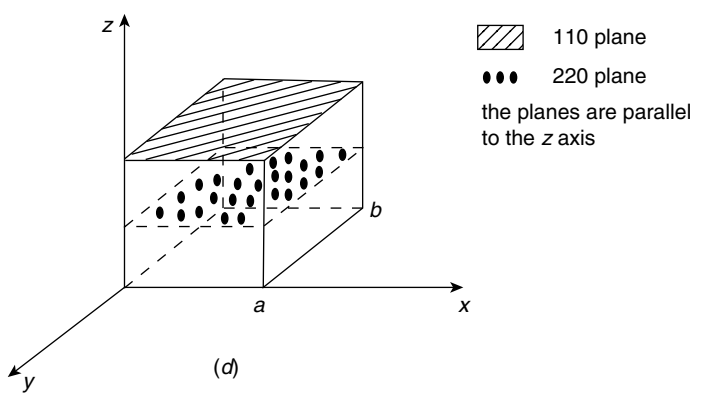
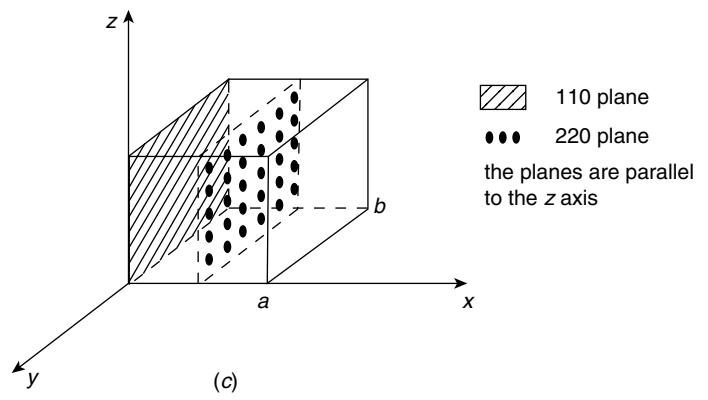
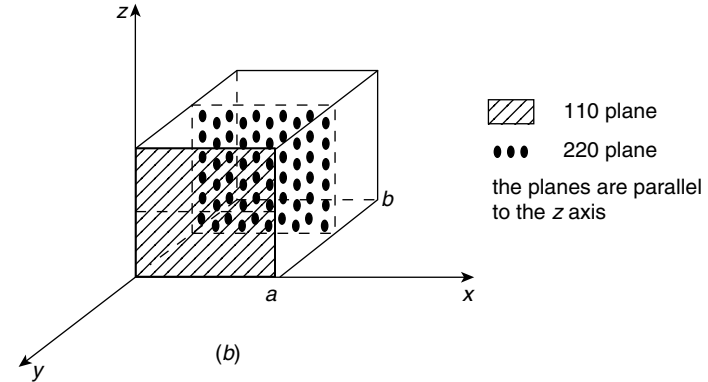


FIGURE 20.4 (Continued)

spacing of planes with indices (100). A very important property of crystals is that for each crystal face there exists three integers h , k , and l such that

$$hx + ky + lz = \text{const} \quad (20.2)$$

20.2.2 Unit Cells or Crystal Systems

The unit cell is the repeating unit in a crystal system. The coordinate system used to describe the unit cell is x , y , and z . The unit of each coordinate is a , b , and c , respectively (Figure 20.5). However, x , y , and z do not have to be Cartesian, that is, α , β , and γ could be any angle, and not necessarily $\pi/2$ (Figure 20.6). For the coordinates x , y , and z and the angles α , β , and γ there are seven different kinds of unit cells, referred to as crystal systems:

Name	Crystal System		Symbols	Symmetry
	Axes	Angles		
Triclinic	$a \neq b \neq c$	$\alpha \neq \beta \neq \gamma$	P	$\bar{1}$
Monoclinic	$a \neq b \neq c$	$\alpha = \gamma = 90^\circ \neq \beta$	PC	$2/m$
Orthorhombic	$a \neq b \neq c$	$\alpha = \beta = \gamma = 90^\circ$	$PIFC$	mmm
Tetragonal	$a = b \neq c$	$\alpha = \beta = \gamma = 90^\circ$	PI	$4/mmm$
Trigonal	$a = b = c$	$\alpha = \beta = \gamma \neq 90^\circ$	R^b	$\bar{3}m$
Hexagonal	$a = b \neq c$	$\alpha = \beta = 90^\circ, \gamma = 120^\circ$	P	$6/mmm$
Cubic	$a = b = c$	$\alpha = \beta = \gamma = 90^\circ$	PIF	$m\bar{3}m$

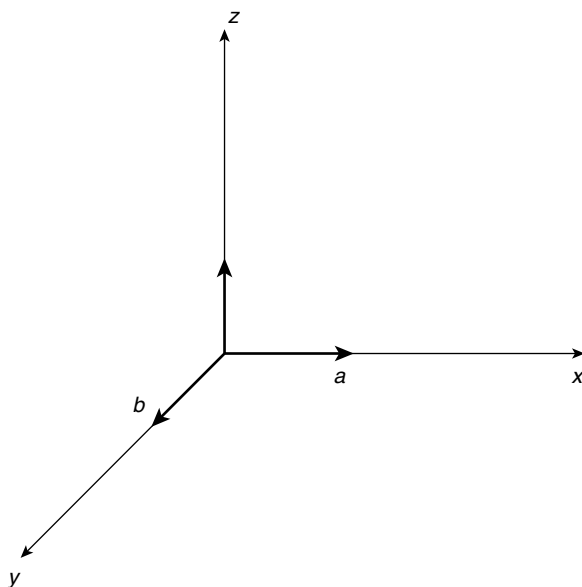


FIGURE 20.5 Crystal coordinates.

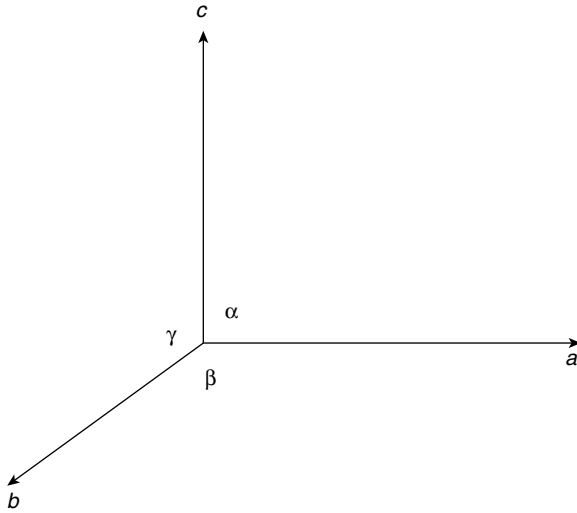


FIGURE 20.6 Crystal angles.

The columns Symbol and Symmetry will be explained in later sections. Trigonal is the same as rhombohedral.

20.2.3 Crystal Drawing

Crystal drawing can be carried out by using the following diagram (Figure 20.7a). Examples of the conventional orientation of crystallographic axes are illustrated with an octahedron and a cube (Figure 20.7b).

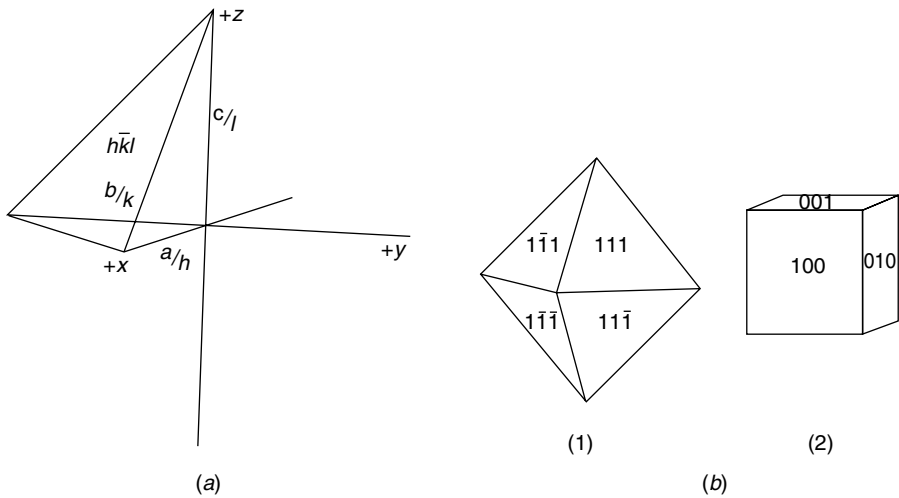


FIGURE 20.7 (a) Example of conventional orientation of crystallographic axes. (b) 1, Octahedron with front faces indexed; 2, cube with front faces indexed.

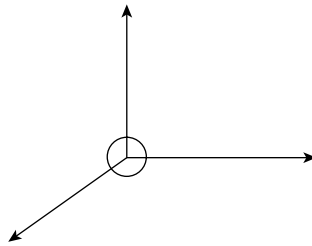
20.3 SYMMETRY IN CRYSTALS

Crystals are characterized by a certain regularity of arrangements called symmetry. There are three kinds of symmetry:

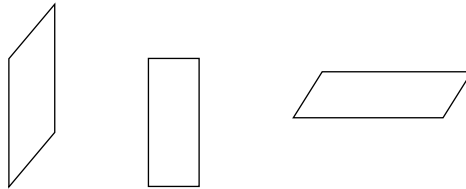
1. Center of symmetry—every face has a similar face parallel to it.
2. Plane of symmetry—the crystal is divided into two equal portions, and these two portions are mirror images of each other with respect to the plane.
3. Axis of symmetry—a line such that after rotation about it through $360^\circ/n$ the crystal assumes a congruent position; the value of n determines the degree of the axis.

Figure 20.8 illustrates the three types of symmetry:

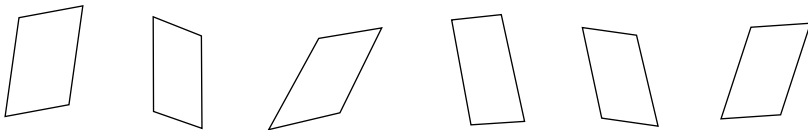
(a) Symmetry center:



(b) Symmetry planes—three planes of symmetry parallel to the faces of a cube:



The six diagonal planes of symmetry in a cube are



(c) Axis of symmetry—line that after rotation about it though $360^\circ/n$ the crystal assumes a congruent position, where $n = 1, 2, 3, 4, 6$.






$n = 1$, an identity axis, through 360° , symbol	
$n = 2$, a diad axis, through 180° , symbol	
$n = 3$, a triad axis, through 120° , symbol	
$n = 4$, a tetrad axis through 90° , symbol	
$n = 6$, a hexad axis, through 60° , symbol	

FIGURE 20.8 Three types of symmetry.

20.3.1 Bravais Lattices

In 1849 Bravais showed that there are only 14 ways to arrange identical points in space such that each point has the same number of neighbors at the same distances and in the same directions. They represent combinations of the seven crystal systems.

The 14 Bravais Lattices are

1. simple (or primitive) cubic,
2. body-centered cubic,
3. face-centered cubic,
4. simple tetragonal,
5. body-centered tetragonal,
6. hexagonal,
7. trigonal,
8. simple orthorhombic,
9. end-centered orthorhombic,
10. body-centered orthorhombic,
11. face-centered orthorhombic,
12. simple monoclinic,
13. end-centered monoclinic, and
14. triclinic.

These 14 lattices are shown in Figure 20.9. In addition, if a unit cell contains only one repeating unit, it is said to be primitive; if a unit cell contains more than one repeating unit, it is said to be centered.

Figure 20.10 shows the four orthorhombic lattice centering types, P , C , F , and I . (Rhombohedral and hexagonal lattices are indicated by the letter R .)

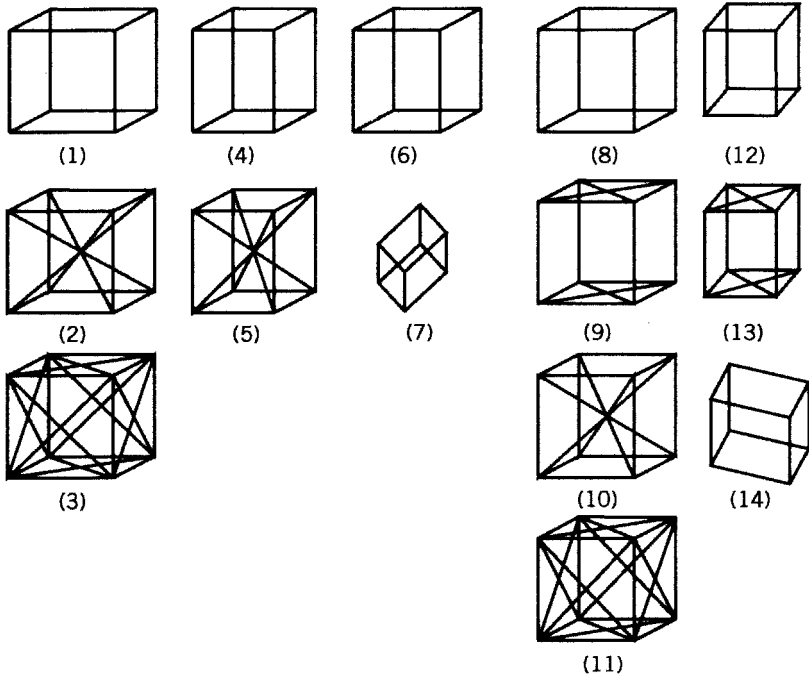


FIGURE 20.9 The 14 Bravais lattices.

20.3.2 Point Group and Space Group

In crystallography, crystals are classified by their lattice symmetry rather than by their shape.

A collection or set of elements that are related to each other is called a group. When symmetry operations are applied about a single point, the result is a point group. When symmetry operations are applied to points arranged periodically on a crystal lattice, the result is a space group.

On this (lattice symmetry) basis, all crystals can be classified into 14 Bravais lattices, 32 unique crystallographic point groups and 230 unique crystallographic space groups.

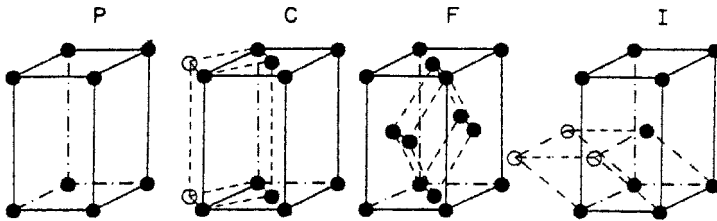


FIGURE 20.10 Orthorhombic Bravais lattices: *P*, primitive; *C*, basis centered; *F*, face centered; *I*, body centered.

20.3.2.1 Point Groups The 32 point groups are built upon four symmetry operators. These operators, which are also called four elements, are as follows:

1. Inversion centers: symbols i .
2. Rotation axis: symbols 1 (identity), 2 (twofold rotation), 3 (threefold rotation), up to 6 (sixfold rotation).
3. Mirror planes: symbols m .
4. Rotation–inversion axes (combination of rotation and inversion) symbols $\bar{1}$ (a simple center of conversion), $\bar{2}$ (a 180° rotation followed by an inversion, $\bar{2} = m$), $\bar{3}$ ($= 3 \cdot \bar{1}$), $\bar{6}$ ($= 3 \cdot m$).

Using the general symbol X to denote a principal axis of any degree, we may have the following combinations:

X	Rotation axis alone: 1, 2, 3, 4, 6
\bar{X}	Inversion axis alone: $\bar{1}$, $\bar{2}$, $\bar{3}$, $\bar{4}$, $\bar{6}$
X/m	Rotation axis <i>normal</i> to a plane of symmetry: $1/m$, $2/m$, $3/m$, $4/m$, $6/m$
Xm	Rotation axis with a <i>vertical</i> plane of symmetry: $1m$, $2m$, $3m$, $4m$, $6m$
$\bar{X}m$	Inversion axis with a <i>vertical</i> plane of symmetry: $\bar{1}m$, $\bar{2}m$, $\bar{3}m$, $\bar{4}m$, $\bar{6}m$
$X2$	Rotation axis with a diad axis normal to it: 12, 22, 32, 42, 62
X/mm	Rotation axis with both kinds of plane of symmetry

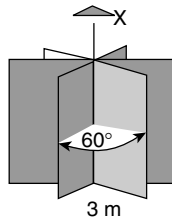
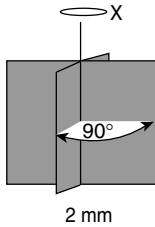
There are no fivefold and sevenfold axes, for 72° ($360^\circ/5 = 72^\circ$) and 51.4° ($360^\circ/7 = 51.4^\circ$) are not symmetric in a circle.

Figure 20.11 summarizes the 32 point groups in graphic portraits.

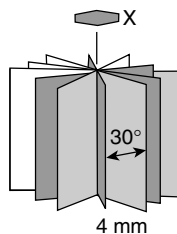
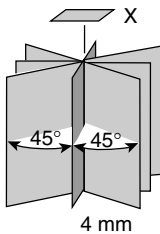
The rules are as follows:

1. Adding m means adding a vertical plane.

- 1 $m = m = \bar{2}$
- 2 $m = 2mm$
- 3 m



- 4 $m = 4mm$
- 6 $m(m)$



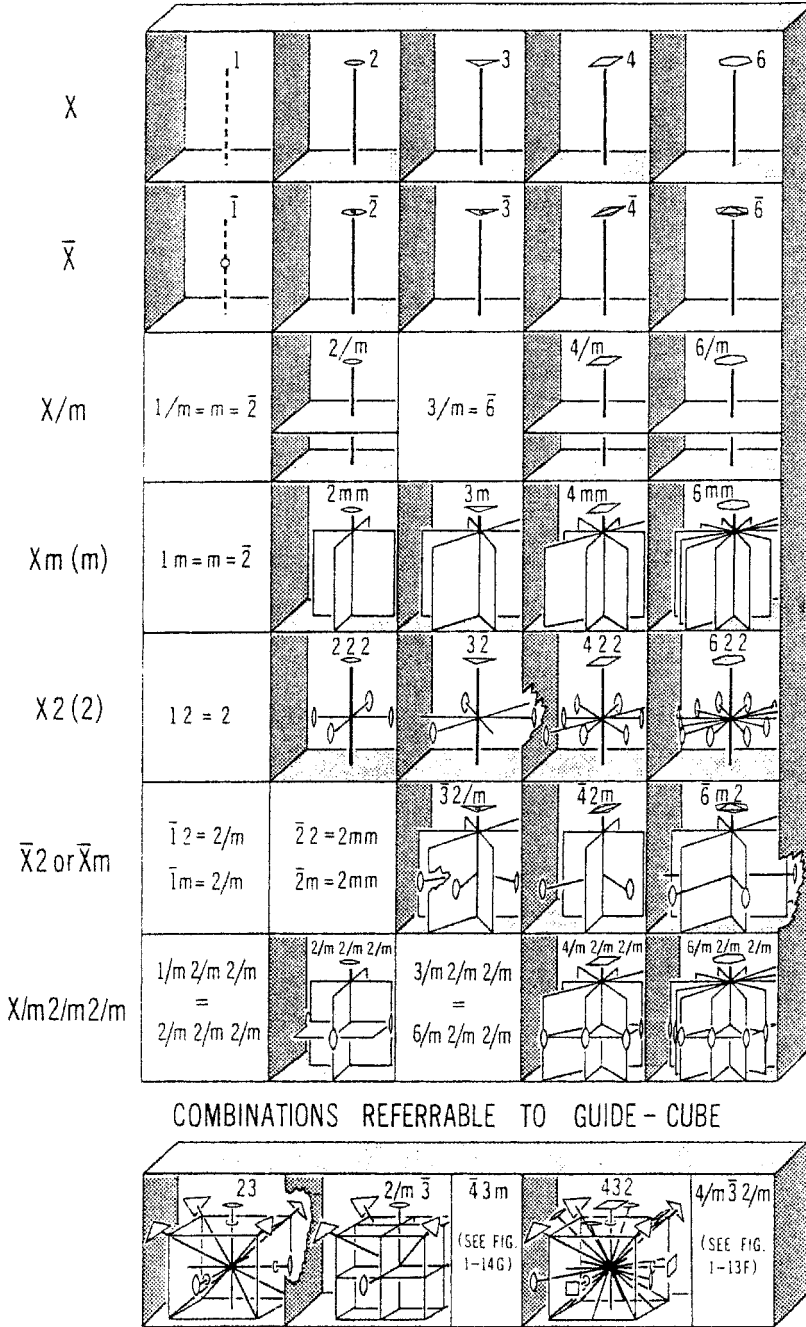
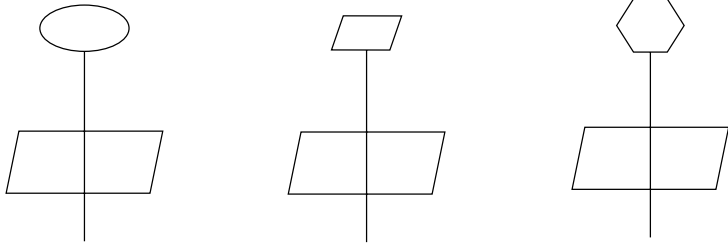


FIGURE 20.11 Graphic portrayal of the geometric relationships between the symmetry elements [Source: Bloss Crystallography and Crystal Chemistry, New York: Holt, Rinehart and Winston, Inc. 1971].

2. Adding $/m$ means adding a horizontal plane:

$1/m = m = \bar{2}$
 $2/m$
 $4/m$
 $6/m$



There is another way to describe the 32 point groups called stereograms. These are related to the two principal axes, X and \bar{X} . Figure 20.12 shows the operation of rotation X (1, 2, 3, 4, 6) and rotoinversion \bar{X} ($\bar{1}$, $\bar{2}$, $\bar{3}$, $\bar{4}$, $\bar{6}$) of the axes. The unfilled circles represent auxiliary points which are not occupied. For each operation, there is an abbreviation in the form of circles and dots (solid or open). These abbreviations constitute the whole stereogram.

Figure 20.13 gives the stereogram of the 32 point groups.

20.3.2.2 Interpretation of Stereogram Figure 20.13 provides an elegant way to summarize some historical discoveries:

(a) Rows 1 and 6 are geometric enantiomorphisms. These classes are

Triclinic	1
Monoclinic	2
Orthorhombic	222
Trigonal	3, 32
Tetragonal	4, 42
Hexagonal	6, 62
Cubic	23, 43

These classes of symmetry show optical activity.

(b) There are 21 classes without a center of symmetry:

Triclinic	1
Monoclinic	2, m
Orthorhombic	mm , 222
Trigonal	3, $3m$, 32
Tetragonal	4, $\bar{4}$, $4mm$, $\bar{4}2m$, 42
Hexagonal	6, $\bar{6}$, $6mm$, $\bar{6}m2$, 62
Cubic	23, $\bar{4}3m$, 43

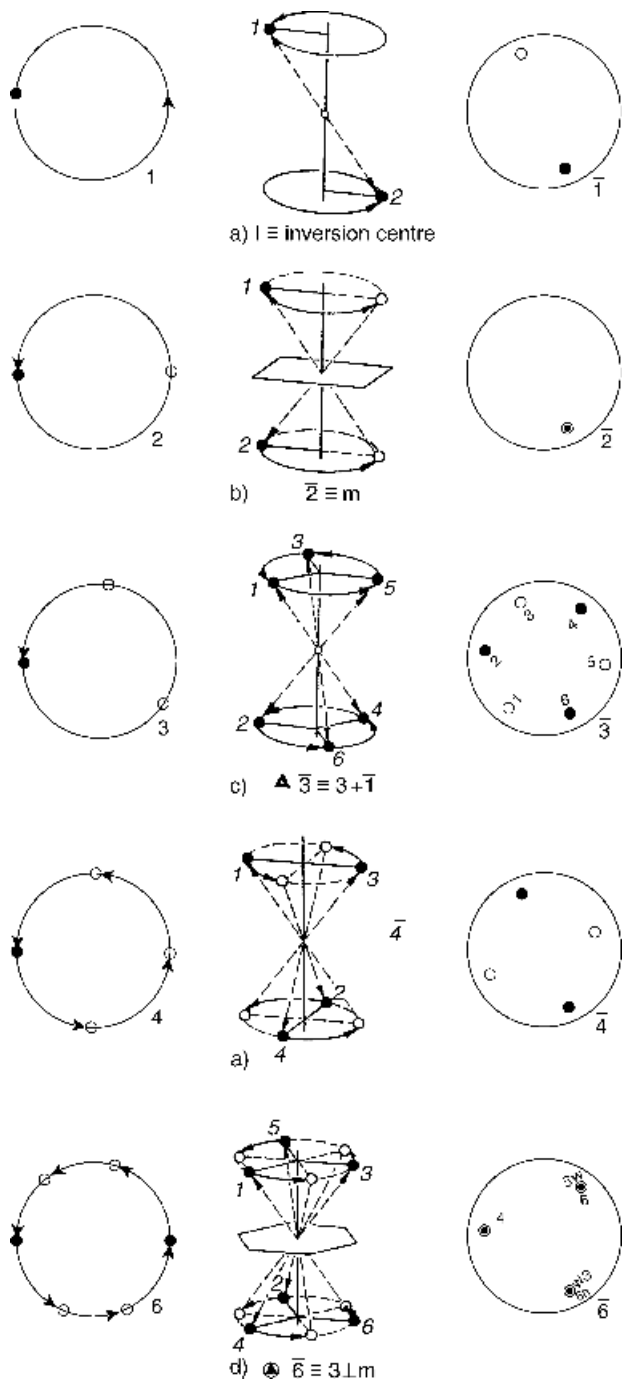


FIGURE 20.12 Operation of rotation X and rotoinversion \bar{X} .

TRICLINIC	MONOCLINIC AND ORTHORHOMBIC	TRIGONAL	TETRAGONAL	HEXAGONAL	CUBIC
 1	 2	 3	 4	 6	 23
 $\bar{1}$	 m ($\bar{2}$)	 $\bar{3}$	 4	 $\bar{6}$	$\bar{2}3 = 2/m3$
$1/m = \bar{2}$	 $2/m$	$3/m = \bar{6}$	 $4/m$	 $6/m$	$m3$ ($2/m3$)
$1m = \bar{2}$	 mm ($2m$)	 $3m$	 $4mm$	 $6mm$	$2m3 = 2/m3$
$\bar{1}m = 2/m$	$\bar{2}m = 2m$	 $\bar{3}m$	 $\bar{4}2m$	 $\bar{6}m2$	 $\bar{4}3m$
$12 = 2$	 222	 32	 42	 62	 43 (432)
$1/m\bar{m} = 2m$	 mmm ($2/m\bar{m}$)	$3/m\bar{m} = \bar{6}m$	 $4/m\bar{m}m$	 $6/m\bar{m}m$	 $m3m$ ($4/m\bar{3}m$)

FIGURE 20.13 The 32 point groups. [Source: Phillips (1971). Reproduced by permission of John Wiley & Sons.]

They show the properties of piezoelectricity and pyroelectricity. Piezoelectricity refers to the separation of electric charges on the surface of the crystal upon mechanical stress, Pyroelectricity is the recovery of electric charges when the crystal is heated or cooled.

(c) *Diffraction pattern*—The 32 classes of symmetry give only 11 different groups distinguishable by means of photographs (due to Laue):

Triclinic	1 and $\bar{1}$ indistinguishable
Monoclinic	2, m and $2/m$ indistinguishable
Orthorhombic	mm , 222 , mmm indistinguishable
Trigonal	3, $\bar{3}$ show trigonal symmetry $3m$, $\bar{3}m$, 32 show ditrigonal symmetry
Tetragonal	4, $\bar{4}$, $4/m$ show tetragonal symmetry $4mm$, $\bar{4}2m$, 42 , $4/mmm$ show ditetragonal symmetry
Hexagonal	6, $\bar{6}$, $6/m$ show hexagonal symmetry $6mm$, $\bar{6}m2$, 62 , $6/mmm$ show dihexagonal symmetry
Cubic	23 , $m\bar{3}$ show a twofold principal axis $\bar{4}3m$, 432 , $m\bar{3}m$ show a fourfold principal axis

20.3.2.3 Space Groups Space groups consist of a symmetry operation of the point group and, in addition, a translation. One set of units of translation in a crystal structure is the three coordinates (a , b , c), which are the unit cell dimensions. Another set is the fractions of these translations, for example, $1/4 a$, $3/4 a$, . . . , $1/4 b$, . . . , $6/1 a$. The translation is the result of a screw operation and a glide operation.

Screw Operation Screw axes are designated as n -fold rotation axes with the fraction of the unit-cell translation by the subscript g : n_g , where n refers to n -fold rotation and g refers to the fraction of unit translation. For example, a fourfold screw axis has a rotation of 90° (i.e., $360/4 = 90$), and is denoted

- 4_1 if the translation is $1/4 a$,
- 4_2 if the translation is $2/4 a$, and
- 4_3 if the translation is $3/4 a$.

Note: 4_1 and 4_3 are enantiomorphic, related as left and right hands. Other examples are

- 2_1 A two-fold screw axis which causes a 180° rotation and a $1/2$ unit cell translation
- 3_1 , 3_2 where the subscript indicates the translation in unit-cell length, e.g., $1/3$, $2/3$ units.
- 6_1 , 6_2 , 6_3 , 6_5

Glide Operation A glide operation involves translation along the unit cell axes with $a/2$, $b/2$, and $c/2$ motion. They are labeled a , b , c , respectively. If

the translation is along a diagonal $1/2 (b + c)$, $1/2 (c + a)$, or $1/2 (a + b)$, the glide plane is denoted n . And if the translation is $1/4 (b \pm c)$, $1/4 (c \pm a)$, or $1/4 (a + b)$, the glide plane is denoted d .

A space group is defined as a set of transformations (symmetry elements) that leave a three-dimensionally periodic, discrete set of labeled points (atoms or molecules) unchanged. The 14 Bravais lattices are combined with the 32 crystallographic point groups plus additional symmetry elements with translational components to give the 230 space groups. It was originally formulated by Lionhard Sohncke in 1879. Table 20.1 gives the 230 space groups.

TABLE 20.1 Space Groups

Point Groups		Space Groups					
<i>Triclinic</i>							
1	$P1$						
$\bar{1}$	$P\bar{1}$						
<i>Monoclinic</i>							
2	$P2$	$P2_1$	$C2$				
m	Pm	Pc	Cm	Cc			
$2/m$	$P2/m$	$P2_1/m$	$C2/m$	$P2/c$	$P2_1/c$	$C2/c$	
<i>Orthorhombic</i>							
222	$P222$	$P222_1$	$P2_12_12$	$P2_12_12_1$	$C222_1$	$C222$	$F222$
	1222	$12_12_12_1$					
$mm2$	$Pmm2$	$Pmc2_1$	$Pcc2$	$Pma2$	$Pca2_1$	$Pnc2$	$Pmn2_1$
	$Pba2$	$Pna2_1$	$Pnn2$	$Cmm2$	$Cmc2_1$	$Ccc2$	$Amm2$
	$Abm2$	$Ama2$	$Aba2$	$Fmm2$	$Fdd2$	$Imm2$	$Iba2$
	$Ima2$						
mmm	$Pmmm$	$Pnmm$	$Pccm$	$Pbam$	$Pmma$	$Pnna$	$Pmna$
	$Pcca$	$Pbam$	$Pccn$	$Pbcm$	$Pnmm$	$Pmmm$	$Pbcn$
	$Pbca$	$Pnma$	$Cmcm$	$Cmca$	$Cmmm$	$Cccm$	$Cmma$
	$Ccca$	$Fmmm$	$Fddd$	$Immm$	$Ibam$	$Ibca$	$Imma$
<i>Tetragonal</i>							
4	$P4$	$P4_1$	$P4_2$	$P4_3$	$I4$	$I4_1$	
$\bar{4}$	$P\bar{4}$	$I\bar{4}$					
$4/m$	$P4/m$	$P4_2/m$	$P4/n$	$P4_2/n$	$I4/m$	$I4_1/a$	
422	$P422$	$P4_22$	$P4_122$	$P4_12_12$	$P4_222$	$P4_24_12$	$P4_322$
	$P4_32_12$	$I422$	$I4_122$				
$4mm$	$P4mm$	$P4bm$	$P4_2cm$	$P4_2nm$	$P4cc$	$P4nc$	
	$P4_2bc$	$I4mm$	$I4cm$	$I4_1md$	$I4_1cd$		
$\bar{4}2m$	$P\bar{4}2m$	$P\bar{4}2c$	$P\bar{4}2_1m$	$P\bar{4}2_1c$	$P\bar{4}m2$	$P\bar{4}c2$	$P\bar{4}b2$
	$P\bar{4}n2$	$I\bar{4}m2$	$I\bar{4}c2$	$I\bar{4}2m$	$I\bar{4}2d$		
$4/mmm$	$P4/mmm$	$P4/mcc$	$P4/nbm$	$P4/nnc$	$P4/mbm$	$P4/mnc$	$P4/nmm$
	$P4/ncc$	$p4_2/mmc$	$P4_2/mcm$	$P4_2/nbc$	$P4_2/nnm$	$P4_2/mbc$	$P4_2/mnm$
	$P4_2/nmc$	$P4_2/ncm$	$I4/mmm$	$I4/mcm$	$I4_1/amd$	$I4_1/acd$	

(Continued)

TABLE 20.1 (Continued)

Point Groups		Space Groups					
<i>Trigonal</i>							
3	$P3$	$P3_1$	$P3_2$	R_3			
$\bar{3}$	$P\bar{3}$	$R\bar{3}$					
32	$P312$	$P321$	$P3_112$	$P3_121$	$P3_212$	$P3_221$	$R32$
$3m$	$P3m1$	$P31m$	$P3c1$	$P31c$	$R3m$	$R3c$	
$\bar{3}m$	$P\bar{3}/m$	$P\bar{3}1c$	$P\bar{3}m1$	$P\bar{3}c1$	$R\bar{m}$	$R\bar{3}c$	
<i>Hexagonal</i>							
6	$P6$	$P6_1$	$P6_5$	$P6_2$	$P6_4$	$P6_3$	
$\bar{6}$	$P\bar{6}$						
$6/m$	$P6/m$	$P6_3/m$					
622	$P622$	$P6_122$	$P6_522$	$P6_222$	$P6_222$	$P6_322$	
$6mm$	$P6mm$	$P6mcc$	$P6_3cm$	$P6_3mc$			
$\bar{6}m2$	$P\bar{6}m2$	$P\bar{6}c2$	$P\bar{6}2m$	$P\bar{6}2c$			
$6/mmm$	$P6/mmm$	$P6/mcc$	$P6_3/mcm$	$P6_3/mmc$			
<i>Cubic</i>							
23	$P23$	$F23$	$I23$	$P2_13$	$I2_13$		
$m\bar{3}$	$Pm\bar{3}$	$Pn\bar{3}$	$Fm\bar{3}$	$Fd\bar{3}$	$Im\bar{3}$	$Pa\bar{3}$	$Ia\bar{3}$
432	$P432$	$P4_232$	$F432$	$F4_132$	$I432$	$P4_332$	$P4_132$
	$I4_132$						
$\bar{4}3m$	$P\bar{4}3m$	$F\bar{4}3m$	$I\bar{4}3m$	$P\bar{4}3n$	$F\bar{4}3c$	$I\bar{4}3d$	
$m\bar{3}m$	$Pm\bar{3}m$	$Pn\bar{3}n$	$Pm\bar{3}n$	$Pn\bar{3}m$	$Fm\bar{3}m$	$Fm\bar{3}c$	$Fd\bar{3}m$
	$Fd\bar{3}c$	$Im\bar{3}m$	$Ia\bar{3}d$				

Symbols: *P*, primitive; *C*, end centered; *F*, face centered; *I*, body centered; *R*, primitive in rhombohedral axes; *a*, *b*, *c*, glide planes; *n*, number of rotation axes. For symmetry elements (e.g., $1,2/m$), see Figure 20.13.

Source: *International Tables for X-ray Crystallography*, Vol. 1, *Symmetry Groups*, Section 4.3, "The 230 Three-Dimensional Space Groups: Equivalent Positions, Symmetry and Possible Reflection." Rearranged in the form of Table 20.2 (in this book), which is taken from Wunderlich (1973). With permission from Dr. Wunderlich and Academic Press.

For illustrations, space groups can be read from Table 20.2 as follows:

$Im\bar{3}M$	Body-centered cubic
$Fd\bar{3}m$	Glide face-centered cubic
$P2_1/m$	Primitive monoclinic space lattice with twofold axis parallel to <i>b</i> axis and mirror plane <i>m</i> perpendicular to this axis

$Cmc2_1$	A c -centered orthorhombic lattice with mirror plane perpendicular to a axis, c glide plane perpendicular to b axis, and 2_1 screw axis parallel to c axis
$P2_12_12_1$	Primitive orthorhombic unit cell (P) with three mutually perpendicular noninteracting twofold screw axes 2_1 in unit cell
$P2_1/a$	Primitive monoclinic unit cell with twofold screw axis along unique axis b and glide plane perpendicular to this axis with translation of $a/2$

The term *asymmetric unit* is the unit on which the space group operations act to produce the entire crystal structure (an infinitely extending pattern). This is the simplest unit that can be selected. The contents of the asymmetric unit combined with the relationships between positions of atoms listed for the space group are needed to derive a picture of the entire atomic contents of the crystal.

20.4 FOURIER SYNTHESIS

Once we have determined the symmetry, the space group, and the unit-cell dimensions of the crystal, we can focus our attention on the intensities that describe the positions of the atoms. These calculations make use of the Fourier transforms as an essential techniques.

20.4.1 Atomic Scattering Factor

If we consider a volume element dV in which the electrons of an atom can be found, we find that a phase difference occurs between the wave scattered by the center of the atom and that scattered by the volume element. This effect is due to the interference of electrons. The atomic scattering factor, which represents the amplitude scattered by the electrons in the atom, is obtained by integrating over the volume elements:

$$f = \int \rho(\mathbf{r}) \exp\left[\frac{2\pi i}{\lambda}(\mathbf{s} - \mathbf{s}_0) \cdot \mathbf{r}\right] dV \quad (20.3)$$

where ρ is the density of electrons. The coordinates of the scattering are described in Figure 20.14. the vector $\mathbf{s} - \mathbf{s}_0$ is normal to the reflecting plane of the crystal.

20.4.2 Structure Factor

By carrying out a summation over all the atoms in a unit cell, we obtain the structure factor $F(hkl)$ of the crystal system:

$$F(hkl) = \sum_i f_i \exp\left[\frac{2\pi i}{\lambda}(\mathbf{s} - \mathbf{s}_0) \cdot \mathbf{r}_i\right]$$

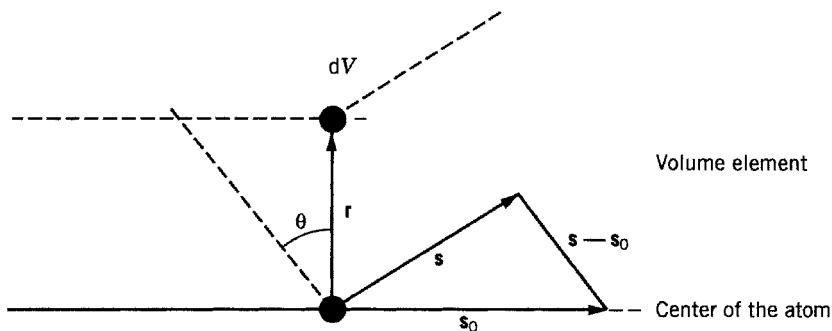


FIGURE 20.14 Coordinates of atomic scattering.

where f_i is the atomic scattering factor of the i th atom. The vector \mathbf{r} is now expressed in terms of the crystal coordinates:

$$\mathbf{r}_i = x_i\mathbf{a} + y_i\mathbf{b} + z_i\mathbf{c}$$

where a , b , and c are coordinates of the unit length and x , y , and z are the Cartesian coordinates at which the (hkl) planes intersect. On the basis of the Laue equations,

$$(\mathbf{s} - \mathbf{s}_0) \cdot \mathbf{a} = h\lambda \quad (\mathbf{s} - \mathbf{s}_0) \cdot \mathbf{b} = k\lambda \quad (\mathbf{s} - \mathbf{s}_0) \cdot \mathbf{c} = l\lambda$$

we can make the vector dot product into the form

$$\mathbf{r}_i \cdot (\mathbf{s} - \mathbf{s}_0) = \lambda(hx_i + ky_i + lz_i)$$

The structure factor now correlates to the Miller indices:

$$F(hkl) = \sum_i f_i \exp[2\pi i(hx_i + ky_i + lz_i)] = \sum_i f_i \exp(i\phi_i) \quad (20.4)$$

where

$$\phi_i = 2\pi(hx_i + ky_i + lz_i) \quad (20.5)$$

However, at this point we still have no knowledge of the phase difference ϕ_i , which we discuss in the next section.

20.4.3 Fourier Synthesis of Electron Density

The electron density $\rho(x, y, z)$ of the whole molecule, existing in the form of a crystal, is a periodic function in three dimensions. For this reason we can write the

density as a Fourier series in summation (not integral) form for the convenience of computer calculations:

$$\rho(x, y, z) = \frac{1}{V} \sum_h \sum_k \sum_l F(hkl) \exp[-2\pi i(hx + ky + lz)] \quad (20.6)$$

The quantities $(1/V)F(hkl)$ are the Fourier coefficients. Here V is the volume of the unit cell. The summation is extended over all diffraction maxima.

20.5 PHASE PROBLEM

If the values of the structure factor $F(hkl)$ were all known, we would calculate the values of ρ and thereby determine the locations of the atoms in a crystal. However, in an actual recorded diffraction pattern, only the intensities and, consequently, the amplitudes of the diffracted rays may be measured. We do not have specific information on the crystal's phase. Since all atoms are not at the same place, the scattering wave from one atom may be in phase or out of phase with that of its neighbor. A value of ϕ has to be assigned to each value of $F(hkl)$. This poses a thorny problem, which has been called the *phase problem*. At one time it was generally believed that crystal structures could not be determined from diffraction intensities alone. In this section we describe two ingenious and successful approaches to this problem.

20.5.1 Patterson Synthesis

In 1934, Patterson suggested that instead of using the structure factors themselves, $F(h, k, l)$, we may use the square modulus of the structure factors, $|F(h, k, l)|^2$, which are the intensities of the diffraction. Equation (20.6) is now modified to the form

$$P(u, v, w) = \frac{1}{V^2} \sum_h \sum_{-\infty}^{\infty} \sum_l |F(hkl)|^2 \exp[-i2\pi(hu + kv + lw)] \quad (20.7)$$

where (u, v, w) refer to all possible vectors between the atoms in the cell and not just those peaks (x, y, z) representing atomic position. The function $P(u, v, w)$ is called the Patterson function. The maxima of a Patterson function give the interatomic factor in a crystal structure.

In an x-ray diffraction experiment, if heavy atoms are introduced as part of the molecule, the scattering from these heavy atoms tends to dominate over the scattering from the light atoms. The summation in Patterson function may be taken only over the heavy-atom positions. The light atoms are considered to be arranged in the form of a random walk around the heavy atoms. Frequently, some light atoms

can be recognized in a diffraction pattern. As a result, a map can be constructed to elucidate the structure of a whole molecule.

20.5.2 Direct Method (Karle–Hauptmann Approach)

The direct method is a mathematical process in which different phase and amplitudes of the molecular transform are related to the contribution of individual atoms. This method is based on statistical procedures used to extract the phase information. The missing phase information is believed to be present in the statistical intensity distribution. One of the most well-known statistical proposals was offered by Karle and Hauptmann (1986). These authors assumed that the Fourier transform of the intensity represents the probability of finding interatomic distances in a molecule and that the transform is nonnegative.

The intensity data collected from an experiment can be transformed into normalized structure factor magnitudes by

$$|E_{\mathbf{h}}| = \frac{|F_{\mathbf{h}}|}{(\varepsilon \sum_{j=1}^N f_{j\mathbf{h}}^2)^{1/2}} \quad (20.8)$$

where $E_{\mathbf{h}}$ is the normalized structure factor and $F_{\mathbf{h}}$ is equivalent to $F(hkl)$. The vector \mathbf{h} (as well as \mathbf{k} and \mathbf{l}) has three integer components: h , k , l (the Miller indices). The symbol ε represents the statistical weighing factor, and the symbol $f_{j\mathbf{h}}$ represents the j th atomic scattering factor, as tabulated in the *International Tables for X-ray Crystallography*.

A formula may be derived for centrosymmetric crystals:

$$sE_{\mathbf{h}} \simeq s \sum_{\mathbf{k}_r} E_{\mathbf{k}} E_{\mathbf{h}-\mathbf{k}} \quad (20.9)$$

The symbol s means “sign of” and the vector \mathbf{k}_r gives the restriction that $|E_{\mathbf{k}}|$ and $|E_{\mathbf{h}-\mathbf{k}}|$ must have large values. If the sign is plus, then the phase is σ ; if the sign is minus, then the phase is π . These two values, σ and π , are the only values possible for centrosymmetric crystals.

Two formulas may also be derived for noncentrosymmetric crystals:

$$\phi_{\mathbf{h}} \cong \langle \phi_{\mathbf{k}} + \phi_{\mathbf{h}-\mathbf{k}} \rangle_{\mathbf{k}_r} \quad (20.10)$$

$$\tan \Phi_{\mathbf{h}} \cong \frac{\sum_{\mathbf{k}} |E_{\mathbf{k}} E_{\mathbf{h}-\mathbf{k}}| \sin(\phi_{\mathbf{k}} + \phi_{\mathbf{h}-\mathbf{k}})}{\sum_{\mathbf{k}} |E_{\mathbf{k}} E_{\mathbf{h}-\mathbf{k}}| \cos(\phi_{\mathbf{k}} + \phi_{\mathbf{h}-\mathbf{k}})} \quad (20.11)$$

The angle $\phi_{\mathbf{h}}$ is the phase associated with the structure factor $F_{\mathbf{h}}$. Equation (20.11) is called the tangent formula. For noncentrosymmetric crystals, certain phases are specified to establish an origin in the crystal. Certain symbols are also assigned for later evaluation, which is done by use of the theory of invariants and

semi-invariants. The procedure continues in a stepwise fashion until a sufficiently reliable set of phase values is built up to solve the structure problem.

20.6 REFINEMENT

The calculated structure factor, whether based on the Patterson synthesis or on the direct method, must be in agreement with the observed structure factor. The uncertainty involved in assigning the positional and thermal parameters in the calculation of the structure factor must be minimized so that the results will be close to the structure factor amplitudes $f_0(\mathbf{h})$ for each reflection \mathbf{h} observed. The minimization procedure is called the *refinement* and is based on Legendre's (1806) classical suggestion. If we have a set of unknown parameters x_1, x_2, \dots, x_n that are related to a set of m observable values O_1, O_2, \dots, O_m by

$$\begin{aligned} O_1 &= a_{11}x_1 + a_{12}x_2 + \cdots + a_{1n}x_n \\ &\vdots \\ O_m &= a_{m1}x_1 + a_{m2}x_2 + \cdots + a_{mn}x_n \end{aligned}$$

then the error E between the set of values x and the set of values O can be expressed by their differences:

$$\begin{aligned} E_1 &= a_{11}x_1 + a_{12}x_2 + \cdots + a_{1n}x_n - O_1 \\ &\vdots \\ E_m &= a_{m1}x_1 + a_{m2}x_2 + \cdots + a_{mn}x_n - O_m \end{aligned}$$

The best values of x are those for which $\sum_{i=1}^m E_i^2$ is at a minimum:

$$\frac{\partial \sum_{i=1}^m E_i^2}{\partial x_1} = \frac{\partial \sum_{i=1}^m E_i^2}{\partial x_2} = \cdots = \frac{\partial \sum_{i=1}^m E_i^2}{\partial x_n} = 0$$

We now have n equations for the n unknown (x 's) to solve. These x 's will give the least errors for our interpretation of the results. In a crystallographic problem, Legendre's procedure may be expressed in the equation

$$F_o(\mathbf{h}) - F_c(\mathbf{h}) = \sum_{j=1}^n \partial x_j \frac{\partial F_c}{\partial x_j}$$

where $F_o(\mathbf{h})$ is the observed factor and $F_c(\mathbf{h})$ is the calculated factor. The refinement is often expressed as a quantity R , called the reliability index:

$$R = \frac{\sum_h |F_o(\mathbf{h}) - F_c(\mathbf{h})|}{\sum_h F_o(\mathbf{h})}$$

Experimentally, modern crystallographic study of the structure of macromolecules may be summarized in three steps:

1. The growth of a single crystal of the macromolecule under study.
2. The preparation of isomorphous heavy-atom derivatives. If only one isomorphous derivative is prepared, the method is known as a single isomorphous replacement; if more than one derivative is prepared the method is known as multiple isomorphous replacement.
3. Data analysis, which includes calculating phases, determining electron density maps, and refinement.

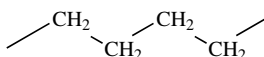
20.7 CRYSTAL STRUCTURE OF MACROMOLECULES

In this section we describe the classical presentation of the crystal structure of macromolecules. These include two synthetic polymers and two biological polymers. They provide us with insight toward the understanding of the three-dimensional structure of a compound.

20.7.1 Synthetic Polymers

Not all polymer chains can be crystallized; only those with stereoregularity can. For example, polyethylene can be crystallized because there is a regular configuration inherent in the monomer. Polypropylene, on the other hand, can be crystallized only under certain conditions. The crystal structures of these two polymers are also quite different. The former is packed in a zigzag form, whereas the latter has helical content (not, of course, 100%). We select these two polymers to illustrate the crystal structure, if any, of synthetic polymers.

Polyethylene The C atoms form a plane of zigzag chain:



The distance between the two carbons C—C is 1.52 Å; the angle —CH₂— is 114°. The unit cell is orthorhombic, with $a = 7.40$ Å, $b = 4.93$ Å, and $c = 2.53$ Å. Taking its position from the c axis, the structure is illustrated in Figure 20.15. The motif, CH₂, has the point symmetry $mm2$. The chain axis (c coordinate) is a 2_1 screw axis. The space group is $Pnam$, that is, the unit cell is primitive with an n glide plane perpendicular to the a axis, an a glide plane perpendicular to the b axis, and a mirror plane perpendicular to the c axis. The four carbon atoms are at positions $x, -y, \frac{1}{4}; -x, y, \frac{3}{4}; -x + \frac{1}{2}, -y + \frac{1}{2}, \frac{3}{4}; x + \frac{1}{2}, y + \frac{1}{2}, \frac{1}{4}$, where $x = 0.038a$ and

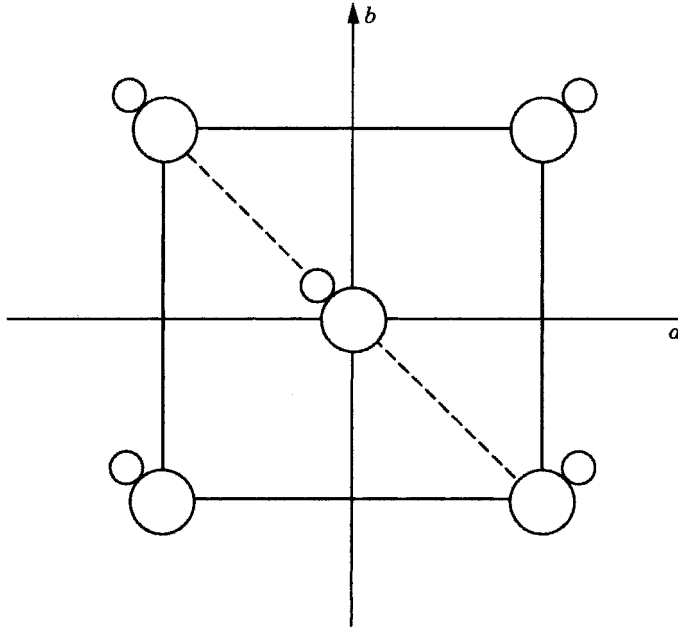


FIGURE 20.15 Structure of polyethylene.

$y = 0.065b$. The helix of polyethylene is represented by the symbol $1 \times 3/1$. The first number, 1, signifies the class of the chain, the 3 signifies the number of motifs, and the last 1 signifies the number of turns. Thus, polyethylene has three CH_2 groups per turn. The width of the Bragg reflections shows polyethylene “crystallites” to be only 100–300 Å in size; hence the polymer is not completely crystallized. A chain contains crystallites as well as an amorphous part.

Polypropylene Unlike polyethylene, which has only one configuration, polypropylene has three configurations: atactic, isotactic, and syndiotactic. We describe syndiotactic and isotactic polypropylene here because their configurations have been studied extensively in crystallography. Syndiotactic polypropylene has an orthorhombic unit cell with $a = 14.50$ Å, $b = 5.60$ Å, and $c = 7.40$ Å. Its space group is $C222_1$. The projection of the unit cell on the 001 plane is shown in Figure 20.16. There are eight monoclinic lattices in the unit cell. The chain has the linear repetition group $S(2/1)2$ symmetry. The model of the chain is in the form shown in Figure 20.17. The chain requires three repeating units for one turn and so it is a $2 \times 3/1$ helix. The isotactic polypropylene has an end-centered monoclinic unit cell with $a = 6.66$ Å, $b = 20.78$ Å, $c = 6.49$ Å, and the angle $\beta = 99.62^\circ$. There are 12 units in the cell. The chain has a $4 \times 2/1$ helix. Figure 20.18 compares the helical structure of isotactic polypropylene with that of syndiotactic polypropylene.

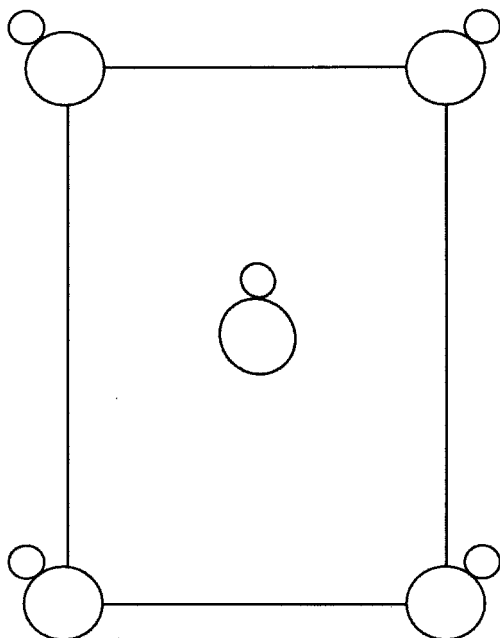


FIGURE 20.16 Projection of the unit cell on the 001 plane of polypropylene.

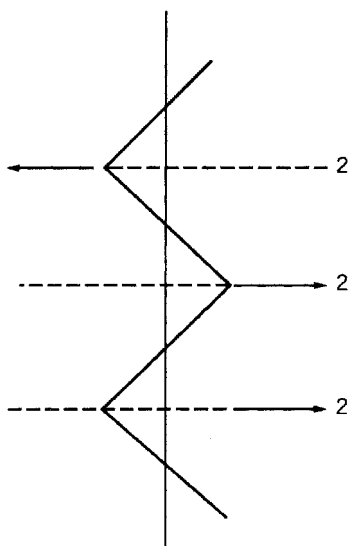


FIGURE 20.17 Linear repetition group $S(2/1)2$ symmetry.

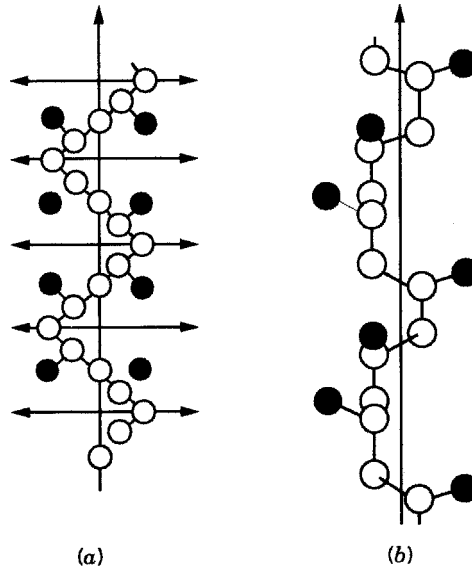


FIGURE 20.18 Helices of polypropylene: (a) syndiotactic; (b) isotactic. [Source: Adapted from Natta et al. (1960) and Wunderlich (1973). With permission from Dr. Wunderlich and Academic Press.]

20.7.2 Proteins

Among the landmarks in the elucidation of crystal structure is the crystallography work on myoglobin. Since 1961, most of the well-known globular proteins, such as ribonuclease, insulin, hemoglobin, lysozyme, β -lactoglobulin, chymotrypsinogen, and carboxypeptidase, have been investigated. Studies on myoglobin have established the general observation on protein structure that nearly all the polar and charged groups lie on the surface, with van der Waal's contact between side groups on the interior of the molecule. Figure 20.19 is a diagram of the conformation of sperm whale myoglobin.

The space group of myoglobin is $P2_1$, with unit cell axes $a = 64.5 \text{ \AA}$, $b = 30.9 \text{ \AA}$, and $c = 34.7 \text{ \AA}$. There are two molecules in a unit cell. Within its folding the molecule contains 20% water. The 153 amino acids and one heme group have all been identified. Among these 153 amino acid residues, 132 form the right-handed α -helices. They constitute a series of straight rods roughly 5 \AA in diameter and $20\text{--}40 \text{ \AA}$ long.

20.7.3 DNA

The DNA molecule, which contains a large percentage of water (up to 40%), exists in three configurations, *A*, *B*, and *C*. The three configurations are of the same

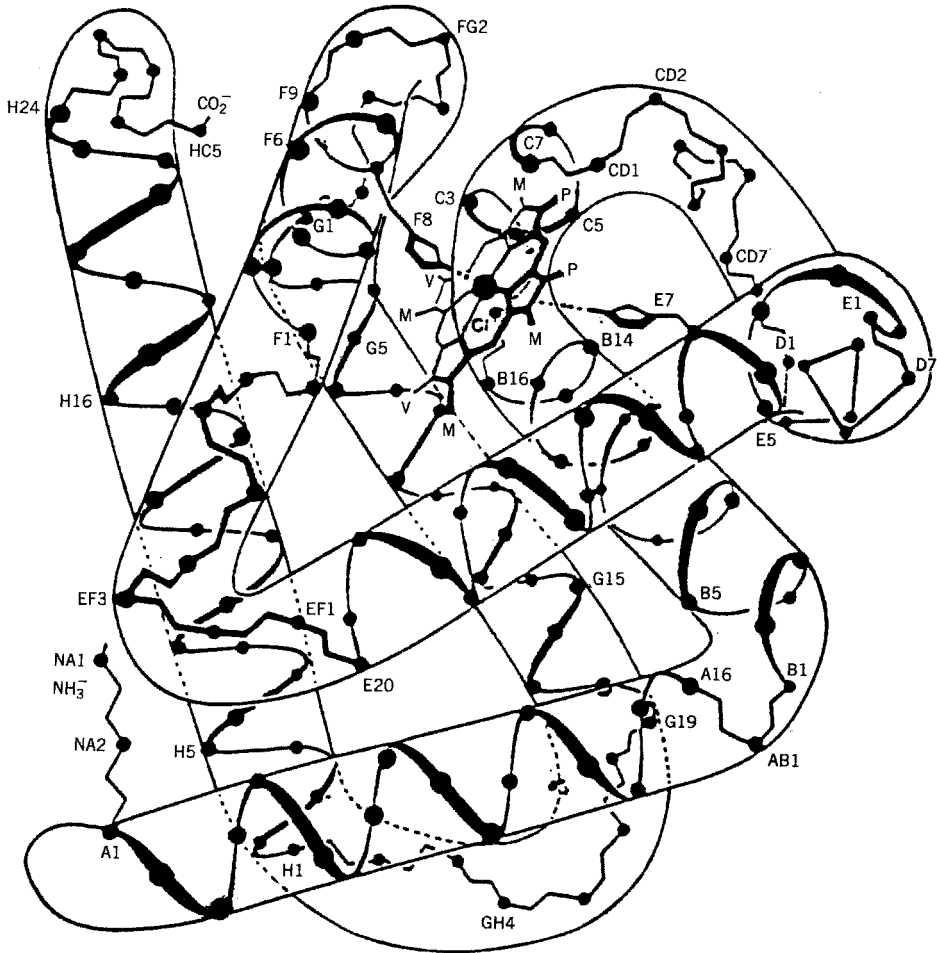


FIGURE 20.19 Crystal structure of sperm whale myoglobin. [Source: Dickerson (1964). Reproduced by permission of Dr. Dickerson and Academic Press.]

structure and differ only in the number of nucleotides per helix turn in helix pitch and in nucleotide conformation. The DNA crystal is monoclinic with the space group $C2$. The molecules occupy special positions $(0, 0, 0)$ $(\frac{1}{2}, \frac{1}{2}, 0)$. Figure 20.20 shows the projection of the ab plane with respect to the arrangement of DNA in the unit cell. The cell axes are $a = 22.2 \text{ \AA}$, $b = 40.6 \text{ \AA}$, and $c = 28.2 \text{ \AA}$ and the cell angles are $\alpha = \gamma = 90^\circ$ and $\beta = 97^\circ$. The molecule possesses a dyad axis that passes through the helix axis of each molecule and is perpendicular to the helix axis. The symmetry is described almost exactly as in the well-known Watson-Crick model.

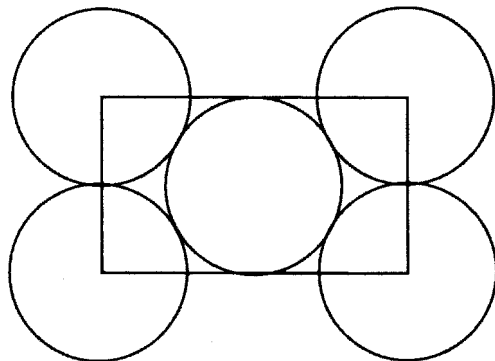


FIGURE 20.20 Projection of the *ab* plane of a DNA crystal.

It has been suggested that the sodium salt of DNA is in the A form with space group $C2$, whereas the lithium salt of DNA is in the B form with the space group $P2_1 2_1 2_1$. Form A belongs to the monoclinic crystal class; form B belongs to the orthorhombic crystal class.

20.8 ADVANCES IN X-RAY CRYSTALLOGRAPHY SINCE 1994

In 1994, the first edition of this book was published. Since then there have been several almost revolutionary advances in the technology of x-ray crystallography. Among them are the x-ray source, new instruments and faster computer programs. The accomplishments of the Human Genome Project pushes a vigorous pursuit for the determination of the structures of both nucleic acid and proteins. X-ray crystallography is the number 1 tool, followed by NMR.

20.8.1 X-Ray Sources

In 1994, the European Synchrotron Radiation Facility (ESRT) in Grenoble, France, was opened to the public. Then in 1996 the advanced photon source (APS) at Argonne National Laboratory, Illinois, United States, was opened. Since then, more x-ray synchrotrons have been constructed in many places and are available to users. The size of a synchrotron to emit the x-rays is as large as a stadium. It can no longer be housed in an ordinary laboratory.

Synchrotrons were originally designed for the study of particle physics. As particles accelerate around a circle, they shed radiation with different wavelengths. Among them are the x-rays. The faster the particles are accelerated, the higher their energy of radiation. With respect of x-rays, in order to generate high intensity, the magnets are bent to keep the beams moving in a circle and 50 or more insertion devices are positioned on a straight section of the electron storage ring. The devices are rows of magnets with alternating polarity to make the electron beams swerve

back and forth, emitting rays with each turn. These devices are also made to modify the rays, for example, to tune the wavelength, to control their polarization and to choose between a single wavelength or a range of wavelength. The beams are so brilliant and so well focused that they allow us to gather data much faster than ever before. The first experiment of an APS beam line, which was very intense, took diffraction patterns of a system at about 30 frames per second; now it can take diffraction patterns in a few nanoseconds with a repetition rate of 100 ps. We can observe what happens in a molecule as it reacts with another molecule or changes its shape.

A device of capillary tubes has been introduced to narrow the beam down to the angstrom level, about 100–1000 Å. The very fine beams provided by the new sources are, in most cases, smaller than the crystal themselves, so that one can now investigate the different parts of a crystal separately.

20.8.2 New Instruments

Before determination of its three-dimensional structure by x-ray crystallography, a protein must be coaxed or grown into crystals. Often, the resultant crystals are either too small or too disorderly to be useful, causing the atomic structure from coming out clearly. By constructing specialized instruments, this problem is partially solved. Enhancing and focusing the beams make it possible to gain a high-resolution x-ray picture even for a newly grown batch of pin-head-sized crystals.

The accomplishments highlight a new frontier in molecular biology; the study of ultrasmall crystals of proteins such as bacteriorhodopsin; the determination of landscapes in protein complexes such as viruses; and equally important, the revelation of hidden events in partially ordered samples, such as the molecular events responsible for muscle contractions.

20.8.3 Structure of Proteins

In the past, it would take months or years to determine the structure of a protein molecule; now it takes a day or even a few hours. Since the wavelength can be changed easily and the intensity of an x-ray is much brighter, more data can be collected. By analyzing the diffraction pattern using software, it becomes much simpler to make a map of the electron density in the crystal. Programs are available or may be devised to have the shape and the structure displayed on a computer screen as a mass of squiggly lines, ribbons, and little balls.

A typical experiment may be described as follows: Native data are collected in-house by using a $\text{CuK}\alpha$ radiation source. Multiwavelength anomalous dispersion (MAD) data are collected at a specific beam line from a synchrotron light source. Data of the sample are collected at a heavy-metal edge by using a selected detector (e.g., ADSC quantum 4 CCD). Then the two data sets are collected from crystals of the sample peptide complex: one from a crystal belonging to a space group, say $C222_1$, and a second that belongs to another space group, $P2_12_12$. All native and

MAD data are indexed. Phases are obtained from the $P2_12_12$ space group and the MAD data set by using a program, for example, SOLVE (automated solution). Molecular graphics of the protein complex are rendered by using a certain selected program, for example, SPOCK.

In the above description, an interesting note should be made about MAD. The phrase "proteins go MAD" means to use mathematical techniques to reconstruct the pattern of atoms that gave rise to the diffraction pattern by using MAD to deal with the phase problem. To solve the problem of the phase of the scattered waves, the usual method is to take multiple images of at least two crystals of the protein, one of which typically has a metal atom inserted into the protein structure such that it produces subtly different patterns. By comparing the two sets of patterns, one finds the precise position of the metal atom as a reference point and the relative phases of the wave scattering from the other atoms in the protein (compare the Patterson synthesis). Now MAD achieves the same result with just a single metal (usually selenium atoms) containing protein. It is done by taking multiple diffraction patterns with x-rays of slightly different wavelengths. The metal atom scatters photons differently if their frequency is tuned slightly above or below a characteristic value, yielding the multiple diffraction images needed to determine the critical phase information.

20.8.3.1 Comparison of X-Ray Crystallography with NMR Spectroscopy Both x-ray crystallography and NMR spectroscopy are indispensable for the study of the three-dimensional structures of macromolecules, particularly with respect to the study of proteins and nucleic acids. Knowledge obtained from x-ray crystallography is almost perfect, leaving little room for any doubt. In the last 40 years, since the publication of the structures of myoglobin, hemoglobin, and others, each time a protein structure is reported from x-ray crystallography, it becomes a major event in the field of protein chemistry. Today, as has been described, methods are so much more advanced that it is no longer sensational to report these kinds of results. Yet it is still x-ray crystallography that provides the final word on protein structure. The knowledge obtained through x-ray crystallography does not need a theoretical calculation for support. Instead, the model of a good theoretical calculation needs experimental support from the x-ray crystallography data. However, x-ray crystallography can only take measurements in crystals and not on samples in solutions. In that respect, NMR spectroscopy must be used to supplement our knowledge.

NMR is the second best technique for studying the structure and functions of nucleic acids and proteins. Originally there was limitation on an NMR sample in that the molecular weight could not be too large (in the past, the limit was 30,000). Now this problem has been partially solved. It is well-known that x-ray crystallography is able to bring us knowledge of the structure of the macromolecule in its entirety. Recent advances show that NMR can also be used for the study of a macromolecule in its entirety. Nevertheless, while NMR is catching up to the precision and speed of x-ray crystallography, there are still some major differences; namely, NMR requires a large amount of computer time and a variety of computer programs. NMR needs computer modeling to assist in the analysis whereas x-ray

crystallography does not. X-ray crystallography needs computer programs only for analyzing the diffraction pattern, making a map of the electron density in the crystal, and displaying the deduced shape on a computer screen.

20.8.4 Protein Examples

As in the previous chapter on NMR, we illustrate two examples of proteins using x-ray crystallography to determine their structure and functions: a polymerase and an anthrax toxin.

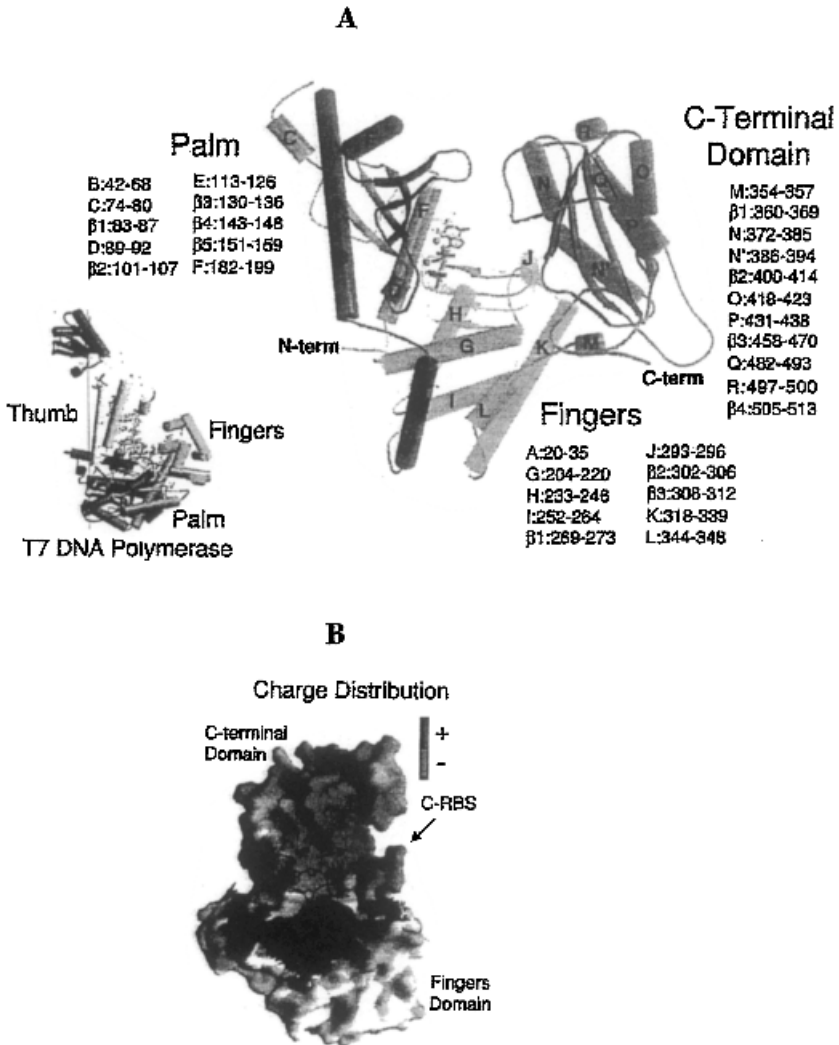


FIGURE 20.21 See color insert. Polymerase (PAD). [Source: Bard et al. *Science* 276, 2016 (1997). With permission from AAAS. Original in color.]

Polymerase Polymerase is an enzyme that catalyzes the addition of nucleotide to DNA or RNA. Figure 20.21a shows the crystal structure of the polyadenylate polymerase (PAP) from *Saccharomyces cerevisiae* (*Pap1*) at 2.6 Å resolution. The crystal contains a large 20 × 30 × 45-Å cleft bounded by three globular domains. The catalytic palm domain and the COOH— terminal domain form the walls of the cleft rather than sitting at its base. The catalytic function of PAP resides in its NH₂— terminal domain. Two divalent cations (orange) are shown bound to the active site and to the phosphates of the incoming 3'-dATP (red). The mononucleotide primer is shown in yellow.

Figure 20.21b shows the charge distribution of the molecular surface of the fingers and COOH— terminal domains of *Pap1*. In this presentation, the palm domain has been removed for clarity.

For both figures, the important crystallographic data are space group, $P2_12_12_1$ (73.8 Å, 109.1 Å, 238.5 Å, 90°, 90°, 90°, 90°); solvent content 70.0% (volume of the asymmetric unit molecular weight of the protein scatters); x-ray source; and APS beam line (19-ID). Both figures are generated using three programs in sequence: MOLSCRIPT, R3D-TO-DOV, and POVRAY.

Anthrax Toxin The anthrax bacterium produces a deadly toxin which has three components: a lethal factor, a protective antigen, and a oedema factor (EF). The lethal factor is involved in the killing of the macrophages by releasing a flood of pent-up cyclokinines. The protective antigen proteins assemble in clusters of seven, forming a barrel-shaped structure with a docking site for either the oedema factor or the lethal factor. The oedema factor binds to a common compound of cells called the calmodulin and becomes activated.

Figure 20.22a shows the secondary structures of (a) oedema alone and (b) complex with calmodulin (CaM).

Figure 20.22b shows a visual representation of the binding structures. These images depict the molecular structure of the EF. The x-ray diffraction models show the molecule before it enters a cell (top left) and inside the cell (top right). The two bottom images show the opposite side of the molecule in each form.

The interface between the helical domain and the remainder of the domain in the EF buries the 16 hydrophobic residues and 3600 Å² of surface area. None of these interactions are preserved in the EF-CaM complex when CaM inserts itself between C_A and the helical domain. In doing so, CaM occupies much of the same volume occupied by the helical domain in the structure of the EF alone. To accommodate CaM, the helical domain, acting as a unit, moves 15 Å and rotates 30° such that C_A, the linker, and the helical domain form a large clamp that almost completely encircles CaM.

The x-ray crystallography data are:

Crystals of nucleotide-free EF-CaM complex $I222$ space group, crystals of EF alone space group $P2_12_12$. The *R* factor/*R* free for the structures of EF-CaM-3'-d-ATP, EF alone and EF-CaM are 21.5/28.6, 22.8/27.6, and 27.8/31.5, respectively. X-ray source APS Biocars 14-BM-C and NSLS X25. Program for process HKL.

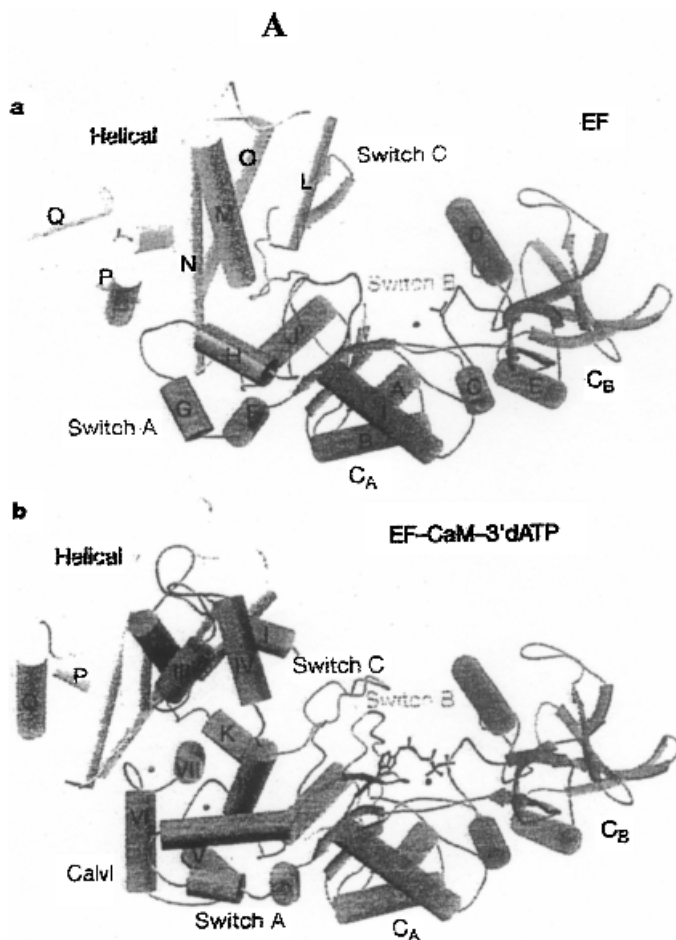


FIGURE 20.22A See color insert. Secondary structures: (a) EF alone; (b) EF-CaM-3'-deoxy-ATP complex color code; CAM (red), CA (green), switch C (magenta), helical domain (yellow), switch A (cyan), switch B (orange), 3'-deoxy-ATP analogue (purple), metal (purple), C_A and C_B (green), D and Q (amino acids 771-799, white). [Source: Drum et al. *Nature* **415**, 396 (2002). Permission from *Nature*. Original in color.]

APPENDIX NEUTRON DIFFRACTION

Neutron diffraction and x-ray diffraction are fundamentally similar. Strong reflections occur when Bragg conditions are satisfied. The experimental data of the wavelength λ and scattering angle θ are needed to calculate the interplanar distance d , and the intensity of the reflection is useful in determining molecular structure. The difference lies in the fact in x-ray diffraction electrons are the principal cause of scattering, whereas in neutron diffraction the scattering involves nuclear rather than electronic processes. For this reason, neutron diffraction can easily distinguish

B

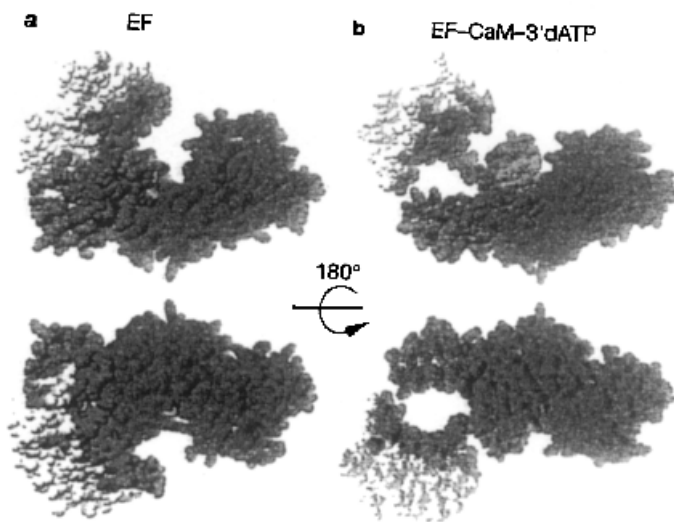


FIGURE 20.22B See color insert. Visual representation EF structures a. EF alone; b. CaM-EF. [Source: Drum et al. *Nature* **415**, 396 (2002). Permission from *Nature*. Original in color.]

between atoms such as carbon and nitrogen in C=N or nitrogen and oxygen in N=O; x-ray diffraction cannot. Neutron diffraction can even distinguish between isotopes. It can be used to observe magnetons and to study the dynamics of the spin state of magnetic crystals.

Neutron Crystallography

The basic equations that apply in the x-ray diffraction pattern also apply in the neutron diffraction:

$$\lambda = 2 \frac{d_{hkl}}{n} \sin \theta \quad (\text{Bragg equation})$$

$$\frac{1}{d_{hkl}} = f(a, b, c, \delta, \beta, \gamma)$$

where, as mentioned before, a , b , and c are the periods of the unit cell, while α , β , and γ are the angles between the coordinate axes.

The Fourier transform for x-ray form factor $F_x(q)$ is slightly different from that for neutron form factor $F_{\text{neutron}}(q)$, as shown in the following equations:

$$F_{\text{x-ray}}(q) = \int_{\tau} e^{iqr} \{N_{\uparrow} |\psi_{\uparrow}(r)|^2 + N_{\downarrow} |\psi_{\downarrow}(r)|^2\} dr$$

$$F_{\text{neutron}}(q) = \int_{\tau} e^{iqr} \{N_{\uparrow} |\psi_{\uparrow}(r)|^2 - N_{\downarrow} |\psi_{\downarrow}(r)|^2\} dr$$

where

$$q = \frac{4\pi}{\lambda} \sin \theta$$

The arrows refer to electron spin: \uparrow in the upward direction and \downarrow in the downward direction. The term N is the number of electrons of an atom and ψ is the wave function of an electron. The radical density of neutron diffraction is in the form

$$U(r) = \frac{2r}{\pi} \int_0^\infty qF(q) \sin(qr) dq$$

which corresponds to the equation of electron density synthesis in x-rays:

$$\rho(x, y, z) = \frac{1}{V} \sum_h^\infty \sum_k^\infty \sum_l^\infty F_{hkl} \exp[-2\pi i(hx + ky + lz)]$$

Because of the high cost of a neutron-diffraction experiment, it has not been used much for polymers, but its potential for the study of polymer structure is obvious.

REFERENCES

- Atkins, P. *Phys. Chem.*, 3rd ed. Freeman: 1986.
- Bloss, F. D., *Crystallography and Crystal Chemistry*. New York: Holt, Rinehart and Winston, 1971.
- Blundell, T. L., and L. N. Johnson, *Protein Crystallography*. London: Academic, 1976.
- Bragg, W. L., *Proc. R. Soc. London Ser. A* **123**, 537 (1929).
- Buerger, M. J., *Elementary Crystallography*. New York: Wiley, 1963.
- Bunn, C. W., *Trans. Faraday Soc.* **35**, 482 (1939).
- Bunn, C. W., *Proc. R. Soc. London Ser. A* **189**, 39 (1947).
- Carradini, P., G. Natta, P. Ganis, and P. A. Temussi, *J. Polym. Sci. C* **162**, 477 (1967).
- Green D. W., V. M. Ingram, and M. F. Perutz, *Proc. R. Soc. London Ser. A* **225**, 287 (1954).
- Hauptmann, H., *Science* **233**, 178 (1986).
- Hauptmann, H., and J. Karle, *The Solution of the Phase Problem, I: The Centrosymmetric Crystal*, ACA Monograph No. 3. Ann Arbor, MI: Edwards Brothers, 1953.
- Izumov, Y. A., and R. P. Ozerov, *Magnetic Neutron Diffraction*. New York: Plenum, 1970.
- Karle, J., *Science* **232**, 837 (1986).
- Karle, J., and H. Hauptmann, *Acta Crystallogr.* **9**, 635 (1956).
- Kavesh, S., and J. M. Schultz, *J. Polym. Sci.* **8**, 243 (1970).
- Kendrew, J. C., H. C. Watson, B. E. Strandberg, R. E. Dickerson, D. C. Phillips, and V. C. Shore, *Nature (London)* **190**, 666 (1961).
- Natta, G., P. Corradini, and P. Gans, *Makromol. Chem.* **39**, 238 (1960).

Patterson, A. L., *Phys. Rev.* **48**, 372 (1934).
 Phillips, F. C., *An Introduction to Crystallography*, 4th ed. New York: Wiley, 1971.
 Spruiell, J. E., and E. S. Clark, *Methods Exp. Phys.* **16B**, 1 (1980).
 Von Laue, M., *Muench. Sitzungsber.*, 363 (1912).
 Wunderlich, B., *Macromolecular Physics*, Vol. 1. New York: Academic. 1973.

PROBLEMS

20.1 A unit cell has two atoms. Their coordinates (x, y, z) are (0.10, 0.10, 0.10) and (0.20, 0.75, 0.40) and their atomic scattering factors are 3.10 and 4.20. Calculate F_{hkl} for the (121) plane.

20.2 The unit-cell constants for human serum albumin and $a = b = 186.5 \text{ \AA}$ and $c = 81.0 \text{ \AA}$. What is the spacing of the (120) and (112) planes?

20.3 The structure factors of ($h00$) planes of a crystal were found as follows:

h	0	1	2	3	4	5	6	7	8	9	10	11	12	13	14	15
F_h	16	-10	2	-1	7	-10	8	-3	2	-3	6	-5	3	-2	2	-3

Construct a plot of the electron density along the x -axis of the unit cell (Atkins, 1986).

20.4 Describe the space groups $Im\bar{3}m$, $Fm\bar{3}m$, and $Fd\bar{3}m$ and the five cubic point groups $F23$, $Fm\bar{3}$, $F43m$, $F432$, and $Fm\bar{3}m$. Note that $Fm\bar{3}m$ is both a space group and a point group.

20.5 Polyorthomethylstyrene forms a crystal with a body-centered lattice. The structure factor at $(\frac{1}{2}, \frac{1}{2}, \frac{1}{2})$ is given by

$$F_{hkl} = \left\{ \sum_m f_m \exp[2\pi i(hx_m + ky_m + lz_m)] \right\} \times \left\{ 1 + \exp \left[2\pi i \left(\frac{h}{2} + \frac{k}{2} + \frac{l}{2} \right) \right] \right\}$$

where m refers to the atoms that compose the motif at each lattice point. Show that if $h + k + l = 2n + 1$, where n is any integer, then

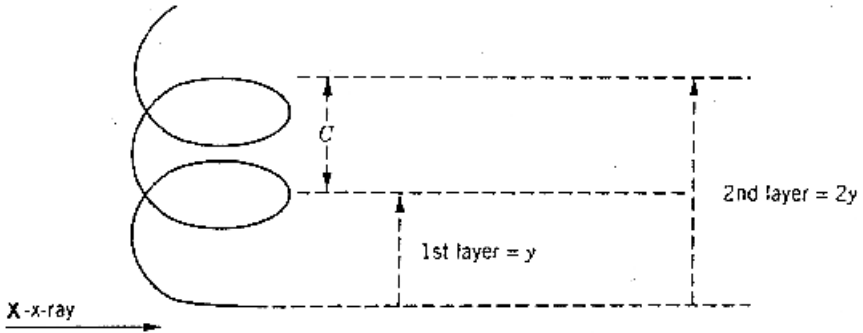
$$F_{hkl} = 0$$

that is, there is no intensity. If $h + k + l = 2n$, then

$$F_{hkl} = \sum_m f_m \exp[2\pi i(hx_m + ky_m + lz_m)]$$

that is, they are still functions of the relative positions of the atoms in the motif (Spruiell and Clark, 1980).

20.6 Following is the diagram of the helical structure of a crystal:



For polyoxymethylene, the intense upper layer line has $l = 5$ at a $2y$ value of 29 mm. The value of $2x$ is also 29 mm. The cylindrical camera diameter ($2D$) was 57.3 mm and $\lambda = 1.54 \text{ \AA}$. Calculate the interplanar distance d and the repeat helix distance c . *Hint:*

$$d = \frac{\lambda}{2 \sin[\frac{1}{2} \tan^{-1}(2x/2d)]} \quad c = \frac{l\lambda}{\sin[\tan^{-1}(y/D)]}$$

(Spruiell and Clark, 1980).

AUTHOR INDEX

- Adam, M., 124
Adamson, A. W., 17
Adler, R. S., 233, 240
Akcasu, A. Z., 395
Aklonis, J. J., 192, 197
Alben, J. O., 430, 435
Albrecht, A. C., 218
Aminabhavi, T. M., 92, 93
Amis, E. J., 393, 395
Andrews, A. T., 317
Anfinson, C. B., 444, 434
Anson, M. L., 240
Archibald, W. J., 262
Atkins, P. W., 496, 532, 533
- Babcock, H. P., 124
Bailey, E. D., 193
Baker, D., 448, 454
Baldwin, R. L., 262, 263
Bard, J., 528
Batley, J. F., 317
- Bawendi, M., 149
Bawn, C. E. H., 218
Baxendale, J. H., 192, 194
Beeman, W. W., 396
Bell, E. T., 368
Benedek, G. B., 396
Benmouna, M., 395
Benoit, H., 317, 332, 345, 395, 396
Berne, B. J., 390, 395
Berry, R. S., 123
Billmeyer, F. W., Jr., 78, 92
Blaschke, F., 171, 193
Bloch, F. W., 494
Bloembergen, N., 495
Bloss, F. D., 508, 532
Blout, E. R., 281, 430
Blundell, T. L., 532
Bly, D. D., 317
Boaz, H., 430, 433
Bodenhausen, G., 494
Boltzmann, L., 224, 240
Borman, S., 453

- Bovey, F. A., 478, 479, 480, 483, 486, 494
Bower, D. I., 430
Bowman, R. L., 430, 433
Bracewell, R. N., 368
Bragg, W. L., 532
Brahms, J., 281, 282
Brand, E. A., 430, 433
Brand, L., 368
Brandrup, J., 92, 192
Brant, D. A., 192, 197
Briggs, D., 430
Bueche, A. M., 177, 178, 179, 192, 376, 396
Bueche, F., 192
Buerger, M. J., 532
Bulouc, V., 149
Bunn, C. W., 532
Burchard, W., 396
Bushuk, W., 332, 345
Bywater, S., 192
- Cabasi, F., 431
Caldwell, K. D., 317
Cantor, C., 281
Caret, R. L., 44, 50
Carlson, F. D., 395
Carlson, R. M. K., 494
Carothers, W. H., 4
Caruthers, M. H., 50
Carradini, P., 532
Cartwright, M., 368
Casassa, E. F., 345
Chandler, D., 218
Chandrasekhar, 99, 123
Chang, T. S., 431
Chapoy, L. L., 430
Chen, R. F., 430, 433
Chen, Y. H., 281
Chervenka, C. H., 262
Chow, C. C., 124
Chu, B., 394, 395
Chu, S., 118, 119, 124
Churchil, R. V., 368
Ciferri, A., 149
- Clark, E. S., 533, 534
Coe, S., 149
Cohen, C., 281
Cohn, J., 92
Cohn-Ginsberg, E., 92, 93
Colowick, S. P., 262
Cooley, J. W., 368, 430
Corey, R. B., 437, 454
Cotton, A., 275, 281
Cotton, J. P., 123, 395, 396
Crank, J., 240
Crawford, F. S., Jr., 368
Croasmum, W. R., 494
Cummins, H. Z., 395
- Daoud, M., 396, 398
Dayhoff, M. O., 92
Davidson, N., 431
Davis, L. G., 377
Debye, P., 177, 178, 179, 192, 324, 335, 345, 375, 396
Decker, D., 395
De Gennes, P. G., 67, 96, 107, 109, 110, 113, 114, 115, 116, 123, 149, 179, 192, 218, 396
De Haseth, J. A., 430
Del Rosario, N. O., 193, 196, 345, 346
Delsanti, M., 124
Des Cloizeaux, J., 209, 210, 211, 218, 395
Deyl, Z., 317
Dibner, M. D., 317
Dickerson, R. E., 524, 532
Doi, M., 116, 123
Dostal, H., 50
Doty, P., 281, 282, 336, 408, 431
Drude, P., 270, 281
Drum, C. L., 530, 531
Dubin, S. B., 396
Duportail, G., 430
- Edelhoch, H., 345
Edelman, G. M., 431
Edsall, J. T., 92, 345

- Edwards, S. F., 109, 110, 116, 123
 Einaga, Y., 123
 Einstein, A., 178, 181, 184, 193, 240
 Eisele, U., 193
 Eisenberg, H., 345
 Epstein, H. F., 431
 Ernst, R. R., 494
 Eyring, H., 317
 Everhart, C. H., 496
- Fager, L. Y., 430, 435
 Fan, J., 124
 Farnoux, B., 123, 395, 396
 Fasman, G. D., 281
 Feller, W., 65
 Ferguson, R. C., 482, 494
 Ferraro, J. R., 430
 Ferry, J. D., 193
 Fick, A., 240
 Fisher, E. W., 149
 Fixman, M., 123, 175, 193
 Flory, P. J., 50, 56, 65, 67, 71, 72, 75, 79,
 80, 81, 84, 85, 92, 93, 94, 96, 107,
 108, 110, 113, 114, 115, 123, 142,
 149, 158, 163, 172, 192, 193, 197,
 204, 205, 218, 219, 221
 Fox, J. C., 193
 Fox, T. G., Jr., 92, 94, 172, 193
 Forster, T., 416, 430
 Fourier, A. B. J., 240, 367
 Fournet, G., 396
 Freed, K. F., 123, 180, 193, 218, 233,
 240
 Freeman, C., 218
 Freifelder, D., 430
 Froelich, D., 430
 Fujii, M., 124
 Fujita, H., 123, 263
 Fulks, W., 368
- Ganis, P., 532
 Gibbs, J. W., 198, 218
 Giddings, J. C., 317
 Gilbert, W., 317
- Goldberg, R. J., 251, 262
 Goodyear, C., 152
 Gosting, L. J., 240
 Grassley, W. W., 123, 151, 163
 Gratzner, W. B., 281
 Green, D. W., 532
 Greenfield, N., 281
 Gregg, R. A., 50
 Griffiths, P. R., 430
 Grim, J. M., 431
 Grimley, T. H., 104, 123
 Grubestic, Z., 294, 317
 Guillemin, E. A., 368
 Guinier, A., 396
 Gupta, A. K., 396, 397
 Guth, E., 161, 163
 Gutts, E., 163
- Haltner, A. J., 240, 242
 Hamition, B. W., 317
 Han, C. C., 393, 395
 Hancock, T., 152
 Hansen, W., 494
 Harrington, W. F., 431, 433
 Harris, R. K., 494
 Hauptmann, H., 578, 532
 Hearst, J. E., 263
 Heftmann, E., 317
 Herbert, T. J., 395
 Hermans, J. J., 104, 123
 Herskovits, T. T., 431
 Hervet, H., 396
 Herzberg, G., 431
 Higgins, J., 395, 396
 Hildebrand, J. H., 76, 77, 78, 80, 81, 92
 Hill, T. L., 163, 218
 Hiratsuda, S., 431
 Hoch, J. C., 368
 Holland-Mortiz, U. K., 426, 431
 Holzwarth, G., 281, 282, 283
 Houwink, R., 172, 193
 Howard, G. A., 317
 Hoy, K. L., 78, 92
 Hsiao, C. L., 317
 Huggins, M. L., 71, 171, 193

- Hummel, J. P., 317
Hunter, B. K., 495
- Iizuka, E., 281
Immergut, E. H., 92, 192
Indrity, J., 368
Ingham, J. D., 92
Ingram, V. M., 532
Inoue, H., 345, 346
Ising, E., 218
Izumov, Y. A., 532
- James, A. T., 317
James, H. M., 163
Janca, J., 317
Jannink, G., 395
Johnson, C. S., 496
Johnson, L. N., 532
Johnson, P., 431
Johnston, J. P., 262
Joule, J. P., 161, 163
- Kaesberg, N. P., 396
Kamaliddin, A., 218
Kaplan, N. O., 262
Karle, J., 518, 532
Karplus, M., 494
Kavesh, S., 532
Kelvin (Thomson, W.), 161, 163
Kendrew, J. C., 532
Kennedy, J. F., 427, 431
Kerker, M., 345
Kerr, J., 140, 149
Khintchine, A., 391, 396
King, J. K., 396
Kirkland, J. J., 317
Kirkwood, J. G., 229
Klinkenberg, A., 317
Koenig, J. L., 431
Koppel, D. E., 395, 396
Kraemer, E. O., 171, 193
Kramers, H. A., 278, 281
- Kratky, O., 105, 123, 385, 396
Krause, S., 92, 93, 345, 347
Kreutz, W., 396
Krigbaum, W. R., 205, 218, 219, 221
Krimm, S., 431
Krishnan, K., 430
Kronig, R., 278, 281
Kuhn, H., 182, 193
Kuhn, W., 123, 182, 193
Kumar, S., 149
Kuo, S. W., 317
Kurata, M., 123, 193, 207, 218, 221
Kutateladze, T., 494
- Laidler, K. J., 50
Lakowicz, J. R., 415, 431
Lam, G. M., 431
Lamm, O., 240
Langevin, D., 262, 266
Laskowski, Jr., M., 431
Lauterbur, P. C., 476
Lawson, D. D., 92
Ledermann, W., 368
Legendre, A. M., 519
Lenz, R. W., 50
Levy, G. C., 494
Lichter, R. L., 494
Lim, H. A., 124
Leger, L., 396
Lontre, R., 345
Lunacek, J. H., 396
Luzzati, V., 377, 380, 396
Lyerla, J. R., 495
- Ma, S. K., 218
MacKnight, W. J., 192
Maddams, W. F., 430
Mandelkern, L., 182, 193
Mano, E. B., 431
Marchal, E., 396
Mark, H., 50, 161, 163, 172, 193
Marmur, J., 431
Matheson, M. S., 50

- Martin, A. F., 92, 171, 193, 286, 289, 317
 Mayer, J. E., 108, 123, 203, 207, 218
 Mayer, M. G., 123
 Mayo, F. R., 35, 50
 McClure, W. O., 431
 McGovern, J. J., 431
 McMillan, W. G., 123, 203, 207, 218
 Merrifield, R. B., 46, 50
 Meselson, M., 262
 Michelson, A. A., 428
 Miller, A. R., 93
 Miller, J., 92
 Mingos, D. M. P., 149
 Miyaki, Y., 123, 126
 Moffit, W., 270, 281
 Mood, A. M., 65
 Morrison, P. R., 345
 Moscowitz, A., 279, 281
 Munk, P., 92

 Nakanishi, K., 431
 Nash, R. A., 124, 317
 Natta, G., 532
 Naumann, A. W., 396
 Nelson, G. L., 494
 Newing, M. J., 93
 Nierlich, M., 123
 Nishijima, Y., 431
 Noolandi, J., 124
 Northrop, J. H., 240
 Nose, T., 394, 395

 Ober, R., 395, 396
 Odian, G., 50
 Ogston, A. G., 262
 O'Konski, C. T., 240
 Onsager, L., 141, 142, 149, 301
 Orofino, T. A., 218
 Oseen, C. W., 176, 193
 Ottewill, R. H., 431
 Overhauser, A. W., 495
 Ozerov, R. P., 532

 Packard, M. E., 494
 Patterson, A. L., 517, 533
 Pauling, L., 437, 454
 Pecora, R., 390, 395
 Pedersen, K. O., 262
 Peebles, L. H., 65
 Penterman, R., 149
 Percec, V., 149
 Perlmann, G. E., 92
 Perkins, T. T., 119, 124
 Perrin, F., 230, 238, 240, 419, 431
 Perutz, M. F., 532
 Perzynski, R., 115, 124
 Peterlin, A., 181, 193
 Phillips, D. C., 532
 Phillips, F. C., 511, 533
 Picot, C., 395, 396
 Piseri, L., 431
 Polson, P., 240
 Poisson, S. D., 185
 Porod, G., 105, 123, 376, 379, 396
 Pound, R. V., 495
 Prusiner, S. B., 495
 Purcell, E. M., 495

 Raff, R., 50
 Randall, J. C., 481, 484, 494
 Rao, C. N. R., 431
 Rao, S. S., 368
 Ravindranath, B., 317
 Rayleigh, Lord, 345
 Read, B. E., 345
 Reddi, K. K., 432
 Rempp, R., 317
 Rice, S. A., 123
 Riseman, J., 176, 193, 196, 197
 Ritland, M., 396
 Rollefson, G. K., 430
 Ronca, G., 149
 Rondelez, F., 262, 266, 396
 Rosenbeck, K., 408, 431
 Rossiten, B. W., 317
 Rouse, P. E., 187, 190, 191, 193, 233, 383

- Safford, G. J., 396
Sameijima, T., 281
Sanders, J. K. M., 495
Sanger, F., 437, 454
Santagata, S., 443, 444, 454
Sarma, G., 396
Scatchard, G., 76, 93, 218, 221
Schachman, H. K., 240, 242, 262
Schiller, P. W., 431, 434
Schnier, I., 281
Schultz, G. W., 171, 193
Schultz, J. M., 532
Schutz, R. C., 149
Scott, R. L., 77, 78
Shechter, E., 281
Shen, M., 192
Sheraga, H. A., 182, 193
Shore, V. C., 532
Siesler, H. W., 426, 431
Sillescu, H. H., 149
Simha, R., 182, 193
Simmons, N. S., 281
Sittel, K., 193
Slater, G. W., 124
Smith, D. E., 119, 124
Sneddon, I. N., 218
Snyder, R. G., 431
Soda, K., 396
Solomon, P. H., 431
Speiss, H. W., 485, 495
Sprutell, J. E., 533, 534
Stacey, K. A., 345
Stahl, F. W., 262
Staudinger, H., 193
Stauffer, D., 124
Steiner, R. F., 345
Stern, A. S., 368
Stern, O., 415, 431
Stockmayer, W. H., 175, 193, 332
Strandberg, B. E., 532
Stryer, L., 431
Studier, F. W., 262
Suda, N., 396
Sun, S. F., 124, 193, 194, 296, 297, 299,
317, 345, 346, 409, 410, 431
Sutherland, W., 240
Svedberg, T., 184, 248, 262
Synge, R. L. M., 286, 289, 317
Szakonyi, G., 443, 444, 454
Szent-Gyorgyi, A. G., 281
Szwarc, M., 50
Tanford, C., 345
Teach, W. C., 431
Teramoto, A., 431
Thompson, H. W., 431
Timasheff, S. N., 345, 346
Temussi, P. A., 532
Tinoco, I., 281
Tiselius, A., 240
Torrey, H. C., 495
Tsuda, T., 396
Tukey, J. W., 368, 430
Tyndall, J., 320, 345
Ursell, H. D., 124
Uspensky, J. V., 124
Valvani, S. C., 93
Van Deemter, J. J., 289, 317
Van Holde, K. E., 262, 263
Van Hove, L., 383, 396
Van Laar, J. J., 93
Vinograd, J., 262, 263
Vollmert, B., 45, 50, 345
Volmer, M., 415, 431
Von Laue, M., 512, 533
Wada, A., 396
Wall, F. T., 93, 163
Watkins, R., 443, 444, 454
Watson, H. C., 532
Weber, G., 240, 415, 417, 431, 433
Weil, G., 430
Wetlaufer, D. B., 281, 431

- Wetmur, J. G., 431
Wiener, N., 391, 396
Willcockson, G. W., 427, 431
Williams, J. W., 263
Wilson, J. N., 289, 317
Wilson, K. G., 110, 124, 218
Wingrove, A. S., 44, 50
Wokaun, A., 494
Wong, E., 296, 317
Wong, F., 299, 317
Woo, W. K., 149
Woods, G., 395
Wunderlich, B., 514, 523, 533
Wuthrich, K., 495
Yalkowsky, S. H., 93
Yang, J. T., 193, 270, 281
Yamakawa, H., 107, 108, 124, 125, 193,
207, 218, 221
Yamamoto, M., 431
Yguerabide, J., 431
Young, L. B., 240, 417, 431
Yphantis, D. A., 263
Yusupov, M. M., 452
Zerbi, G., 431
Zimm, B. H., 107, 108, 190, 193, 218,
233, 345, 383, 385
Zuiderwig, F. J., 317

SUBJECT INDEX

- Absorption system (sedimentation), 258
- Activity a_1 , 198
- Adsorption chromatography, 291
- Advances in NMR since 1994, 487
- Advances in X-ray crystallography since 1994, 525
- Agarose gel electrophoresis, 307
- Aggregation of polypeptide chains, 450
- α -helix, 437–439
- Amino acids, 8, 9
- Anionic polymerization, 25
- Anisotropic interaction, 127
- Applications of size-exclusion chromatography, 293
- Approach to equilibrium method, 244
- Archibald method, 251
- Atactic polymers, 6
- Atomic scattering factor, 515
- Autocorrelation and power spectrum, 390, 391, 392
- Auxochromes, 404
- Basic Fourier series, 350
- Binomial distribution, 53
- Bernoulli probability, 98, 99
- Bessel function, 377
- β -sheet, 437, 438, 440
- Biological polymers, 7
- Boltzmann-Planck law, 74
- Brain diseases, 450
- Bravais lattices, 505, 506
- Butyl rubber, 153
- Capacity factor (HPLC), 287
- Capillary viscometers, 166
- Cationic polymerization, 27
- Chain collapses, 113
- Chain crossover and chain entanglement, 109
- Chain entanglement, 179

- Chain length, 40
Chain reactions, 35
Chaperones, 448
Characteristic frequency of functional groups, 425
Chemical potential μ , 82, 83
Chemical shift and spin-spin coupling constant, 461–466
Chromophores, 403
Circular dichroism, 267, 272, 279
Classification of proteins, 439
Cluster expansion method, 108
Coherently elastic neutron scattering, 384
Cohesive energy density, 76
Columnar mesophase, 137
Colloids, 1
Comb-shaped polymer, 6
Comparison of ORD and CD, 280
Comparison of small-angle neutron scattering with light scattering, 384
Comparison of X-ray crystallography with NMR spectroscopy, 527
Complex Fourier series, 353
Complication in chain termination, 22
Complication in chain transfer, 22
Complication in propagation, 21
Computer simulation, 445
Concentration dependence of diffusion coefficient, 231
Condensation reactions, 34
Contact energy, 79
Continuous-wave (CW) method, 470
Continuity equation, 224
Contrast factor, 386
Conversion from α -helices to β -sheets, 449
Convolution, 359
Convolution theorem, 361
Coordination polymerization, 30
Copolymer, 6
Copolymers (light scattering), 331
Correlation between ORD and CD, 277
Correlation function, 121, 363
Correlation length, 112
Cotton effect, 275, 276, 277
Cross-linking, 151
Crystal drawing, 503
Crystal coordinates, 502
Crystal structure of macromolecules, 520
Crystals, 498
Cumulant analysis, 395
Debye-Bueche theory, 177, 178
Deformation and recoverability, 151
De Gennes' fluctuation theory, 144
Degree of addition polymerization (DP), 38
Denaturation and renaturation of DNA, 411, 412
Density gradient at equilibrium, 244, 259
De Novo prediction, 447
Des Cloizeaux-de Gennes scaling theory, 209
Determination of molecular weight (light scattering), 329
Deuterium NMR spectra, 482
Dichroic bands, 274
Difference spectra, 409
Diffusion, 223
Direct method (Karle-Hauptmann approach), 518
Discrete Fourier transform, 364, 365
DNA, 14
DNA synthesis, 48
DP, 50
Drude equation, 270
Eddy diffusion, 290
Effective residue rotation, 271
Einstein-Svedberg equation, 184
Einstein's equation of diffusion, 226
Einstein equations for spherical molecules, 181
Electrolyte buffer, 305
Electronic devices, 147

- Electronic spectroscopy, 399
 Electrophoresis, 284, 300
 Electrophoresis since 1994, 313
 Elliptically polarized light, 268
 Emission, excitation, and visible
 absorption (fluorescence), 414
 Emission and excitation spectra, 413
 Energy transfer, 416
 Ensembles, 215
 Entropy of dilution parameter, 4, 85
 Equation of $\alpha^5 - \alpha^3$, 115
 Equivalent hydrodynamic sphere model,
 178
 Experimental methods for determining
 molecular weight distribution, 64
 Even function, 349
- Fast Fourier transform, 366
 Fick's first law and second law, 223,
 238, 243
 Field-flow fractionation, 314, 315, 316
 First law of thermodynamics, 70
 First-order perturbation theory, 108
 Flory-Fox equation, 172, 173, 174
 Flory-Krigbaum theory, 205, 207, 219
 Flory's mean-field theory, 106
 Flory theory of osmotic pressure, 204,
 207, 211, 212
 Flory viscosity constant, 173, 174
 Flow birefringence, 239
 Fluctuation theory (Debye), 324–329
 Fluorescence depolarization, 239
 Fluorescence spectra, 399, 412
 Forced Rayleigh scattering, 394
 Forster's theory, 416
 Four types of electron transitions, 401
 Fourier cosine series, 352
 Fourier integrals, 354, 355
 Fourier sine series, 352
 Fourier series, 348
 Fourier synthesis of electron density,
 516
 Fourier transform infrared spectroscopy
 (FTIR), 428
- Fourier transform pairs, 356, 357, 358
 Free-energy landscape, 446
- Gaussian distribution, 55
 Gaussian distribution function, 100
 Gel filtration chromatography, (GFC),
 293
 Gel permeation chromatography,
 (GPC), 293
 Gels, 162
 Genomics, proteomics, and
 bioinformatics,
 451
 Gibbs-Duhem equation, 198, 326
 Gouy interference method, 235
 Good solvent, 86
 Green's function, 217
 Guinier plot, 373, 374, 378, 379
- Heat, 68
 Heat-of-dilution parameter K_1 , 85
 High-performance liquid
 chromatography (HPLC), 284
 Hildebrand-Scatchard equation, 79
 Homolog modeling, 447
 Homopolymer, 6
 Huggins constant, 171
 Hummel and Dreyer chromatogram,
 297, 298
 Hydrophobic, 1
 Hypochromism, 405
- Ideal rubber, 157, 161
 Ideal temperature θ , 85
 Images of individual polymer chains,
 118
 Infrared spectra, 400
 Infrared spectroscopy, 399, 420
 Inner product, 349
 Interaction contacts, 112
 Interaction energy of the solvent χ_1 , 81
 Interference factor $p(\theta)$, 335

- Internal interference (light scattering), 333, 334, 335
Interferometer, 428
Interpretation of stereogram, 509
Intra- and inter-molecular interaction (protein misfolding), 449
Intrinsic viscosity, 170
Intrinsic viscosity molecular weight, 62, 64
Ion-exchange chromatography, 291
Ionic atmosphere and mobility, 301
Isobestic point, 404
Isoelectric focusing and isotachopheresis, 310, 311, 312, 313
Isotactic polymers, 6
- Johnston-Ogston effect, 248
Junction points, 151
- Kerr effect, 140
Kinetics of synthesis of polymers, 33
Kirkwood-Riseman equation, 173, 176, 177, 195, 196
Kohlrausch's equation, 319
Kronig-Kramers transform, 278
Kuhn length, 233
Kuhn-Kuhn equation for rigid rods and disks, 182
Kurata-Yamakawa theory, 207
- Lagrange equation, 420
Lagrangian theory, 209, 217
Lambert-Beer law (u.v. spectroscopy), 402
Laplace transform, 367
Larmor precession, 459, 471
Laser light scattering, 371, 389
Lattice model, 142
Light scattering, 320
Linear polymers and branched polymers, 5
- Linewidth analysis, 394
Liquid crystals, 127
Liquid crystal displays, 146
Liquid crystalline phase, 127
Living polymers, 27
Long-range interaction, 117
Lorentz line shape, 362, 363, 388, 468
Lorentzian equation, 392
Low-molecular-weight liquid crystals, 131
Lyotropic liquid crystals, 138, 139, 141
- Macromolecular science, 18
Macromolecular thermodynamic, 67
Magnetic field and magnetic moment, 455
Magnetic properties of nuclei, 456
Magnetic resonance imaging (MRI), 475
Main-Chain liquid crystalline polymers, 132
Mark-Houwink equation, 172, 173, 174
Markov chain, 96, 98, 101
Maxwell's model of a mechanical body, 184
McMillan-Mayer theory of osmotic pressure, 203
Mean-field theory, 216
Mean residual rotation, 269
Measurement of translational diffusion coefficient, 234
Mellin transform, 367
Mesogenic core, 127
Mesogens, 128, 132
Mesomorphic phase, 127
Mesophases, 134
Micelle, 2
Miller indices, 498, 500, 501
Mobile phase and stationary phase, 284
Modeling of chemical shift, 488
Moffit-Yang equation, 270, 271
Molar ellipticity, 273
Molar rotation, 269

- Molecular weight and second virial coefficient, 199
 Molecular weight distribution of addition polymers, 58
 Molecular weight distribution of condensation polymers, 57
 Moving boundary (electrophoresis), 303, 304
 Moving-boundary methods (sedimentation), 246

 Natural rubber, 153
 Nematic phase, 134, 136
 Neutron diffraction, 530
 Neutron spectroscopy, 388
 Newtonian fluid, 166
 NMR spectra of macromolecules, 477
 NMR spectroscopy, 470
 Normal phase chromatography, 291, 292
 Northern blot, 309
 Nuclear magnetic resonance, 455, 460
 Nuclear quadrupole relaxation, 469
 Number average molecular weight, 61, 64
 Nylon (66), 32

 Odd function, 349
 One-dimensional NMR, 472
 One-parameter equation, 56
 Operation of rotation X and rotoinversion \bar{X} , 510
 Optical rotatory dispersion, 267, 270
 Order and mobility, 134, 151
 Osmometers, 199
 Osmotic pressure, 198
 Orthogonality, 349
 Overhauser effect, 469

 Partial molar volume, 82
 Partial specific volume, 82, 83
 Partition coefficient (HPLC), 286
 Partition function, 142, 203, 205, 215
 Path, 69
 Patterson synthesis, 517
 Pearl string model, 177
 Periodic function, 348
 Perturbation theory, 107
 Peterlin equation for ellipsoids of revolution in general, 181
 Phase equilibrium, 89
 Plastics, 7, 23
 Point groups, 506, 507, 508
 Poiseuille's law, 167
 Poisson distribution, 54, 58
 Poisson's ratio, 185
 Polarization and depolarization, 418
 Polarized light, 267
 Polyacrylamide gel electrophoresis, 307, 308
 Polycarbonate, 33
 Polyester (fiber), 4
 Polyethylene, 5, 20, 23
 Polymeric liquid crystals, 130
 Polymer of sugars (polysaccharides), 15
 Poly (methyl methacrylate) 5, 6, 25
 Polypeptide synthesis, 40
 Polypropylene, 24, 31
 Polystyrene, 5, 6, 24
 Polyurea, 4
 Polyurethane (fiber), 4, 33
 Poly (vinyl chloride), 5, 24, 25
 Poor solvent, 86
 Power theorem, 361
 Preferential binding (light scattering), 330
 Presvel's equality, 361
 Protein folding and refolding, 444
 Protein misfolding, 448
 Proteins, 10
 Protein sequence and structure, 436
 Protein structure determination (by NMR), 489
 Protein structure representation, 441
 Pulsed Fourier transform method, 471

- Quantum yield, 414
Quenching, 413, 414
- Radical polymerization, 19
Random-flight chains, 103
Random walk, 98, 99
Raoult's law, 75
Rayleigh interference method, 235
Rayleigh ratio, 323
Rayleigh scattering, 320, 321, 322, 323, 324
Red shift and blue shift, 405
Refinement, 519
Relaxation processes, 466
Renormalization group theory, 216
Reversed phase chromatography, 291, 292
Resolution (HPLC), 288
Resonance, 458
Retention (HPL), 285
Review of mathematical statistics, 53
Review of thermodynamics, 68
Ribbon diagrams, 442, 443
Ribosomes: site and function of protein synthesis, 452
Riemann-Stieltjes integral, 354
Rigid-rod model, 141
RNA, 14
Rotational diffusion, 237
Rotation frame of reference, 471
Rouse theory, 187
Rouse-Zimm model, 383
- Scaling relation for translational diffusion coefficient, 233
Scaling theory, 260
Scaling and universality, 119
Scatchard's equation for macroions, 213
Scaling law, 383
Scheraga-Mandelkern equation, 182
Screen length, 112
SDS-polyacrylamide gel electrophoresis, 308
- Second law of thermodynamics, 70
Sedimentation, 243
Segmented-chain polymer liquid crystals, 131, 133
Sedimentation equilibrium method, 244, 250
Sedimentation velocity method, 244, 246
Semidilute solutions, 111, 393
Sequencing DNA fragments, 310
Shapes of mesogens, 133, 134
Shear creep, 186
Side-chain polymer liquid crystals, 131, 132
Simha equations, 182
Size-exclusion chromatography, 291, 293
Small-angle X-ray scattering, 371, 372
Smectic phase, 134, 136
Solubility parameter, 77
Southern blot, 309
Space-filling assembly, 442, 444
Space groups, 506, 512, 513, 514
Space lattices, 499
Specific rotation, 269
Spectrophotometric titration, 408
Spin-lattice relaxation and spin-spin relaxation, 467, 468
Spring-bead model, 188
Star-shaped polymer, 5
Statistical theory of rubber elasticity, 158
Stepwise polymerization, 32
Stern-Volmer equation, 415
Stockmayer-Fixman equation, 175
Structure factor, 515
SBR (styrene-butadiene-rubber), 153
Stoke's law, 176, 238, 419
Stokes-Einstein equation, 230
Stress, strain, and modulus, 165, 166
Stretching and bending, 421
Svedberg equation, 249
Symmetry in crystals, 504
Syndiotactic polymers, 6

- Temperature effect on chain conformation, 114
- Tensile creep, 186
- The 90° pulse, 471, 472
- Theory of chromatography, 289
- Thermodynamics and critical phenomena, 91
- Thermodynamics of rubber, 154
- Thermotropic liquid crystals, 138, 139
- Three-dimensional network, 151
- Torsion angles, 140
- Two-dimensional NMR, 473, 474, 475
- Tube length, 117
- Tube theory (repatation theory), 116
- Turbidity, 323
- Two-parameter equations, 59
- Ultraviolet (UV) and visible spectra, 399, 400
- Unit Cells, 502
- Van Deemter equation, 290
- Van der Waals force, 3, 75
- Van Holde-Baldwin equation, 254
- Van Laar expression, 80
- Van't Hoff's equation of osmotic pressure, 199, 200, 201, 210
- Vapor pressure, 87
- Viscoelastic state, 150
- Viscoelasticity, 184
- Viscosity, 165, 168
- Vulcanization, 152
- Watson-Crick model of DNA, 15
- Weight average molecular weight, 61, 64
- Wiener-Khintchine theorem, 369, 391
- Western blot, 309
- Wormlike chains, 105
- X-ray crystallography, 497
- X-ray diffraction, 497, 498
- Yphantis method, 256
- Z average molecular weight, 62, 64
- Zeta potential, 302, 303
- Ziegler-Natia catalysts, 4
- Zimm plot, 337–345

Publisher's Note:

Permission to reproduce this image online was not granted by the copyright holder. Readers are kindly requested to refer to the printed version of this article.

FIGURE 5.9 Conformation-dependent rate of stretching. Image spaced every 0.13 at the highest strain rate investigated. [Source: T.T. Perkins, D.E. Smith, and S. Chu, *Science* **276**, 2016 (1997). With permission from AAAS.]

Publisher's Note:

Permission to reproduce this image online was not granted by the copyright holder. Readers are kindly requested to refer to the printed version of this article.

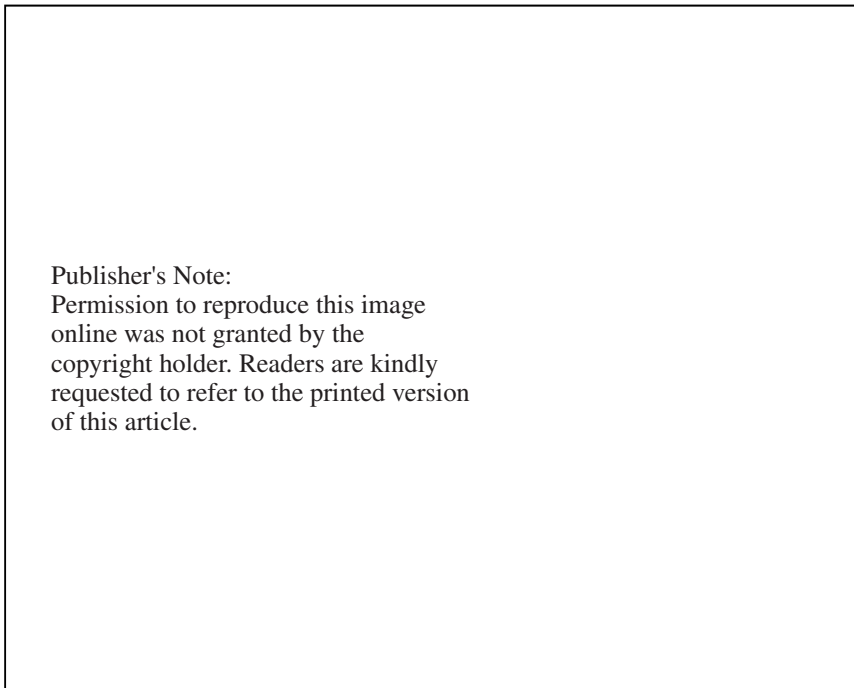
FIGURE 18.6 Ribbon diagrams of three proteins. [Source: (1) Santagata, et al., *Science* **292**, 2041 (2001); (2) Szakonyi, et al., *Science* **292**, 1725 (2001); (3) Watkins, et al., *Science* **292**, 2329 (2001). With permissions from AAAS.]

Publisher's Note:
Permission to reproduce this image
online was not granted by the
copyright holder. Readers are kindly
requested to refer to the printed version
of this article.

FIGURE 18.7 Protein assemblies. [Source: (1) Santagata, et al., *Science* **292**, 2041 (2001); (2) Szakonyi, et al., *Science* **292**, 1725 (2001); (3) Watkins, et al., *Science* **292**, 2329 (2001). With permissions from AAAS.]

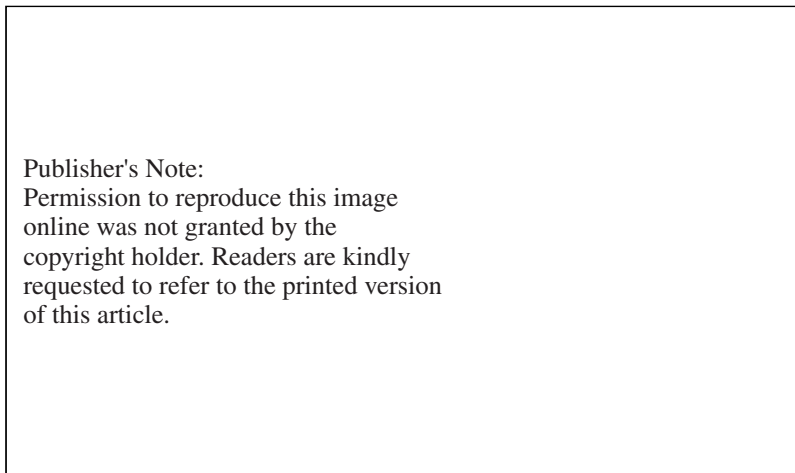
Publisher's Note:
Permission to reproduce this image
online was not granted by the
copyright holder. Readers are kindly
requested to refer to the printed version
of this article.

FIGURE 18.9 Protein structure models: (a) a model of a complex between a fatty acid and a brain protein; (b) a model colored by the surface electrostatic potential. [Source: Baker, et al., *Science* **294**, 93 (2001). With permissions from AAAS.]



Publisher's Note:
 Permission to reproduce this image
 online was not granted by the
 copyright holder. Readers are kindly
 requested to refer to the printed version
 of this article.

FIGURE 18.10 Case 1: Sequence not identified, function similar. Case 2: Sequence and function predicted (left) and experimentally confirmed (right). [Source: Baker, et al., *Science* **294**, 93 (2001). With permissions from AAAS.]



Publisher's Note:
 Permission to reproduce this image
 online was not granted by the
 copyright holder. Readers are kindly
 requested to refer to the printed version
 of this article.

FIGURE 18.13 Structure of a ribosome. [Source: Yusupov, et al., *Science* **292**, 883 (2001). With permissions from AAAS.]

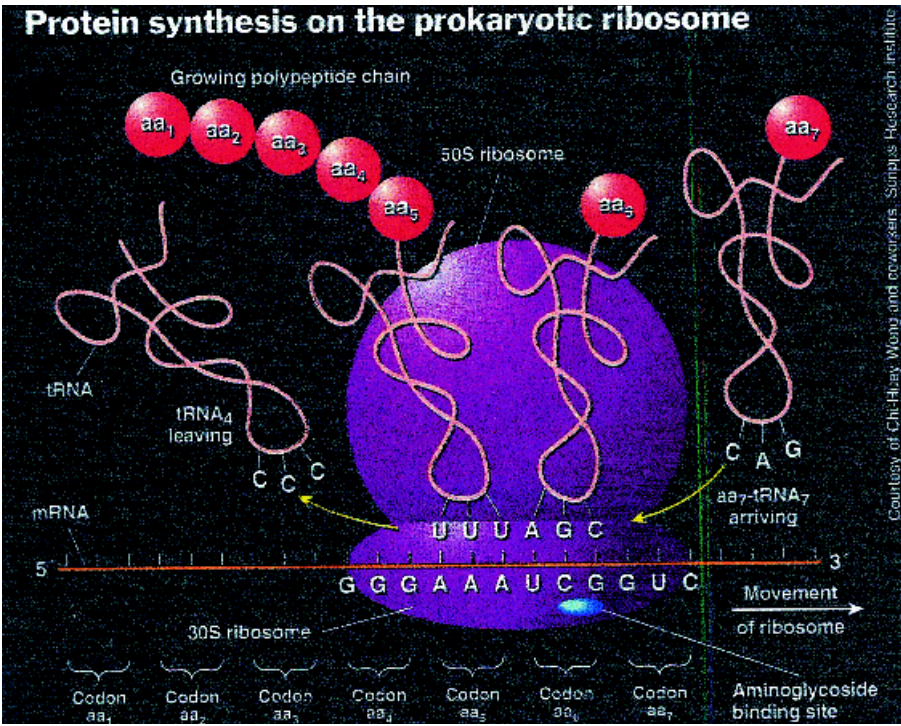


FIGURE 18.14 Protein synthesis on the prokaryotic ribosome. [Source: Borman, S., *C & EN (ACS)* 54, October 2 (2000).]

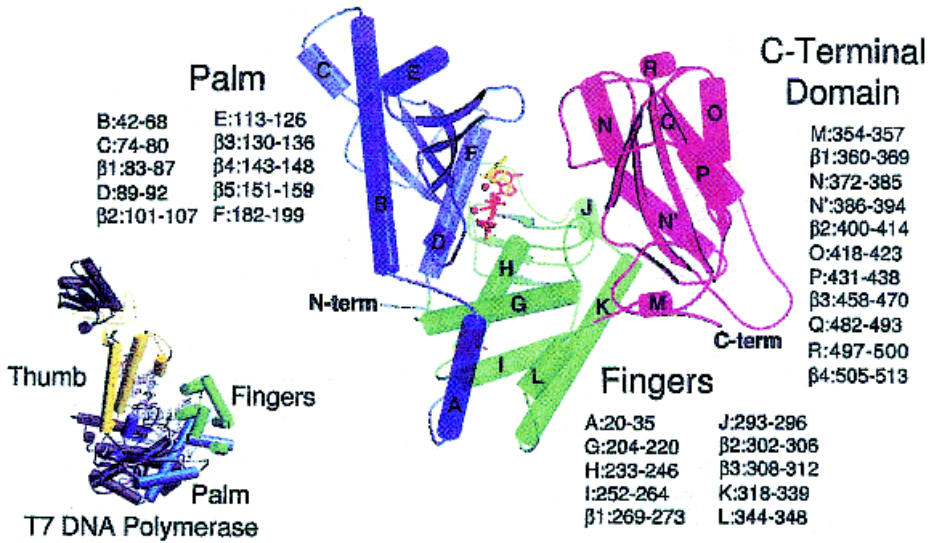
Publisher's Note:
Permission to reproduce this image
online was not granted by the
copyright holder. Readers are kindly
requested to refer to the printed version
of this article.

FIGURE 19.18 A membrane protein: (a) ribbon diagram; (b) recognition; (c) interaction.
[Source: Kuteteladze, et al., *Science* **291**, 1793 (2001). With permission from AAAS.]

Publisher's Note:
Permission to reproduce this image
online was not granted by the
copyright holder. Readers are kindly
requested to refer to the printed version
of this article.

FIGURE 19.19 NMR molecular modeling of prions: (a) NMR structure of PrP^C: (b) binding of protein x to PrP^C: (c) plausible model for the tertiary structure of PrP^{Sc}. Color codes are : red, S1; gray, -helices H³ and H⁴; yellow, loop. Four residues implicated in the species barrier (Asn¹⁸⁸, Met¹²⁹, and Ala¹³⁴) are shown in ball-and-stick form. [Source: Prusiner, S.B., *Science* **278**, 245 (1997). With permission from AAAS.]

A



B

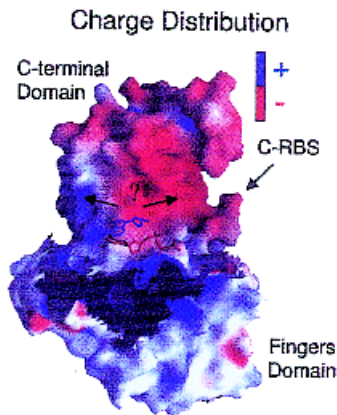


FIGURE 20.21 Polymerase (PAD). [Source: Bard et al., *Science* 276, 2016 (1997). With permission from AAAS.]

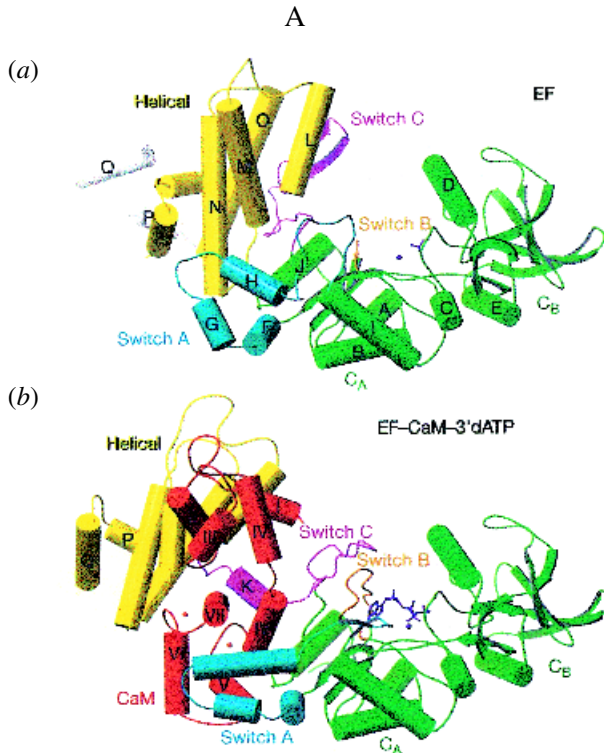


FIGURE 20.22A Secondary structures: (a) EF alone; (b) EF-CaM-3'-deoxy-ATP complex color code; CAM (red), CA (green), switch C (magenta), helical domain (yellow), switch A (cyan), switch B (orange), 3'-deoxy-ATP analogue (purple), metal (purple), C_A and C_B (green), D and Q (amino acids 771–799, white). [Source: Drum et al., *Nature* **415**, 396 (2002). Permission from *Nature*.]

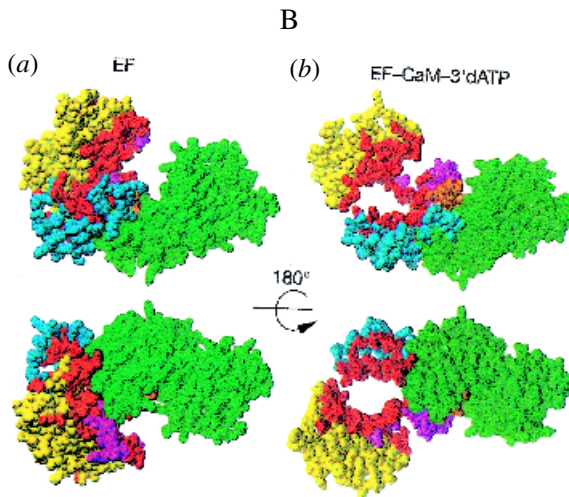


FIGURE 20.22B Visual representation EF structures. (a) EF alone; (b) CaM-EF. [Source: Drum et al., *Nature* **415**, 396 (2002). Permission from *Nature*.]